Lecture Notes in Mechanical Engineering

Vijay Kumar Gupta
Prabhakar V. Varde
P. K. Kankar
Narendra Joshi *Editors*

Reliability and Risk Assessment in Engineering

Proceedings of INCRS 2018

Springer

Lecture Notes in Mechanical Engineering

Lecture Notes in Mechanical Engineering (LNME) publishes the latest developments in Mechanical Engineering - quickly, informally and with high quality. Original research reported in proceedings and post-proceedings represents the core of LNME. Volumes published in LNME embrace all aspects, subfields and new challenges of mechanical engineering. Topics in the series include:

- Engineering Design
- Machinery and Machine Elements
- Mechanical Structures and Stress Analysis
- Automotive Engineering
- Engine Technology
- Aerospace Technology and Astronautics
- Nanotechnology and Microengineering
- Control, Robotics, Mechatronics
- MEMS
- Theoretical and Applied Mechanics
- Dynamical Systems, Control
- Fluid Mechanics
- Engineering Thermodynamics, Heat and Mass Transfer
- Manufacturing
- Precision Engineering, Instrumentation, Measurement
- Materials Engineering
- Tribology and Surface Technology

To submit a proposal or request further information, please contact the Springer Editor in your country:

China: Li Shen at li.shen@springer.com
India: Priya Vyas at priya.vyas@springer.com
Rest of Asia, Australia, New Zealand: Swati Meherishi at swati.meherishi@springer.com
All other countries: Dr. Leontina Di Cecco at Leontina.dicecco@springer.com

To submit a proposal for a monograph, please check our Springer Tracts in Mechanical Engineering at http://www.springer.com/series/11693 or contact Leontina.dicecco@springer.com

Indexed by SCOPUS. The books of the series are submitted for indexing to Web of Science.

More information about this series at http://www.springer.com/series/11236

Vijay Kumar Gupta · Prabhakar V. Varde ·
P. K. Kankar · Narendra Joshi
Editors

Reliability and Risk Assessment in Engineering

Proceedings of INCRS 2018

Springer

Editors
Vijay Kumar Gupta
Discipline of Mechanical Engineering
PDPM Indian Institute
of Information Technology, Design
and Manufacturing, Jabalpur
Jabalpur, Madhya Pradesh, India

P. K. Kankar
Discipline of Mechanical Engineering
Indian Institute of Technology Indore
Indore, Madhya Pradesh, India

Prabhakar V. Varde
Reactor Group
Bhabha Atomic Research Centre
Mumbai, Maharashtra, India

Narendra Joshi
Research Reactor Services Division
Bhabha Atomic Research Centre
Mumbai, Maharashtra, India

ISSN 2195-4356 ISSN 2195-4364 (electronic)
Lecture Notes in Mechanical Engineering
ISBN 978-981-15-3745-5 ISBN 978-981-15-3746-2 (eBook)
https://doi.org/10.1007/978-981-15-3746-2

This Springer imprint is published by the registered company Springer Nature Singapore Pte Ltd.
The registered company address is: 152 Beach Road, #21-01/04 Gateway East, Singapore 189721, Singapore

International Advisory Committee

Prof. A. Parey, IIT Indore, India
Prof. A. S. Sekhar, IIT Madras, India
Prof. A. K. Verma, University of Applied Sciences, Haugesund, Norway
Prof. C. G. Soares, Institute Superior Tecnico Lisbon, Portugal
Prof. Ming J. Zuo, University of Alberta, Canada
Prof. Navin Kumar, IIT Ropar, India
Prof. P. Mahajan, IIT Delhi, India
Prof. P. K. Kapur, Amity University, Gurgaon, India
Prof. P. S. V. Nataraj, IIT Bombay, India
Prof. R. Prakash, IIT Madras, India
Prof. R. Tiwari, IIT Guwahati, India
Prof. R. K. Pandey, IIT Delhi, India
Prof. S. Ahmad, IIT Delhi, India
Prof. S. Chakrabarti, IIT Kanpur, India
Prof. S. Dharmaraja, IIT Delhi, India
Prof. S. Mukhopadhyay, IIT Kharagpur, India
Prof. S. C. Sharma, IIT Roorkee, India
Prof. S. K. Chaturvedi, IIT Kharagpur, India
Prof. S. K. Maiti, IIT Bombay, India
Prof. S. P. Harsha, IIT Roorkee, India

Organizing Committee

Patron

Dr. Kota Harinarayana, Chairman, Board of Governors
Prof. Pramod K. Jain, Director, PDPM IIITDM, Jabalpur
Shri. S. P. Dharne, Vice President, SRESA

Keynote Speakers

Prof. Ajit Kumar Verma, Western Norway University of Applied Sciences, Haugesund, Norway
Dr. JezdimirKnezevic, MIRCE Akademy, Exeter, UK
Prof. Ming J. Zuo, University of Alberta, Edmonton, Alberta, Canada
Dr. Suraj P. Harsha, Indian Institute of Technology Roorkee, India

Conference Chair

Dr. Prabhakar V. Varde, BARC, Mumbai
Prof. V. K. Gupta, PDPM IIITDM, Jabalpur

Conference Co-chair

Dr. P. K. Kankar, PDPM IIITDM, Jabalpur
Dr. P. Vaishnavi, Anna University, Chennai

Conference Convener

Dr. S. Patel, PDPM IIITDM, Jabalpur
Shri. N. S. Joshi, BARC, Mumbai

Conference Secretary

Dr. P. K. Kankar, PDPM IIITDM, Jabalpur
Shri. V. Mishra, BARC, Mumbai

Conference Treasurers

Dr. H. Singh, PDPM IIITDM, Jabalpur
Shri. P. K. Ramteke, BARC, Mumbai

Local Organizing Committee

Prof. A. Ojha, PDPM IIITDM, Jabalpur
Dr. Deepmala, PDPM IIITDM, Jabalpur
Mr. J. B. Singh, PDPM IIITDM, Jabalpur
Dr. H. S. Nanda, PDPM IIITDM, Jabalpur
Dr. K. K. Bharti, PDPM IIITDM, Jabalpur
Dr. M. Ghosh, PDPM IIITDM, Jabalpur
Dr. M. Z. Ansari, PDPM IIITDM, Jabalpur
Mr. N. Joshi, PDPM IIITDM, Jabalpur
Dr. N. K. Jaiswal, PDPM IIITDM, Jabalpur
Dr. P. K. Jain, PDPM IIITDM, Jabalpur
Dr. P. Khanna, PDPM IIITDM, Jabalpur
Prof. P. Tandon, PDPM IIITDM, Jabalpur
Mr. R. Ahmad, PDPM IIITDM, Jabalpur
Dr. R. Panwar, PDPM IIITDM, Jabalpur
Dr. S. K. Jain, PDPM IIITDM, Jabalpur
Mr. S. Mahobia, PDPM IIITDM, Jabalpur
Dr. S. Mukherjee, PDPM IIITDM, Jabalpur
Dr. S. P. Singh, PDPM IIITDM, Jabalpur
Prof. T. Sheorey, PDPM IIITDM, Jabalpur
Mr. V. K. Dubey, PDPM IIITDM, Jabalpur
Dr. Y. S. Katharria, PDPM IIITDM, Jabalpur

Sponsors

Board of Research in Nuclear Sciences (BRNS), Mumbai, India
Atomic Energy Regulatory Board
Bharatiya Nabhikiya Vidyut Nigam Limited (BHAVINI)
SAGE Publications
ARK Infosolutions Pvt. Ltd.

Preface

Reliability and risk assessment has attracted much attention in recent years and plays an important role right from product design, manufacturing, and maintenance phases of any engineering system. It finds various applications in the fields of aerospace, automobile, power plants, security, navy, software, electrical distribution, etc. This book is a collection of articles on reliability and risk assessment presented in the 1st International and 4th National Conference on Reliability and Safety Engineering (INCRS 2018) held at PDPM Indian Institute of Information Technology, Design and Manufacturing, Jabalpur, India. This book consists of eight parts based on specific research areas which include big data analytics and software reliability, condition monitoring techniques and applications, data analytics for reliability, design for reliability, diagnostics and prognostics of mechanical system, health monitoring and management using multi-sensors, optimization and machine learning techniques for industrial applications, performance/failure analysis of materials in service, and reliability issues in electrical distribution systems. A brief description of the parts is as follows:

1. The first part is on *Big Data Analytics and Software Engineering*. Big data analytics has become a major decision support factor in industry and government organizations. In critical system environment, the time factor plays a major role. Many issues are raised when integrating the data across the different platforms of data analytics.

   Right from the analysis and design stage to the maintenance of software-based systems, reliability remains one of the major concerns. This part covers the various factors affecting software reliability and their early assessment.
2. Data analytics has become a major decision support for reliability and maintenance in industry and government organizations. In order to monitor the condition of a machine or plant, a large number of data are acquired from various sensors and analyzed. With the increase in the available data, there is a need for smart data analysis for decision making. Many issues are raised when integrating the data across different platforms. Data analytics can effectively deploy data mining tools and techniques to find hidden patterns in the datasets to

ensure reliability and maintenance of the system. Research topics related to *Data Analytics for Reliability: Applications* will be covered under the first part.

3. Condition monitoring is widely used for monitoring of various components and machines to improve the reliability and life. A number of condition monitoring techniques have been developed based on vibration, acoustics, oil analysis, and thermography. One or more of these techniques can be used for any application based on the critical nature of the machine, plant, etc. This part on *Condition Monitoring Techniques and Applications* includes articles on condition monitoring techniques.
4. The healthy operation of the system is closely allied with the functioning of other linked machine elements. It is always of prime importance to diagnose the fault at the early stage and perform prognosis analysis. Aspects related to health monitoring are covered in two parts on *Diagnostics and Prognostics of Mechanical Systems* and *Health Monitoring and Management Using Multi-sensors.* These parts include articles related to prognostics and uncertainty, accelerated life testing, measurement methods, nonlinear and bifurcation theory, prognostics and health management of machines, etc.
5. The design of a product itself has a strong influence on reliability. Design insufficiencies affect both subcomponent and component. These insufficiencies need to be identified and critically analyzed at the design stage itself, as it is challenging to correct them at later stages. Therefore, reliability-based design is essential to avoid the defects and possibilities of failures. This part on *Design for Reliability* covers topics such as reliability analysis during design, failure mode, effects and criticality analysis, product life cycle assessment, stochastic analysis, failure mechanisms and modeling, and product life extension analysis.
6. Optimization and machine learning techniques have emerged as a powerful tool in recent years. Broadly, meta-heuristics and machine learning can be used for optimization, classification, prediction, and regression analysis. The part titled as *Optimization and Machine Learning Techniques for Industrial Applications* covers the articles discussing these techniques to solve a variety of problems in industrial applications and to determine remaining useful life, reliability of components, and the most economical design of various industrial equipment.
7. Topics such as engineering failure analysis, failure mode effect analysis, and failure logic model are discussed in the part on *Performance/Failure Analysis of Materials in Service*.

Jabalpur, India — Vijay Kumar Gupta
Mumbai, India — Prabhakar V. Varde
Indore, India — P. K. Kankar
Mumbai, India — Narendra Joshi

Contents

Editors and Contributors

About the Editors

Dr. Vijay Kumar Gupta is currently working as a Professor in the discipline of Mechanical Engineering at PDPM-Indian Institute of Information Technology, Design and Manufacturing, Jabalpur. He has more than 25 years of teaching and research experience. He obtained his PhD in Mechanical Engineering from Indian Institute of Technology Bombay, India. His research interests include smart structure, vibration, design, reliability, finite element analysis, mechatronics and robotics, etc. He has published more than 30 papers in refereed journals and conferences and one book. He is recipient of ISAME K. Suryanarayan Rao Memorial Senior Student Award for R&D in Smart Technology for year 2003. He is a member of ASME, SPIE, IEEE, SRESA and other professional bodies.

Dr. Prabhakar V. Varde was Associate Director of Reactor Group, Bhabha Atomic Research Center, Mumbai, India and is Senior Professor, Homi Bhabha National Institute, Mumbai. He completed his PhD from IIT Bombay in 1996. He worked as post-doctoral fellow at Korea Atomic Energy Research Institute, South Korea in 2002 and was visiting professor at CALCE, University of Maryland, USA in 2012. His research interests are development of prognostic models for nuclear plants components in general and electronic components in particular. He worked as a consultant with several international organizations such as OECD/NEA (WGRISK) Paris, International Atomic Energy Agency, Vienna, etc. He is a chief editor for International Journal of Life Cycle Reliability and Safety Engineering. He has over 250 publications, which includes 10 conference proceedings/books, in national and international publications.

Dr. P. K. Kankar is an Associate Professor in the discipline of Mechanical Engineering, Indian Institute of Technology Indore. He has over 14 years of teaching and research experience. He obtained his PhD from Indian Institute of Technology Roorkee, India. His research interests include vibration, design,

condition monitoring of mechanical components, nonlinear dynamics, soft computing, etc. He has published more than 100 papers in refereed journals and conferences. His work has been cited more than 1500 times. He also served as a guest editor of special issues of various journals of national and international repute. He is a member of professional bodies like American Society of Mechanical Engineers, Society for Reliability and Safety (SRESA), Tribology Society of India and International Institute of Acoustics & Vibration (IIAV).

Mr. Narendra Joshi is working as Secretary and founder member of the Society for Reliability & Safety, and is the Managing Editor of SRESA-Springer International Journal on Life Cycle Reliability and Safety Engineering. He has over 20 publications to his credit in journals and conferences. Mr. Joshi is currently looking after the activities of Human Resource Development, Simulator Training, Root Cause Analysis and safety documentation in research reactors at the Bhabha Atomic Research Centre, Mumbai. He has also worked in Operation and Maintenance of research reactors for 13 years. He was involved in preparation of Probabilistic Risk Assessment of research reactors at Trombay and Risk Informed In-Service Inspection.

Contributors

Pavan Agrawal Madhav Institute of Technology & Science, Gwalior, MP, India

Suhail Ahmad Indian Institute of Technology Delhi, New Delhi, India

A. Alagesan A. D. Agricultural College & Research Institute, Tamil Nadu Agricultural University, Tiruchirappalli, India

M. Amarnath Department of Mechanical Engineering, PDPM Indian Institute of Information Technology, Design and Manufacturing, Jabalpur, India

S. Ananthi Anna University Chennai—BIT Campus, Tiruchirappalli, India

Atul B. Andhare Department of Mechanical Engineering, VNIT, Nagpur, India

Prashant Athanker Department of Mechanical Engineering, MNIT, Jaipur, Rajasthan, India

Mradul Awasthi Indian Institute of Technology Delhi, New Delhi, India

Saurabh Bhalerao Rajarambapu Institute of Technology, Rajaramnagar, India

Sharad Bhardwaj Department of Mechanical Engineering, ABES Engineering College, Ghaziabad, U.P., India

Mahesh Bhiwapurkar O. P. Jindal University, Raigarh, India

Neeraj Kumar Bhoi Department of Mechanical Engineering, PDPM IIITDM Jabalpur, Jabalpur, India

Abhishek Chavan Rajarambapu Institute of Technology, Rajaramnagar, India

N. J. Chotai Department of Mechanical Engineering, Marwadi Education Foundation Group of Institutions, Rajkot, India

A. A. Darji Department of Mechanical Engineering, C. U. Shah University, Surendranagar, Gujarat, India;
Department of Mechanical Engineering, LDRP Institute of Technology, Gandhinagar, India

P. H. Darji Department of Mechanical Engineering, C. U. Shah University, Surendranagar, Gujarat, India

N. Dave Department of Mechanical Engineering, PDPU, Gandhinagar, India

Vipul Dave Pandit Deendayal Petroleum University, Gandhinagar, India

V. Deenadayalan Anna University, Tiruchirapalli, India

J. V. Desai Paher University, Udaipur, Rajasthan, India;
Department of Mechanical Engineering, LDRP Institute of Technology and Research, Gandhinagar, Gujarat, India

Nishant Doshi Pandit Deendayal Petroleum University, Gandhinagar, Gujarat, India

Pratiksha Gautam Department of Computer Science & Engineering, Amity School of Engineering and Technology, Amity University Madhya Pradesh, Gwalior, Madhya Pradesh, India

A. B. Gholap Marathwada Mitra Mandal's College of Engineering Pune, Pune, India

Ashish Gupta Discipline of Electrical Engineering, NIT Agartala, Agartala, Tripura, India

Karunesh Kumar Gupta Birla Institute of Technology and Science, Pilani, Rajasthan, India

S. P. Harsha Indian Institute of Technology Roorkee, Roorkee, India

Ankush C. Jahagirdar Birla Institute of Technology and Science, Pilani, Rajasthan, India

Arihant Jain Research Reactor Services Division, Reactor Group, Bhabha Atomic Research Centre, Trombay, India

Arvind Kumar Jain Discipline of Electrical Engineering, NIT Agartala, Agartala, Tripura, India

Pratesh Jayaswal Madhav Institute of Technology & Science, Gwalior, MP, India

M. D. Jaybhaye Department of Production Engineering and Industrial Management, College of Engineering Pune, Pune, India

N. S. Joshi Research Reactor Services Division, Reactor Group, Bhabha Atomic Research Centre, Trombay, India

U. Kagathara Department of Mechanical Engineering, PDPU, Gandhinagar, India

P. K. Kankar Discipline of Mechanical Engineering, Indian Institute of Technology Indore, Indore, India;
PDPM Indian Institute of Information Technology, Design and Manufacturing, Jabalpur, India

M. Karthick AERB-Safety Research Institute, Kalpakkam, India;
College of Engineering, Anna University, Chennai, India

R. Karthikeyan Anna University Chennai—BIT Campus, Tiruchirappalli, India

Abhay Khalatkar Department of Mechanical Engineering, G. H. Raisoni College of Engineering, Nagpur, India

M. B. Kiran Department of Industrial Engineering, PDPU, Gandhinagar, India

K. L. A. Khan Department of Mechanical Engineering, KIET Group of Institutions, Muradnagar, Ghaziabad, U.P., India

Basavraj S. Kothavale Department of Mechanical Engineering, MAEER's MIT College of Engineering, Kothrud, Pune, Maharashtra, India

Harshwardhan Kulkarni Indian Institute of Technology, Mumbai, India

Prabhat Kumar Bharatiya Nabhikiya Vidyut Nigam (BHAVINI), Kalpakkam, Tamilnadu, India

Sachin Kumar Department of Mechanical Engineering, Indian Institute of Technology Ropar, Rupnagar, India

Devesh Kumar Lal School of Computer Science & IT, Devi Ahilya University, Indore, India

Rashmi Lalwani Manipal University Jaipur, Jaipur, Rajasthan, India

V. B. Lalwani Department of Mechanical Engineering, LDRP-ITR, Gandhinagar, Gujarat, India

A. R. Majmudar Department of Mechanical Engineering, LDRP Institute of Technology and Research, Gandhinagar, Gujarat, India

Ashish Malik Department of Mechanical Engineering, ABES Engineering College, Ghaziabad, U.P., India

D. P. Mavani Department of Mechanical Engineering, LDRP Institute of Technology and Research, Gandhinagar, Gujarat, India

S. P. Mehta Department of Mechanical Engineering, LDRP Institute of Technology and Research, Gandhinagar, Gujarat, India

C. J. Mevada Department of Mechanical Engineering, LDRP Institute of Technology, Gandhinagar, India

R. K. Mishra CEMILAC, Defence R&D Organization, Bangalore, India

M. Monica Bhavani Department of CSE, Anna University, BIT Campus, Trichy, Tamilnadu, India

D. H. Pandya Department of Mechanical Engineering, LDRP Institute of Technology and Research, Gandhinagar, Gujarat, India

Adesh Paramane Rajarambapu Institute of Technology, Rajaramnagar, India

Anand Parey Department of Mechanical Engineering, Indian Institute of Technology Indore, Indore, India

S. Parsana Pandit Deendayal Petroleum University, Gandhinagar, Gujarat, India

Chintan Patel Pandit Deendayal Petroleum University, Gandhinagar, Gujarat, India

Jaydeep Patel Department of Mechanical Engineering, Pandit Deendayal Petroleum University, Gandhinagar, Gujarat, India

Rajesh Patel Department of Mechanical Engineering, Pandit Deendayal Petroleum University, Gandhinagar, India

Rhythm Patel Department of Mechanical Engineering, Pandit Deendayal Petroleum University, Gandhinagar, Gujarat, India

S. A. Patel Department of Mechanical Engineering, LDRP Institute of Technology and Research, Gandhinagar, Gujarat, India

Shivdayal Patel Discipline of Mechanical Engineering, Indian Institute of Information Technology, Design and Manufacturing, Jabalpur, India

Vivek Patel Department of Mechanical Engineering, Pandit Deendayal Petroleum University, Gandhinagar, Gujarat, India

Rajkumar Bhimgonda Patil Center for Advanced Life Cycle Engineering (CALCE), University of Maryland, College Park, USA;
Department of Mechanical Engineering, Annasaheb Dange College of Engineering and Technology, Ashta, Sangli, Maharashtra, India

T. Paul Robert College of Engineering, Anna University, Chennai, India

N. B. Prajapati Department of Mechanical Engineering, LDRP Institute of Technology and Research, Gandhinagar, Gujarat, India

Saurabh Pratap Department of Mechanical Engineering, PDPM IIITDM Jabalpur, Jabalpur, India

N. Radadia Pandit Deendayal Petroleum University, Gandhinagar, Gujarat, India

B. D. Raja INDUS University, Ahmedabad, Gujarat, India

T. Ramprabhu Materials and Manufacturing Processes, Palakkad, Kerala, India

K. S. Ramprasad Sathyabama Institute of Science and Technology, Chennai, India

Arun Kumar Rouniyar Department of Mechanical Engineering, Motilal Nehru National Institute of Technology, Allahabad, Uttar Pradesh, India

Neelesh Kumar Sahu Department of Mechanical Engineering, Medi-Caps University, Indore, India

D. Saikiran Department of Mechanical Engineering, Motilal Nehru National Institute of Technology, Allahabad, Uttar Pradesh, India

Hemraj Saini Jaypee University Information Technology, Waknaghat, Solan, Himachal Pradesh, India

Poonam Savsani Department of Mechanical Engineering, Pandit Deendayal Petroleum University, Gandhinagar, Gujarat, India

Vimal Savsani Department of Mechanical Engineering, Pandit Deendayal Petroleum University, Gandhinagar, Gujarat, India

Prakash Kumar Sen O.P. Jindal University, Raigarh, India

C. Senthil Kumar AERB-Safety Research Institute, Kalpakkam, India

Pragya Shandilya Department of Mechanical Engineering, Motilal Nehru National Institute of Technology, Allahabad, Uttar Pradesh, India

Aditya Sharma Department of Mechanical Engineering, Faculty of Engineering, Dayalbagh Educational Institute, Dayalbagh, Agra, India

Vikas Sharma Department of Mechanical Mechatronics Engineering, The LNM Institute of Information Technology, Jaipur, India

Mohak Sheth Canadore college, North Bay, Canada

N. Sheth Pandit Deendayal Petroleum University, Gandhinagar, Gujarat, India

Parnika Shrivastava Mechanical Engineering Department, National Institute of Technology Hamirpur, Hamirpur, India

Amit Singh Department of Mechanical Engineering, MNIT, Jaipur, Rajasthan, India

Harpreet Singh Department of Mechanical Engineering, PDPM IIITDM Jabalpur, Jabalpur, India

Suneet Singh Indian Institute of Technology, Mumbai, India

R. B. Solanki Atomic Energy Regulatory Board, Mumbai, India

Ugrasen Suman School of Computer Science & IT, Devi Ahilya University, Indore, India

Puneet Tandon Mechanical Engineering Department, PDPM Indian Institute of Information Technology, Design and Manufacturing, Jabalpur, India

V. K. Tapas Research Reactor Services Division, Reactor Group, Bhabha Atomic Research Centre, Trombay, India

H. M. Trivedi Department of Mechanical Engineering, LDRP Institute of Technology, Gandhinagar, India

N. Upadhyay Department of Mechanical Engineering, Indian Institute of Technology Delhi, New Delhi, India

O. G. Vaghela Department of Mechanical Engineering, LDRP Institute of Technology and Research, Gandhinagar, Gujarat, India

P. Vaishnavi Department of Computer Applications, Anna University, Chennai—BIT Campus, Tiruchirappalli, India

S. Vaishnavi Department of Computer Applications, Anna University, Chennai—BIT Campus, Tiruchirappalli, India

V. Vakharia Department of Mechanical Engineering, Pandit Deendayal Petroleum University, Gandhinagar, India

A. Valarmathi Department of MCA, Anna University, BIT Campus, Trichy, Tamilnadu, India

P. V. Varde Bhabha Atomic Research Center, Mumbai, India;
Research Reactor Services Division, Reactor Group, Bhabha Atomic Research Centre, Trombay, India

Akash Vasani Department of Mechanical Engineering, Pandit Deendayal Petroleum University, Gandhinagar, Gujarat, India

A. K. Verma Western Norway University of Aplied Sciences, Haugesund, Norway

Jay Govind Verma PDPM Indian Institute of Information Technology, Design and Manufacturing, Jabalpur, India

G. Vidhyalakshmi Department of Computer Applications, Anna University, Chennai—BIT Campus, Tiruchirappalli, India

Anurag Vijaywargiya O.P. Jindal University, Raigarh, India

Venkata Ravi Vusa Discipline of Mechanical Engineering, Indian Institute of Information Technology, Design and Manufacturing, Jabalpur, India

H. K. Yadav Department of Mechanical Engineering, LDRP Institute of Technology and Research, Gandhinagar, Gujarat, India

Big Data Analytics and Software Engineering

A Survey of Real-Time Big Data Processing Algorithms

Devesh Kumar Lal and Ugrasen Suman

Abstract Data collection and processing in real time is one of the most challenging domains for big data. The sustainable proliferation of unbounded streaming data has become arduous for data collection, data pre-process, data optimization, etc. Real-time streaming for data collection can effectively be performed by windowing mechanism. In this communication, we have discussed various windowing mechanisms such as sliding window, tumbling window, landmark window, index-based window, adaptive size tumbling window, and partitioned-based window. The reliability measure, which depends upon selection of appropriate windowing mechanism, has also been discussed. These window-based algorithms have been compared on the basis of CPU utilization, memory consumption, time efficiency, and operation compatibility. In this paper, we have surveyed various aggregation algorithms such as reactive aggregator, flatFAT, flatFIT, B-Int, DABA, and two stacks aggregator and compared them based on time complexity. Remarkably, a hybrid window mechanism has been introduced in this study which can handle the most recent data stream and variable rate of data stream by sliding window and tumbling window, respectively.

Keywords Aggregation algorithms · Big data · Real-time data processing · Streaming data · Window algorithms

1 Introduction

Big data is used for enormous data sets, which become arduous to process by traditional methods like distributive mechanisms. Big data processing challenge gets intensified as data sets acquire velocity (also known as streaming data). Streams of data may be generated from IoT sensor network, internetwork traffic data, stock market, etc. The performance of streaming data analytics in real time with minimum

D. K. Lal (✉) · U. Suman
School of Computer Science & IT, Devi Ahilya University, Indore, India
e-mail: devesh2222@gmail.com

U. Suman
e-mail: ugrasen123@yahoo.com

V. K. Gupta et al. (eds.), *Reliability and Risk Assessment in Engineering*,
Lecture Notes in Mechanical Engineering,
https://doi.org/10.1007/978-981-15-3746-2_1

latency becomes intricate. Unbounded streams of data from various sources continuously proliferate over time. This sustainable proliferation of data stream needs to process in a real-time mode, to minimize the accumulation of data sets in a particular node. Processing of data stream cannot be performed at once; it requires some finite data elements, from unbounded data set.

Sliding window is the most common mechanism for data selection. It gives a finite window particularly based on time or space [1–6]. Time-based window accumulates data sets depend upon number of clock cycle, while space-based window depends upon its size. Increase in coarse window is directly proportional to its latency so that it is adjusted between coarse and fine size of a window. Window accumulations are primarily of two types; namely count-based window and time-based window [7, 8]. Stream of data resides in window for a fixed number of counts, which is termed as count-based window. A window is specified by a fixed-size temporal extent, which usually, most recent time interval and comes under time-based window [9, 10]. Figure 1 depicts a typical windowing mechanism for streaming data. In this mechanism, fixed windows slide over unbounded data streams.

Infeasibility to process entire data stream at once procreates the concept of windowing. Here, the most recent data streams reside into a window. Windowing is widely accepted mainly because of two benefits. Firstly, window makes it possible to implement streaming version of aggregation, and secondly, the most recent data stream can be availed, which is predominant in real-time analytics as compared to historical data. Centralized and distributive window are the two types of processing mechanisms of windowing system. Centralized window creates bottleneck, where data streams are accumulated at a single node, which may discard the new stream data gathered at a node. The rate of incoming data stream might be equal or less than the processing time of the outgoing stream, else creates the accumulation of data streams [11, 12].

Distributive window partitions the window into smaller multiple sub-windows to be deployed into different nodes, for parallel processing. There exist various window techniques such as sliding window, tumbling window, hopping window, partitioned window. [5, 13–17]. The existing window techniques deal with the smaller chunks

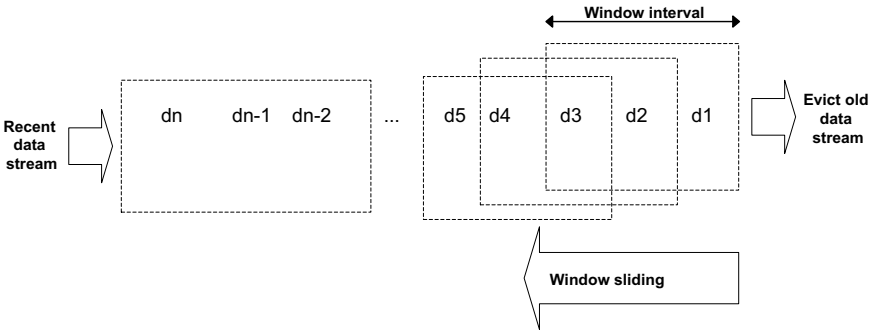

Fig. 1 Windowing system in real-time big data

of data, formed from unbound sets of data stream, which considers the entire data stream in a sequential order, resulting in the enhancement of reliability.

Sliding window is the most widely used technique in data streaming. It uses aggregation mechanisms, which are applied over a window [18]. In this paper, we have applied window algorithms and aggregate algorithms for data streaming. Also, these algorithms are compared with their time and space complexity. Various challenges exist in windowing and aggregators algorithms to design a holistic aggregation for real-time data streams. Many aggregator algorithms are based on operators applied over single data stream node. The challenges get intensified for scalable nature of data stream. Therefore, we have introduced a scalable approach of aggregation sliding-window algorithm able to process into multiple nodes at a time.

2 Windowing Algorithms

Real-time unbound data stream can be evaluated with a fixed size of deterministic window where all types of aggregation and filter operations are performed. A finite number of data chunks can reside in the main memory at a particular time. This data chunk is termed as window, which contains multiple tuples. This window can be processed in centralized or distributed manner. Balkesen et al. [19] propose common dependent tuples require serial manner processing, whereas independent tuples process in parallel manner. Input streams are partitioned into independent chunks known as panes. These collective panes belong to similar window are processed and managed by same process instance.

Balkesen et al. [19] proposed sliding-window partitioning mechanism, where window is broken down into smaller multiple chunks. These multiple chunks are processed in parallel. In tumbling window, elements are assigned to a fixed length, non-overlapping windows of a specified window size such that only, one particular window evicts and inserts at a time [20].

Chen et al. [21] proposed the two classifications of sliding-window algorithm. First classification is based on data independent mode, which is extricated by equivalence partition with round-robin technique. Second approach, classifies data-dependent mode of data streams using a sliding-window index technique. In this approach, data-dependent stream uses a sliding-window index that maintains the window size. It maintains the window by inserting the new data stream into the window and evicting the old data stream resulting in low resource utilization and high system latency.

Tangwongsan et al. [22] and Hirzel et al. [23] proposed the outlining of a chunked-array queue implementation for FIFO windows. The main operations based on queues, such that insert from the back of the queue and evict the front element of the queue. Additionally, the queue provides a bidirectional iterator, which serves as pointers into the queue. The complexity is managed by maintaining a doubly-linked list of chunks, each a fixed-size array of elements.

Patroumpas et al. [18] proposed landmark window where windows have their lower or upper bound fixed at a specific time known as a landmark letting others bound

Table 1 Comparison of windowing mechanisms

Parameter	Window algorithm			
	CPU utilization	Memory consumption	Time efficiency	Operation compatibility
Sliding window	Low	Moderate	High	High
Tumbling window	Moderate	Moderate	Low	Low
Landmark window	Low	Moderate	Low	Low
Index-based window	Low	Moderate	High	High
Adaptive-sized tumbling window	High	Moderate	High	Moderate
Partitioned-based window	High	Low	High	High

to follow the evolution of time. The existing windowing techniques are compared on the basis of CPU utilization, memory consumption, time efficiency, and operation compatibility. Comparison of various windowing algorithms is depicted in Table 1.

Smaller finite sets from unbound data stream procreate window, which become significant by applying operations such as aggregation, joins. Among them, aggregation is a common important feature in streaming applications. Such applications often need an aggregated summary of the most recent data in a stream, which is deemed the most relevant. A poorly chosen algorithm can cause high latencies and high memory consumption, leading to losses, missed opportunities, and quality-of-service violations. Aggregation operation depends on its window, which aims the most efficient algorithm. The most commonly used aggregation algorithms are discussed in the following sections.

3 Aggregation Algorithm

In traditional approach, aggregation is performed from scratch on a chunk window of streaming data. These windows are aggregated as per user-defined query. Increase in window size may reflect enhancement of overall complexity because entire window gets aggregated at a time. Tangwongsan et al. [24] proposed reactive aggregator; it manages values irreversibility, handles non-commutative of processed stream, and provides solution from out-of-order window semantics. In this aggregator, a constant stride maintains which applies over entire window. The length of stride is smaller so that instance aggregated value is stored in a flat array. A user-defined aggregated value is fetched from a query. Reactive aggregator uses FlatFAT aggregator operator mechanism, which stores aggregated results in a pointer-less and tree-based data

structure. These mechanisms reduce the overhead cost such as size of pointer, inclusion of tree-based aggregation. In FlatFAT, aggregated operator allows processing of multiple queries at time into a particular window. These aggregations are performed by storing partial aggregated values in tree leaf node. Final aggregated values are retrieved through applying multiple queries over partial aggregated results. The leaf node of a tree contains partial aggregated values while root node consists of maximum range allowed for a result.

Shein et al. [25] proposed an incremental sliding-window aggregator for real-time analytics. Here, they have introduced a flat and fast index traverse such as FlatFIT approach. FlatFIT maintains indexing structures using a two circular array and a stack. Here, stack maintains and stores indices, whereas circular array interconnected with the help of indices.

The partial aggregated results are stored in an index structure, which reduces recalculation at the time of performing final aggregation. Tangwongsan et al. [22] proposed a De-Amortized Banker's Aggregator (DABA) sliding-window aggregator. DABA uses chunked-array queue data structure for performing sliding-window aggregator operation. Here, every chunk represents a linear size array, which is interlinked with different reference pointers. In this algorithm, various reference pointers help to calculate partial aggregated results. These partial results recombine to form a complete desired aggregated result.

Base Intervals (B-Int) proposed by Arasuand Widom [26] is a final aggregation technique. It uses a multi-level data structure that consists of dynamic intervals of different lengths. The number of partial depends upon the level, such as first level consists of one partial, the second level has two partial, and so on, until we reach to maximum supported range length. The whole data structure is organized in a circular fashion so that the rightmost interval on any level is followed by the leftmost interval from the same level. When producing the final aggregate, B-Int also determines the minimum number of intervals needed to represent the desired range and aggregates the entire range. During insertions, B-Int only updates the intervals that end with the inserted value, instead of updating the entire structure bottom up until reaching the top layer. However, this slows down look-ups, since more intervals are needed to be aggregated to produce result.

Two-stack algorithm is proposed and implemented by Tangwongsan et al. [24] using FIFO window mechanism. In this approach, aggregation is performed over stack, by storing aggregated value in stack-based manner. Two-stack approach spends linear time in evict and storage. A comparative chart of aggregation algorithms is presented in Table 2. The comparison is based on time complexity and usage of its window mechanism.

The comparison of different aggregators on the basis of their time complexity indicates the adaptation of suitable windowing mechanisms. In real-time big data processing, aggregation operation applies on a fraction of window. Therefore, it becomes essential to determine appropriate window and aggregator algorithms. Table 2 shows FlatFIT aggregation approach is best suitable for sliding window and tumbling window. These aggregators may be compared with space complexity as well.

Table 2 Comparison of aggregation algorithms

Algorithm	Time complexity	Windowing
Traditional aggregators	O(n)	Smaller window
Reactive aggregators	Average (log n)	TW, SW, LW
FlatFIT	$n - 1$	SW, TW
B-Int	n . log(n)	Shared window
DABA	Worst O(1)	SW, TW, LW
Two stacks	Average O(1)	IBW, SW

TW—Tumbling window, SW—Sliding window, LW—Landmark window, IBW—Index-based window

4 Challenges and Proposed Work

Windowing mechanisms bind with various challenges such as selection of appropriate window size. If selection of proper window with relative aggregation is not specific, then approach will become costly. A coarse size window may perceive higher latency as compared to fine-sized window. It has some limitation based on eviction and insertion of data streams in window. Aggregations approaches may be distributive, non-distributive, commutative, etc. Generalized aggregator requires specifically designed algorithms, which can contribute number of use cases. Aforementioned aggregator algorithm is based on single data stream node [27].

Here, we introduce the hybrid window model with the combination of sliding window and tumbling window. Sliding window accumulates recent data streams, while tumbling window keeps a fixed interval of data stream that is responsible for the rate of change. Tumbling window slices short interval from sliding window. Tumbling window is executed in distributed manner. Unbound data stream arrives in multiple nodes at a time, which may be extricated by distributive mode and it may also handle generalized holistic aggregation operations. Window can be distributed over multiple nodes. Partitioned window is computed separately in different node. Results are reassembled to get the aggregated value.

5 Conclusions

In real-time data processing, latency can be minimized by using a suitable windowing and aggregation mechanism. The selection of appropriate window and aggregation algorithm is based on various factors such as aggregation operation, type of window, requirements for latency, type of processing, and size of data streams. A generalized solution for all types of use cases in real-time stream processing is rare. Individual algorithm for window and aggregator mechanism cannot satisfy all types of requirements. This paper presents a brief study and comparison of various data stream algorithms, also identified research gaps in aforesaid algorithms.

Acknowledgements I offer most sincere gratitude to the Council of Scientific and Industrial Research (CSIR), Government of India, for financial support in the form of Junior Research Fellowships.

References

1. Gibbonsand BP, Tirthapura S (2002) Distributed streams algorithms for sliding windows. In: Proceedings of the fourteenth annual ACM symposium on parallel algorithms and architectures. ACM
2. Rivetti N, Busnel Y, Mostefaoui A (2015) Efficiently summarizing data streams over sliding windows. In: 2015 IEEE 14th international symposium on network computing and applications (NCA). IEEE
3. Mousavi H, Zaniolo C (2013) Fast computation of approximate biased histograms on sliding windows over data streams. In: Proceedings of the 25th international conference on scientific and statistical database management. ACM
4. Badiozamany S, Orsborn K, Risch T (2016) Framework for real-time clustering over sliding windows. In: Proceedings of the 28th international conference on scientific and statistical database management. ACM
5. Wei Z, Liu X, Li F, Shang S, Du X, Wen JR (2016) Matrix sketching over sliding windows. In: Proceedings of the 2016 international conference on management of data. ACM
6. Wu F, Wu Q, Zhong Y, Jin X (2009) Mining frequent patterns in data stream over sliding windows. In: 2009 international conference on computational intelligence and software engineering, 2009, CiSE. IEEE, New York
7. Zaharia M, Das T, Li H, Hunter T, Shenker S, Stoica I (2013) Discretized streams: fault-tolerant streaming computation at scale. In: Proceedings of the twenty-fourth ACM symposium on operating systems principles. ACM
8. Epasto A, Lattanzi S, Vassilvitskii S, Zadimoghaddam M (2017) Submodular optimization over sliding windows. In: Proceedings of the 26th international conference on world wide web international world wide web conferences steering committee
9. Zhang L, Zhanhuai L, Yiqiang Z, Min Y, Yang Z (2007) A priority random sampling algorithm for time-based sliding windows over weighted streaming data. In: Proceedings of the 2007 ACM symposium on applied computing. ACM
10. Braverman V, Ostrovsky R, Zaniolo C (2009) Optimal sampling from sliding windows. In: Proceedings of the twenty-eighth ACM SIGMOD-SIGACT-SIGART symposium on principles of database systems ACM
11. Balazinska M, Hwang JH, Shah MA (2009) Fault-tolerance and high availability in data stream management systems. In: Encyclopedia of database systems. Springer US, 1109–1115
12. Liberty E (2013) Simple and deterministic matrix sketching. In: Proceedings of the 19th ACM SIGKDD international conference on knowledge discovery and data mining. ACM
13. Patroumpas K, Sellis T (2009) Window update patterns in stream operators. In: East European conference on advances in databases and information systems. Springer, Berlin
14. Bhatotia P, Acar UA, Junqueira FP, Rodrigues R (2014) Slider: incremental sliding window analytics. In: Proceedings of the 15th international middleware conference. ACM
15. Badiozamany S (2016) Real-time data stream clustering over sliding windows. Diss. Acta Univ Ups
16. Zhang L, Lin J, Karim R (2017) Sliding window-based fault detection from high-dimensional data streams. IEEE Trans Syst Man Cybernet Syst 47(2):289–303
17. Golab L (2004) Querying sliding windows over online data streams. In: International conference on extending database technology. Springer, Berlin

18. Patroumpas K, Sellis T (2006) Window specification over data streams. In: Current trends in database technology–EDBT, pp 445–464
19. Balkesen C, Tatbul N (2011) Scalable data partitioning techniques for parallel sliding window processing over data streams. In: International workshop on data management for sensor networks (DMSN)
20. Marcu OC, Tudoran R, Nicolae B, Costan A, Antoniu G, Hernandez MSP (2017) Exploring shared state in key-value store for window-based multi-pattern streaming analytics. In: Proceedings of the 17th IEEE/ACM international symposium on cluster, cloud and grid computing. IEEE Press
21. Chen H, Wang Y, Wang Y, Ma X (2016) GDSW: a general framework for distributed sliding window over data streams. In: IEEE 22nd international conference on parallel and distributed systems (ICPADS). IEEE
22. Tangwongsan K, Hirzel M, Schneider S (2017) Low-latency sliding-window aggregation in worst-case constant time. In: Proceedings of the 11th ACM international conference on distributed and event-based systems. ACM
23. Hirzel M, Schneider S, Tangwongsan K (2017) Sliding-window aggregation algorithms: tutorial. In: Proceedings of the 11th ACM international conference on distributed and event-based systems. ACM
24. Tangwongsan K et al (2015) General incremental sliding-window aggregation. In: Proceedings of the VLDB endowment vol 8(7), pp 702–713
25. Shein AU, Chrysanthis PK, Labrinidis A (2017) FlatFIT: accelerated incremental sliding-window aggregation for real-time analytics. In: Proceedings of the 29th international conference on scientific and statistical database management. ACM
26. Arasu A, Widom J (2004) Resource sharing in continuous sliding-window aggregates. In: Proceedings of the thirtieth international conference on very large data bases, vol 30. VLDB Endowment
27. Cormode G, Yi K (2011) Brief announcement: tracking distributed aggregates over time-based sliding windows. PODC 11

The Internet of Renewable Energy: Big Data-Driven Smart Grid Management with the Reliability and Security Analysis

P. Vaishnavi and V. Deenadayalan

Abstract Renewable energy sources as the solar and wind power are transforming the energy landscape across the world, especially in India. As the government is planning to install 80 GW of solar power generation and 50 GW of wind power generation by 2020, we are presently in an era of increasing solar and wind power generation. The solar and wind energy, along with the associated sensor devices, generate huge amount of data that our traditional warehousing system is unable to store, manage and analyze smart grid, and big data technology provides an answer. Big data is a major research and development direction which provides data storage, retrieval, real-time processing, analytical modeling and visualization. In this paper, we propose the renewable energy architecture along with the integration of big data and power grid. This integration realizes high degree of network connectivity, along with complex security vulnerabilities into the grid. These security challenges, as well as reliability of the system in terms of privacy, integrity authentication and third-party protection have also been discussed in this paper.

Keywords High performance · Computing (IoT) · Renewable energy · Big data analytics

1 Introduction

Renewable energy is an energy which is generated from various natural sources. These sources constitute energy from sunlight, energy from wind, ocean waves, flowing water and geothermal heat [1]. We considered environment as the source. Source will produce an energy, which will be utilized by us either directly or indirectly. The

P. Vaishnavi (✉)
Department of Computer Applications, Anna University, Chennai—BIT Campus, Tiruchirappalli, India
e-mail: vaishmk@gmail.com

V. Deenadayalan
Anna University, Tiruchirapalli, India
e-mail: deenatau@gmail.com

V. K. Gupta et al. (eds.), *Reliability and Risk Assessment in Engineering*,
Lecture Notes in Mechanical Engineering,
https://doi.org/10.1007/978-981-15-3746-2_2

term in-direct refers to the source (sun, water, etc.) which has been converted into a useful energy by using some devices like solar panels.

Before the electricity is delivers to target station (home, office, industry), the source of the electricity is managed by substation for accurate distribution automation. The double power source will be able to switch over to another power source if one has failed to ensure continuous electricity supply to the target stations. So, the traditional grid operation method needs to be changed due to greener power generation. Today, energy is produced everywhere and transported in all the direction in the power system. The intelligent power grid or smart grid is the key to realize this transformation [2]. The green and intelligent power system of the feature is composed of several elements, namely (i) flexible production (solar, wind, biogas); (ii) a strong power grid will be required that is able to transport the large amount of renewable energy to where the energy will be consumed in an international energy market and (iii) demand response. The smart grid in renewable energy enforces for economic and optimum usage of renewable energy using intelligent power system [3].

Reliability is theoretically defined as the probability of success (Reliability $= 1 -$ Probability of Failure) [4] as the frequency of failures; or in terms of availability, as probability derived from reliability, testability and maintainability. Testability, maintainability and maintenance are often defined as a part of "reliability engineering" in reliability programs [5]. Reliability plays a key role in the cost-effectiveness of the systems.

Collecting and analyzing large amounts of data, primarily unstructured data, are not an easy task. Current company systems are not equipped to process 500 terabytes of data per week that can help companies create new products and services that customers want [6]. IoT offerings are generally run on large and costly supercomputers with hundreds or even thousands of servers [7]. The reliability of electricity supply refers to the ability of the bulk electricity supply system to provide electricity within the accepted standards of power quality (i.e., frequency and waveform) when it is demanded. In general, reliability problems fall into two distinct categories—service interruptions/outages and power quality disturbances (i.e., momentary interruptions and voltage disturbances) (Fig. 1).

2 Streamlining Operation and Maintenance Processes

The large-scale wind/solar energy plants enforce for high production in energy resources. The wind/solar energy requires a very large phase of maintaining its energy production. In order to sort the issue of high maintenance, the power plant dataset has to be evaluated to extract the information based on the health condition of the plant. The architectural pattern of solar/wind energy plant is interconnected with many solar panels, sensor extracted data, inverters and connected with complex wired structure.

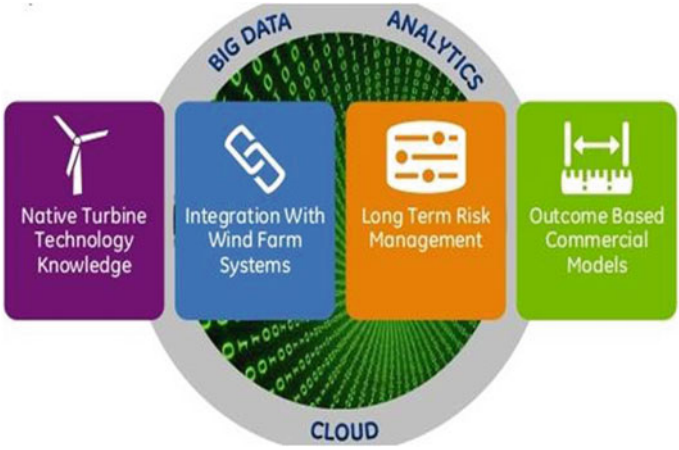

Fig. 1 Industrial Internet for renewable power

The complexity of the plant structure affects routine maintenance in the operation process of plant. Consequently, the energy measurement in the plant on a regular basis will be affected.

The future is on the way with advancements in technology, especially on data analytics (big) on datasets. The datasets received from solar/wind have to be under the solar/wind operations and management (O&M). The virtual irradiance (VI) is a software program for maintenance in the operations of PV panels. It captures the ground-level dataset based on the big data technology. The panels are measured for its outperformance by using analytical tools that reveal the work conditions of the panels interns of over-/underperformance category.

The operators of the group can analyze the problem in ground level of the panels with reliable datasets. The software system analyzes the datasets which enforce the maintenance operations with lesser cost.

The researchers are working exhaustively to ensure the health conditions of the equipments/panels of the plant. They focus on to cut off the parameters to measure the roughness in WEDM of Inconel-825.

3 Internet of Things in Vivid Cortex

Internet of Things(IoT) is connected by physical devices which produces large volume of data and the key challenge in the process is fetching relevant data from the dataset [8]. However, our analytics solution will do the predictive and reliability analysis from the gathered data. This will be achieved through machine learning and artificial intelligence, to work in conjunction with analytics. Vivid Cortex will sit in the top of the Hadoop ecosystem, and this is the best way to understand what

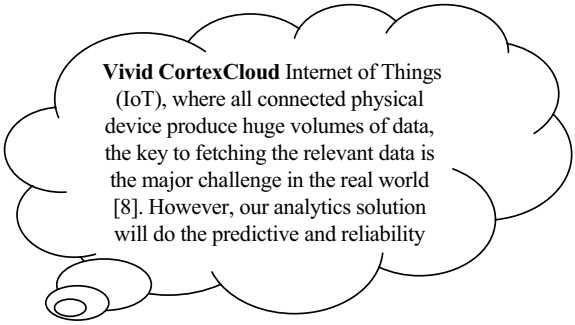

Fig. 2 Implementing big data in Vivid Cortex cloud

happens inside the databases. The characteristics of Vivid Cortex are to perform database operations with backend as MySQL, MongoDB, Cassandra PostgreSQL and Redis. The queries are retrieved through the databases, and the extracted information measures the performance. The major performance between Vivid Cortex and other performance monitoring is showing the performance by charts and gives the alarm by messages [9]. It supports multiple messaging interfaces for remote data logging which includes Kafka, ActiveMQ, MSMQ, MQTT (Fig. 2).

4 Big Data: The Reliability Challenge

Due to technological advancements in data analytics platform, there is a concern on challenges on reliability. The field datasets are considered as highly informative with excessive extraction of useful information from the field. The real-time possibilities are to install various sensors to find the root analysis, predict the future performance, analyze load balancing along with the environmental factors as parameters. Other measurements are the components failure analysis, physical device performance and analysis of imminent component failure [1].

The energy extracted from solar/wind is very large with higher growth of 30% per year continuously for 10 years. This vast growth is a challenge in reliability of components in panels, equipments and physical devices. The operational and maintenance of the devices are moved under very high repair category.

In order to overcome the issues of the reliability of the devices in solar/wind, a predictive mechanism for repair maintenance has to be adopted. Our proposal on the above factors is considered with collection of real-time datasets to measure the performance of the plant by considering the various parameters to enforce reliability challenges.

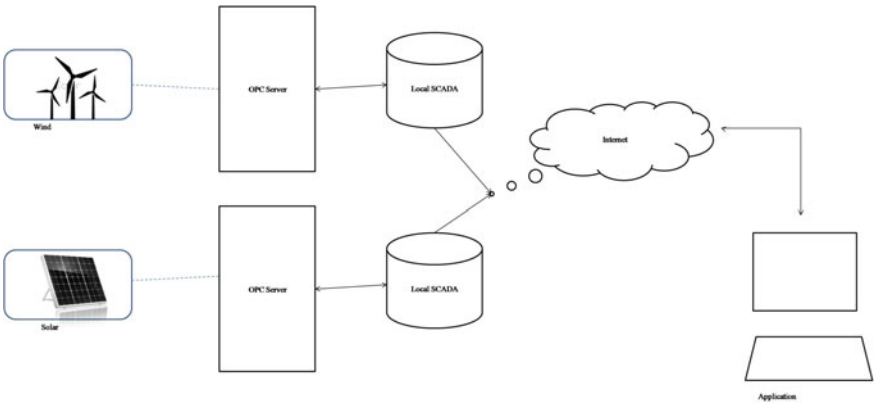

Fig. 3 OPC server with local SCADA integration

5 Solution Design and Outcome

Our proposed analytics solution gives an operation benefit of the application to do the in-depth real-time information about all devices and its alarm notification. During further iteration, the reliability of the devices can be found. It can be found by diagnosing faults and taking decision in real time. Our application will help to identify the underperforming devices by doing digital real-time plant performance analysis. Since we are using waterfall loss diagram, we can identify losses across different stages of solar/wind plant hierarchy.

In Fig. 3, flow diagram displays the information on renewable energy generated from the device data which will in turn send to OPC server. The Open Platform Communications is a software module to run software standards that allow programs to communicate with industrial hardware devices (solar/wind) on supervisory control and data acquisition (SCADA) systems.

The software in the SCADA systems fetches the data from in-build tags and enables the logger to run the OPC server to display the data. Those clients can run on PC with TCP/IP connection in the logger net. The generated data from the logger is displayed through the Internet for analysis and information extraction.

6 Results and Discussion

Based on the sampling data which is generated by the (wind) renewable energy devices, the data processing was done in the HPC environment. The application is to calculate the generated energy which is emitted by the wind plant. The measurement (Figs. 4, 5 and 6) shows the future prediction of renewable energy performance. Based

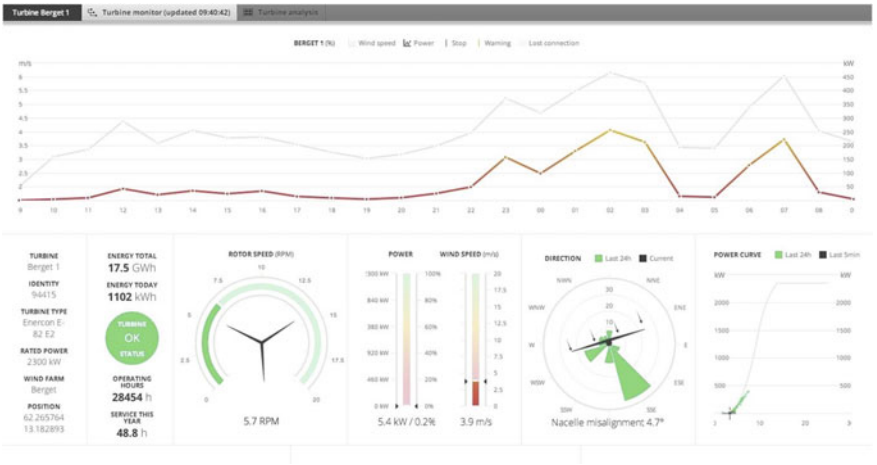

Fig. 4 Analysis of a single wind unit

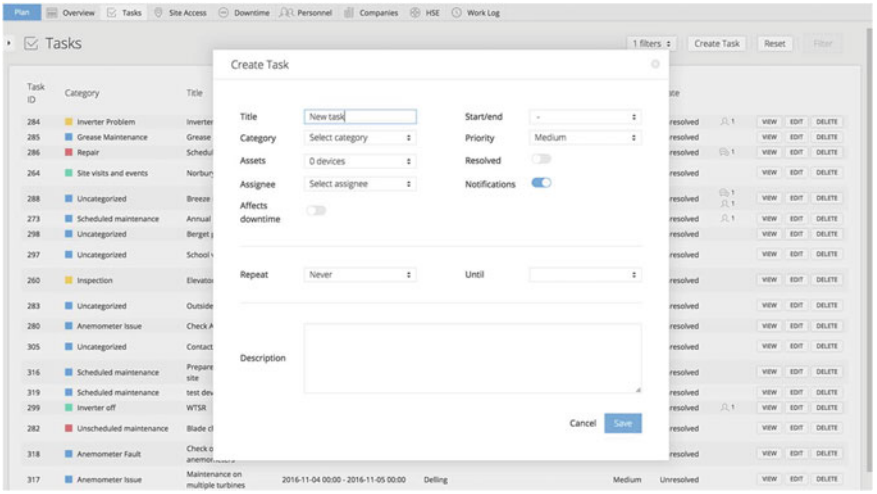

Fig. 5 Task scheduler and maintenance window

on the result, we can identify/predict the future wind generation rate, performance, etc.

The application helps to do all wind farm maintenance tasks using pre-scheduled task window. It will help to find the O&M tasks, site accessibility and turbine downtime status. We can create N number of tasks in the scheduler that depends on the requirement and measures. The monitor dashboard view will show the real-time view of the turbine which includes error logs and warnings (Fig. 7).

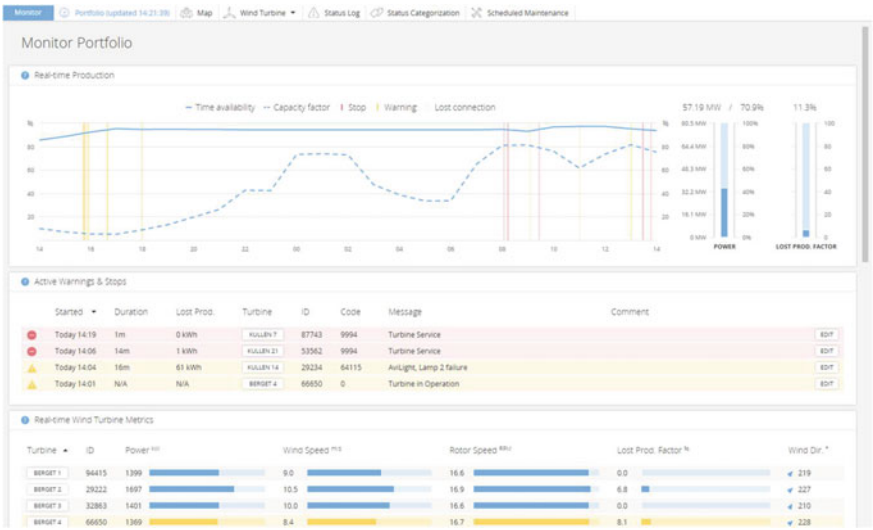

Fig. 6 Monitor dashboard

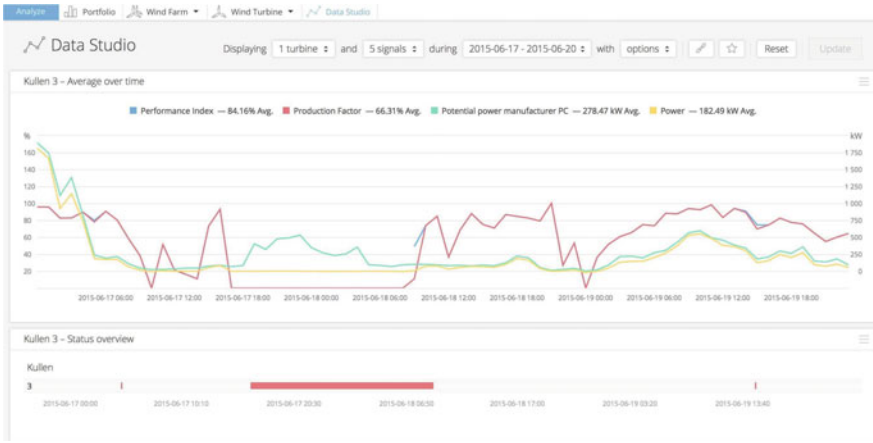

Fig. 7 Data analysis

The wind data analysis will be calculated based on performance metric and production factor. Performance metric will be calculated only when turbine is up and running, and it does not have any stop alarms (Figs. 8 and 9).

The production metric will be calculated only during downtime. During the downtime, turbine performance is 0% and power generation is also 0 kW. The performance metric is always greater than production metric, or both will be the same. The performance analysis on the dashboard helps to understand the turbine performances. Based on this analysis, the turbines will go for the optimization or under-maintained

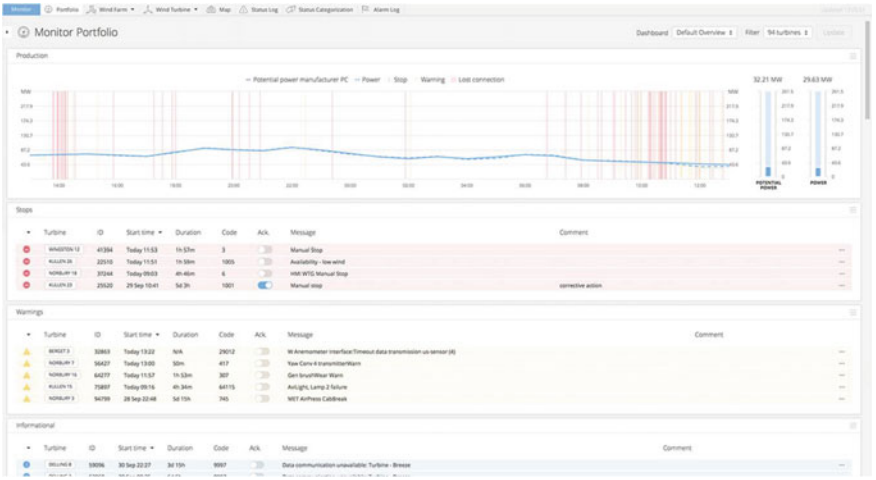

Fig. 8 Turbine reliability monitoring

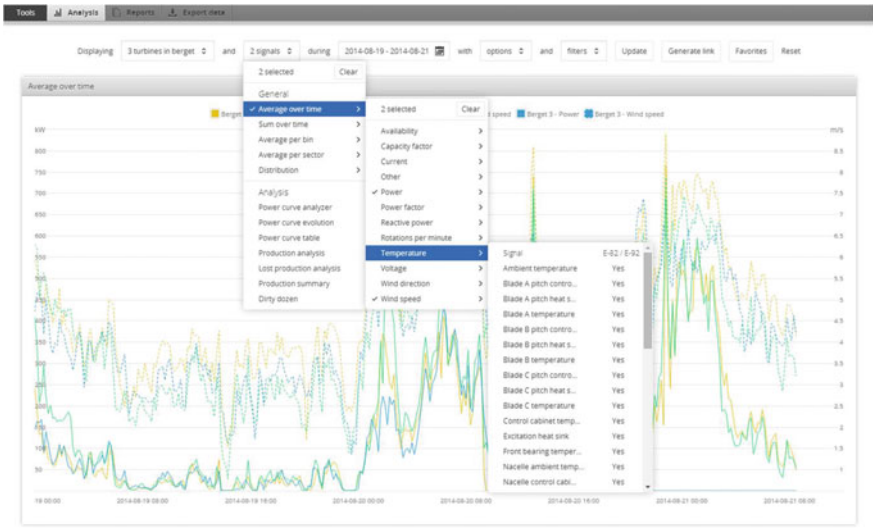

Fig. 9 Performance and alarms

phases. Also, it helps to do the root cause analysis of the turbine if it fails to do the intended operation (Fig. 10).

The turbine availability will be calculated based on the status code and device configuration codes. Each and every device within turbine has their own configuration and its codes. To do the category wise availability, we need to do the detailed analysis of each and every component/devices within the turbine. So, this can be sorted out

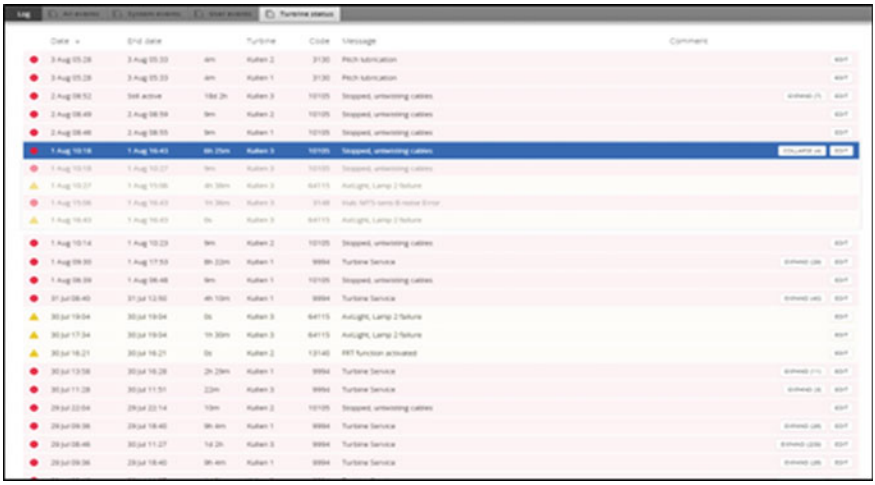

Fig. 10 Turbine availability and perdition

by doing system study and configuration updates of the components. It will help to find the turbine availability, downtime and prediction of failure.

7 Conclusion

In this paper, we have worked on real-time datasets for analysis and discussed the challenges in reliability in data extraction in energy production of solar/wind. The main focus of this paper is working on big data for power grid. The big data-driven smart grid enhances the performance analysis from real-time datasets. The operational and maintenance of the devices in power grid is monitored to extract the uptime and downtime of devices connected in the network. The reliability of the components connected with power grid is measured from the extracted information by providing alarm notification from the software system.

References

1. Zio E (2016) Some challenges and opportunities in reliability engineering. IEEE Trans Reliab 65:1769–1782
2. Bui N, Castellani AP, Casari P, Zorzi M (2012) The internet of energy: a web-enabled smart grid system. IEEE Netw 26:39–45 (2012)
3. Ye Z-S, Xie M (2015) Stochastic modelling and analysis of degradation for highly reliable products. Appl Stoch Models Bus Ind 31:16–32
4. Jarad M, Jarrah M, Bousselham A, Jararweh Y, Al-Ayyouba M (2015) The internet of energy: smart sensor networks and big data management for smart grid. Proc Comp Sci 56:592–597

5. Yin J, Sharma P, Gorton I, Akyoli B (2013) Large-scale data challenges in future power grids. In: IEEE seventh international symposium on service-oriented system engineering, pp 324–328
6. Vellaithurai C, Srivastava A, Zonouz S, Berthier R (2015) CPINDEX: cyber-physical vulnerability assessment for power-grid infrastructures. IEEE Trans Smart Grid 6:566–575
7. Usharani S, Saravanan D, Parthiban R (2017) Resource allocation through energy in IoT network. Int J Sci Res Comp Sci Eng Inf Technol 2:84–86
8. Foradis T, Thramboulidis K (2017) From mechatronic components to industrial automation things: an IoT model for cyber-physical manufacturing systems. J Soft Eng Appl 10:734–753
9. Hu J, Vasilakos AV (2016) Energy big data analytics and security: challenges and opportunities. IEEE Trans Smart Grid 7

Mutation Testing-Based Evaluation Framework for Evaluating Software Clone Detection Tools

Pratiksha Gautam and Hemraj Saini

Abstract Mutation testing has become a prominent research area in the past few decades. The mutation testing has been basically used in the testing society. It is a type of software testing where we mutate (small change, modification in the program) source code using mutant operators by introducing potential new bugs in the program code without changing its behavior. Analogously, mutant operators generate new clones by copy/paste editing activities. However, several software clone detection tools and techniques have been introduced by numerous scientists and a large number of tools comprises for a perceivable evaluation. Moreover, there have been a lot of efforts to empirically assess and analyze variant state-of-the-art tools. The current abstraction exhibits that various aspects that could leverage the legitimacy of the outcome of such assessment have been roughly anticipated due to lack of legitimized software clone benchmark. In this paper, we present a mutation testing-based automatic evaluation structure for valuating software clone detection tools and techniques. The proposed framework uses the edit-based taxonomy of mutation operator for assessing code clone detection tools. The proposed structure injects software clones in the source code automatically, and after that, we evaluate clone detection tools. The clone detection tools are evaluated on the basis of precision (number of corrected clones) and recall (total number of clones). We visualize that such a framework will present a valuable augmentation to the research community.

Keywords Mutation analysis · Software clone · Mutation techniques · Mutation operators

P. Gautam (✉)
Department of Computer Science & Engineering, Amity School of Engineering and Technology, Amity University Madhya Pradesh, Gwalior, Madhya Pradesh, India
e-mail: pratikshamtech20@gmail.com

H. Saini
Jaypee University Information Technology, Waknaghat, Solan, Himachal Pradesh, India
e-mail: hemraj1977@yahoo.co.in

V. K. Gupta et al. (eds.), *Reliability and Risk Assessment in Engineering*,
Lecture Notes in Mechanical Engineering,
https://doi.org/10.1007/978-981-15-3746-2_3

1 Introduction

The experiential estimation of testing techniques plays a vital role in software testing as well as in software clone detection research. One frequent usage is inserting flaws, either manually or by using mutation operators [1]. Generally, empirical evaluations are used to actuate two or more approaches, which are exclusive for complying with some detection-related activity. Testing experiments usually entail a set of subject programs with known faults or errors. Furthermore, in software clone detection, it also requires some faulty version or duplicated code, to evaluate software clone detection approaches. Many researchers consequently have taken the methods of introducing bugs into the correct program to generate faulty variants. These bugs can be pioneered by hand or generated automatically through a faulty version of program text. Typically, we view an automatically generated version as an outcome of employing some editing activities in the source code. However, these editing activities are performed according to well-defined rules which are called mutant operators, and the resulting flawed variants are called mutation generation [2]. The mutation operators are identically used to generate potential bugs in software code clones so as to change the original source code [3, 4]. Reusing source code segment by copying and pasting is a common practice in software development. As a consequence, similar copied code fragments are called software clones, and the process is called software cloning [3]. Earlier study exhibits that a major portion (20–59) of program code in the software code was duplicated [5–10]. An error detected in one segment of code, and then, all segments of source code should be checked for the same error [11]. Copied code can also considerably augment the effort to be thorough when intensifying or complying source code [8]. However, several software clone detection approaches have been anticipated, and there have been a number of comparisons and valuation abstractions relating them in different contexts [12–16]. Nonetheless, it is ambitious to analyze different software clone detection tools, due to software clone detection techniques having specific features, and thus, these researches present considerable contributions to the software clone detection research [17]. Typically, insufficient assessment is aggravated as there are no universal evaluation benchmarks. It is thorny to find such a general norm as each technique has its own tunable features and is designed for distinctive reasons.

In this paper, we present a layout of mutation testing-based evaluation framework. The main objective of our abstraction is to draft a mutation-based evaluation framework which has been used to assess clone detection tools and techniques. The proposed framework is still under implementation and is manifested for quantifying and expanding various software clone detection tools. In this paper, we start off by abstracting the basic introduction of software code cloning and mutation testing from which an editing taxonomy of mutant operators can be derived. Moreover, on the basis of these mutation operators, we assert a framework for valuating code clone detection tools.

2 Background

Copying source code fragments from one section of source text and reusing them into another section with or without minor adaptation are frequent activities in software development process [5]. Software clones can be classified on the basis of their attributes as textual similarity and functional similarity. Further, the textual similarity-based clones are also categorized into three types such as (1) type 1(identical code segment except some variations in whitespace and comments), (2) type 2 (structurally similar code segments except some modifications in variable names, white spaces and comments) (3) type 3 (similar code segments with further alterations as statements deleted, inserted). Functional similarity-based clones are type 4 which have similar functionality but different structures.

3 Mutation Testing Overview

Mutation is a type of white-box testing, which is mainly used for unit testing where we transform (mutate) certain statements of a program text and verify if the test cases are able to find the fault. The adaptation in a mutant program is kept enormously small, so that it does not change the overall intention of the program. The perception of mutation testing is to introduce a syntactic transformation into the original source code, to create a flawed variant (termed as a mutant) as stated by well-defined rules (mutant operators) [18]. The mutation testing first time emerged in the 1970s by [19], in a class term paper. The first research paper was published by the authors 1 [20–22]. The author [23] conducted a survey work on the subarea of mutation testing, which was a weak survey, while the firm mutation provided by [24–27] and they gave an introductory chapter on mutation testing in their books. In 2000, [28] carried out a survey work on mutation testing as well as they recapitulated the history of mutation testing and presented an outline of the existing optimization techniques for mutation testing. Authors [29] defined mutation testing as a fault-based testing, which presents a testing standard known as "mutationcompetence score." The potency of test set can be quantified by using this score in terms of its facility to detect flaws. A recent review was accomplished [30]. They provide a methodical literature survey on application perception of mutation testing. The mutation testing approaches are classified into three types, and mutant operators can be assorted into two types which are shown in Fig. 1. Figure 1a depicts the classification of mutation testing techniques such as (1) the value mutation testing, which alters the key parameter's value as well types of mutation operators. (2) The decision mutation testing, modification in the control statement of the source code using and, or, not. (3) The statement mutation testing method, reorder statements of the program. Figure 1b demonstrates types of mutant operators. The mutant operators can be categorized as traditional mutation operators and class mutant operators. (1) The traditional mutant operators are further classified as arithmetic, logical, relational, conditional, etc. (2) The class mutant operator as

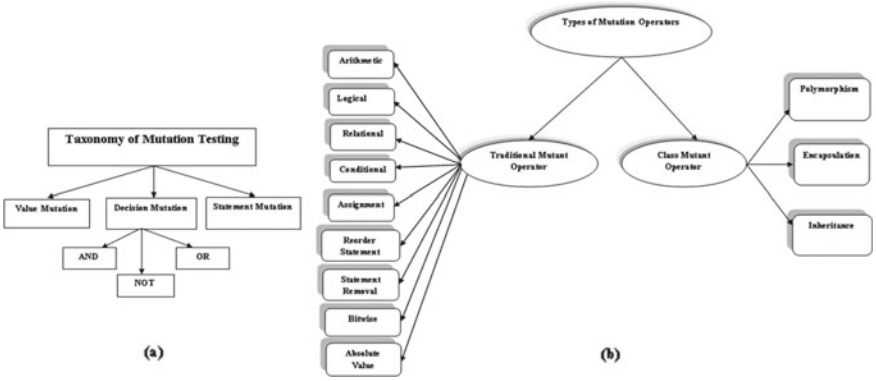

Fig. 1 Taxonomy of **a** mutation testing, **b** mutation operators

inheritance (delete a hidden variable), polymorphism (to check methods have the same name) and encapsulation (transforms, delete and insert instance variables for generating mutants).

The mutation testing is used to create flawed variants from an original program. Further, we used mutation operators for creating various types of software clones which are shown in Fig. 2. Figure 2 shows the mutation operators for software clones. Software clones can be classified into four types. Type-1 clones can be generated by using several mutation operators as mCW removes white space, mCW—changes in blank spaces, mCC—changes in comments, mCF—changes in formatting and mCNWs—changes in new line spaces. Type-2 clones can be generated by using mutation operators as mARV—arbitrary renaming variables, mRPE—replacement of parameters with expressions, mARDT—renaming data types and mARL—arbitrary renaming of literals. Type-3 clones can be generated by mSDL—small deletions within a line, mSIL—small insertions within a line, mMLs—modification in the whole line, mAOR—changes in arithmetic operators and mDSV—variation data statements. Type-4 clones can be created by using mROS—reorder the statements, mCR—replaces one type of control statement with another type of control statement, mCSS—constant substitution.

4 Related Work

The basic idea behind mutation testing is creating exactly similar variants from original program. Each mutant contains at least one artificial modification [31]. There is no mutation testing-based assessment structure presented in the literature; however, there are a number of experiments that contrast and valuate software clone detection

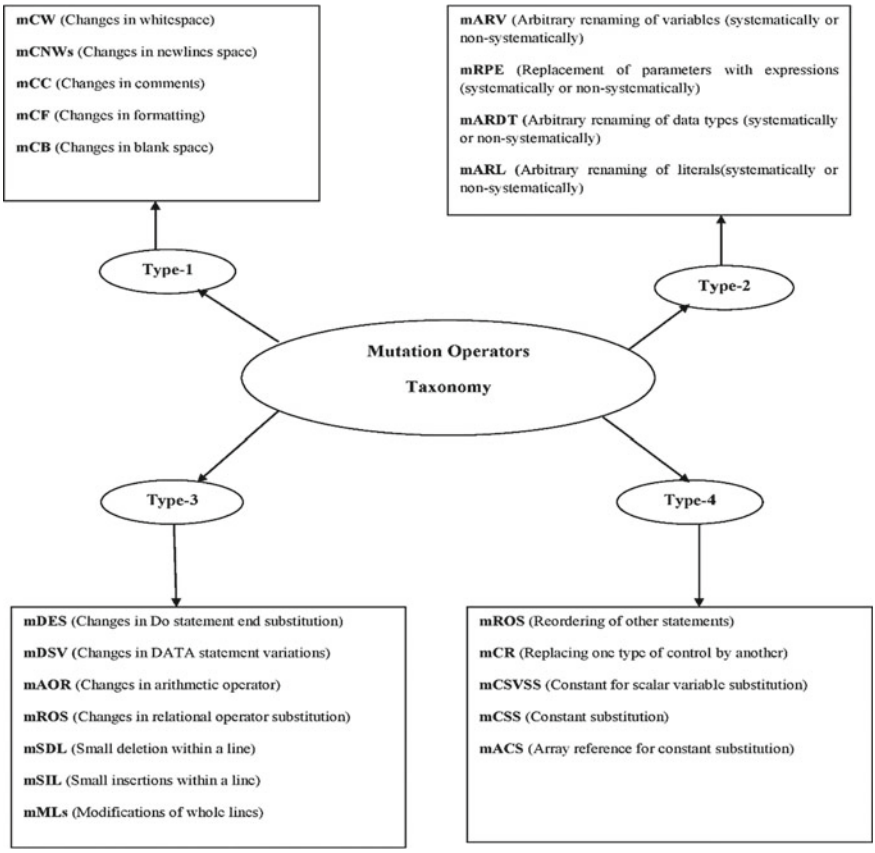

Fig. 2 Taxonomy of mutation operators for software clones

techniques/tools. We present an outline of the existing tool assessment experimentation from the literature. The first experiment was accomplished [14] on two plagiarism detection tools and three state-of-the-arts clone detection tools to evaluate their performance. The first thing they did was verifying the entire duplicated code clones using all the techniques of their experimentation. Various techniques were then compared against various parameters by a human oracle, which in turn uses several metrics that are responsible for measuring different facets of the detected code clones. Though they efficiently identified all the candidate clones, the main constraints of this case study are in terms of size and system quality. The primary objective of their study was to help in a preventive maintenance task which had leverage in validating the candidate clone. Authors have [12] accomplished tool comparison which was invented after considering the limitations of [14] experiment. Further, the authors [12] conducted this experiment with similar three software clone detection tools which are used [14] in their experiment, and they also used three additional clone detection tools in their experiments. The system software [14] had used a diverse set,

accounting to four Java and four C. Moreover, when the authors' [14] studies were taken under consideration while validating the candidate clones, a human oracle was then used for the same. Although being the most comprehensive study till now, the clone candidate being oracled was only a small proportion considering that other factors might have affected the results [17]. However, authors [15] extended this study with a prototype application of several tools, but without addressing anything to conquer the shortcomings of Bellon et al.'s study. The three envoy software clone detection techniques valuated [16], and they presented relative fallouts in perspective of portability, types of replication addressed, scalability, a number of false test matches and the number of ineffectual matches. Nevertheless, the little size cases and paradigm implementation were used by them instead of the actual tools. They intended to conclude appropriateness of the detection technique for a meticulous task as a substitute to the perceptible evaluation of the detection approaches. The researchers [13] carried out an interesting study; they evaluated numerous clone detection techniques in respect of detecting crosscutting apprehensions.

Recently, various researchers proposed number of techniques for mutation testing. Author [32] proposed an efficient mutation testing framework for multi-threaded code which can reduce time required for mutation testing of multi-threaded code. They proposed a tool named as MuTMuT which is based on four optimizations and one heuristic. The mutation testing method used mutation testing in safety-critical industry using high-integrity subsets of C and ADA [33]. They recognized most adequate mutant types and analyzed main reasons of failure in test cases. Moreover, they also provided a practical evaluation of the application of mutation testing to airborne software system. One of the main issues regarding mutation testing was high cost, due to the creation of mutants, execution of mutants and calculation of their scores. Mateo and Usaola [34] proposed a mutant schema with extra code (MUSIC) which reduces the mutation cost through uncovered mutants. Though this technique defines the statements enclosed by the tests in the original system, in order to out the mutant executions, because tests are only executed against the mutants whose mutated statement is covered by tests. Authors [35] measured the complexity of mutants and prioritized them on the basis of how easy or hard to manifest them. The mutation testing is presented in perspective of Python program [36]. They showed how mutation testing can be effectively handled in Python environment. A mutation reduction method is proposed in terms of program structure [37]. Although they used two path-aware heuristic rules named as loop-depth and module-depth rules and combined these two rules with operator-based selection and statements for the development of four mutant reduction approaches. In addition to this, the researchers [38] have also evaluated mutation at the class level while the existing method analyzes mutation at the traditional level. Further, they proposed a MuCPP system which is based on the class mutation operators of C++ programming language. An improved genetic algorithm is presented [39] which is a search-based approach to reduce the computational cost of mutation testing. However, they used state-based and control-oriented fitness function in their tool eMuJava and compared it with other standard fitness functions. However, aforementioned mutation-based testing approaches have been presented in the literature. All these approaches were focused on mutation

testing, while mutation word first time was used [3, 4] in clone detection research field in a brief way. Although they provided an editing taxonomy for various types of clone generation and also proposed a mutation/injection-based framework for evaluation clone detection tools.

As per the authors' best knowledge, there is no thorough work on mutation testing operators in perspectives of software clone detection tools. Yet, there is no standard benchmark available for evaluating clone detection, and there is no empirical evaluation, which explicitly determines the utilization of mutants in clone detection research field. The author contribution in this manuscript is summarized as follows:

- We used mutation testing concept in clone detection research area.
- We used mutation operators for generating various types of software clones.
- Proposed an evaluation framework using mutated code clones.

We evaluated clone detection tools on the basis of mutated code.

5 Proposed Evaluation Framework

This section presents details of our proposed framework which is based on mutation testing as shown in Fig. 5. We start with the basic components of the proposed framework and then thrash out clones terminology, precision and recall of the tools. Although, this framework is based on mutation testing and it acts in accordance with the principle of mutation testing.

Figure 5 illustrates conceptual layout of the proposed framework. The proposed framework is categorized into two main phases. Firstly, Clone Generation Phase, in this phase, software clones are generated from original code with the help of mutation operator-based editing taxonomy. The second phase is Tools Evaluation Phase, in which mutated codes are used to evaluate the software clone detection tools performance. The detailed discussions of the proposed framework are shown below.

5.1 Validation Study

Input Original Code Base: At the primary step of the framework, we input the target code base which is shown in Fig. 3. To find out which tool would be significant for such a valuation in terms of recall and precision.

Figure 3 shows an example of code base which is taken as input in the proposed framework. The original code is retrieved from an open-source project named as wet lab [40] which is an open-source project of C++ language.

Figure 4 depicts an illustration of duplicated code which is generated using mutation operators-based editing taxonomy as well as original source code.

```
//Date: Oct 4 Start :5:23PM End :5:30PM
//Find The Pair With Given Sum
//Complexity : O(n)
#include<iostream>
#include<vector>
using namespace std;
int main()
{
vector<int> v = {1,2,4,5,6,7};
int sum ,left =0 ,right=v.size()-1;
cin>>sum;
while(left<right)
{
  if(v[left]+v[right]==sum)
  break;
  else if(v[left]+v[right]>sum)
  right--;
  else
  left++;
}
if(left<right)
cout<<"Pair Having Sum  "<<sum <<" found at location "<<left+1<<" and "<<right+1<<" value
s are "<<v[left]<<" and "<<v[right];
else
```

Fig. 3 An example of original code base

```
//Date: Oct 4 Start :5:23PM End :5:30PM
//Find The Pair With Given Sum
\\Testing Comment Inserted//Complexity : O(n)
#include<iostream>
#include<vector>
using namespace std;
int main()
{
vector<int> v = {1,2,4,5,6,7};
int sum ,left =0 ,right=v.size()-1;
cin>>sum;
while(left<right)

{
  if(v[left]+v[right]==sum)
  break;
  else if(v[left]+v[right]>sum)
  right--;
  else
  left++;
}
if(left<right)
cout<<"Pair Having Sum  "<<sum <<" found at location "<<left+1<<" and "<<right+1<<" value
s are "<<v[left]<<" and "<<v[right];
```

Fig. 4 An illustration of code clone (type-1)

Random Selection of Code Segment

Once the source code is elected, then any preferred fractional number of accessible source code segment is either selected automatically or randomly from the code base for clone mutation.

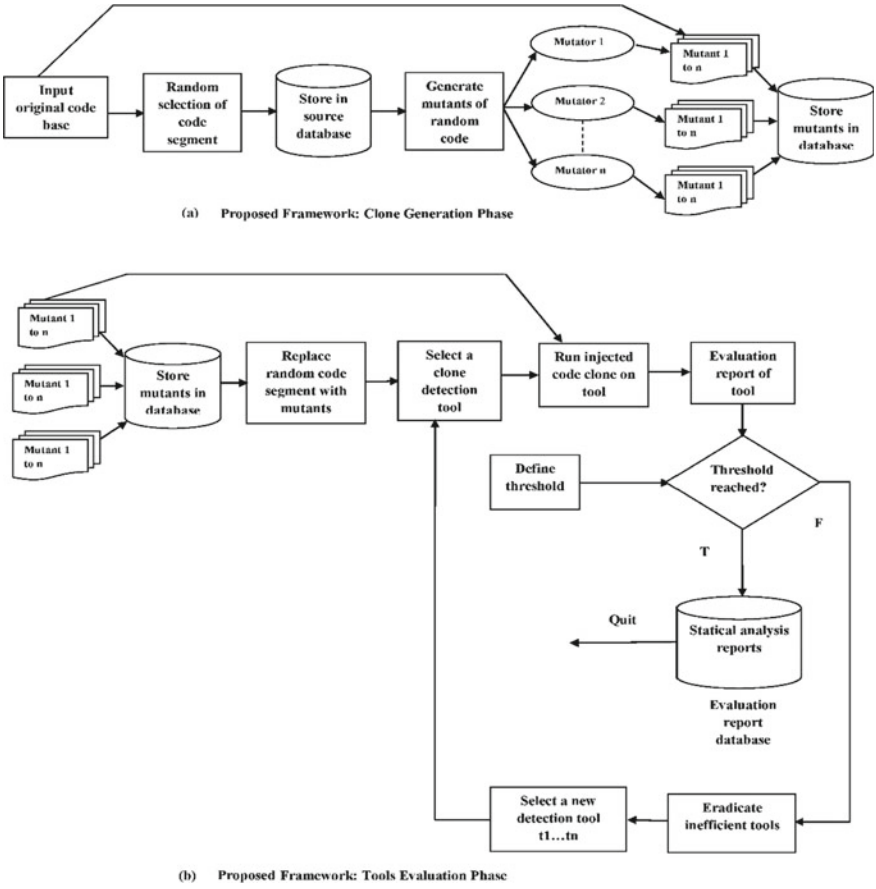

Fig. 5 Proposed mutation-testing-based automatic evaluation framework **a** Clone Generation Phase **b** Clone Tools Evaluation Phase

Stored in Source Database

Randomly selected code segments are stored in the source database, and then, mutants will be created by using these randomly selected code segments.

Generate Mutant of Random Code Segment

The edit-based taxonomy of mutation operators is used for generating mutant versions of randomly or sequentially selected code fragments which are stored in the mutant source database. An example of mutant-version of original code base is shown in Fig. 4. A number of mutants can be generated for one code segment.

The mutated version of the code base after replacement will be fed as input to clone detection tool. The detection tool will be evaluated on the basis of how many clones it will detect accurately and how fast they detect clones.

5.2 Tools Evaluation Phase

In this phase, each of the mutated code is stored in the database, and then, each mutated code is fed into clone detection tools as an input for evaluating and comparing clone detection tools. The main key feature of this phase is threshold. We defined threshold for clone detection tools. If a tool does not fulfill the threshold limit, then that will be eradicated and a new tool will be selected for evaluation.

Replace Random Code Segment with Mutants
The mutated code is generated for each of the mutant code variants of the source code. The generated mutated version of the original code base is replaced with the randomly selected code segments in the original code base.

Select a Clone Detection Tool
In this phase, a tool will be selected, and then, mutated code base is given as input into the selected tool.

Run Injected Code Clones on Tool
The mutated version of code base after replacement will be given as input on clone detection tool. The detection tool will be evaluated on the basis of how much clone it will detect accurately and how fast they detect clone.

Evaluation Report of Tool
The evaluation report makes a decision for the tool. It analyzes the performance of the tool on the basis of precision (number of accurately detected clones) and recall (total number of clones), scalability (tool supports large database) and portability (language support).

Define Threshold
The key objective of this phase is to diminish the execution time and cost of this process. A threshold will be defined by a user for a clone detection tool, and the tool crossing the threshold will be eliminated, and it will select a new tool for evaluation. Further, the tool which has low precision and recall will be discarded and the high precision–recall tool will be evaluated. It will be useful for those users who are seeking high precision and recall-based tools.

Eradicate Inefficient Tool
Most of the tools have low accuracy in the sense that they did not detect all clones (recall), as they returned a large number of false positive (precision). This led to the cognizance which is a step of valuating the results of tools that should be saved at the end.

Statistical Analysis Report
Once the experimentation is accomplished, then evaluation database is used to calculate clone detection tools accuracy as precision, recall, portability and scalability for each type of clone.

6 Clone Terminology

The clone detection tool returns clones in the form of clone pairs (CP), clone classes (CC) or both. The similarity relation between two or more clone fragments is illustrated by these two terms. Further, the clone similarity relation between code segments is an equivalence relation which is described in [41]. The clone relation exists between two segments if they are similar structurally or semantically. A pair of code fragments is called clone pair if there exists a clone relation, while clone class is a union of all clone pairs [42].

Definition 1 (*Code Segment*) A code segment (CS) consists of any subsequence of code string. It is defined by any type of granularity as fixed (predefined syntactic boundary as function, begin-end block) or free (no syntactic boundary). A CS is detected on the basis of granularity in the original program, and it is implied as (CS.Filename, CS.BeginLine, CS.EndLine).

Let $P = \{0, 1, 2, \ldots)$ and $P{+}= \{1, 2, \ldots)$. For $p \in P$, denoted by $O\ (p)\ A$ the set of n operations on A and set $OA{:} = Up \in P{+}\ O(p)A$. A subset CS $\subseteq OA$.

Definition 2 (*Software Clone*) A code segment CS2 is a duplicated software clone of another source segment CS1 if they are identical on the basis of some given definition of similarity that is $f(\text{CS1}) = \text{CS2}$, where f is a similarity function (textual or semantic). Further, when two code segments are similar with each other, they are called clone pairs.

$$\text{CP} = (\text{CS1}, \text{CS2})$$

Definition 3 (*Software Clone Types*) Software clones are classified on the basis of their attributes as textual similarity-based or syntactic-based, and other is functional similarity-based or semantic-based [5].

Definition 4 (*Code Segment Encompassment*) If two or more code segments are contained within same file or the boundary of line numbers of CS1 is within the boundary of line numbers of CS2.

File contained (CS CS1, CS CS2)

If((CS1.FileName==CS2.FileName) && (CS1.BeginLine>=CS2.BeginLine) && (CS1EndLine<=CS2.EndLine))

7 Measuring Recall

The main objective of our proposed framework is to automatically inject software clones in the source code which are generated by using mutation operators. Further, we evaluate clone detection tool's accuracy in terms of precision and recall. The proposed framework addresses recall for each type of software clones and for each

type of mutation operators for all the tools. In this proposed framework, the detectable clones are our injected mutant clone versions of the original source code, and that will be inserted into mutated source code base, randomly or automatically. The mutation testing-based techniques make recall simpler. Moreover, if the mutated code segment as moCS of original code segment oCS inserted into the mutated code base mioCB of original source code base oCB is "killed," oCScs and moCS are detected by clone detector and their threshold level value which returns 1 if detector's minimum threshold value is greater than 1 and maximum value less than 100, otherwise it will return to 0. The main objective of threshold value is to minimize the execution time and complexity. The threshold value depends on user's requirements, and the user can define threshold value between 1 and 100 because recall cannot be less than 1 and cannot be greater than 100.

$$\text{Recall} = (\text{Number of detected clones} * 100)/\text{Total number of clones}$$

R T (oCS, moCs) = {return 1, if (oCS, moCS) is detected by tool T in mioCB $\rightarrow$ THLV (minimum value>=1 & maximum value<=100) otherwise 0.

Where THLV means threshold level value. The similar code segments can be inserted or injected randomly, any number of times, in the original code base oCB and generate n different mutated variants of oCB as mioCB1, mioCB2, …, mioCBn. The proposed framework used mutation operators for creating various types of mutated versions of source code and then inserting them randomly several times to check the sensitivity of clone detector. However, the random segment selector selects m code base, and each of them will be mutated by mutation operators dmOP for generating mutated versions of code segments as moCS1, moCS2, …, moCSm.

Hence, the recall for mutation operator dmOP for clone detector is given as follows.

$$\text{RTdmOP} = \sum_{i=1} n * \text{mRT(oCSi)}/n * m$$

The type-1 software clones used four types of mutation operators (mCW, mCNWs, mCC, mCF, mCB) and their combination (mCW + mCNWs), (mCC + mCF), (mCF + mCB), (mCW + mCC), (mCW + mCF), (mCW + mCB), (mCNW + mCC), (mCNWs + mCF), (mCNW + mCB), (mCC + mCB) and mCF + mCB) can be applied to the m code segments (if we allow operator repetition, then a number of combination can be generated), and each of which is inserted n times into the code base. Therefore, the recall of clone detector tool T for type-1 can be defined as:

RTdmOP = $\sum_{i=1} n * m * (5 + 11)$ RT(oCSi, moCSi)/$m*n*(5+11)$ = {return H, if (n, m) is detected by clone detector tool T in mioCBTHLV (minimum value>=1 & maximum value<=100) otherwise L.

Where H means high recall, L means low recall and 5 indicates number of operators and 11 indicates number of combinations.

The overall recall of clone detectors can be defined as:

RTdmOP $= \sum_{i=1} n * m * (S + C)$ RT(oCSi, moCSi)$/m{*}n{*}(S{+}c) = \{$return H, if (n, m) is detected by tool T in mioCB $\rightarrow$ THLV (minimum value>=1 & maximum value<=100) otherwise L.

Where H means high recall, L means low recall and S indicates number clone mutation operators and C indicates number of combinations.

8 Measuring Precision

Precision measures irrelevant items which appeared in the results. Preferably, precision should be high when recall increases, but practically, it is difficult to accomplish. The precision definition is shown below.

Precision = (Number of correctly detected clones $*$ 100)/Total number of detected clones

The precision of a tool can be calculated as a mutated code segment moCS generated by using mutation operators dmOP, and clone detector tool T returning k clone pairs, (moCS, CS1), (moCS, CS2)…(moCS, CSK) in mutated code base mioCB.

PTdmOP = w.r.t. t. single insertion of moCS = a/k {return 1, if (oCS, moCS) is detected by tool T in mioCB $\rightarrow$ THLV (minimum value>=1 & maximum value<=100) otherwise 0.

Where a means accurate detection and k means number of clone pairs returned by a clone detector T.

The overall precision of clone detector tool in terms of number of mutation operators and number of combinations which is applied n times to m code segments is shown below.PTdmOP $= \sum_{i=1} n * m * (S + C) \Big/ \sum_{i=1} n * m * (S + C) = \{$return H, if (n, m) is detected by clone detector tool T in mioCBTHLV (minimum value>=1 & maximum value<=100) otherwise L. Where H means high precision and L means low precision.

9 Conclusion and Future Work

The valuation of code clone detection tools and techniques is an emerging issue in today's scenario. The previous studies for experimentally valuating clone detection tools and techniques had various constraints and hence, cannot present a persuasive comparable survey. Thus, in this paper, we proposed a peculiar mutation testing-based evaluation layout, for valuating code clone detection tools which are used by testing society over the past thirty years. Moreover, this paper encompasses mutation testing, operators and provides insight into related work on mutation testing. However, we have not accomplished the execution of the framework until now; we are assured that such a framework can present truthful analogous outcome for distinct tools, in finding deliberately generated software code clones. In the proposed structure,

thousands of mutated clone pairs are injected into large systems which are generated by using mutation operators taxonomy (Fig. 1). Further, software clone detection tools will be assessed on the basis of how many duplicated code clones they can identify which is inserted in the software code. In the future, we empirically evaluate mutation testing-based proposed framework for evaluating clone detection tools.

References

1. Andrews JH, Briand LC, Labiche Y (2005) Is mutation an appropriate tool for testing experiments? In: Proceedings of the 27th international conference on software engineering. ACM, pp 402–411
2. Offutt AJ, Lee A, Rothermel G, Untch RH, Zapf C (1996) An experimental determination of sufficient mutant operators. ACM Trans Softw Eng Methodol 5(2):99–118
3. Roy CK, Cordy JR (2009) A mutation/injection-based automatic framework for evaluating code clone detection tools. In: International conference on software testing, verification and validation workshops. IEEE Computer Society, Washington, DC, USA, pp 157–166
4. Roy CK, Cordy JR (2008) Towards a mutation-based automatic framework for evaluating code clone detection tools. In: Proceedings of the 2008 C3S2E conference. ACM, New York, NY, USA, pp 137–140
5. Gautam P, Saini H (2016) Various code clone detection techniques and tools: a comprehensive survey. In: International conference on smart trends for information technology and computer communications. Springer, Singapore, pp 655–667
6. Baker BS (1995) On finding duplication and near-duplication in large software systems. In: Proceedings of 2nd working conference on reverse engineering. IEEE, pp 86–95
7. Ducasse S, Rieger M, Demeyer S (1999) A language independent approach for detecting duplicated code. In: Proceedings of software maintenance. IEEE, Oxford, UK, pp 109–118
8. Mayrand J, Leblanc C, Merlo E (1996) Experiment on the automatic detection of function clones in a software system using metrics. In: ICSM, vol 96, p 24
9. Kontogiannis KA, DeMori R, Merlo E, Galler M, Bernstein M (1996) Pattern matching for clone and concept detection. Autom Softw Eng 3(1–2):77–108
10. Lague B, Proulx D, Mayrand J, Merlo EM, Hudepohl J (1997) Assessing the benefits of incorporating function clone detection in a development process. In: Proceedings of software maintenance. IEEE, Washington, DC, USA, pp 314–321
11. Li Z, Lu S, Myagmar S, Zhou Y (2006) CP-Miner: finding copy-paste and related bugs in large-scale software code. IEEE Trans Softw Eng 32(3):176–192
12. Bellon S, Koschke R, Antoniol G, Krinke J, Merlo E (2007) Comparison and evaluation of clone detection tools. IEEE Trans Softw Eng 33(9):577–591
13. Bruntink M, Van Deursen A, Van Engelen R, Tourwe T (2005) On the use of clone detection for identifying crosscutting concern code. IEEE Trans Softw Eng 31(10):804–818
14. Burd E, Bailey J (2002) Evaluating clone detection tools for use during preventative maintenance. In: Proceedings of second IEEE international workshop on source code analysis and manipulation. IEEE Computer Society, Washington, DC, USA, pp 36–43
15. Koschke R, Falke R, Frenzel P (2006) Clone detection using abstract syntax suffix trees. In: 13th working conference on reverse engineering. IEEE Computer Society, Washington, DC, USA, pp 253–262
16. Van Rysselberghe F, Demeyer S (2004) Evaluating clone detection techniques from a refactoring perspective. In: Proceedings. 19th international conference on automated software engineering, 2004. IEEE Computer Society, Washington, DC, USA, pp 336–339
17. Baker BS (2007) Finding clones with dup: analysis of an experiment. IEEE Trans Software Eng 33(9):608–621

18. Offutt J (2011) A mutation carol: past, present and future. Inf Softw Technol 53(10):1098–1107
19. Lipton RJ (1971) Fault diagnosis of computer programs. Student report, Carnegie Mellon University
20. Budd T, Sayward F (1977) Users guide to the Pilot mutation system. Technique report 114, Yale University, New Haven, CT
21. Hamlet RG (1977) Testing programs with the aid of a compiler. IEEE Trans Softw Eng 4:279–290
22. DeMillo RA, Lipton RJ, Sayward FG (1978) Hints on test data selection: help for the practicing programmer. Computer 11(4):34–41
23. DeMillo RA (1989) Completely validated software: test adequacy and program mutation (panel session). In: Proceedings of the 11th international conference on software engineering. ACM, Pittsburgh, PA, pp 355–356
24. Woodward MR (1990) Mutation testing—an evolving technique. In: IEE colloquium on software testing for critical systems, p 3-1
25. Woodward MR (1993) Mutation testing—its origin and evolution. Inf Softw Technol 35(3):163–169
26. Mathur AP (2013) Foundations of software testing, 2/e. Pearson Education India
27. Ammann P, Offutt J (2016) Introduction to software testing. Cambridge University Press, Cambridge
28. Offutt AJ, Untch RH (2001) Mutation 2000: uniting the orthogonal. In: Mutation testing for the new century. Springer, USA, pp 34–44
29. Jia Y, Harman M (2011) An analysis and survey of the development of mutation testing. IEEE Trans Softw Eng 37(5):649–678
30. Zhu Q, Panichella A, Zaidman A (2016) A systematic literature review of how mutation testing supports test activities (No. e2483v1). PeerJ Preprints, pp 1–57
31. Reales P, Polo M, Fernandez-Aleman JL, Toval A, Piattini M (2014) Mutation testing. IEEE Softw 31(3):30–35
32. Gligoric M, Jagannath V, Luo Q, Marinov D (2013) Efficient mutation testing of multithreaded code. Softw Test Verification Reliab 23(5):375–403
33. Baker R, Habli I (2013) An empirical evaluation of mutation testing for improving the test quality of safety-critical software. IEEE Trans Softw Eng 39(6):787–805
34. Mateo PR, Usaola MP (2015) Reducing mutation costs through uncovered mutants. Softw Test Verification Reliab 25(5–7):464–489
35. Namin AS, Xue X, Rosas O, Sharma P (2015) MuRanker: a mutant ranking tool. Softw Test Verification Reliab 25(5–7):572–604
36. Derezinska A, Hałas K (2015) Improving mutation testing process of python programs. In: Software engineering in intelligent systems. Springer, Cham, pp 233–242
37. Sun CA, Xue F, Liu H, Zhang X (2017) A path-aware approach to mutant reduction in mutation testing. Inf Softw Technol 81:65–81
38. Delgado-Pérez P, Medina-Bulo I, Palomo-Lozano F, García-Domínguez A, Domínguez-Jiménez JJ (2017) Assessment of class mutation operators for C++ with the MuCPP mutation system. Inf Softw Technol 81:169–184
39. Bashir MB, Nadeem A (2017) Improved genetic algorithm to reduce mutation testing cost. IEEE Access 5:3657–3674
40. Wet Lab (1989) Retrieved from http://ftp.gnu.org/gnu/wget/
41. Kamiya T, Kusumoto S, Inoue K (2002) CCFinder: a multilinguistic token-based code clone detection system for large scale source code. IEEE Trans Softw Eng 28(7):654–670
42. Roy CK, Cordy JR (2007) A survey on software clone detection research. Queen's School of Computing TR, 541(115), pp 64–68

Data Analytics for Reliability: Applications

Optimal Traffic Route Finder System

M. Monica Bhavani and A. Valarmathi

Abstract The main aim of this traffic route finder system is to reduce the number of re-computations for finding optimized route and alternate routes. This is to obtain less memory consumption and less wastage of resources that result in minimal response times. On the development of intelligent transport system (ITS), this increasing intensive on-demand of routing guidance system in the real time coincides with increasing growth of roads in the real world. This paper is about the values of the real-time traffic data obtained for arriving at an optimal vehicle routing solution within dynamic transportation networks. Our proposal is to implement an optimal vehicle routing algorithm in order to incorporate the dynamically changing traffic flows. Thus, we present a dynamic approach in selecting the paths for the implementation of our proposed algorithm for the effective road traffic transportations routing system by providing dynamically changing traffic flow of information and the historical data using GIS.

Keywords Shortest path · Geographical information system · Optimal route · Real-time traffic

1 Introduction

This paper gives the optimal traffic routes for the road traffic using the Geographical Information System (GIS). The method has been determined for the calculation of the shortest path using the modified Dijkstra's algorithm with the usage of the fuzzy logic. The Dijkstra's algorithm is the frequently used the shortest path calculating algorithm so far. The fuzzy logic is used with the Dijkstra's algorithm in order to find

M. Monica Bhavani (✉)
Department of CSE, Anna University, BIT Campus, Trichy, Tamilnadu, India
e-mail: mmonicabhavani@gmail.com

A. Valarmathi (✉)
Department of MCA, Anna University, BIT Campus, Trichy, Tamilnadu, India
e-mail: valar1030@gmail.com

V. K. Gupta et al. (eds.), *Reliability and Risk Assessment in Engineering*,
Lecture Notes in Mechanical Engineering,
https://doi.org/10.1007/978-981-15-3746-2_4

out the various other paths of the source node to the destination node, to be selected with the various weights of the paths to be found.

With the improvements in the Geographic Information System (GIS) technology, it is much possible to calculate the fastest and optimized route. This is because a path on a real road network in the city can have various different levels of the traffic, at different time periods of the day, and it is not at all an easy task to locate the shortest path. Thus, the fastest and optimal path can only be calculated in the real time. In some of the cases, the fastest and optimal route has to be calculated in various other ways. Whenever the larger area of road networks is involved in any of the application, the calculation of the shortest paths and optimal path can computationally be very tough.

With the help of the Geographic Information System (GIS) and the Global Positioning System (GPS), logs of information needed in the real-time are dynamic. The changing information has been collected and has become a common practice in many such applications. This paper provides the real-time traffic information of the system, integrated with the historical data which can be used to develop various routing strategies in order to provide both the travel time between the source to destination and the fuel consumption or the traveling cost. This paper aims to develop the new algorithm to reduce the traveling time and cost between every source and destination, by providing an optimal routing path.

We thereby propose the fastest and optimal transportation path routing algorithm, called modified Dijkstra's algorithm, with the fuzzy logic in order to select various routing paths, which defines these conditions. Thus, we present an approach to provide the implementation of the proposed algorithm to an optimal road transportation routing system, where it will be integrated with GIS providing real-time traffic flow information. Thus, we consider getting the shortest path on a road network with various travel times, where the resultant paths for traffic flow are observed in a dynamic way with the help of GIS. This proposed algorithm is designed in a manner to provide the optimal fastest path by using the fuzzy logic, in selecting the next shortest path for every source to the destination.

2 Related Works

The shortest path problem finding with the lower or minimal cost [1] and time from a source to a destination is the fundamental problem [2] in the pathfinding in a road network. Most of the papers deal with finding the shortest path with the algorithms like Bellmann–Ford, Dijkstra's algorithm [3], etc., for the traffic routing between source and destination [4]. Our problem is to find the shortest path with the more optimal algorithms [5] like Dijkstra's algorithm. Many of the literatures emphasize Dijkstra's algorithm as the best-suited algorithm [6] for the shortest path calculation. From the Dijkstra's algorithm, most of the advantageous parts are obtained for creating this new algorithm [7] called modified Dijkstra's algorithm with fuzzy logic [8] which optimize decision making in finding the next shortest destination path to be

selected, as an optimal route [9], to find the destination by considering the dynamic traffic flows information and so on.

Traffic congestion [10] can be of two types: recurring traffic and nonrecurring traffic [11]. Recurring traffic is the place where traffic occurs all the time, and thus, they can be easily predictable. But, the nonrecurring traffic is the place where traffic occurs occasionally which cannot be predictable by most of these systems in providing the most optimal path selection in between a source and destination.

The development of this communication has deciphered dynamic routing as a reality, by providing the Global Positioning System (GPS) for positioning the traffic flows and the Geographical Information System (GIS) to map the features of the traffic routing system. The research publication [12] which is the extended work of the paper [13] determines the special case where network traffic status updating is completely available to all the vehicle drivers. The regular state-space compression technique for the dynamic and flexible stochastic optimal path problems is with real-time traffic information, which is provided to efficiently increase the computational and the implementation processes. This research paper is an extended work of the paper [12] and helps determine the different issues like combining the vehicle routing with the various real-time traffic flow information, from Geographical Information System.

3 Problem Statement

The shortest path calculation is the main problem in the transportation network. Our aim is to create a shortest path algorithm, which is more advantageous than other algorithms, for calculation of the shortest path. This calculation contains various constraints. Some of them are real-time traffic information, that is of the dynamic traffic flow and time-dependent information that is available. In the dynamic transportation network, the network can be of dynamic traffic flow of information with the network path weight changes. This can be of either deterministic or the stochastic dynamic network which is dynamic.

The optimal path problem has been immensely examined and cited in the literature of paper [14] which also gives a modified Dijkstra's algorithm that can be used to calculate the minimum cost for the route in a network, which is static. The paper [15] depicts that the standard shortest path algorithms (such as Dijkstra's algorithm [16]) do not find the minimum expected weight path on a non-stationary or a stochastic network which is dynamic, and that the optimal path chosen cannot be calculated as a simple path but examined based on constraints. There are many dynamic parameters which require constraint-based decision making using the fuzzy logic systems.

4 Methodology

The methodology deals with various constraints and characteristics of the dynamic traffic flow of information, like the time-dependent traffic flow of information which is dynamic, and the historical information which are the GPS datasets of the road traffic information. The methodology is to collect the GPS datasets of the information from the vehicles which traverse through various parts of the city. The routes of the whole city can be noted down for a week's time. This traffic information is gathered from the GPS dataset which is noted down with timing constraints and transformed into a GIS database. From this GIS database, the traffic flow of information is gathered, which is able to detect the traffic in peak hours and during weekends, where the traffic values are high and low, respectively.

From this GIS database, the shortest path is calculated with various clustering techniques and with the proposed algorithm which is modified Dijkstra's algorithm using fuzzy logic in order to detect the traffic route from source to destination. The clustering techniques use the time constraints and travel time of the vehicles, and thus, the optimal shortest path is calculated with the modified Dijkstra's algorithm using fuzzy logic for the decision-making purpose. The shortest path calculated from these techniques and algorithms has to be mapped with the GIS software for visualization of results of specific regions. This methodology provides us with the optimal traffic route.

The implementation of this methodology is done with the help of fuzzy condition-based modified Dijkstra's algorithm. The methodology diagram above provides the implementation steps of the algorithm, which dynamically updates the real-time traffic information with that of the historical collection of the data (GPS logs) collected from GPS-enabled vehicles. The new algorithm has been proposed which is the fuzzy-based modified Dijkstra's algorithm as fuzzy routing algorithm (FRA).

4.1 Fuzzy Routing Algorithm

The fuzzy-based routing algorithm first calculates the intensity of the road traffic within the city for every source and destination. This can be done with the help of the historical dataset, which are GPS logs, for a particular city and the real-time traffic information. The fuzzy logic is to provide the details regarding intensity estimation of every road segment.

Algorithm FRA (G, R, C, ingress, egress, b)

Notation
G = G (N,L) = Input Graph.
R = Set of link residual bandwidth r_i
C = Set of link capacities c_i.
Ingress = Ingress node.
Egress = Egress node.
b = Bandwidth demand.
$Path_y$= Set of nodes in the path from ingress to node y
Begin

1. Remove all links which does not satisfy bandwidth constraint "b" from G
2. Run Dijkstra's Algorithm to calculate H_{min} for each node
3. P = {}, $Path_y$ = {} ∀y, $m^r_{ingress}$=1, and m^r_i = 0 ∀i ≠ ingress.

Loop

4. Find x ∉ P such that m^r_x is maximum ∀x∉ P;
5. P = P U {x}. If P contains egress then exit loop;

Loop

6. ∀y∉ P having a link xy **Update**

$test_y = \beta \times \min(p_{xy}, l_{xy}, h_{xy}) + (1-\beta) \times 1/3(p_{xy}, l_{xy}, h_{xy})$
If
$test_y > m^r_y$
then
$Path_y = Path_x$ U {x};
$m^r_y = \max(m^r_y, test)$;
End If
End Loop
End Loop

7. **Return** $Path_{egress}$
8. **End** FRA

5 Implementation

The implementation of this work is to provide the optimal and shortest path, based on various conditions like traffic intensity estimation, cost of traveling path, the shortest time to reach the destination and so on. This can be done with the help of modified Dijkstra's algorithm and the application of fuzzy logic. The modified Dijkstra's algorithm based on fuzzy logic is to find the shortest and an optimal path to every source and destination. This algorithm is proposed as the fuzzy routing algorithm (FRA).

The various implementation steps of this process are (1) collection of datasets, which are the historical datasets from the GPS logs (2) integration of the real-time

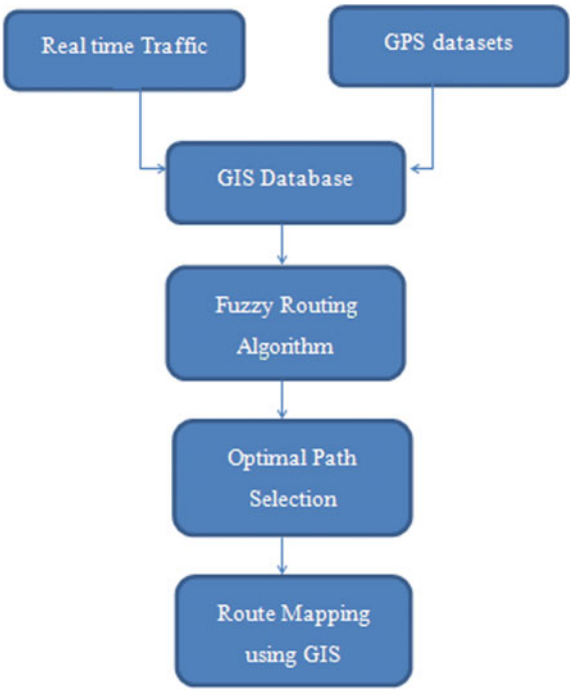

Fig. 1 Methodology diagram

data of traffic information (3) formation of the GIS database (4) execution of the fuzzy-based routing system which provides the traffic intensity estimation, which is the application of the fuzzy logic (5) finding an optimal route between source and destination.

Figure 1 is the implementation output of the fuzzy-based routing algorithm/(FRA). This implementation is done with the Quantum GIS Software (QGIS) which is the open-source software. With the help of QGIS software and execution of the shortest and an optimal path calculating algorithm are taken to calculate the shortest and an optimal path selection. The fuzzy logic provides the traffic estimation prediction in the range of low, very low, moderate, high, very high and so on (Figs. 2, 3 and 4).

6 Conclusion

This paper gives an approach for providing an optimal routing in transportation system and that combined with GIS technology provides the real-time changing and dynamic traffic flows. We have observed that when there are number of paths for the same source to same destination, increased with real-time dynamic traffic flow information, then finding of an optimal routing path for the changing traffic flows is predictable, based on the decision-making process using the fuzzy logic technique.

Table

Road_Centerline

FID	Shape *	Layer	street_nam	Length
0	Polyline ZM	Bituminous Road center	NETHAJI ROAD	638.855481824686
1	Polyline ZM	Bituminous Road center	EAST HANUMANTHARAYAN KOIL STREET	160.938823744309
2	Polyline ZM	Bituminous Road center	MELA AVANI MOOLA STREET	372.545209450986
3	Polyline ZM	Bituminous Road center	VADAKU KOBURAM STREET	113.892723675815
4	Polyline ZM	Bituminous Road center	PATTAMMAL STREET	116.685974415501
5	Polyline ZM	Bituminous Road center	KELA PATTAMMAL STREET	119.885173501993
6	Polyline ZM	Bituminous Road center	NORTH AVANI MOOLA STREET	515.012563410224
7	Polyline ZM	Bituminous Road center	SUNNAMBUKKARA STREET	223.336532452277
8	Polyline ZM	Bituminous Road center	ARISEKARA STREET	154.580751618058
9	Polyline ZM	Bituminous Road center	SOUTH MASI STREET	153.145786143881
10	Polyline ZM	Bituminous Road center	EAST MASI STREET	597.330891837267
11	Polyline ZM	Bituminous Road center	THERKKU MADA VEDHI	88.5929021918555
12	Polyline ZM	Bituminous Road center	THERKKU MADA VEDHI	78.9046227343667
13	Polyline ZM	Bituminous Road center	JADAMUNI KOIL STREET	137.829655847011
14	Polyline ZM	Bituminous Road center	THERKKU MADA VEDHI	586.734208942544
15	Polyline ZM	Bituminous Road center	THOTTIYAN KINATRU STREET	147.366700148313
16	Polyline ZM	Bituminous Road center	SOUTH AVANI STREET	565.149909070298
17	Polyline ZM	Bituminous Road center	THALAVAI STREET	577.792066168771
18	Polyline ZM	Bituminous Road center	VENGALAKADAI STREET	258.669339475449

Fig. 2 Dataset

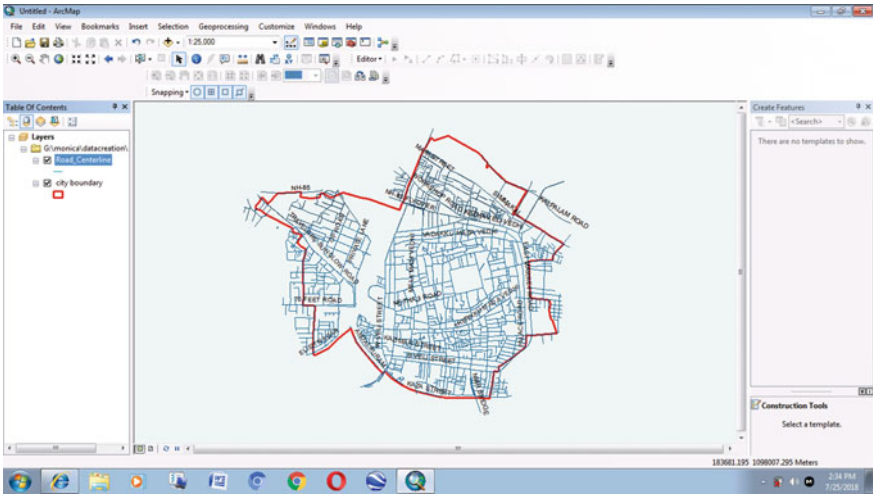

Fig. 3 Shortest path map

Hence, routing algorithm based on the shortest path calculation has been possible with the modified Dijkstra's algorithm with fuzzy logic. It concludes that real-time traffic information from GIS which is incorporated can significantly reduce expected costs and usage of the vehicle during times of heavy congestion.

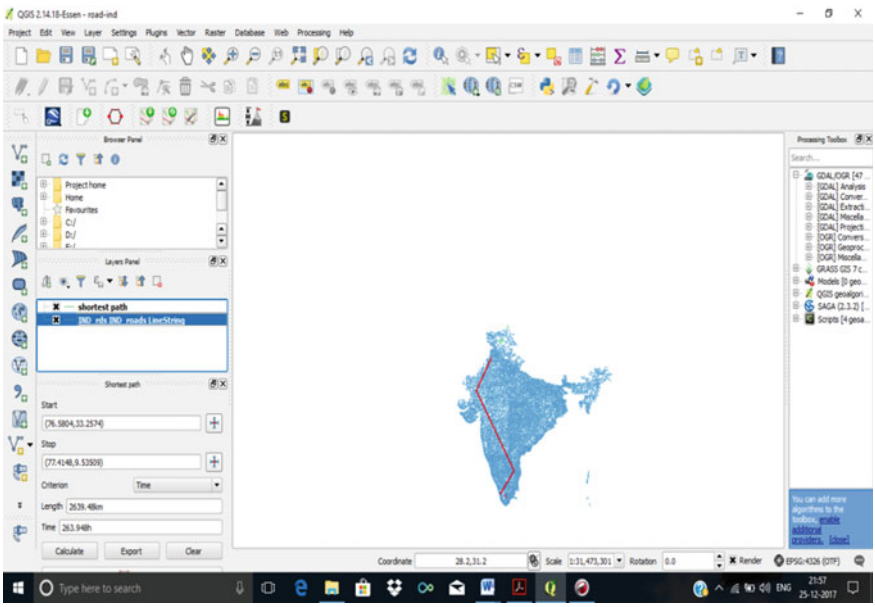

Fig. 4 Shortest path computation using fuzzy routing algorithm (FRA)

7 Future Work

Our aim is to work on with real-time traffic flow of information to obtain the optimal traffic information using GIS by dynamically changing values of information. This will provide dynamic, time to time varying, dependent information, with the real-time traffic flow. This scenario will be created as an application with the most optimal shortest path

References

1. Bander J, White C (2002) A heuristic search approach for a nonstationary stochastic shortest path problem with terminal cost. Transp Sci 36:218–230
2. Hashemi S, Mokarami S, Nasrabadi E (2010) Dynamic shortest path problems with time-varying costs. Optim Lett 4:147–156
3. Likhachev M, Ferguson D, Gordon G, Stentz A, Thrun S (2008) Anytime search in dynamic graphs. Artif Intell 172:1613–1643
4. Opasanon S, Miller-Hooks E (2006) Multicriteria adaptive paths in stochastic, time-varying networks. Eur J Oper Res 173:72–91
5. Zeng W (2009) Finding shortest paths on real road networks: the case for A*. Int J Geogr Inf Sci Taylor Fr 23:531–543
6. Feldman R, Valdez-Flores C (2010) Applied probability and stochastic processes. Springer, Berlin

7. Sarkar A, Sahoo G, Sahoo UC (2012) Application of fuzzy logic in transport planning. Int J Soft Comput (IJSC) 3(2):1–21
8. Sasikala KR, Petrou M, Kittler J (1996) Fuzzy classification with a GIS as an aid to decision making. University of Surrey, Guildford, Surrey GU2 5XH, UK
9. Viswarani CD, Vijayakumar D, Subbaraj L, Umashankar S, Kathirvelan J (2014) Optimization on shortest path finding for underground cable transmission lines routing using GIS. J Theor Appl Inf Technol 65(3):639–643
10. Cherkassky B, Goldberg A, Radzik T (1996) Shortest paths algorithms: theory and experimental evaluation. Math Program 73:129–174
11. Dial R (1969) Algorithm 360: Shortest-path forest with topological ordering. In: Communications of the ACM, ACM, vol 12, pp 632–633
12. Kim S, Lewis M III, White C (2005) State space reduction for non stationary stochastic shortest path problems with real-time traffic information. IEEE Trans Intell Transp Syst 6:273–284
13. Psaraftis H, Tsitsiklis J (1993) Dynamic shortest paths in acyclic networks with Markovian arc costs. Oper Res, JSTOR 41:91–101
14. Fan Y, Kalaba R, Moore I (2005) Shortest paths in stochastic networks with correlated link costs. Comput Math Appl 49:1549–1564
15. Delling D, Wagner D (2009) Time-dependent route planning. In: Robust and online large-scale optimization, Springer, Berlin, vol 5868, pp 207–230
16. Alazab A, Venkatraman S, Abawajy JL, Alazab M (2011) An optimal transportation routing approach using GIS-based dynamic traffic flows. In: International conference on information and financial engineering, IPEDR, vol 12

Failure Modes and Effects Analysis of CNC Turning Center

Rajkumar Bhimgonda Patil and Basavraj S. Kothavale

Abstract CNC turning center is one of the significant CNC-assisted machine tools, widely used for different machining operations. The quality, reliability and maintainability of such CNC turning centers are critical for both the manufacturers and users. In this context, it is decided to carry out failure modes and effects analysis (FMEA) of a typical CNC turning center manufactured and used in India. A FMEA framework is proposed for the analysis of the CNC turning center. The main objective of analysis was to identify critical failure modes and their effects on the components and sub-systems. This study uses the field failure data from more than 50 CNC turning centers and opinions from more than five industrial experts. CNCS, EES, XZAS, ChS, MT, HS, CS and SS are found to be the critical sub-systems of the CNC turning center.CNCS, HS, MT, EES, ChS, TS, XZAS and CS are the critical sub-systems from reliability and maintainability perspective.

Keywords CNC turning center · Reliability · FMEA · Risk priority number

1 Introduction

Computerized numerical control (CNC) turning center is an important CNC-assisted machine tool and used for machining operations [1, 2]. The CNC turning center should be highly reliable and maintainable in order to achieve weekly/monthly/yearly manufacturing targets by smooth and uninterrupted machining operations. The fast-growing manufacturing industries are increasing the demand of such CNC turning

R. B. Patil (✉)
Center for Advanced Life Cycle Engineering (CALCE), University of Maryland, College Park 20742, USA
e-mail: rajkumarpatil2009@gmail.com

Department of Mechanical Engineering, Annasaheb Dange College of Engineering and Technology, Ashta, Sangli, Maharashtra 416301, India

B. S. Kothavale
Department of Mechanical Engineering, MAEER's MIT College of Engineering, Kothrud, Pune, Maharashtra 411038, India

V. K. Gupta et al. (eds.), *Reliability and Risk Assessment in Engineering*,
Lecture Notes in Mechanical Engineering,
https://doi.org/10.1007/978-981-15-3746-2_5

centers [3]. Therefore, the manufacturers of the CNC turning center should allocate suitable reliability and maintainability value in order to sustain in competitive marketplace [4, 5]. Reliability and maintainability ultimately minimize the life cycle cost (LCC) of the CNC turning center and maximize the attention of the user [6]. Time-to-failure, time-to-repair and expert opinion are generally used for reliability, maintainability and availability analysis [7–9].

Failure modes and effects analysis (FMEA) is a qualitative reliability analysis tools used at design as well as operation stage [10, 11]. At design stage, it is used to identify critical failure modes of the system and minimize their occurrence by certain design modifications [12]. FMEA is used at operation stage to improve manufacturing capability and maintenance scheduling [13]. This paper presents the FMEA of a typical CNC turning center manufactured and used in India. The main objective of this analysis is to identify critical failure modes and their effects at component and sub-system level. CNC turning center consists of a large number of components and requires time, cost and detailed knowledge to carry out FMEA. Therefore, it is decided to select only those components and their failure modes which are significant from reliability and maintainability perspective. The effect of failure modes on the component level, assembly level, sub-system and system level is considered to avoid complexity, as well as to maintain consistency, in the FMEA. In this context, FMEA of CNC turning center is carried out with the following objectives.

- To develop FMEA procedure for CNC turning center.
- To prepare severity rating (SR), occurrence rating (OR) and detection rating (DR) using standards.
- Identification of critical failure modes and root causes.
- To develop FMEA worksheet using developed SR, OR and DR and calculate risk priority number (RPN) of each failure mode, component and sub-system.
- To identify the critical components and sub-systems of CNC turning center.

2 Configuration of CNC Turning Center

Figure 1 shows the configuration of a typical CNC turning center. It is composed of mechanical, electrical, electronic, hydraulic, pneumatic and software systems. Chuck is one of the important mechanical sub-systems of CNC turning center, mounted on spindle. The machining component is mounted on the chuck. The clamping and de-clamping of the component are done by hydraulic sub-system through drawbar. The spindle is rotated by a servomotor with step-less speed regulation through main transmission. The encoder is provided on spindle, for thread turning. Cutting tools are mounted on the turret which is moved along *X*- and *Z*-axes. AC or DC servomotors are used to drive *X*- and *Z*-axes through ball lead screws and controlled simultaneously. The turret may change the tools automatically. The other sub-systems of the CNC turning center are cooling, pneumatic, tail-stock, pedestal and lightening.

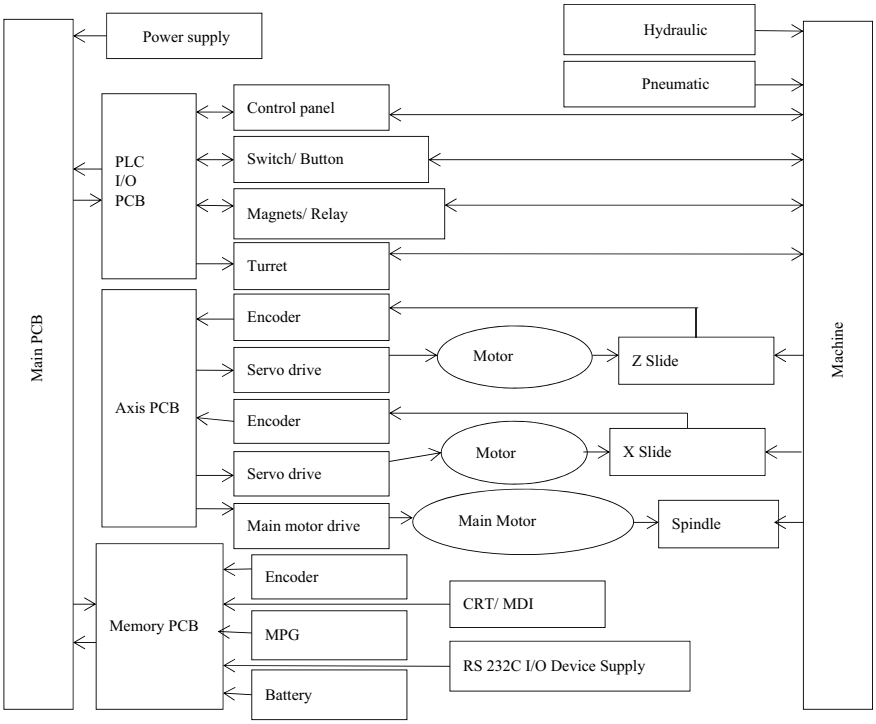

Fig. 1 Configuration of CNC turning center

The various sub-systems are precisely controlled by the CNC system. Therefore, CNC sub-system is considered as the heart of the turning center. It consists of programmable logic control (PLC), printed circuit board (PCB) and power supply. The input/output (I/O) PCB connects the control panel, buttons, limit switch, magnets, turret and other sub-systems. The axis PCB controls the slide axes and the spindle through semi-closed or closed-loop electronic control motor drive and photoelectric encoder. Memory PCB connects additional encoder, CRT/MDI, manual pulse generator (MPG), backup battery and RS-232 serial communication device. There are some electronic components, such as relays, contactor switches, regulators and buttons, fixed in a cabinet. Limit switches, proximity switches and encoders are located on the machine. The CNC sub-system is considered as software sub-system. For analysis purpose, the whole CNC turning center is classified into 14 different sub-systems as shown in Table 1.

Table 1 Sub-systems of the CNC turning center

S. No.	Sub-system	Code	S. No.	Sub-system	Code
1	Main transmission	MT	8	Hydraulic sub-system	HS
2	Spindle sub-system	SS	9	CNC sub-system	CNCS
3	Chuck sub-system	ChS	10	Electrical and electronic sub-system	EES
4	*X*- and *Z*-axis sub-system	HS	11	Swarf conveyor	SC
5	Turret sub-system	TS	12	Pneumatic sub-system	PS
6	Cooling sub-system	CS	13	Tail-stock sub-system	TSS
7	Lubrication sub-system	LS	14	Other sub-system	OS

3 Development of FMEA Framework for the Analysis of CNC Turning Center

In this section, a FMEA framework is developed for the analysis of CNC turning center using standards. The required data for FMEA of CNC turning center are collected from the users, domain experts and published research papers. A multi-disciplinary FMEA team is formed consisting members from different departments such as design, reliability, production, materials, maintenance and planning, and also, persons from management, operators, suppliers and customers. The team is generally selected based on several factors such as experience, expertise and domain knowledge [14]. Risk priority number (RPN) and military standard technique (MST) are the two methods used for failure analysis. Defense, aerospace and nuclear industries use MST, and automotive industries widely use RPN. MIL-STD-1629A (1980), SAE J 1739 and SMC REGULATION 800-31 are the standards developed for FMEA. It is developed by the Defense Department of the United States [15]. The ratings and the layout may change from one standard to another; however, the fundamental procedure remains same. In this context, FMEA of CNC turning center is presented using the guidelines presented in MIL-STD-1629A (1980). However, to make FMEA more appropriate to CNC turning center, necessary modifications are made in severity, occurrence and detection rating criteria.

FMEA uses a numerical value to each risk causing a failure. The RPN of a failure mode is calculated using following three factors: (1) the severity of the failure effect, (2) probability of occurrence of the failure mode and (3) the detection probability. The RPN of a failure mode is calculated by taking the product of corresponding severity rating, occurrence rating and detection rating. The severity, occurrence and detection ratings are allocated with a minimum rating of 1 and maximum rating of 10. Therefore, the minimum and maximum RPN are 1 and 1000, respectively. A high value of RPN for a failure mode indicates a poor score, and such failure modes are critical failure modes. Therefore, a higher priority is given to these failure modes. However, the ratings and criteria for criticality of failure modes are different for different organization.

Table 2 presents the proposed severity rating used for CNC turning center FMEA. Five different categories are formed to define failure effect severity, and the rating scale 1–10 is maintained with certain modification. Table 3 shows the modified occurrence rating with a clear distinction between Levels A to E. The scale for occurrence probability is defined using field failure data and verified by expert opinions. The modified detection rating is shown in Table 4. It considers the detection levels with number 1, 3, 5, 7 and 10 in order to make clear distinction between several detection measures.

4 FMEA of CNC Turning Center

The main drawback of the collected field failure database of the CNC turning center is the inappropriate record of the failure modes and their root causes. Therefore, the failure modes and corresponding root causes are linked using expert opinion [16–18]. Table 5 shows the FMEA of three sub-systems of the CNC turning center. Each sub-system of a CNC turning center consists of a large number of components. However, FMEA of the components having higher failure rates is carried out. Furthermore, the failure of a component occurs due to several root causes. However, the dominating failure modes associated with a component are considered as the main failure modes of that component. There are several effects of a failure mode at component and sub-system level. However, only prominent effects of each failure mode are taken into consideration [19–21]. The RPN of a root cause is calculated by multiplying corresponding SR, OR and DR. The sum of RPN of each of the root cause gives the RPN of the failure mode, and the sum of RPN of each failure mode gives RPN of the component. Finally, the RPN of each sub-system of the CNC turning center is calculated by taking summing components RPN. The critical components and sub-systems of the CNC turning center are identified using corresponding RPN.

Some failure modes are common for various components of the CNC turning center. These common failure modes of the CNC turning center are presented in Table 6. The root causes corresponding to common failure modes are summarized in Table 7.

5 Interpretation of FMEA Results

The proposed SR, OR and DR are used to calculate the RPN value of each failure mode, component and sub-system of the CNC turning center. Table 8 shows the RPN, SR * OR and OR * DR of thirteen sub-systems of the CNC turning center. Figure 2 compares the RPN of thirteen sub-systems and identifies the critical sub-systems of CNC turning center. CNCS, EES, XZAS, ChS, MT, HS, CS and SS are found to be the critical sub-systems. CNCS, HS, MT, EES, ChS, TS, XZAS and CS are the critical sub-systems from reliability and maintainability perspective. However,

Table 2 Proposed severity rating for CNC turning center FMEA

Failure effect severity category	Description of severity category	Rank
Very high category I	Failure of CNC turning center may endanger the operator without warning	10
	Failure of CNC turning center may endanger the operator with warning	09
	Failure may endanger CNC turning center without a warning; CNC turning center is required to be scrapped	08
High category II	Failure may endanger CNC turning center with a warning; Major maintenance is required to recondition the system; Time required for maintenance activity is more than 100 h; Weekly/monthly machining targets are not achieved; Cost of maintenance and production loss is very high (more than Rupees 01 lakh)	07
	Loss of primary function of sub-system/component; Time required for maintenance activity is between 50 and 100 h; Weekly/monthly machining targets are not achieved; Cost of maintenance and production loss is high (between Rupees 25 thousand to 01 lakh)	06
Moderate category III	Reduced primary function or performance of a sub-system/components; Time required for maintenance activity is between 20 and 50 h; Weekly/monthly machining targets may not be achieved; Cost of maintenance is moderate (between Rupees 10 thousand to 25 thousand)	05
	Component requires repair or major variance/possible scrap; Time required for maintenance activity is between 05 and 20 h; Weekly/monthly machining targets might not be achieved; Cost of maintenance is moderate (between Rupees 02 thousand to 10 thousand)	04
Low category IV	Component requires minor or low repair; Time required for maintenance activity is between 02 and 05 h; Weekly/monthly machining targets are achieved; Cost of maintenance is minor (less than Rupees 02 thousand)	03
Remote category V	Minor failure in CNC turning center; Failure has little effect on system; Cost of maintenance is less than Rupees 500	02
	Minor failure in CNC turning center; Failure has no or little effect on system	01

Table 3 Estimates of occurrence ratings for CNC turning center FMEA

Ranking level	Ranking term meaning	Occurrence probability	Rank
Level A—Very frequent	Occurrence of failure is almost inevitable	>0.0360	10
		0.0321–0.0360	9
Level B—Frequent	Repeated failures will occur	0.0281–0.0320	8
		0.0241–0.0280	7
Level C—Occasional	Occasional failures are expected	0.0201–0.0240	6
		0.0161–0.0200	5
		0.0121–0.0160	4
Level D—Remote	Relatively few failures are expected	0.0081–0.0120	3
		0.0041–0.0080	2
Level E—Extremely	Occurrence of failure is quite unlikely	<0.0040	1

Table 4 Proposed detection ratings for CNC turning center FMEA

Likelihood of detection	Rank meaning	Rank
Almost certain	Present monitoring method almost always will detect the existence of a failure	1
High	High probability that the current monitoring method will detect the existence of the failure	3
Moderate	Current monitoring method is possibly detecting the failure	5
Low	Low probability current monitoring methods will detect the failure	7
Detectability absolutely uncertain	The present monitoring method cannot detect the failure	10

it is difficult to conclude the severity information obtained from the comparison of RPN. In this context, the product of SR and OR for each sub-system is calculated and compared to get severity information. Figure 3 compares the SR * OR values of all sub-systems of the CNC turning center and identifies severity information.

6 Conclusions

This paper presents FMEA of a typical CNC turning center. The main objective of this paper was to identify critical failure modes, components and sub-system by determining RPN value. As compared to traditional FMEA, this FMEA approach uses the field failure data as well as experts' knowledge and experience. The accuracy and effectiveness of FMEA are proved through this paper. The results of the FMEA are useful for system reliability improvement of CNC turning center at design stage.

Table 5 FMEA of CNC turning center

Component	Failure mode/Location	Failure effect	SR	Failure cause	OR	Detection techniques	DR	RPN
Main transmission RPN = 305								
Motor	Overheating	Accelerate motor life, motor failure, motor trips	05	Cooling fan failure, frequent starts, overload	02	Overheating alarm 9001	03	30
	Noisy operation	Motor heat built-up	05	Bearing failure, vibration	04	Inherent noise of motor, overheating alarm 9001	03	60
Motor cooling system	Shorted winding	Motor will not start, spindle motor overheating	05	Insulation breakdown, dirt built-up	03	overheating alarm 9001, spindle will not rotate	03	45
Spindle Belt	Worn belt	Noisy operation, uneven speed and torque transmission	03	Repetitive stresses, pulley/sheave misalignment	10	Noise of belt, incorrect speed and feed alarm	05	150
Pulley	Worn sheave	Belt failure (belt cut), accelerate belt life	04	Surface worn-out, Maintenance of spindle bearing	01	Inherent noise level, during replacement of belt or spindle bearing	05	20
Spindle sub-system = 210								
Spindle Bearing	Bearing deformation, fatigue	Chatter mark on job, job run-out	07	Deformation of elements of bearing	10	Noise, chatter mark on job, job run-out	03	210
Chuck sub-system = 320								
Chuck	Worn-out	Job run-out, improper job clamping	04	Collect surface fatigue	10	Inspection using special gauge (10–50 micron)	05	200
Drawbar	Thread damage	Improper job clamping	04	Extension treading failure at either end	10	Improper clamping of the component or job	03	120

Table 6 CNC turning center failure modes

Mechanical	Electrical	Material
Deformation, fracture, thermal, detachment, misalignment, blockage	Electrical failure, electrical insulation, software fault, output inaccuracy, intermittent output	Fatigue, material, structural

Table 7 CNC turning center root causes

Mechanical	Electrical	Material
Design fault, maintenance fault, external damage, mechanical overload, manufacturing defect, presence of debris, mechanical overload collision	Connection and insulation failure, calibration error, short circuit, electrical overload, loss of power input, software design fault, conducting debris	Corrosion, wear, fatigue, vibration fatigue, pipe puncture, insufficient lubrication, overheating

Table 8 RPN values of various sub-systems of CNC turning center

S. No.	Sub-system	RPN	SR * OR
1	CNC sub-system (CNCS)	448	138
2	Electrical and electronic sub-system (EES)	333	105
3	*X*- and *Z*-axis sub-system (XZAS)	327	81
4	Chuck sub-system (ChS)	320	80
5	Main transmission (MT)	305	79
6	Turret sub-system (TS)	294	60
7	Hydraulic sub-system (HS)	282	80
8	Cooling sub-system (CS)	221	51
9	Spindle sub-system (SS)	210	70
10	Pneumatic sub-system (PS)	110	34
11	Lubrication sub-system (LS)	90	16
12	Other sub-system (OS)	79	37
13	Swarf conveyor (SC)	40	8

The maintenance can be also optimized at operation stage. The study uses field failure data from more than 50 CNC turning centers and more than five industrial experts. Therefore, the results of FMEA can help manufacturers and users of CNC turning center. Some critical conclusions are (1) the failure probability of electrical and electronic components is more than that of mechanical components; (2) It is observed that the material corrosion and fatigue are the key factor of failures. This result is confirmed from the data collected from the industry and expert opinion; (3) The study has identified the critical sub-systems and components from reliability perspective and system reliability can be improved through certain design improvements; (4)

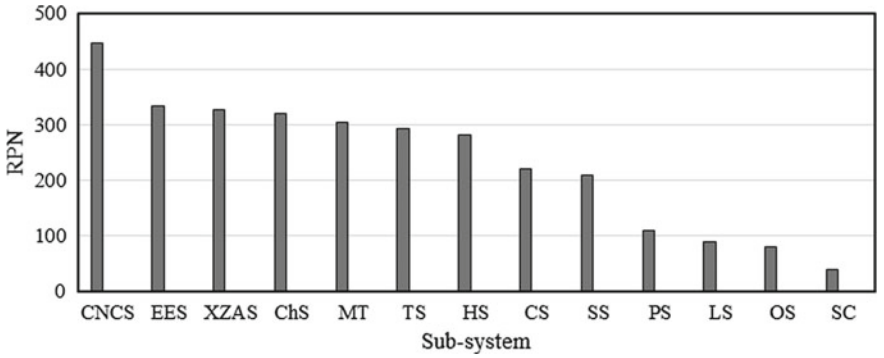

Fig. 2 Comparison of RPN values of thirteen sub-systems of CNC turning center

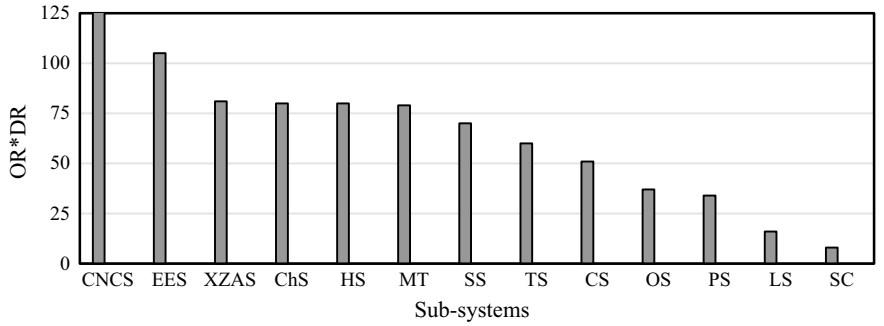

Fig. 3 Comparison of SR * OR values of sub-systems of CNC turning center

CNCS, MT, XZAS, HS, ChS and SS are found to be critical sub-systems, (5) CNCS, HS, MT, EES, ChS, TS, XZAS and CS are the critical sub-systems from reliability and maintainability perspective, and (6) the developed severity, occurrence and detection rating can be used for the FMEA of other CNC-assisted machine tools.

Acknowledgements The authors would like to thank SPM Tools, Ichalkaranji, India, for supporting this work. Authors would like to thank Dr. S. G. Joshi, former Head and Professor, Walchand College of Engineering, Sangli and Dr. L. Y. Waghmode, Professor and Vice-Principal, Annasaheb Dange College of Engineering and Technology, Ashta, for their valuable suggestions and guidance.

References

1. Zhang HB, Jia YZ, Zhou GW (2007) Time between failures model and failure analysis of CNC system. J Harbin Inst Technol (New Ser) 14(2):197–201
2. Mejia DAT, Medjaher K, Zerhouni N (2012) CNC machine tool's wear diagnostic and prognostic by using dynamic Bayesian networks. Mech Syst Sig Process 29:167–182

3. Dai Y, Jia Y (2009) Reliability of a VMC and its improvement. Reliab Eng Syst Saf 74:99–102
4. Yang Z, He J, Wang J, Li G, Tian H, Du X, Kan Y (2016) Bayesian method to solve the early failure period of numerical control machine tool. Proc IMechE Part B: J Eng Manuf 1–10
5. Keller AZ, Kamath RR, Perera UD (1982) Reliability analysis of CNC machine tools. Reliab Eng 3(6):449–473
6. Patil RB, Kothavale BS, Waghmode LY, Joshi SG (2017) Reliability analysis of CNC turning center based on the assessment of trends in maintenance data: a case study. Int J Q Reliab Manage 34(9):1616–1638
7. Zhao-Jun Y, Hai-Chen C, Fei-Chen Bo-Hao Q, Bin-Bin X (2013) Reliability analysis of machining center based on the field data. Maint Reliab 15:147–155
8. Wang Y, Jia Y, Yu J, Zheng Y, Yi S (1999) Failure probabilistic model of CNC lathes. Reliab Eng Syst Saf 65:307–314
9. Hai-Bo Z, Ya-Zhou J, Guang-Wen Z (2007) Time between failures model and failure analysis of CNC system. J Harbin Inst Technol 14:197–201
10. Cicek K, Celik M (2013) Applications of failure modes and effects analysis to main engine crankcase explosion failure on-board ship. Saf Sci 51:6–10
11. Kurt L, Ozilgen S (2013) Failure mode and effect analysis for dairy product manufacturing: practical safety improvement action plan with cases from Turkey. Saf Sci 55:195–206
12. Lolli F, Gamberini R, Rimini B, Messori M (2015) Flow sort-GDSS—a novel group multi-criteria decision support system for sorting problems with application to FMEA. Expert Syst Appl 42:6342–6349
13. Hoseynabadi HA, Oraee H, Tanver PJ (2010) Failure modes and effects analysis (FMEA) for wind turbines. Electr Powers Energy Syst 32:817–824
14. Spreafico C, Russo and D, Rizzi C (2010) A state-of-the-art review of FMEA/FMECA including patents. Comput Sci Rev 25:19–28
15. United States Department of Defense. 'MIL-STD-1629A—Military standard procedures for performing a failure mode, effects and criticality analysis', 24th November 1980. 'System Reliability Center PDF Directory'. http://src.alionscience.com/pdf/MIL-STD-1629RevA.pdf
16. Wang Y, Jia Y, Jiang W (2001) Early failure analysis of machining centers: a case study. Reliab Eng Syst Saf 72:91–97
17. Lad BK, Kulkarni MS (2010) A parameter estimation method for machine tool reliability analysis using expert judgment. Int J Data Anal Tech Strat 2(2):155–169
18. Colli A (2015) Failure mode and effect analysis for photovoltaic systems. Renew Sustain Energy Rev 50:804–809
19. Waghmode LY, Patil RB (2016) Reliability analysis and life cycle cost optimization: a case study from indian industry. Int J Q Reliab Manage 33(3):414–429
20. Teng SH, Ho SY (1996) Failure mode and effects analysis – an integrated approach for product design and process control. Int J Q Reliab Manage 13(5):8–26
21. Xu K, Tang LC, Xie M, Ho SL, Zhu ML (2002) Fuzzy assessment of FMEA for engine systems. Reliab Eng Syst Saf 75(1):17–29

Criticality Analysis of CNC Turning Center Using Analytic Hierarchy Process

Rajkumar Bhimgonda Patil and Basavraj S. Kothavale

Abstract Computerized numerical control (CNC) turning center plays an important role in manufacturing industries. Reliability and maintainability are the key activities in any manufacturing industry to complete weekly/monthly/yearly manufacturing targets by maintaining the health of the CNC turning center. Therefore, it is essential to prioritize sub-systems of the CNC turning center according to criticality. In this context, analytic hierarchy process (AHP), one of the multiple criteria decision-making (MCDM) tool, is used for prioritizing sub-systems of the CNC turning center for four different criteria, viz. failure frequency, sub-system downtime, maintenance cost, and customer inconvenience. The major 14 sub-systems of the CNC turning center are considered for the analysis. SS, CNC, XZAS, TS, EES, and MT are the critical sub-systems of CNC turning center for the selected criteria and should be monitored carefully. The critical sub-systems for individual criteria are also identified. This case study shows that the AHP is a simple and effective tool for prioritizing the sub-systems and beneficial for maintenance managers to decide optimum maintenance strategies.

Keywords Criticality analysis · Analytic hierarchy process · CNC turning center · Frequency of failure · Maintenance cost

R. B. Patil
Center for Advanced Life Cycle Engineering (CALCE), University of Maryland, College Park, USA
e-mail: rajkumarpatil2009@gmail.com

Annasaheb Dange College of Engineering and Technology, Ashta, Sangli, Maharashtra 416301, India

B. S. Kothavale (✉)
Department of Mechanical Engineering, MAEER's MIT College of Engineering, Kothrud, Pune, Maharashtra 411038, India
e-mail: basavraj.kothavale@mitcoe.edu.in

V. K. Gupta et al. (eds.), *Reliability and Risk Assessment in Engineering*,
Lecture Notes in Mechanical Engineering,
https://doi.org/10.1007/978-981-15-3746-2_6

1 Introduction

CNC turning center is a computerized numerical control (CNC) machine tool used for various machining operations in manufacturing industry. It is a complex system that consists of various sub-systems such as mechanical, hydraulic, pneumatic, electrical, and electronics. The failure of a single sub-system can lead to failure of the whole CNC turning center. Therefore, the failure-free operation can be achieved by implementing suitable maintenance policy such as preventive, predictive, and breakdown. It is also required to design and manufacture economical, reliable, and maintainable CNC turning center, in order to survive in the market as a manufacturer. Reliability and maintainability tools help to achieve these objectives and optimize machining as well as life cycle cost [1]. In this context, it is decided to identify the critical sub-systems of the selected CNC turning center. These sub-systems need to be monitored closely for avoiding catastrophic failure.

Several multiple criteria decision-making (MCDM) tools are used for making complex decisions by considering quantitative and qualitative factors [2–4]. MCDM approach can give the best alternative from possible options by considering several relevant criteria. Among the various MCDM methods, AHP is popular and used by many researchers as it is intuitive, easy, and understandable [5]. It is possible to select the most suitable trade-off among different criteria, even when some of the criteria are contrasting. AHP assigns a weight for each evaluation criteria. The more the weight, the more significant the corresponding criteria. In the case of fixed criteria, the AHP assigns a score to each option, according to the decision-maker's pairwise comparisons of the options based on those criteria. Finally, weight of each of the criteria is combined and normalized, and the global score is determined to decide severity ranking.

In this context, it is decided to analyze the CNC turning center using AHP for four different criteria, viz. failure frequency, sub-system downtime, and maintenance cost, and customer inconvenience has been used for decision making. The main objective of this paper is to identify critical sub-systems of CNC turning center. In this context, the following studies have been carried out.

- Literature review revealing AHP analysis of various industrial systems;
- Development of AHP methodology for analyzing CNC turning center;
- Identification of critical sub-systems of CNC turning center using developed AHP methodology.

2 Literature Review

In this section, the relevant published literature of AHP and other MCDM techniques are collected, analyzed, and summarized. The AHP tool is proposed in [6] and thereafter, it is popularly applied in a wide variety of areas including engineering,

planning, selecting the best alternative, resolving conflicts, and resource allocation [6]. AHP tool is vastly applied for solving various problems and based on it more than 1300 papers and 100 doctoral dissertations are published [7–10]. However, in this section, relevant literature is discussed in order to develop AHP methodology for the analysis of CNC turning center and can be used for the analysis of other CNC-assisted machine tools. The applications of the AHP in engineering and operations management are categorized into five classes: operations strategy, process and product design, planning and scheduling resources, project management, and managing the supply chain [11–14]. Table 1 summarizes the AHP and other MCDM methods used for the analysis of various systems. It includes the purpose of analysis, criteria considered, and tool used. It is concluded from the literature survey that AHP is the most suitable method for analyzing various engineering systems and the analysis results are encouraging.

3 Development of AHP Methodology for CNC Turning Center

Literature review reveals that the AHP allows decision-makers to model a problem in a hierarchical structure determining the relationships between the goals, objectives (criteria), and alternatives [15–27]. The effectiveness of AHP depends on the careful selection of decision-making criteria and proper classification of the system or equipment [28, 29]. Therefore, in this section, an AHP methodology is proposed for ranking the sub-systems of CNC turning center. The methodology for the identification of critical sub-systems of CNC turning center and their ranking according to criticality is developed by modifying the existing methodologies. The AHP methodology used for the analysis of CNC turning center is discussed below.

- Classify the whole CNC turning center into various sub-systems according to their functions.
- Decompose the problem definition into three levels: goal, criteria, and alternatives and then decide hierarchy of the same.
- Define the score scale for each criterion.
- Based upon the defined scale, develop a comparison matrix.
- Convert the comparison matrix into a normalized matrix.
- Suppose, X represents the comparison matrix: $X = [x_{ij}]$. Where i stands for sub-system of the CNC turning center ($i = 1 \ldots n$) and j stands for criteria ($j = 1 \ldots m$). Then, the normalized matrix (r_{ij}) from X can be obtained by:

$$r_{ij} = \frac{x_{ij}}{\sum_{i=1}^{n} x_{ij}} \tag{1}$$

where r_{ij} gives the value of (ij)th element of the normalized matrix.

Table 1 Literature survey of AHP and other MCDM methods

Author (year)	Tools used	Findings
Chang et al. (2007) [15]	AHP and Delphi	The main purpose of this study is to select the best slicing machine based on four criteria: machine-related, human-related, management, and measurement
Si et al. (2009) [16]	AHP	The operational competitiveness studied and identified the development route of Chinese high-tech manufacturing companies, know-how, flexibility, delivery, quality, customer, focus, and cost are the selected criteria
Chatzim-ouratidis and Pilavachi (2009) [17]	AHP	Research objective was to evaluate critical sub-systems in power plants of power plants by considering technological, economical, and sustainability aspects
Suebsomran (2010) [18]	FMEA and AHP	Used FMEA and AHP approaches to find the critical ranking priority of failure mode relating to three criteria such as men per hour working, maintenance cost, and line priority of thermal power plant
Samvedi et al. (2012) [19]	Fuzzy AHP and GRA	Integrated fuzzy AHP and gray relational analysis (GRA) approaches for the selection of a machine tool from a given set of alternatives. The analysis results are found to be better
Singh and Kulkarni (2013) [20]	AHP	Analyzed thermal power plant using AHP tool. Raking of equipment and their criticality is based on multiple criteria, viz. environmental impact, customer inconvenience, and maintenance cost

(continued)

Table 1 (continued)

Author (year)	Tools used	Findings
Adhikary and Bose (2014) [21]	COPRAS-G	Present a multi-criteria failure mode effect and criticality analysis for coal-fired thermal power plants using uncertain data and substituting the traditional risk priority number estimation method
Govindan et al. (2015) [22]	MCDM with fuzzy theory	Reviewed several MCDM methods used for the analysis considering environmental factors. Gaps in the current literature are identified and suggested future directions
Bologa et al. (2016) [23]	Fuzzy AHP	An AHP-based is proposed for selecting the most beneficial variant for the process. Future researches will be oriented to a comparison between the two tools used in this work, the fuzzy tool and AHP
Kokangul et al. (2017) [24]	Hybrid AHP	Presented risk assessment of a large manufacturing company considering experience and 10 years statistical records
Jagtap and Bewoor (2017) [25]	AHP	Applied AHP for the identification of critical equipment of thermal power plant. Effect of failure on equipment on power generation, environment and safety, frequency of failure, and maintenance costs are the parameters selected for the analysis
Bian et al. (2017) [26]	AHP	AHP-based methodology to identify the influence of the node is proposed. The efficiency and practicability of the proposed method is presented based on the experiments on four real networks and an informative network

(continued)

Table 1 (continued)

Author (year)	Tools used	Findings
Breaz et al. (2017) [27]	AHP and fuzzy	The AHP method was used for selecting between the three variants of manufacturing processes: CNC milling, robot milling, and a process of additive manufacturing (DMLS)

- Define a pairwise comparison of relative importance between the n rating criteria. This results in an n-by-n matrix $A(a_{ij})$ with i and $j = 1, 2, \ldots, n$.

$$A = \begin{bmatrix} a_{11} & a_{12} & \ldots & a_{1n} \\ a_{21} & a_{22} & \ldots & a_{2n} \\ \ldots & \ldots & \ldots & \ldots \\ \ldots & \ldots & \ldots & \ldots \\ \ldots & \ldots & \ldots & \ldots \\ a_{n1} & a_{n2} & \ldots & a_{nn} \end{bmatrix} \tag{2}$$

where $a_{ij} > 0, a_{ij} = 1/a_{ij}, a_{ij} = 1$ and a_{ij} is the user-defined rating of relative importance criteria i with respect to criteria j. In case, i and j have equal relative importance, then $a_{ij} = a_{ji} = 1$. The values of relative rankings a_{ij} can be assumed as: (a) Criteria i and j are equally important: 1, (*b*) Criteria i is slightly more important than criteria j: 3, (c) Criteria i is significantly more important than criteria j: 5, (d) Criteria i is strongly more important than criteria j: 7, (e) Criteria i is extremely more important than criteria j: 9, and (f) 2, 4, 6, and 8 are used for intermediate numerical values.

- Check the pairwise comparison matrix for consistency and also calculate the weight of the different criteria. The judgement matrix should be a consistent. The consistency ratio (CR) should be less than 0.10 to ensure a consistent judgement [5].
- Find out criticality rank of sub-systems of CNC turning center.

4 Analysis of CNC Turning Center Using Developed AHP Methodology

In this section, the selected CNC turning center is analyzed using developed AHP methodology. For analysis purpose, the whole CNC turning center is classified into fourteen sub-systems, viz. CNC sub-system (CNCS), electrical and electronic sub-system (EES), main transmission (MT), spindle sub-system (SS), chuck sub-system

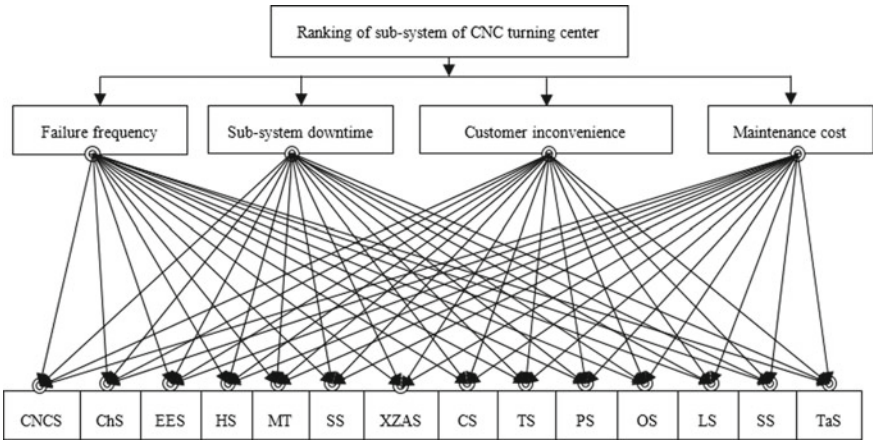

Fig. 1 AHP hierarchy structure diagram for CNC turning center

(ChS), *X-axis* and *Z*-axis sub-system (XZAS), turret sub-system (TS), hydraulic sub-system (HS), pneumatic sub-system (PS), coolant sub-system (CS), lubrication sub-system (LS), swarf conveyor (SC), tail-stock sub-system (TSS), and other sub-system (OS). Assemblies, sub-assemblies, and components of each sub-system are not considered to avoid unnecessary complexity of the analysis. During brainstorming session and detailed discussion with domain experts, four criteria are selected for the analysis: failure frequency, sub-system downtime, maintenance cost, and customer inconvenience. The required data for this analysis is collected from domain experts, service and maintenance engineers, maintenance register, and customer opinion. The entire problem is decomposed into three levels: goal, criteria, alternatives and making a hierarchy of the same. AHP hierarchy structure diagram for CNC turning center is presented in Fig. 1.

4.1 Criterion I—Failure Frequency (FF)

In this criterion, failure frequency of a sub-system is categorized into four classes: once a year, twice a year, thrice a year, and frequent failures according to its impact on annual manufacturing target. Four numerical scales are assigned: (1) for annual manufacturing target will be achieved, (2) for light to medium impact on manufacturing target, (3) for medium to high impact on manufacturing targets, and (4) for manufacturing target will not be achieved. Table 2 shows the severity for the failure frequency of a sub-system on manufacturing target. Table 3 gives the weight estimation of failure frequency criteria. Here, the rows are compared with columns. If the row parameter is more important than column parameter, a weight value 3 is assigned, if the row and column are of equal importance, a weight value 2 is assigned and if the row parameter is of less importance, a weight value 1 is assigned.

Table 2 Severity rating for the failure frequency of a sub-system on manufacturing target

S. No.	Sub-system	Failure frequency class			
		Once a year	Twice a year	Thrice a year	Frequent failures
1	CNCS	2	2	3	4
2	ChS	1	1	2	3
3	EES	1	1	2	3
4	HS	1	1	2	3
5	MT	2	2	3	4
6	SS	2	3	4	4
7	XZAS	2	2	3	4
8	CS	1	1	2	2
9	TS	1	2	3	3
10	PS	1	1	2	2
11	OS	1	1	1	1
12	LS	1	1	1	2
13	SC	1	1	1	1
14	TaS	1	1	1	1

Table 3 Weight estimation of failure frequency criterion

S. No.	Failure frequency	Weight for failure frequency				Sum	Percentage	Weight
		Once a year	Twice a year	Thrice a year	Frequent failures			
1	Once a year	2	1	1	1	5	15.63	0.16
2	Twice a year	3	2	1	1	7	21.88	0.22
3	Thrice in year	3	3	2	1	9	28.13	0.28
4	Frequent failure	3	3	3	2	11	34.38	0.34

Table 4 shows the overall impact of failure frequency criteria and it is calculated by multiplying the severity rating (Table 2) and the corresponding weight value (Table 3). The overall impact of failure frequency criteria for various sub-systems is presented in Table 4. It also gives the overall impact of failure frequency of each sub-system on CNC turning center.

Table 4 Overall impact of failure frequency criterion

S. No.	Sub-system	Impact of failure frequency				Overall impact
		Once a year	Twice a year	Thrice a year	Frequent failure	
1	CNCS	0.32	0.44	0.84	1.36	2.96
2	ChS	0.16	0.22	0.56	1.02	1.96
3	EES	0.16	0.22	0.56	1.02	1.96
4	HS	0.16	0.22	0.56	1.02	1.96
5	MT	0.32	0.44	0.84	1.36	2.96
6	SS	0.32	0.66	1.12	1.36	3.46
7	XZAS	0.32	0.44	0.84	1.36	2.96
8	CS	0.16	0.22	0.56	0.68	1.62
9	TS	0.16	0.44	0.84	1.02	2.46
10	PS	0.16	0.22	0.56	0.68	1.62
11	OS	0.16	0.22	0.28	0.34	1
12	LS	0.16	0.22	0.28	0.68	1.34
13	SC	0.16	0.22	0.28	0.34	1
14	TaS	0.16	0.22	0.28	0.34	1

4.2 Criterion II—Sub-system Downtime (SD)

System complexity, availability of spare, skill of maintenance team, resources, and work environment decide the total time required for the maintenance. Considering these aspects, four classes are formed to define severity of sub-system downtime: sub-system downtime is less than 05 h (sub-system is easily restored), sub-system downtime is between 05 and 10 h (sometimes maintenance is slightly complex and require moderate time), system downtime is between 10 and 15 h (maintenance is complex), and system downtime is more than 15 h (external agency should be hired for maintenance due to high complexity). Table 5 shows the severity of each sub-system downtime. Table 6 shows the weight estimation for sub-system downtime criteria. The process of weight estimation for this criterion is same as discussed in Sect. 4.2. Table 7 shows the overall impact of sub-system downtime criteria for various sub-systems of CNC turning center.

4.3 Criterion III—Customer Inconvenience (CI)

The production loss due to maintenance and frequent failures of CNC turning center causes inconvenience to the customer. Inconvenience is more when the maintenance activity requires large time to restore the system from failure state to operational

Table 5 Severity of sub-system downtime

S. No.	Sub-system	Sub-system downtime (in h)			
		<05	05–10	10–15	>15
1	CNCS	2	3	3	4
2	ChS	1	2	2	2
3	EES	1	2	2	2
4	HS	1	1	1	1
5	MT	1	1	1	1
6	SS	3	3	4	4
7	XZAS	2	3	4	4
8	CS	1	1	1	1
9	TS	2	2	3	4
10	PS	1	1	1	1
11	OS	1	1	1	1
12	LS	1	1	2	3
13	SC	1	1	2	2
14	TaS	1	1	1	1

Table 6 Weight estimation for sub-system downtime criterion

S. No.	Sub-system downtime (in h)	Weight for sub-system downtime (in h)				Sum	Percentage	Weight
		<05	05–10	10–15	>15			
1	<05	2	2	1	1	6	18.18	0.18
2	05–10	3	2	2	1	8	24.24	0.24
3	10–15	3	3	2	1	9	27.27	0.27
4	>15	3	3	2	2	10	30.30	0.30

state. Ultimately, the failure and large maintenance time lead is responsible for production loss and the customer may not receive the required lot of finished goods. The customer inconvenience is expressed in terms of weekly production loss. The customer inconvenience and the corresponding scale are shown in Table 12.

4.4 Criterion IV—Maintenance Cost (MC)

The cost associated with maintenance activity is considered as maintenance cost. This maintenance cost includes spare cost, maintenance person charges, cost of production loss, and cost of consumables. The total maintenance cost again increases considerably when maintenance is carried out with external agency. Table 8 shows the maintenance cost and corresponding scale.

Table 7 Overall impact of sub-system downtime criterion

S. No.	Sub-system	Impact of sub-system downtime				Overall impact
		<05 h	05–10 h	10–15 h	>15 h	
1	CNCS	0.36	0.72	0.81	1.2	3.09
2	ChS	0.18	0.48	0.54	0.6	1.8
3	EES	0.18	0.48	0.54	0.6	1.8
4	HS	0.18	0.24	0.27	0.3	0.99
5	MT	0.18	0.24	0.27	0.3	0.99
6	SS	0.54	0.72	1.08	1.2	3.54
7	XZAS	0.36	0.72	1.08	1.2	3.36
8	CS	0.18	0.24	0.27	0.3	0.99
9	TS	0.36	0.48	0.81	1.2	2.85
10	PS	0.18	0.24	0.27	0.3	0.99
11	OS	0.18	0.24	0.27	0.3	0.99
12	LS	0.18	0.24	0.54	0.9	1.86
13	SC	0.18	0.24	0.54	0.6	1.56
14	TaS	0.18	0.24	0.27	0.3	0.99

Table 8 Scale for the severity measurement of the four identified criteria

Overall impact of failure frequency	Overall impact of sub-system downtime	Customer inconvenience due to weekly production loss (in %)	Maintenance cost (in Rupees)	Scale
3.8–4.2	3.8–4.2	>35	>60 thousand	9
3.4–3.8	3.4–3.8	30–35	50 thousand–60 thousand	8
3–3.4	3–3.4	25–30	40 thousand–50 thousand	7
2.6–3	2.6–3	20–25	30 thousand–40 thousand	6
2.2–2.6	2.2–2.6	15–20	20 thousand–30 thousand	5
1.8–2.2	1.8–2.2	10–15	10 thousand–20 thousand	4
1.4–1.8	1.4–1.8	5–10	5 thousand–10 thousand	3
1–1.4	1–1.4	1–5	1 thousand–5 thousand	2
<1	<1	<1	<1 thousand	1

Table 9 Comparison matrix of sub-systems of CNC turning center

S. No.	Sub-system	FF	SD	CI	MC
1	CNCS	6	7	7	7
2	ChS	4	4	2	4
3	EES	4	4	3	3
4	HS	4	1	2	2
5	MT	6	1	2	2
6	SS	8	8	8	8
7	XZAS	6	7	8	5
8	CS	3	1	2	2
9	TS	5	6	4	3
10	PS	3	1	2	2
11	OS	2	1	1	1
12	LS	2	4	5	3
13	SC	2	3	1	2
14	TaS	2	1	1	1

5 Development of Normalized Matrix

In this section, comparison matrix and normalized matrix for the sub-systems of CNC turning center are developed using the severity of four identified criteria. Table 8 summarizes the scale for the severity measurement of the four identified criteria. The comparison matrix of sub-systems of the CNC turning center for the four identified criteria is prepared using the scale (Table 8) and the overall impact of each criteria. Table 9 shows the comparison matrix for the sub-systems of CNC turning center. The scale value of each sub-system for each criterion is normalized by dividing the sum of scale values of the corresponding criteria (Table 10).

6 Criticality Rank Estimation of Sub-systems of CNC Turning Center

A pairwise comparison matrix of the selected criteria (A) is defined for checking their consistency. The values of relative rankings a_{ij} can be assumed as follows: criteria i and j are equally important: 1; criteria i is slightly more important than criteria j: 3; criteria i is significantly more important than criteria j: 5; criteria i is strongly more important than criteria j: 7; criteria i is extremely more important than criteria j: 9; and 2, 4, 6, and 8 are used for intermediate numerical values. Table 11 shows the estimation of eigenvector for FF, SD, CI, and MC, respectively. The entries in each row of the comparison matrix are multiplied together and the nth root of the

Table 10 Normalized matrix obtained from comparison matrix

S. No.	Sub-system	FF	SD	CI	MC
1	CNCS	0.1053	0.1429	0.1458	0.1556
2	ChS	0.0702	0.0816	0.0417	0.0889
3	EES	0.0702	0.0816	0.0625	0.0667
4	HS	0.0702	0.0204	0.0417	0.0444
5	MT	0.1053	0.0204	0.0417	0.0444
6	SS	0.1404	0.1633	0.1667	0.1778
7	XZAS	0.1053	0.1429	0.1667	0.1111
8	CS	0.0526	0.0204	0.0417	0.0444
9	TS	0.0877	0.1224	0.0833	0.0667
10	PS	0.0526	0.0204	0.0417	0.0444
11	OS	0.0351	0.0204	0.0208	0.0222
12	LS	0.0351	0.0816	0.1042	0.0667
13	SC	0.0351	0.0612	0.0208	0.0444
14	TaS	0.0351	0.0204	0.0208	0.0222

Table 11 Estimation of eigenvector

	FF	SD	CI	MC	4th root	Eigenvector
FF	1	3	5	7	3.2011	0.5638
SD	0.3333	1	3	5	1.4953	0.2634
CI	0.2	0.3333	1	3	0.6687	0.1178
MC	0.1429	0.2	0.3333	1	0.3124	0.0550
Total					5.6775	1.0

product is taken, where n is the order of the matrix. Then, the roots thus calculated are summed. Further, each of the roots is normalized with the help of this sum to get eigenvectors.

A =

	FF	SD	CI	MC
FF	1	3	5	7
SD	1/3	1	3	5
CI	1/5	1/3	1	3
MC	1/7	1/5	1/3	1

Each row of the comparison matrix (A) is multiplied by the eigenvector column from Table 11, just like a matrix multiplication. For all the four rows, the calculation yields: 2.3280, 1.0797, 0.4834, and 0.2275, respectively. Now, divide each yield value by corresponding eigenvector to get the corresponding values of λ: 4.1291, 4.0991, 4.1036, and 4.1364. The average of the four values of λ gives λ_{max}. Here, $\lambda_{max} = 4.1170$. Now, consistency index (CI) is calculated as: CI = $(\lambda_{max} - n)/(n - 1)$

Table 12 Final criticality rank of sub-systems of CNC turning center

S. No.	Sub-system	Name of the criteria				Weighted score	Rank
		FF	SD	CI	MC		
1	CNCS	0.0593	0.0376	0.0172	0.0086	0.1227	2
2	ChS	0.0396	0.0215	0.0049	0.0049	0.0709	7
3	EES	0.0396	0.0215	0.0074	0.0037	0.0721	5
4	HS	0.0396	0.0054	0.0049	0.0024	0.0523	9
5	MT	0.0593	0.0054	0.0049	0.0024	0.0721	6
6	SS	0.0791	0.0430	0.0196	0.0098	0.1515	1
7	XZAS	0.0593	0.0376	0.0196	0.0061	0.1227	3
8	CS	0.0297	0.0054	0.0049	0.0024	0.0424	10
9	TS	0.0495	0.0323	0.0098	0.0037	0.0952	4
10	PS	0.0297	0.0054	0.0049	0.0024	0.0424	11
11	OS	0.0198	0.0054	0.0025	0.0012	0.0288	13
12	LS	0.0198	0.0215	0.0123	0.0037	0.0572	8
13	SC	0.0198	0.0161	0.0025	0.0024	0.0408	12
14	TaS	0.0198	0.0054	0.0025	0.0012	0.0288	14

$= 0.0390$ and consistency ratio (CR) is calculated as: CR $=$ CI/RI $= 0.0433$. Using random index (RI) for different orders of the judgment. For $n = 4$, the value of RI is taken as 0.9. Here, a CR value is less than 0.10, and it indicates the judgment is consistent. Further, using values of eigenvectors, the relative weights of each sub-system for the selected four criteria are calculated. Table 12 shows the total weighted score of each sub-system and the corresponding criticality rank. Table 12 reveals that SS is the most critical sub-system for the selected criteria followed by CNCS, XZAS, TS, EES, MT, ChS, LS, HS, CS, PS, SC, OS, and TaS, respectively.

7 Result and Discussion

The AHP method is applied for criticality analysis of sub-systems of the CNC turning center and the results are encouraging. It shows the critical sub-systems for each of the selected criteria and overall criticality. It is seen that failure frequency of SS, CNCS, MT, XZAS, and TS are very high as compared to other sub-systems. The maintenance time required for SS, XZAS, MT, CNCS, and TS is more responsible for most of the production loss and customer inconvenience. The maintenance cost of SS, CNCS, and XZAS dominates the total maintenance cost associated with CNC turning center. Table 12 provides the overall criticality rank for the sub-systems of CNC turning center for the selected criteria. SS and CNCS are the two most critical sub-systems with first rank and second rank, respectively, which need to be monitored very closely. The failure of these two sub-systems may lead to catastrophic failure of

the plant, requires considerable maintenance time and cost, and causes inconvenience to the customer. Similarly, AHP method provides the ranking of sub-systems from three to fourteen for XZAS, TS, EES, MT, ChS, LS, HS, CS, PS, SC, OS, and TaS, respectively.

8 Conclusion

From the above case study, it is concluded that the AHP proved to be a simple, effective, and powerful tool for prioritizing the sub-systems of the CNC turning center. In this paper, fourteen sub-systems of CNC turning center were considered for criticality analysis, viz. SS, CNCS, XZAS, TS, EES, MT, ChS, LS, HS, CS, PS, SC, OS, and TaS. The criticality analysis is carried out with AHP for the selected four criteria: failure frequency, sub-system downtime, customer inconvenience, and maintenance cost. The overall criticality rank of each sub-system is estimated. AHP analysis also provides the critical sub-systems for individual criteria. The results of this analysis can be used for reliability, maintainability, and life cycle cost analysis of CNC turning center. Furthermore, the results of this analysis can be compared with failure rate, repair rates, and failure modes and effects analysis (FMEA).

Acknowledgements The authors would like to thank Mr. Amod Kulkarni, Technical Director, SPM Tools, Ichalkaranji, Mr. Hemant Kulkarni, Director, H. K. Group, domain experts of SPM Tools as well as H. K. Group, Dr. S. G. Joshi, former Head and Professor, Walchand College of Engineering, Sangli and Dr. L. Y. Waghmode, Professor, ADCET, Ashta for their guidance and critical suggestions.

References

1. Patil RB, Kothavale BS, Waghmode LY, Joshi SG (2017) Reliability analysis of CNC turning center based on the assessment of trends in maintenance data: a case study. Int J Qual Reliab Manag 34(9):1616–1638
2. Ivanco M, Hou G, Michaeli J (2017) Sensitivity analysis method to address user disparities in the analytic hierarchy process. Expert Syst Appl 90:111–126
3. Wang L, Chua J, Wub J (2007) Selection of optimum maintenance strategies based on a fuzzy analytic hierarchy process. Int J Prod Econ 107:151–163
4. Cimren E, Catay B, Budak E (2007) Development of a machine tool selection system using AHP. Int J Manuf Technol 35:363–376
5. Saaty TL (1990) How to make a decision: the analytic hierarchy process. Eur J Oper Res 48(1):9–26
6. Saaty TL (1980) The analytic hierarchy process. McGraw-Hill, New York
7. Subramanian N, Ramanathan R (2012) A review of applications of analytic hierarchy process in operations management. Int J Prod Econ 138:215–241
8. Manglaa SK, Govindan K, Luthrac S (2017) Prioritizing the barriers to achieve sustainable consumption and production trends in supply chains using fuzzy analytical hierarchy process. J Clean Prod 51:509–525

9. Vaidya OS, Kumar S (2006) Analytic hierarchy process: an overview of applications. Eur J Oper Res 169:1–29
10. Zyoud SH, Fuchs-Hanusch D (2017) A bibliometric-based survey on AHP and TOPSIS techniques. Expert Syst Appl 78:158–181
11. Dıaz VG, Fernandez JG, Marquez AC (2011) Practical application of an analytic hierarchy process for the improvement of the warranty management. J Qual Maint Eng 17(2):163–182
12. Deng Y (2016) Fuzzy analytical hierarchy process based on canonical representation on fuzzy numbers. J Comput Anal Appl 22:201–228
13. Sergaki A, Kalaitzakis K (2002) A fuzzy knowledge based method for maintenance planning in power system. Reliab Eng Syst Saf 77:19–30
14. Ho W (2008) Integrated analytic hierarchy process and its applications—a literature review. Eur J Oper Res 186:211–228
15. Chang C, Wu C, Lin C, Chen H (2007) An application of AHP and sensitivity analysis for selecting the best slicing machine. Comput Ind Eng 52:296–307
16. Si S, Takala J, Liu Y (2009) Competitiveness of Chinese high-tech manufacturing companies in global context. Ind Manag Data Syst 109(3):404–424
17. Chatzimouratidis AI, Pilavachi PA (2009) Sensitivity analysis of technological, economic and sustainability evaluation of power plants using the analytic hierarchy process. Energy Policy 37:778–798
18. Suebsomran A (2010) Critical maintenance of thermal power plant using the combination of failure mode effect analysis and AHP approaches. Asian Int J Sci Technol Prod Manuf Eng 3:1–6
19. Samvedi A, Jain V, Chan FTS (2012) An integrated approach for machine tool selection using fuzzy analytical hierarchy process and grey relational analysis. Int J Prod Res 50:3211–3221
20. Singh RK, Kulkarni MS (2013) Criticality analysis of power-plant equipments using the analytic hierarchy process. Int J Ind Eng Technol 3:1–14
21. Adhikary DD, Bose GK (2014) Multi criteria FMECA for coal-fired thermal power plants using COPRAS-G. Int J Qual Reliab Manag 31:601–614
22. Govindan K, Rajendran S, Sarkis J, Murugesan P (2015) MULTI criteria decision making approaches for green for green supplier evaluation and selection: a literature review. J Clean Prod 98:66–83
23. Bologa O, Breaz R, Racz S, Crenganis M (2016) Using the analytic hierarchy process (AHP) in evaluating the decision of moving to a manufacturing process based upon continuous 5 axes CNC machine-tools. Procedia Comput Sci 91:683–689
24. Kokangul A, Polat U, Dagsuyu C (2017) A new approximation for risk assessment using the AHP and fine kinney methodologies. Saf Sci 91:24–32
25. Jagtap HP, Bewoor AK (2017) Use of analytic hierarchy process methodology for criticality analysis of thermal power plant equipments. In: 5th International conference of materials processing and characterization, materials today: proceedings, vol 4, pp 1927–1936
26. Bian T, Hu J, Deng Y (2017) Identifying influential nodes in complex networks based on AHP. Phys A Stat Mech Appl 479:422–436
27. Breaz RE, Bologa O, Racz SG (2017) Selecting between CNC milling, robot milling and DMLS processes using a combined AHP and fuzzy approach. Procedia Comput Sci 122:796–803
28. Waeyenbergh G, Pintelon L (2002) A framework for maintenance concept development. Int J Prod Econ 77:299–313
29. Wang YJ, Leeb HS (2007) Generalizing TOPSIS for fuzzy multiple-criteria group decision making. Comput Math Appl 53:1762–1772

Condition Monitoring Techniques and Applications

Tool Condition Monitoring in End Milling of Ti-6Al-4V Using Multisensory Approach

Neelesh Kumar Sahu, Atul B. Andhare, and Abhay Khalatkar

Abstract The present work focuses on cutting tool condition monitoring of end milling cutter, using multisensory approach in machining of Ti-6Al-4V. Indirect process parameters such as cutting forces and spindle current are measured as responses using different sensors. Face milling operations are performed on CNC vertical milling center and correlation coefficients are determined to associate tool wear with multiresponse. Systematic plan of experiments was developed using central composite design (CCD) under response surface methodology (RSM) with cutting speed, feed rate, and depth of cut as design variables. Subsequently multisensor-based response surface model was developed in addition to cutting variables. Analysis of variance (ANOVA) was performed to evaluate statistical validity as well as significant variables over the tool wear. Coefficient of determination (R^2_{adj}) value of 98.28% shows that model correctly explains the experimental results and it behaves well even when adjustment is made in factors, or some factors are added or eliminated. The analysis shows that the measured responses such as cutting forces and spindle current can be used as indirect process parameters for tool wear monitoring in end milling operation of Ti-6Al-4V.

Keywords Tool condition monitoring · Cutting force · Spindle current · Ti-6Al-4V

N. K. Sahu (✉)
Department of Mechanical Engineering, Medi-Caps University, Indore, India
e-mail: neeleshmecher@gmail.com

A. B. Andhare
Department of Mechanical Engineering, VNIT, Nagpur, India
e-mail: abandhare@mec.vnit.ac.in

A. Khalatkar
Department of Mechanical Engineering, G. H. Raisoni College of Engineering, Nagpur, India
e-mail: abhay.khalatkar@raisoni.net

V. K. Gupta et al. (eds.), *Reliability and Risk Assessment in Engineering*,
Lecture Notes in Mechanical Engineering,
https://doi.org/10.1007/978-981-15-3746-2_7

1 Introduction

Condition monitoring is an important tool to avoid catastrophic failure of system. Indirect, online process parameter measurement, can give indication in change of behavior of the process. Metal cutting processes are very common in manufacturing. One of the most important elements in machining is the cutting tool. Every cutting tool wears out with time during machining, and tool wear has large effect on the machining process. Every tool needs to be replaced after some usage due to wear, to avoid loss of product quality and machining efficiency. The tool replacement should be a planned event and for this purpose, it is essential to have knowledge of tool wear and its progress. This helps in eliminating product loss and unplanned stoppages of machines. This ultimately leads to cost savings. Therefore, tool condition monitoring is a topic of wide interest and many attempts have been made to diagnose the condition of tool at any instant of time while machining. This paper is focused on tool condition monitoring while machining of Ti-6Al-4V using multisensor approach. Ti-6Al-4V is selected because it is one of the difficult to machine materials and condition monitoring of tool is more important here due to lesser tool life. Also, multisensor approach is used as most of the earlier works are based on single-parameter-based tool condition monitoring.

Bhattacharyya et al. [1] presented combinations of signal processing techniques, for real-time estimation of tool wear in face milling using cutting force signals. They used probabilistic neural network (PNN) approach for decision making. Saglam and Unuvar [2] introduced the application of a multilayered neural network for tool condition monitoring in face milling using cutting force data. Lee et al. [3] used spindle current for tool wear monitoring. Sevilla-Camacho et al. [4] used discrete wavelet transform and statistical methodologies for monitoring condition of the tool. Method based on spindle motor current was also used by Bhattacharyya et al. [5]. They used multiple linear regression model, built on the filtered features, to estimate tool wear in real time. Patra et al. [6] applied a multilayer neural network with backpropagation algorithm (BPNN) to predict the average flank wear of a high-speed steel (HSS) drill bit for drilling on a mild steel work piece. Al-Sulaiman et al. [7] presented a method for online monitoring, which is based on monitoring the differential electrical power consumption. Haber et al. [8] investigated tool wear monitoring in a high-speed machining process on the basis of analysis of different signals signatures in the time and frequency domains. Andhare and Kumar [9] also used ANN for tool wear monitoring in turning. Thus, it is seen that cutting force, tool vibration, spindle current, surface roughness, etc., are generally used as indicators for monitoring tool wear and ANN is successfully used for classifying the tool wear data. Therefore, in the present work, cutting force and spindle current are taken as indicators along with cutting parameters for TCM using multisensory approach.

2 Experimentation

To get correlation among cutting parameters and the responses, experiments were designed using response surface methodology for end milling of Ti-6Al-4V. Three control parameters—cutting speed, feed and depth of cut—were used and two levels of each parameter as shown in Table 1 were considered. This resulted in twenty sets of experiments using central composite design of RSM. The designed experiment matrix is shown in Table 2. Tool wear, cutting force, and spindle motor current were the responses measured.

Table 1 Control factors and factor levels

S. No.	Factors	Nomenclature	Low value	High value
1	Cutting speed (m/min)	V_c	100	125
2	Feed (mm per tooth)	f	0.15	0.2
3	Depth of cut (mm)	a_p	2	2.5

Table 2 Matrix of experiments

Std order	Run order	Speed (rpm)	Feed (mm/tooth)	Doc (mm)
5	1	636.60	0.150	2.50
6	2	795.80	0.150	2.50
4	3	795.80	0.200	2.00
14	4	716.20	0.175	2.67
1	5	636.60	0.150	2.00
2	6	795.80	0.150	2.00
19	7	716.20	0.175	2.25
20	8	716.20	0.175	2.25
7	9	636.60	0.200	2.50
3	10	636.60	0.200	2.00
9	11	582.33	0.175	2.25
10	12	850.07	0.175	2.25
8	13	795.80	0.200	2.50
17	14	716.20	0.175	2.25
11	15	716.20	0.133	2.25
18	16	716.20	0.175	2.25
15	17	716.20	0.175	2.25
16	18	716.20	0.175	2.25
13	19	716.20	0.175	1.83
12	20	716.20	0.217	2.25

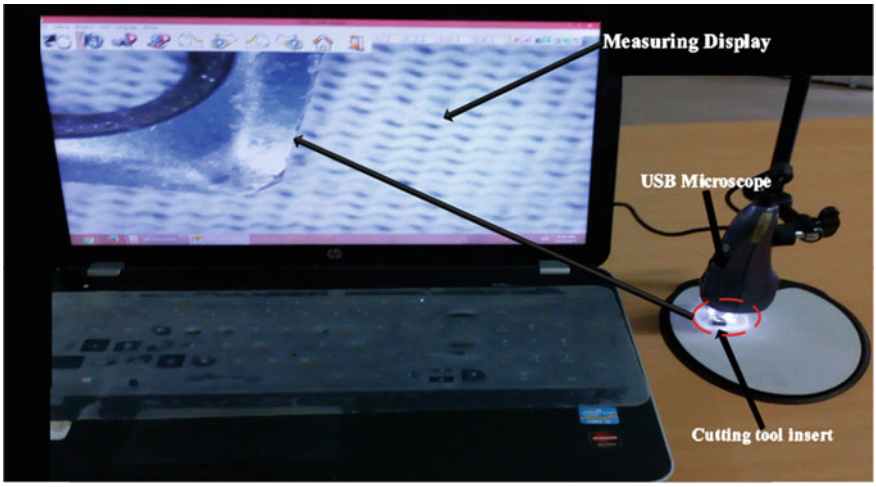

Fig. 1 Tool wear measurement setup

End milling was performed on plates of Ti-6Al-4V (Hardness 36 HRc) work pieces with length of cut as 95 mm in a single pass. Tungsten carbide inserts (SPMT09T308-F55WSM35) having Grade-WSM35 with PVD coating of ZrCN, rake angle of 11°, and nose radius of 0.79 mm were used for machining. Separate cutting edge was used for each run of the experiment and following responses were measured. Tool wear is measured by USB microscope—ISM-PM600SB—in which microscope gets connected to computer by its interface software ISM-PRO. It is a program designed by Insize for ISM-PM600SB digital microscope as shown in Fig. 1. Spindle current is measured using power quality analyzer. Three-phase 4-wire method of current measurement is used where electric current in all the three phases are measured with three wires and extra channel is used as reference channel during current measurement as shown in Fig. 2. The analyzer has a current measuring range from 500 mA to 5 kA with sampling frequency 20 kHz and current sensor accuracy of ±0.2% reading (rdg.) ±0.1% full scale (f.s.). All the measurement data during machining was recorded in memory card, which could later be used for further data analysis. Data analysis of current was done with the Hioki 9424-50 PQA-HI View-pro software application, which analyses binary format measurement data from PW3198 power quality analyzer on a computer. Cutting forces are measured using Kistler 9257BA dynamometer as shown in Fig. 3. Output of dynamometer is given to NI cDAQ-9178 (Data acquisition card) which can be continuously monitored using LabVIEW 2012 software.

Fig. 2 Setup for current measurement

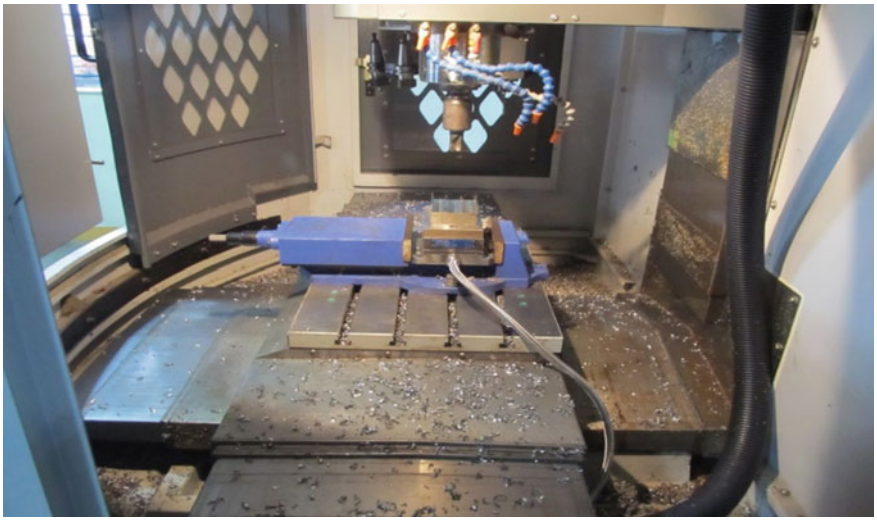

Fig. 3 Setup for cutting force measurement

3 Results and Discussions

Experiments were performed based on design of experiment similar to Table 2. Cutting forces and spindle current were recorded and saved during machining as shown in Fig. 1. Each experiment was performed with new insert tip, for measurement of tool flank wear. Figure 2 shows wear of tool insert. Reading of tool wear for each experiment was determined by calculating average of, number of selected points, in

Table 3 Data of measured responses

Exp. No.	Tool wear (mm)	Current (A)	Normal force, F_y (N)	Feed force, F_x (N)
1	0.133	8.84	828	742
2	0.139	8.85	860	773
3	0.17	8.96	930	750
4	0.153	9.07	950	833
5	0.131	8.62	687	517
6	0.135	8.59	780	694
7	0.148	8.85	837	722
8	0.149	8.88	848	736
9	0.162	9.12	928	843
10	0.159	8.76	840	702
11	0.141	8.76	776	684
12	0.163	8.89	925	850
13	0.172	9.04	1010	880
14	0.146	8.84	830	725
15	0.128	8.65	705	649
16	0.148	8.98	843	733
17	0.151	8.89	845	740
18	0.143	8.86	833	716
19	0.139	8.66	715	633
20	0.179	9.08	952	840

wear area. All measured values of tool wear, cutting force, and spindle current are shown in Table 3.

3.1 Response Surface Methodology

As an important subject in the statistical design of experiments, the response surface methodology (RSM) is a collection of mathematical and statistical techniques, useful for the modelling and analysis of problems in which a response of interest is influenced by several variables [10].

Model developed between control parameters and response as shown in Eq. 1.

$$y = \beta_0 + \sum_{i=1}^{n} \beta_i x_i + \sum_{i=1}^{n} \beta_{ii} x_i^2 + \sum_{i=1}^{n-1} \sum_{j=i+1}^{n} \beta_{ij} x_i x_j + \varepsilon \tag{1}$$

Table 4 Estimated regression coefficients for tool wear

Term	Coefficient	SE coefficient	T	P
Constant	0.145452	0.001361	106.869	0.000
Speed (v_c)	−0.00576	0.001449	−3.974	0.003
Doc (a_p)	−0.02096	0.001692	−12.39	0.000
Normal force (F_y)	0.019738	0.004744	4.16	0.002
Feed force (F_x)	0.011662	0.004424	2.636	0.025
Current (I)	0.008627	0.002577	3.348	0.007
Current * current (I^2)	0.001998	0.001519	1.315	0.218
Speed * Doc (v_c * a_p)	0.007611	0.002654	2.868	0.017

where y is measured response; β_0, β_i are regression coefficients; x_i is input factors, and ε error in measurement. The method of least squares is used to estimate the parameters in the approximating polynomials. The response surface analysis is then performed using the fitted surface. The model parameters can be estimated most effectively if proper experimental designs are used to collect the data. In the present work, model for tool wear was developed using multisensory approach, in which sound, pressure, and vibration are taken as control parameters in addition to cutting parameters.

Analysis of variance was performed to find out the significant parameters based on p value as shown in Table 4. Non-significant parameters are eliminated using stepwise backward elimination method. Parameters having the p-value greater than 0.1 are removed from the model.

3.2 Response Surface Model

Response surface model to predict tool wear with cutting speed, feed rate, depth of cut, sound emission, and vibration amplitude with significant parameters is shown in Eq. 2:

$$V_b = 2.444 - 5.4786e-4 \times V_c - 0.146 \times a_p * 4.71e-5 \times F_y + 6.425 \times e-5F_x - 0.471 \times I + 0.000135 \times V_c \times a_p \quad (2)$$

where V_b = tool flank wear (mm); f = feed rate (mm/tooth); a_p = depth of cut (mm); F_y = normal force (N); F_x = feed force, and I is current in ampere. Correlation coefficient (R^2_{adj}) of 98.28% shows that 99.2% data can be explained by the developed model. Model adequacy was checked by residual plots as shown in Fig. 4. In normal probability plot, all the points lie along the straight line. It shows that 95% of the fitted data calculated from the model are close to experimental data. Residual versus

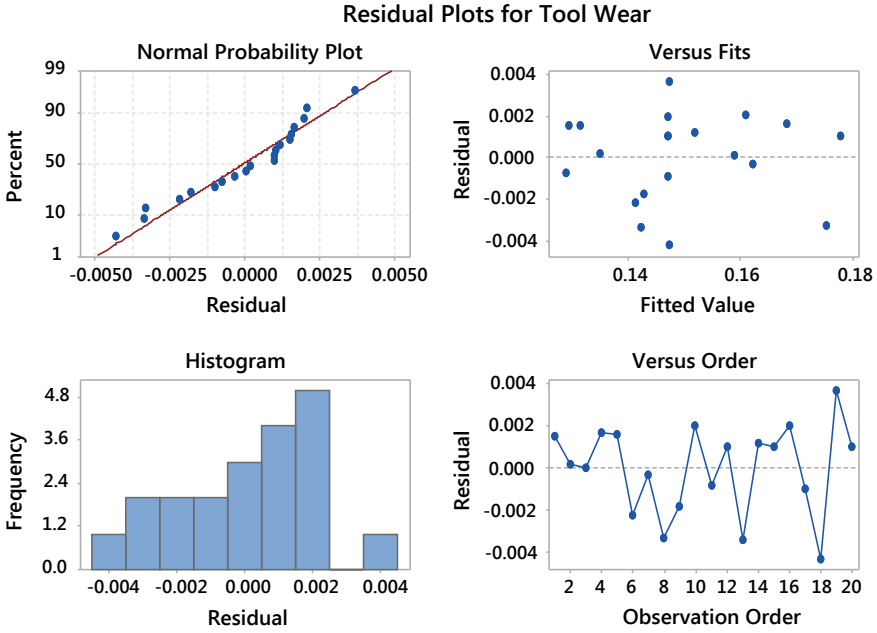

Fig. 4 Residual plot for tool wear

fitted data, histogram and residual versus observation order also show fitted values are closer to experimental values.

Tool wear occurs on the tool flank as a result of friction between the machined surface of the workpiece and the tool flank. As process parameters increases, friction also increases. Figure 5 shows that tool wear is increasing with increase in speed, feed, and depth of cut. Slope of graphs clearly indicates that the machining parameter which had the highest influence on tool wear is the feed rate, followed by the cutting speed and depth of cut. Cutting forces and spindle current also show uniform effect over tool wear. The possible reasons for the above trend are, as the sharpness of tool reduces, it requires large forces to penetrate inside the workpiece for particular depth of cut. As the cutting forces increase, power consumption required for machining is increased for machine tool. Therefore, value of cutting forces as well as spindle current increase with increase in tool wear. This model is still the best example for proving importance of multisensory approach in tool condition monitoring. This is so because, in most cases, signals coming from only one sensor are typically insufficient to give enough information for machining and tool condition monitoring. Hence, two signals from different sources are integrated to provide the maximum information needed for tool condition monitoring.

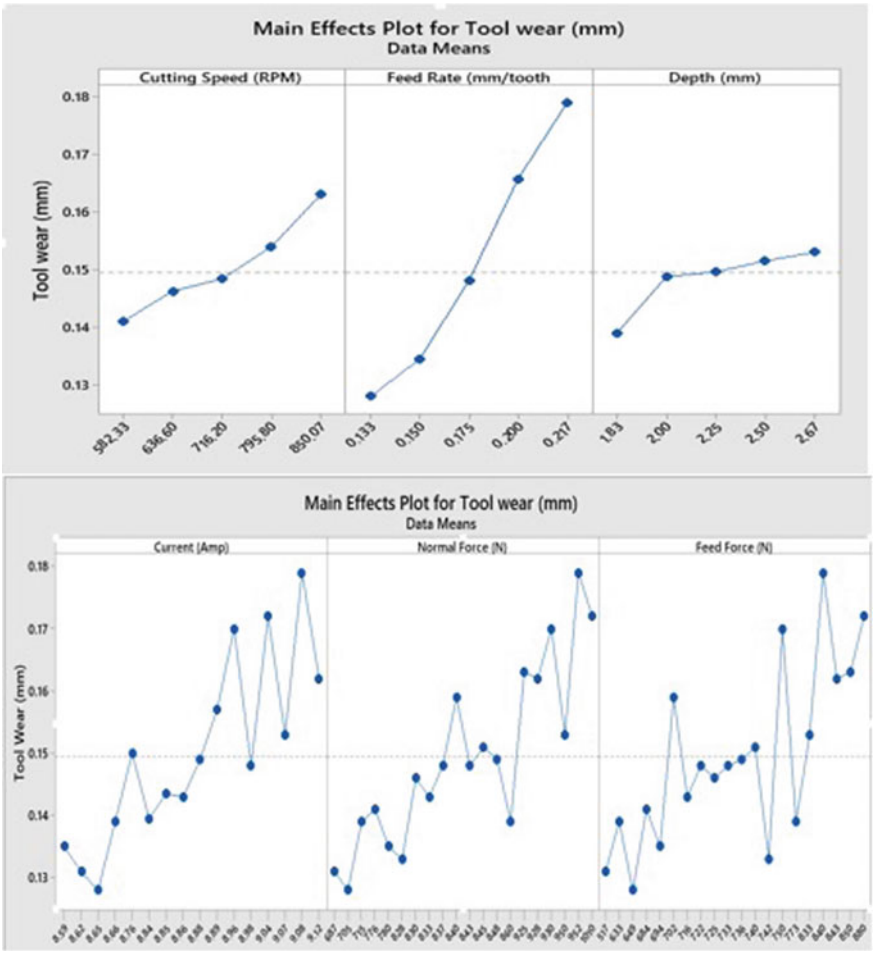

Fig. 5 Main effect plot for tool wear

3.3 Confirmation Experiments

In order to verify the adequacy of model, additional experiment was performed. The conditions were those which have not been used previously but are within the range of the levels defined previously, as shown in Table 5. The predicted value from model and the actual experimental value for tool flank wear were compared. Percentage error between actual and predicted value was found to be 4.5% which is acceptable.

Table 5 Details of validation experiment

Speed (rpm)	Feed rate (mm/tooth)	Doc (mm)	Spindle motor current (A)	Normal force (N)	Feed force (N)	Tool wear Exp. (mm)	Tool wear model (mm)	% error
780.3	0.197	2.366	8.97	984.3	865	0.168	0.176	4.5

4 Conclusion

Milling process was studied and three process control variables, namely cutting speed, feed, and depth of cut were chosen for tool condition monitoring. Design of experiments was done using central composite method and 20 machining experiments were carried out. Spindle current and cutting forces were measured during experiments. Tool flank wear was measured for each experiment performed with new insert. Tool wear prediction model was developed using multisensory approach and a verification experiment was conducted for checking the accuracy of generated models. The following concluding remarks can be drawn from the experiments conducted and repeated in the paper:

1. RSM-based design of experiments is a very structured methodology for planning and designing a sequence of experiments.
2. Prediction model for tool wear is developed using spindle current, cutting forces, and process parameters. Its % error in prediction of tool wear is 4.5. Hence, this method can be used for prediction of tool wear. Correlation coefficient (R^2) of 98.28% shows that model best explains the experimental data.
3. The prediction of tool wear concludes that multisensory approach for tool condition monitoring gives more accuracy as compared to TCM which uses single sensor.

References

1. Bhattacharyya P, Sengupta D, Mukhopadhyay S (2007) Cutting force-based real-time estimation of tool wear in face milling using a combination of signal processing techniques. Mech Syst Signal Process 21(6):2665–2683
2. Saglam H, Unuvar A (2003) Tool condition monitoring in milling based on cutting forces by a neural network. Int J Prod Res 41(7):1519–1532
3. Lee K-J, Lee T-M, Yang M-Y (2007) Tool wear monitoring system for CNC end milling using a hybrid approach to cutting force regulation. Int J Adv Manuf Technol 32(1):8–17
4. Sevilla-Camacho PY, Herrera-Ruiz G, Robles-Ocampo JB, Jáuregui-Correa JC (2011) Tool breakage detection in CNC high-speed milling based in feed-motor current signals. Int J Adv Manuf Technol 53(9):1141–1148
5. Bhattacharyya P, Sengupta D, Mukhopadhyay S, Chattopadhyay AB (2008) On-line tool condition monitoring in face milling using current and power signals. Int J Prod Res 46(4):1187–1201

6. Patra K, Pal SK, Bhattacharyya K (2007) Artificial neural network based prediction of drill flank wear from motor current signals. Appl Soft Comput 7(3):929–935
7. Al-Sulaiman FA, Baseer MA, Sheikh AK (2005) Use of electrical power for online monitoring of tool condition. J Mater Process Technol 166(3):364–371
8. Haber RE, Jiménez JE, Peres CR, Alique JR (2004) An investigation of tool-wear monitoring in a high-speed machining process. Sens Actuators A 116(3):539–545
9. Andhare A, Kumar R (2015) Condition monitoring of turning tool using Artificial Neural Network. Paper presented at the National Conference on Condition Monitoring, Vishakhapatnam
10. Myers RH, Montgomery DC, Anderson-Cook CM (2016) Response surface methodology: process and product optimization using designed experiments. Wiley, New York, NY

Envelope Spectrum Analysis with Modified EMD for Fault Diagnosis of Rolling Element Bearing

A. A. Darji, P. H. Darji, and D. H. Pandya

Abstract Selection of demodulation resonant frequency band for envelope analysis is often made by spectrum examination of all frequency band during the fault diagnosis process in time-frequency analysis. To overcome this limitation, a new criterion to select a suitable resonant frequency band for concern bearing defect frequencies has been examined experimentally in present work. Synchronized resonant frequency band is obtained based on orthogonal reverse biorthogonal wavelet RBIO 5.5 for decomposition of signal, using wavelet packet transform for time-frequency analysis. Concept of pseudo-IMF has not been explained by earlier researchers and the authors are interested to study the effectiveness of subsequent IMF with different resonant frequency band. The experimental results from set up indicate that the present concept is a validated tool, to develop an efficient online fault diagnosis system to diagnose the incipient bearing faults.

Keywords Ball bearing · Hilbert hung transform · Localized defect · Spectral kurtosis · Wavelet packet transform

A. A. Darji (✉) · P. H. Darji
Department of Mechanical Engineering, C. U. Shah University, Surendranagar, Gujarat, India
e-mail: ankitdarjildrp@gmail.com

P. H. Darji
e-mail: pranav_darji@rediffmail.com

D. H. Pandya
Department of Mechanical Engineering, LDRP Institute of Technology and Research, Gandhinagar, Gujarat, India
e-mail: veddhrumi@gmail.com

V. K. Gupta et al. (eds.), *Reliability and Risk Assessment in Engineering*,
Lecture Notes in Mechanical Engineering,
https://doi.org/10.1007/978-981-15-3746-2_8

1 Introduction

Rolling bearings are the most important elements in rotating machinery. Modern bearings have vital role in various process industries which make it one of the reliable and long-lasting elements. This reliability of rolling element bearing is affected by advance materials, newer design criteria, lubrication, proper installation and maintenance. Requirement of industries is to implement incipient fault diagnosis techniques and avoid catastrophic failure of ball bearing. Condition-based monitoring techniques have touched new horizons of real-time analysis, with advanced sensors and improved signal processing techniques. Time-based, time-frequency-based techniques have significant importance in vibration measurement and analysis for real-time fault diagnosis of ball bearing [1]. Localized fault in rolling element bearings produces a series of impacts which repeat periodically, at a rate dependent on bearing geometry. These repetition rates are known as the characteristic defect frequency (CDF). Researchers are interested to diagnose these low frequencies which are modulated with bearing's high resonant frequencies. To demodulate these CDF, number of techniques like shock pulse method (SPM), high-frequency resonant technique, FFT, wavelet transform, etc. are being effectively diagnosed for the bearings. The low-frequency modulating signal can effectively filter out, from high-frequency raw signal, with high-frequency resonance technique. Proposed technique has better performance due to absence of low-frequency mechanical noise, compared to demodulated vibration signal. Thus, present technique provides a low-frequency demodulated signal with a high signal-to-noise ratio, with a high-frequency system resonance [2]. Later, HFRT is modified as envelope analysis technique. The traditional envelope analysis has two disadvantages, one fast Fourier transform is widely used for analyzing envelope spectrum which could give general energy-frequency distribution hence it had failed to give particulars of characteristic defect frequency (CDF) from signal. Also, FFT considers all type of signals as harmonic signals and analysis with such assumption may mislead the information specially in case of non-stationary and nonlinear vibration responses from inner race defect or ball defect [3]. Ball bearing is a multi-body nonlinear dynamic mechanism, where non-linearity in the system is induced due to clearance, waviness, nonlinear stiffness, nonlinear damping, uneven loading conditions, etc. [4]. Nonlinear signals are effectively investigated with time-frequency domain which provides time, frequency and amplitude information. Wavelet transform is one of the well-known time-frequency techniques to examine non-stationary signals, where energy distribution changes with time, along each frequency band. It is like a FFT with multiple window size [5]. However, Peng et al. [6] have noticed some expected limitations of wavelet transform, including border distortion and energy leakage. Thus, modulation limitation will modulate little noisy data for the entire range of frequency scales, which will be difficult to diagnose. WPT is extension of WT, considering the fixed level of decomposition, irrespective of intrinsic characteristic of non-stationary and nonlinear bearing signals. Hilbert–Huang Transformation (HHT), first proposed by Huang et al. [7], is an effective time-frequency-based adaptive approach. Thus, HHT is considered as one

of the effective signal processing technique to analyze non-stationary and nonlinear signals. The HHT consists of the well-known EMD and IMF. WPT-based Hilbert–Huang transforms can produce effective result but there is more computing time required for envelope detection. Dejie et al. [3] have represented combined envelope analysis method and EMD technique for condition monitoring of roller bearings. In that method, raw data signal from targeted bearings was transformed into time-scale representation by using the wavelet transformation. High-scale wavelet coefficient received by wavelet transformation would be analyzed with Hilbert transform, which would signify the high-frequency components of transform signal. Thus envelope spectrum analysis was done using EMD and Hilbert transform which work out the local marginal spectrum to represent condition of roller bearing. Application of data mining was used to identify pattern of the fault condition. Peng et al. [8] have made comparison of Hilbert–Huang transformation with the wavelet transformation spectrum, evaluated for computer-generated signal validated with rubbing rotor model. Characteristics defect frequency of rolling bearing has been recorded with time interval between successive impacts produced with nonlinear responses. The difference in frequency range from simulated signal has produced only 2 IMFs and authors have also recorded the complexity in identification of inner race defect (IRD) in the bearing, due to number of non-stationary transfer segments as compared to the outer race defect (ORD) and ball defect. Rai and Mohanty [9] have presented a comparative analysis to indicate the usefulness of frequency-domain approach. DFT has shown it to be less efficient while wavelet transformation has intrinsic limitation of longer computational time and fixed-scale frequency resolution. Hilbert–Huang Transform (HHT) technique has additional edge to overcome above-listed limitations and offer multi-resolution in various frequency scales which consider variation of frequency in processed signals. Sheen [10] has demonstrated the signal processing method to extract impulse response from the modulated signal for condition monitoring and fault diagnosis of rotating systems is carried out in two stages. First, envelope spectrum analysis would be carried out and then impulse response function modulated, to process the signal, and estimated from the linear least square analysis. Thus, reversed signal processing can be reconstructed and the sidebands in impulse response spectrum could be theoretically eliminated. Thus, overall effectiveness could be improved. Sheen [11] has proposed an algorithm based on the resonance modes of system. Tsao et al. [12] represented a newel idea using EMD technique as effective fault diagnosis tool of ball bearing, for process industries. A band-pass filtering nature of decompose signal with EMD have to select mono-component of signal, recognized as IMF. Optimized IMF selection has proposed using EMD with a swept-sine excitation and concluded as effective tool for fault diagnosis, where specific IMF have been selected with a spectrogram. Conclusion of above review suggested that there are various methods and techniques suggested for fault diagnosis of ball bearing. HHT with wavelet packet transform was the effective fault diagnosis method for ball bearing. HHT is perfect tool for nonlinear and non-stationary signals of ball bearing but it has some deficiencies, like at end of orthogonal representation (IMF), large swings will occur due to curve fitting limitation. Secondly, if the first IMF does not satisfy the mono-component definition, but

even then IMF1 is utilized by the researchers in envelope spectrum because considering that first two IMF as real component and rest are the pseudo-IMF, concept of pseudo-IMF was not explained. Hence, authors intended to study the effectiveness of subsequent IMF with different resonant frequency band. Synchronized resonant frequency band is selected using the WPT noise reduction technology that separates the high-frequency resonance components and the modulating unwanted signals at less amplitude SNR.

2 Experimental Data Acquisition

The experimental setup utilized for the present research is shown in Fig. 1. Rigid structure of mild steel has designed and mounted on experimental table with bolted joints. Suitable rubber packing was installed between rigid structure and table, to minimize additional vibrations from surroundings. As shown in Fig. 1, rotating system has design mounted on ball bearing and driven by a DC motor with external servo controller. A flexible spring type coupler has been used to minimize the effect of misalignment, if any, present in the system. SKF 6205 deep groove ball bearing has been used for the present research. The localized defects are implemented through laser machining with defect size of 300 × 300 × 20 μ as shown in Fig. 2. Authors have experimented four test bearings for the present research like (A) healthy bearing (B) bearing with outer race defect (ORD), (C) bearing with inner race defect (IRD) and (D) bearing with ball defect. Data acquisition was done with latest vibration analyzer. Pickup type of sensors with frequency range of 1–30 kHz were used Piezoelectric sensors were calibrated to measure range of ±500 g with resolution of 0.005 g. Calibration of variable speed motor with vibration analyzer was established up to resonant frequency of 70 kHz. Post-processer of present analyzer is easy to operate with its GUI interface and MATLAB integrity. Vibration signals have been collected with four input channels at sampling rate of 20.480 kHz.

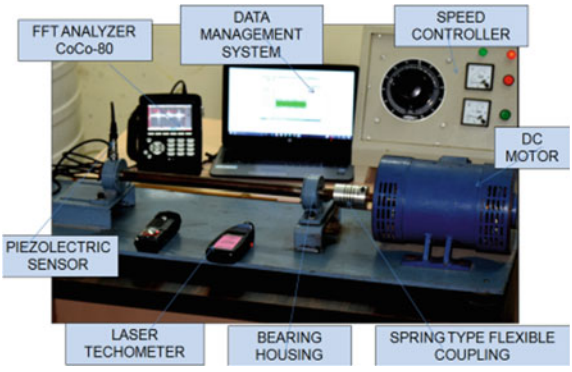

Fig. 1 Experimental setup

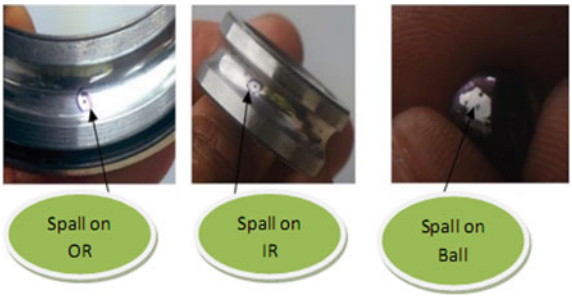

Fig. 2 Localized defect on bearing element

3 Methodology

In this paper, original time series data is decomposed with wavelet packet using real reverse biorthogonal 5.5 wavelet, where selection of RBIO 5.5 wavelet was recommended by Pandya et al. [13]. Thus decompose signal has been employed to check spectral kurtosis of each decompose segment. Larger kurtosis is indicative of impulsive responses in that synchronized frequency band. The original time series data was decomposed in intrinsic oscillation mode, using the empirical mode decomposition. Finally, the envelope spectrum is applied to the IMF with resonant frequency band, which coordinated with preceding selected frequency band.

The process of selection of IMF based on synchronized resonant frequency band for ball bearing diagnosis was listed stepwise as follows:

(1) Collecting raw vibration signal.
(2) Decompose signal: Choosing a wavelet and decomposition level J. The total decomposition levels (J) can be calculated according to the following relationship:

$$J \geq \log_2\left(\frac{f_s}{f_c}\right) + 1$$

where f_s is sampling frequency and f_c characteristic defect frequency.
(3) The WPT resonant frequency band with maximum kurtosis was selected to obtain maximum impulse frequency in this band. Spectral kurtosis has effective ability to analyze frequency domain and to identify concern frequency bands where the fault signal can be best detected [14–18].
(4) Performed band-pass filtering with EMD on time series data.
(5) Optimized IMF and set of IMFs of definite frequency band were selected.
(6) The IMF with resonant frequency band, which synchronized with frequency band was obtained with WPT and spectral kurtosis.
(7) Processed selected signal for extracting fault features.

4 Results and Discussion

Vibration measurement is more difficult when faults may locate on rotating inner race and ball, in case of rolling element bearing. When inner race fault comes in load zone once in the revolution, it generates low frequency as compared to same size of outer race fault, even it may not generate any impulses when inner race fault is out of load zone. Ball pass frequency of inner race is generally modulated with rotating frequency of rotor. BPFI is generally modulated with rotating frequencies and BSF, resulting in generation of fundamental train frequency, which modulates other frequencies such as BPFI, BSF and rotating unit frequency. These modulations generate number of sidebands around the CDF which sometimes are difficult to recognize in low-frequency range.

In this paper, proposed concept is experimentally demonstrated at bearing with IRD condition. The traditional envelope analysis with fast kurtogram and the developed technique are used to compare effectiveness at different bearing conditions, with SKF 6205 single deep groove ball bearing at 4000 rpm.

4.1 Inner Race Defect

When bearing with IRD operate, it will execute non-linear signal due to material & geometric non-linearity and non-stationary signal due variable location of defect in a revolution. Figure 3a shows fast kurtogram with decomposition level 2.5, which shows high, non-stationary responses around carrier frequency of 4266.67 Hz. The dyad which maximizes the kurtosis is (f_c, BW), that is, the frequency band of (3413.33–5119 Hz). Here, a characteristic defect frequency (BPFI) is 361 Hz for rotational frequency of 66.67 Hz. Envelope analysis spectrum with fast kurtogram is recorded significant peaks at X, 2X and modulating peak (BPFI-2X) 227 Hz as shown in Fig. 3b. Figure 3c shows the spectral kurtosis at three decomposition level, which shows the maximum kurtosis at 2880 Hz and at decomposition level 5 of WPT corresponding resonant frequency band is (2720–3040 Hz). Sudden impulses were also observed in terms of SK at 3840 Hz and corresponding resonant frequency band at (3680–4000 Hz). EMD procedure is computed waveform spectra of 18 IMFs, out of those first four Fourier spectra of IMFs are shown in Fig. 3d. Now, the Fourier spectra synchronized with resonant frequency bands is IMF2. Traditional HHT envelope analysis is based on IMF1, even through IMF1 cover a wide frequency range at high-frequency region and not satisfy the mono-component definition. Figure 3e, f shows the envelope spectrum of IMF1 and IMF2, respectively. The comparison clearly indicates the effectiveness of proposed concept. Envelope spectrum with IMF2 shows the significant and clear peaks at X, 2X, BPFI-2X (227 Hz) and BPFI (361 Hz), while envelope spectrum of IMF1 shows the significant peaks at X and 2X. Other peaks are observed as sidebands at 240, 278 Hz and at other segment near to BPFI peak is modulated with half of FTF frequency, which shows lower peak at (BPFI)

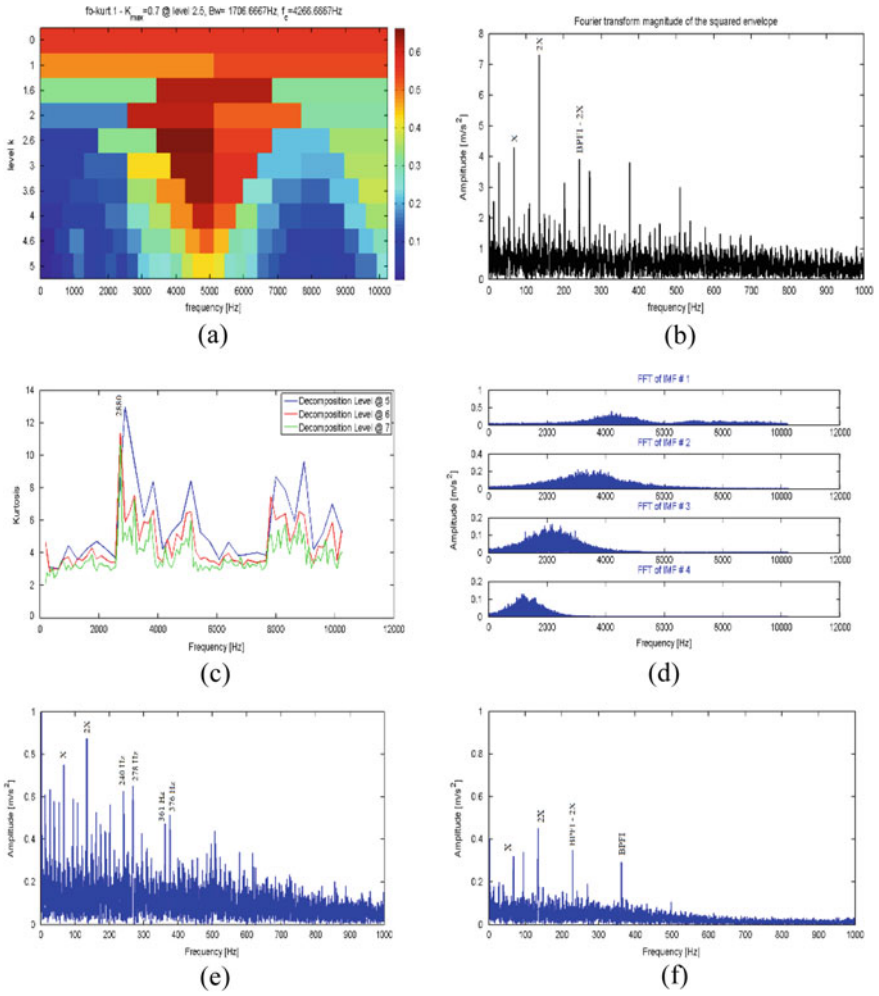

Fig. 3 Data from bearing with inner race fault. **a** Fast kurtogram, **b** squared envelope spectrum, **c** spectral kurtosis versus frequency, **d** Fourier spectra of first four IMFs, **e** envelope spectrum of IMF1 and **f** envelope spectrum with synchronized frequency band (IMF2)

361 Hz and adjacent higher peak at 376 Hz. Bearing fault diagnosis of bearing with IRD is more effective with proposed technique at resonant frequency band of IMF2, than fast kurtogram with resonant frequency band at (3413.33–5119 Hz) and poor resolutions with IMF1 envelope spectrum at high-frequency region and also poor curve fitting limitation, at the end of first intrinsic function.

5 Conclusion

The present research work leads to conclude the following outcomes based on experimental analysis with the proposed technique.

- In this research work, the HHT technique is used as an effective tool for analyzing non-stationary and nonlinear vibration signals with intrinsic mode function. Resonant frequency band determined through WPT and spectral kurtosis enhance an additional edge to Hilbert–Huang transform, as an effective fault diagnosis tool.
- Basically, IMFs are a kind of complete, adaptive, almost orthogonal and mono-component representation for the analyzed signal. But even then, IMF1 is utilized for envelope analysis. This research is concluding the effectiveness of IMF2 and IMF3 for effective analysis of nonlinear and non-stationary signals.
- Here in the proposed concept researchers suggested effective and faster technique to select IMF as compare to earlier conventional envelope analysis and/or fast kurtogram.

References

1. Tandon N (1994) A comparison of some vibration parameters for the condition monitoring of rolling element bearings. Measurement 12(3):285–289
2. Sheen YT (2004) A complex filter for vibration signal demodulation in bearing defect diagnosis. J Sound Vib 276(1–2):105–119
3. Dejie Y, Junsheng C, Yang Y (2005) Application of EMD method and hilbert spectrum to the fault diagnosis of roller bearings. Mech Syst Signal Process 19(2):259–270
4. Harsha SP (2005) Nonlinear dynamic response of a balanced rotor supported on rolling element bearing. Mech Syst Signal Process 19(3):551–578
5. Junsheng C, Dejie Y, Yu Y (2005) Time-energy density analysis based on wavelet transform. NDT E Int 38(7):569–572
6. Peng Z, Chu F, He Y (2002) Vibration signal analysis and feature extraction based on reassigned wavelet scalogram. J Sound Vib 253(5):1087–1100
7. Huang N, Shen Z, Long S, Wu M, Shih H, Zheng Q, Yen NC, Tung C, Liu H (1998) The empirical mode decomposition and the hilbert spectrum for nonlinear and non-stationary time series analysis. Proc R Soc A 454(1971):903–995
8. Peng ZK, Tse PW, Chu FL (2005) A comparison study of improved hilbert–hung transform and wavelet transform: application to fault diagnosis for rolling bearing. Mech Syst Signal Process 19(5):974–988
9. Rai VK, Mohanty AR (2007) Bearing fault diagnosis using FFT of intrinsic mode functions in hilbert–huang transform. Mech Syst Signal Process 21(6):2607–2615
10. Sheen YT (2007) An impulse-response extracting method from the modulated signal in a roller bearing. Measurement 40(9–10):868–875
11. Sheen YT (2010) An envelope analysis based on the resonance modes of the mechanical system for the bearing defect diagnosis. Measurement 43(7):912–934
12. Tsao WC, Li Y, Le D, Pan MC (2012) An insight concept to select appropriate IMFs for envelope analysis of bearing fault diagnosis. Measurement 45(6):1489–1498
13. Pandya DH, Upadhyay SH, Harsha SP (2014) Fault diagnosis of rolling element bearing by using multinomial logistic regression and wavelet packet transform. Soft Comput 18(2):255–266

14. Dwyer RF (1998) A technique for improving detection and estimation of signals contaminated by under ice noise. J Acoust Soc Am 74(1):124–130
15. Antoni J (2006) The spectral kurtosis: a useful tool for characterizing non-stationary signals. Mech Syst Signal Process 20(2):282–307
16. Antoni J (2007) Fast computation of the kurtogram for the detection of transient faults. Mech Syst Signal Process 21(1):108–124
17. Randall RB (2005) Applications of spectral kurtosis in machine diagnostics and prognostics. Key Eng Mater 293–294:21–30
18. Xiao Y, Ding E, Chen C, Liu X, Li L (2015) A novel characteristic frequency bands extraction method for automatic bearing fault diagnosis based on hilbert huang transform. Sensors 15(11):27869–27893

Experimental Investigation of Chatter in CNC Turning Using Different Shim Materials

C. J. Mevada, H. M. Trivedi, A. A. Darji, and D. H. Pandya

Abstract The most widely used machining operation in the manufacturing is the turning. Machining Vibration or chatter is one of saviour outcome of non-linear motion of cutting operation which has immense effect on tool wear and surface roughness. Chatter in machining will ultimately reducing the productivity of system because of involvement of post processing or finishing operation. The different methods for chatter reduction are categorized into two types, active and passive chatter control techniques. One of the passive chatter control techniques is proposed in this paper. The chatter is reduced by using different shim materials between insert and tool holder, which causes change in damping value of the cutting tool. The different shim materials used are carbide, aluminum and brass. The harmonic analysis is used for finding the damping ratio for different shim materials, and computational simulation has been performed with the corresponding Rayleigh damping coefficient. Experiments were conducted for gathering the acceleration data, which is helpful in generating different plots such as fast Fourier transformation (FFT) plot, Poincare plot and Orbit plot using MATLAB. The surface roughness was also measured. All these data are helpful in predicting chatter reduction. The experimental data will be useful for design of the cutting tool and operating condition by operators.

Keywords ANSYS · Chatter · CNC turning · Finite element method · Shim

C. J. Mevada · H. M. Trivedi · A. A. Darji · D. H. Pandya (✉)
Department of Mechanical Engineering, LDRP Institute of Technology, Gandhinagar, India
e-mail: veddhrumi@gmail.com

C. J. Mevada
e-mail: chiragmevada9@gmail.com

H. M. Trivedi
e-mail: hemant_trivedi@ldrp.ac.in

A. A. Darji
e-mail: ankitdarjildrp@gmail.com

V. K. Gupta et al. (eds.), *Reliability and Risk Assessment in Engineering*,
Lecture Notes in Mechanical Engineering,
https://doi.org/10.1007/978-981-15-3746-2_9

1 Introduction

The chatter is one of the major obstacles in achieving the automation of machining operations such as turning, boring, drilling and milling. The chatter in machining causes problems like inferior surface finish, excess amount of noise, reduction in tool life and in worst case breakdown of the tool components, which hampers productivity.

Siddhpura and Paurobally [1] reviewed the status of current research in chatter vibration in turning and summarized the methods for stability prediction of chatter, detection of chatter and techniques to control chatter for the most widely used turning operation. Different methods for stability prediction of chatter, detection of chatter and techniques to control chatter are compared for finding the most preferable technique/s and to find the scope of research in chatter vibration.

2 Chatter in CNC Turning

A nonlinear delay differential equation (DDE) with two degree of freedom model was proposed by Chandiramani and Pothala [2], where researchers were analyzed for self-excited vibration of cutting tool during the orthogonal turning operation. Clancy and Shin [3] introduced a model for face turning operation using the three-dimensional frequency domains for chatter, which includes the process damping and the effect of tool wear. The direction and magnitude of the damping force during process are accurately predicted for tools with complex geometries. Mahdavinejad et al. [4] presented the dynamic model giving instability analysis for the machining processes for the turning machine. The model in which it consists of structure of machine tool was provided by ANSYS software and finite element method, so the machine's structural flexibility, tool and workpiece have been taken into consideration.

Hajikolaei et al. [5] suppressed regenerative chatter using adaptive force control and variation of spindle speed for turning process. Two strategies of control were developed, to minimize turning operation also using a worn-out tool. The results gathered in the delayed resonator (DR) study of vibration can be extended to the chatter vibration. Tansel et al. [6] proposed S-transformation for detection of the chatter. S-transformation is used for the preparation of the 3D plots, which display change in the amplitude into the sensory signals, for the turning process inside of the frequency and time domain, simultaneously. The S-transformation results are helpful in obtaining the frequency versus time versus damping index graph.

Tarng et al. [7] presented a method of mounting the piezoelectric-inertia actuator on a cutting tool and perform as a vibration absorber with tuning to reduce the chatter in turning process. In which, the natural frequency of the cutting tool must be equal to the natural frequency of the vibration absorber. Further, a larger amount of damping ratio is required for vibration absorber. Cardi et al. [8] investigated a method of regenerative chatter reduction for compliant workpiece material. A neural network trained with particle swarm optimization is used to transform the radial displacement,

measured at cutting tool, to an approximation of the workpiece's radial displacement. In addition to this, the change in the thickness of uncut chip is measured over time, to find the transition of stable cut to chatter vibration through experiment. Orra et al. [9] developed and implemented an electro magneto rheological damper that is used for monitoring and controlling vibrations of machine tool. Also, they have used a well-known half-power bandwidth method, which provides damping ratio, given by equation $\zeta = f2 - f1/2\text{fr}$. Where ζ is the damping ratio, $f1$ and $f2$ are the half-power frequencies for the amplitude of $fr/\sqrt{2}$; fr is the undamped natural frequency for the highest peak. In present work, this method to find damping ratio is used.

The main aim of this work is to mitigate chatter by varying the damping ratio of the cutting tool, using different shim materials. The shim materials provided by manufacturers are made of carbide on demand, which is replaced by materials with different damping characteristics such as aluminum and brass. The damping ratio is found using all three shims; also experiments were conducted to validate the results. Damping ratio was calculated from the frequency response plot generated using harmonic analysis.

3 Harmonic Analysis and Damping Ratio

To perform harmonic analysis, the software used is ANSYS-15. The geometric model prepared in PRO-E of cutting tool with insert and shim is shown in Fig. 1a. The half tool is used for analysis, only to consider hanging portion in tool post. The meshing method used is sweep and tetrahedral patch conforming method. The natural frequencies and modes of vibrations are found using modal analysis of cutting tool. The mode frequencies are used in harmonic analysis, for generating frequency response graph.

4 Problem Statement

The pick point in frequency response graph shows the maximum amplitude and natural frequency point as shown in Fig. 1b–d. The half-power bandwidth method is used for finding the damping ratio for cutting tool with different shim. The various calculated values of damping ratio by half-power bandwidth method for tool holder with different shim materials are given in Table 1.

From harmonic analysis of cutting tool, it is proved that the tool with brass shim shows lower damping ratio as compared to aluminum and carbide shim. These values of damping ratios are helpful in finding Rayleigh damping coefficient, α damping (mass coefficient) and β damping (stiffness coefficient). The α damping also known as mass damping coefficient in which friction or viscous damping is considered to be zero ($\alpha = 0$).

The β damping coefficient can be calculated from equation $\beta = 2\zeta/\omega$ for known values of ζ (damping ratio) and ω (natural circular frequency) which gives structural

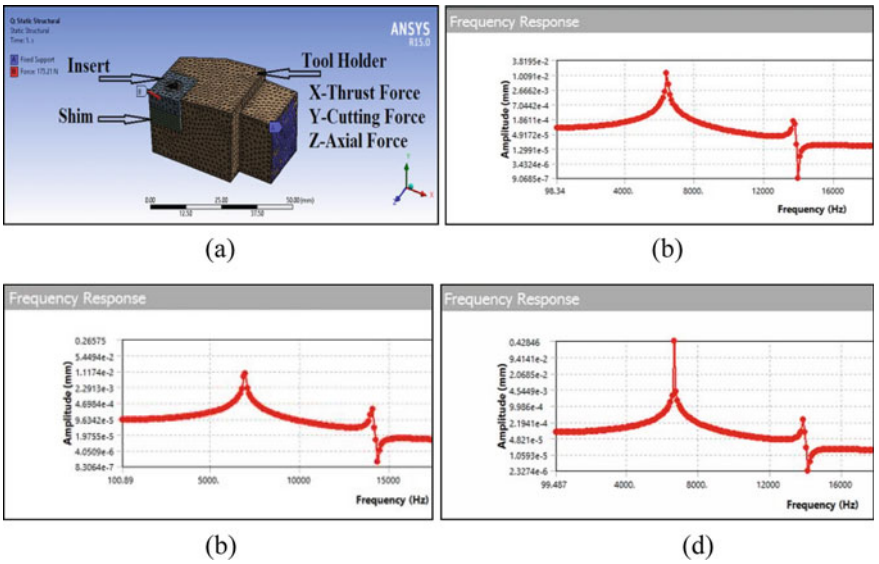

Fig. 1 **a** Cutting tool model with meshing and nomenclature, **b** frequency response plot for cutting tool with carbide shim, **c** frequency response plot for cutting tool with aluminum shim, **d** frequency response plot for cutting tool with brass shim

Table 1 Damping ratio of cutting tool with various shim materials

Shim	Max amplitude (mm)	Natural frequency Fr (Hz)	Half-power Point (mm)	$f1$ (Hz)	$f2$ (Hz)	Damping ratio
Carbide	1.21E–02	6392.2	8.55E–03	6356.812	6437.238	0.0063
Aluminum	8.66E–03	6961.3	6.14E–03	6884.755	7000.120	0.0083
Brass	4.27E–01	6665.7	3.04E–01	6636.273	6695.013	0.0044

damping of material. The value of β damping (or stiffness coefficient) is used in ANSYS, as damping control input for simulation of amplitude versus frequency plot for tool holder with different shim materials.

5 Setup for Experimental Work

The turn master GF 165-A CNC lathe machine was used to carry out experiments. The workpiece material is of 45 HRC En 31 mild steel bar used for turning operation. The length and diameter of workpiece are 40 mm and 50 mm, respectively. The insert used for cutting is CBN 650. The carbide shim used was provided by the cutting tool manufactures. The aluminum shim is made of al 2024 or duralumin, and the brass

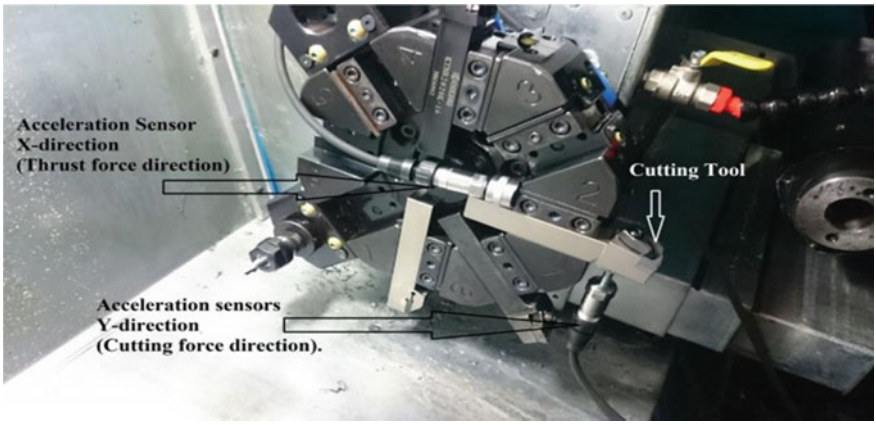

Fig. 2 Sensors mounting and cutting tool setup

shim is made of C 26000 cartridge brass. These two materials are used because of their damping characteristics and availability.

The Kyocera's manufacturers catalog was used for selecting feed, cutting speed and depth of cut. The minimum value of feed 0.08 mm/rev was selected and kept constant for all readings. The two cutting speeds used are 150 m/min and 200 m/min. The various depth of cut used are 0.3, 0.4 and 0.5 mm for each shim of carbide, aluminum and brass for performing experiments.

The acceleration data are measured with the help of acceleration sensors connected to the CO CO80 dynamic analyzer. The forces acting on tool produce vibration, and these vibration readings are taken using two uni-axial piezoelectric accelerometers. The vibration was measured in X the direction of thrust force and Y the direction of cutting force. The sampling frequency used for analyzing the data is 5.12 kHz. The surface roughness tester SJ 210 of Mitutoyo with measuring range of −200 to 150 μm is used. Figure 2 shows the sensors mounting and cutting tool setup.

6 Results of Experiment and Discussion

The total 18 number of experiments are conducted for each shim material with two cutting speed and three depth of cut. The acceleration data collected using CO CO80 dynamic analyzer to plot the Fast Fourier Transformation (FFT) plot, Poincare plot and Orbit plot are plotted for finding the behavior of cutting tool. Since, the Time response and FFT plot are not sufficient to define cutting tool behavior, hence two different plots such as Poincare plot and Orbit plot are generated, using MATLAB. The three types of responses which are discussed for cutting tool behavior are chaotic, multi periodic and quasi periodic. Figure 3 shows the different plots for the dynamic motion behavior analysis.

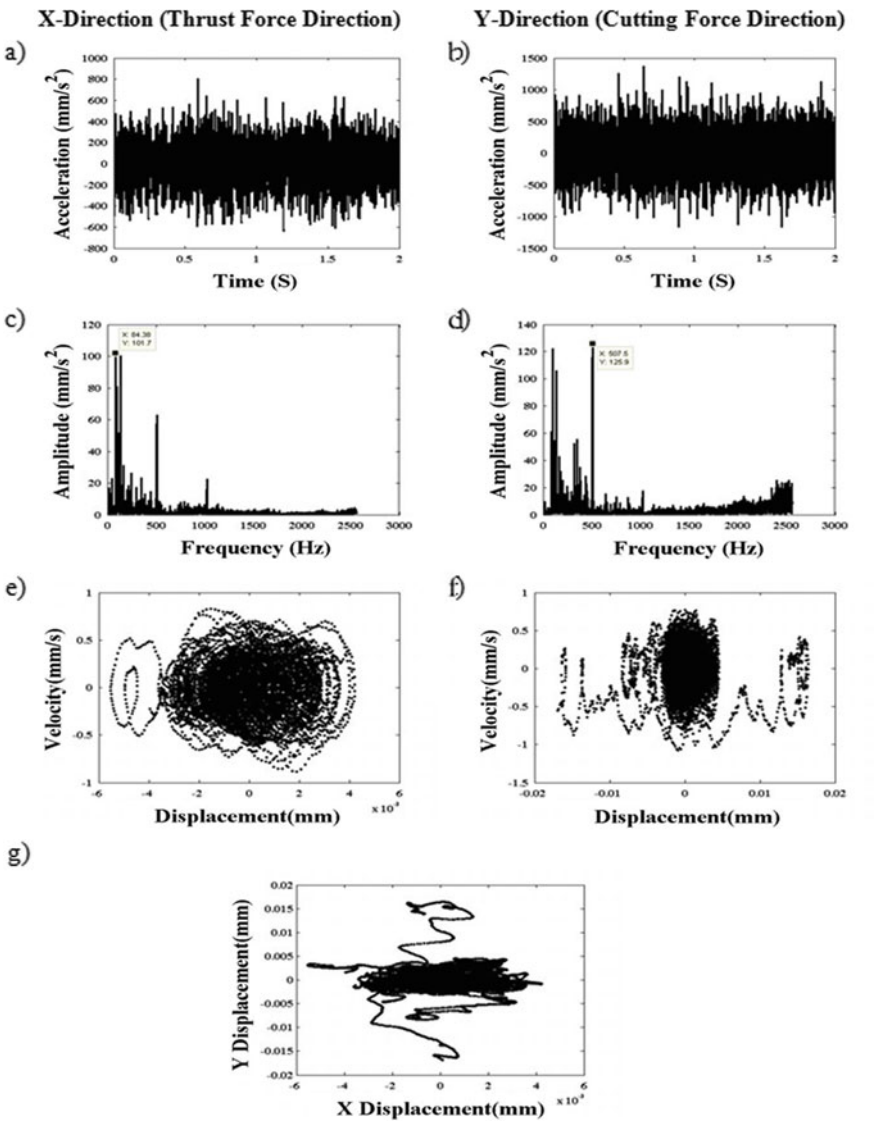

Fig. 3 Experimental result: Time response plot (**a**, **b**), fast Fourier transformation plot (**c**, **d**), Poincare plot (**e**, **f**) and Orbit plot (**g**) shows the response of quasi-periodic for brass shim at 150 m/min of cutting speed and 0.3 mm of depth of cut

In this paper, the cutting tool behavior is observed for different machining conditions which are given in Table 2.

As per experimental results more number of multi periodic responses are provided by the cutting tool with aluminium shim. Whereas more number of quasi periodic responses are provided by the cutting tool with brass shim. The surface roughness

Table 2 Cutting tool behavior, peak acceleration data and surface roughness values

Sr. No	Shims	Cutting speed (m/min)	Depth of cut (mm)	Peak values of acceleration (mm/s^2)		Behavior	Surface roughness (μm)
				X-direction	*Y*-direction		
1	Carbide	150	0.3	600	1000	Quasi-periodic	0.42
2		150	0.4	15,000	40,000	Chaotic	2.75
3		150	0.5	2000	3000	Quasi-periodic	0.41
4		200	0.3	6000	11,000	Chaotic	1.58
5		200	0.4	15,000	30,000	Multi-periodic	2.74
6		200	0.5	11,000	20,000	Multi-periodic	2.70
7	Aluminum	150	0.3	4000	10,000	Multi-periodic	1.51
8		150	0.4	15,000	40,000	Multi-periodic	3.20
9		150	0.5	17,000	60,000	Multi-periodic	3.81
10		200	0.3	4000	10,000	Chaotic	1.12
11		200	0.4	15,000	40,000	Multi-periodic	3.76
12		200	0.5	14,000	40,000	Multi-Periodic	2.26
13	Brass	150	0.3	600	1300	Quasi-periodic	0.41
14		150	0.4	400	600	Quasi-periodic	0.41
15		150	0.5	650	2500	Quasi-periodic	0.38
16		200	0.3	1000	4000	Quasi-periodic	0.61
17		200	0.4	550	1500	Quasi-periodic	0.45
18		200	0.5	1400	2500	Quasi-periodic	0.64

data were also collected during experiment for validating the chatter behaviors by surface roughness values. The cutting tool behavior, peak acceleration data, and surface roughness values are shown in Table 2.

7 Conclusion

In this work, the harmonic analysis was done and damping ratio of cutting tool with carbide, aluminum and brass shim materials. Dynamic motion behavior analysis was performed to know the behavior of cutting tool under different cutting conditions, for performing dynamic motion behavior analysis. The acceleration data were collected through experiments. From simulated computational work and through experiments, the following results were obtained.

- From the harmonic analysis of cutting tool, it is proved that the tool with brass shim shows lower damping ratio, as compared to carbide and aluminum shim. The tool with aluminum shim gives higher damping ratio, in comparison with carbide and brass. Simulated results for various shim material show significant comparison with the experimental results.
- The tool with brass shim provides better results than carbide and aluminum for turning operation at 0.3, 0.4 and 0.5 mm depth of cut. The tool with carbide shim is justified to use for 150 m/min of cutting speed and 0.3 mm of depth of cut. While the tool with aluminum shim does not justify to be used for machining operations.
- So the cutting tool having brass shim provides chatter reduction as verified from the dynamic motion behavior analysis. The measurement of surface roughness is instrumental in indirect validation of the chatter suppression. This data are helpful in reducing the chatter or machining vibrations, in turning of hard material at high speed.
- The experimental data obtained will be useful to design machine tool and cutting tool as well as operating condition with reduction in chatter.

References

1. Siddhpura M, Paurobally R (2012) A review of chatter vibration research in turning. Int J Mach Tools Manuf 61:27–47
2. Chandiramani NK, Pothala T (2006) Dynamics of 2-d of regenerative chatter during turning. J Sound Vib 290(1–2):448–464
3. Clancy BE, Shin YC (2002) A comprehensive chatter prediction model for face turning operation including tool wear effect. Int J Mach Tools Manuf 42(9):1035–1044
4. Mahdavinejad R (2005) Finite element analysis of machine and workpiece instability in turning. Int J Mach Tools Manuf 45(7–8):753–760

5. Hajikolaei KH, Moradi H, Vossoughi G, Movahhedy MR (2010) Spindle speed variation and adaptive force regulation to sup-press regenerative chatter in the turning process. J Manuf Process 12(2):106–115
6. Tansel IN, Wang X, Chen P, Yenilmez A, Ozcelik B (2006) Transformations in machining. Part 2. Evaluation of machining quality and detection of chatter in turning by using s-transformation. Int J Mach Tools Manuf 46(1):43–50
7. Tarng YS, Kao JY, Lee EC (2000) Chatter suppression in turning operations with a tuned vibration absorber. J Mater Process Technol 105(1–2):55–60
8. Cardi AA, Firpi HA, Bement MT, Liang SY (2008) Workpiece dynamic analysis and prediction during chatter of turning process. Mech Syst Signal Process 22(6):1481–1494
9. Orra K, Choudhury SK, Kishore R (2018) On-line control of machine tool vibration in turning operation using electro-magneto rheo-logical damper. J Manuf Process 31:187–198

Condition-Based Maintenance Modeling Using Vibration Signature Analysis

A. B. Gholap and M. D. Jaybhaye

Abstract The paper deals with condition-based maintenance modeling using vibration signature analysis. In manufacturing industry, due to continuous operation of machinery, the wear and tear occur in rotating/sliding elements of the system. Vibration signature analysis is an important tool for monitoring condition of these elements by analyzing complete system. In general, vibration analysis is an important way to detect and respond to maintenance needs. The elements in various mechanical power transmission system have a specific pattern of vibration that depends on the construction and condition of machine. An attempt is made in present work to monitor gearbox using the VA 12 analyzer, with FFT analysis through piezoelectric accelerometer PV 57I equipped with magnetic attachment. The signals are taken from experimental setup consisting of two-stage spur gear system. The vibration signals recorded from mechanical power transmission system with the help of accelerometer are in time domain. The variation in transmitted force is one of the most important mechanisms responsible for vibration. The type of fault/defect causes variation in the vibration signal. The monitoring of vibration signal gives the condition of system and predicted life of the system. This also helps in preventive maintenance policies to be adopted for prolonged usage of the system.

Keywords Vibration · Condition-based maintenance · Wear · Defect

A. B. Gholap (✉)
Marathwada Mitra Mandal's College of Engineering Pune, Pune, India
e-mail: anandagholap@gmail.com

M. D. Jaybhaye
Department of Production Engineering and Industrial Management, College of Engineering Pune, Pune, India
e-mail: mdj.prod@coep.ac

V. K. Gupta et al. (eds.), *Reliability and Risk Assessment in Engineering*,
Lecture Notes in Mechanical Engineering,
https://doi.org/10.1007/978-981-15-3746-2_10

1 Introduction

In continuous production systems, vibration analysis is a very powerful predictive maintenance technique used for early problem detection in rotary machinery. Condition monitoring techniques and its applications are constantly evolving and greatly enhanced by scientific and advanced instruments that allow the scientific analysis of industrial equipment's health or condition. Problems can be detected early in their phase of development and fixed by proper maintenance before they become sufficiently serious to cause system failure. It involves designing and using monitoring systems in conjunction with tools for data collection and analysis. It consists of predictive and diagnostic techniques with the goal of using real condition information to execute equipment/system maintenance in a scheduled manner.

There is inadequate knowledge in the current situation to understand and predict machinery actions in actual-life situations. Close attention is thus required to monitoring and controlling vibration and noise in hydraulic systems and high-speed machines. CBM is most commonly used in the industry of manufacturing refining of oil, chemicals, and related products. Higgs et al. [1] mentioned that vibration analysis is the most widely used CBM and NDT technique.

Peng et al. [2] in their work claimed that variation in transmitted force is one of the most important mechanisms responsible for the vibration. Ebersbach et al. [3] discussed various vibration analysis techniques such as time-domain analysis, frequency domain, time–frequency analysis, and envelope analysis. Saxena et al. [4] stated that simple symptoms of any equipment malfunction can hardly be detected from the time domain only if the defect is at an early stage.

The most common method for diagnosing gear faults is the frequency-domain analysis. Frequency-domain techniques use a fast Fourier transform (FFT) to transform time-domain vibration signals into distinct frequency components. Frequency domain carries no information in the time domain. The frequency domain is simply another way to look at the information about the signal. The key advantage of frequency-domain analysis to time-domain analysis is that, as peaks in the frequency spectrum, the repetitive nature of the vibration signals is clearly disrupted, and it has the ability to easily detect such important frequency components. Figure 1 demonstrates the conversion of the time-domain signal to the frequency-domain signals by fast Fourier. This is the way to take a time-varying signal from the actual world and break it into parts, each with amplitude, phase, and frequency.

Antoniadou et al. [5] proposed the Empirical Mode Decomposition (EMD) approach for decomposing vibration signals into usable signal components related to different signal frequency bands. Igba et al. [6] suggested three-model techniques (signal correlation, intense vibration, and RMS frequency) and validated with a time-domain data approach using condition monitoring information from operating wind turbines. Conclusions from this study show that tracking RMS and intense values uses extreme value theory as a leading indicator of early detection of faults. Aval et al. [7] discussed the wind turbine system condition monitoring and fault diagnosis. Jayaswal et al. [8] via vibration analysis gave a brief overview of the art of machine

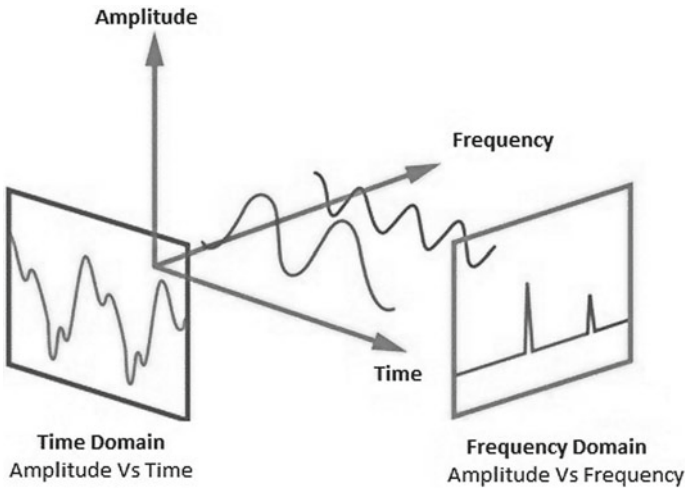

Fig. 1 Time- and frequency-domain technique

fault detection. Weqerich et al. [9] developed a smart signal nonparametric modeling technique that illustrates the use of this method to detect faults in rotating machinery through the extraction of vibration signals characteristics.

2 Vibration Analysis Techniques

2.1 Vibration Signature

The term signature is used to identify signal trends that describe a system from which they are obtained from the state or condition. Signatures are commonly used as a mechanical system diagnostic tool. The method and range of transducers used are very important factor for capturing vibration signal. Mechanical vibration main causes are misalignment, unbalance, distortion and looseness, faulty bearings, reliability gear and coupling, crucial speeds, etc. Mechanical vibrations can be interpreted as a dynamic spring and weight combination. Acceleration, velocity, and displacement are the basic physical factors that describe vibration. The vibration condition can be measured by evaluating each of these values.

2.2 Vibration Meter Mode

Evaluating the frequency of vibrations is a useful diagnostic tool to assess the normal operation of machinery and to test for signs of potential faults. For example, when

vibrations in the velocity range beyond the reference value (up to 1000 Hz) are observed, the presence of an misalignment, loose condition, or imbalance condition may be reported, while vibrations in the acceleration zone (1 kHz to approximately 12–15 kHz) may signify possible gear and bearing problems.

2.3 Crest Factor

The crest factor (C.F.) is an example of a waveform's influence characteristics. The ratio between the RMS and peak values is calculated. Higher values of the crest function imply a higher level of impact. The acceleration calculation crest factor is useful to identify the early stages. The crest factor is calculated by formula as given in Eq. (1)

$$\text{Crest factor} = \text{Peak value}/\text{RMS value} \tag{1}$$

2.4 Definition of Classes

According to the specifications ISO 10816 and type of motor used or type of base of the system, the following classification is used for setting representative value zone of velocity.

Class I: 0–15 kW small motors.
Class II: 15–75 kW motors, equipment mounted on a rigid frame up to 300 kW.
Class III: Rigid base heavy machinery.
Class IV: Flexible base large machinery equipment.

Table 1 shows zone values representation of velocity for the motors.

2.5 Using a Relative Evaluation Standard—Trend Management

The minimum values for warning and danger conditions are set using normal condition as a guideline. When the level of caution is surpassed, monitoring is strictly required and a thorough analysis is done when the level of hazard reaches. A commonly used factor for setting the levels is as follows: caution level = 2–3 times the normal value, hazard level = 2–3 times the caution value. A widely used level setting variable is as follows: level of caution = 2–3 times the normal RMS value, level of hazard = 2–3 times the value of caution. A time series graph as shown in Fig. 2 is

Table 1 Zone values of velocity for the motor class [10]

Class boundary value (mm/s)	Class-I	Class-II	Class-III	Class-IV
0.28 0.45 0.71	A	A	A	A
1.12 1.8	B	B		
2.8 4.5	C	C	B	B
7.1 11.2 18.0 28.0 45.0	D	D	C D	C D

Category A: Good, Category B: Satisfactory, Category C: Unsatisfactory, Category D: Unacceptable

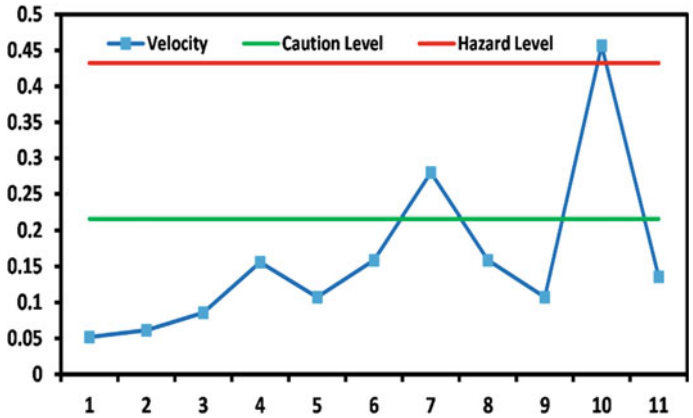

Fig. 2 Trend management diagram

typically used for trend analysis, including measurement frequency and other data, after deciding on the location of the vibration measurement [11].

2.6 FFT Analyzer Mode

Machinery usually includes a variety of sources of vibration such as gears, motors, fans and bearings. While developing steps to mitigate vibrations and attempting to find the causes of problem vibrations, often only calculating the frequency of vibrations will not provide sufficient information. Frequency analysis is also required to

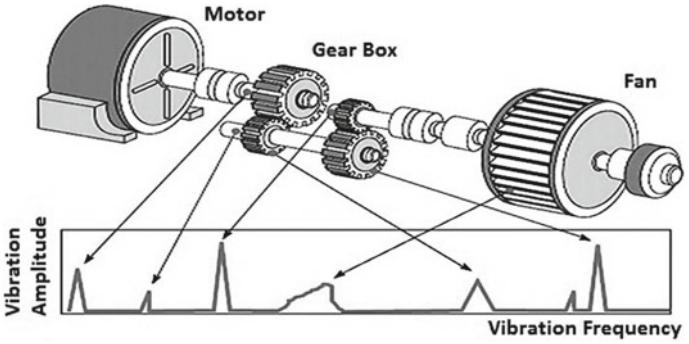

Fig. 3 FFT analysis mode

determine that vibration types exist and what their levels are. As shown in Fig. 3, vibration intensity will be influenced by the locations where vibrations occur. Analysis of frequency makes it possible to more accurately identify vibration sources. The fast Fourier transform (FFT) is a class of special algorithms implementing the discreet Fourier transformation with significant time savings. Fourier's discrete transformation is known as

$$X(k) = \sum_{n=0}^{n-1} x(n) \mathrm{e}^{-j\left(\frac{2\pi nk}{N}\right)} \tag{2}$$

where

X The frequency-domain representation of time series signal 'x';
k The frequency component; $k = 0, 1, 2, \ldots, n-1$;
N The total number of samples in signal 'x'; x: The time series signal;
n The nth sample (in the time domain);
j The imaginary unit.

3 Experimental Setup

The experimental setup is shown in Fig. 4. It consists of a motor and compound (two-stage incremental) gearbox. The input shaft of gearbox is connected to 1 HP, 3 phase 60 Hz, induction electric motor through rubber coupling. All drive shafts are supported at its ends with anti-friction bearings. Using the RPM sensor, a VFD is used to adjust the speed of the electric motor and the speed of the motor or output shaft. The vibration data are collected from the X, Y, and Z surface of gearbox using the accelerometer PV 57I. The collected vibration data are processed in VA 12 excel

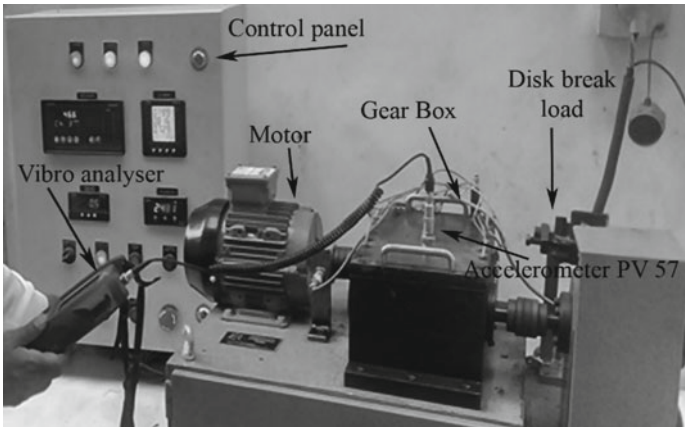

Fig. 4 Experimental setup

macron sheet for signal processing. The vibration signals from a healthy gear are collected at a shaft speed of 250, 420, 710, 1200, 1600, 2000, and 2400 rpm.

The VA 12 analyzer with FFT measuring functions designed specifically for vibration field analysis [11]. It comes with the magnetically attached piezoelectric accelerometer PV 57I. It offers three vibration meter mode, time waveform mode, frequency mode, and FFT mode. Displacement, velocity, acceleration peak, and crest factor can be measured simultaneously in vibration meter mode. The waveform of the envelope curve of velocity, velocity, displacement, or acceleration can be viewed in time waveform mode. In FFT mode, it is possible to view the frequency analysis of the velocity displacement or the acceleration envelope curve.

A variable frequency drive (VFD) is used to set desired RPM. The PIC101A-VI-230 Process Indicator is used for indication of set pressure on disk brake. RPM range is selected as 250, 420, 710, 1200, 1600, 2000, and 2400 as per standard machine tool. The vibration readings are taken in three directions namely *X*-, *Y*-, and *Z*-direction.

Load is set from no load condition to 5 kgf/cm^2 in step of 1 kgf/cm^2 on brake system using screw adjustment.

For each reading, VA 12 Excel macron gives around 1020 instantaneous values of velocity. Store interval is 1 min. Vibration analyzer parameters are set as given in Table 2.

For sensitive analysis, root mean square value is calculated for all instantaneous values, i.e., 1024 values for each reading, in each *X*-, *Y*-, and *Z*-direction.

Table 3 shows the RMS values of velocity for each RPM value in *X*-, *Y*-, and *Z*-direction, respectively.

Graphs are plotted as shown in Figs. 5, 6, and 7 which show the normal values of RMS, caution level, and hazard level of velocity for each RPM value in *X*-, *Y*-, and *Z*-direction, respectively. Figure 8 shows time-domain velocity plot.

Table 2 VA 12 parameters set before experimentation

Range (mm/s)	3160
Frequency span (Hz)	200
Number of samples	1024
High-pass filter (Hz)	10
Low-pass filter (kHz)	1
Overload	Off
Sensitivity (mV/ms^2)	4.81

4 Conclusions

- In this work, an attempt is done to analyze the gearbox system through vibration signature analysis. It has been observed that at no load condition with maximum RPM, velocity is high and reduces with increase in loading.
- Normal level can be set by using regular loading condition using root mean square values (RMS) of values obtained by VA 12 Vibro Analyzer.
- Caution level can be set at twice that of normal values of RMS.
- Hazard level can be set at twice that of caution values.
- No action is needed if the condition is close to normal, but monitoring is required.
- If the condition is close to the level of caution, it may be necessary to close monitoring and maintenance earlier.
- If condition is close to hazard level, condition is hazardous, and immediate action is required.
- The vibration signals are recorded with periodic interval of 2 h for a week's span, and it was observed that as time increases, the noise factor is getting introduced, which increases the level of vibration signal. The wearing of gears gives alarming signal in terms of increased vibration along the axis and system as a whole.

Table 3 RMS values of velocity for each RPM value in *X*, *Y*, and *Z*

RPM	No load			Load 1 kgf/cm^2			Load 2 kgf/cm^2			Load 3 kgf/cm^2			Load 4 kgf/cm^2			Load 5 kgf/cm^2		
Axis	*X*	*Y*	*Z*	*X*	*Y*	*Z*	*X*	*Y*	*Z*	*X*	*Y*	*Z*	*X*	*Y*	*Z*	*X*	*Y*	*Z*
250	0.1215	0.1239	0.1419	0.1235	0.1184	0.1217	0.1209	0.1270	0.1220	0.0498	0.0380	0.0449	0.0539	0.0382	0.0462	0.0539	0.0503	0.0517
420	0.1402	0.1856	0.2232	0.1737	0.1880	0.2169	0.1827	0.1725	0.2288	0.0620	0.0528	0.0625	0.0681	0.0605	0.0666	0.0696	0.0613	0.0615
710	0.2262	0.2897	0.5627	0.2573	0.2793	0.5300	0.2609	0.2891	0.5619	0.0629	0.0798	0.0827	0.0835	0.0638	0.0843	0.0871	0.0686	0.0858
1200	0.6555	0.6846	1.7920	0.7669	0.9843	1.7773	0.7843	0.9907	1.8268	0.1244	0.1165	0.1513	0.1229	0.1208	0.1551	0.1304	0.1248	0.1559
1600	0.5328	0.6779	0.6553	0.5350	0.6280	0.6996	0.6553	0.8156	0.1141	0.1213	0.1113	0.1123	0.1171	0.1156	0.1132	0.1284	0.1166	0.1073
2000	0.8156	1.2045	1.8598	0.9264	1.3268	2.1095	0.1449	0.1441	0.1629	0.1444	0.1387	0.1632	0.1507	0.1446	0.1726	0.1469	0.1432	0.1588
2400	2.4721	2.5603	1.0230	2.3139	2.3844	1.1087	0.1809	0.1661	0.1356	0.1845	0.1679	0.1349	0.1868	0.1606	0.1394	0.1837	0.1686	0.1356

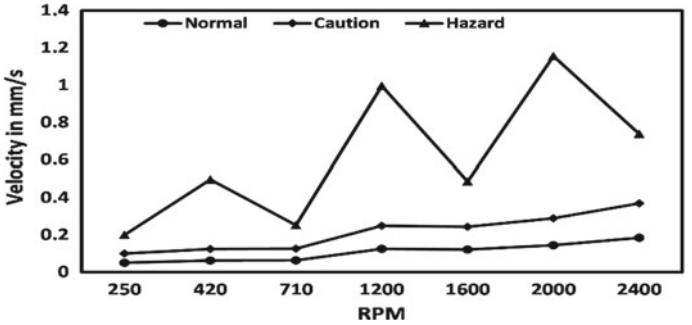

Fig. 5 Velocity versus RPM at 3 kgf/cm^2

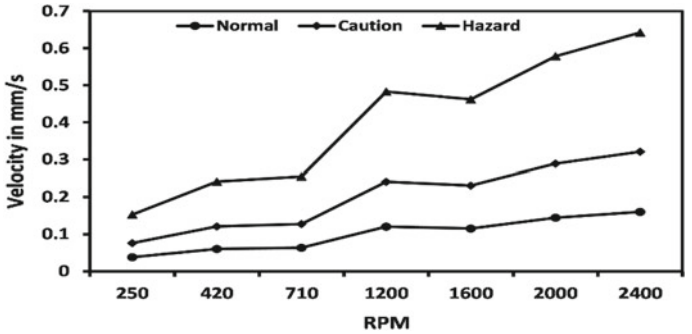

Fig. 6 Velocity versus RPM at 4 kgf/cm^2

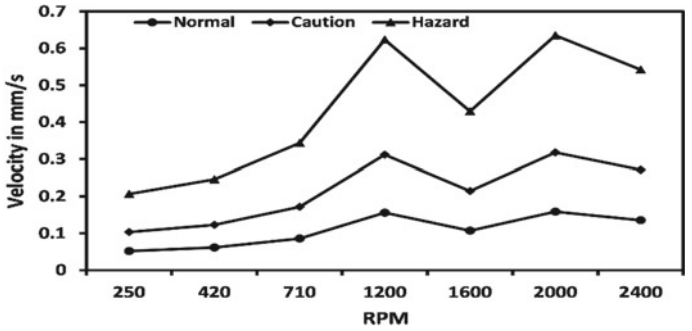

Fig. 7 Velocity versus RPM at 5 kgf/cm^2

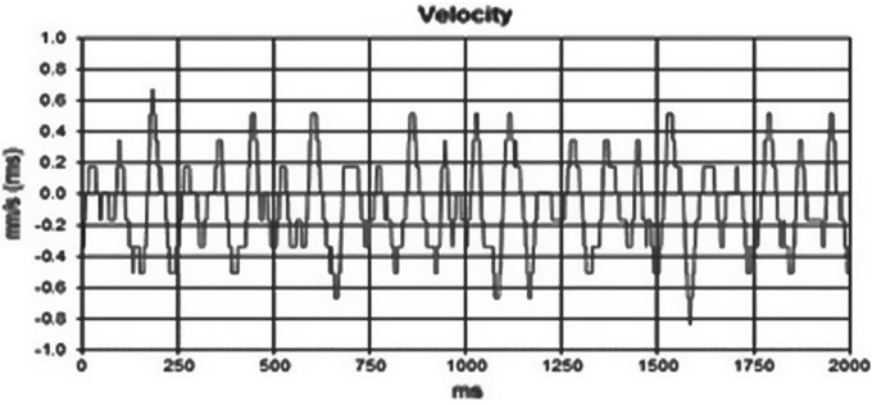

Fig. 8 Time-domain velocity plot

Acknowledgements This research work is supported by AICTE New Delhi (India) under the RPS project on Condition Monitoring using ferrography and Vibration Signature Analysis. The authors gratefully acknowledge the support and guidance of Dr. B. B. Ahuja, Director, College of Engineering Pune, Dr. Rajiv B., Head of Production Engineering and Industrial Management Department, and Dr. S. K. Basu, Professor Emeritus, College of Engineering Pune during the experimental work.

References

1. Higgs PA, Parkin R, Jackson M (2004) A survey on condition monitoring systems in industry. In: Proceedings of ESDA 2004: 7th Biennial ASME conference engineering systems design and analysis, Manchester, UK, ESDA2004-58216, 19–22 July 2004
2. Peng Z, Kessissoglou N (2003) An integrated approach to fault diagnosis of machinery using wear debris and vibration analysis. Wear 255:1221–1232
3. Ebersbach S, Peng Z, Kessissoglou NJ (2006) The investigation of the condition and faults of a spur gearbox using vibration and wear debris analysis techniques. Wear 260:16–24
4. Saxena V, Chowdhury NK, Devendiran S (2013) Assessment of gearbox fault detection using vibration signal analysis and acoustic emission technique. IOSR J Mech Civ Eng (IOSR-JMCE) 7(4):52–60
5. Antoniadou I, Manson G, Staszewski WJ, Barszcz T, Worden K (2015) A time–frequency analysis approach for condition monitoring of a wind turbine gear box under varying load conditions. Mech Syst Signal Process 64–65:188–216
6. Igba J, Alemzadeh K, Durugbo C, Eiriksson ET (2016) Analyzing RMS and peak values of vibration signals for condition monitoring of wind turbine gearboxes. Renew Energy 91:90–106
7. Aval SMM, Ahadi A (2016) Wind turbine fault diagnosis techniques and related algorithms. Int J Renew Energy Res 6(1):80–88
8. Jayaswal P, Wadhwani AK, Mulchandani KB (2008) Machine fault signature analysis. Int J Rotating Mach. Article ID 583982. https://doi.org/10.1155/2008/583982
9. Weqerich SW, Wilks AD, Pipke RM (2003) Nonparametric modeling of vibration signal features for equipment health monitoring. In: Proceedings of the IEEE aerospace conference, vol 7, pp 3113–3121

10. Instructional Manual, Vibration analyzer, VA 12, RION CO., LTD, 3-20-41 Higashimotomachi, Kokubunji, Tokyo 185-8533, Japan
11. VA-12 Quick Instruction Manual, VA 12, RION CO., LTD, 3-20-41 Higashimotomachi, Kokubunji, Tokyo 185-8533, Japan

Health Monitoring and Management Using Multi-sensors

Experimental Investigation of Nonlinear Dynamic Motion Analysis of Balanced Rotor Supported by Cylindrical Roller Bearing

O. G. Vaghela, A. R. Majmudar, D. P. Mavani, S. A. Patel, S. P. Mehta, H. K. Yadav, and D. H. Pandya

Abstract Rolling contact bearings are widely used in rotating types of machinery. Many researchers have worked on a mathematical model by considering Hertzian contact stress theory at its roller and race contact points by generating its mathematical equivalent. In the present study, the dynamic behaviour of motion of healthy cylindrical roller bearing SKF NJ305 class C3 having 11 rollers which is supported on a balance rotor system has been investigated. Experimental motion analysis was carried out using FFT analyser and developed experimental set up at our laboratory. FFT, Orbit plots and Poincaré plots have been analysed to diagnose the dynamic motion behaviour of roller bearing at various speeds. Experimental multiperiodic, quasiperiodic and chaotic motion behaviour have been identified which will be useful for design and maintenance, whereas the database may be useful for future endeavours.

Keywords Balanced rotor · Chaos · Cylindrical bearing · Internal radial clearance · Quasiperiodic

1 Introduction

A wide range of industrial type equipments have rotating machinery for their applications. Among them, the most commonly used parts are the cylindrical roller bearing, due to their better load carrying capacity and low friction characteristic. Such bearings account as a source of vibration and noise which affects the dynamic response of rotating machinery. The main cause of such undesirable vibrations is varying compliance, localised defect and internal clearance. For a specific bearing,

O. G. Vaghela (✉) · A. R. Majmudar · D. P. Mavani · S. A. Patel · S. P. Mehta · H. K. Yadav · D. H. Pandya
Department of Mechanical Engineering, LDRP Institute of Technology and Research, Gandhinagar, Gujarat, India
e-mail: omvaghela.info@gmail.com

D. H. Pandya
e-mail: veddhrumi@gmail.com

V. K. Gupta et al. (eds.), *Reliability and Risk Assessment in Engineering*,
Lecture Notes in Mechanical Engineering,
https://doi.org/10.1007/978-981-15-3746-2_11

the clearance remains the same after manufacturing and does not change. Such clearance is facilitated for compensating thermal expansion. But as a by-product, it also leads to vibration and nonlinearity in the system behaviour. Some mathematical models have been presented by different researchers which give frequencies induced by such vibrations of bearings. As an experimental study in the paper, the authors have made efforts to understand the behaviour of a balanced rotor, with speed as the input parameter.

The machine performance is majorly dependent on the rolling element of bearings, and thus, their good working condition is necessary. The vibration spectrum of the rotor bearing assembly supported by the perfect cylindrical roller is dominated by vibrations at two different frequencies, i.e. natural frequency and varying compliance (VC) frequency. Parametric vibrations, viz. clearance and frequency generate strong nonlinearity in the dynamic behaviour of components.

Study of the effect of unbalanced forces for cylindrical roller bearing having eight number of rollers was done by Harsha [1]. According to which a route to chaos in intermittent mechanism due to periodic doubling was calculated. Many researchers have analysed the nonlinear behaviour with the help of the mathematical model, Poincaré plot, time displacement plot, FFT plot and Orbit plot. Some researchers have also analysed nonlinear vibration response with fluctuating speed and unbalanced effect, concluding that the unbalanced rotor results in various regions of unbalance with higher amplitude of vertical vibration [2]. Researchers also studied the effect of the number of rolling elements, in case of cylindrical roller bearing, by developing the mathematical model. This concluded that with an increase in the number of rollers, the effect of varying compliance frequency reduces, and thus, the system becomes stiffer due to the reason that the centre of oscillation approaches zero. Liu and Shao [3] have examined vibration responses due to the effect of maximum amplitude and nonlinearity due to uneven distribution of the surface waviness of the hydrodynamic bearing.

The behaviour of an unbalanced rotor with deep groove ball bearing has also been studied by Yadav et al. [4]. The superposition method is utilised to get the stiffness equation for a crowned roller. Horng [5] has investigated rollers with circular, quadratic, cubic, fourth-order power and exponential profiles. Applied researches have established a numerical model for roller-pocket rotation and mechanics analysis to examine the hydrodynamic lubrication between rollers and straight-sided cage pockets in a cylindrical roller bearing [6]. Effects of inner ring rotation speed, roller cage angular acceleration, roller profile and cage geometry are numerically studied.

The effect of IRC for balanced rotor has been studied [7]. The numerical model has been proposed with the nonlinear damping and stiffness at the Hertzian contact. It has been concluded by authors that at 9000 RPM the system becomes chaotic [8]. Researchers have studied the unbalanced rotor supported by a ball bearing to investigate the effect of preloading. It was concluded that chaotic phenomena can be prevented by applying preload. Yadav et al. [9] have developed the mathematical model for balanced rotor system which is supported by cylindrical roller bearing (SKF NJ 305 C3 clearance). The numerical results have been obtained, and different

nonlinear behaviour has been identified with unbalanced rotor bearing conditions [10].

As an outcome of a detailed literature study, the authors have found that different researchers have attempted theoretical study by considering the distributed/local defects or off-sized ball defect for ball bearing. It has been observed that there is a lack of literature review related to the behaviour of a healthy cylindrical roller bearing. Thus, the available study is based on analytical study. The authors have decided to study the balanced rotor supported by the cylindrical roller bearing (SKF NJ 305 C3 clearance) experimentally.

2 Experimental Setup

In this study, experimentation is carried out on a shaft-bearing test rig, with speed as a control parameter. The speed is controlled with the help of a DC Controller. An optic-tachometer is used to measure the RPM of a shaft, and the shaft is connected with the motor through a spring coupling which also compensates any misalignment. The connection of data acquisition is made on the housing surface, where the piezoelectric sensors are connected. The tools used in the analysis are frequency responses whose speed range is taken up to 5000 RPM. The system of rotor and bearing is assumed to be perfectly rigid and is supported by a cylindrical roller bearing. The objective of the study is to analyse the effect of speed variation for the dynamic behaviour of cylindrical roller bearings supported on balanced rotor system (Fig. 1).

To acquire and analyse the data, CoCo-80 is used. The frequency range of a sensor is 1–30 kHz, and the measurement range is ±500 g peak, resolution is 0.005 g, and resonance frequency is 70 kHz. The test figure has been well supported in order to minimise vibrations, using adjustable rubber pad having MS base plate.

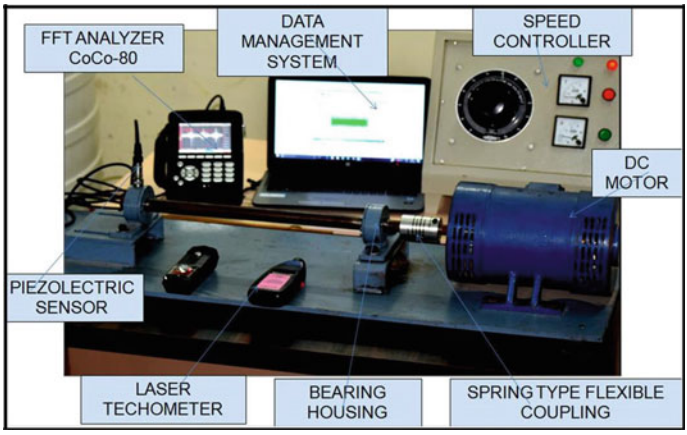

Fig. 1 Experimental setup

3 Results and Discussion

The bearing system is centrally located in housing, and sensors are adhering to the outer faces of the housing. The study has been carried with speed as a control parameter. The sensor is attached to the housing in horizontal and in vertical directions which is at the far end of the shaft from the motor. The study has been done over the speed range from 0 to 5000 RPM with the help of tools like FFT plot and Poincaré plots. Cylindrical roller bearing (SKF NJ 305) has shown superharmonic responses up to 1000 RPM, and then onwards, up to 4000 RPM significant peaks have shown subharmonic responses of the system. Researchers have investigated dynamic motion behaviour of the system for all speed ranges as shown in Table 1.

Transient chaos has been observed at 500 RPM with superharmonic responses, as shown in Fig. 2. As operating speed increases. the system tends to subharmonic peaks as shown in Fig. 3 and net structure of Poincaré plots clearly indicates the quasiperiodic behaviour of the system. Responses plotted at 4000 RPM lead to conclude chaotic behaviour of the system as clearly indicated by broad sidebands in FFT responses, in horizontal and vertical directions; and dense irregular Poincare plots endorse the same as shown in Fig. 4. At 4500 RPM, the system has shown chaotic behaviour with subharmonic responses as shown in Fig. 5. Poincare plot of vertical direction has indicated a trend towards the multiperiodic behaviour of the system.

Table 1 List of balance (VC) peak

Speed (RPM)	Significant peak horizontal vertical		Motion behaviour
500	7/4VC, 3VC, 9/4VC	1/3VC	Transient chaotic
1000	3/2VC, 17/4VC	1/4VC, VC	Multiperiodic
1500	1/4VC, 1/2VC, 1VC	1/4VC, 1VC, 9/5VC	Quasiperiodic
2000	1/4VC, 1/2VC, 7/10VC	1/4VC, 2/3VC	Multiperiodic
2500	1/4VC, 1/2VC, 3/5VC	1/4VC, 1VC, 11/4VC, 9/10VC	Multiperiodic
3000	1/4VC, 1/2VC, 7/10VC	1/2VC, 4/5VC	Quasiperiodic
3500	1/4VC, 2/5VC	1/4VC, 3/5VC, 7/4VC, 3VC	Beginning of chaos
4000	7/20VC, 9/20VC	1/4VC, 5/3VC, 8/3VC	Chaotic
4500	1/4VC	1/3VC, 5/2VC, 3VC	Subharmonic route to chaos
5000	1/4VC, 12/5VC	1/3VC	Multiperiodic

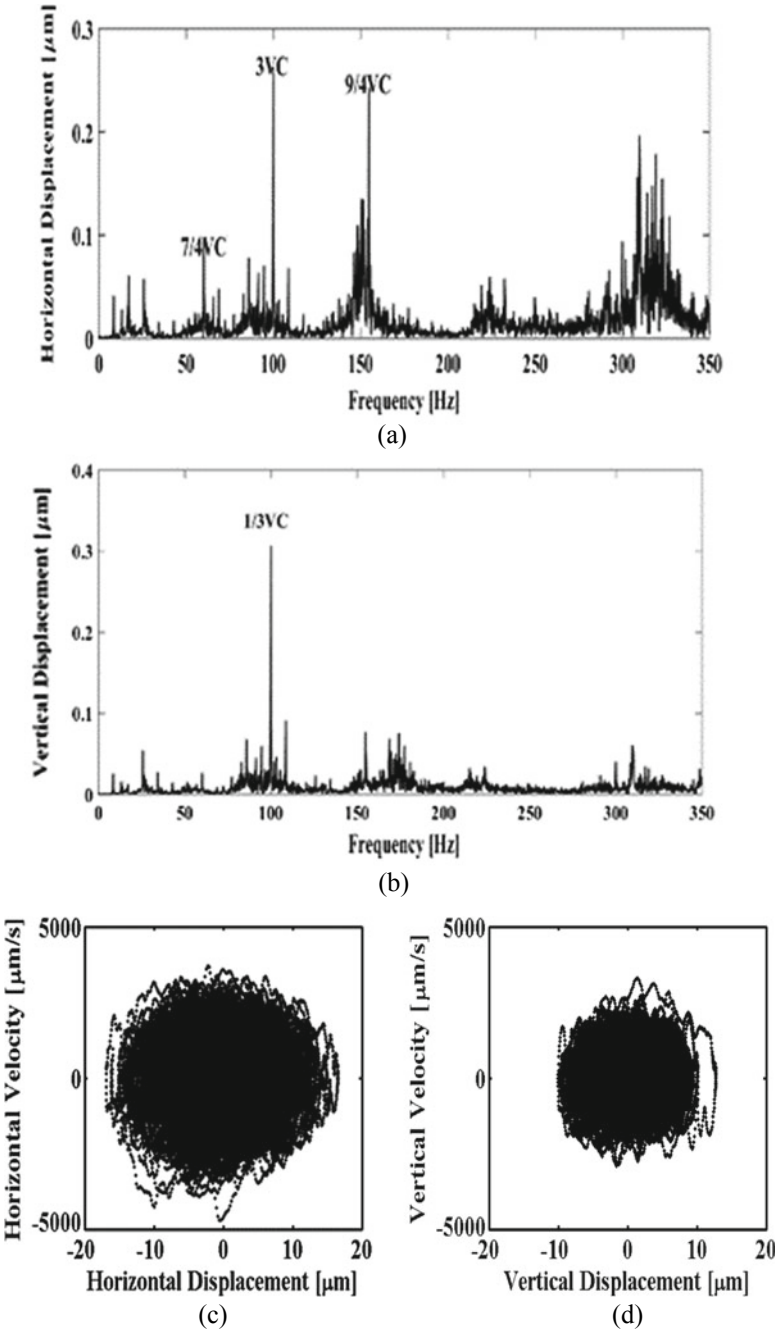

Fig. 2 Experimental results at 500 RPM. **a** Horizontal FFT. **b** Vertical FFT. **c** Horizontal Poincaré. **d** Vertical Poincaré

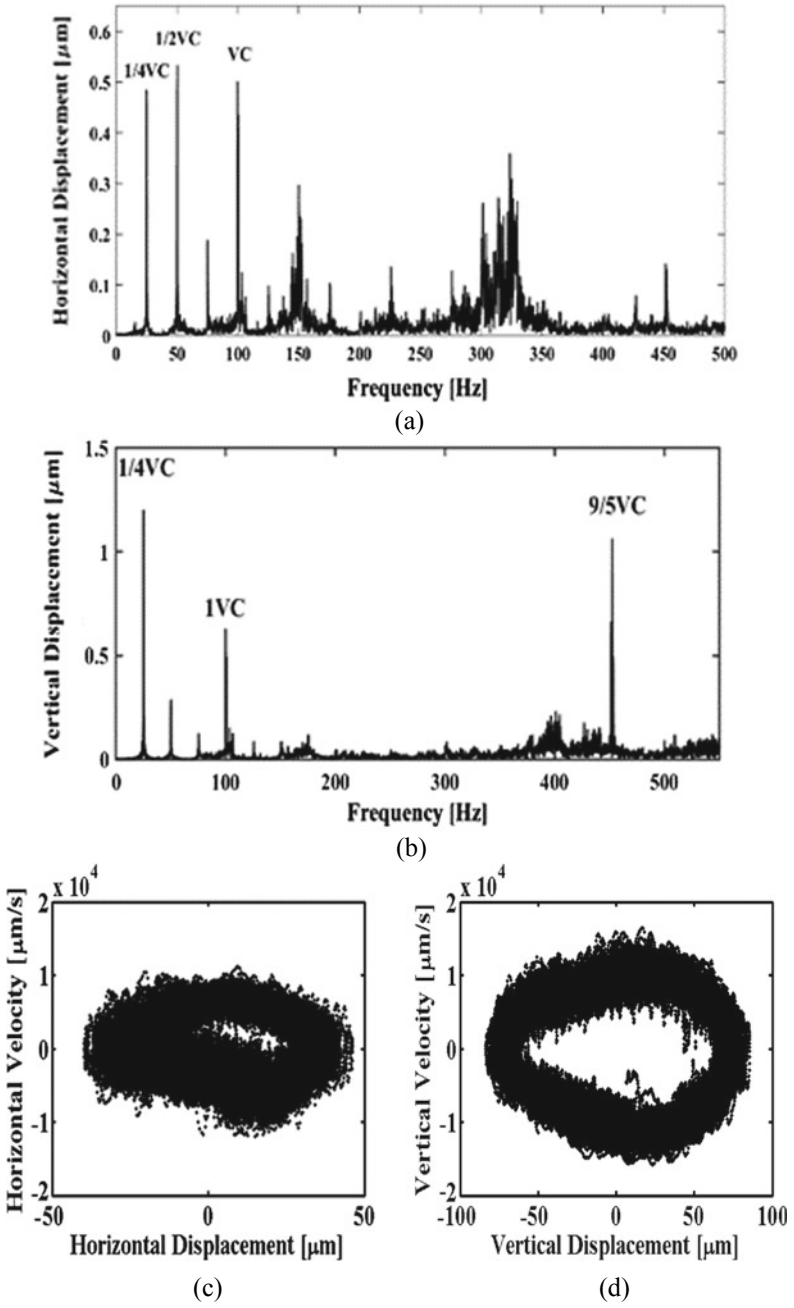

Fig. 3 Experimental results at 1500 RPM. **a** Horizontal FFT. **b** Vertical FFT. **c** Horizontal Poincaré. **d** Vertical Poincaré

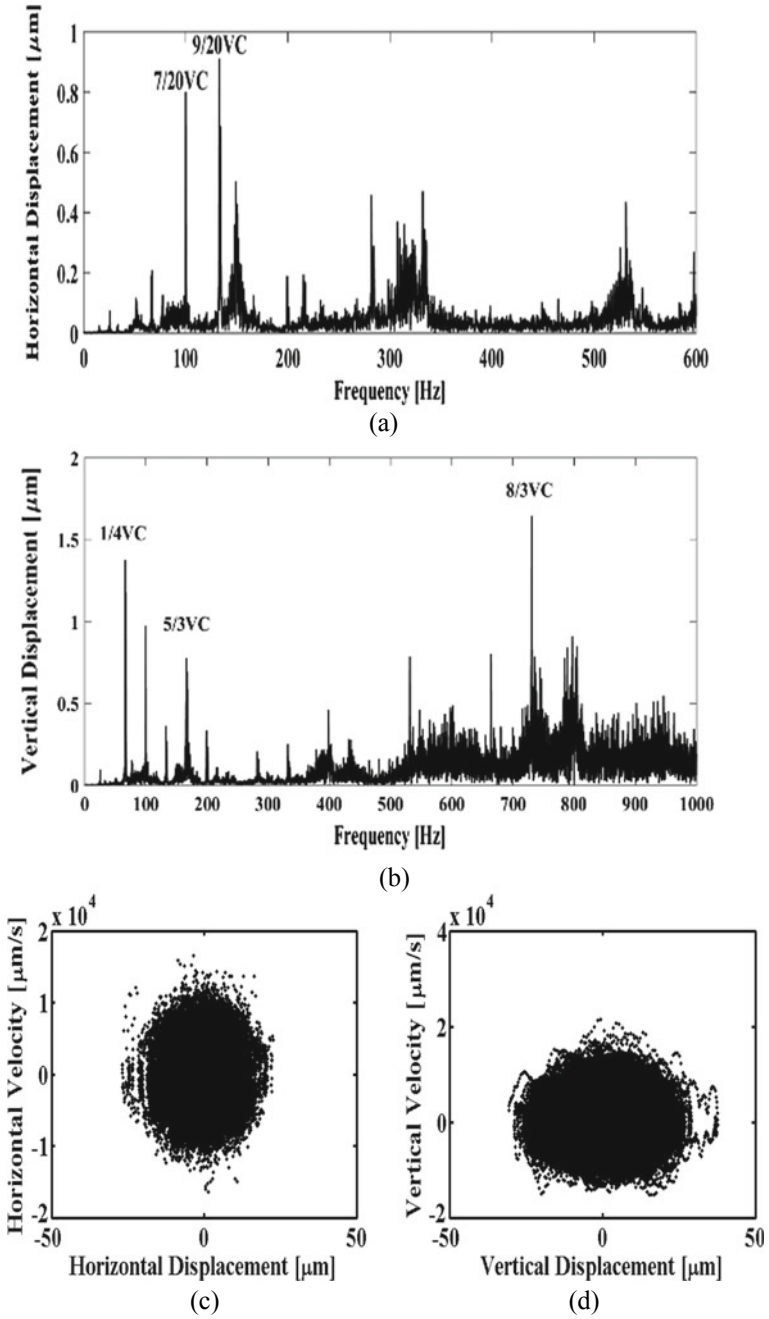

Fig. 4 Experimental results at 4000 RPM. **a** Horizontal FFT. **b** Vertical FFT. **c** Horizontal Poincaré. **d** Vertical Poincaré

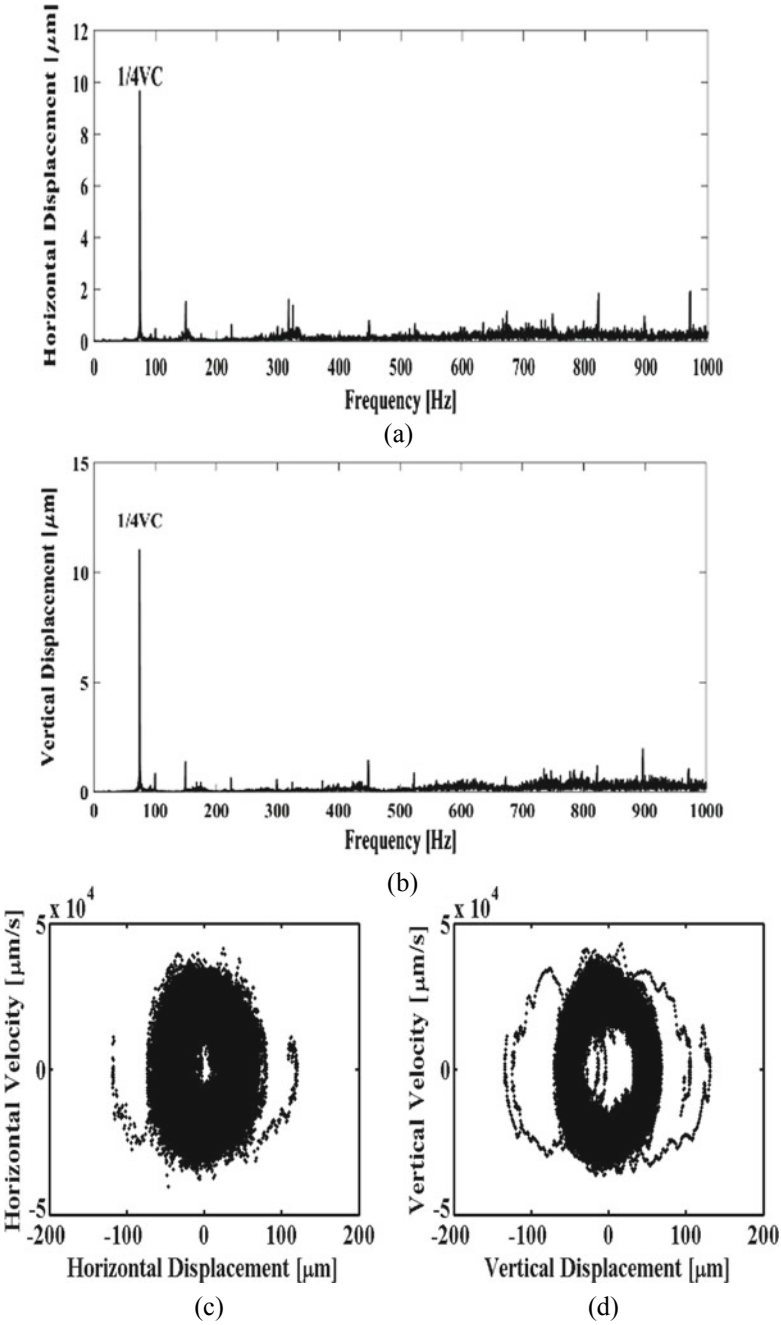

Fig. 5 Experimental results at 4500 RPM. **a** Horizontal FFT. **b** Vertical FFT. **c** Horizontal Poincaré. **d** Vertical Poincaré

4 Conclusions

- It has been inferred that system has transient chaotic behaviour up to 1000 RPM.
- At 1500 RPM and at 3000 RPM, the system behaves with quasiperiodic motion which would be desired range of operation and design.
- The beginning of chaos and subharmonic route to chaos is observed between 3500 and 4500 RPM and the region is avoided.
- Hence, this research work leads to conclude that present experimental data will be useful for the designer and condition monitoring people of process industries.

References

1. Harsha SP (2004) Non-linear dynamic analysis of an unbalanced rotor supported by roller bearings. Chaos, Solitons Fractals 26:47–61
2. Sharma A, Amarnath M, Kankar PK (2014) Effect of varying the number of rollers on dynamics of a cylindrical roller bearing. In: Proceedings of the ASME 2014 international design engineering technical conferences & computers and information in engineering conference IDETC/CIE, pp 1–8
3. Liu J, Shao Y (2015) Vibration modelling of nonuniform surface waviness in a lubricated roller bearing. J Vibr Control, pp 1–18
4. Yadav HK, Pandya DH, Harsha SP (2017) Nonlinear vibration signature analysis of rotor supported ball bearing. Int J Non Linear Dyn Control (Inderscience Publication) 1(1):1–26
5. Horng TL (2008) An analytical solution of the stiffness equation for linear guide way type recirculating roller with arbitrarily crowned profiles. Proc Inst Mech Eng Part C J Mech Eng 223:1351–1358
6. Ma Fangbo, Jiang Fengyuan, An Qi (2015) Simulation of hydrodynamic lubrication between cage pockets and rollers in cylindrical roller bearings. Proc Inst Mech Eng Part C J Mech Eng 229:2551–2560
7. Harsha SP, Nataraj C, Kankar PK (2006) The effect of ball waviness on nonlinear vibrations associated with rolling element bearings. Int J Acoust Vibr 11(2):56–66
8. Harsha SP, Kankar PK (2004) Stability analysis of a rotor bearing system due to surface waviness and number of balls. Int J Mech Sci 46(7):1057–1081
9. Yadav K, Pandya DH (2017) Nonlinear dynamic analysis of cylindrical roller bearing. Proc Eng 173:1878–1885. In: Proceedings of 11th international symposium on plasticity and impact mechanics, Implast, IIT Delhi
10. Sharma A, Amarnath M, Kankar PK (2015) Effect of unbalanced rotor on the dynamics of cylindrical roller bearings. Proceedings of the 9th IFToMM international conference on rotor dynamics. Mechanisms and Machine Science, vol 21, pp 1653–1663

Safety and Crashworthiness Analysis of Composite Tube Under Impact Loading

Shivdayal Patel and Venkata Ravi Vusa

Abstract Crashworthiness effects and axial collapse with damage propagation behavior of GFRP/CFRP composite circular hollow tube were investigated under dynamic axial crushing load. Energy absorption and peak force for the composite circular tubes mainly depends on the ply orientations and materials. In this study, focus on crushing analysis of circular tube under axial loading with different ply orientations and materials namely glass fiber-reinforced plastic (GFRP), carbon fiber reinforced polymer (CFRP). In this dynamic analysis, damage initiation and propagation models are implemented in the finite element code of ABAQUS/Explicit. At the onset of study, numerical results are obtained using the progressive damage model and validated against the existing experimental study in the literature. During crash, the in-plane damage modes such as matrix cracking, fiber failure and shear cracking are modeled using failure initiation and propagation criteria. The out of plane delamination is modeled using cohesive surfaces. Numerical results were compared based on both energy absorption and peak force of these cases. The GFRP quasi-isotropic composite circular tubes exhibited the superior energy absorption and peak force than the CFRP.

Keywords Safety of vehicles · Crashworthiness · Failure prediction · Progressive damage modeling · Structural health monitoring

1 Introduction

Vehicle crashworthiness and occupant protection are imperative and demanding design considerations in the automotive industry. At present, automobile structures

S. Patel (✉) · V. R. Vusa
Discipline of Mechanical Engineering, Indian Institute of Information Technology, Design and Manufacturing, Jabalpur 482005, India
e-mail: shivdayal@iiitdmj.ac.in

V. R. Vusa
e-mail: 1613111@iiitdmj.ac.in

V. K. Gupta et al. (eds.), *Reliability and Risk Assessment in Engineering*,
Lecture Notes in Mechanical Engineering,
https://doi.org/10.1007/978-981-15-3746-2_12

are fabricated mostly of pressed steel panels and assembled using different binding techniques. Designers produce vehicles to offer occupant safety by maintaining reliability of the customer section. Consequently, the aim of crashworthiness is an optimized automobile structure that can absorb collide energy by prohibited automobile deformations and also reduce collide loads shift to the automobile occupants. Marzbanrad and Keshavarzi [1] performed the numerical and experimental studies on the aluminum crash box with elastic support. It was found that elastic support is reasonable under crash box instead of a rigid wall during the crash of tested tube in the numerical and experimental analysis. Actually, in-vehicle crash absorbers do not have rigid support and these are experienced support from S-rail and firewall while collision. Researchers concluded that elastic support has better agreement with experimental work when stiffness ratio is 1000 MN/m. Energy absorption and deformation are changing with different stiffness ratio and even behavior of crash box also varies with the support of plastic elements. Kumar and Manikandaraja [2] as well as Nia and Hamedani [3] performed the computational study for aluminum tube subjected to axial and oblique impact to evaluate the superior geometry shapes and mesh sizes by using finite element code of ABAQUS. In this study, they discussed deformation mode, absorbed energy, maximum collapse mode, maximum and mean force. Circular sections are capable of absorbing more energy because energy absorption is based on number of corners but these are having maximum peak loads. Conical and pyramidal samples have less difference between peak and mean. Quasi-static crush behavior of foam-filled aluminum tubes was performed by Guden et al. [4]. Before this study, some of the research work has been done on composites to understand and predict the behavior under crushing loads but those simulation techniques are not good enough to predict the behavior of composites. Reuter et al. [5] investigated material detection parameters and an insensitive simulation model. In this study, researchers observed that fiber orientations of UD-layers are strongly influenced the specific energy absorption (SEA) of carbon fiber-reinforced plastic (CFRP) crash tube. In actual world, vehicle collisions are happening not in exact longitudinal front crashes and deformation is happening in progressive and bending mode. Djamaluddin et al. [6] and Santosa et al. [7] investigated on FE analysis of foam-filled circular tubes subjected to tilted loading. In this study, tube placed in an inclined manner varies from 0° to 40°. In 0°, 10° and 20° loading model failed in progressive mode and rest of them in bending mode. In the partially filled model, the specific energy absorption is high, and reducing the crest force concurrently subjected it to dissimilar impact angles, compared to the empty and fully foamed tube. Nia and Parsapour [8] as well as Pirmohammad and Marzdashti [9] numerically and experimentally investigated an energy absorption capacity of simple and multi-cell thin-walled tubes with different shapes. Sample tubes were made by aluminum sheets and edges of sheets are connected with adhesive in order to reduce the effect of binding which is assumed to be symmetric. They were studied on different varieties of tubes first one is simple geometry, the second type is multi-cells in the middle of the tube side and finally, multi-cells in the corners of the tube along with numbering codes are given for all varieties. It was found that the multi-cell samples are greater than simple geometries samples in mass, mean crushing force, specific energy absorption (SEA) and

average SEA especially in triangle compared to other geometries. Numerical modeling of different geometry tubes was done with straight columns and different aspect ratio of inner shapes. Experiments are conducted on the square shape of proposed design under the longitudinal and oblique loadings, using the universal test machine equipped with a suitable compression fixture. In this study, they found that square multi-cell with 0.5 aspect ratio giving good result among all based on a decision-making method namely COPRAS was implemented on the LS-DYNA results to rank the multi-cell members in terms of crashworthiness capability.

Numerical analysis has been performed to determine the failure behavior of FRP tube [10]. FRP material under the impact loading the failure initiation is predicted by various criteria, such as maximum principal stress, maximum principal strain, Tsai-Wu, Tsai-Hill, Puck and Schurmann [11, 12]. The continuum damage mechanics approach is investigated to accurately predict the fracture behavior of the FRP composites materials. Intra-laminar failure behavior of the FRP material is determined to incorporate the cohesive surfaces [13, 14].

This research paper presents the progressive damage modeling approach for lightweight fiber-reinforced plastic (FRP) structures which is strong enough to sustain impact force. Fabrication of such lightweight FRP tubes is a tough task. Presently, a significant difference is observed in energy absorption and peak force among the different combination of materials and ply orientations. The deterministic design methodology was performed to attain insubstantial FRP tube design using FEA. In the current study, damage propagation (fiber, matrix cracking and delamination)-based failure criteria were implemented in user define subroutine to estimate the deterministic response such as peak loads, deformations and energy absorption.

2 Composite Damage Modeling

An impact on FRP material the damage started within the plies. The damage starts grow as an intra-lamina matrix break due to shear or bending, which propagates further into the interface causing delamination between different plies and fiber breakage.

In the dynamic, explicit analysis is performed based on the central difference method to calculate time step, strain and stress respectively. The governing equation is used to determine outcome parameters in the explicit dynamic analysis is

$$[M]\{\ddot{u}\} + [K]\{u\} = \{(F)(t)\} \tag{1}$$

here

$[M]$	mass matrix,
$[K]$	stiffness matrix and
F	external forces.
$\{\ddot{u}\}$, $\{u\}$ and t	acceleration, displacement and time

The explicit analysis followed the central difference method to find the stress and strain values at a particular time internal so time step calculated by using this equation.

$$\Delta t = \frac{2}{\omega_{\max}} \tag{2}$$

$\omega_{\max}$ maximum frequency.

In the central difference method, acceleration calculated first with inversion of the mass matrix as follows

$$\{\ddot{u}\} = [M]^{-1}(\{(F)(t)\} - [K]\{u\}) \tag{3}$$

From the initial acceleration, displacement and velocity estimated for another step by using formulas according to the central difference method until completion of the whole process.

The failure of fiber-reinforced plastic consists of two phases; failure initiation and propagation. Failure initiation occurs in the fiber-reinforced plastic when the Hashin [15] and Puck and Schurmann [16], failure models are satisfied. Consequently, the damage growth is leading up to the final failure of the structure.

2.1 Damage Initiation

Damage initiation possible in fiber plastic composite when satisfying anyone among mentioned below equations

- Tensile fiber failure for $\sigma_{11} \geq 0$

$$\left(\frac{\sigma_{11}}{X^T}\right)^2 + \alpha\left(\frac{\tau_{12}}{S^L}\right)^2 = \begin{cases} \geq 1 \text{ failure} \\ < 1 \text{ No failure} \end{cases} \tag{4}$$

- Compressive fiber failure for $\sigma_{11} < 0$

$$\left(\frac{\sigma_{11}}{X^C}\right)^2 = \begin{cases} \geq 1 \text{ failure} \\ < 1 \text{ No failure} \end{cases} \tag{5}$$

- Tensile matrix failure for $\sigma_{22} > 0$

$$\left(\frac{\sigma_{22}}{Y^T}\right)^2 + \left(\frac{\tau_{12}}{S^L}\right)^2 = \begin{cases} \geq 1 \text{ failure} \\ < 1 \text{ No failure} \end{cases} \tag{6}$$

- Compressive matrix failure for $\sigma_{22} < 0$

$$\left(\frac{\sigma_{22}}{2S^T}\right)^2 + \left[\left(\frac{Y^C}{2S^T}\right)^2 - 1\right]\frac{\sigma_{22}}{Y^C} + \left(\frac{\tau_{12}}{S^L}\right)^2 = \begin{cases} \geq 1 \text{ failure} \\ < 1 \text{ No failure} \end{cases} \tag{7}$$

Here,

σ_{11}, σ_{22} and τ_{12}	Stress in longitudinal, transverse and shear direction
X^T, X^C	Strength properties of fiber in longitudinal, transverse
Y^T, Y^C	Strength properties of matrix in longitudinal, transverse
S^L, S^T	Shear strength properties in longitudinal, transverse.
α	1.

2.2 Damage Propagation

Damage propagation of the FRP materials for fiber and matrix cracking damaged modes is determined for the following equation
Fiber and Matrix tensile failure,

$$d_{f,m}^T = \frac{\varepsilon_{f,m}^{fT}}{\varepsilon_{f,m}^{fT} - \varepsilon_{f,m}^{0T}}\left(1 - \frac{\varepsilon_{f,m}^{0T}}{\varepsilon_{f,m}}\right) \tag{8}$$

where $\varepsilon_f^{fT} = \frac{2G_{fc}^T}{X^T \times l^*}$ and $\varepsilon_f^{0T} = \frac{X^T}{E_1}$
$\varepsilon_m^{fT} = \frac{2G_{mc}^T}{Y^T \times l^*}$ and $\varepsilon_m^{0T} = \frac{Y^T}{E_2}$
Compressive fiber failure,

$$d_f^C = \frac{\varepsilon_f^{fC}}{\varepsilon_f^{fC} - \varepsilon_f^{0C}}\left(1 - \frac{\varepsilon_f^{0C}}{\varepsilon_f}\right) \tag{9}$$

here $\varepsilon_f^{fC} = \frac{2G_{fc}^C}{X^C \times l^*}$ and $\varepsilon_1^{0C} = \frac{X^C}{E_1}$
Compressive matrix failure,

$$d_m^C = \frac{\varepsilon_m^{fC}}{\varepsilon_m^{fC} - \varepsilon_m^{0C}}\left(1 - \frac{\varepsilon_m^{0C}}{\varepsilon_m}\right) \tag{10}$$

where $\varepsilon_m^{fC} = \frac{2G_{mc}^C}{\sigma_m^{0C} \times l^*}$ and $\varepsilon_m^{0C} =$ compressive matrix failure.
T, *C* represents tension or compression and *f, m* represents fiber or matrix
here

$\varepsilon_{f,m}$	equivalent displacement in between damage initiation, propagation

$\varepsilon_{f,m}^{fT,fC}$ equivalent displacement at final failure in tension or compression
$\varepsilon_{f,m}^{0T,0C}$ equivalent displacement at damage initiation in tension or compression
σ_{m}^{0C} equivalent stress at damage initiation
$G_{fc,mc}^{T,C}$ critical fracture energy of element

characteristic length, $l^* = \frac{\sqrt{A_{IP}}}{\cos\theta}$ $|\theta| \leq 45°$

A_{IP} area associated with integration point, θ = angle between mesh line and crack the direction.

3 Finite Element Modeling

The composite tube consists of the individual layers of CFRP and GFRP with internal dimension of the tube is 50 mm. CFRP and GFRP tubes with the preferential plies orientations (0°, ±45°, 90°) consist of 28 laminates with thickness of 0.15 mm. The total tube wall thickness is 4.2 mm. GFRP and CFRP consist of different ply orientations performed as shown in Table 1. Fibers orientation of 0° is parallel to the loading direction and 90° is tangential to the loading directions of the crash tube. All tubes have the same length of 150 mm. The mass of each circular tube is 160 g.

Explicit FE code was used to perform dynamic FE simulations in ABAQUS/EXPLICIT. Numerical modeling of the circular tube is based on a multi-layered shell approach of continuum shell elements. The crash tubes are modeled by four layers of continuum shell element (SC8R). Material properties of the used material are linear in nature, until strength properties of fiber and matrix are reached. These properties are presented by Reuter et al. [5], while fiber is in parallel and matrix is in perpendicular to the loading direction. The rigid impactor of circular shape has radius and mass of 45 mm and 380 kg, respectively. Cohesive surfaces based on traction and separation law are investigated to determine the extent of damage due to delamination. The general contact model is investigated to reproduce the crush force in FEA. Explicit analysis is performed to determine the dynamic response of the GFRP and CFRP tubes.

Table 1 Composite materials and orientations

Notations	Carbon fiber-reinforced plastic (CFRP)		Glass fiber-reinforced plastic (GFRP)	
Fiber angles	$[0]_{28}$	$[90_2/(0_2/45_2/-45_2)_2]_s$	$[0]_{28}$	$[90_2/(0_2/45_2/-45_2)_2]_s$

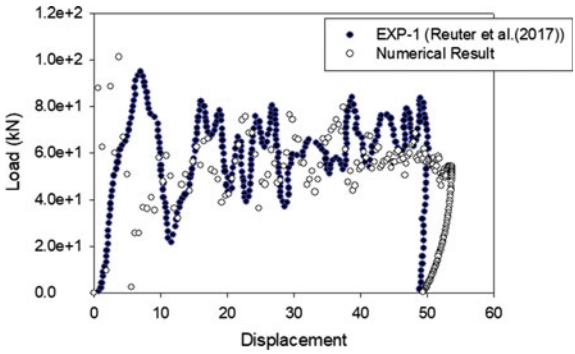

Fig. 1 Load versus displacement curve of the CFRP tube

3.1 Validation Study

Numerical results are performed using the user-defined subroutine code to validate the FE results with available experimental results in Reuter et al. [5]. The complete data details of composite tube, used for validation, are given in Sect. 3.

The load versus displacement response is predicted by FE simulation using the impactor velocity at 3.94 m/s and mass 380 kg showed the same trend and the magnitude of the present results slightly larger than the literature result [5] (Fig. 1). This variation shows due to the effect of damping parameters and the trigger offset effect does not consider in the FE simulation [5].

4 Results and Discussion

Dynamic response of FRP plate due to crush force considering the material properties and impactor velocity, following relevant cases are studied. FEA has been performed to obtain the deterministic results of FRP tubes.

4.1 Effect of Stacking Sequence

The energy absorption and peak force capability were influenced by stacking sequence, shape of the tube and materials. Modes of collapse mechanism are different in two cases, load versus displacement graphs are shown in Fig. 2. In 0° composite tube, fibers are normal to the loading direction. In quasi-isotropic tube, fiber assists in different orientation [90°, 0°, 45°, −45°], each orientation of fiber has their own mechanism. Collapse mechanisms of each composite tube for different ply orientations are as follow

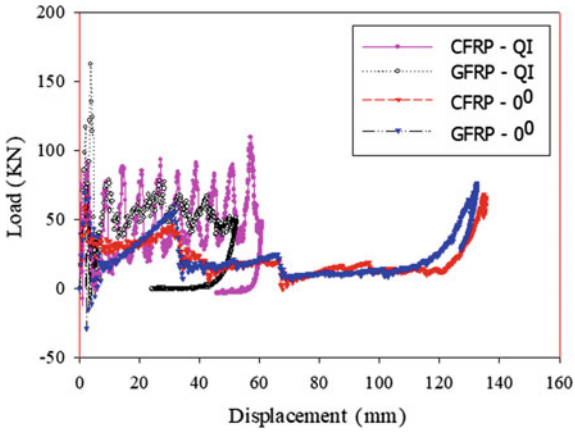

Fig. 2 Load versus displacement result of the composite tubes

First, in the CFRP $[0]_{28}$ and GFRP $[0]_{28}$ composite circular tubes, the fiber reinforcement mechanisms were normal to the loading direction. In loading, direction fiber has resistance to bend and absence to prevent severe damage as well as delamination between layers. Delamination between the layers occurred severely and broken easily and it is leading to get different modes damage. After 15 ms of simulation time, progressive damage shifted to mixed damage mode.

In the CFRP $\left[90_2^\circ/\left(0_2^\circ/45_2^\circ/-45_2^\circ\right)_2\right]_s$ and GFRP $\left[90_2^\circ/\left(0_2^\circ/45_2^\circ/-45_2^\circ\right)_2\right]_s$ composites circular tubes, the fiber reinforcement mechanisms were stacked in the different ply orientation to the loading direction. In loading direction, 0° fiber were avoiding the severe damage and delamination in the matrix of 90° fiber layers and secured 90° fiber giving resistance to the applied loading along with 45° and −45° fiber were keeping the load in high for more time after peak loads. Good synergetic effect was obtained coming from these various collapse mechanisms. Therefore, this tube showed the best crashworthiness characteristics.

4.2 Energy Absorption Characteristics

In 00 cases, fiber direction is normal to the loading direction and damage occurring in both progressive mode and bending mode. Due to mixed damaging mode, the length of the deformation is high and low efficiency in CFRP and GFRP. The internal energy versus time plots is shown in Fig. 3. The crest forces and energy absorption are fiber direction dependent with respect to the loading direction. After 15 ms of simulation time, material degradation exhibits different modes of collapse mechanism. Each simulation collapsed specimen is presented in Figs. 4 and 5. Based on this plots, glass fiber reinforced polymer composite showed that 10% high peak force, 5% less deformation and 6% more energy absorption compared to the carbon fiber reinforced polymer composite tube.

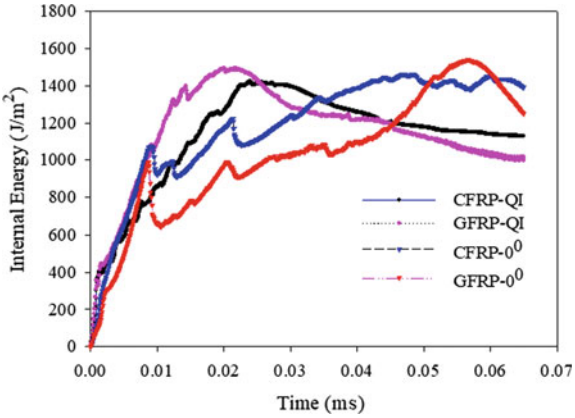

Fig. 3 Energy dissipations of the composite tubes

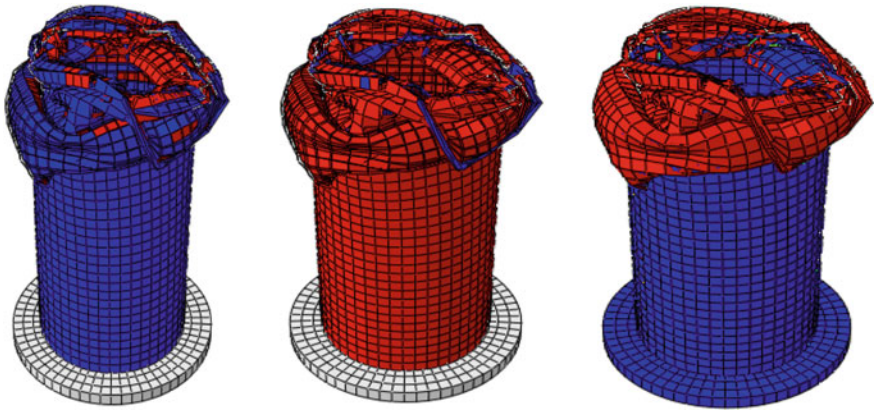

Fig. 4 Deformation modes of GFRP quasi-isotropic laminates tube for fiber, matrix and delamination

The quasi-isotropic composite tube has four fiber orientations and these are mutually sharing the strength, giving support to each other. In the quasi-isotropic composite tube, deformation length is fewer and peak forces are high compared to 0° fiber directions and the load-displacement curve is shown in Fig. 2. In this case, material degradation occurs only in progressive mode. This damage mode gives the best energy absorbing capabilities out of all other damage modes occurred in crushing. The internal energy plots are shown in Fig. 3. Glass fiber reinforced polymer composite tube has 6% high energy.

Absorption capabilities, 34% high peak forces and 17.5% less deformation compared to carbon fiber reinforced polymer composite tube. In this study, it was also

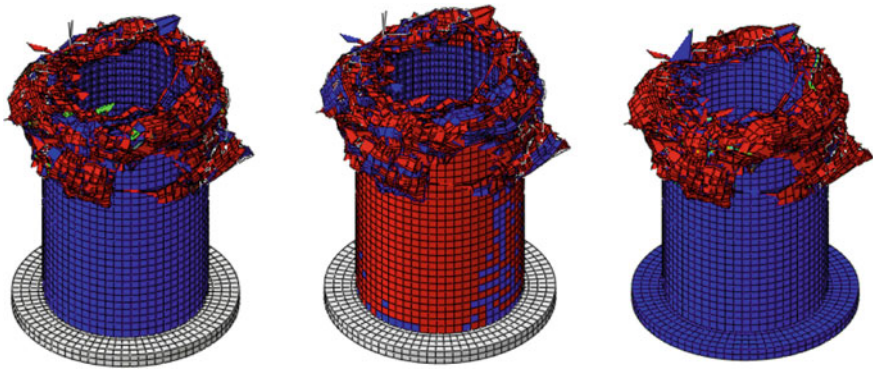

Fig. 5 Deformation modes of CFRP quasi-isotropic laminates tube for fiber, matrix and delamination

found that the GFRP circular cross-section composite tube shows superior energy absorption ability compared to CFRP composite tube. In energy absorption of the composite structures in terms of fiber failure, matrix failure and delamination are very important components. Energy dissipation of the composite materials mainly depends upon the stacking sequence, fiber, matrix and delamination failures. In 0° composite tube, most of the energy are dissipated in terms of fiber and matrix failures. The delamination failure very small energy is dissipated by 0° composite tubes because of the same ply orientations. Quasi-isotropic composite tube showed the better energy absorption result in comparison to the other ply orientation of composite tubes. The energy dissipation through fiber failure, matrix failure and delamination is more compared to 0° composite tubes.

5 Conclusions

In this study, crushing analysis of a composite circular tube under axial impact loading was investigated with CFRP and GFRP composites tubes. Energy absorption, peak loads and deformation are dependent on stacking sequence and materials changing accordingly. Quasi-isotropic composite tube has all fiber orientation benefits hence cause it has better results compared to 0° fiber orientation as shown in load versus displacement plot. In this study, glass fiber reinforced polymer has less deformation, maximum energy absorption and value of crest force is also more compared to carbon fiber reinforced polymer in both of the cases. The GFRP quasi-isotropic stacking sequence showed the best energy absorption and crest force. The crest force and energy absorption of the GFRP composite tube are 34% and 6% greater than that of the CFRP composite tube, respectively, for the quasi-isotropic ply orientation.

References

1. Marzbanrad J, Keshavarzi A (2014) Numerical and experimental study on the crash behaviour of the extruded aluminum crash box with elastic support. Lat Am J Solids Struct 11(8):1329–1348
2. Santhoshkumar V, Manikandaraja G (2016) Numerical study on energy absorbing characteristics of thin-walled tube under axial and oblique impact. Alexandria Eng J 55(1):187–192
3. Nia AA, Hamedani JH (2010) Comparative analysis of energy absorption and deformations of thin walled tubes with various section geometries. Thin-Walled Struct 48(12):946–954
4. Aktay L, Toksoy AK, Guden M (2006) Quasi-static axial crushing of extruded polystyrene foam-filled thin-walled aluminum tubes: Experimental and numerical analysis. Mater Des 27(7):556–565
5. Reuter C, Sauerland KH, Tröster T (2017) Experimental and numerical crushing analysis of circular CFRP tubes under axial impact loading. Compos Struct 174:33–44
6. Djamaluddin F, Abdullah S, Ariffin AK, Nopiah ZM (2016) Finite element analysis and crashworthiness optimization of foamfilled double circular under oblique loading. Lat Am J Solids Struct 13(11):2176–2189
7. Santosa S, Wierzbicki T, Hanssen AG, Langseth M (2000) Experimental and numerical studies of foam-filled sections. Int J Impact Eng 24(5):509–534
8. Nia AA, Parsapour M (2014) Comparative analysis of energy absorption capacity of simple and multi-cell thin-walled tubes with triangular, square, hexagonal and octagonal sections. Thin-Walled Struct 74:155–165
9. Pirmohammad S, Marzdashti SE (2016) Crushing behavior of new designed multi-cell members subjected to axial and oblique quasi-static loads. Thin-Walled Struct 108:291–304
10. Singh H, Namala KK, Mahajan P (2015) A damage evolution study of E-glass/epoxy composite under low velocity impact. Compos Part B Eng 76:235–248
11. Patel S, Guedes SC (2018) Reliability assessment of glass epoxy composite plates due to low velocity impact. Compos Struct 200:659–668
12. Patel S, Guedes SC (2017) System probability of failure and sensitivity analyses of composite plates under low velocity impact. Compos Struct 180:1022–1031
13. Patel S, Ahmad S (2017) Probabilistic failure of graphite epoxy composite plates due to low velocity impact. J Mech Des 139(4):044501–44504
14. Patel S, Vusa VR, Soares CG (2019) Crashworthiness analysis of polymer composites under axial and oblique impact loading. Int J Mech Sci 156:221–234
15. Hashin Z (1980) Failure criteria for unidirectional fiber composites. J Appl Mech 47(2):329–334
16. Puck A, Schurmann H (2002) Failure analysis of FRP laminates by means of physically based phenomenological models. Compos Sci Technol 62(12–13):1633–1662

Strategies for Controlling the Accuracy and Reliability of Abrasive Water Jet Machining

Neeraj Kumar Bhoi, Harpreet Singh, and Saurabh Pratap

Abstract The abrasive water jet machining (AWJM) process utilized a wide industrial application due to its unique capabilities of cutting any soft or hard material. AWJM uses high-velocity water and abrasives to remove the material with the concept of the impact of high kinetic energy jet on the work material. During AWJM, the accuracy of cutting geometry primarily depends on the size of nozzle orifice and then on standoff distance (SOD), tool path and slurry velocity. In order to reach an accurate and reliable quality control of a mechanical part produced using AWJM, material and process parameter-based control strategies have developed with the objective to reduce down the nozzle erosion. Furthermore, these strategies help to achieve low-cost machining, high level of productivity and increased reliability due to reduced scrap rate by increasing the nozzle life span. In this paper, various developed strategies made by researchers to monitor the nozzle condition during machining are summarized. It is found that to improve the reliability and performance of the AWJM operation, more efforts should be paid to developing nozzles, and a relationship between the work surfaces and the nozzles must be listed.

Keywords Abrasive water jet machining · Nozzle wear · Reliability · Geometrical accuracy · MRR · Surface quality

1 Introduction

Non-conventional machining methods are gaining applications in wider engineering areas due to their capability to produce complex shapes on difficult-to-cut, especially hard materials. Abrasive water jet machining (AWJM) process is a non-conventional

N. K. Bhoi (✉) · H. Singh · S. Pratap
Department of Mechanical Engineering, PDPM IIITDM Jabalpur, Jabalpur, India
e-mail: neerajbitd@gmail.com

H. Singh
e-mail: hps.dme@iiitdmj.ac.in

S. Pratap
e-mail: s.pratapiitkgp@gmail.com

V. K. Gupta et al. (eds.), *Reliability and Risk Assessment in Engineering*,
Lecture Notes in Mechanical Engineering,
https://doi.org/10.1007/978-981-15-3746-2_13

machining process used to cut virtually any type of material, e.g., metals, alloys, ceramics and composites [1]. This is due to the presence of fine abrasive particles which exerts a lower mechanical load during erosion and lower thermal stresses (no heat-affected zones) because of water flow. Owing to its unique capabilities, AWJM has received considerable attention from industry worldwide [2]. A pie chart shown in Fig. 1 represents the percentage of the global market of AWJM.

The health and life of the abrasive nozzle are a major concern to take care of, as it directly affects the performance of the whole abrasive water jet system. Wear in nozzle causes poor jet quality, ineffective mixing of abrasive and water resulting in a poor cutting performance with reduced nozzle life. The wear in the nozzle can be assessed by a number of parameters such as tube weight loss, the incidents of the wear pattern on the inner surface, changes in the outlet geometry and exit diameter increase at the outlet of the jet. Dispersion of exit jet diameter is a major monitoring method to check the quality of a nozzle used, reported in [3]. The wear of nozzle can be assessed directly by measuring the jet diameter, the internal diameter of the nozzle, etc., while there are some factors by which we can correlate the nozzle life such as level of forces that are impacting on the surface, noise factor and machine vibration [4]. AWJM process parameters which affect directly or indirectly the total accuracy of the product can be categorized as hydraulic, abrasive, mixing and cutting parameters. Figure 2 shows various input parameters which affect the performance of AWJM. This paper reviews the major research activity which was carried out to determine the different causes of wear in the nozzle, and methods which were employed to determine the life of nozzle, various design aspects in the nozzle and different process optimization techniques by which the accuracy of the product is maintained.

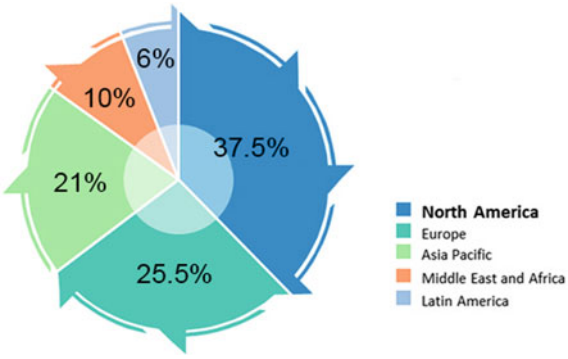

Fig. 1 Percentage of the global market of AWJM

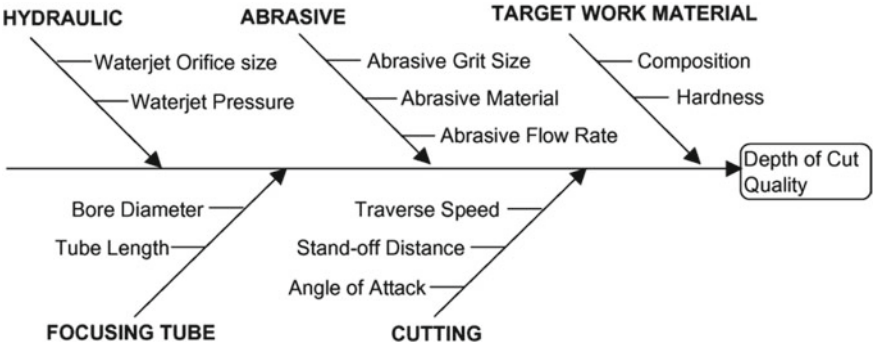

Fig. 2 Process parameters influencing the AWJ cutting process (adapted from Rozario et al. [5])

2 Discussion on Developed Strategies to Control the Accuracy and Reliability of AWJM

2.1 Based on Design and Material of the Nozzle

The sustainability and energy conservation are a prime consideration nowadays in any manufacturing process. Researchers are always looking for a process which is more reliable, viable and feasible to work with. AWJM has always been a simple and cost-effective process due to its unique ability to cut any type of material with highly precision, very less cutting force, less thermal damage to material and very less deformation stress in the processed workpiece [2]. Modification in the basic design of the water jet nozzle, for improved product quality and higher productivity, has always been a challenging task. From the inception of water jet cutting process, various modifications in orifice and mixing tube have been done. Figure 3 depicts a comparison of original patent drawings from the 1930s and a modern abrasive

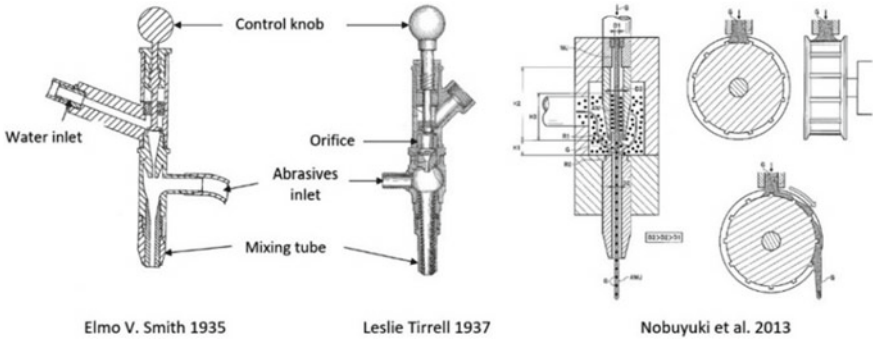

Fig. 3 Evolution of the abrasive water jet nozzle [6–8] (available from freepatentonline.com)

water jet nozzle cut in half, showing the evolution of the design. Generally, two basic designs of the nozzle are widely used: first one, where abrasive is mixed in the mixing tube and the other one where abrasive and water are premixed and added to the orifice. Abrasive slurry jet (ASJ) system uses premixed slurry, causing lower entrapment of air bubble in the mixing tube, thus resulting in coherent jet and improved surface quality. The amount of slurry mixture to be used is always a difficult work to handle, due to variation in solubility and other aspects of the material, such as hardness and toughness.

Hashish studied the effect of premixed abrasive slurry in place of AWJ for cutting of aluminium material, keeping other parameters constant [9]. It was observed that with ASJ the surface with better quality, more width of cut and less striation on the cutting surface is obtained. Long-chain polymer type of non-ionic polyacrylamide flocculants was added with alumina particle, to find the jet stability during AWJM in [10], used. Based on the dimensional analysis and developed model, partial factorial design was suggested. It was found that with higher concentration and decreasing jet pressure, the jet compact length improved. With improved jet compact length, the machining quality enhanced. With more the jet dispersion, the striation and rough machined surface were obtained. The modified process by applying a DC potential voltage between the nozzle and workpiece for higher improved surface quality and material removal is discussed in [11]. Tungsten carbide (WC) material was tested in this process for electrochemical slurry jet machining (ESJM) process. When compared to electrochemical jet machining (ECJM), the surface roughness improved by 13% and material removal improved up to 50%. Madhu and Balasubramanian in 2017 [12] redesigned the nozzle with internal threading to know the effect of whirling of the jet on the surface quality of the carbon fibre composite material. With internal threading, the nozzle provides better surface quality and minimum diameter. The size of the abrasive particle affects much on the machined zone. Lowering the particle size improves the quality of the surface (Figs. 4, 5 and 6).

2.2 Based on the Nozzle Wear Monitoring Techniques

The nozzle wear in AWJM can be analogous to cutting tool wear in the convention machining process, which directly affects the output performance and total productivity. It is essential to monitor the nozzle conditions regularly for maintaining the quality and reliability of the product and AWJM system. There are a number of monitoring methods developed such as direct and indirect sensing methods and real-time control strategies, to monitor the wear in the AWJ nozzle [2]. Nozzle wear can be divided into two different categories: regular and accelerated wear test. Based on that Hashish in 1994 compares the different grade of tungsten carbide and boron carbide tubes for wear testing using aluminium oxide and garnet as the abrasive material. It was observed that the hardness and toughness of the abrasive water jet nozzle material are the most important factor which governs the efficiency of the nozzle. Actual test condition with garnet shows that boron carbide deteriorates

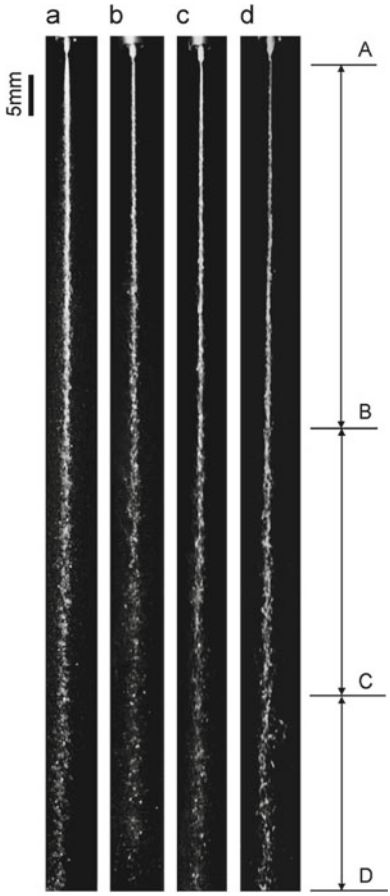

Fig. 4 Effect of chemical concentration on the jet stability: $P = 2$ MPa, $d =$ 0.84 mm and 0 (water), 0.1, 0.25 and 0.5% for (a–d) (respectively, taken from [10])

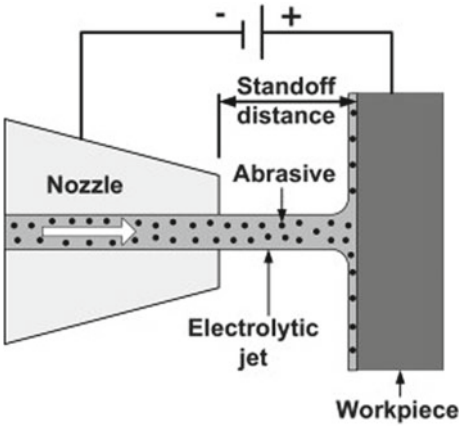

Fig. 5 Schematic of electrochemical slurry jet micro-machining (ESJM) (taken from [11])

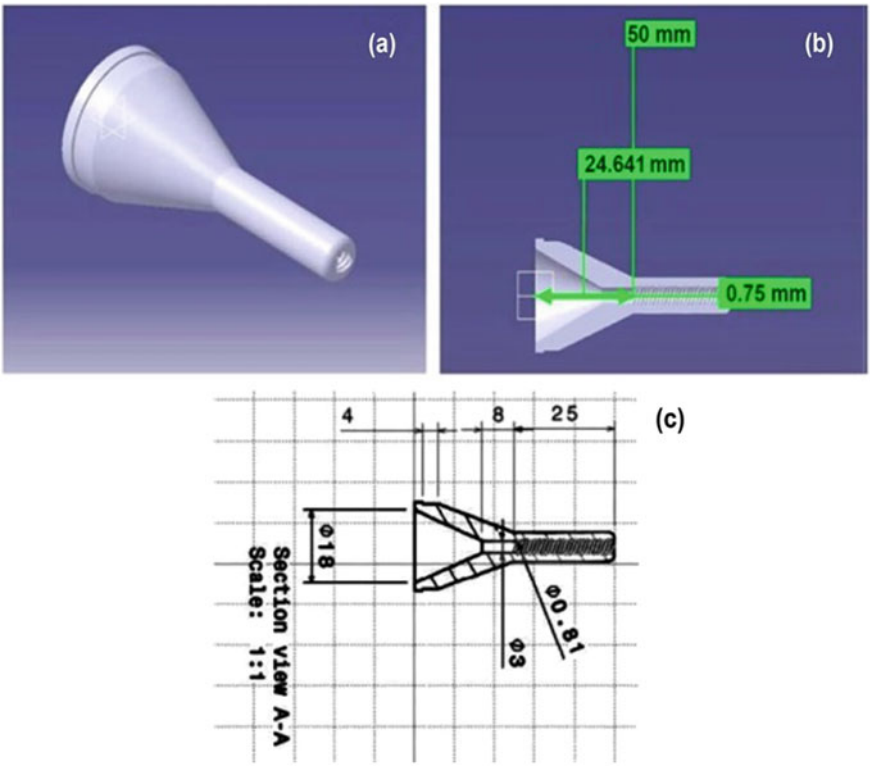

Fig. 6 **a** Internal threaded nozzle. **b** Thread profile inside the nozzle. **c** Dimensions of the nozzle (taken from [12])

faster, which is in contrary to, when aluminium oxide was used. A smaller particle with longer mixing tube length reflects the slower wear rates [13]. Kovacevic in 1991 [3] proposed a method to determine wear in the nozzle by introducing a sensory loop circuit. The loop is attached to the tip of the AWJ nozzle with a spacing of 0.05 mm in each of the four quadrants. The inside diameter change at the outlet of the AWJ nozzle was used to measure the wear. Figure 7 shows the conductive loops used for measuring wear in the nozzle. Prijatelj et al. [14] measure the nozzle wear by measuring AWJ diameter. The diameter is measured with Keyence digital display compact laser through beam sensor, LX2-V10W series. Figure 8 shows the images taken before and after experimentation with different sets of the nozzle. Perfect round shape was observed in case of the new nozzle, and as the wear progresses the roundness slowly decreases. In case of the abrasive water jet, the air entrapment is more, causing more wear to that of the pure water jet. Larger diameter nozzle produces more wear and worn asymmetrically.

Ness and Zibbell [15] studied the three different hard materials (i.e., tungsten carbide/cobalt, boron carbide and composite carbide) which are commonly used in

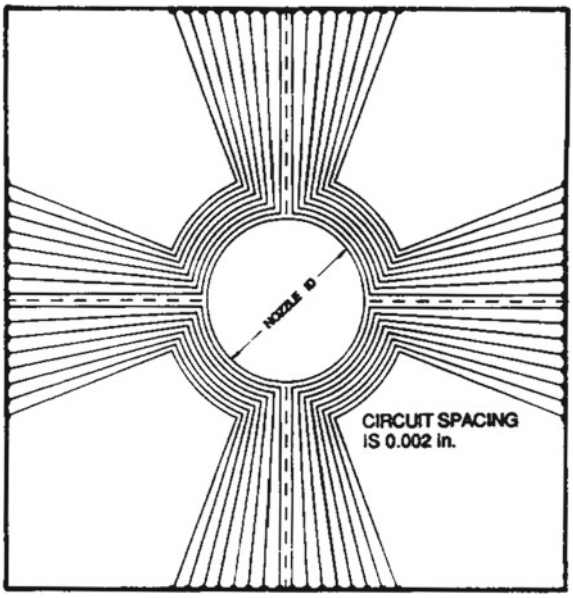

Fig. 7 Abrasive water jet nozzle wear probe (taken from [3])

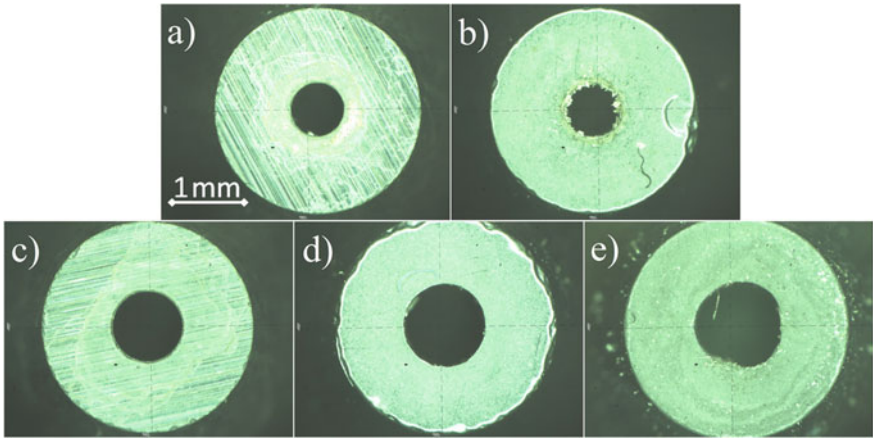

Fig. 8 Images of focusing nozzles taken with the Mitutoyo microscope: **a** 0.76 mm new, **b** 0.76 mm worn, **c** 1.02 mm new, **d** 1.02 mm worn, **e** 1.02 mm very worn (taken from [11])

mixing tube in AWJ applications. Hardness and toughness of the material prevent the nozzle wear as observed during ASTM G76 erosion test. The loss in weight of composite ROCTEC100 (WC/Mo_2C) is very less compared to the other two used in the test. From the micrograph, it is evident that ROCTEC100 is having a smaller scar which shows a superior material in abrasion and erosion environment.

Nanduri et al. [16] analysed the nozzle wear in AWJM using accelerated wear test, using two different nozzle materials WC/Co and ROCTEC100 (R100, REXP) with two different abrasive materials (i.e., garnet and aluminium oxide). Figures 9 and 10 show the validity of accelerated wear test using two different abrasives. During experimentation, a number of AWJ test parameters were considered such as nozzle length, inlet angle, nozzle diameter, orifice diameter, abrasive flow rate and pressure. It was observed that with the increase in inlet angle, nozzle diameter,

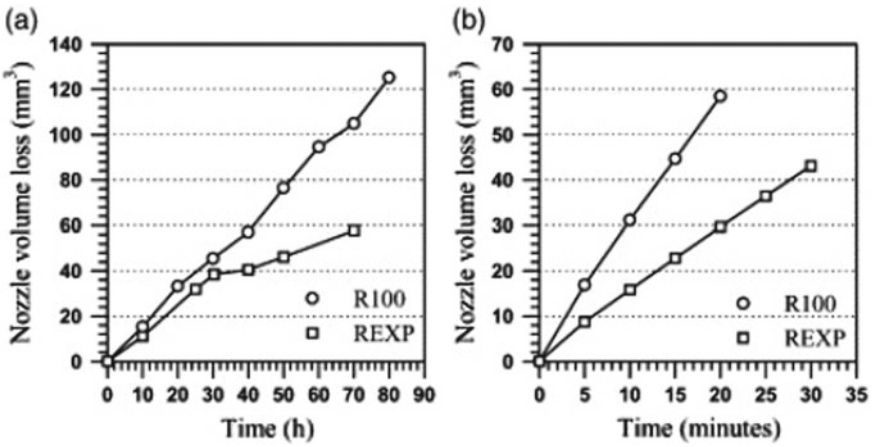

Fig. 9 Validity of accelerated wear tests: **a** long-term data using garnet abrasives; **b** short-term data using aluminium oxide abrasives (taken from [13])

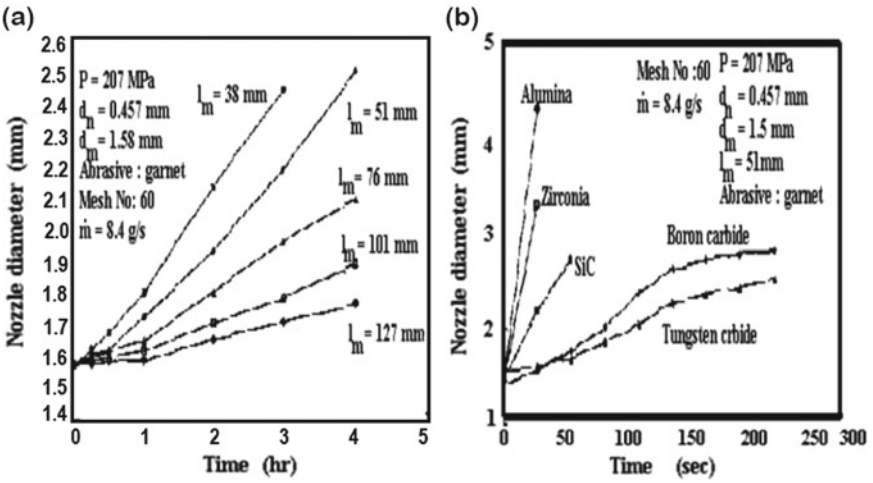

Fig. 10 **a** Reduced wear rates with increased nozzle length. **b** Wear of different nozzle materials using garnet abrasives (taken from [13])

Table 1 Test parameters and values

Parameter	Values tested	Typical value
Nozzle length	32.5, 50.8, 76.2 and 101.6 mm	50.8 mm
Nozzle inlet angle	10°, 20°, 30°, 40°, 50° and 180°	60°
Nozzle diameter	0.79, 1.14 and 1.63 mm	1.14 mm
Orifice diameter	0.28, 0.33, 0.38 and 0.43 mm	0.38 mm
Water pressure	172, 241, 310 and 359 MPa	310 MPa
Abrasive flow rate	1.9, 3.8, 5.7, 7.6, 9.5 and 11.4 g/s	3.8 g/s

orifice diameter and abrasive flow rate, the wear rate in nozzle increases, whereas with other parameters it tends to reduce with increase in nozzle length and pressure of the system. An empirical model was developed for nozzle weight loss, considering the AWJ system and nozzle parameters. Table 1 shows the typical test condition used in the experimentations.

2.3 Based on the AWJM Input Process Parameters

Higher productive and desired surface qualities are two basic requirements of any manufacturing process. The controlling parameters, which affect the machining process, need to be controlled precisely. Most of the researchers are always trying to modify the combination of the process parameters and various optimization strategies to determine the best possible method for enhancing quality and reliability in the products. Various investigators tried working with AWJM to get the optimized and higher accuracy in the outcomes and analysis. Some of the studies are summarized here in brief, keeping other parameters constant. Boud et al. [17] assessed the effect of soluble abrasive material during machining of brass, copper, steel and Inconel with varying traverse speed. Three different types of abrasives were used during machining: as garnet, maxxstrip and softstrip. With the use of soluble abrasive material, the material removal rate is improved up to 20 times for brass and five times for copper, compared to plain water jet machining. Using soluble abrasive material improves the surface finish but for hard material like Inconel, the material removal rate is very low compared to the use of garnet as abrasive. Haghbin et al. [18] analysed the effect of submerged water during AWJM for glass, aluminium 6061-T6 and stainless steel 316L with varying nozzle angle SOD and abrasive flow rate. Two different environments like air and water were taken into consideration during experimentation. During submerged water studies, higher resolution can be achieved with reduced noise and debris. Figure 11 represents a schematic of the submerged

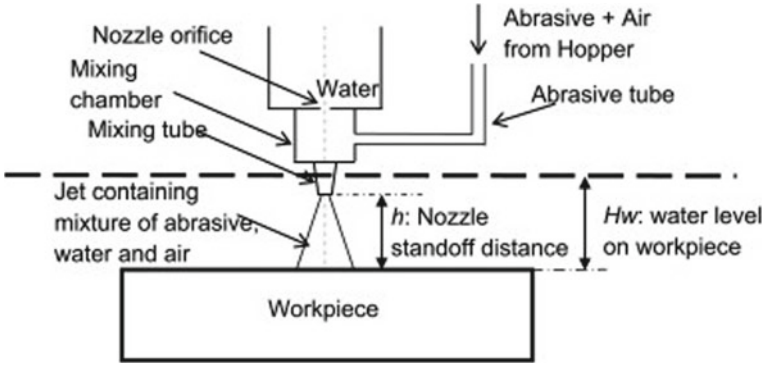

Fig. 11 Schematic of the submerged abrasive water jet (taken from [18])

abrasive water jet. Patel and Tandon [19] studied the effect of the external heating source during AWJM for improvement of surface quality and material removal rate. Three different materials, i.e., Inconel 718, titanium Ti6Al4V and mild steel MS A36 were investigated experimentally with varying SOD, pressure and temperature during machining. It was found that material removal is improved but thermal damages are a prime factor to be taken care of, a low thermally conductive material distorts with external heating. The suggested method is useful for higher material removal rate but applicable only when the surface quality of machining is not a prime consideration. Figure 12 shows the schematic representation of the developed set-up for thermally enhanced water jet machining. Babu and Muthukrishnan [20] investigated using the brass-360 material for minimizing surface roughness in AWJM. Taguchi L27 experimental design was used with parameter abrasive flow rate, pump pressure

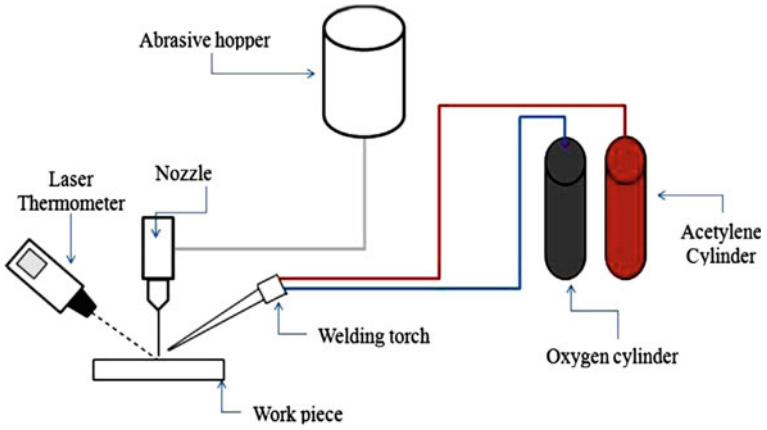

Fig. 12 Schematic of the set-up of thermally enhanced abrasive water jet machining taken from [19]

and SOD with response surface methodology for deciding optimal parameter during machining. For better surface accuracy, higher pump pressure with a low abrasive flow rate is suggested. The optimal machining condition is found as pump pressure of 399 MPa, the abrasive flow rate of 75.37 g/min, SOD of 1 mm and a feed rate of 557 m/min. The pump pressure was found as the most influencing factor in AWJM for brass, as investigated experimentally.

3 Conclusions

This paper highlights the novel strategies developed for enhancing the reliability of abrasive water jet machining (AWJM) operations. From the literature, it is evident that the appropriate design of the nozzle, a suitable material of the nozzle and proper controlling of input process parameters during machining, gives accurate and reliable products. Based on the developed strategies, the following conclusions could be drawn.

- For efficient product quality, reliable machining system of the nozzle material and jet stability is a prime concern. The type of additives, material for the nozzle and process modification must be chosen carefully for enhanced performance. Some additional research is required in this direction for the proper selection of abrasive and nozzle material.
- For continuous run monitoring of nozzle, wear control is necessary for desired product accuracy, to avoid mean time between failure of cutting head assembly. Highly sensitive sensing elements are required to develop for accurate measurement of wear process monitoring.
- Selection of control parameters during machining is very crucial as the product accuracy and overall system reliability are totally dependent upon the input conditions. The level of noise, vibration in the system, fixture unit, etc., totally depends upon the input given to the system. A strategy must be developed to control all affecting variables, which affect the overall accuracy and reliability of AWJM.

Research in the direction of the total cost of machining, mean time between failures, total machining time for the product, failure frequency of each machine component and assessment of life cycle needs to be analysed more in AWJM. In addition, to improve the reliability and performance of the AWJM operation, more efforts should be directed to develop nozzles, and the relationship between work surfaces and nozzles must be listed properly.

References

1. Kovacevic AWM (1998) Principles of abrasive water jet machining
2. Kovacevic R, Hashish M, Mohan R, Ramulu M, Kim TJ, Geskin ES (1997) State of the art of research and development in abrasive waterjet machining. J Manuf Sci Eng 119:776
3. Kovacevic R (1991) A new sensing system to monitor abrasive waterjet nozzle wear. J Mater Process Technol 28:117–125
4. Baralic J, Nedic B, Marusic V (2008) Focusing tube wear and quality of the machined surface of the abrasive water jet machining. Tribol Ind 30:55–58
5. Jegaraj JJR, Ramesh Babu N (2006) A soft computing approach for controlling the quality of cut with abrasive waterjet cutting system experiencing orifice and focusing tube wear. J Mater Process Technol 185:217–227
6. Smith EV (1936 May 12) Liquid blasting. US Patent No. 2040715
7. Tirrell LL (1939 Oct 17) Sandblast device. US Patent No. 2176577
8. Nobuyuki T, Masashi T, Takuya A, Nobuhide T, Abrasive water jet nozzle and abrasive water jet machine. US 20130267152 A1
9. Hashish M (2007) Comparative evaluation of abrasive liquid jet machining systems. J. Eng. Ind. 115:44–50
10. Nguyen T, Shanmugam DK, Wang J (2008) Effect of liquid properties on the stability of an abrasive waterjet. Int J Mach Tools Manuf 48:1138–1147
11. Liu Z, Nouraei H, Spelt JK, Papini M (2015) Electrochemical slurry jet micro-machining of tungsten carbide with a sodium chloride solution. Precis. Eng. 40:189–198
12. Madhu MS, Balasubramanian M (2017) Influence of nozzle design and process parameters on surface roughness of CFRP machined by abrasive jet. Mater Manuf Process 32:1011–1018
13. Hashish M (1994) Observations of wear of abrasive-waterjet nozzle materials. J Tribol 116:439
14. Prijatelj M, Jerman M, Orbanic H, Sabotin I, Valentincic J, Lebar A (2017) Determining focusing nozzle wear by measuring AWJ diameter. J Mech Eng 63:597–605
15. Ness E, Zibbell R (1996) Abrasion and erosion of hard materials related to wear in the abrasive waterjet. Wear 196:120–125
16. Nanduri M, Taggart DG, Kim TJ (2002) The effects of system and geometric parameters on abrasive water jet nozzle wear. Int J Mach Tools Manuf 42:615–623
17. Boud F, Murray JW, Loo LF, Clare AT, Kinnell PK (2014) Soluble abrasives for waterjet machining. Mater Manuf Process 29:1346–1352
18. Haghbin N, Spelt JK, Papini M (2015) Abrasive waterjet micro-machining of channels in metals: comparison between machining in air and submerged in water. Int J Mach Tools Manuf 88:108–117
19. Patel D, Tandon P (2015) Experimental investigations of thermally enhanced abrasive water jet machining of hard-to-machine metals. CIRP J Manuf Sci Technol 10:92–101
20. Naresh Babu M, Muthukrishnan N (2014) Investigation on surface roughness in abrasive water-jet machining by the response surface method. Mater Manuf Process 29:1422–1428

Environmental Impact Study on Carbon Footprint Emission and Development of Software Architectural Framework to Measure the Level of Emission in Cloud Services

P. Vaishnavi and S. Ananthi

Abstract Demand of data storage and processing of datasets in cloud computing consumes a huge volume of power and energy. Exhaustive usage of power and energy by the cloud service providers globally increases carbon footprint which is an environmental concern. Latest research results on carbon emission indicate a warning sign for environmental sustainability. Data centers, their resources and the digital waste created in the cloud environment have created a major impact on the environment. Taking this as an alarm sign on a global perspective, we rigorously worked on to develop "green software" in order to minimize the carbon waste from the environment. The design of this software focuses on to measure energy consumption and the carbon footprint level. This green software shall motivate the cloud services to uphold the concern on carbon emission and to take immediate attention to predict the waste of CPU power. This green software design framework provides a separate track session on energy consumption by the data center and cloud service provider along with the acquired energy efficiency level by the specific center. The software architecture insights are the working elements to analyze the level of emission, time period of the effect and the impact assessment of the carbon footprint. We propose an energy-efficient and cost-effective solution to minimize carbon emission and its impact on the environment.

Keywords Data centers · Data storage · Energy consumption · Green software

1 Introduction

Green computing is a technology also termed as green IT. The concept improved its popularity in recent decades because of its need in the field. In 1991, the Environmental Protection Agency (EPA) designed a terminology green light for

P. Vaishnavi (✉) · S. Ananthi
Anna University Chennai—BIT Campus, Tiruchirappalli, India
e-mail: vaishmk@gmail.com

S. Ananthi
e-mail: anthi.ms@gmail.com

V. K. Gupta et al. (eds.), *Reliability and Risk Assessment in Engineering*,
Lecture Notes in Mechanical Engineering,
https://doi.org/10.1007/978-981-15-3746-2_14

energy efficiency [1]. Nowadays, many computer data have switched over from the desktop to larger data centers [2] because of its emerging needs. Many organizations implement cloud technology to offer unimaginable and uninterruptable services and resources to the client for better performance and cost association [3].

During the last few years, the utilization of HPC framework has increased tremendously to process the business and IT applications. In recent survey, top 500 super computers used HPC, 9.2% for finance and 6.2% for logistics [4]. Green cloud is a technique to provide resource efficiently and also aims to reduce hazardous element and emission. Cloud computing technology with different service models is classified as IaaS, Saas, PaaS and SEaaS. All these models are managed under the platform called virtual machine (VM). If a client demands the resources, the host machine in turn creates a demand on VM. This results in high-power consumption and loss of efficiency of the machine.

According to the survey, the data centers consume 0.5% of world total electricity [5]. In 2010, it increased to 1.5% of data centers in the USA. High-power consumption of data centers leads to huge emission of CO_2. According to Gartner, the total CO_2 emission from data centers is equal to the aviation industry [6]. To control the emission, we require load balancing scheduling technique. This technique will promptly allocate and utilize the resources efficiently. The performance of cloud computing has to be increased, and meanwhile, the concept of green cloud computing is also ascertained. The objective of the proposed work is to design a new scheduler, to maximize profit and minimize the environmental impacts. New heuristic algorithms for load balancing are also analyzed.

2 Literature Review

A research on green cloud computing substantiate improves the application of green computing in real-life parameters. Pinheiro et al. [7] introduced methodology for improvising the energy factor of data green grid terminology proposed parameters like data center efficiency (DCE) metrics [7] for enhancing energy efficiency. According to Wikipedia, the parameters define the efficient use of energy resources. In recent years, companies like Google achieved low level of DCE [8]. The value of DCE is 1.5 means energy consumption in 1 kWh and 0.5 Wh wasted like the process of cooling and other works. Pinheiro et al. [7] which illustrate that of the 22 measured, PUE values were obtained in the range of 1.3–3.0 [9]. QOS of the cloud system maintains high quality only when the energy utilization is minimal [10, 11]. Klienrock [12] an American scientist proposed the concept of computation utility in cloud computing. Garg and Buyya [13] have introduced the concept of framework for market-based resource utilization.

3 Problem Statement

Recent survey states that the carbon emission rate will increase nearly 20% by the end of 2020. Because of the utilization of data centers in the cloud computing framework, data center requires a huge amount of resources for providing a fast response to the client. So, the emission of carbon footprint is unavoidable too. Another report provided by Green ICT Standardization in India states that around 4% of GHG emission is from ICT sector. India also plans to reduce the GDP by 20–25% by the year 2020. The cloud technology reduces the carbon emission by reduced utilizations of energy resource. Recent research from CDP states that offsite server produces nearly 85.7 million metric tons of annual carbon emission.

So to reduce the carbon emission, implementing green computing in cloud is the only solution. To design data center on the basis of green computing, we can save billions of dollar through energy saving. To adopt high-performance computing with less utilization of energy resources is suitable for both firm and environment. At its initial step, Google designed their own server and data center for reducing energy usage and also for low emission profile.

There are numerous techniques proposed by the researchers to solve the issue of power consumption. But the solution for this issue is difficult to ascertain, because the amount of power consumed by the resource is purely proportional to the accuracy of the task. So, the technology needs a technique to satisfy the constraint of both provider and user. The table below shows the technique to solve the issue of power consumption, but the technique is not efficient. The comparative analyses are as follows (Fig. 1 and Table 1).

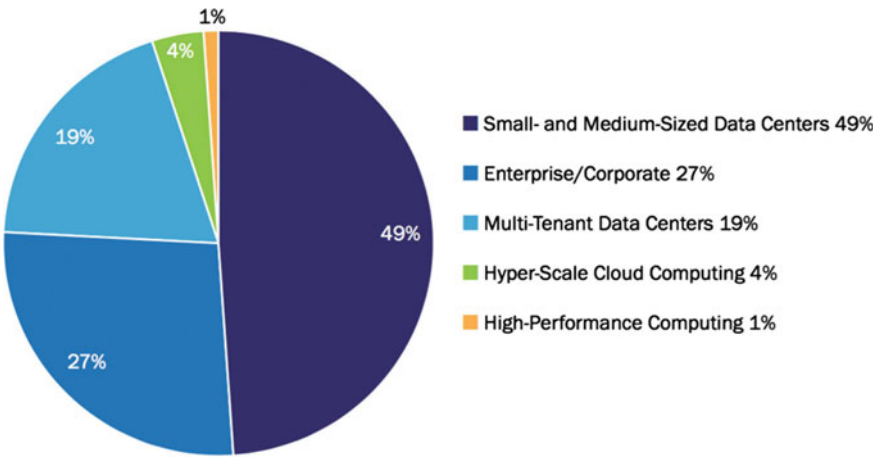

Fig. 1 Estimated US data center electricity consumption by market segment (2011)

Table 1 Different power reduction techniques in cloud

Title of paper	Reduction of power consumption technique used	Limitations
Energy-saving approaches for green cloud computing	Workloads and server allocation	Technique implements without virtualization
Energy aware cloud service provisioning approach for green computing environment	Proposed an energy model for allocation of server to the task	Scalability of the model is not efficient
Reduction of power consumption in cloud data centers via dynamic migration of virtual machines	Migration technique of virtual machine is implemented	Breaches of SLA are unlimited
Green computing: analyzing power consumption using local cooling	Software is implemented to analyze the energy consumption	It fully depends on software. Virtualization does not have a scope in this model
The strategic plan founded on the efficiency of using green computing techniques in data centers	Technique design to consolidate the resources	Implementation of the proposed technique is not ascertain

4 Proposed Framework

Resource allocation in cloud computing entirely varies from other scheduling techniques. Normally, the server shares the resources globally, but in the case of cloud computing, it shares resource to the nearest server.

In this paper, resource scheduling technique proposed is based on power consumptions. The proposed work is divided into two levels. In the first level, the scheduler algorithm receives the request from the user. Then, the task is forwarded into the carbon emission calculator.

These CO_2 emission calculators analyze the eco metrics and calculate the carbon footprint by the following equation

$$CO_2E = COE + SE \tag{1}$$

Another derivation CO_2Em is one, which is fixed for the limit of emission according to their productivity. This Co2E is compared with the CO_2Em to identify the emission rate. Emission rate is categorized as higher, normal and lower. If carbon emission calculator is satisfied, the constraint fixed by the organization is allowed to proceed with the deadline of the task.

Task deadline calculator analyzes by using the following equation

$$TDL = VMC - Atk \tag{2}$$

$$TDL = TL/VMC \tag{3}$$

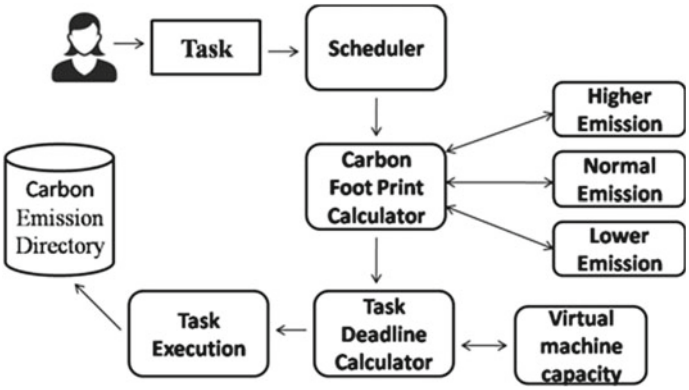

Fig. 2 Proposed framework for green HPC

After allocating task to the system, scheduler will check the factor whether it will satisfy the constraint or it moves on to the resource scheduling. If not, it will reallocate the task and also try to reduce the emission rate. Emission rate is the ultimate constraint, and at the same time it lays to focus on energy efficiency too (Fig. 2).

Algorithm 1: Pseudo code of scheduling algorithm

```
1. flag ← FALSE; VM^STATUS ← NULL;
2. For each tkin the host do
3. Calculate Co2E usingEq(1);
4. If Co2E > Co2Em , then
5. flag← FALSE; Higher
6. else if Co2E = Co2Em , then
7. Flag ←TRUE; then
8. Calculate TDL using Eq (2,3);
9. else flag ←TRUE ; then
10.   repeat 8;
11.   Select TDL with Minimum utilization of
   resources
12.   end
13. Update the allocation resulting of tk and
   remove it from queue.
```

The above algorithm is implemented based on many parameters as performance aware, energy aware and QOS aware. It has the peculiar technique to allocate the task resources. It is appropriate for the virtual machine in a distributed system and also provides simulation framework to compile all the particulars together. Its aim is to provide the optimal solution, to be both user friendly and environmental friendly.

5 Conclusion

The usage of cloud computing has increased vigorously, and at the same time environmental pollution has also increased. It is our duty to enjoy the ultimate growth of technology without disturbing the environment resources. So, this proposed technique ultimately achieves the objectives of reduction in carbon footprint by implementing the load balancing algorithm. Furthermost in the future, we will plan to implement a cloud simulator and also compare with various algorithms like FCFS or round-robin to know the accuracy of our proposed algorithm.

References

1. Fanara A (2007) Report to congress on server and data center efficiency public law 109-431. US, Environmental Protection Agency Energy star program, pp 133
2. Ambrust M, Fox A, Griffith R, Joseph A, Katz R, Konwinski A, Lee G, Patterson D, Rabkin A, Stocia I, Zaharia M (2009) Above the clouds: A Berkeley view of cloud computing. EECS Dept., University of California, Berkely, Technical report No., UCB/EECS
3. Kelenrock L (2005) A vision for the internet. ST J Res, 4–5
4. Belonglazov A et al (2010) Energy efficient allocation of virtual machine in cloud data center. In: International conference on cluster, cloud and grid computing, pp 577–578
5. Younge AJ et al (2010) Efficient resource management for cloud computing environments. In: International conference on green computing
6. Gartner (2007) Gartner estimates ICT industry accounts for @ percent of global carbon emission
7. Pinheiro E, Bianchini R, Carrera EV, Heath T (2003) Dynamic cluster reconfiguration for power and performance. In: Compilers and operating systems for low power, pp 75–93
8. Heo DH, Liu X, Abdelzaher T (eds) (2007) Integrating adaptive components: an emerging challenge in performance-adaptive systems and a server farm case-study. In: IEEE international conference of the real-time systems symposium (RTSS), pp 227–238
9. Chase JS, Anderson D, Thakar P, Vahdat A, Doyle R (2001) Managing energy and server resources in hosting centers. In: 8th ACM symposium on operating system principles, pp 103–116
10. Atrey A, Jain N, Iyengar N (2013) A study on green cloud computing. Int J Grid Distrib Comput
11. Kelenrock L (2005) A vision for the internet. ST J Res, pp 4–5
12. NRDC Issue Briefing (2014) America's data centers are wasting huge amounts of energy, IB:14-08-A. https://www.nrdc.org/sites/default/files/data-center-efficiency-assessment-IB.pdf
13. Garg SK, Buyya R (2012) Green cloud computing and environmental sustainability. IEEE Press Ebook, vol 1, no 3, pp 76–87
14. Cloudweaks (2013) Cloudweaks, the free research portal. http://research.cloudtweaks.com/technology/networking/cloud_computing

Comparative Study of Cepstral Editing and Unitary Sample Shifted Probability Distribution Function Method for Bearing Fault Diagnosis

Ankush C. Jahagirdar and Karunesh Kumar Gupta

Abstract This paper presents a comparative study of cepstral editing and unitary sample shifted probability distribution function method used for bearing fault diagnosis. Traditionally, different signal processing techniques are employed for this application. This study compares recent methods including cepstral editing and unitary sample shifted Laplacian window method. The superiority of these methods under different conditions and fault types is discussed based on the squared envelope spectrum (SES) feature and kurtosis. It is concluded from this study that use of cepstral pre-whitening (CPW) before the unitary sample shifted Laplacian window method significantly improves the performance for the diagnosis of ball faults.

Keywords Cepstral editing · Hilbert transform · Probability distribution function · Rolling element bearing

1 Introduction

1.1 A Subsection Sample

Machine condition monitoring is a classical problem, being attempted to be solved, using knowledge from various fields of science and engineering. Given the criticality of bearing health, many researchers are working on the diagnosis of bearing faults—inner race, outer race and ball faults—through analysis of vibration signals. Due to the interaction of various machine components, the vibration signal is often amplitude-modulated or frequency-modulated or both. It is also found to be non-stationary, mainly due to speed variations or deterioration of fault. Also, the presence of high-frequency components during the surface-to-surface impact of the faulty component is highly undesirable. Diagnosis of fault relies on bearing fault frequencies, which are specific to the geometry of the bearing and rotational speed.

A. C. Jahagirdar (✉) · K. K. Gupta
Birla Institute of Technology and Science, Pilani, Rajasthan, India
e-mail: ankush.chandrakant@pilani.bits-pilani.ac.in

V. K. Gupta et al. (eds.), *Reliability and Risk Assessment in Engineering*,
Lecture Notes in Mechanical Engineering,
https://doi.org/10.1007/978-981-15-3746-2_15

Various signal processing techniques are being explored to extract features which can faithfully represent the magnitude and type of bearing fault. A detailed analysis of different cepstral editing methods is discussed in [1]. As opposed to magnitude cepstral editing, phase editing is also being explored recently, as potentially a better fault diagnostic technique [2]. On the other hand, researchers are also trying an altogether different approach which relies on probability distribution function of the data samples for the inner race, outer race and ball defects [3]. Cepstral analysis is used by many authors as a tool of bearing fault diagnosis [4–8]. Randall [9] provides history of few such methods. Two of such important techniques—cepstral pre-whitening (CPW) [6] and automated cepstral editing procedure (ACEP) [10]—act as signal pre-processing and try to improve the diagnostic performance by removing the harmonic noise in the signal.

2 Theory

2.1 Cepstral Editing

Bearing signal is often corrupted by harmonic noise, for instance from a fan nearby. Cepstral editing provides an efficient way to remove such noise. Cepstrum of a signal, which is defined as inverse Fourier transform (IFFT) of log spectrum of the signal, concentrates all the harmonics of one fundamental frequency in a signal peak in the cepstrum domain. Liftering out such a peak in the cepstrum domain ensures filtering of all the corresponding harmonics from the signal, thus reducing the interference of other machine components.

Simplest method of cepstral editing is cepstral pre-whitening [6]. It makes entire real magnitude cepstrum equal to zero. Though computationally less demanding, it is blunt way of signal pre-processing. Automated cepstral editing procedure (ACEP) is modification of cepstral pre-whitening, in which only selected peaks are liftered out [10]. ACEP is an automated procedure of fault detection and consists of various steps including long-pass liftering, wavelet denoising, thresholding and comb liftering.

2.2 Unitary Sample Shifted PDF

The method of unitary sample shifted, probability distribution function is based on observing the probability distribution function (PDF) of the data samples obtained from bearing vibration signal [3]. One of the important observations of this paper is that the PDF changes significantly based on number of samples and bit-by-bit shift over the entire data. Impacts of inner race and outer race faults are found to follow Laplacian distribution, whereas ball faults are observed to follow normal distribution.

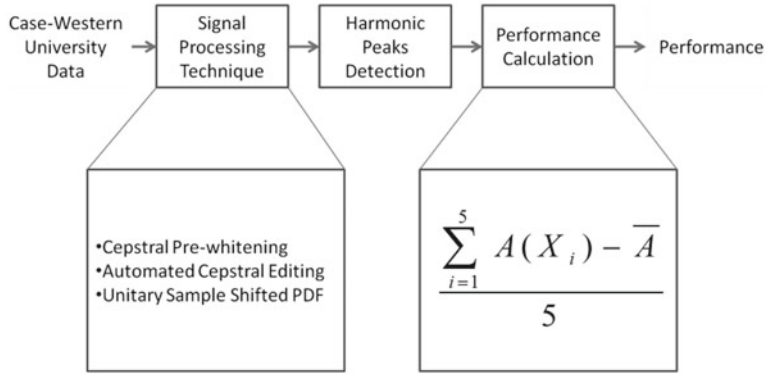

Fig. 1 Methodology

Taking this hint, [3] uses Laplacian window and sweeps it over the data bit-by-bit to extract maximum fault information from the signal. Three features are used to generate new time-domain signals—frame-based crest factor, frame-based kurtosis and frame-based energy—which are later analyzed by taking Fourier transform.

3 Methodology

The methodology adapted for this study is depicted in Fig. 1. This study uses Case Western Reserve University (CWRU) bearing data available online [11]. All the computations are carried out using MATLAB®. The signal processing technique block shown in the figure includes signal pre-processing methods under study and Fourier transform. Hilbert transform is also used for envelope detection after CPW and ACEP steps. Harmonic peak detection is a step in which magnitudes of first five fault harmonics are calculated, which are later used in performance calculation. The methods are compared based on squared envelope spectrum (SES) feature, which is nothing but average deviation of first five fault harmonics from spectrum average.

4 Results

Figure 2 shows the simulation results for comparison of cepstral editing and unitary sample shifted PDF for inner race, outer race and ball faults based on SES feature, whereas Fig. 3 shows the comparison based on kurtosis values.

The ACEP method implemented for this study takes 3 s cut-off for long-pass liftering in the cepstrum domain. The denoising method used is wavelet denoising with ‘db3’ wavelets, whereas unitary sample shifted probability distribution method considers a boundary of [−3, 3] for Laplacian window and frame-based kurtosis

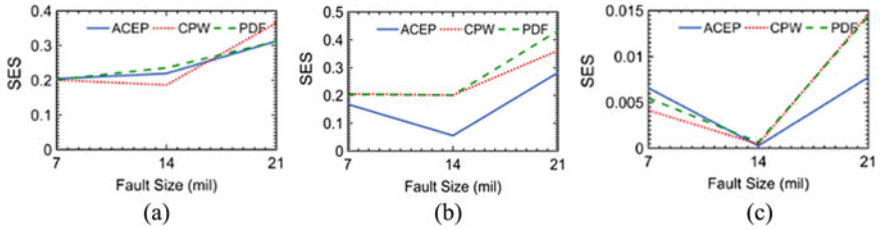

Fig. 2 SES-based comparison for **a** inner race fault, **b** outer race fault and **c** ball fault

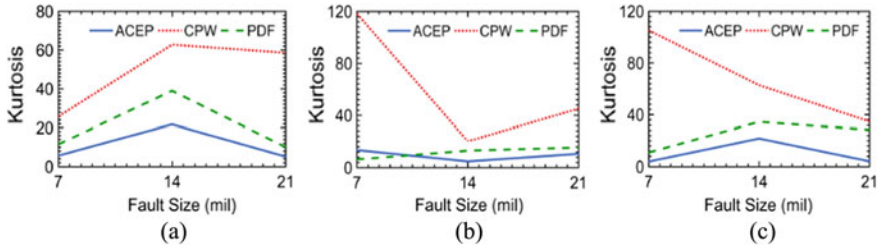

Fig. 3 Kurtosis-based comparison for **a** inner race fault, **b** outer race fault and **c** ball fault

signal for Fourier analysis. Some of the important observations of this comparison are cepstral pre-whitening (CPW) is computationally very less demanding but performs better both based on SES feature as well as kurtosis and in all fault types. CPW significantly improves kurtosis values for all three fault types—inner race, outer race, ball—and for all three fault sizes—7, 14 and 21 mil. Squared envelope spectrum (SES) feature value is significantly less for ball faults. From the definition of the feature, this clearly means that magnitude of first five harmonics of the ball fault frequencies is very less, almost close to the spectrum average. Thus, ball faults are difficult to detect.

With these observations in mind, performance of cepstral pre-whitened and unitary sample shifted PDF filtered (CPW–PDF) method is investigated below.

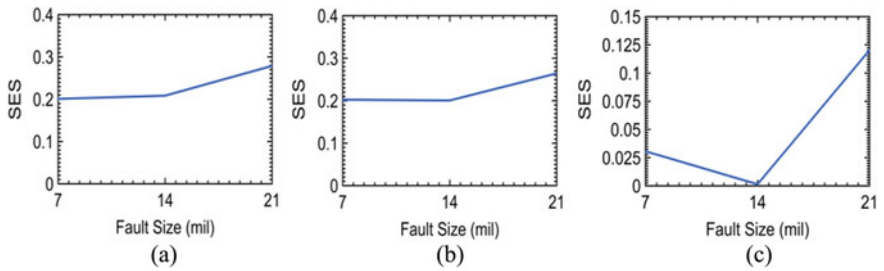

Fig. 4 SES-based performance of CPW–PDF method for **a** Inner race fault, **b** Outer race fault and **c** Ball fault

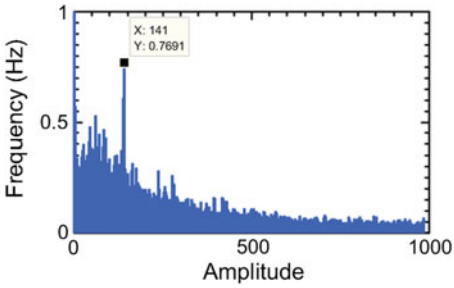

Fig. 5 Spectrum of vibration signal modified after CPW–PDF (Drive end bearing, 12,000 samples/s, ball fault, 21 mil)

Figure 4 clearly shows that though the SES values for 21 mil inner race and outer race faults are less than CPW of PDF alone, there is significant improvement in the SES values for the ball fault. This improvement is more visible in the spectrum, as shown in Fig. 5. It can be clearly seen that the 1X which fault frequency corresponds to 141 Hz for ball fault has a significant peak.

5 Conclusion

This paper compares two important signal pre-processing techniques for bearing fault diagnosis—cepstral editing and unitary sample shifted probability distributed function. The methods are compared primarily based on the squared envelope spectrum (SES) feature. Performance of these methods based on kurtosis values is also investigated. As cepstral pre-whitening is computationally less demanding and performs better on kurtosis scale, it was used before the PDF method to try and improve the performance. Obtained results show significant improvement in the diagnosis of ball faults, especially 21 mil fault. However, the performance of CPW–PDF is to be further investigated under different conditions.

References

1. Peeters C, Guillaume P, Helsen J (2017) A comparison of cepstral editing methods as signal pre-processing techniques for vibration-based bearing fault detection. Mech Syst Signal Process 91:354–381
2. Barbini L, Ompusunggu AP, Hillis AJ, du Bois JL, Bartic A (2017) Phase editing as a signal pre-processing step for automated bearing fault detection. Mech Syst Signal Process 91:407–421
3. Mohanty S, Gupta KK, Raju KS (2017) Effect of unitary sample shifted laplacian and rectangular distributions in bearing fault identifications of induction motor. IET Sci Meas Technol 11(4):516–524
4. El Morsy M, Achtenova G (2015) Rolling bearing fault diagnosis techniques—autocorrelation and cepstrum analyses. In: Proceedings of 23th mediterranean conference on control and automation (MED), Torremolinos, Spain, pp 328–334

5. Salah M, Bacha K, Chaari A (2014) Cepstral analysis of the stator current for monitoring mechanical unbalance in squirrel cage motors. In: Proceedings of first international conference on green energy ICGE, Sfax, Tunisia, 290–295
6. Borghesani P, Pennacchi P, Randall RB, Sawalhi N, Ricci R (2013) Application of cepstrum pre-whitening for the diagnosis of bearing faults under variable speed conditions. Mech Syst Signal Process 36(2):370–384
7. Hwang YR, Jen KK, Shen YT (2009) Application of cepstrum and neural network to bearing fault detection. J Mech Sci Technol 23(10):2730–2737
8. Li H, Ai S (2009) Application of order bi-cepstrum to gearbox fault detection. In: Proceedings of international conference on measuring technology and mechatronics automation, ICMTMA, Zhangjiajie, Hunan, China, pp 590–593
9. Randall RB (2017) A history of cepstrum analysis and its application to mechanical problems. Mech Syst Signal Process 97:3–19
10. Ompusunggu AP (2015) Automated cepstral editing procedure (ACEP) as a signal pre-processing in vibration-based bearing fault diagnostics. In: Proceeding of international conference of surveillance, France, pp 1–11
11. Loparo KA, Bearings vibration data set. Case Western Reserve University [Online Available] http://csegroups.case.edu/bearingdatacenter/pages/12k-drive-end-bearing-fault-data

Study of Emission Pattern of ICs Using Photon Emission Microscopy

Rashmi Lalwani, Arihant Jain, V. K. Tapas, N. S. Joshi, and P. V. Varde

Abstract Photon emission microscopy (PEM) acts as a useful tool for defect localization in integrated circuits (ICs). It detects very low-level photon emissions generated as a result of an electroluminescence process. The emission pattern of a faulty IC can be compared to that of a healthy one to get an idea about fault location. This requires a database of emission patterns corresponding to healthy ICs. The objective of the current work is to generate a database of emission patterns of healthy ICs that can further be used to compare and study the emission patterns obtained from faulty IC. The database is generated for four ICs that include NPN transistors IC, quad 2-input NOR gate, digital-to-analog convertor and non-inverting buffer. Photon emission microscope is used to obtain the emission image which is then overlaid on the optical image to obtain a realistic image of emission patterns. The image obtained in this manner acts as the signature for comparing faulty IC with healthy one. This paper presents the emission pattern of various ICs.

Keywords Photon emission microscopy · Emission pattern · Fault localization · Fault identification

R. Lalwani
Manipal University Jaipur, Jaipur, Rajasthan 303007, India
e-mail: rashmilalwani567@gmail.com

A. Jain (✉) · V. K. Tapas · N. S. Joshi · P. V. Varde
Research Reactor Services Division, Reactor Group, Bhabha Atomic Research Centre, Trombay, India
e-mail: arihantj@barc.gov.in

V. K. Tapas
e-mail: vktapas@barc.gov.in

N. S. Joshi
e-mail: nsjoshi@barc.gov.in

P. V. Varde
e-mail: varde@barc.gov.in

V. K. Gupta et al. (eds.), *Reliability and Risk Assessment in Engineering*,
Lecture Notes in Mechanical Engineering,
https://doi.org/10.1007/978-981-15-3746-2_16

1 Introduction

The advances made in semiconductor technology and manufacturing have enabled the manufacture of integrated circuits (ICs) having very large numbers of devices on the die. During the mid-1970s to mid-1980s, significant advances in the field of silicon technology [1] took the industry from large-scale integration (LSI) with 2^{11}–2^{16} devices on a die to very large-scale integration (VLSI) with 2^{16}–2^{21} devices on a die [2]. Industry is now moving forward to ultra-large-scale integration (ULSI) and gigantic-scale integration (GSI) with over 2^{26} devices per chip. Increasing number of devices is causing great challenges to the physical analysis of components when a failure occurs. Fault localization and failure identification of defects in complex ICs are becoming more difficult with time. Emergence of flip-flop packaging has further complicated the job by making front-side analysis of the circuit almost impossible without removing the chip bounds physically.

Photon emission microscopy (PEM) attempts to address the difficulties in fault localization. PEM uses photon wavelengths in the infrared (IR) and near-infrared regions exploiting transparency of such wavelengths to silicon. It can be used for defect localization and defect characterization in ICs. It is mainly applicable for defects that exhibit leakage of electrical current. Emission patterns of some ICs are presented by Nath et al. [3]. This work is in continuation of the work presented in [3] with an objective to prepare a database of emission pattern of various ICs that can be used for fault localization and characterization.

Emission patterns of four ICs have been observed in this work using INSCOPE labs PEM 1200 for emission detection. The emission patterns observed are discussed in Sect. 2 of the paper. The conclusion inferred from the work and future scope are discussed in Sect. 3 and 4, respectively.

2 Emission Patterns of Tested Integrated Circuit (IC)

Four different ICs were tested in this work. The ICs were biased in line with the specifications mentioned in the respective datasheets. The four ICs tested are:

- CA2083—NPN transistor
- MC14001BCP—2-input NOR gate
- AM1408L8—Digital-to-analog convertor
- 4050BDM—Non-inverting buffer

The detailed observations are presented in this section. A brief description of each IC is presented followed by details about the electrical biasing conditions. Emission spectrum of the IC for each biasing is then presented followed by a discussion on observations.

2.1 CA2083—NPN Transistors

The CA3083 is a versatile array of five high-current NPN transistors on a common monolithic substrate. Independent connections for each transistor plus a separate terminal for the substrate permit maximum flexibility in circuit design [4]. Pinout diagram is shown in Fig. 1. There are five independent transistors on the IC. The transistor marked in Fig. 1 (Q1) is biased for experimentation.

NPN transistor can operate in two regions, i.e., saturation region and cutoff region. In saturation region, the base-emitter and base-collector junctions are forward biased, while in cutoff region, the two junctions are reverse biased. Base, emitter and collector of a typical transistor on CA3083 are shown in Fig. 2.

2.1.1 Saturation Region

NPN transistor will operate in saturation region if:

- Base-emitter and Base-collector junctions are forward biased.
- $V_{BE} > 0$ and $V_{BC} > 0$.
- $V_{BE} > V_{th}$ (Threshold Voltage), V_{th} is reported as 0.64 V in datasheet.

Pin configuration is:

- Pin 16 (Base): 0.7 V
- Pin 1 (Collector): 0 V
- Pin 15 (Emitter): 0 V

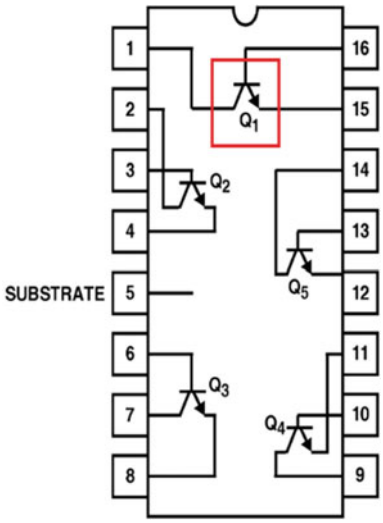

Fig. 1 Pin out diagram of CA3083. Q1 is biased for experimentation

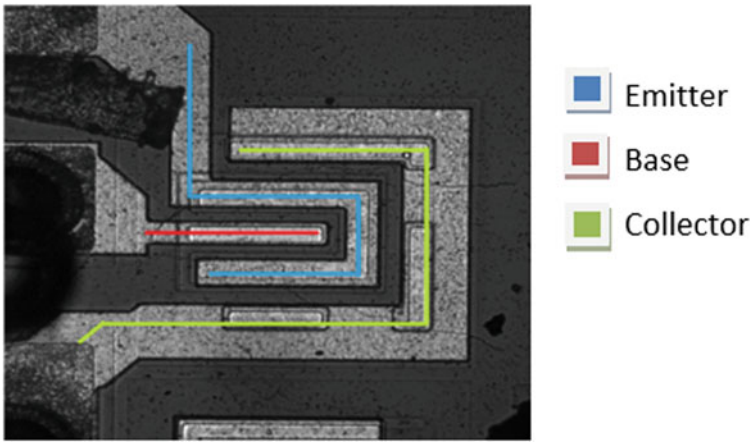

Fig. 2 A typical transistor present on CA3083

The relative intensity of photons emitting from the circuit is represented by false-color image with red signifying maximum photon intensity. The emission pattern for saturation region is shown in Fig. 3.

The emission pattern shows the flow of the current through base-emitter and base-collector junction.

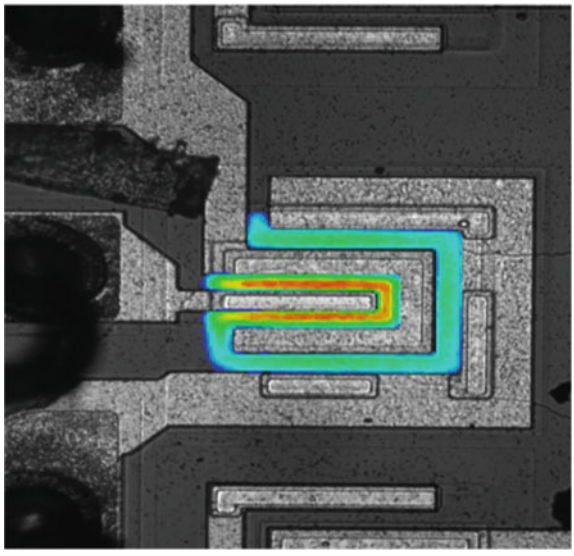

Fig. 3 Emission pattern for NPN transistor operating in saturation region

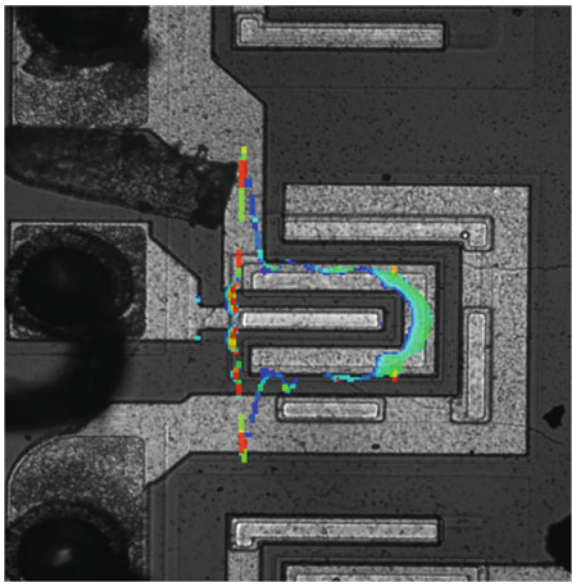

Fig. 4 Emission pattern for NPN transistor operating in cutoff region

2.1.2 Cutoff Region

NPN transistor will operate in cutoff region if:

- Base-emitter and Base-collector junctions are reverse biased.
- $V_{BE} < 0$ and $V_{BC} < 0$.
- $V_{BE} >$ reverse breakdown voltage. Base-emitter breakdown voltage is reported as 6.9 V in datasheet.

Pin configuration is:

- Pin 16 (Base): 0 V
- Pin 1 (Collector): 7.5 V
- Pin 15 (Emitter): 7.5 V

The emission pattern for cutoff region is shown in Fig. 4.

2.1.3 Observations

One NPN transistor on CA3083 IC is biased in two regions, i.e., saturation region and cutoff region. Emission pattern is observed in saturation region when base-emitter (V_{BE}) voltage greater than threshold voltage (0.64 V) is applied. Emission pattern shows that the current flow is established at base-emitter and base-collector junction. In cutoff region, $V_{BE} > 6.9$ V reverse-biased voltage gives an emission pattern. The current flow is established at base-emitter junction due to reverse breakdown.

2.2 MC14001BCP—2 Input NOR Gate

MC14001BCP is an IC having four 2-input NOR gates. The logic gates are constructed with P- and N-Channel enhancement mode devices in a single monolithic structure (complementary MOS) [5]. Pinout diagram is shown in Fig. 5. The NOR gate marked in Fig. 5 with inputs A1 and B1 and output Q1 is biased for the study.

Two cases are considered in the study. In the first case, the inputs are high (logic 1) resulting in low output (logic 0). In the second case, the inputs are low resulting in high output.

2.2.1 Case 1—Inputs at 5 V

The inputs applied to the IC are:

- Pin 1 (A1): 5 V
- Pin 2 (B1): 5 V
- Pin 7 (V_{ss}): 0 V
- Pin 14 (V_{dd}): 5 V

Output of NOR gate is observed at Pin 3 (Q1). The output in this case is low (0 V). No photon emission is observed for this case.

2.2.2 Case 2—Inputs at 0 V

The inputs applied to the IC are:

- Pin 1 (A1): 0 V
- Pin 2 (B1): 0 V

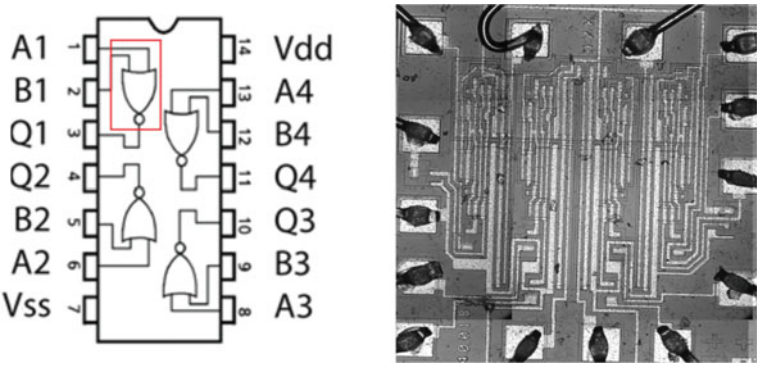

Fig. 5 Pinout diagram for MC14001BCP (left). The marked NOR gate is biased for experiment. Optical image of the IC is shown in right image

- Pin 7 (V_{ss}): 0 V
- Pin 14 (V_{dd}): 5 V

Output of NOR gate is observed at Pin 3 (Q1). The output in this case is low (5 V). This case also did not generate any detectable photon emission from the IC. In order to initiate a flow of current through the IC, a resistor is connected between Q1 and GND (V_{ss}). The current flow is detected through the IC, but still, no photon emission is generated.

2.2.3 Observations

MC14001BCP IC has four 2-input NOR gates. One NOR gate is biased for this experiment. The two inputs (A1 and B1) are kept high for case 1 and low for case 1, respectively. Expected outputs are observed on output pin (Q1). None of the two cases generate any detectable photon emission in the IC. Even when the current flow exists though the IC, emission is not observed. It can be concluded that MC14001BCP does not generate any detectable photon emission when working properly.

2.3 AM1408L8—Digital-to-Analog Convertor

AM1408L8 is an 8-bit monolithic multiplying digital-to-analog convertor consisting of a reference current amplifier, an R-2R ladder and eight high-speed current switches [6]. R-2R ladder divides the reference current into eight binary-related components which are fed to the switches. It is used in many applications like waveform synthesizers, digitally programmable gain, CRT character generation, etc. (Fig. 6).

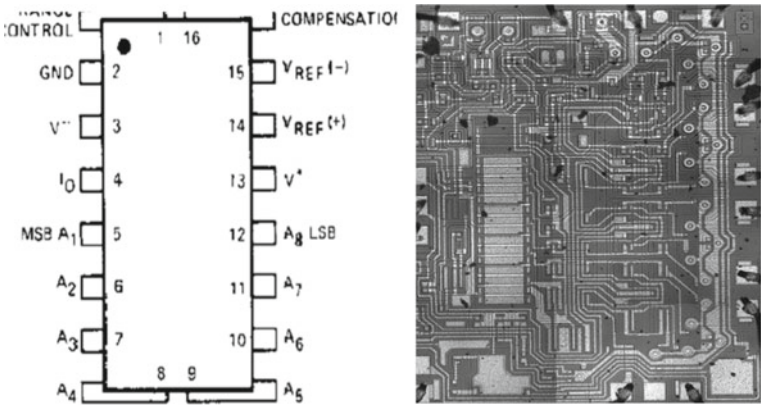

Fig. 6 Pinout diagram of AM1408L8 DAC (left). Optical image of IC is shown on right

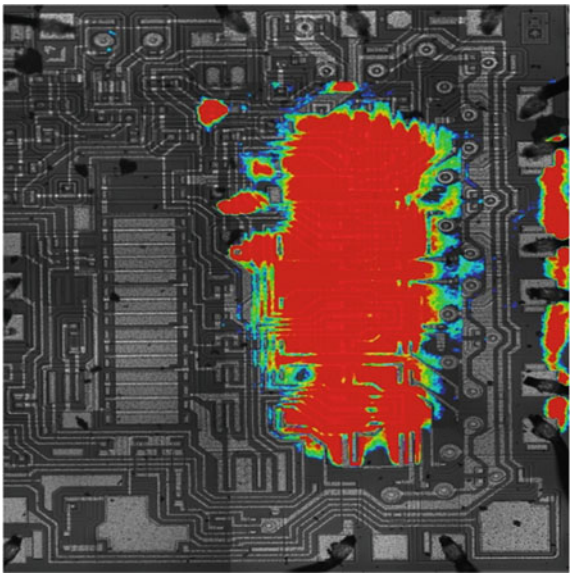

Fig. 7 Emission pattern observed in AM1408L8 IC

2.3.1 Experiment

Pins 5–12 serve as digital inputs to the IC, while Pin 4 gives analog output. For the study, Pin 5 (most significant bit) is provided high input (5 V), while the other input pins are kept low. The binary input provided corresponds to 10000000 binary logic. Pin configuration is:

- Pin 2 (GND): 0 V
- Pin 3 (V−): 0 V
- Pin 5 (A1): 5 V
- Pins 6–12: 0 V
- Pin 13 (V+): 5 V
- Pin 14 ($V_{\text{ref+}}$): 5 V
- Pin 15 ($V_{\text{ref}-}$): 0 V

Emission pattern observed is shown in Fig. 7. Very high intensity of photon emission was observed from the IC. This does not indicate failure as the IC was working properly (indicated by output measurement).

2.3.2 Observations

AM1408L8 is an 8-bit digital-to-analog convertor. Input binary logic of 10000000 is applied to the IC. Logically, correct analog output is observed at Pin 4 indicating healthiness of the IC. Emission pattern observed shows very high intensity of photon being emitted from the IC as shown in Fig. 7.

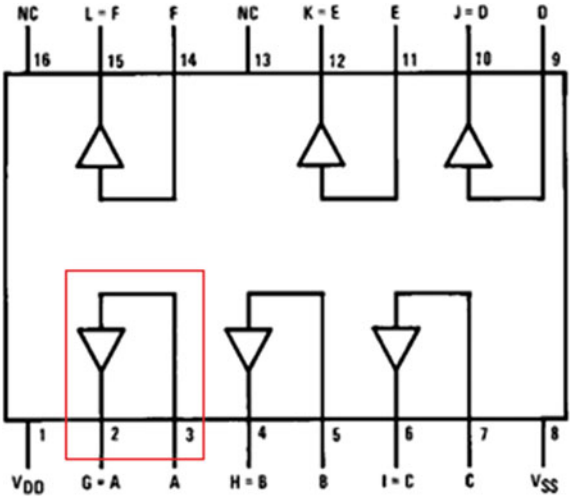

Fig. 8 Pinout diagram of 4050BDM IC. The marked buffer is used for study

2.4 4050BDM—Non-inverting Buffers

4050BDM (hex non-inverting buffers) is monolithic complimentary MOS (CMOS) integrated circuit constructed with N- and P-channel enhancement mode transistors. It features logic level conversion using only one supply voltage (V_{dd}) [7]. Pinout diagram of the IC is shown in Fig. 8. The buffer marked in Fig. 8 is considered for the study.

2.4.1 Experiment

Pins 3, 5, 7, 9, 11, 14 (A, B, C, D, E, F) are used as inputs while Pins 2, 4, 6, 10, 12, 15 (G, H, I, J, K, L) are output pins. For this study, only one buffer with input at Pin 3 (A) and output at Pin 2 (G) is used. The pin configuration is:

- Pin 8 (V_{ss}): 0 V
- Pin 1 (V_{dd}): 5 V
- Pin 3 (Input of buffer A): 5 V

The emission pattern observed is shown in Fig. 9. Localized photon emission is observed from buffer A. Similar emission is observed when input is applied to other buffers with emission location shifting accordingly.

2.4.2 Observations

4050BDM has six buffers and features logic level conversion using only one supply voltage (V_{dd}). For the study, input is applied at Pin 3 and output is observed at Pin

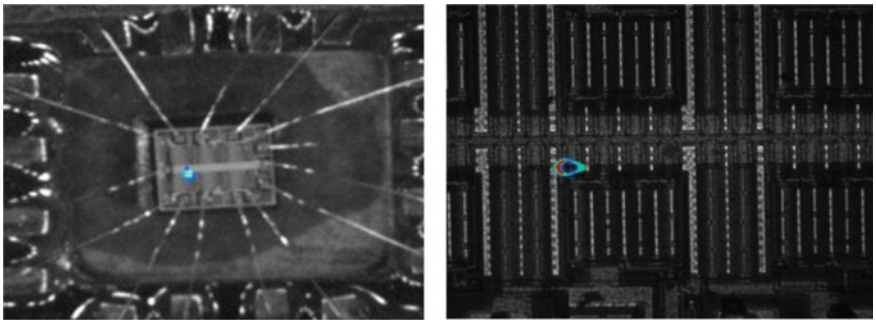

Fig. 9 Emission pattern observed for 4050BDM when input is applied to buffer A. 1× image which is shown on left and 20× image on right

2. Localized photon emission is observed from the IC as shown in Fig. 9. Similar emission pattern is observed when other buffers are biased. Emission location shifts according to the buffer being used.

3 Conclusion

The spectroscopic mode of the photon emission microscope offers capability for failure identification using the photon spectrum as a defect fingerprint or defect signature. Experiments are performed on four ICs, and the emission patterns are observed under specified biasing conditions. Photon emission from CA2083 NPN transistor shows the flow of current in the transistor under forward- and reverse-biased conditions. No emission is observed in MC14001BCP NOR gate. Very high-intensity photon emission is observed from AM1408L8 DAC which spreads over a wide area, while localized emission is observed in 4050BDM non-inverting buffer.

4 Future Scope

Photon emission microscopy is very useful technique for fault identification and characterization. A reference database is being prepared so that emission patterns of faulty ICs can be compared with that of healthy ones. Experiments need to be performed to expand the database further. Emission patterns of known faults should also be included in the database to aid in fault identification and characterization.

References

1. Fair R (1990) Challenges to manufacturing submicron, ultra-large scale integrated circuits. Proc IEEE 78(11):1687
2. Reisman A (1983) Device, circuit and technology scaling to micron and submicron dimensions. Proc IEEE 71(5):550
3. Nath D, Jain A, Tapas V, Joshi N, Varde P (2020) A study on emission pattern of semiconductor ICs using photon emission microscopy. In: Varde P, Prakash R, Vinod G (eds) Reliability, safety and hazard assessment for risk-based technologies
4. Renesas, 15 December 2011 (Online). Available: https://www.intersil.com/content/dam/Intersil/documents/ca-3/ca-3083.pdf
5. Motorola (Online). Available: http://pdf1.alldatasheet.com/datasheet-pdf/view/90052/MOTOROLA/MC14001BCP.html
6. Advanced Micro Devices (Online). Available: https://www.digchip.com/datasheets/parts/datasheet/013/AM1408L8-pdf.php
7. Fairchild Semiconductors Corporations, October 1987. (Online). Available: http://www.datasheetlib.com/datasheet/1249318/4050bdm_fairchild-semiconductor.html

Diagnosis and Prognosis of Mechanical Systems

Effect of Lubricant on the Stiffness and Damping Characteristics in a Single-Stage Gearbox: A Theoretical Analysis

Vikas Sharma and Anand Parey

Abstract Gearbox is the most used mechanism to transmit the energy positively. Ignorance of any localized faults like crack, pitting, spalling, scuffing and wear could be responsible for the occurrence of any catastrophe. The odd operating conditions of a gearbox result in the initiation of the aforementioned faults. Such faults and operating conditions influence both noise and vibration levels. This article describes the role of lubricant in the gearbox. In this article, a theoretical model and a finite element method (FEM) have been presented to exhibit the characteristics of lubricant. The variation in the stiffness between the gears with and without lubricant has been evaluated using FEM. The results of simulation studies discussed and it has been found that the thickness of lubricant film affects both stress distribution and the mesh stiffness of the gear pair.

Keywords Finite element method · Gearbox faults · Lubricant · Stiffness · Vibrations

1 Introduction

Ignorance of the incipient fault and the possible reason for its cause could lead to the failure of a gearbox of a machine. Literature reports that such failures could be as dreadful as a catastrophe [1, 2]. A lubricant film plays a vital role in between the contact surfaces of any rotating machine elements such as bearings and gearboxes. No, or inadequate, lubrication causes high amount of wear which leads to degradation of components and the entire system could fail. It has been reported that failures in heavy machineries were due to lubrication problems [3]. Monitoring of lubricating

V. Sharma (✉)
Department of Mechanical Mechatronics Engineering, The LNM Institute of Information Technology, Jaipur, India
e-mail: s.vikasiiti@gmail.com

A. Parey
Department of Mechanical Engineering, Indian Institute of Technology Indore, Indore, India
e-mail: anandp@iiti.ac.in

V. K. Gupta et al. (eds.), *Reliability and Risk Assessment in Engineering*,
Lecture Notes in Mechanical Engineering,
https://doi.org/10.1007/978-981-15-3746-2_17

systems and lubricants in a gearbox could prevent breakdown/failures of machines and preventive measures could be suggested timely [4].

Lubricant in a gearbox is essential in maintaining efficient and effective operations under harsh speed and load conditions [5]. Lubricant damps the noise generated by the gear mesh. Harsh operating conditions due to variation in speed and load provoke gear tooth failures such as pitting, scuffing and wear. Gearbox vibration signals are dependent on gear mesh stiffness and if a fault in gear tooth initiates the mesh stiffness changes. As a result of change in gear mesh stiffness due to gear fault, the vibration signals of the gearbox change. This change in gearbox vibration signal highlights the fault occurred. In other words, reduction in gear mesh stiffness and severity of damage can be assessed by evaluating the same using vibration-based signals. Lubricating oils reduce wear and friction at these contact surfaces and separate them by maintaining proper lubrication and ensuring wear-less operation to avoid failures. Lube oil also affects gearbox behaviour in terms of vibration generated, heat absorbed and power characteristics [6]. Therefore, continuous monitoring of changes in lubricant properties could prove to be vital in avoiding propagation of defects within machines [7] and by preventing unexpected breakdowns.

Studies show that churning and splashing of lubricant in between the mating surfaces considerably affect the behaviour and performance of gearbox [8]. Churning of oil causes significant power losses in the gearbox and the losses due to churning increase with increasing viscosity at low speeds; however, these losses decrease at higher speeds [9, 10]. Further, due to internal friction in the lube oil, layers decrease with rise in temperature [11]. Further, an increase in temperature increases chemical activities, formation of tribological layers and decrease in oil film thickness.

Gear mesh stiffness is one of the fundamental parameters in the physics of gear. It further helps in determination and load-carrying capacity of gears, dynamic tooth loads and vibration characteristics of geared systems. If the meshing surfaces of gear and pinion tooth contain a surface fault, then there will be a loss in tooth contact. Due to the loss of contact, stiffness will reduce gradually, and as a result, vibration signal will change. Particularly, due to the absence/minimal thickness of lubricating film, surface faults/error appears in the original involute profile of gear. Due to gear tooth faults, a change in gear mesh stiffness and occurrence of impulses have been observed in between meshing gears, which have lost the original involute profile, thus leading to change the vibration levels of the system [12].

For gearbox vibration analysis, most of the researchers have discussed that time-varying gear mesh stiffness is one of the important parameters that affect the vibration response of the gearbox [13–15]. A reduction in gear tooth stiffness with an increase in teeth wear shows a linear relationship with wear severity. Further, increase in the vibration levels occurs due to reduction in oil film thickness between the meshing surfaces due to reduced damping effect [16].

The literature presents the studies considering gears under static conditions only; thus, the stiffness has been evaluated without considering the lubrication. However, in the present manuscript, this gap has been attempted to address. Further, the effect of no or less lubrication on the gear vibration can be understood from the results obtained. In the above-mentioned literature, the gear mesh stiffness

is calculated without considering the characteristics of lubricant. However, in the practical environment, there is always a lubricating film in between a gear mesh pair and its role cannot be neglected while deriving the equivalent gear mesh stiffness of a gear pair. An attempt to exhibit the effect of lubricating film on the gear mesh stiffness has been addressed in the present manuscript. In this study, the theoretical model for evaluating gear mesh stiffness is presented. A simulation study has been performed to illustrate the effect of lubrication on gear mesh stiffness.

2 Gear Mesh Stiffness of a Single-Stage Spur Gear Pair

In the present study, single-tooth contact pair of gear system is investigated. In a single pair, two teeth are meshed and share equal force. In case of single-tooth contact pair, the gear mesh stiffness consists of the tooth stiffness of gear 1 (gear) and gear 2 (pinion). The gear mesh stiffness expression is considered by many researchers to study the gear defects such as crack, pitting and spall is given by [13, 17–19]:

$$\frac{1}{K_{\mathrm{m}}} = \frac{1}{k_{\mathrm{p}}} + \frac{1}{k_{\mathrm{g}}} \tag{1}$$

where k_{p} is the tooth stiffness of pinion, k_{g} is the tooth stiffness of gear and K_{m} is gear mesh stiffness.

But, for the real circumstances, a stiffness component of lubricant film will also be added to Eq. (1) as suggested by Yuan et al. [20]. Figure 1 presents the model of an actual gear pair. The equivalent gear mesh stiffness of the gear pair in mesh with lubrication can be denoted by K_{e} which can be express as:

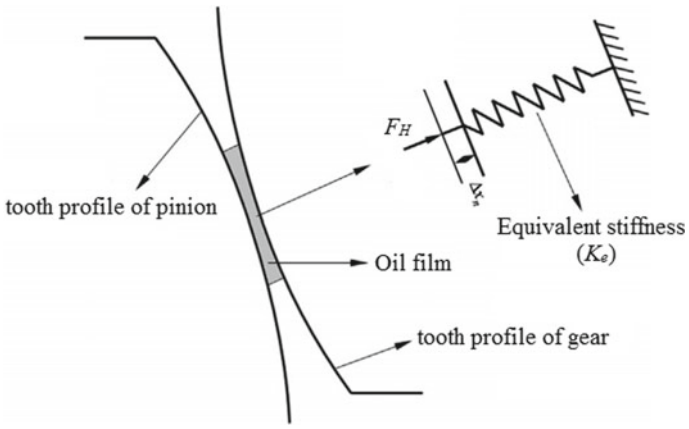

Fig. 1 Model of spring stiffness of a gear pair

$$\frac{1}{K_e} = \frac{1}{K_m} + \frac{1}{K_l} \tag{2}$$

where K_l is lubricant film stiffness, described as $K_l = \partial F_H / \partial h_c$, where F_H is the hydrodynamic force or the contact mesh force and h_c is the thickness of the lubricating film between the two meshing surfaces. K_m is the gear mesh stiffness of gear pair without lubrication, which is evaluated as $K_m = k_p k_g / (k_p + k_g)$.

Further, the damping of lubricant film plays a crucial role in gear dynamics. The critical viscous damping ratio ζ is inversely proportional to gear mesh stiffness and can be expressed as [21]:

$$\zeta = \frac{c}{2\sqrt{K_m m_e}} \tag{3}$$

where c is the damping coefficient of viscous lubricant and m_e is the gear pair's equivalent mass. It can be observed from Eq. (3) that the damping ratio is inversely proportional to the stiffness. Also, the damping ratio is dependent on the excitation frequency ω. Nevertheless, viscous damping also depends on the physical parameters of the gear-lubricant system, viz. tooth profile and geometry, sliding velocity of teeth as well as the tooth meshing force. The contact mesh force FH will act on a gear pair as [21]:

$$F_H = F_k + F_c \tag{4}$$

where F_k is the amount of force disbursed to stiffness components and F_c towards the damping effect.

In a gear mesh during teeth contact, the oil squeeze action between the gear teeth controls the damping behaviour of lubricant [21]; parameters such as the viscosity of lubricant, temperature of lubricant as well as the velocity of the gear pair play a significant role. It has been observed that for a given temperature, the damping ratio (lubricant viscous damping capacity) increases with higher operating speed. A decrease in the minimum film thickness leads to augmentation of the dissipative energy and severe teeth vibro-impacts.

3 Discussion of Simulation Studies of a Single-Stage Gear Pair

The major parameters of gear pair and lubricant used in the simulation studies are given in Table 1. In the present article, two simulation studies have been carried out to study the behaviour of lubricant. First one is the finite element method-based simulation study that has been performed to highlight the stress distribution under the effect of lubricated film. The second one is the MATLAB simulation of numerical expressions to exhibit the behaviour of mesh stiffness under the effect of lubrication.

Table 1 Gear geometry and lubricant parameters

Parameters related to gear pair		Parameters related to lubrication	
Young's Modulus (E)	206.8 GPa	Damping ratio (ζ)	0.17
Poisson's ratio (ν)	0.3	Viscosity at ambient pressure (η_0)	0.08 Pa s
Pressure angle (φ)	20°	Density at ambient pressure (ρ_0)	870 kg/m^3
Face width (B)	16 mm	Pressure–viscosity component (α_0)	2.2×10^{-8} Pa^{-1}
Tooth number (Z_p/Z_g)	32/81	Ambient temperature (T_0)	30 °C
Module (m)	2 mm		
Material density (ρ)	7800 kg/m^3		

3.1 Finite Element Method

A three-dimensional model of spur gears with involute tooth profile has been adopted to analyze the effect of stress distribution with and without lubrication. The film of lubrication in between the gear tooth meshing surfaces has been treated as mass-less spring-damper link. The finite element modelling of gear pair with lubricating film has been performed in Ansys. The FEM-based model of spur gear has been analyzed from engagement to disengagement point. The main parameters of spur gears used for finite element modelling are shown in Table 1. Figure 2 shows the FEM-based model of gear and pinion. The contact regions of pinion and gear wheel are fine meshed than the remaining body of the gears. The internal diameter of gear wheel is fixed and internal diameter of pinion is supported by frictionless support. The moment of 19.8 Nm is applied on pinion. The deflections along the y-axis and x-axis are obtained using FEM. In Fig. 2, only mesh position is shown; however, the other mesh positions from engagement to disengagement are modelled and applied same procedure at each position.

Figure 3 shows the Von-Mises stresses developed at the contact of the gear mesh for both the conditions, i.e. with lubrication and without lubrication. For the case of without lubrication, the maximum value of stress is 1.229 GPa, whereas for the case of with lubrication, the value of maximum stress 1.18 GPa. On comparing the stress distribution at the gear mesh point, it has been observed that the lubricant bears 49 MPa of stress. It is worth noting that the distribution of the stresses for both the cases remains more or less same. A possible reason behind this behaviour could be because of the simulation conditions. To analyze the effect of lubrication in between the gears, MATLAB simulation has also been performed and presented subsequently. It can also be observed that the applied moment of 19.8 Nm exerts the force at the tooth root of gear.

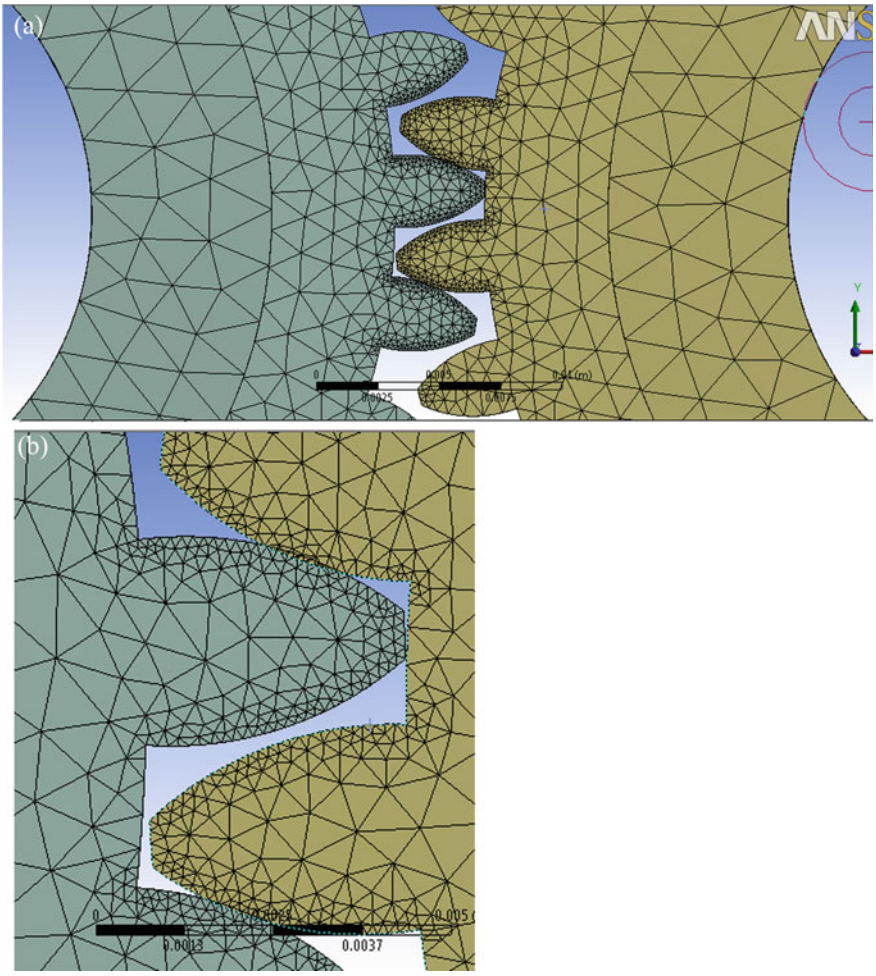

Fig. 2 Finite element method of pinion gear pair. **a** Full model, **b** zoomed view

3.2 MATLAB Simulation of Numerical Expressions

The main parameters of the pinion and the gear used to evaluate the gear mesh stiffness are listed in Table 1. Figure 4 shows the mesh stiffness values for healthy gear pair for both the cases, viz. without lubrication and with lubrication. A change in stiffness value has been observed when there is lubrication between the meshing surfaces, as compared to the stiffness value without lubrication. Due to lubrication, the friction coefficient in between the meshing surfaces varies. It has been observed that for the case of without lubrication, the stiffness increases linearly for the double contact region of gear meshing. Whereas for the case of with lubrication, the mesh stiffness increases for the approach part of double tooth contact and then decreases

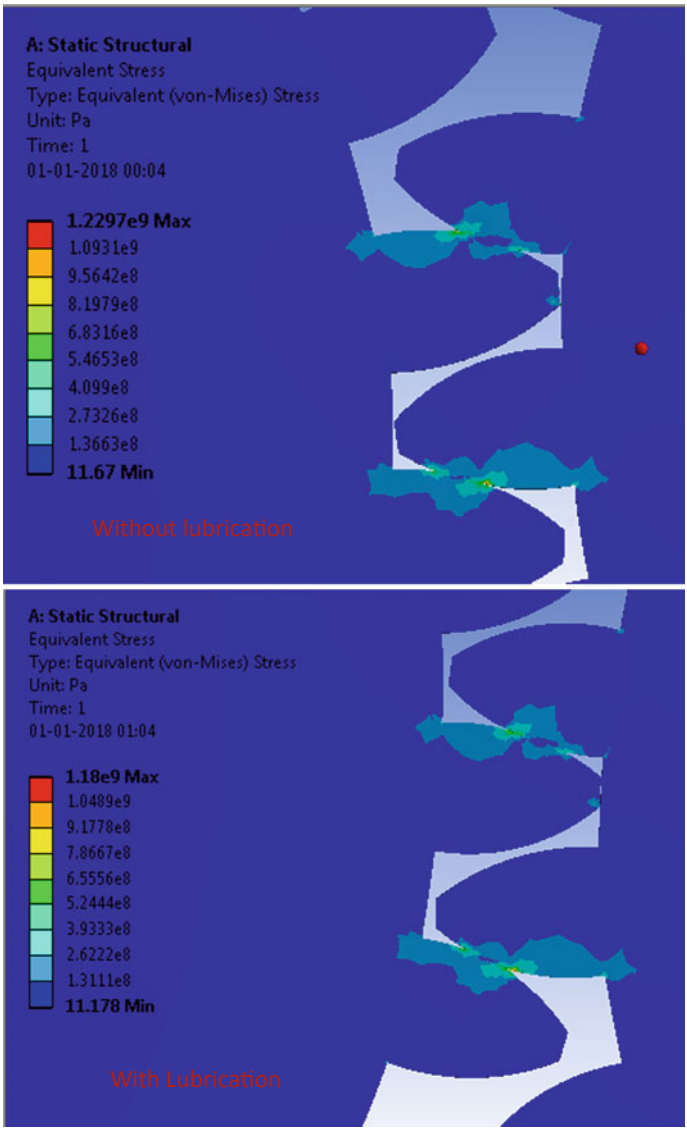

Fig. 3 Stress distribution at contact point of mesh

for the recess part of double tooth contact. The variation in mesh stiffness is due to the nonlinear characteristics of lubricant, i.e. damping and stiffness. The gear mesh stiffness has been plotted for three mesh cycles and is shown in Fig. 4. An increase in the gear mesh stiffness has been observed for both approach and recess for the duration of single point tooth contact with lubrication. On the other hand, the

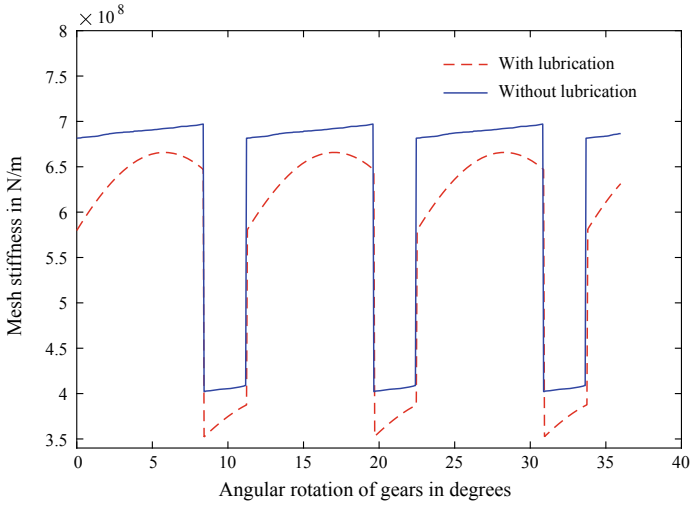

Fig. 4 Effect of lubricant on mesh stiffness for healthy gear tooth

mesh stiffness without lubrication is reflected by a very steep curve, which is due to increased friction in between the meshing surfaces.

4 Conclusion

The lubricant film in between the gear tooth meshing surface plays a pivotal role. Simulation studies highlight that lubrication affects the application of force on the gear mesh surfaces, contact teeth and minimizes the level of stress. The distribution of the stress at the contact point of teeth in gear mesh remains nearly same. Further, lubrication also affects the mesh stiffness of the gear pairs. The mesh stiffness increases with decrease in the lubricant film thickness. In the presence of lubrication, the variation in equivalent gear mesh stiffness occurs from single-to-double and double-to-single-tooth contact nonlinearly. Further, experimental evaluations need to perform to prove the effect of lubrication on the vibration characteristics. A relationship exhibiting connection between gear vibration and lubrication can be further addressed mathematically.

References

1. Samuel PD, Pines DJ (2005) A review of vibration-based techniques for helicopter transmission diagnostics. J Sound Vib 282(1):475–508
2. Sharma V, Parey A (2016) A review of gear fault diagnosis using various condition indicators. Procedia Eng 144:253–263

3. Smith R, Mobley RK (2011) Rules of thumb for maintenance and reliability engineers. Butterworth-Heinemann
4. Zhu X, Du L, Zhe J (2014) An integrated lubricant oil conditioning sensor using signal multiplexing. J Micromech Microeng 25(1):015006
5. Zhu J, He D, Bechhoefer E (2013) J Chem Sci Technol 2:100–115
6. Perera, PABA (1986) Effect of lubricating oil characteristics on gear vibrations. Ph.D. thesis
7. Abusaad S, Benghozzi A, Brethee K, Gu F, Ball A (2014) In: 3rd international workshop and congress on eMaintenance, Lulea, Sweden, 17–18th June 2014
8. Mehta NS, Parekh NJ, Dayatar RK (2013) Int J Eng Adv Technol (IJEAT) 2:120–123
9. Michaelis K, Höhn BR, Hinterstoißer M (2011) Ind Lubr Tribol 63:46–55
10. Michaelis K, Winter H (1994) In: 48th annual meeting, tribology transactions, Alberta, vol 37, pp 161–167
11. Höhn R, Michaelis K (2004) Tribol Int 37:103–109
12. Sheng S, Veers PS (2011) Wind turbine drivetrain condition monitoring—an overview. National Renewable Energy Laboratory
13. Raghuwanshi NK, Parey A (2017) Experimental measurement of spur gear mesh stiffness using digital image correlation technique. Measurement 111:93–104
14. Chaari F, Baccar W, Abbes MS, Haddar M (2008) Effect of spalling or tooth breakage on gearmesh stiffness and dynamic response of a one-stage spur gear transmission. Eur J Mech A/Solids 27(4):691–705
15. Chen Z, Shao Y (2013) Mesh stiffness calculation of a spur gear pair with tooth profile modification and tooth root crack. Mech Mach Theory 62:63–74
16. Amarnath M, Sujatha C, Swarnamani S (2009) Experimental studies on the effects of reduction in gear tooth stiffness and lubricant film thickness in a spur geared system. Tribol Int 42(2):340–352
17. Liang X, Zhang H, Liu L, Zuo MJ (2016) The influence of tooth pitting on the mesh stiffness of a pair of external spur gears. Mech Mach Theory 106:1–15
18. Liang X, Zuo MJ, Feng Z, Liu L (2016) A mesh stiffness evaluation model to reflect tooth pitting growth of a pair of external spur gears. In: Prognostics and system health management conference (PHM-Chengdu). IEEE, pp 1–6
19. Ma H, Li Z, Feng M, Feng R, Wen B (2016) Time-varying mesh stiffness calculation of spur gears with spalling defect. Eng Fail Anal 66:166–176
20. Yuan SH, Dong HL, Li XY (2012) Analysis of lubricating performance for involute gear based on dynamic loading theory. J Mech Des 134(12):121004
21. Liu FH, Theodossiades S, Bergman LA, Vakakis AF, McFarland DM (2015) Analytical characterization of damping in gear teeth dynamics under hydrodynamic conditions. Mech Mach Theory 94:141–147

Dynamic Motion Analysis of Reciprocating Vibro-separator

V. B. Lalwani, J. V. Desai, and D. H. Pandya

Abstract In this paper, dynamic motion behavior of the reciprocating vibro-separator model has been developed and analyzed. Effect of three different elasticity of vibro-pad material has been computed and nonlinear dynamic motions investigated. Based on previous empirical data, the computational model was validated with elasticity value of 25 MPa, vibro-motor at 1000 rpm, and vibro-motor angle (α) 30° has resulted in minimum horizontal displacement and periodic motion of the system. For the motion analysis, Poincaré, fast Fourier transit (FFT) and time data graphs have been used. The computational model of reciprocating vibro-separator has observed significant resemblance with the industrial case study.

Keywords Dynamic motion analysis · Model validation · Material property

1 Introduction

We are living in a world where technology is the most important part of life. Everyday new techniques are implemented in different fields, but still some areas lack behind in the usage of modern technology. Agriculture is one of them, where some processes had to improve. Many modern-day researchers on separating process are being carried out, some using reciprocating vibro-separator too, aimed at achieving useful outputs. Some work has been performed for improving its efficiency and its strength.

Here, Zhao et al. [1] have noticed that during testing average velocities of simulations for both spherical and non-spherical particle, models show similar trends for each case. Result concluded that during each case, due to the simplification of

V. B. Lalwani (✉) · D. H. Pandya
Department of Mechanical Engineering, LDRP-ITR, Gandhinagar, Gujarat, India
e-mail: viplalwani@gmail.com

D. H. Pandya
e-mail: veddhrumi@gmail.com

J. V. Desai
Paher University, Udaipur, Rajasthan, India
e-mail: jayesh.svit@gmail.com

V. K. Gupta et al. (eds.), *Reliability and Risk Assessment in Engineering*,
Lecture Notes in Mechanical Engineering,
https://doi.org/10.1007/978-981-15-3746-2_18

particle shapes, the velocities of spherical particles are highly predicted than those of non-spherical ones.

Du et al. [2] have analyzed the screening process of three different vibration screens and concluded that the variable linear vibration screen has better power distribution. The flexible screen surface is having advantage over fixed one, and that is experimentally proven with results of the experiment on screen surface. Li and Ma [3] concluded that amplitude value of the nonlinear system is compensated when vibrating system mass has small fluctuation. This will not affect the amplitude value of the system. Lala et al. [4] indicated that the vibration direction angle affects more on the particles' average velocity, and the average throw height is considered over a range of linear screen. The vibration frequency and inclination angle plate are found to have not much effect on it. They concluded that it is difficult to sieve the frequency and its amplitude value of vibration for ideal sieving effect of materials. The optimum value that was founded of motor angle, vibration frequency and amplitude is 6° and 40°, 13 Hz, 6.6 mm, respectively. Soldinger [5] has used the Monte Carlo simulation for analysis purpose of angle between horizontal line and bottom layer line of separator box. After experiment, she concluded that the value for the β is of 5° and the speed range is from 1000 to 800 rpm. Liu et al. [6] have tried to get the optimum angle between horizontal line and bottom layer line of separator box (β) and concluded that inclination of discharge end has the same effect on banana screening process, as an increment of the screen deck. The range of angle β that described is between 10° and 5°.

Dong et al.'s [7] study conducted on linear, circular and elliptical motion of the screen. They concluded that during linear screening, the travel velocity of the particles is the fastest and this will affect the lowest overall efficiency of screening. The circular mode motion has the highest particle efficiency and the lowest velocity Jianzhang and Xin [8] investigated the effect of vibration parameters like frequency and declination angle, on screening efficiency. After the simulation, the empirical formula is generated to describe the relationship between vibration parameter and efficiency of vibration screen.

Golovanevskiy et al. [9] have mentioned that to ensure the highest efficiency of material using vibration, it was suggested that the value of vibration factor w has to be selected for the amplitude and frequency. The value for w is of $w \approx 3$ or slightly higher. Further, it needs to focus on the development of model and describe the flow of material behavior under vibration.

Wang et al. [10] have found regimes of the different particle behaviors such as stable periodic motion, period-doubling bifurcation motion, bifurcation motion and the chaotic motion. Chaotic motion was found to be beneficial in separating particles effectively from other agricultural threshed materials and at the same time avoids particles accumulating on the screen and enhances the probability that the particle penetrates the screen hole. A detailed investigation on this aspect (passage rate) was not performed and it remained an open problem.

Li et al. [11] concluded that more work focus will be on the implementation of advanced experimental techniques besides using DEM simulation to measure the process and validate it.

Lala et al. [12] found that vibration parameters have significant effects on the circularly vibrating screening process. Large values of these parameters will also reduce screening efficiency. He and Liu [13] have studied a theoretical kinematic analysis of the vibrating screen that shows how the screen motion gets affected due to different parameters. Linear, circular or elliptical type's motion traces are obtained. They also concluded that the position of the exciter axle center of vibrating screen extremely affects the screening efficiently that will lead to design, by adjusting the relative position of the axle. This will result in increased capacity of a vibrating screen without consuming more power.

The present work is to investigate the dynamic motion behavior of reciprocating vibro-separator by using ANSYS software. In present work, the motor is placed on two sides of the separator box at the center position. As previous works concluded that motion has a significant effect on product efficiency and velocity, so the author tried to focus on the amplitude and dynamic motion behavior of reciprocating vibro-separator. From the study conducted, authors have attempted to validate the computational model with experimental model, in the industrial case study.

2 Computational Analysis and Responses

The reciprocating vibro-separator has three types of vibration mode, out of which elliptical vibration mode gave good results of screening, as compared to others. To observe that elliptical motion, the computational model of reciprocating vibro-separator is modeled out in CRE-O 3.0 and analyzed in ANSYS 14.5. The main parts of reciprocating vibro-separator are motor, connecting plate, rubber pad, separator box and unbalanced mass. The attached unbalanced set of mass having total weight of 14 kg is rotating at 1000 rpm on both sides of separator box. This will create a centrifugal force value of 5373.4512 N.

Mainly, three materials are used in analysis. They are rubber, gray cast iron and structural steel where assumption is that the property of structural steel has mild steel properties, which are nearly same with structural steel, so the mild steel material is replaced with structural steel in analysis.

The mesh used for analysis purpose is called tetrahedral shape type mesh. The mesh generation is coarse type, where mesh size of separator box is manually taken as 120 mm and the remaining part is as the default size. Number of meshed elements is 27,840 for the whole setup, and for foundation rubber, it is 2347, where the box mesh size is taken larger than the default mesh size for reducing complicity and reducing in number of nods.

In the ANSYS, harmonic analysis module is used to get the failure frequencies. Out of six modes of failure, it has been imperially concluded that the mode 3 is a critical mode of failure. Corresponding critical frequencies have been observed as 185.35 Hz, and similarly, based on half-power bandwidth concept the damping ratio (ζ) of vibro-pad has been investigated and the calculated value is 0.0017. Frequency response graph for mode 3 at 185.35 Hz has been analyzed at 70% marginal amplitude

of peak, which is in response to the concerned frequencies, as shown in enlarged view in Fig. 1. From the calculated value of the damping ratio, the authors calculated the damping coefficient for stiffness (β), which was further used in the structural module of ANSYS input parameter. For Analysis Using Transiant module in ANSYS, Value of β has to input as one of the important parameter in material property. Equation for β is given by the method of Rayleigh. β is called as Beta damping (input on BETAD command) $\beta = 2\zeta/\omega$.

Computational analysis of developed model is performed with different input parameters like motor angle (α), motor speed and properties of vibro-pad as varying parameters, and the dynamic motion behavior of vibro-separator is observed.

3 Industrial on Sight Experiment

The setup was prepared as per the computational work. Here, the two vibro-motors are running at 1000 rpm. The variation in motor speed is ± 20 rpm.

Each vibro-motor is having 0.5 horse power. The experimental setup is running in between 980 and 1020 rpm motor speed, with 30° motor angle. The entire work for the experiment is done at Gajanand Industries.

In the design of separator box, there are two motors connected at two sidewall in the middle position of wall. Total (3.34 * 4) 13.36 kg unbalanced mass is connected for centrifugal force generation. The experimental results are taken at three points, i.e., one point is at the top center place of vibro-separator box and the remaining two points are at top side end position of separator box as shown in Fig. 2. The piezoelectric accelerometer sensor (uniaxial) is used for picking up the vibration signals from the point on separator box. This special piezoelectric pickup type sensor is used with a frequency of range from 1 to 10 kHz. The sensitivity of sensor is 107 mV/(m/s^2) and Input Mode of sensor is integral electronics piezoelectric accelerometer (IEPE). The analyzer used to measure the acceleration data is made by Crystal Corporation. The model of the analyzer is CoCo-80 (Fig. 3).

4 Discussion of Result

To observe the dynamic motion of separator, the time domain data, fast Fourier transform (FFT) and Poincaré tools are used. These three are preferable tools of study for motion behavior analysis. The experimental data as well as computational model data were observed using these tools and fixed a point on separator box. For common sampling rate in computational data and experimental data, 10 kHz sampling frequency is considered. Three different values of vibro-pad were used for computational work. The values taken for elasticity were 10, 25 and 40 MPa. Second consideration that was common between experiment and computation is that

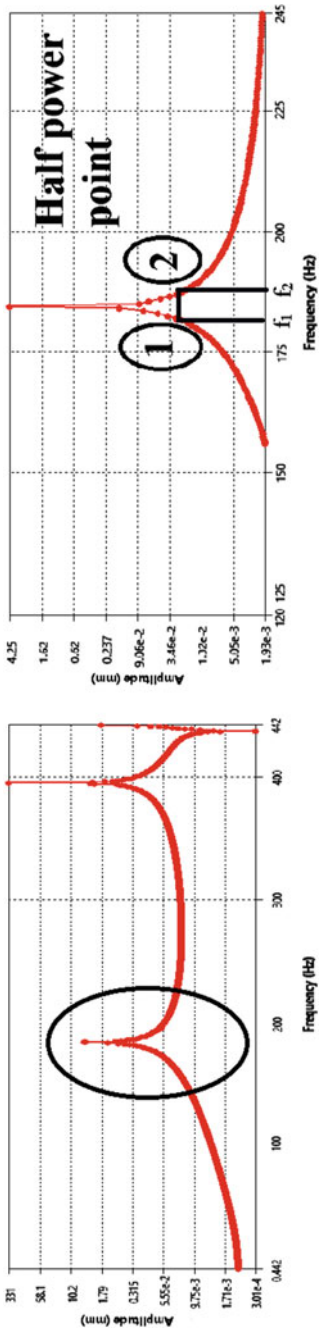

Fig. 1 Frequency response graph

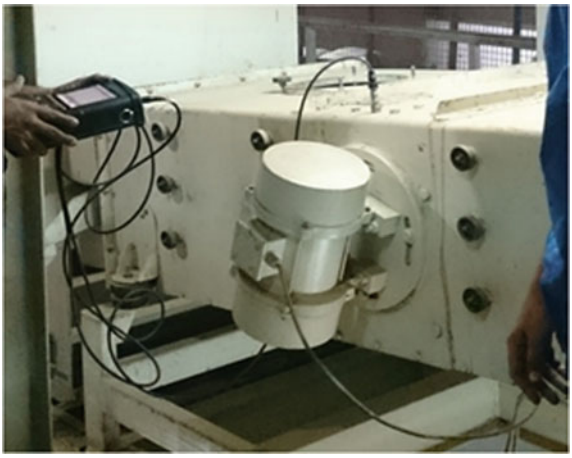

Fig. 2 Experimental setup in Gajanand Industries

Fig. 3 Vibro Analyzer Model-CoCo 80

the model is analyzed for 30° motor angle and 1000 rpm speed. The range of speed of the motor in experiment is, from 920 to 1020 rpm.

Figure 4a, b is the acceleration graphs that indicate that the acceleration value of vibro-separator is higher in vertical direction, as compared to horizontal direction. Figure FFT plot has indicated the super-harmonic response in horizontal direction. Neither sub-harmonic nor super-harmonic responses have been observed in vertical direction, as shown in Fig. 4c, d, which would lead to conclude the periodic behavior of system. Figure 4e, f is the Poincaré graph that it shows that the motion of reciprocating vibro-separator has periodic motion in vertical and multi-periodicity observed in horizontal direction. Horizontal Poincaré responses have displacement of $+3$ to -4 mm.

Figure 5a, b shows that the value of acceleration in horizontal direction is approximately doubled than in vertical direction. As we decrease the elasticity, the clear stable equilibrium time response has been observed in horizontal, as compared to horizontal time response for elasticity of 40 MPa. Vertical time responses have

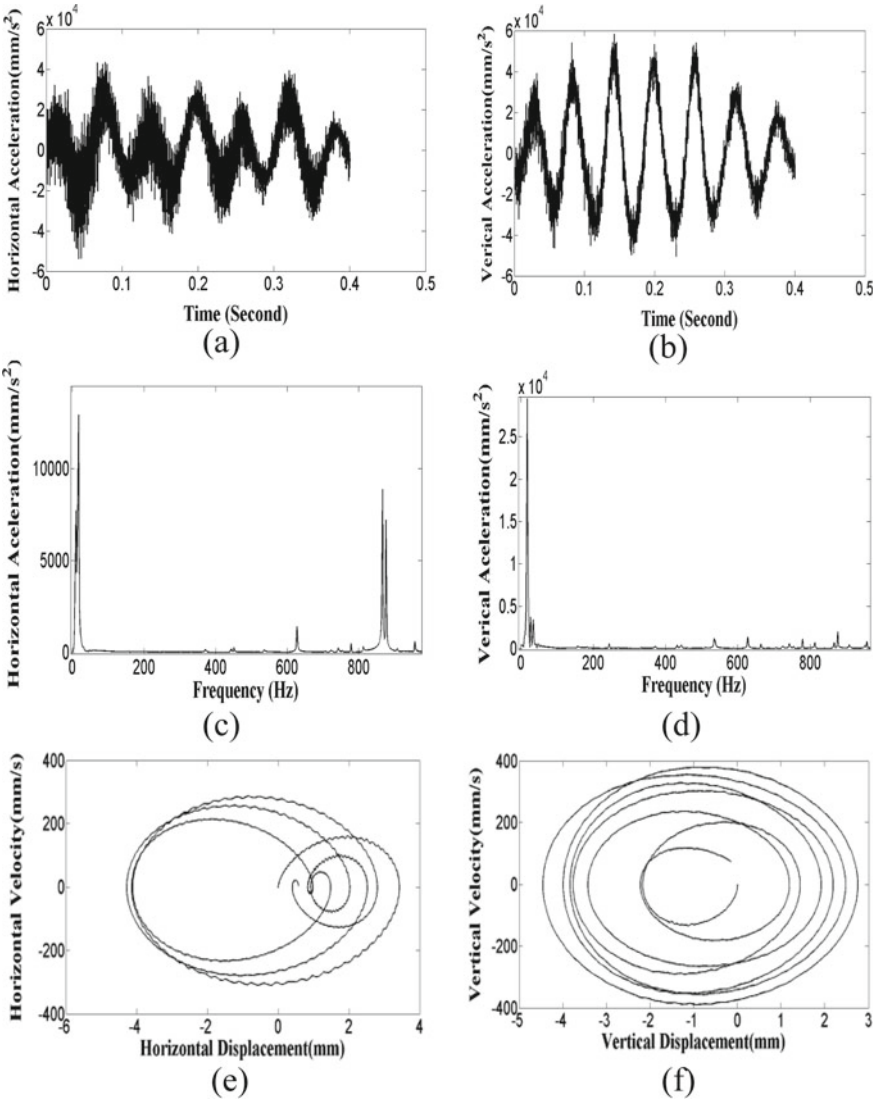

Fig. 4 Computational model 40 MPa elasticity

a clear indication of the periodic motion behavior of the system. FFT plots have mentioned that the motion is periodic as no such super-harmonic or sub-harmonic peaks have been observed as shown in Fig. 5c, d. Figure 5e, f is the Poincaré maps for horizontal and vertical direction, that clearly indicated periodic motion with less multi-periodicity, as compare to rubber elasticity of 40 MPa. Horizontal Poincaré responses have displacement of $+2.2$ to -3.5 mm.

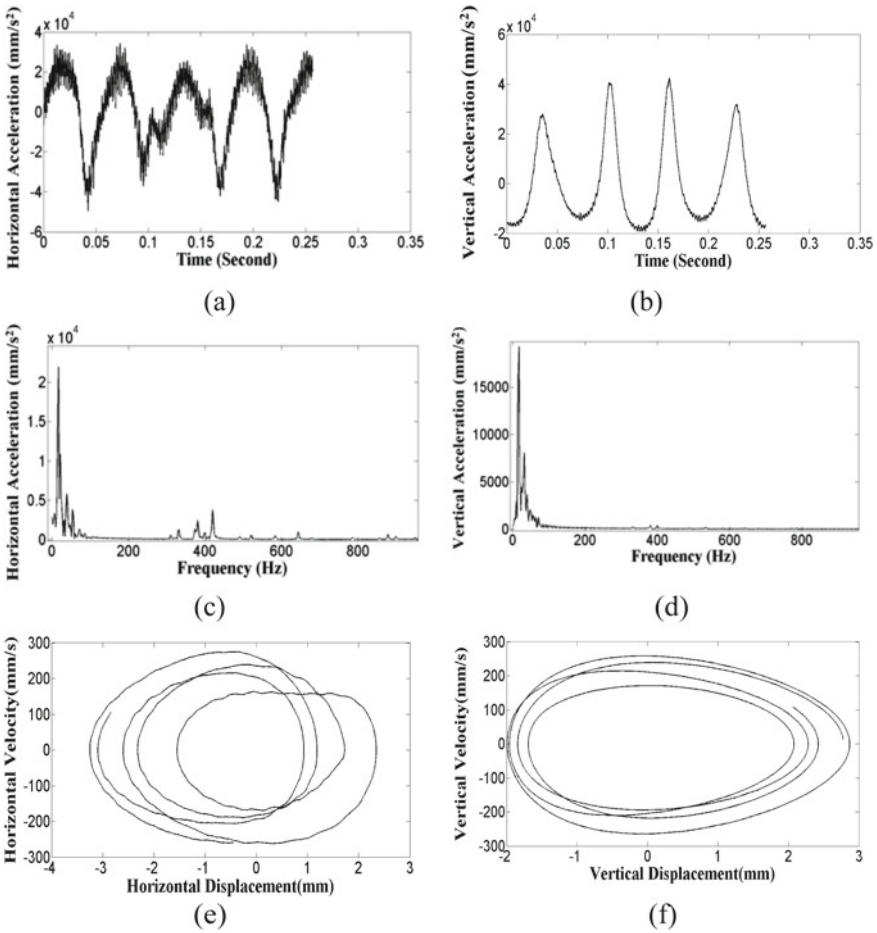

Fig. 5 Computational model 25 MPa elasticity

On the further decrease in elasticity, more instable responses in both directions are observed as shown in Fig. 6a, b. Figure 6c, d are the FFT plots having sub-harmonic responses with significant sidebands in horizontal responses, while the vertical responses have been observed with higher range super-harmonic responses. Poincaré maps clearly indicated 5T periodicity in horizontal responses and multiple periodicities in vertical responses. Horizontal Poincaré responses have displacement of $+7$ to -6.3 mm.

Experimental time responses have concluded stable and periodic response to system as shown in Fig. 7a, b. Figure 7c, d is the FFT plot that indicates that the motion is periodic. Figure 7e, f is the Poincaré maps which clearly indicate periodic motion behavior of system. Horizontal Poincaré responses have displacement of $+1.8$ to -1.75 mm.

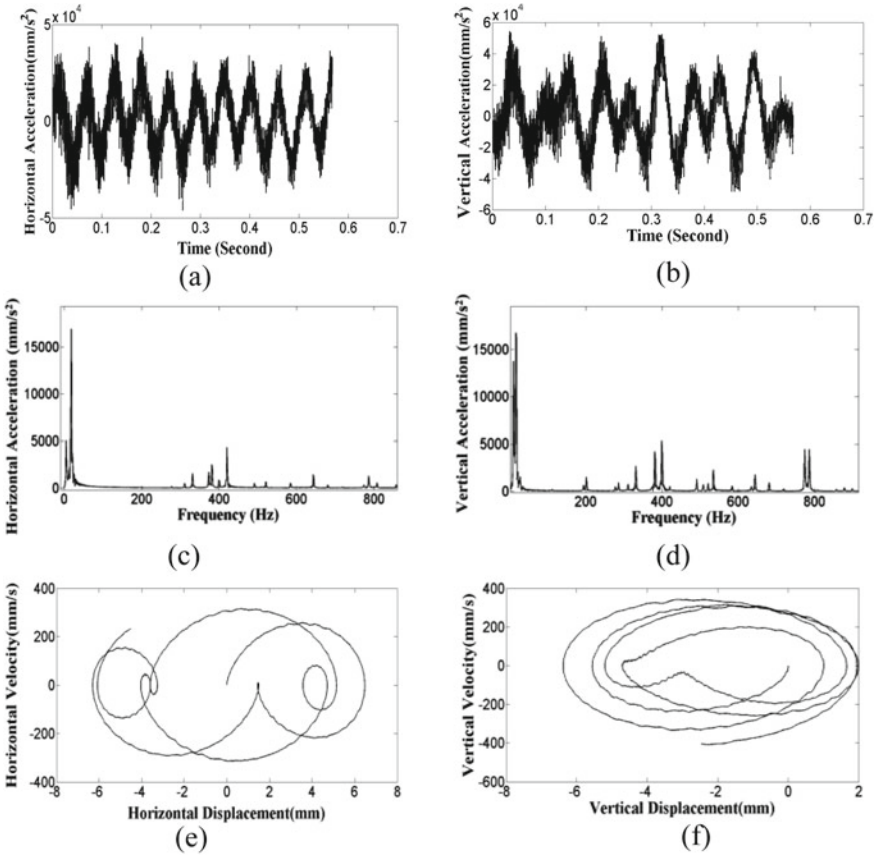

Fig. 6 Computational model with 10 MPa elasticity

Computational model with elasticity value of 25 MPa, vibro-motor at 1000 rpm and vibro-motor angle (α) 30° has resulted in horizontal displacement of 5.7 mm with periodic responses. As elasticity increases, horizontal displacement of the system has been increased to 7 mm and multi-periodicity has been reported. Contrarily, as elasticity of vibro-pad decreases, horizontal displacement of system has increased to 13.3 mm and multi-periodicity has also been reported. Horizontal amplitude responses have reported more than the vertical amplitude responses in time domain responses in computational and experimental as well. Computational model has validated with industrial experiments.

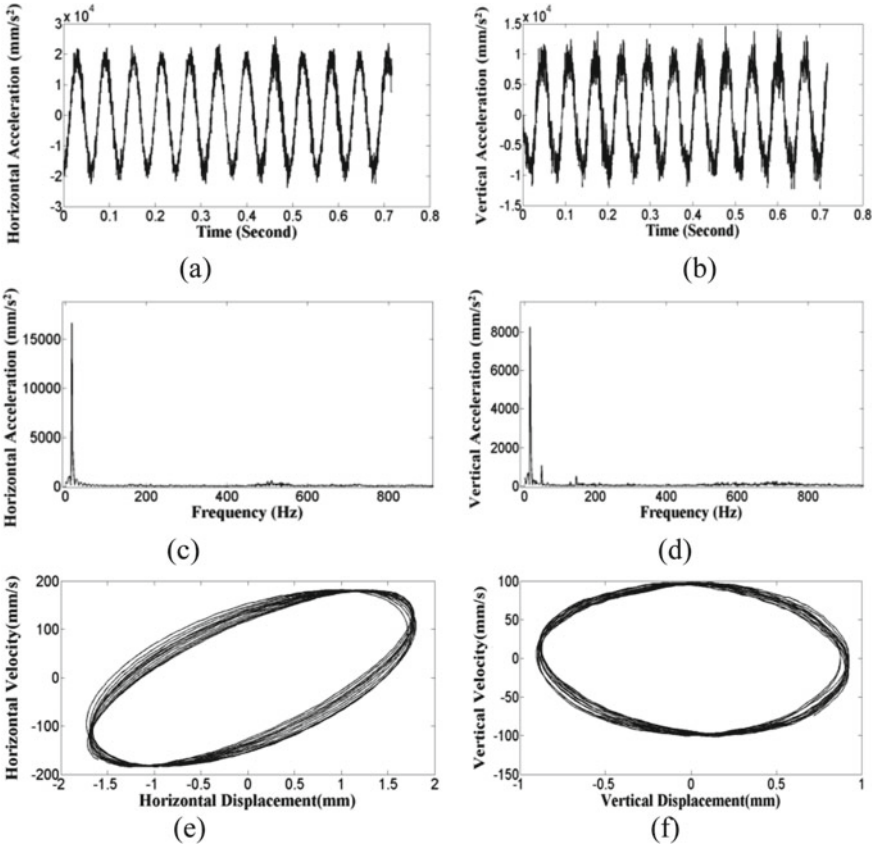

Fig. 7 Computational model

5 Conclusions

In the present work, the computational model has been developed and analyzed for different nonlinear motion behavior of vibro-separator with three different elasticity of vibro-pad. Required damping coefficient of mass and stiffness has been evaluated using half-power bandwidth method. Analyzed computational model has shown significant validation with industrial case study, which leads to conclude the following:

1. Decreasing the elasticity of vibro-pad material, it will make the system more and more unstable as shown in Figs. 4a, b, 5a, b and 6a, b.
2. Nonlinear motion behaviors of the system have concluded that the system has less multi-periodicity with at 25 MPa elasticity of vibro-pad in computational model, which shows more resemblance with experimental Poincaré responses.

3. Effective operating parameters to be concluded from computational model with elasticity value of 25 MPa, vibro-motor at 1000 rpm and vibro-motor angle (α) 30° have resulted in minimum horizontal displacement of 5.7 mm bidirectional with periodic responses.

Authors would like to further extend this work for varying motor angle for future work.

Acknowledgements The authors would like to acknowledge the Gujarat Council of Science and Technology (GUJCOST) (grant no GUJCOST/MRP/2016-17/527).

References

1. Zhao L, Zhao Y, Bao C, Hou Q, Yu A (2016) Laboratory-scale validation of a DEM model of screening processes with circular vibration. Powder Technol 303:269–277
2. Du C, Gao K, Li J, Jiang H (2014) Dynamics behavior research on variable linear vibration screen with flexible screen face. Adv Mech Eng 2014, Article ID 957140, 12 p
3. Li X, Ma M (2014) Dynamics analysis of the double motors synchronously exciting nonlinear vibration machine based on acceleration sensor signal. Sens Transducers 176(8):290–295
4. Lala Z, Chusheng LIU, Junxia YAN (2010) A virtual experiment showing single particle motion on a linearly vibrating screen-deck. Min Sci Technol 20(2):276–280
5. Soldinger M (2002) Transport velocity of a crushed rock material bed on a screen. Miner Eng 15(1–2):7–17
6. Liu C, Wang H, Zhao Y, Zhao L, Dong H (2013) DEM simulation of particle flow on a single deck banana screen. Int J Min Sci Technol 23(2):273–277
7. Dong H, Liu C, Zhao Y, Zhao L (2013) Influence of vibration mode on the screening process. Int J Min Sci Technol 23(1):95–98
8. Jianzhang X, Xin T (2012) Particle stratification and penetration of a linear vibrating screen by the discrete element method. Int J Min Sci Technol 22(3):357–362
9. Golovanevskiy VA, Arsentyev VA, Blekhman II, Vasilkov VB, Azbel YI, Yakimova KS (2011) Vibration-induced phenomena in bulk granular materials. Int J Miner Process 100(3–4):79–85
10. Wang L, Ding Z, Meng S, Zhao H, Song H (2017) Particuology Kinematics and dynamics of a particle on a non-simple harmonic vibrating screen. Particuology 32:167–177
11. Li J, Webb C, Pandiella SS, Campbell GM (2002) A numerical simulation of separation of crop seeds by screening—effect of particle bed depth. Food Bioprod Process 80(2):109–117
12. Lala Z, Yuemin Z, Chusheng L, Jun L, Hailin D (2011) Mining Science and Technology (China) simulation of the screening process on a circularly vibrating screen using 3D-DEM. Min Sci Technol 21(5):677–680
13. He XM, Liu CS (2009) Dynamics and screening characteristics of a vibrating screen with variable elliptical trace. Min Sci Technol 19:508–513

A Review of Fault Detection, Diagnosis, and Prognosis of Rolling Element Bearing Using Advanced Approaches and Vibration Signature Analysis

Pavan Agrawal and Pratesh Jayaswal

Abstract Rolling element bearing is the most significant component of the rotating machines. In most of the cases, machines failed due to the failure of rolling element bearing. The aim of the present paper is to provide a brief review of the advanced approaches like condition-based monitoring, wavelet transform, energy entropy ratio, artificial neural network, support vector machine, fuzzy logic, and vibration signature analysis techniques used to find the fault detection and diagnosis of rolling element bearing. The several techniques of vibration signature analysis have been given by several researchers. It is the most reliable non-destructive health monitoring technique used to detect the location and severity of the faults. Bearing faults and its classifications have already been reviewed. Time, frequency, time–frequency domain, and wavelet transform types signal processing methods have also been developed for fault detection. Term prognosis is used to estimate the remaining useful life of the faulty bearing and has been reviewed by various investigators. Advance approaches like energy, entropy, and energy entropy ratio criterion have been used for the classification of different types of signal waves. Higher energy and lower entropy criteria are favorable for the selection of mother wavelets in signal processing. Soft computing techniques like ANN, SVM, fuzzy logic, and ANFIS are used as decision-making tools and classifiers.

Keywords Bearing health monitoring · Vibration signature analysis · Energy entropy approaches · ANN · ANFIS

1 Introduction

Generally, all rotating machines failed due to failures in rolling element bearing. Therefore, it is necessary to find the fault of bearings at an incipient stage before failure. The bearing health monitoring techniques have been given by various investigators. Vibration signature analysis is one of the best techniques among

P. Agrawal (✉) · P. Jayaswal
Madhav Institute of Technology & Science, Gwalior, MP, India
e-mail: pavanmits2012@gmail.com

V. K. Gupta et al. (eds.), *Reliability and Risk Assessment in Engineering*,
Lecture Notes in Mechanical Engineering,
https://doi.org/10.1007/978-981-15-3746-2_19

the other condition monitoring techniques like lubricant analysis, current signature analysis, and oil debris, etc. It is a non-destructive technique, which may be applied in online or running condition of bearing, without any restriction of the process. A lot of research work has been done by many researchers on the development of an expert system for fault detection and classification of bearings. Tandon et al. [1] have reviewed the vibration signature analysis and acoustic measurement methods to find out the defects in bearings using time and frequency domain and signal processing techniques such as acoustic emission and sound intensity. Azeez and Naseel [2] have presented the review of the method of detection of a fault of bearings by comparison of signals of healthy and faulty bearings using time-domain signal peaks and frequency domain characteristics. Marichal et al. [3] have proposed the intelligent system for detection and classification of faulty bearings using the artificial neural network and neuro-fuzzy systems. The objective of the research is to meet out the gap between the old and present research and update the reviews by incorporating of recent methodologies and advance approaches which have been adopted in bearing fault detection and diagnosis and develop the idea for expert system which is used to find out the real-time incipient fault of the bearing automatically.

2 Rolling Element Bearing Failure

Several types of research [4–9] have been done to explain the fault detection methodologies, the severity of faults and its classification in bearings. Mainly, bearing faults are divided into two categories localized and distributed defects [9]. Localized defects induced on the rolling surface that pits cracks and spalls. However, the distributed defects developed the surface roughness, misaligned races, and waviness. Generally, rolling element bearings failed due to contaminants like dirt, abrasive foreign particles, etc. Pandya et al. [5] have proposed a method for diagnosis of rolling element bearing faults, for single-point defects using wavelet packet decomposition and neural network. Qtpax [6] showed the investigation of operating conditions of bearing operation and different types of faults and its effects on railways. The International Organization for Standardization (ISO) has proposed a methodology for classifying rolling element bearing damage and faults (ISO 15243). The standard recognizes six primary damage modes, sub-modes, and their causes in bearings as shown in Table 1.

3 Condition Monitoring

Condition monitoring is a valuable preventive maintenance tool to extend the operating life of a machine. Detection, diagnosis, and prognosis are three major areas in which we can classify condition monitoring. In condition monitoring, there are various techniques like optical, thermal, vibration, and current, but vibration

Table 1 Mode of failure of bearings [6]

Mode of damage/failures	Sub-modes of damage/failures	Causes of damage/failures
Fatigue	• Subsurface fatigue • Surface initiated fatigue	Repeated stresses developed in the rolling component
Wear	• Abrasive wear • Adhesive wear	Due to insufficient lubrication
Corrosion	• Moisture corrosion • Frictional corrosion	Due to the looseness of rolling components and relative movement between races and shaft or housing
Electrical erosion	• Excessive voltage • Current leakage	Due to passes of electric current through a bearing
Plastic deformation	• Overload • Indentation from debris • Indention by handling	Due to shock loading or incorrect mounting of rolling elements, rings or seals
Fracture and cracking	• Forced fracture • Fatigue fracture • Thermal cracking	Due to stress concentration in excess of the material and incorrect mounting and dismounting

monitoring techniques are having edge over others. Gaud et al. [10] have reviewed that in the present industrial scenario 70% vibration signature analysis, 20% wear particles, and remaining 10% covers all the non-destructive testing techniques including eddy current measurement. These are used as health condition monitoring of bearings and rotary machines. Mathew and Alfredson [11] have studied the condition monitoring techniques to analyze the vibration signals of rolling element bearings and shown that frequency domain parameters are more useful to the detection of bearing faults than time-domain parameters. Jayaswal et al. [12] have developed the techniques for automatic condition-based maintenance procedure of bearings. They have proposed two criteria based on wavelet transforms and neuro-fuzzy systems for early detection of bearing faults over the conventional vibration signature analysis techniques using time and frequency domain.

4 Vibration Signature Analysis

To monitor the health of the running bearing without any destruction, vibration signature analysis is the most constructive technique. Jayaswal et al. [13] have presented a detailed review of vibration analysis techniques such as time domain, frequency domain, and time–frequency domain. A hybrid intelligent system is developed using wavelet transforms, artificial neural network, and fuzzy logic for fault diagnosis of bearings in online condition. Kankar et al. [14] have presented the methodology to diagnose the severity of faults in ball bearings using time-domain statistical features such as skewness, kurtosis, log energy entropy, and Shannon

entropy. The machine learning techniques such as support vector machine and artificial neural network were used as faults classifier. They have found that fault classification efficiency, achieved by the proposed methodology, is better than other conventional methodologies. To detect and diagnose bearing defects, vibration-based monitoring technique has been used for several decades. These techniques had been applied conventionally according to time and frequency domains. Orhan et al. [15] have presented a comparative case study of vibration monitoring and analysis. They also examined the machinery in real-operating conditions. The vibration signature analysis has been predominantly allocated to the following categories.

4.1 Time Domain

The time domain is used to analyze the vibration signal data as a function of time. In time-domain analysis statistical features are calculated for vibration signals. By comparing the statistical features, the fault of the bearing may be identified [16]. Statistical features of the time domain are used as input for the training of the neural network, and the system is able to classify the rolling element bearing faults effectively [17]. The major benefit of this technique is that before inspection little or no data is lost. It helps in detailed analysis and direct fault diagnosis. The disadvantage of this technique is that there is often too much data. A time domain included statistical attributes of vibration signals such as root mean square, standard deviation, peak level, crest factor, kurtosis, and skewness as a trait to detect emergent faults in bearings [18]. These statistical features are as follows [17, 19–21].

1. Root mean square (RMS):

$$\text{RMS} = \sqrt{\frac{1}{N}\sum_{n=1}^{N} f_n^2} \tag{1}$$

2. Mean value:

$$\text{Mean} = \frac{1}{N}\sum_{i=1}^{N} f_n \tag{2}$$

3. Peak value:

$$P_{\text{v}} = \frac{1}{2}[\max(f_n) - \min(f_n)] \tag{3}$$

4. Crest factor:

$$\text{Crest factor} = \frac{P_{\text{v}}}{\text{RMS}} \tag{4}$$

5. Skewness:

$$\text{Skewness} = \frac{\frac{1}{N}\sum_{n=1}^{N}\left(f_n - \overline{f}\right)^3}{\text{RMS}^3} \tag{5}$$

6. Kurtosis:

$$\text{Kurtosis} = \frac{\frac{1}{N}\sum_{n=1}^{N}\left(f_n - \overline{f}\right)^4}{\text{RMS}^4} \tag{6}$$

7. Variance:

$$\text{Variance} = \sigma^2 = \frac{\sum_{n=1}^{N}\left(f_n - \overline{f}\right)^2}{N} \tag{7}$$

8. Standard deviation:

$$\text{SD} = \left(\frac{1}{N-1}\sum_{n=1}^{N}\left(f_n - \overline{f}\right)^2\right)^{\frac{1}{2}} \tag{8}$$

4.2 Frequency Domain

Frequency domain technique plays an important role in fault detection and diagnosis of the rolling element bearings. The frequency domain is referred to where repetitive vibration signals occur. Fast Fourier transform algorithm is used to convert the time-domain vibration signal into a frequency domain [13]. Jayaswal et al. [21] have reviewed the various frequency domain techniques, such as envelop spectrum, band passes analysis, signature spectrum, and spike energy, are used to find the indication of bearing health condition. The fault frequencies of rolling element bearings are as follows [22, 23].

1. Shaft rotational frequency

$$\text{FSR} = \frac{N}{60} \tag{9}$$

2. The frequency of inner race defect

$$\text{FIRD} = \left(\frac{n}{2}\right)\left(\frac{N}{60}\right)\left[1 + \left(\frac{b_\text{d}}{p_\text{d}}\right)\cos\varnothing\right] \tag{10}$$

3. The frequency of outer race defect

$$\text{FORD} = \left(\frac{n}{2}\right)\left(\frac{N}{60}\right)\left[1 - \left(\frac{b_\text{d}}{p_\text{d}}\right)\cos\varnothing\right] \tag{11}$$

4. The frequency of ball defect

$$\text{FBD} = \left(\frac{p_\text{d}}{b_\text{d}}\right)\left(\frac{N}{60}\right)\left[1 - \left(\frac{b_\text{d}}{p_\text{d}}\cos\varnothing\right)^2\right] \tag{12}$$

5. The frequency of cage defect

$$\text{FCD} = \frac{1}{2}\left(\frac{N}{60}\right)\left[1 - \left(\frac{b_\text{d}}{p_\text{d}}\right)\cos\varnothing\right] \tag{13}$$

where n = number of balls, $\varnothing$ = contact angle, p_d = pitch diameter, b_d = diameter of ball, N = rotational speed in rpm.

4.3 Time–Frequency Domain (Wavelet Transforms)

Wavelet analysis is the new approach and it is used to test the health of the bearing and solving the critical problems in engineering applications. The main functions of the wavelet transform are small waves located at different times or increasing the resolution of complex signals. It also provides information about a signal in both modes (time and frequency domain). The wavelet transform is subdivided into the following categories such as continuous wavelet transform, discrete wavelet transform, and wavelet packet transform. There are various real and complex base wavelets like Meyer wavelet, Morlet wavelet, complex Morlet wavelet, and Daubechies wavelet, etc. [19, 24, 25]. Rodrigues et al. [26] have proposed the method of mother wavelet selection for vibration signature analysis of titanium alloy material during high-speed machining. The following are the different wavelets shown in Fig. 1 [24].

5 Energy Entropy Approaches

Advanced energy entropy approaches are used for optimal base wavelet selection. The mother wavelet results may differ for different applications. Therefore, the selection of appropriate mother wavelet is important. The maximum value of energy and a minimum value of Shannon entropy criterion are favorable for base wavelet selection corresponding to the wavelet coefficient [27]. He et al. [28] have proposed

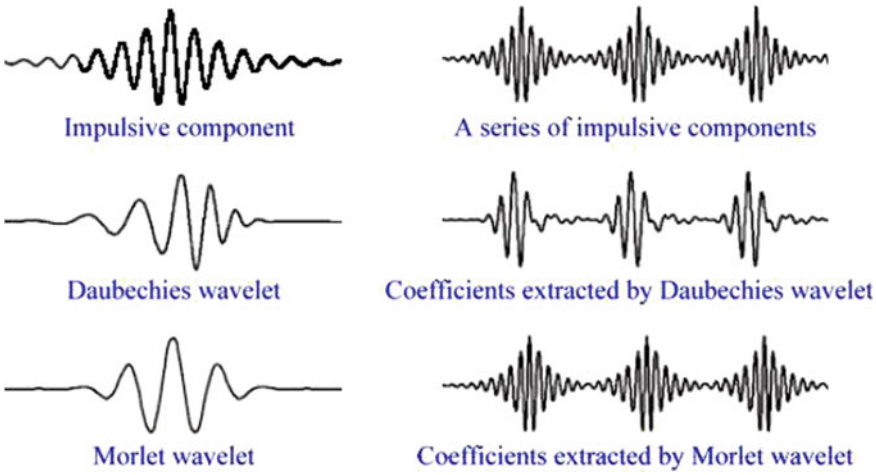

Fig. 1 Different types of wavelets and its coefficients [24]

extensive multiple criteria based on energy and entropy approaches to search for a mother wavelet for a certain electrocardiogram (ECG) signals.

5.1 Energy Entropy Ratio (EER)

The energy and entropy ratio criterion is used for the selection of mother wavelet. For a selection of appropriate mother wavelet, the maximum value of energy and entropy ratio is considerable [19]. Sample graph between maximum energy to Shannon entropy ratio and scale number of wavelet coefficient for various bearing fault conditions [27] is shown in Fig. 2.

5.2 Relative Wavelet Energy (RWE)

The relative wavelet energy criterion is considered for the selection of mother wavelet. To detect a specific characteristic in time and frequency planes maximum value of feature extraction of relative wavelet energy, for mother wavelet, is considered as time-scale density. It gives information about relative energy and associated frequency bands and detects the degree of similarity between different signals [29]. Sample graph between maximum relative wavelet energy and scale number of wavelet coefficient for different bearing faults [30] is shown in Fig. 3.

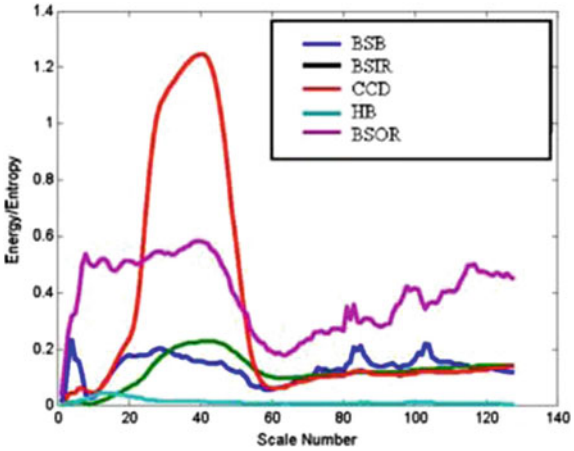

Fig. 2 Graph of energy to entropy ratio to scale number [27]

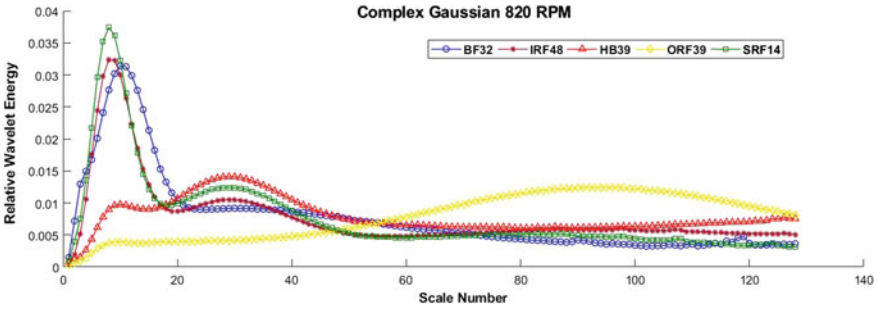

Fig. 3 Graph of relative wavelet energy to scale number [30]

6 Advanced Signal Processing Techniques

In different areas of engineering, the interest has grown and researchers apply the approaches such as an artificial neural network (ANN), fuzzy logic, and time encoded signal processing and recognition. The contemporary intensification of curiosity to overcome the individual weakness is merging and combing neural network and fuzzy logic system into a functional system [31].

6.1 Artificial Neural Network (ANN)

The human brain has an outstanding ability to contemplate, recall, and logical quality which has motivated many investigators to enhance artificial models whose basic

learning process is similar to that of a biological neuron. Rao et al. [25] have presented a critical review of the structure and history of the artificial neural network. ANN is employed for the classification of faults and prognosis of rolling element bearing. Gaud et al. [10] have proposed the various condition monitoring methods and backpropagation neural network for fault classification in bearings. Tiwari et al. [32] have proposed the hybrid system using multi-scale permutation entropy and adaptive neuro-fuzzy classifier for automated fault diagnosis of bearing. Multi-scale permutation entropy is used for feature extraction and adaptive neuro-fuzzy classifier works as an expert system for detecting faults of bearing. Bhavaraju et al. [20] compared the artificial neural network (ANN) and self-organizing maps (SOM) for a finding of fault classification in bearings and found that ANN identifies the better classification than SOM.

6.2 Support Vector Machine (SVM)

Support vector machine is a supervised machine learning technique. It is incorporated into learning algorithms that inspect data used for classification and regression analysis. A multi-fault SVM classifier has been used for recognition of bearing fault [33]. The SVM algorithm finds the maximum margin separating hyperplane. Kankar et al. [27] have compared the machine learning techniques ANN, SVM, and SOM and found that Meyer wavelet has given the best results with SVM than other techniques. Barakat et al. [34] proposed the best selective parameters (BSP), binary decision tree (BDT) methods based on multi-class support vector machines, and found higher classification efficiency than ANN. Li et al. [35] have presented the hybrid system using the wavelet packet decomposition and SVM techniques. Wavelet packet decomposition is used to decompose the vibration signals. Widodo and Yang [36] have reviewed that support vector machine techniques have been successfully applied to verification, face recognition, test detection, and categorization, information and image retrieval, etc. Support vector machine classification is shown in Fig. 4 [37].

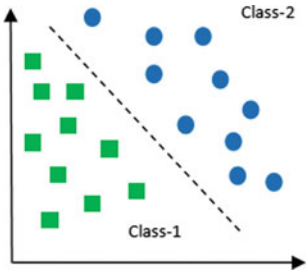

Fig. 4 Support vector machine classification [37]

6.3 Fuzzy Logic

The fuzzy logic was incorporated as a means for constituting, operating, and employing uncertain information. Fuzzy logic is a problem-solving control system technique [38]. Sugumaran and Ramachandran [39] have proposed a fuzzy classifier and decision tree machine learning technique for pattern recognition and fault classification. Marichal et al. [3] have given the method having a neuro-fuzzy system and vibration analysis in the frequency domain for a finding of bearing fault classification. Lou and Loparo [40] have given an automatic detection of the fault diagnosis system based on wavelet transform and neuro-fuzzy classifier for localized defects in bearing. An adaptive neural fuzzy interface system is used as a diagnostic classifier.

7 Experimental Test Rig

Experimental test rig design and development have been given by a number of researchers for acquiring signals for health monitoring of bearings [20, 41, 42]. It consists of a double row, self-aligning ball bearings mounted on a shaft driven by a three-phase electric induction motor (1 HP, 220–240 V) of an experimental setup. This experimental setup has a facility for easy removal of bearings to be tested. The bearings housing of the experimental setup has a facility for the placement of the sensor (accelerometer) on it. The motor connected to the shaft rated max 2900 rpm. FFT analyzer is used to collect the vibration signatures from bearing through the accelerometer. After the collection of data, we will analyze the signal through various signal processing techniques and extract the features to calculate the frequency and classify the healthy and faulty bearings. Experimental test rig for acquiring of vibration signals of different bearings is shown in Fig. 5 [37].

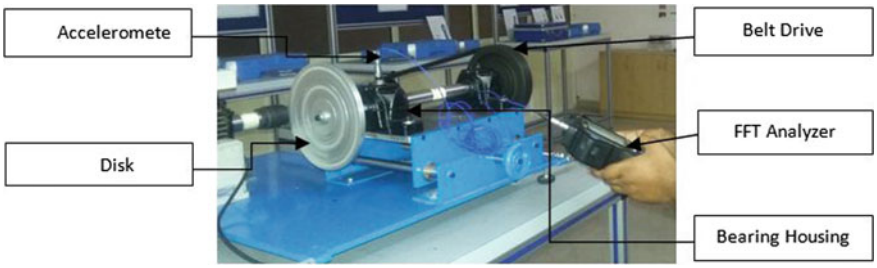

Fig. 5 Experimental test rig [37]

8 Conclusions

A brief review of the application of vibration signature analysis along with wavelet transform and machine learning techniques like ANN, SVM, and fuzzy logic, in the area of fault diagnosis, have been presented. Time-domain techniques are used for finding the fault of the bearing, and frequency domain methods are used to identify the fault locations. Time–frequency techniques (wavelet transforms) have been found better techniques for fault diagnosis of bearings, due to its high resolution, than other techniques. The emphasis has been put on various advanced approaches of energy entropy for the selection of mother wavelets. A number of research papers on vibration signature analysis and machine learning techniques have been reviewed by various researchers for bearing fault diagnosis. An expert system using ANFIS for a finding of bearing faults and classification has been reviewed. Attoui et al. [43] have presented the ANFIS system in order to detect, identify and classify different fault bearing conditions like an outer race defect, and inner race defect at different shaft rotation speed and for different defect conditions. After a detailed review of research papers, it has been found that system using advanced approaches like wavelet transform, energy entropy criterions, machine learning techniques, and neuro-fuzzy system perform better than traditional fault diagnosis method.

Acknowledgements The authors are indebted to the SKF Reliability Maintenance Center, Madhav Institute of Technology and Science, Gwalior, India for their unconditional support in research work and for providing the facility of literature review.

References

1. Tandon N, Choudhury A (1999) A review of vibration and acoustic measurement methods for the detection of defects in rolling element bearing. Tribol Int 32:469–480
2. Azeez NI (2014) Detection of rolling element bearing defects by vibration signature analysis: a review. In: ICMMD
3. Marichal GN, Artes M, Garcia-Prada JC (2010) An intelligent system for faulty-bearing detection based on vibration spectra. J Vib Control 17(6):931–942
4. McFadden PD, Smith JD (1985) The vibration produced by multiple point defects in a rolling element bearing. J Sound Vib 98(2):263–273
5. Pandya DH, Upadhyay SH, Harsha SP (2012) ANN based fault diagnosis of rolling element bearing using time-frequency domain feature. Int J Eng Sci Technol 4(6):2878–2886
6. Qtpax T (2012) Bearing investigation. In: Railway technical handbook, vol 1, pp 122–135
7. James Li C, Ma J (1997) Wavelet decomposition of vibrations for detection of bearing-localized defects. NDT E Int 30(3):143–149
8. Kankar PK, Sharma SC, Harsha SP (2012) Vibration signature analysis of a high speed rotor supported on ball bearings due to localized defects. J Vib Acoust ASME 10(12):1833–1853
9. Stack JR, Habetler TG, Harley RG (2004) Fault classification and fault signature production for rolling element bearings in electric machines. IEEE Trans Ind Appl 40(3):735–739
10. Gaud DK, Agrawal P, Pradesh M (2016) Fault diagnosis of rolling element bearing based network parameter selection. IEEE, pp 8–12

11. Mathew RJAJ (1984) The condition monitoring of rolling element bearings using vibration analysis. J Vib Acoust Stress Reliab Des 106(July):2016
12. Jayaswal P, Verma SN, Wadhwani AK (2010) Development of EBP—artificial neural network expert system for rolling element bearing fault diagnosis. J Vib Control 17(8):1131–1148
13. Jayaswal P, Verma SN, Wadhwani AK (2015) Application of ANN, Fuzzy Logic and Wavelet Transform in machine fault diagnosis using vibration signal analysis. J Qual Maint Eng 16(2):190–213
14. Kankar PK, Sharma SC, Harsha SP (2011) Expert systems with applications fault diagnosis of ball bearings using machine learning methods. Expert Syst Appl 38(3):1876–1886
15. Orhan S, Aktu N (2006) Vibration monitoring for defect diagnosis of rolling element bearings as a predictive maintenance tool: comprehensive case studies. NDT E Int Elsevier 39:293–298
16. Lakshmi Pratyusha P, Shanmukha Priya V, Naidu VPS (2014) Bearing health condition monitoring: time domain analysis. Int J Adv Res Electr Electron Instrum Eng 75–82
17. Lakshmi Pratyusha P, Shanmukha Priya V, Naidu VPS (2014) Bearing health condition monitoring: time domain analysis. In: 2008 IEEE region 10 colloquium and the third international conference on industrial and information systems, pp 75–82
18. Shakya P, Darpe AK, Kulkarni MS (2013) Vibration-based fault diagnosis in rolling element bearings: ranking of various time, frequency and time-frequency domain data-based damage identification parameters. Int J Cond Monit 3(2):53–62
19. Bafroui HH, Ohadi A (2014) Application of wavelet energy and Shannon entropy for feature extraction in gearbox fault detection under varying speed conditions. Neurocomputing 133:437–445
20. Bhavaraju KM, Kankar PK, Sharma SC, Harsha SP (2010) A comparative study on bearings faults classification by artificial neural networks and self-organizing maps using wavelets. Int J Eng Sci Technol 2(5):1001–1008
21. Jayaswal P, Wadhwani AK (2015) Application of artificial neural networks, fuzzy logic and wavelet transform in fault diagnosis via vibration signal analysis: a review. Aust J Mech Eng 7(2):157–171
22. Garad A, Sutar KB, Shinde VJ, Pawar AC (2017) Analysis of vibration signals of rolling element bearing with localized defects. Int J Curr Eng Technol 7(1):37–42
23. Jayaswal P, Wadhwani AK, Mulchandani KB (2008) Machine fault signature analysis. Int J Rotating Mach 2008
24. Yan R (2007) Base wavelet selection criteria for non-stationary vibration analysis in bearing health diagnosis
25. Rao BKN, Pai PS, Nagabhushana TN (2012) Failure diagnosis and prognosis of rolling-element bearings using artificial neural networks: a critical overview. J Phys 364:012023
26. Rodrigues AP, D'Mello G, Srinivasa Pai P (2016) Selection of mother wavelet for wavelet analysis of vibration signals in machining. J Mech Eng Autom 6(5A):81–85
27. Kankar PK, Sharma SC, Harsha SP (2011) Fault diagnosis of ball bearings using continuous wavelet transform. Appl Soft Comput J 11(2):2300–2312
28. He H, Tan Y, Wang Y (2015) Optimal base wavelet selection for ECG noise reduction using a comprehensive entropy criterion. Entropy 17:6093–6109
29. Rosso OA et al (2001) Wavelet entropy: a new tool for analysis of short duration brain electrical signals. J Neurosci Methods 105:65–75
30. Agrawal P, Jayaswal P (2019) Fault investigation of rolling element bearing using soft computing. J Artif Intell Res Adv 6(1):8–22
31. Samanta B, Al-Balushi KR (2003) Artificial neural network based fault diagnostics of rolling element bearings using time-domain features. Mech Syst Sig Process 17(2):317–328
32. Tiwari R, Gupta VK, Kankar PK (2013) Bearing fault diagnosis based on multi-scale permutation entropy and adaptive neuro fuzzy classifier. J Vib Control 2013
33. Sui W, Zhang D (2009) Rolling element bearings fault classification based on SVM and feature evaluation. In: Eighth international conference on machine learning and cybernetics July, pp 450–453

34. Barakat M, Lefebvre D, Khalil M, Mustapha O, Druaux F (2010) BSP-BDT classification technique: application to rolling elements bearing. In: Conference on control and fault tolerant system, vol 4, no. 3, pp 654–659
35. Li P, Jiang Y, Xiang J (2014) Experimental investigation for fault diagnosis based on a hybrid approach using wavelet packet and support vector classification. Sci J Hindawi 2014
36. Widodo A, Yang BS (2007) Support vector machine in machine condition monitoring and fault diagnosis. Mech Syst Sig Process 21:2560–2574
37. Agrawal P, Jayaswal P (2019) Selection of best classification algorithm for fault diagnosis of bearing using vibration signature analysis. Int J Innov Technol Explor Eng 8(5):538–546
38. Marichal G, Artes M, Garcia-Prada J (2011) An intelligent system for faulty-bearing detection based on vibration spectra. J Vib Control 17(6):931–942
39. Sugumaran VÃ, Ramachandran KI (2007) Automatic rule learning using decision tree for fuzzy classifier in fault diagnosis of roller bearing. Mech Syst Sig Process 21:2237–2247
40. Bhavaraju KM, Kankar PK, Sharma SC, Harsha SP (2009) Fault diagnosis of ball bearings using soft computing. In: IDETC/CIE 2009, no. 91, pp 1–5
41. Kappaganthu K, Nataraj C (2016) Feature selection for fault detection in rolling element bearings using mutual information. J Vib Acoust ASME 133:1–11
42. Wang H, Chen J, Dong G (2014) Weak fault feature extraction of rolling bearing based on minimum entropy de-convolution and sparse decomposition. J Vib Control 20:1148–1162
43. Attoui I, Fergani N, Boutasseta N, Oudjani B, Deliou A (2017) A new time-frequency method for identification and classification of ball bearing faults. J Sound Vib 397:241–265

Integrated Model and Machine Learning-Based Approach for Diagnosis of Bearing Defects

N. Upadhyay and P. K. Kankar

Abstract Rolling element bearings are the furthermost precarious mechanical components and used in almost all types of rotating machineries. Due to continuous operation, fatigue stresses are developed over the bearing contact surfaces which result, defects emerging over the rolling element bearing surfaces. For the continuous and smooth operation of rotating machines, it is necessary to detect these defects at their early development stage to avoid the catastrophic failure of rotating machines. In this study, an integrated model and data driven-based methodology for the diagnosis of bearing defect is presented. Data have been collected from the simulation of the mathematical model as well as from experiment. Further, statistical time domain features are calculated from the data to train the machine learning technique, i.e., artificial neural network, support vector machine and decision tree. The features vector is prepared by combining the features extracted from both simulation and experimental data. It has been found that integration of model and machine learning-based technique provides good diagnosis efficiency.

Keywords Diagnosis · Feature extraction · Machine learning techniques · Rolling element bearing

1 Introduction

Rolling element bearings are the most critical components that play an important role in the health of machinery and its life in modern production system. Condition monitoring methods are required to predict health state of rolling element bearings

N. Upadhyay (✉)
Department of Mechanical Engineering, Indian Institute of Technology Delhi, New Delhi 110016, India
e-mail: nitin.upadhyay7@gmail.com

P. K. Kankar
Discipline of Mechanical Engineering, Indian Institute of Technology Indore, Indore 453552, India
e-mail: pkankar@iiti.ac.in

V. K. Gupta et al. (eds.), *Reliability and Risk Assessment in Engineering*,
Lecture Notes in Mechanical Engineering,
https://doi.org/10.1007/978-981-15-3746-2_20

during the operation. Various condition monitoring techniques are vibration analysis, stator current, oil-debris analysis acoustic emission, etc. Out of these techniques, vibration analysis is an efficient and extensively used method for the monitoring of bearing's health. The condition monitoring process comprises detection, diagnosis and prognosis analysis. This requires feature extraction from raw vibration signal to determine the state of the rolling element bearing.

The bearing defects are majorly classified into the two groups: distributed defects and localized defects. Distributed defects are bearing surface waviness, misaligned races, and off-sized rolling elements. The localized defects comprise cracks, spalls, corrosion pitting, etc. on the various bearing components. Defects in bearings generate a series of impulses at regular intervals.

A large amount of works are presented on diagnosis of bearing defects using signal processing and machine learning techniques. Samanta et al. [1] presented a comparative study of artificial neural network (ANN) and support vector machine (SVM) for fault diagnosis of the ball bearing and genetic algorithm had been used for selection of most appropriate features. Yang et al. [2] developed a procedure for the diagnosis of bearing defects by intrinsic mode decomposition of envelope spectrum and SVM. In their work, the defects are considered in both inner and outer races, and vibration response of the normal and defective bearings was recorded. Kankar et al. [3] compared the classification result of ANN and SVM. Authors concluded that SVM gives the higher classification efficiency as compared to ANN. Randall and Antoni [4] presented a brief review of various rolling element bearing defect diagnostic techniques. Tiwari et al. [5] used multiscale permutation entropy with adaptive neuro-fuzzy classifier for bearing fault classification. Authors found that ANFC combined with MPE provides 100% classification accuracy. Vakharia et al. [6] presented feature ranking technique to find out the optimal features for the effective diagnosis of bearing defects. Kavathekar et al. [7] presented rotation forest technique for effective diagnosis of bearing defects. Based on the literature, it has been observed that existing method still needs to be improved.

Based on the previous research, it has been found that when the system is new and the number of data is less, accuracy of diagnosis techniques is poor. In this paper, an integrated diagnostic approach combining mathematical model and data driven-based approach has been presented. To achieve this objective, classical statistical features are calculated from both mathematical model and experiments' results. These features are combined together to make the features vector. Then, this features vector is used as input to the machine learning such as SVM, ANN and decision tree; overview of proposed approach is shown in Fig. 1.

2 Mathematical Model

Schematic of a rotor-bearing system is demonstrated in Fig. 2. In the mathematical model, contact between ball and races is taken as nonlinear spring-damper system. Stiffness can be calculated using Hertzian contact theory [8, 9]. The inner race is

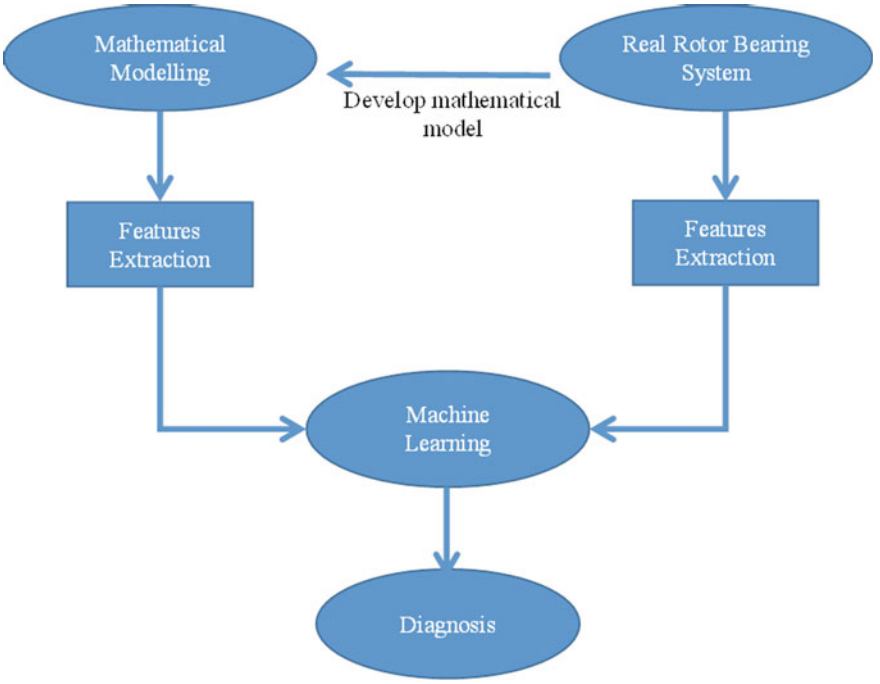

Fig. 1 Overview of proposed methodology

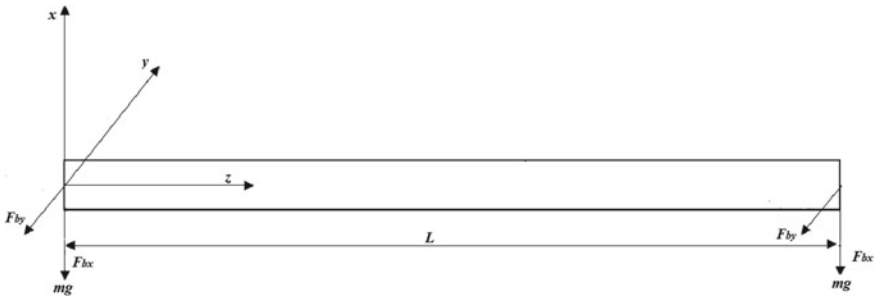

Fig. 2 Schematic of rotor-bearing system

rotating at shaft speed and outer race is fixed in housing. A constant vertical force is assumed to act on the system.

Mostly, the modeling of rotor-bearing system is very challenging. Therefore, the following assumptions are considered for accurate modeling:

1. No friction between races and balls.
2. Balls are equal-spaced and there is no contact between the balls and races.

Symbols in Fig. 2 are explained as follows m is the mass of rotor bearing assembly; k and c are stiffness and damping of shaft, respectively; F_{bx} and F_{by} are the bearing restoring force acting on bearing in x and y directions, respectively, c_{bx} and c_{by} are the nonlinear contact stiffness in x and y direction, respectively [10]. Values of the parameters are taken from Upadhyay et al. [9].

According to Newton's second law, the governing differential equation of motion along x and y direction can be expressed as:

$$m\ddot{x} + (c + c_{bx})\dot{x} + kx + F_{bx} = mg \tag{1}$$

$$m\ddot{y} + (c + c_{by})\dot{y} + ky + F_{by} = 0 \tag{2}$$

Equations 1 and 2 are nonlinear differential equations of motion. In the equations, the terms x and y are the displacement of the bearing in x and y direction, respectively. First and double derivative in the equations signifies velocity and acceleration, respectively. To obtain the results of dynamics system, sixth-order Runge–Kutta method has been used [10]. Details about sixth-order Runge–Kutta method can be found in Luther [11].

3 Experimental Setup

Experiments have been performed to acquire the vibration signals. The setup has a 3HP induction motor whose speed is measured using variable frequency drive (VFD). One end of the shaft is connected to motor with the help of flexible coupling and other end supported on test bearing. Data is acquired using an accelerometer at 48,000 Hz sampling frequency for various defect conditions such as bearing with no defect (ND), with inner race defects (ID) and with outer race defects (OD). An accelerometer is used to obtain the vibration signals. DEWESOFT data acquisition system has been used to record the vibration response over the speed range 500–1500 rpm. Experimental setup is presented in Fig. 3. Detail specification of bearing are listed in Table 1.

4 Feature Extraction

Time-domain statistical features have been calculated from the both mathematical model and experimental data. Features extracted from mathematical model and experimental investigation are combined together to make the features vector. The following features are considered for the classifications of bearing defect which are explained below [12]:

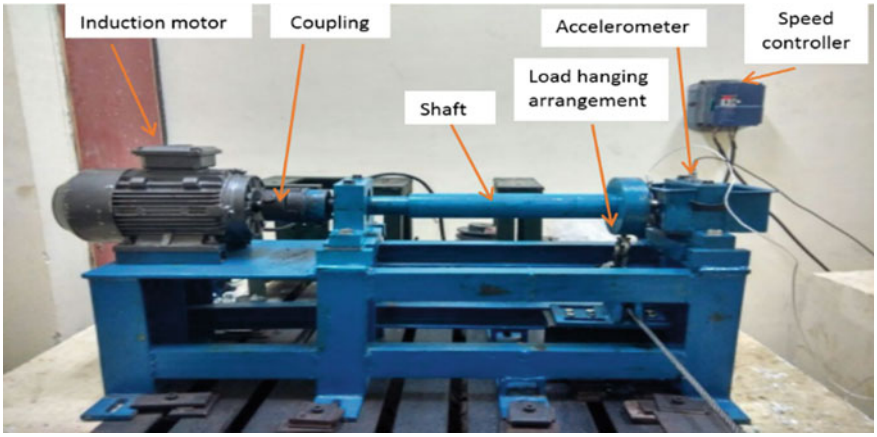

Fig. 3 Experimental setup

Table 1 Bearing specifications

Parameters	Values
Bearing number	NBC 6307 (single row deep groove ball bearing)
Bore diameter	35 mm
Diameter of outer race	80 mm
Diameter of ball	11.25 mm
Width	21 mm
Number of balls	8

1. **RMS value**: It is defined as the square root of the arithmetic mean of squares of original values.

$$\text{RMS} = \sqrt{\frac{\sum_{i=1}^{m} (x_i)^2}{m}} \tag{3}$$

2. **Standard deviation(s)**: Standard deviation represents the amount of energy present in the signal.

$$s = \sqrt{\sum_{i=1}^{m} (x_i - \overline{x})^2 \Big/ m} \tag{4}$$

3. **Kurtosis**: It is a measure of peakedness of data.

$$\text{Kurtosis} = \frac{1}{m} \times \left\{ \frac{\sum_{i=1}^{m} (x_i - \bar{x})^4}{s^2} \right\} \tag{5}$$

4. **Skewness**: It is a degree of symmetry in data. A distribution is called symmetric if it seems similar to the right and left of the centre point.

$$\text{Skewness} = \frac{1}{m} \times \left\{ \frac{\sum (x_i - \bar{x})^3}{s^{3/2}} \right\} \tag{6}$$

5. **Minimum value**: It signifies minimum value in a specific data set of signal.
6. **Peak value**: The maximum value of the signal above the reference value, which usually used is zero.
7. **Crest factor**: It is defined as the ratio of peak to its RMS value known as Crest factor.

$$\text{Crest factor} = \text{Peak/RMS} \tag{7}$$

8. **Form factor**: Ratio of RMS to mean value is known as Form factor.

$$\text{Form factor} = \text{RMS}/x \tag{8}$$

5 Classification Techniques

For the classification of bearing defects, machine learning techniques, i.e., ANN, SVM, and decision tree are used.

5.1 Support Vector Machine

Support vector machine is one of the most majorly used machine learning techniques. It is a kind of supervised learning technique used for the classification and regression when the number of data point is less. In this technique, a hyperplane is created between the classes to be separable. The data points nearby to the plane are known as support vectors. For the least generalization error, SVM maximizes the margin from support vectors. The brief of SVM techniques is presented in Cortes and Vapnik [13].

5.2 Artificial Neural Network

Artificial neural network involves the bunch of interconnected neurons. These neurons are used to transfer the information from input to output neurons via hidden

neurons. It is an information-based structure which changes its structure depending on the flow of information via network [14].

Each neuron consists of synapses, summation junction and activation function. Synapses sustained the connection between the jth neuron and input signal x_i and the weighting factor w_{ki}. Adder sum off the input signals multiply by respective weight of neuron. Activation function is used to transform the total output into a small range of output.

A general mathematical expression of ANN can be expressed as:

$$y_k = \sum_{i=1}^{n} w_{ki} x_i + w_{ko} \tag{9}$$

5.3 Decision Tree

Decision tree involves number of roots, nodes, branches, and leaves. Nodes signify the features and each branch signifies outcome. A branch contains a series of nodes from root to leaf which indicate the class label. The features exist in a tree delivers the information about decision tree [15]. It is an information-based machine learning techniques used for the classification. J48 algorithm is majorly used to algorithm to build.

Efficiency of Classifier: It is the ratio of correctly classified cases to total number of cases.

$$\text{Classification efficiency} = \frac{\text{Correctly classified instances}}{\text{Total instances}} \tag{10}$$

6 Results

The outcomes of the test data are presented in the form of two-dimensional confusion matrices. The detailed information of classification by each machine learning technique by test set and tenfold cross-validation is shown in Tables 2, 3 and 4. For the test set, 66% of features are used to train the machine learning techniques and remaining 33% are used to test the performance of the machine learning techniques model.

Tenfold cross-validation is a standard way for finding the classification efficiency of a machine learning technique. Tenfold cross-validation is selected because it eliminates the biasness while assigning data into training and testing set. Tables 2, 3, and 4 show the results of machine learning techniques using both test set and tenfold cross-validation.

Table 2 Confusion matrix of SVM

Test set				Tenfold			
ND	ID	OD	Classified as	ND	ID	OD	Classified as
13	5	0	ND	50	16	0	ND
0	18	0	ID	0	66	0	ID
0	0	18	OD	0	1	65	OD

Table 3 Confusion matrix of ANN

Test set				Tenfold			
ND	ID	OD	Classified as	ND	ID	OD	Classified as
16	1	1	ND	63	3	0	ND
2	16	0	ID	1	64	2	ID
1	1	16	OD	2	1	63	OD

Table 4 Confusion matrix of decision tree

Test set				Tenfold			
ND	ID	OD	Classified as	ND	ID	OD	Classified as
18	0	0	ND	65	1	0	ND
0	18	0	ID	0	66	0	ID
0	0	18	OD	2	1	63	OD

For the testing purpose, the overall testing efficiency for SVM, ANN, and decision tree is 90.74%, 88.88%, and 100%, respectively, and for tenfold cross-validation, the classification accuracies are 91.41%, 96.46%, and 97.97%, respectively, for SVM, ANN, and decision as shown in Table 5. It is clear from the above results that integrated approach provides good classification accuracy. Classification accuracy of decision tree is higher than the other machine learning techniques used in this work.

Table 5 Classification results

Parameters	SVM		ANN		Decision tree	
	Test set	Tenfold	Test set	Tenfold	Test set	Tenfold
Correctly classified instances	49 (90.74%)	181 (91.41%)	48 (88.88%)	191 (96.46%)	54 (100%)	194 (97.97%)
Incorrectly classified instances	5 (9.26%)	17 (8.58%)	6 (11.22%)	7 (3.54%)	0 (0%)	4 (2.02%)

7 Conclusions

Presented an integrated model and data driven-based technique for the accurate diagnose of bearing defects. In this study, SVM, ANN, and decision tree are used for the classification of bearing defects. Statistical time-domain feature is calculated from the data obtained by mathematical model and experimental investigation. Integration of model and data-driven techniques are giving good classification accuracy. Based on the classification result, it has been observed that decision tree gives better efficiency as compared to SVM and ANN. Since both test set and cross-validation technique are used for the classification, tenfold cross-validation is more accurate than the test set because it eliminates the biasness in training and test data. In future, we can apply proposed technique with combination of different signal decomposition methods.

References

1. Samanta B, Al-Balushi KR, Al-Araimi SA (2003) Artificial neural networks and support vector machines with genetic algorithm for bearing fault detection. Eng Appl Artif Intell 16:657–665. https://doi.org/10.1016/j.engappai.2003.09.006
2. Yang Y, Yu D, Cheng J (2007) A fault diagnosis approach for roller bearing based on IMF envelope spectrum and SVM. Meas J Int Meas Confed 40:943–950. https://doi.org/10.1016/j.measurement.2006.10.010
3. Kankar PK, Sharma SC, Harsha SP (2011) Fault diagnosis of ball bearings using machine learning methods. Expert Syst Appl 38:1876–1886. https://doi.org/10.1016/j.eswa.2010.07.119
4. Randall RB, Antoni J (2011) Rolling element bearing diagnostics—a tutorial. Mech Syst Sig Process 25:485–520. https://doi.org/10.1016/j.ymssp.2010.07.017
5. Tiwari R, Gupta VK, Kankar PK (2015) Bearing fault diagnosis based on multi-scale permutation entropy and adaptive neuro fuzzy classifier. J Vib Control 21:461–467. https://doi.org/10.1177/1077546313490778
6. Vakharia V, Gupta VK, Kankar PK (2016) A comparison of feature ranking techniques for fault diagnosis of ball bearing. Soft Comput 20:1601–1619. https://doi.org/10.1007/s00500-015-1608-6
7. Kavathekar S, Upadhyay N, Kankar PK (2016) Fault classification of ball bearing by rotation forest technique. Procedia Technol 23:187–192. https://doi.org/10.1016/j.protcy.2016.03.016
8. Metsebo J, Upadhyay N, Kankar PK, Nana Nbendjo BR (2016) Modelling of a rotor-ball bearings system using Timoshenko beam and effects of rotating shaft on their dynamics. J Mech Sci Technol 30:5339–5350. https://doi.org/10.1007/s12206-016-1101-x
9. Upadhyay N, Metsebo J, Kankar PK, Nbendjo N (2017) An improved theoretical model of unbalanced shaft-bearing system for accurate performance prediction of ball bearing due to localized defects. Iran J Sci Technol Trans Mech Eng. https://doi.org/10.1007/s40997-017-0098-9
10. Kankar PK, Sharma SC, Harsha SP (2012) Vibration based performance prediction of ball bearings caused by localized defects. Nonlinear Dyn 69:847–875. https://doi.org/10.1007/s11071-011-0309-7
11. Luther HA (1968) An explicit sixth-order Runge-Kutta formula. Math Comput 22:434–434. http://www.ams.org/jourcgi/jour-getitem?pii=S0025-5718-68-99876-1
12. Sharma A, Amarnath M, Kankar PK (2016) Novel ensemble techniques for classification of rolling element bearing faults. J Braz Soc Mech Sci Eng 39:709–724. https://doi.org/10.1007/s40430-016-0540-8

13. Cortes C, Vapnik V (1995) Support-vector networks. Mach Learn 20:273–297
14. Haykin S (1998) Neural networks—a comprehensive foundation, 2nd edn. Prentice Hall, New Jersey
15. Quinlan JR (1996) Improved use of continuous attributes in C4.5. J Artif Intell Res 4:77–90

Performance Assessment of Dual Fuel Engine Operated with Agricultural Waste and Diesel

Sharad Bhardwaj, Aditya Sharma, Ashish Malik, and K. L. A. Khan

Abstract To find out the replacement of fossil fuel, numbers of alternative fuels have been developed. It has been observed that in a stationary diesel engine, producer gas is a better substitute for diesel. Through the process of gasification which is a thermo-chemical process, the solid biomass can be converted into a mixture of combustible gases that can be used in various applications. In the present work, while operating in dual fuel mode, a significant reduction in diesel fuel was detected. A 5 kW downdraft gasifier and a four-stroke diesel engine are used to conduct the experiments. Three types of biomasses (rice husk, rice straw and sugarcane bagasse) are considered to study the effect of producer gas on specific consumption of diesel in the dual mode of the engine. The producer gas is generated by using the biomasses and used along with diesel to run the engine in dual mode. The results obtained from the biomasses are compared to find the saving of diesel in dual mode. Results highlighted the better performance of engine when operated with the biofuels, obtained from the biomasses.

Keywords Dual fuel engine · Agricultural waste · Alternative fuel · Sugarcane bagasse

S. Bhardwaj · A. Malik
Department of Mechanical Engineering, ABES Engineering College, Campus 1, NH 24, Ghaziabad, U.P. 201009, India
e-mail: sharadbhardwaj24@gmail.com

A. Malik
e-mail: ashish.abes@yahoo.com

A. Sharma (✉)
Department of Mechanical Engineering, Faculty of Engineering, Dayalbagh Educational Institute, Dayalbagh, Agra 282005, India
e-mail: aditya.me02@gmail.com

K. L. A. Khan
Department of Mechanical Engineering, KIET Group of Institutions, Ghaziabad-Meerut Road, NH-58, Muradnagar, Ghaziabad, U.P. 201206, India
e-mail: kla.khan@kiet.edu

V. K. Gupta et al. (eds.), *Reliability and Risk Assessment in Engineering*,
Lecture Notes in Mechanical Engineering,
https://doi.org/10.1007/978-981-15-3746-2_21

1 Introduction

Fossil fuels such as petroleum, coal and natural gas are the main sources which fulfill the major fraction of the total need of world's energy. But, the stocks of fossil fuels are limited and likely to exhaust. Also, the burning of fossil fuels generates harmful greenhouse gases which in turn causes harm to the environment [1]. For the generation of electricity through the use of fossil fuels, a remarkable amount of carbon dioxide is emitted from the energy sector. A rapid emission of carbon dioxide is expected to increase from energy sector as the demand of electricity is continuously increasing. So, we have to search out the replacement of these fossil fuels. Therefore, to fulfill this increasing demand of energy and to solve the environmental-related issues, the whole world has to move in the direction of non-conventional energy resources [2]. In spite of being pollution-free, renewable fuels are never ending. In case of solar energy, the commercial prospects of larger thermal power plant is uncertain due to the high cost per kW of installed capacity, low operating hours per day, larger ground area requirement, etc. Wind energy though it is a cheap energy generation source, it may not be always available at all the places. Only heavy wind zones and a few places in medium wind zone provide economic sites for wind energy production. Ocean energy can also be generated at few locations. Therefore, the situation of energy is shifting quickly in favor of biomass.

Siemons [3] investigated the possibility of biomass gasification for the electrification of rural areas in developing countries. For the investigation, they follow the way of an annuity costing model, by taking proper explanation of the time value of money. The outcome of the investigation tells about the viability of biomass gasification under different situations. Uma et al. [4] focused on the emission characteristics of a diesel engine at different load conditions in diesel mode and as well as in dual mode (with producer gas). Study was focused on the concentration of pollutants. As a result, the authors concluded that the emissions increase at low-rate conditions. Nouni et al. [5] examined for both dual fuel engine-based biomass gasifier power projects and 100% producer gas engine-based biomass gasifier power projects, the initial capital cost and unit capital cost in India. The cost of biomass gasifier to the diesel generator was compared. Results indicated that the capital cost of the 100% producer gas engine-based biomass gasifier power project was almost twice that of the dual fuel-based gasifier power project. So, according to the results of study, the two smaller capacity systems were expected financially more attractive than the single large capacity systems. Deshmukh et al. [6] investigated the performance and emission characteristics of an engine that was operated in single fuel mode and in dual fuel mode operation at different load conditions. The study concluded that the specific energy consumption in dual fuel mode was in the higher side at all local conditions and the brake thermal efficiency was found to be on greater side for Hingan oil methyl ester or diesel than that of dual fuel mode operation.

Gai and Dong [7] have investigated how the temperature profiles, release of chlorine and sulfur compounds during gasification of corn straw and the composition distribution of producer gas of the gasifier got affected by the operating conditions,

which in turn directly influence the gasification performance. Results show that the composition distribution of the product gas and temperature profiles of the gasifier is greatly influenced by operating conditions. Prashant et al. [8] performed experimental investigations to monitor the effect of methanol blend on the combustion parameters of dual fuel diesel engine. The authors utilized response surface methodology and highlighted the superior performance of the dual fuel engine over the diesel engine. Chintala et al. [9] studied the performance of dual fuel diesel engine, operated by Jatropha seeds. The biofuel obtained from the Jatropha seeds was blended with the diesel in the proportions of 20, 40 and 60% for the examinations. The authors analyzed the combustion and emission characteristics in their investigations and observed significant increment in brake thermal efficiency and reduction in carbon-based emissions of the engine. Dubey and Gupta [10] performed an extensive study to examine the performance of biofuel obtained from Jatropha and Turpentine. The authors carried out the experiments on a diesel engine and obtained a significant reduction in fuel when the engine was operated by biofuel at various loads. Recently, Dubey and Gupta [11] analyzed the effect of biofuels on single-cylinder variable compression ratio diesel engine. The authors investigated the performance of engine at various compression ratios and observed that the engine produces very less emissions when operated on biofuels.

Most of the previous work is focused on woody biomass. However, in actual practice, agricultural waste is available in abundance in most of the states of India. At present, most of the agriculture biomass especially in Uttar Pradesh, Punjab and Haryana are either burned in the fields itself or used for cooking purpose with direct combustion [12]. This method pollutes the environment and is very less energy efficient. Therefore, there is a need to explore the suitable technology to use the available agricultural wastage effectively and economically. Hence, the present study has been conducted on the agriculture/nonwoody biomass to produce energy.

2 Biomass Energy and Its Indian Perspective

The term biomass is used to explain all biologically created matter, and it is the name given to all living substance on earth. Naturally, all biomass decomposes ultimately to its molecules with the release of heat and the combustion of biomass imitates. So, the energy obtained from biomass is a form of renewable energy. It is unique that the biomass efficiently stores solar energy naturally. Also, it is the only renewable energy source of carbon and is able to convert into convenient solid, liquid and gaseous fuels [13]. Unlike any other energy resource, use of biomass for the production of energy is often a way to dispose off biomass waste materials, otherwise it can generate environmental risks. About 600 million tons of agricultural waste, consisting chiefly of rice husks, paddy straw, sugarcane waste, wheat residues and cotton stalks, produce in India. It has been found that about 300 million tons of agricultural waste is not being utilized and is being disposed off by burning it into the open fields, which is creating environmental threats. Government of India makes strict law every year, so

Table 1 Total availability of crop residues in India [15]

Crop	Grain: straw ratio	Estimated crop residues (million ton)
Rice	1.5	123.45
Wheat	1.5	98.87
Sorghum	2.0	15.96
Pearl millet	2.0	15.38
Maize	1.5	16.28
Pulses	1.0	13.07
Pigeon pea	2.0	4.88
Oilseeds	2.0	44.04
Groundnut	1.5	11.78
Cotton	2.0	22.28
Jute and mesta	2.0	22.24
Sugarcane	0.1	27.63
Total	–	415.86

that this agricultural waste could not burn in an open field, but these laws and warnings are overlooked. As a solution to it, these wastes can be used by transforming them into a gaseous combustible fuel named as "producer gas or syngas" in appropriate designed reactors (biomass gasifiers).

India is a country of agriculture land. A variety of crop residues are available in the country, and some of them are given in Table 1. Presently, biomass shares 15% of the total energy supply worldwide and 40% of this energy is consumed in developing countries, generally in rural areas. As the potential of biomass is 19,500 MW, a maximum amount of 4272 MW has been commissioned till December 2014 [14]. If the biomass is burned in a competent way, oxygen from the atmosphere reacts with the carbon present in plants and produces carbon dioxide and water. This is a cyclic process as the carbon dioxide is then available to produce new biomass. Biomass is not only the renewable source of energy but also has the potential to be clean and safe for the environment. Since in biomass there are organic substances which can be converted into heat and power without contributing to carbon dioxide emission, we must enable the biomass to function as a carbon-neutral source of energy [13].

3 Experimental Setup and Procedure

Three types of biomass, rice husk, rice straw and sugarcane bagasse, were selected as raw material. The brief outlines of the experimental setup are shown in Fig. 1, and the image of complete experimental setup is shown in Fig. 2. It mainly consists of a diesel engine, gasifier, gas filter, gas cooler and eddy current dynamometer. About 5 kg of three biomasses is utilized to drive the gasifier. A set of radially directed air

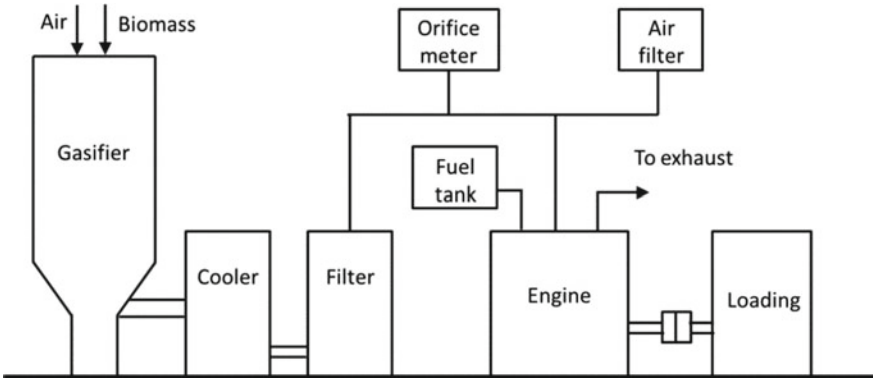

Fig. 1 Outlines of the experimental setup along with the gasifier and test engine

Fig. 2 Engine experimental test rig

nozzles permit the air to be drawn into the biomass, as it moves down to be gasified. The nozzles are attached to a distribution manifold, which in turn is attached to the outer surface of the inner can. This manifold is connected through the outer can to a large air-entry port. The incoming air burns some of the wood, most of the tars and oils, and some of the charcoal that fills gasifier below the nozzles get pyrolyzed. Mostly, mass of the biomass is converted into gas. The gasifier is self-adjusting in many ways. If no sufficient charcoal is there in the air nozzles, more biomass is burned and pyrolyzed to make more charcoal. If char forms in excess during high-load conditions, then the level of char increases above the nozzles, so that incoming air burns the char to reduce the level of char. Thus, at the nozzles, reaction zone

is maintained. After the completion of combustion, the producer gas obtained was supplied to the engine along with the diesel. As a result, change in specific fuel consumption of diesel amount was observed. The engine is single-cylinder, four-stroke, water-cooled diesel engine (Kirloskar make) and is operated at 1500 rpm. The rated power of the engine is 3.5 kW.

4 Results and Discussion

The syngas produced from the gasifier is supplied to the dual fuel engine. As a result, the dual fuel engine starts consuming the syngas, and due to this, the consumption of diesel is decreased. This is how fuel is saved using the syngas. The consumption which is reduced after the use of this produced gas depends upon the composition of the gas. The composition of fuel further depends upon the type of biomass used.

Table 2 gives the consumption of diesel at different loads in diesel mode of engine. These results are also shown in Fig. 3. The data obtained from the experiments by using the rice husks in dual fuel mode is summarized in Table 3. Figure 4 shows the effect of varying load on specific diesel consumption in diesel only and dual fuel mode, in which producer gas of rice husk was used with diesel. It shows the benefit of using dual mode, as at highest load, i.e., 4 kW, in diesel only mode, consumption

Table 2 Consumption of diesel at various loads in diesel mode of engine

Electric load (kW)	Diesel consumption (mL)	Time (s)	Specific diesel consumption (SDC) (mL/s)
1	10	42	0.2481
2	10	28	0.3611
3	10	19	0.5326
4	10	14	0.7204

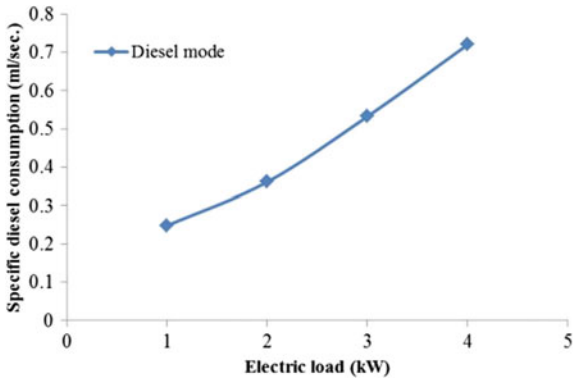

Fig. 3 Effect on specific fuel consumption on varying load in diesel mode

Table 3 Consumption of diesel at various loads in dual mode of engine (rice husk)

Electric load (kW)	Diesel consumption (mL)	Time (s)	Specific diesel consumption (SDC) (mL/s)
1	10	88	0.1145
2	10	62	0.1596
3	10	45	0.2237
4	10	35	0.2901

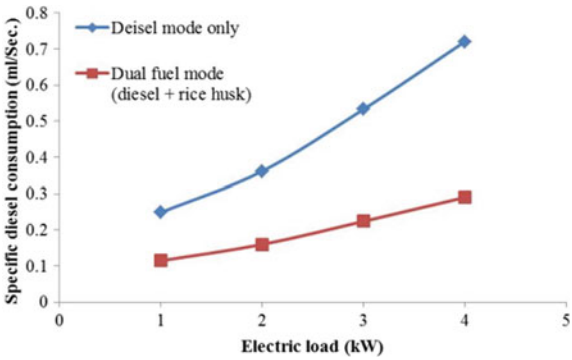

Fig. 4 Effect on specific fuel consumption on varying load in diesel mode and dual fuel mode (diesel + rice husk)

of diesel was more than 0.72 mL/s. However, in case of dual mode, the consumption of diesel was 0.2901 mL/s. Therefore, it is clear that 59.73% diesel consumption can be saved by using the dual fuel mode (producer gas of rice husk + diesel).

Rice straws are cut down into small pieces, and then, those small pieces are fed to the gasifier to generate the producer gas. The observations, given in Table 4, are taken after performing the experiments. Figure 5 shows the effect of varying load on specific diesel consumption in diesel only and dual fuel mode, where producer gas of rice straw was used as second fuel along with primary fuel—diesel. At 1 kW load, diesel consumption was approximately 0.25 mL/s and in dual mode approximately 0.1396 mL/s was observed. It shows that 43.74% diesel consumption is reduced. However, at maximum load, i.e., 4 kW load, the diesel consumption is reduced to 0.3863%, and it results in 0.4637% reduction of the diesel.

Table 4 Consumption of diesel at various loads in dual mode of engine (rice straw)

Electric load (kW)	Diesel consumption (mL)	Time (s)	Specific diesel consumption (SDC) (mL/s)
1	10	71	0.1396
2	10	49	0.2035
3	10	34	0.2951
4	10	26	0.3863

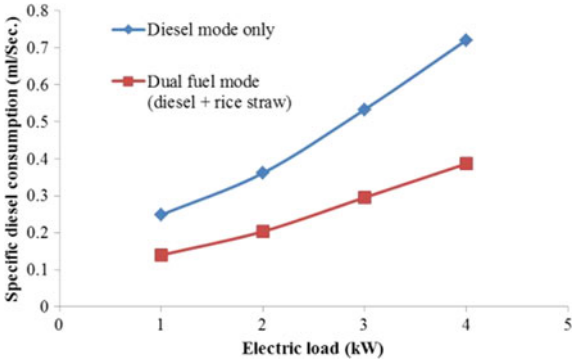

Fig. 5 Effect on specific fuel consumption on varying load in diesel mode and dual fuel mode (diesel + rice straw)

Table 5 Consumption of diesel at various loads in dual mode of engine (sugarcane bagasse)

Electric load (kW)	Diesel consumption (mL)	Time (s)	Specific diesel consumption (SDC) (mL/s)
1	10	173	0.0587
2	10	134	0.0741
3	10	105	0.0957
4	10	81	0.1211

Table 5 gives the results obtained from sugarcane bagasse fuel being used in the gasifier for producer gas generation. The result shows that the specific consumption of diesel is increasing as the load is increasing. In Fig. 6, both dual mode and diesel only mode are shown, and it is clear from the figure that dual fuel mode is showing better results because in the dual mode, specific consumption of diesel is less as compared to diesel only mode. At 1 kW load, diesel consumption was approximately 0.25 mL/s in diesel only mode, but in dual mode, dual consumption was reduced to approximately 0.06 mL/s. So, this is apparent that 76.34% diesel consumption can

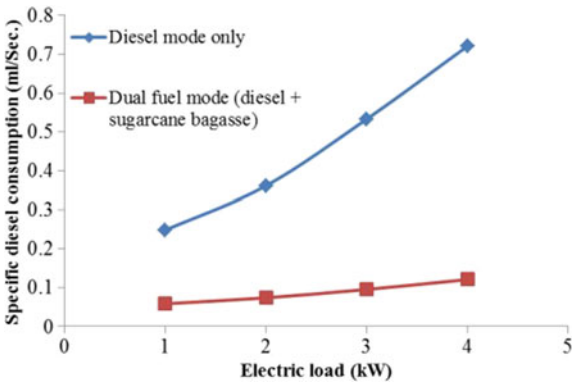

Fig. 6 Effect on specific fuel consumption on varying load in diesel mode and dual fuel mode (diesel + sugarcane bagasse)

be reduced by using the dual fuel mode, where along with diesel, producer gas from sugarcane bagasse was used. Similarly, at 4 kW load, diesel consumption was 0.72 mL/s in diesel only mode, and in the dual mode, it was reduced to 0.12 mL/s. Therefore, 83.19% of diesel consumption can be saved. Results indicate that for the same volume of fuel, the operating time of engine is increased significantly when operated through biofuels (Tables 3, 4 and 5) as compared to the diesel only mode (Table 2). It shows the usefulness of biofuels over the diesel fuel.

5 Conclusions

In the present study, the performance of four-stroke diesel engine is investigated experimentally using diesel and syngas obtained from three biofuels at various loads. Out of the three biomasses, the best results are obtained by using the sugarcane bagasse because of the properties of sugarcane bagasse. After sugarcane bagasse, the results obtained from the rice husks are good as compared to rice straw. However, all the three biofuels indicate superior results over the diesel only mode of the engine. A significant amount of diesel fuel can be saved by replacing it with producer gas. It is observed that consumption of diesel can decrease up to 83.19%, 59.73% and 46.37% by using sugarcane bagasse, rice husk and rice straw, respectively, which not only saves money, but also can help to handle the waste from agricultural crops.

Acknowledgements Authors would like to thank the Faculty and Staff Members of Department of Mechanical Engineering of Thapar University, Patiala (Punjab), for their support in this work.

References

1. Houghton JT, Ding Y, Griggs DJ, Noguer M, van der Linden PJ, Dai X, Maskell K, Johnson CA (eds) (2001) Climate change 2001: the scientific basis, Intergovernmental panel on climate change. Cambridge University Press, Cambridge
2. McNeils B, Roekel VG, Presier K (2002) Renewable energy technology for developing countries, the future for renewable energy: prospects and directions. EUREC Agency, London
3. Siemons RV (2001) Identifying a role for biomass gasification in rural electrification in developing countries: the economic perspective. Biomass Bioenerg 20(4):271–285
4. Uma R, Kandpal TC, Kishore VVN (2004) Emission characteristics of an electricity generation system in diesel alone and dual fuel modes. Biomass Bioenerg 27(2):195–203
5. Nouni MR, Mullick SC, Kandpal TC (2007) Biomass gasifier projects for decentralized power supply in India: a financial evaluation. Energy Policy 35(2):1373–1385
6. Deshmukh LBB, Thakre SB (2008) Investigation on performance and emission characteristics of CI engine fuelled with producer gas and esters of hingan (Balanites) oil in dual fuel mode. Int J Aerosp Mech Eng 2:148–153
7. Gai C, Dong Y (2012) Experimental study on non-woody biomass gasification in a downdraft gasifier. Int J Hydrog Energy 37(6):4935–4944
8. Prashant GK, Lata DB, Joshi PC (2016) Investigations on the effect of methanol blend on the combustion parameters of dual fuel diesel engine. Appl Therm Eng 103:187–194

9. Chintala V, Kumar S, Pandey JK (2017) Assessment of performance, combustion and emission characteristics of a direct injection diesel engine with solar driven Jatropha biomass pyrolysed oil. Energy Convers Manag 148:611–622
10. Dubey P, Gupta R (2017) Effects of dual bio-fuel (Jatropha biodiesel and Turpentine oil) on a single cylinder naturally aspirated diesel engine without EGR. Appl Therm Eng 115:1137–1147
11. Dubey P, Gupta R (2018) Influences of dual bio-fuel (Jatropha biodiesel and turpentine oil) on single cylinder variable compression ratio diesel engine. Renew Energy 115:1294–1302
12. Jain N, Bhatia A, Pathak H (2014) Emission of air pollutants from crop residue burning in India. Aerosol Air Qual Res 14:422–423
13. Demirbas A (2001) Biomass resources facilities and biomass conversion processing for fuels and chemicals. Energy Convers Manag 42:1357–1378
14. Ministry of new and renewable energy (MNRE), Government of India, Annual report 2014–15. Available at: http://mnre.gov.in/file-manager/annual-report/2014-2015/EN/Chapter%201/chapter_1.htm. Accessed on 20 Oct 17
15. Mohapatra SK, Singh L (2003) Bio energy potential and management in India with emphasis on biomass gasification. In: Proceedings of national conference on recent development in mechanical engineering, TIET Patiala, 31 Oct and 1 Nov 2003

Investigations on Nonlinearity for Health Monitoring of Rotor Bearing System

Aditya Sharma, P. K. Kankar, and M. Amarnath

Abstract In this work, the nonlinear dynamic analysis of rotor bearing system is carried out. The combined effects of the parametric excitation such as nonlinear stiffness, varying compliance and Hertzian contact force are considered and formulated in the mathematical model. The analysis is carried out at various rotor speeds to monitor and predict the behavior of the system. This work also represents the vibration frequencies arising from the nonlinear dynamic responses of unbalanced rotor supported on cylindrical roller bearing. The qualitative and quantitative assessments of nonlinearity of the rotor bearing system have been performed using Poincaré maps and Higuchi's fractal dimensions, respectively. The developed mathematical model is also validated with the experimental analysis, and results are presented in the form of frequency spectrums and fractal dimensions.

Keywords Higuchi's fractal dimension · Poincaré maps · Rotor bearing system · Unbalanced effect

1 Introduction

In today's competitive environment, very precise and safe operations of rotating machines are of prime importance. This makes the nonlinear vibration analysis of rotor bearing system more essential. Nonlinear analysis of rolling element bearings

A. Sharma (✉)
Department of Mechanical Engineering, Faculty of Engineering, Dayalbagh Educational Institute, Dayalbagh, Agra 282005, India
e-mail: aditya.me02@gmail.com

P. K. Kankar
Discipline of Mechanical Engineering, Indian Institute of Technology, Indore 453552, India
e-mail: pkankar@iiti.ac.in

M. Amarnath
Department of Mechanical Engineering, PDPM Indian Institute of Information Technology, Design and Manufacturing, Jabalpur 482005, India
e-mail: amarnath.cmy@gmail.com

V. K. Gupta et al. (eds.), *Reliability and Risk Assessment in Engineering*,
Lecture Notes in Mechanical Engineering,
https://doi.org/10.1007/978-981-15-3746-2_22

includes detailed physical modeling and is a useful tool for insight analysis. The nonlinear analysis of rotor bearing system also helps to understand the system's dynamics and predicts the system's behavior under various operating conditions. Bearings are one of the major sources of nonlinearity in rotating machines which considerably affect the performance of the system. It leads to focus on the nonlinear behavior of rolling element bearings. Having several sources, the nonlinearity arises in rotor bearing system mainly due to the presence of unbalanced forces, internal radial clearance, damping and stiffness. This leads to the generation of nonlinear vibrations. Moreover, during continuous operation, many localized and distributed defects are originated. These are also responsible for development of nonlinear vibrations in bearing.

Various studies are available [1–8] in which the researchers have developed the mathematical models and investigated the responses of rotor bearing system. However, less work is reported for the quantification of nonlinearity in a rotor bearing system. The stability of rotor bearing system can be classified in three categories: periodic, quasi-periodic and chaotic. The qualitative assessment of stability of rolling element bearings has been performed using Poincaré maps or phase trajectory in most of the studies. On the other hand, the quantitative assessment has been carried out using Lyapunov exponent, correlation dimension, fractal dimension and others. Jiang et al. [9] explored the applicability of correlation dimensions for gearbox condition monitoring. The authors summarized that the proposed methodology can be effectively used for health diagnostics but is significantly affected in presence of noise. Changqing and Qingyu [10] carried out extensive study to observe the nonlinearity of balanced rotor bearing system with varying clearance. The authors employed Lyapunov exponent to diagnose the nonlinearity. Results highlighted that Lyapunov exponent can be effectively used to identify the nonlinearity of the system. Ghafari et al. [11] examined the effects of localized defects on ball and roller bearings. The authors carried out experimental investigations and employed Lyapunov exponent and correlation dimension for the analysis. The study summarized that chaotic parameters have great potential and can be used to monitor the health of rolling element bearings. Caesarendra et al. [12] used Lyapunov exponent as a feature for condition monitoring of bearings. The authors concluded that proposed methodology can be used to monitor the health of rolling element bearings that have low energy nonlinear vibrations.

In the previous studies of nonlinear dynamic analysis of rolling element bearings, varying compliance, flexible supports, damping and number of rolling elements, etc., have been considered as sources of nonlinearity. The effects of localized and distributed defects in bearing components were also discussed. However, to establish the baseline data, it is essential to examine the healthy system prior to the defective one. Few investigations have been reported that discuss the dynamic analysis of healthy rotor bearing system at various speeds. Due to the reason of operating the rotating machines at various speeds to meet the operational demands, speed is one of the important parameters that have considerable impact on the responses of rotor bearing system. In the present work, the nonlinear dynamic analysis of healthy cylindrical roller bearing has been carried out. The mathematical model of

the rotor bearing system is developed. This model considers the combined effects of excitations such as varying compliance, Hertzian contact force and varying rotational speed. Besides that, in most of the previous studies, Poincaré maps and Lyapunov exponents have been extensively used for the characterization of nonlinearity. In the present work, Poincaré maps and Higuchi's fractal dimensions are used for the qualitative and quantitative assessment of nonlinearity of the rotor bearing system. Experimental investigations are also performed for the validation of the developed analytical model. The results in the form of frequency spectrums and fractal dimensions, obtained from the numerical analysis and experimental analysis, are compared.

2 Mathematical Model Description

The authors utilized their previously developed mathematical model here for the examination of structural vibrations in cylindrical roller bearing. The details of the model can be accessed in [13]. The governing equations of motions of the system are summarized as:

$$m\ddot{x} + c\dot{x} + \sum_{j=1}^{N} k[(x\cos\theta j + y\sin\theta j) - (R_{\mathrm{cr}})]_{+}^{1.08}\cos\theta j = W + U_{\mathrm{f}}\cos(\omega t) \quad (1)$$

$$m\ddot{y} + c\dot{x} + \sum_{j=1}^{N} k[(x\cos\theta j + y\sin\theta j) - (R_{\mathrm{cr}})]_{+}^{1.08}\sin\theta j = U_{\mathrm{f}}\sin(\omega t) \quad (2)$$

where m is the mass of the rotor supported on the bearings, c is the damping force (450 N s/m), W is the radial load acting on the bearing and U_{f} is the unbalance force and is considered as 5% of the radial load (W) acting on the rotor bearing system. Various other physical values corresponding to the analysis are listed in Table 1.

Table 1 Physical values of bearing

Parameter	Value
Mass of rotor (m)	8 kg
Radius of inner race (R_{ir})	23.1 mm
Radius of outer race (R_{or})	35.1 mm
Pitch circle radius (R_{p})	29.1 mm
Effective length of roller (L_{u})	11.6 mm
Radius of roller (R_{r})	6 mm
Number of rollers (N_{r})	12
Contact angle (β)	0°

3 Higuchi's Algorithm for Fractal Dimension Calculation

Fractal dimension (FD) is an approach for quantifying the nonlinearity of irregular time series system. The basic idea about fractal dimensions (FDs) has been proposed by Mandelbrot [14]. FDs provide a quantitative measure of chaos unlike Fourier transform and bifurcation diagram which provide a general indication of change in response from periodic to chaotic and vice versa. Higuchi's algorithm for fractal dimension estimation is based on the calculations of curve length measurement and calculates the FD with high temporal resolution. It evaluates the mean length of the curve by taking a segment of p samples as a unit of measure. HFD estimation requires following steps for the calculation of FDs [15]:

Step 1: Define a fixed set of time series data at a regular interval as:

$$q(1), q(2), q(3), \ldots, q(M), \ldots, q(N) \tag{3}$$

where $M = 1, 2, 3, \ldots, N$.

In this study, the time series is successive displacement values, respectively, in horizontal and vertical directions.

Now, construct a new time series q_p^v, for a range of p values from 1 to $p_{\max}$ as:

$$q_p^v = q(v), q(v+p), q(v+2p), \ldots, q\left(v + \text{int}\left(\frac{N-v}{p}\right) \cdot p\right) \tag{4}$$

where $v = 1, 2, 3, \ldots, p$.

Step 2: Determine the length of $L_v(p)$ of each curve q_p^v as:

$$L_v(p) = \left[\left(\sum_{M=1}^{\text{int}\left(\frac{N-v}{p}\right)} |q(v + M \cdot p) - q(v + (M-1) \cdot p)| \right) \cdot \frac{N-1}{\text{int}\left(\frac{N-v}{p}\right) \cdot p} \right] \cdot p^{-1} \tag{5}$$

where the term $(N-1) \cdot \left(\text{int}\left(\frac{N-v}{p}\right) \cdot p\right)^{-1}$ indicates the regularization factor for the curve length of q_p^v.

Step 3: Estimate the mean length of the curve for each value of p, $\langle L(p) \rangle$, as the average value over p sets of $L_v(p)$, for $v = 1, 2, 3, \ldots, p$ and repeat the iteration for p ranging from 1 to $p_{\max}$.

Step 4: If $\langle L(p) \rangle \alpha(p)^{-\text{FD}}$, then the curve is fractal with dimension FD.

In the present study, the value of $p_{\max}$ is obtained from a wide range of p values, ranging from 1 to 40,000, in each of horizontal and vertical directions, using the method proposed by Polychronaki et al. [15].

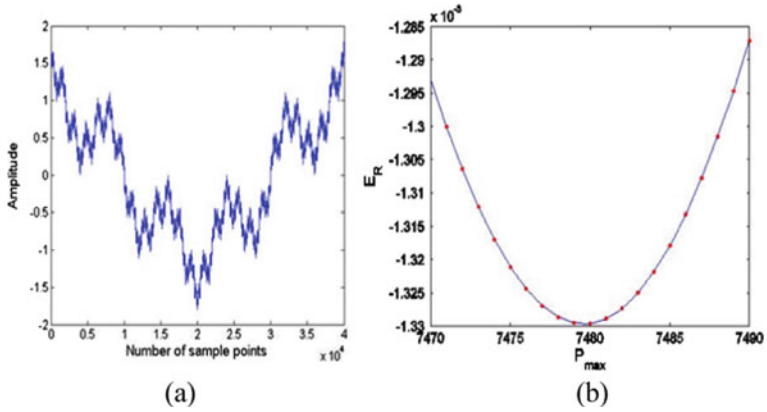

Fig. 1 **a** Weierstrass cosine function for theoretical fractal dimension ($FD_{th} = 1.5$), **b** relative error (E_R) for Higuchi's fractal dimension estimations with p_{max}

The HFD is calculated for each of p values for a synthetic signal (Weierstrass sequence). To estimate the accuracy of the proposed algorithm, relative error (E_R) is computed for different p_{max} values as follows:

$$E_R = FD_{est} - FD_{th} \tag{6}$$

where FD_{est} is the estimated fractal dimension and FD_{th} is the theoretical fractal dimension.

The synthetic Weierstrass sequence with $FD_{th} = 1.5$ is used in the present study and is shown in Fig. 1a. The plot of relative error for Weierstrass sequence is shown in Fig. 1b. It can be easily observed from Fig. 1b that relative error is minimum for $p_{max} = 7480$ (as p has a wide range from 1 to 40,000, only a segment of this range in which E_R is minimum is shown here). Values lower and higher than 7480 clearly lead to higher relative error for the dataset. Hence, HFD is estimated using $p_{max} = 7480$. The value of FDs for a two-dimensional time series data varies between 1 and 2, where the FDs near to 1 indicate the periodic nature and FDs near to 2 indicate the chaotic nature of the system [16].

4 Experimentation and Data Acquisition

In this work, experiments are also carried out to analyze the responses of the rotor bearing system. An experimental test rig is developed to conduct the tests on cylindrical roller bearing. The detailed experimental test rig is shown in Fig. 2. The SKF NJ307ECP bearing has been taken for the study. The physical specifications and parameters of the test bearing are same as taken in theoretical investigations. The physical specifications and parameters of the bearing are summarized in Table 2.

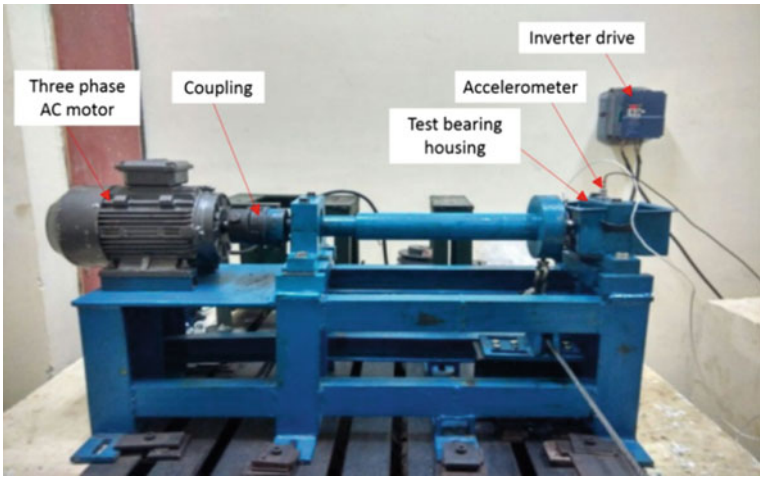

Fig. 2 View of experimental test rig

Table 2 Physical values of bearing

Parameter	Value
Radius of inner race	23.1 mm
Radius of outer race	35.1 mm
Pitch circle radius	29.1 mm
Radius of roller	6 mm
Effective length of roller	11.6 mm
Number of rollers	12
Contact angle	0°
Weight	0.494 kg

The test rig consists of a healthy shaft mounted between two supports. One end of the shaft is connected to a three-phase AC motor of 2.2 kW using mechanical coupling. The rotating speed of the shaft is varied using an inverter drive. The other end of the shaft is connected to the test bearing, and the inner race of the bearing is rigidly fixed with the shaft. The experiments are conducted at various speeds. The vibration signals are acquired using MMF KS78.100 accelerometer and DEWE soft data acquisition system. Further, the data is processed and stored in a personal computer. The accelerometer is attached at the top of the bearing housing using magnetic base, and the sampling frequency is kept 12 kHz.

5 Results and Discussion

5.1 Theoretical Results and Discussion

The rotational speed is one of the key factors which significantly affect the dynamic response of the rotor bearing system. Several rotating machines are operated at various speeds, which make it essential to operate the machines under safe speed limits, otherwise it may affect the system's performance and may reduce the efficiency of the machine.

The response plots of the system at 600 rpm are shown in Fig. 3. The peak amplitude of vibrations in frequency spectrum is appeared at varying compliance (VC) frequency (47.6 Hz) in both the horizontal and vertical directions, and other major peaks are noticed at superharmonics of VC as 2VC and 4VC in vertical direction. The multiorbit periodic nature of Poincaré maps shows the stable nature of the system. HFDs are obtained as 1.0811 and 1.0602, respectively, in horizontal and vertical directions and confirm the stable nature of the system. The system shows stable nature with multiorbit periodic structure up to 2846 rpm. The response of the system at 2900 shows the net structured shape of Poincaré maps which show

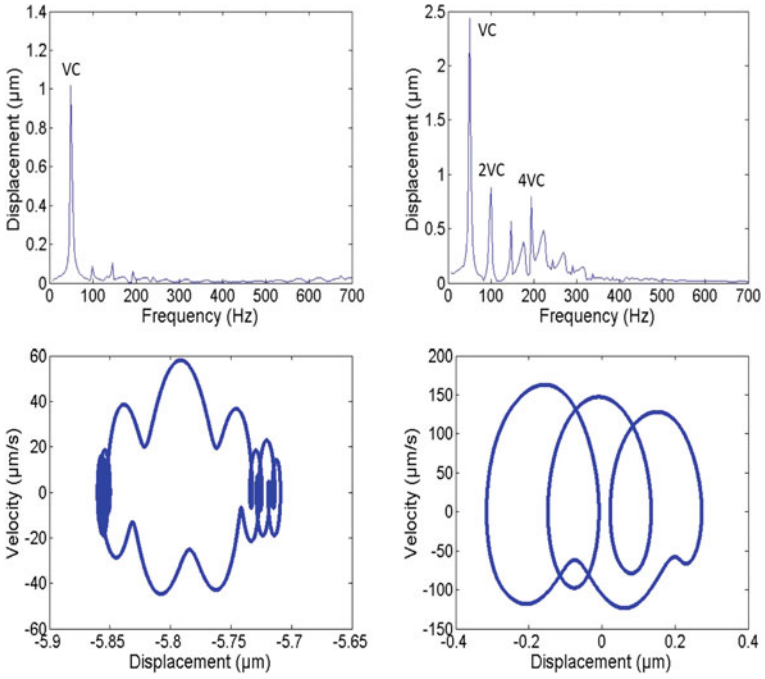

(a) Horizontal (b) Vertical

Fig. 3 Response plots of bearing at 600 rpm

the quasi-periodic nature of the system, and HFDs are quantified as 1.4378 and 1.4829, respectively, in horizontal and vertical direction. As the speed is increased beyond 2934 rpm, the system comes out from unstable region and becomes stable. The system remains in stable region from 2935 to 3496 rpm. As the speed is further increased to 3497 rpm, the system loses its stability again and remains in unstable region up to 3555 rpm. With further increment in the speed as 3556 rpm, the system regains its stability and remains stable up to 4466 rpm. In this region, the HFDs of the system at 3700 rpm are found as 1.0463 and 1.0211, respectively, in horizontal and vertical direction, and periodic nature of the system is observed. The system exhibits quasi-periodic nature with further increment in speed from 4467 to 4573 rpm.

The system regains its stability in the range 4574–5459 rpm; however, the system again enters into unstable region in speed range from 5460 to 5943 rpm. The next stable region is recognized with further increment in speed. This region ranges from 5944 to 6506 rpm. In this region, the HFDs at 6400 rpm are calculated as 1.0937 and 1.0904, respectively, in horizontal and vertical directions. As the speed is further increased to 6507 rpm, the system loses its stability. The system enters into chaotic regime due to sudden attack of chaotic attractor, and system remains in this regime up to 6656 rpm. In this region, the response plots at 6600 rpm are shown in Fig. 4, where the peak amplitude of vibrations is identified at VC (524 Hz) and 0.5VC, respectively, in horizontal and vertical directions. The other major peaks are observed at VC +

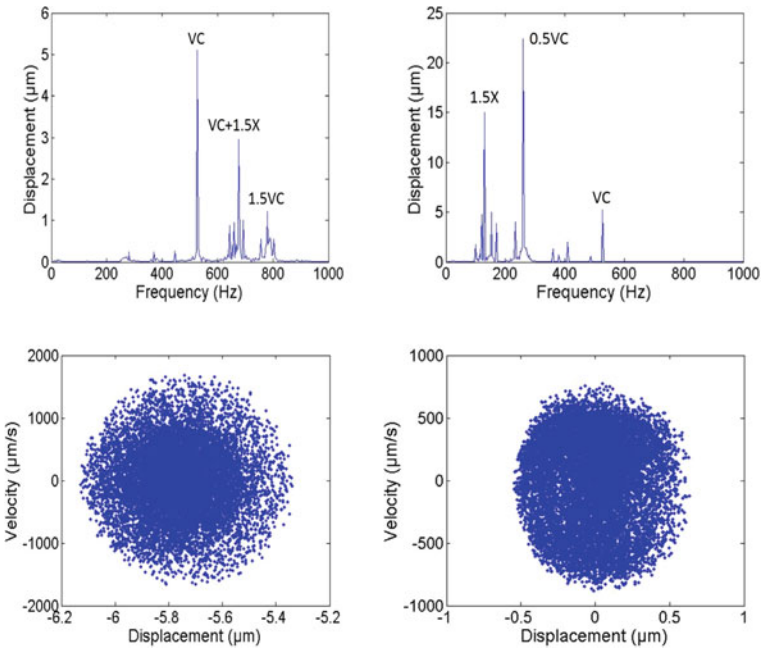

(a) Horizontal (b) Vertical

Fig. 4 Response plots of bearing at 6600 rpm

1.5X and 1.5VC in horizontal direction. In vertical direction, other major peaks appear at 1.5X and VC. The fractal nature of the Poincaré maps shows the chaotic nature of the system, and the HFDs also indicate the unstable chaotic nature of the system as 1.7839 and 1.7265 in horizontal and vertical directions, respectively. The system regains stability with further increment in speed to 6657 rpm and remains stable up to 9516 rpm. This region is recognized as sixth stable region of the system. In this region, the HFDs at 7700 rpm are observed as 1.0735 and 1.0449, respectively, in horizontal and vertical directions which confirm the periodic nature of the system. With further increment in speed to 9519 rpm, the system loses its stability and enters into unstable region. This region, 9517–9816 rpm, is identified as sixth unstable region of the system. In this region, the Poincaré maps at 9700 rpm are obtained in form of net structure, and the HFDs for this speed are calculated as 1.5526 and 1.4813, respectively, in horizontal and vertical directions. As the speed is further increased to 9817 rpm, the system achieves the stability and remains stable up to 10,577 rpm. However, the system shows unstable nature as the speed is further increased to 10,578 rpm and remains unstable up to 11,000 rpm. In this region, the Poincaré maps also show the quasi-periodic nature of the system at 11,000 rpm.

5.2 *Experimental Results and Discussions*

In this work, the responses of healthy bearing at various speeds are analyzed experimentally. Experiments are carried out for rotor speeds ranging from 500 to 1000 rpm. For the comparison of experimental and theoretical frequency responses, the acceleration response is converted to displacement [17]. For the validation purpose, the experimental frequency responses are plotted and compared with the numerical results at same speed.

The frequency responses of the healthy bearing at 500 rpm are shown in Fig. 5.

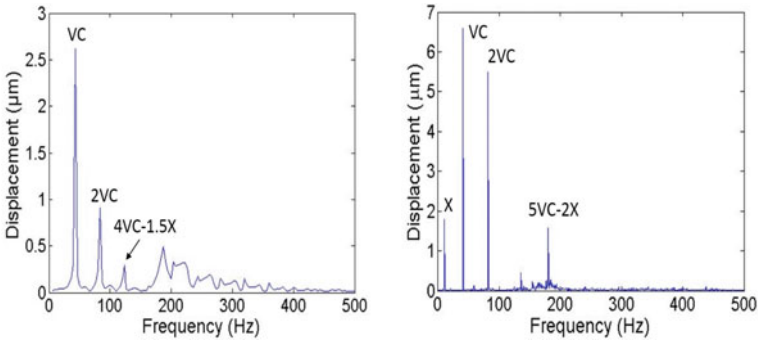

(a) Theoretical (b) Experimental

Fig. 5 Response plots of bearing at 500 rpm

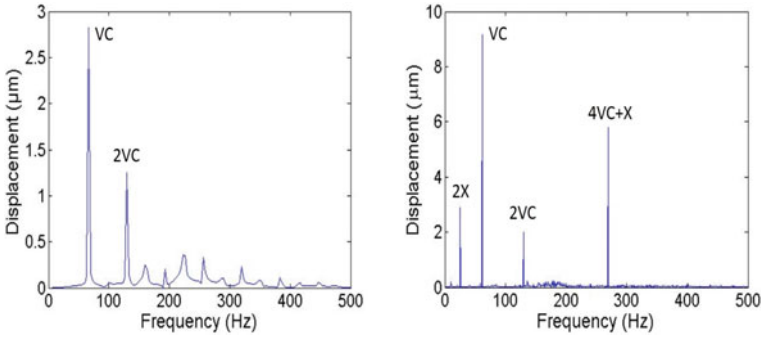

(a) Theoretical (b) Experimental

Fig. 6 Response plots of bearing at 800 rpm

Figure 5a shows the response obtained from the numerical investigation, in which peak amplitude of vibration is observed at varying compliance frequency (VC = 39.7 Hz), and other major peaks are noticed at 2VC and 4VC-X. The experimental results at the same speed are shown in Fig. 5b, and good agreement between the theoretical and experimental results is observed. The peak amplitude of vibration in the experimental results is observed at VC, and the other major peaks are noticed at 2VC, X and 5VC-2X. As the speed is further increased to 800 rpm, the peak amplitude is noticed at VC (VC = 63.5 Hz) in frequency spectrum, when analyzed theoretically. The other peak is perceived at 2VC and shown in Fig. 6a. The experimental result at 800 rpm is shown in Fig. 6b and confirms the nature of system as examined through numerical simulation. In Fig. 6b, the major peak is observed at VC, and other peaks are observed at 4VC + X, 2X and 2VC. A good synchronization between the theoretical and experimental results is observed. The results obtained from the numerical simulation and experimental investigation at various rotor speeds are summarized and compared in Table 3.

6 Conclusions

The following conclusions can be drawn from this work;

1. The experimental investigations have been performed and the vibration responses are presented in the form of FFTs for various rotational speeds. The nonlinearity of the obtained experimental responses is assessed through Higuchi's fractal dimensions and compared with the theoretical responses. Although there are minor differences in the experimental results and theoretical results, these are in close agreement.

Table 3 Summary of theoretical and experimental investigations

S. No.	Rotor speed (rpm)	Peak amplitude at		Difference (%)	HFDs		Difference (%)
		Theoretical investigation	Experimental investigation		Theoretical investigation	Experimental investigation	
1	500	VC (39.7 Hz)	VC (40.89 Hz)	−2.99	1.0716	1.0628	0.82
2	700	VC (55.6 Hz)	VC (57.98 Hz)	−4.28	1.0875	1.0615	2.39
3	800	VC (63.5 Hz)	VC (61.65 Hz)	2.92	1.0322	1.0413	−0.88
4	1000	VC (79.4 Hz)	VC (81.18 Hz)	−2.24	1.0387	1.0526	−1.34
5	1400	VC (111.2 Hz)	VC (111.7 Hz)	−0.45	1.0174	1.0225	−0.51
6	1500	VC (119.1 Hz)	VC (122.7 Hz)	−3.03	1.0186	1.0259	−0.72

2. The qualitative and quantitative assessment of nonlinearity of rotor bearing system has been performed, and both are capable to identify the stability of the system. Higuchi's fractal dimensions are successfully employed to identify and quantify the nonlinearity of the rotor bearing system.
3. Results indicate that Higuchi's fractal dimensions can be used as a diagnostic tool for health monitoring of rotor bearing system and maintenance strategies can be planned accordingly. Moreover, it can be used as a powerful tool for chaos quantification and helps the design/service engineers to deal with the high unstable regimes precisely.

References

1. Wensing J, van Nijen GC (2001) The dynamic behaviour of a system that includes a rolling bearing. Proc Inst Mech Eng, Part J: J Eng Tribol 215(6):509–518
2. Ashtekar A, Sadeghi F, Stacke L (2008) A new approach to modeling surface defects in bearing dynamics simulations. Trans ASME J Tribol 130(4):041103-1-8
3. Kankar PK, Harsha SP, Kumar P, Sharma SC (2009) Fault diagnosis of a rotor bearing system using response surface method. Eur J Mech A Solids 28(4):841–857
4. Bai C, Zhang H, Xu Q (2010) Experimental and numerical studies on nonlinear dynamic behavior of rotor system supported by ball bearings. Trans ASME J Eng Gas Turbines Power 132(8):082502-1-5
5. Shao Y, Liu J, Ye J (2014) A new method to model a localized surface defect in a cylindrical roller-bearing dynamic simulation. Proc Inst Mech Eng Part J: J Eng Tribol 228(2):140–159
6. Ghalamchi B, Sopanen J, Mikkola A (2016) Modeling and dynamic analysis of spherical roller bearing with localized defects: analytical formulation to calculate defect depth and stiffness. Shock Vib 2016:1–11
7. Tiwari M, Gupta K, Prakash O (2000) Dynamic response of an unbalanced rotor supported on ball bearings. J Sound Vib 238(5):757–779

8. Sharma A, Amarnath M, Kankar PK (2014) Effect of varying the number of rollers on dynamics of a cylindrical roller bearing. In: Proceedings of the ASME international design and engineering technical conferences & computers and information in engineering conference (IDETC/CIE 2014), vol 8: 26th conference on mechanical vibration and noise, Buffalo, 17–20 Aug 2014, paper no. DETC2014-34824, pp V008T11A067, 8 p. ASME, New York
9. Jiang JD, Chen J, Qu LS (1999) The application of correlation dimension in gearbox condition monitoring. J Sound Vib 223(4):529–541
10. Changqing B, Qingyu X (2006) Dynamic model of ball bearings with internal clearance and waviness. J Sound Vib 294(1–2):23–48
11. Ghafari SH, Golnaraghi F, Ismail F (2008) Effect of localized faults on chaotic vibration of rolling element bearings. Nonlinear Dyn 53(4):287–301
12. Caesarendra W, Kosasih B, Tieu AK, Moodie CAS (2015) Application of the largest Lyapunov exponent algorithm for feature extraction in low speed slew bearing condition monitoring. Mech Syst Signal Process 50–51:116–138
13. Sharma A, Amarnath M, Kankar PK (2015) Effect of unbalanced rotor on the dynamics of cylindrical roller bearings. Mech Mach Sci 21:1653–1663
14. Mandelbrot B (1967) How long is the coast of Britain? Statistical self-similarity and fractional dimension. Science 156(3775):636–638
15. Polychronaki GE, Ktonas PY, Gatzonis S, Siatouni A, Asvestas PA, Tsekou H, Sakas D, Nikita KS (2010) Comparison of fractal dimension estimation algorithms for epileptic seizure onset detection. J Neural Eng 7(4):1–18
16. Chang-Jian C-W (2010) Strong nonlinearity analysis for gear-bearing system under nonlinear suspension-bifurcation and chaos. Nonlinear Anal: R World Appl 11(3):1760–1774
17. Grant E (2017) How to convert accelerometer data to displacements. http://in.mathworks.com/matlabcentral/answers/17611-how-to-convert-a-accelerometer-data-to-displacements#answer_23739. Accessed on 5 Apr 2017

Experimental Investigation of Chatter in Boring Operation Using Shim

N. B. Prajapati, J. V. Desai, and D. H. Pandya

Abstract In boring process, casted, forged, or extruded holes in components are finished with a boring bar having cutting insert at its frontend. Dynamic and static deflections are always there in the boring bar due to its slenderness. The generating force for chatter is supplied by the cutting process itself, so it creates problems in achieving desired productivity. The main goal of this research work is to amend the rendition of boring tool with the help of shim having good damping capacity, which is placed under the tool insert. Here, brass shim is used and experiments are performed with and without shim one by one on CNC machine. Whole experimental data of acceleration is collected using CoCo80 dynamic signal analyzer. Using this data, various plots like time response plot, frequency response plot, Poincare plot, orbit plot are obtained to check for motion behavior. Surface roughness is also measured using surface roughness tester. The proposed concept shows effective chatter suppression strategy in boring operation.

Keywords Boring · Chatter · Damping · Motion behavior · Shim

1 Introduction

Boring is a finishing process, where a hole is finished or enlarged using single-point cutting tool. The process is mostly used in applications where close dimensional tolerances and good surface finish are required [1]. The vibration in tool–workpiece system is a critical issue in machining operations, because it can decrease the productivity of tool life and deteriorate the workpiece surface finish. More *L*/*D* ratio

N. B. Prajapati (✉) · J. V. Desai · D. H. Pandya
Department of Mechanical Engineering, LDRP Institute of Technology and Research, Gandhinagar, Gujarat, India
e-mail: prajapatinikunj9@gmail.com

J. V. Desai
e-mail: jayesh.svit@gmail.com

D. H. Pandya
e-mail: veddhrumi@gmail.com

V. K. Gupta et al. (eds.), *Reliability and Risk Assessment in Engineering*,
Lecture Notes in Mechanical Engineering,
https://doi.org/10.1007/978-981-15-3746-2_23

is the main cause of high amplitude vibrations in boring tool. Boring process is also known as internal turning process. Chatter is one of the most common limitations for productivity and part quality in boring operation. The generating force for chatter is supplied by the cutting process itself. It comes from work–tool interaction. Chatter produces effects like an increase in wear rate of tool, reduction in tool life, vibration of the machine–tool–workpiece system, and poor surface finish.

Various researchers have been given various methods to reduce chatter during machining. By applying those methods, one can obtain higher productivity, good tool life, and better surface finish of the product. Following data revel that the direction of work toward chatter reduction in boring operation [2].

Alammari et al. [3] investigated the shifting of boring bar's natural frequency using semi-active fluid control. At the back end of boring bar, mass is connected. Natural frequency of that mass is modulated by setting fluid's level in reservoir. At the end of research, authors observed that by adding different materials inside the boring bar, deformation resistance of the bar against external loads increases and also increases in static stiffness of boring. Thakkar and Pandya [4] made design and done analysis of tunable holder for boring bar. Here, analytical receptance coupling (ARC) is used to join assembly of holder and boring bar. In this experiment, chatter is reduced by matching natural frequency of the tool with the same of flexible holder. Boring bar's vibration amplitudes with different conditions and frequencies have been predicted by MATLAB. For boring tool, this holder assembly method is worked as a dynamic absorber. Mohan et al. [5] proposed an approach which reduces chatter on boring tool with magnetorheological (MR) fluid damper. MR fluid contains small iron particles in a fluid. The particles form linear pattern parallel to the applied field on the exposure of fluid to a magnetic field. It is observed by authors that boring tool having MR damper shows a meaningful enhancement in the dynamic behavior of the structural analysis, in comparison with ordinary boring tool.

Saindane et al. [6] made an attempt to increase the damping capacity of boring bar by decreasing the loss of static stiffness, and for that, they have been implemented passive damper. Here, tool with passive damper of nylon and polyurethane is compared with boring tool of conventional type. Results presented after this research are the reduction of deflection and improvement in surface finish. Wadhwankar et al. [7] made a boring tool which was laminated with carbon fiber with different fiber orientation. This type of boring bar proffers reduction in noise level and frequency during operation of cutting. Houck et al. [8] proposed a new approach for improvement in boring bar's flexibility, and for that, they have been matched natural frequencies of holder and boring bar. Rao et al. [9] have been introduced ANN approach to predict befitting cutting parameters. The forecasted results have been compared with the gathered data of experiment, and percentage error was computed. They concluded that set up of LDV is easy compared to accelerometer, and there is relationship between cutting parameters and vibration amplitude. Prasannavenkadesan et al. [10] made a boring tool with passively fixed cartridge brass (copper of 70% and zinc of 30%). Boring tool having brass damper gives better results compared to the same without damper. Quintana and Ciurana [11] reviewed

existing methods for ensuring stable cutting, and those methods are out-of-process method, in-process method, passive method, and active method.

Based on the above discussion on chatter suppression strategies, we can make a clear classification of strategies which ensure chatter-free boring operation. Strategies for ensuring stable boring process are classified as follows [11]:

1. By selecting cutting parameters combinations (using lobbing effect)
   - Out-of-process strategies
   - In-process strategies.
2. By changing the system behavior
   - Passive strategies
   - Active strategies.

Category of this research work falls under passive strategy of chatter suppression strategies in boring operation.

2 Experimental Details

The experiments were performed in a CNC machine to machine the aluminum alloy hollow workpiece of 60 mm outside diameter, 40 mm inner diameter, and 60 mm in length. Two boring bars of 25 mm diameter, one with shim and second without shim, are used for this experiment. Boring bar material is tool steel. Here, shim of brass material is used. Experimental setup is incorporated with CoCo80 dynamic signal analyzer unit in order to measure the cutting vibration responses during boring process. "Mitutoyo SJ-201" contact-type surface roughness measuring instrument is used. Measuring range of this surface roughness tester is 17.5 mm, and this amount of machined length is considered for measuring surface roughness. Table 1 shows the specifications of the instruments.

It is clear from the literature survey that, boring process mainly depends upon parameters such as depth of cut, cutting speed, material of damping, type of damping method, slenderness of bar, damper position. Here, after knowing all these effects, cutting parameters have been selected. Experiments with shim and without shim are performed with combinations of cutting parameters. A total of 18 experiments

Table 1 Specification table

CoCo80 dynamic signal analyzer		Mitutoyo SJ-201 surface roughness tester	
Max. sampling rate	0.48 Hz to 102.4 kHz, with 54 stages	Stylus and tip radius	Diamond tip of radius 5 μm
Dynamic range	100 dB	Measuring range	−200 to +150 μm
Frequency accuracy	Better than 1/100,000	Measuring force	4 mN
Amplitude accuracy	0.1% typical	Measuring range	17.4 mm

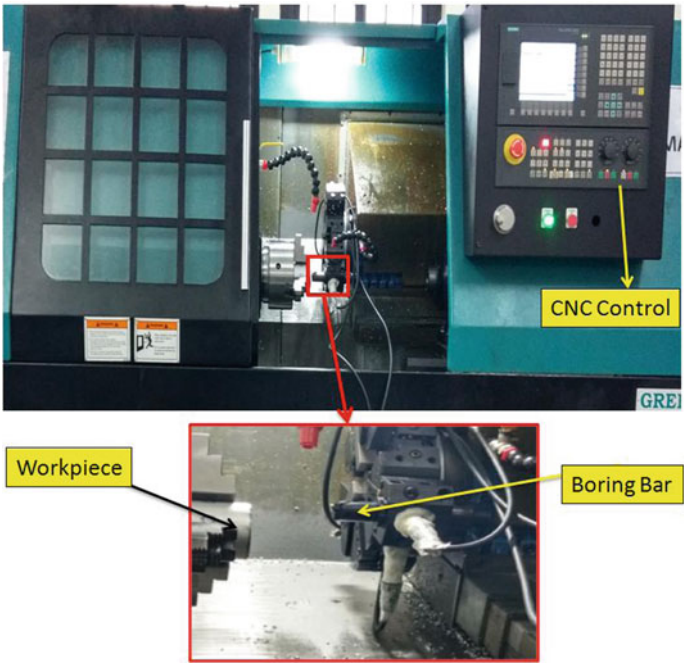

Fig. 1 Experimental setup

(9—with shim and 9—without shim) are performed. Here values of cutting speed (m/min) and depth of cut (mm) are 150, 220, 300 and 0.5, 0.75, 1.0, respectively. Feed of 0.15 mm/rev is taken as constant.

Figure 1 shows experimental setup of this research work in which CNC machine is incorporated with dynamic signal analyzer.

3 Results and Discussion

During experiment, acceleration data is collected for different cutting conditions. The acceleration peak value in radial force and cutting force directions is measured. Acceleration data is converted into displacement data and velocity data. Using these data, different graphs like time response (TR) plot, frequency response (FR) plot, Poincare plot, and orbit plot are plotted. Table 2 gives vibration amplitude data in two directions, type of motion behavior, and surface roughness value for different combinations of the depth of cut and cutting speed.

Dynamic motion analysis is the tool for checking the motion behavior of any system based on different graphs. In the present work, TR plot, FR plot, Poincare, and orbit plot are used for the prediction of behavior of boring tool with and without

Table 2 Type of motion behavior and surface roughness value for different cutting conditions

S. No.	Shim	Cutting speed (m/min)	Depth of cut (mm)	Value of peak ac. (mm/s^2)		Motion behavior	Surface roughness (μm)
				Cutting force direction	Radial force direction		
1	Without	150	0.5	3140	1380	Quasi-periodic	0.420
2		150	0.75	11,910	13,020	Quasi-periodic	0.411
3		150	1.0	20,680	9220	Multi-periodic	2.750
4		220	0.5	8980	3960	Multi-periodic	1.001
5		220	0.75	19,250	9320	Multi-periodic	2.225
6		220	1.0	25,450	23,290	Multi-periodic	2.146
7		300	0.5	15,180	7350	Multi-periodic	1.581
8		300	0.75	31,400	26,040	Chaotic	2.627
9		300	1.0	49,500	33,600	Chaotic	2.701
10	With	150	0.5	2360	1040	Quasi-periodic	0.673
11		150	0.75	8600	4870	Quasi-periodic	0.416
12		150	1.0	12,610	7140	Quasi-periodic	0.399
13		220	0.5	5730	3250	Quasi-periodic	0.204
14		220	0.75	9950	6450	Multi-periodic	1.100
15		220	1.0	12,620	8290	Multi-periodic	1.038
16		300	0.5	9600	6140	Quasi-periodic	0.958
17		300	0.75	13,270	8740	Multi-periodic	1.436
18		300	1.0	14,100	9950	Quasi-periodic	0.986

shim. Here, three types of responses are observed in boring tool with and without shim, and these three responses are quasi-periodic, multi-periodic, and chaotic. In Fig. 2, these plots are compared for trials with shim and without shim.

4 Conclusions

Intend of this, research work is to explore the influence of shim in boring cutting operation. A passive strategy for reducing chatter in boring process is proposed, whose crucial considerations are cutting parameters and damping material (shim). The following conclusions are obtained after experimental analysis:

- The boring tool equipped with shim have reduced amplitude of vibration in acceleration mode by 28.48% and surface roughness by 36.5% as compare to boring tool without shim at cutting speed of 300 m/min and depth of cut of 1.00 mm.

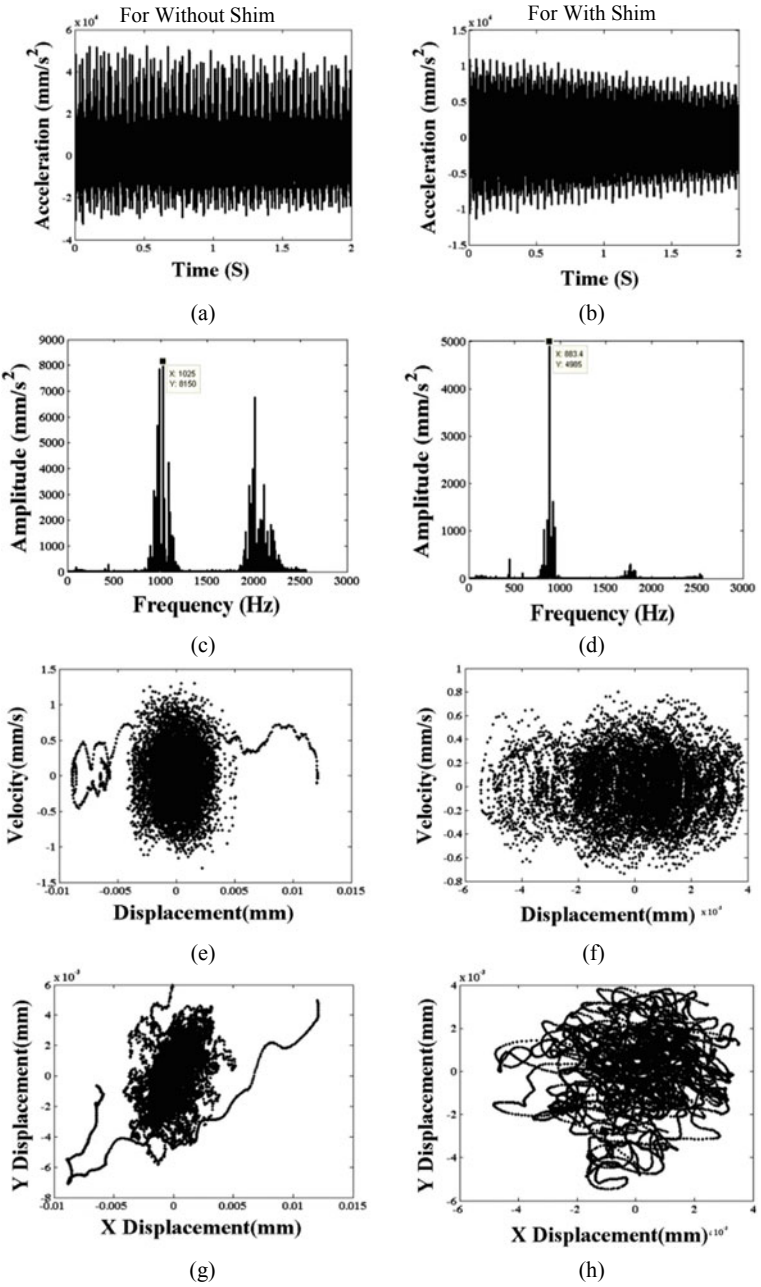

Fig. 2 Results of vibration in cutting force direction: time response plots (**a**, **b**), frequency response plots (**c**, **d**), Poincare plots (**e**, **f**), orbit plots (**g**, **h**) at cutting speed of 300 m/min and depth of cut of 1.0 mm for both without shim and with shim

- 63.49% of maximum reduction in surface roughness is achieved by reducing chatter using boring tool with shim.
- After experiment, a crucial relationship among cutting parameters, damping material (shim), chatter, and surface finish is achieved. If we take cutting speed constant, then with the increase in depth of cut chatter behavior changes from quasi-periodic to multi-periodic or chaotic, and for the same condition, surface roughness is also increased with depth of cut. So, by putting shim and controlling cutting parameters one can achieve chatter-free less-chattered boring operation.
- This experimental work will be useful to operate machine–tool with reduced chatter condition, and hence, by doing this one will achieve a good surface finish.

References

1. Yussefian NZ, Imani BM, Mounayri H (2008) The prediction of cutting force for boring process. Int J Mach Tools Manuf 48:1387–1394
2. Waghmare PJ, Patil RV, Waghmare GS (2015) A review on vibration mitigation of boring bar using passive damping techniques. Int J Res Eng Technol 04:07138–141
3. Alammari Y, Sanati M, Freiheit T, Park SS (2015) Investigation of boring bar dynamics for chatter suppression. In: 43rd Proceedings of the North American Manufacturing Research Institution of SME, vol 1, pp 768–778
4. Thakkar AD, Pandya DH (2014) Analytical investigation of boring bar for chatter. Int J Adv Eng Res Sci (IJAERS) 1(7). ISSN: 2349-6495
5. Mohan E, Natarajan U, Prasanth CS (2017) Investigation of damping effect of magneto-rheological fluid damper on internal turning operation. SSRG Int J Mech Eng (ICEHS) 23–28. ISSN: 2348-8360. Special Issue
6. Jakikore A, Saindane G, Umbarkar A (2014) Experimental investigation of vibration damping in boring operation using passive damper. Int J Res Eng Adv Technol 2(3)
7. Wadhwankar D, More K, Bajaj V (2016) Experimental investigation of boring tool vibration for improving surface finish by using passive damper. Int J Curr Eng Technol. E-ISSN 2277-4106, P-ISSN: 2347-5161. Special Issue-6
8. Houck L, Schmitz TL, Smith KS, Tunable holder for boring bars. Research gate, Department of Mechanical and Aerospace Engineering University of Florida, Gainesville, FL, USA
9. Rao KV, Murthy BSN, Rao NM (2014) Prediction of work piece vibration in boring of AISI 316 steel using artificial neural network. Int J Mech Prod Eng 2(2). ISSN: 2320-2092
10. Prasannavenkadesan V, Elango A, Chockalingam S (2015) Chatter suppression in boring process using passive damper. Int J Mech Aerosp Ind Mechatron Manuf Eng 9(11)
11. Quintana G, Ciurana J (2011) Chatter in machining processes: a review. Int J Mach Tools Manuf 51:363–376

Methodology to Incorporate the Effect of Plant Operating State During Surveillance Testing in Determining Optimal Surveillance Test Interval

Arihant Jain, N. S. Joshi, and P. V. Varde

Abstract Periodic surveillance tests are performed on standby systems to maintain operational preparedness of the safety-critical systems in nuclear plants. Test intervals are mostly decided qualitatively based on operational experience and expert advice in line with manufacturer's recommendations. Probabilistic techniques allow to take risk-informed decision on surveillance test interval (STI) that aims at minimising mean system unavailability. System unavailability during testing is an important parameter influencing optimum STI. The contribution of testing time on system mean unavailability depends on demand occurrence frequency during testing. Many safety systems are tested during plant shutdown or low-power operation which significantly reduces demand occurrence frequency during testing. Traditional approaches towards STI optimisation do not consider this effect and consider either no demand during testing or take demand occurrence frequency similar to that during power operation. This paper discusses a methodology to incorporate the effect of reduced demand occurrence frequency during testing, in the determination of optimum STI using a factor that gives the ratio of demand occurrence frequency during system testing to that during standby condition. It is an approach balanced between the two extreme traditional approaches. A case study is performed on the Emergency Core Cooling System of Dhruva Reactor to study the effect of this parameter on optimum STI.

Keywords Optimisation · Reliability · Surveillance test interval · System unavailability

A. Jain (✉) · N. S. Joshi · P. V. Varde
Research Reactor Services Division, Reactor Group, Bhabha Atomic Research Center, Trombay, India
e-mail: arihantj@barc.gov.in

N. S. Joshi
e-mail: nsjoshi@barc.gov.in

P. V. Varde
e-mail: varde@barc.gov.in

V. K. Gupta et al. (eds.), *Reliability and Risk Assessment in Engineering*,
Lecture Notes in Mechanical Engineering,
https://doi.org/10.1007/978-981-15-3746-2_24

1 Introduction

Safety systems employed in various nuclear plants are generally standby systems. Periodic inspection and testing of such systems is important to maintain operational preparedness of the safety-critical systems. Surveillance test interval (STI) is very important for the standby systems. With an objective to minimise system unavailability, optimisation of STI plays a very important role in risk-informed maintenance.

Test intervals are mostly decided qualitatively based on operational experience and expert advice in line with manufacturer's recommendations. Probabilistic techniques allow to take risk-informed decision on surveillance test interval (STI) that aims at minimising mean system unavailability. Early STI optimisation work [1–4] focused on minimising mean unavailability of single components. STI optimisation of systems with multiple components is very complex and requires numerical solutions using computer codes. Various numerical coded like ICARUS [5] and FRANTIC [6] were developed for this purpose. Risk-based STI optimisation can also be carried out by using results of probabilistic safety assessment (PSA) [7]. Core damage frequency (CDF) is then considered as optimising criteria. PSA results allow to selectively tackle the safety systems based on their effect on CDF. Apart from probabilistic criteria, such as mean unavailability of component and system, core damage frequency and risk factors, some works also use cost as a parameter for optimisation [8, 9].

During surveillance testing, the system remains unavailable to cater any demand occurrence. This factor pushes the optimum surveillance interval higher, as frequent testing causes higher unavailability due to increased contribution of testing time. The problem with current models is that they do not take into account the existing plant conditions during testing. As is observed in many plants, the surveillance testing of safety-critical systems is carried out during plant shutdown. This is a common case for many nuclear research reactors (e.g. Dhruva). During shutdown, the pressure and temperature are significantly lower than that during full-power operation. This reduces the possibility of any demand occurrence on the safety systems. Current models either take similar demand occurrence frequency during shutdown as that during normal operation or do not consider demand occurrence at all during shutdown. It was felt that neither of the two scenarios take into account the actual plant conditions and hence give results that are on extreme ends.

The model presented in this paper captures the effect of reduction in demand occurrence frequency during surveillance testing to evaluate mean system unavailability. This is accomplished using a parameter p that gives the ratio of demand occurrence frequency during testing to the demand occurrence frequency during normal operation. The mathematical modelling is presented in Sect. 2. In Sect. 3, a simple case study is carried out on the Emergency Core Cooling System of Dhruva Research Reactor to observe the change in optimum STI with p and to get any idea about impact of p on STI.

2 Mathematical Modelling

Surveillance tests are conducted on standby safety systems periodically to ensure system readiness and effectiveness in case of any emergency. During the surveillance testing and maintenance time, the system remains unavailable for normal use. Hence, any emergency condition occurring in this interval cannot be dealt with.

Consider that for a standby safety system, total time is divided into two parts corresponding to the respective time spent in standby condition and surveillance testing. As shown in Fig. 1, the total time (surveillance test interval, T) is divided into the time spent in standby state (t_1) and time spent during testing (t_2). I and II are the two operating states, i.e. standby and testing, respectively.

Mean unavailability of the system $P(U)$ is given as:

$$P(U) = P(\mathrm{I})P(U|\mathrm{I}) + P(\mathrm{II})P(U|\mathrm{II}) \tag{1}$$

where
$P(\mathrm{I})$ is the probability that demand occurs in state I.
$P(\mathrm{II})$ is the probability that demand occurs in state II.
$P(U|\mathrm{I})$ is the mean unavailability in state I.
$P(U|\mathrm{II})$ is the mean unavailability in state II.

During surveillance testing, the system is unavailable. It can be represented as:

$$P(U|\mathrm{II}) = 1 \tag{2}$$

If demand frequency is considered constant during the two operating states, then the probability of demand occurring in a specific state is given by the fraction of time spent in that state, which for the current situation is

$$P(\mathrm{I}) = \frac{t_1}{T} \tag{3}$$

$$P(\mathrm{II}) = \frac{t_2}{T} \tag{4}$$

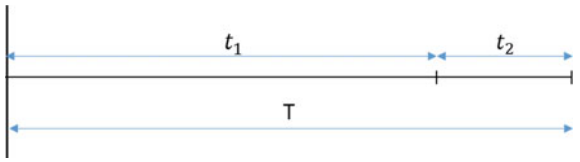

Fig. 1 Time spent by standby safety system in various states

The problem with assumption of constant demand frequency is that it does not take into account the system conditions during testing. For example, if we consider that surveillance testing of ECCS is carried out during plant shutdown condition (as in the case of many research reactors), the possibility of LOCA during testing is diminished due to low pressure and temperature conditions. Such effects are not captured by the traditional approach which either assume same frequency or consider no LOCA possibility during testing.

In this work, we introduce a factor p to include the effect of system conditions during testing. p is the ratio of demand frequency during testing to the demand frequency during normal operation, i.e.

$$p = \frac{\nu_{\mathrm{II}}}{\nu_{\mathrm{I}}}$$

where ν_{I} and ν_{II} are the demand occurrence frequencies in operating conditions I and II, respectively.

The value of p ranges from zero to one, corresponding to the relative frequency of demand occurrence during testing to that during standby operation. Values of p greater than one represent a situation in which demand probability is higher during testing. This situation is not common and hence is ignored afterwards.

The probability of demand occurrence during testing is hence modified as:

$$P(\mathrm{II}) = p\frac{t_2}{T} \tag{5}$$

As there exist only two states for the system, demand will occur either in state I or II only, hence,

$$P(\mathrm{I}) + P(\mathrm{II}) = 1$$

Using Eq. (5) we get

$$P(\mathrm{I}) = 1 - p\frac{t_2}{T}$$

$P(\mathrm{I})$ can be modified using a factor q to satisfy the above equation. Taking

$$P(\mathrm{I}) = q\frac{t_1}{T}$$

We get

$$q = p + \frac{T}{t_1}(1 - p) \tag{6}$$

Using above relations in Eq. (1), we get

$$P(U) = q\frac{t_1}{T}P(U|\mathrm{I}) + p\frac{t_2}{T}$$
$$P(U) = P(U|\mathrm{I}) + p\frac{t_2}{T}\{1 - P(U|\mathrm{I})\} \tag{7}$$

Equation (7) gives the mean unavailability of the system taking into consideration the effect of demand occurrence possibility during testing or maintenance.

The value of p ranges from zero to one with zero corresponding to no possibility of demand occurrence during testing and one corresponding to no effect of testing on demand.

The effect of p on mean unavailability of a system with constant failure rate is shown in Fig. 2.

3 Case Study

We do a case study on the Emergency Core Cooling System of Dhruva Research Reactor. The objective is to study the trend of system unavailability with surveillance test interval. Surveillance test interval is the time spent by a system between two surveillance testing. It is referred to as T in Fig. 1.

3.1 Brief Description

Dhruva is a 100 MWt high flux nuclear research reactor. It was commissioned in 1985. Natural uranium is used as fuel and heavy water as primary coolant, moderator and reflector. The reactor is being used to carry out research work in the fields of Nuclear Science and Engineering.

It also produces radioisotopes for research and industrial applications including medical sciences.

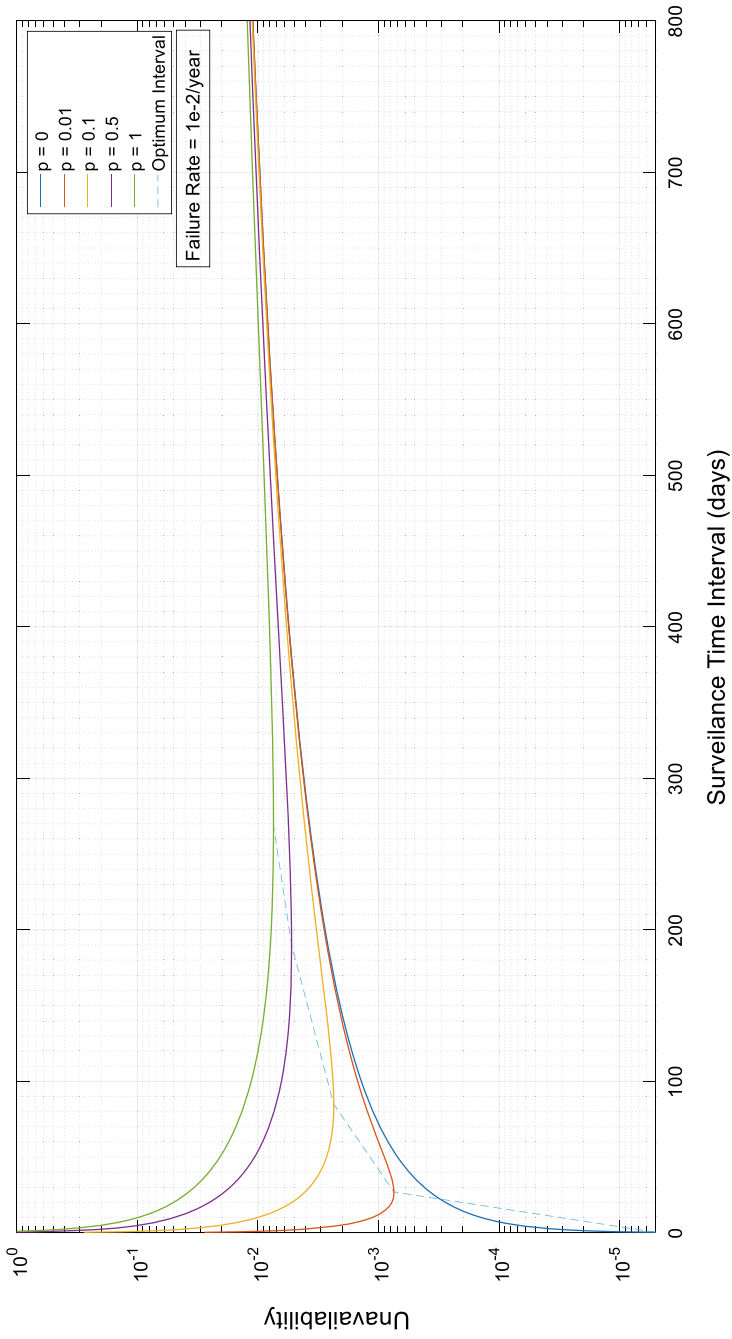

Fig. 2 Effect of 'p' on unavailability of a system with STI

During normal operation of the reactor, the heat generated in the core is removed by heavy water circulated by three main coolant pumps (MCPs). The heavy water is then cooled in heavy water/process water heat exchangers. In the event of loss-of-coolant accident (LOCA), which will result in depletion of coolant inventory from the system, a stage may reach when cooling may get adversely affected resulting in core damage. To prevent this situation, ECCS is installed to carry out the following objectives:

- Detection of loss-of-coolant inventory;
- Collection of leaked out inventory;
- Injection of leaked out inventory back to system;
- Sustain adequate coolant flow through the core.

Loss of heavy water inventory gives LOCA signal initiating reactor trip. The leaked out heavy water is collected in a tank (SDT) connected to inlet of recirculating pumps. The pumps recirculate the leaked water into reactor core through two injection lines simultaneously connected to inlet and outlet of the core, respectively. In case the leaked heavy water is not collected in the tank, there exists a provision to manually inject light water into the tank. In that case, light water is circulated in the core.

A simplified fault tree for ECCS is shown in Fig. 3. Failure rates for various events are given in Table 1. Hypothetical values are considered for this study.

3.2 Surveillance Test Interval Optimisation

ECCS is tested quarterly to ensure readiness in case of any emergency. During testing, the system remains unavailable to cater any demand. Testing is only carried out during reactor shutdown. The temperature and pressure in the primary heat transport system are significantly lower than that during reactor operation. Hence, the possibility of demand occurrence (LOCA) is also lower during ECCS testing. This effect is considered by taking appropriate value of parameter p in Eq. 7. Figure 4 shows the variation of ECCS unavailability with surveillance test interval (STI) for various values of p. The increasing value of parameter p indicates that the LOCA frequency during reactor shutdown is increasing relative to the possibility of LOCA during reactor full-power operation with $p = 1$ indicating that there is reactor shutdown does not affect LOCA frequency.

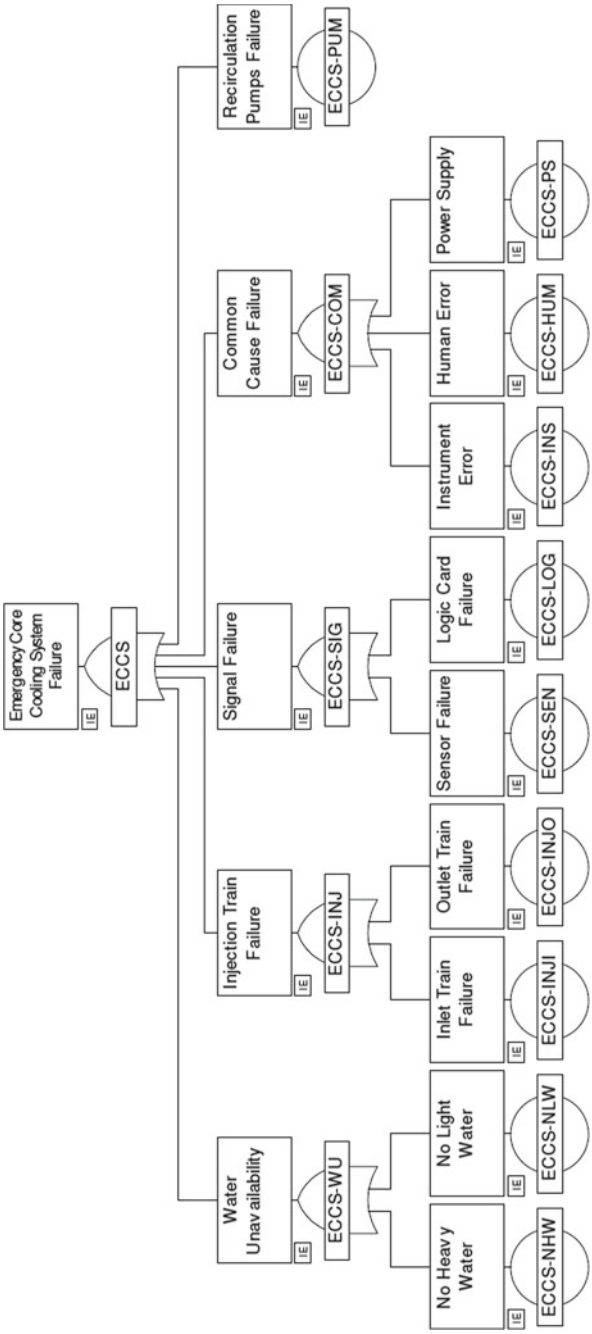

Fig. 3 Simplified fault tree for ECCS

Table 1 Failure rate of basic events in fault tree

S. No.	Event	Failure rate (per year)
1	ECCS-NHW	3.28E−03
2	ECCS-NLW	8.23E−04
3	ECCS-INJI	3.36E−04
4	ECCS-INJO	3.36E−04
5	ECCS-SEN	8.20E−04
6	ECCS-LOG	1e−5 (fixed unavailability)
7	ECCS-INS	1e−5 (fixed unavailability)
8	ECCS-HUM	1e−6 (fixed unavailability)
9	ECCS-PS	1e−6 (fixed unavailability)

Surveillance test interval is optimum when ECCS unavailability is lowest. Figure 4 shows that optimum STI increases with an increase in p. Optimum test interval is given in Table 2. The increase in optimum STI is attributed to the increased contribution of unavailability during testing with increase in p.

The significance of parameter p is clearly visible in the result reported in Table 2.

4 Conclusion

Available methods for determining optimum STI of standby systems do not take into account the actual system conditions existing during surveillance testing. In some cases, e.g. ECCS of Dhruva Research Reactor, the demand frequency (LOCA) during testing is significantly lower than that during system standby condition. The model presented in this paper captures this effect through a parameter p that gives the ratio of demand frequency during testing, to that during standby condition. A simple case study of Dhruva ECCS shows that optimum STI is very strongly dependent on p.

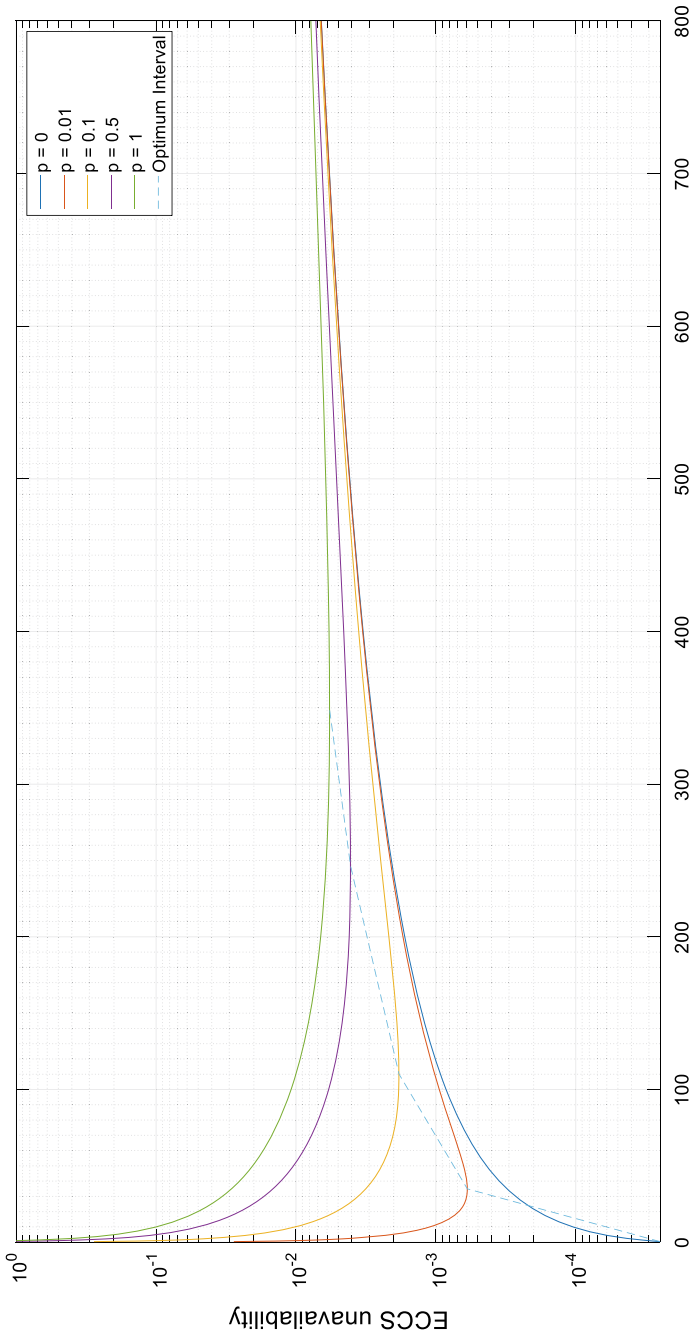

Fig. 4 ECCS unavailability versus STI for various values of 'p'. Testing time = 24 h

Table 2 Optimum STI (minimum unavailability) of ECCS for various values of p

S. No.	p	Optimum STI (days)
1	0.00	0
2	0.01	34
3	0.10	110
4	0.50	246
5	1.00	348

Acknowledgements We thank Shri S. Bhattacharya, Associate Director, Reactor Group, for his encouragement and support during the work. We also thank Reactor Operations Division, BARC, for their guidance in understanding working and surveillance testing of Dhruva ECCS system.

References

1. Hirsch H (1971) Setting test intervals and allowable bypass times as a function of protection system goals. IEEE Trans. Nucl Sci 18:488–494
2. Jacobs I (1968) Reliability of engineered safety features as a function of testing frequency. Nucl Saf 9:303–312
3. Signoret J (1976) Availability of a periodically tested standby system. NUREG/TR-0027
4. Vaurio J (1991) Comments on system availability analysis and optimal test intervals. Nucl Eng Des 128:401–402
5. Vaurio J, Sciaudone D (1979) Unavailability modelling and analysis of redundant safety systems. ANL-79-87. Argonne National Laboratory
6. Vesely W, Goldberg F (1977) FRANTIC—a computer code for time dependent unavailability analysis. NUREG-0193
7. Cepin M, Mavko B (1995) Risk based surveillance test interval optimisation. In: Nuclear Society of Slovenia, pp 206–213
8. Vaurio J (1995) Optimisation of test and maintenance intervals based on risk and cost. Reliab Eng Syst Saf 49:23–36
9. Harunuzzaman M, Aldemir T (1996) Optimisation of standby safety system maintenance schedules in nuclear power plants. Nucl Technol 113:354–367

Design for Reliability

Design and Development of Steering System for Formula-Styled Vehicle

Saurabh Bhalerao, Adesh Paramane, and Abhishek Chavan

Abstract The abstract should summarize the contents of the paper in short terms, i.e., 150–250 words. The main aim of this paper is design and development of Ackermann steering system for formula-styled vehicle and use bevel gears for making steering ratio adjustable. In the formula-styled vehicle, it requires aggressive steering, as compared to other conventional vehicles. The steering column is linkage between rack and pinion gearbox and steering wheel. To avoid the problem regarding to steering wheel free play, bevel gear arrangement is used because bevel gear has constant velocity ratio and it has better efficiency compared to other types of gears. By using bevel gears of different diameters, steering ratio can be adjusted.

Keywords Ackermann · Bevel gear · Steering system · Steering ratio · No slip rate · Steering efforts

1 Introduction

The steering system is one of the most important parts of any car. Primary function of steering system is to achieve angular motion of the front wheels to negotiate a turn. This can be done through linkage and steering gear which convert the rotary motion of the steering wheel into angular motion of the front road wheels. A failure on this mechanism can be fatal to the health of the driver [1].

The basic function of steering system is to provide comfort to driver by reducing steering efforts. Some technical aspects affect the steering system like minimum turning radius, easy steering retainability and less lock-to-lock wheel rotation. Steering wheel design (diameter) also affects the efforts required to steer the vehicle. In the formula-styled vehicle, generally, Ackermann and anti-Ackermann steering systems are used. Due to high speed and less time required to turn the vehicle (during dynamic condition), 100% Ackermann is not preferable for race cars. To avoid this problem, aggressive steering is required. Aggressive steering reduces steering reaction time

S. Bhalerao · A. Paramane (✉) · A. Chavan
Rajarambapu Institute of Technology, Rajaramnagar, India
e-mail: adesh.paramane@gmail.com

V. K. Gupta et al. (eds.), *Reliability and Risk Assessment in Engineering*,
Lecture Notes in Mechanical Engineering,
https://doi.org/10.1007/978-981-15-3746-2_25

and steering ratio [2]. Vehicle weight on the front and rear axle also affects steering system.

In the steering system, universal joint is used to connect upper end of steering column with quick release assembly and lower end to the rack and pinion gearbox. During static as well as dynamic condition, some amount of free play is available in the steering wheel assembly. To avert this problem, bevel gear should be the best solution because power transmission efficiency is up to 98% (2% frictional losses) and approximately zero percentage of slip rate because of constant velocity ratio.

2 Design Considerations

Some important design parameters to design Ackermann steering geometry are as mentioned in Sect. 2.1.

2.1 Ackermann Design

Design parameters:
Turning radius = 2500 mm.
Wheelbase = 1700 mm (for 100% Ackermann).
Design for 85% Ackermann.
Track width = 1300 mm.
Inner angle = 37.990.
Outer angle = 24.640.
Ackermann angle = 37.980.
Ackermann percentage = 85%.
Steering arm angle = 20.920 [3, 4].
Rack travel = 81 mm for 195.75° steering wheel rotation.
Available rack travel = 120 mm for 290° wheel rotation, steering ratio = 3:1.

In Ackermann steering geometry, inner angle of wheels is greater than outer angle of wheels, in order to reduce scrub radius. The steering arm length connects to the tie rods; tie rods selected are of lightweight fiber plastic to get massive reduction in weight. The tie rods are capable enough to sustain the load acting on them.

For determining this geometry, AutoCAD software is used (Fig. 1).

2.2 Pinion Torque and Steering Effort Calculation

The weight of the vehicle is distributed 45% on front axle and 55% in rear axle. The actual weight of vehicle is 300 kg. By 45% weight on front axle, i.e., 135 kg, weight is distributed on front wheels and 165 kg on rear wheels of the vehicle [4, 5].

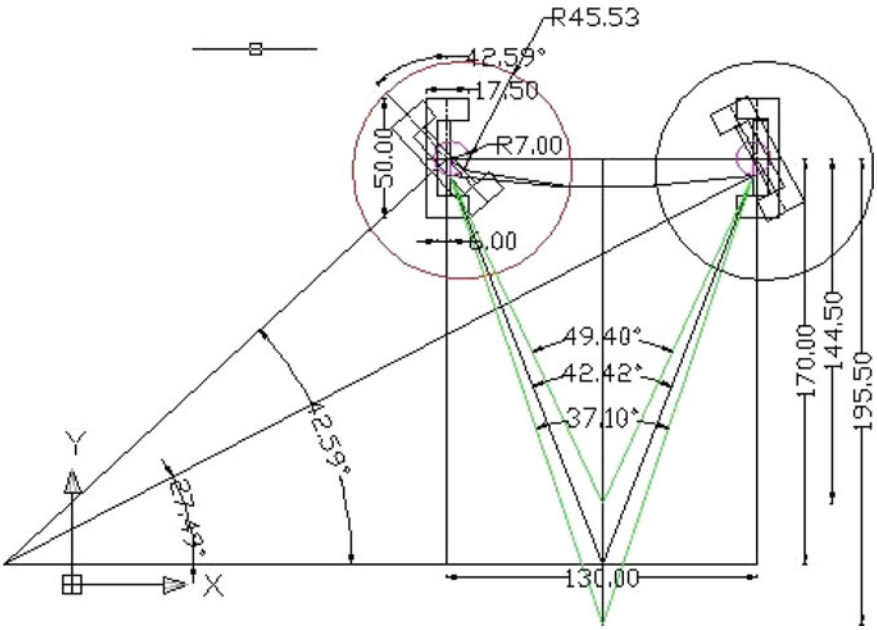

Fig. 1 Steering geometry

$\therefore$ Force on front wheels = 135 * 9.81 = 1324.35 N.
$\therefore$ Force on each wheel = 1324.35/2 = 662.175 N.
Now, force required to steer the vehicle

$$T = F * r$$

where,
T = torque required to steer the vehicle.
F = force on each wheel.
r = radius of pinion.
$\therefore T = 662.175 * 0.025$
$= 16{,}554.37$ Nmm.
Efforts required to steer the vehicle (F1):

$$F_1 = T/D$$

D = diameter of steering wheel.
$\therefore F_1 = 16{,}554.37/210$
$= 78.83$ N
Finally, effort required to steer the vehicle,
$F_1 = 7.88$ kg.

2.3 Proposed System

In the formula-styled vehicle, generally, steering system uses universal joints to connect the whole assembly. But, by using the UV joint, some amount of free play is always available during dynamic condition. According to FSAE rulebook, free play in steering wheel is not acceptable as per concern of driver safety [3].

In the proposed system, bevel gear arrangement is used to connect the assembly. The bevel gears are meshed. The two shafts are used to transmit the motion. One shaft is used to connect one bevel with steering hub and quick release set, and another one is used to connect other bevel with rack and pinion gears. Mountings are used to hold these two shafts. Bearings are used to reduce frictional resistance and provide angular motion.

After using this mechanism, there is no chance of any slippage in assembly because gears have constant velocity ratio. The secondary advantage of this system is that we can adjust the steering ratio by changing bevel gear ratio (Fig. 2).

The main aim of this system is achieved by using gears of variable diameters, of one of the bevel gears or both of the bevel gears in system of same module.

We can test this system for different cases

Case 1. If diameter of bevel connecting rack and pinion is increased and other kept constant, then efforts required to steer the vehicle are more and steering ratio is increased.

Case 2. If diameter of bevel connecting quick release mechanism of steering wheel is increased and other kept constant, then efforts required to steer the vehicle are less and steering ratio is reduced.

Case 3. By changing both the diameters of bevels and keeping both the diameters same, there is no effect on steering efforts as well as steering ratio.

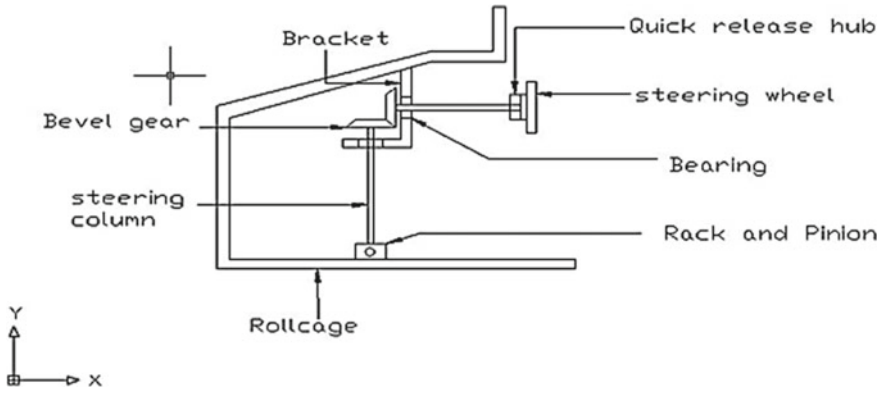

Fig. 2 Proposed design

2.4 Design of Bevel Gears

Bevel gears are gears where the axes of two shafts intersect, and the tooth-bearing faces of the gears themselves are conically shaped. Bevel gears are most often mounted on shafts that are at 90°. Two important concepts in the gearing are pitch surface and pitch angle. The pitch surface of a gear is the imaginary toothless surface. The pitch angle of a gear is between face of pitch surface and axes.
Bevels are classified in the following types:

1. Straight bevel gear
2. Spiral bevel gear
3. Zero bevel gear
4. Hypoid bevel gear [6].

Generally, cast iron is used to manufacture the bevel gears due to its wear resistance and excellent machinability.
Grades of cast iron used for manufacturing bevel gear:
ASTM grade 20, 25, 30, 40, 50 and 60.
Design calculations for bevel gear:
Material selected for manufacturing bevels is ASTM grade 40.
Material properties:
Brinell hardness number: 160–300.
Compressive strength: 570–1290 MPa.
Young's modulus: 80–170 GPa.
Elongation: 0.52 mm, Density: 7.2 gm/cm^3.
Fatigue strength: 69–190 MPa, Tensile strength: 150–420 MPa.
Shear strength: 180–610 MPa.

Table 1 shows the gear terminologies which are used to transmit the motion from steering wheel to rack and pinion gearbox. By using this bevel arrangement, there is no need to use upper universal joint which connects quick release assembly and steering column.
Advantages of using bevel gear:

1. Bevel gear has no slip rate because of constant velocity ratio.
2. Because of smooth operation as compared to universal joint, it is easy to steer the steering wheel.
3. Steering free play is minimized because of reduction in UV joint.
4. Compact and comfortable design.

Disadvantages:

1. Manufacturing cost of bevel gear is high as compared to UV joint.
2. Extra mountings are needed to hold the bearing to hold shafts of bevels.

Table 1 Design parameters

Parameters	Pinion	Gear
Diametral pitch	0.5	0.5
Teeth	20	40
Pitch diameter	40	80
Whole depth	40.37	4.37
Addendum	2	2
Dedendum	2.37	2.37
Clearance	0.37	0.37
Circular tooth thickness	3.14	3.14
Pitch angle	26.56	63.43
Pitch cone radius	44.72	44.72
Face width	14.90	14.90
Outside diameter	43.57	81.78
Back cone angle	22.36	89.44
Virtual number of teeth	22.36	89.44

2.5 Actual View (CAD View)

For a given system, we want to make system as simple as possible. As desired, we made two splined shafts, one having external splines and other one is having internal splines for adjusting the position of pinion gear with respect to gear. Splined shafts are provided for varying the length of steering column with respect to different diameters of bevel gear (Figs. 3, 4 and 5).

Another advantage of these splined shafts is that it makes steering system easy to assemble and disassemble. For adjusting the variable steering ratio, fixture was

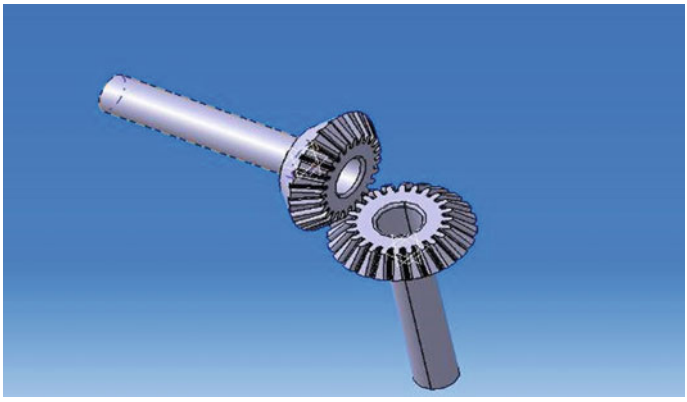

Fig. 3 Bevel gear arrangement

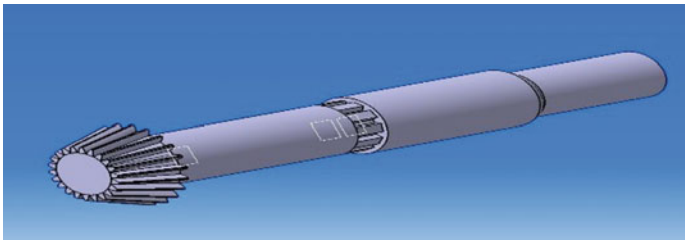

Fig. 4 Splined shaft (assembled)

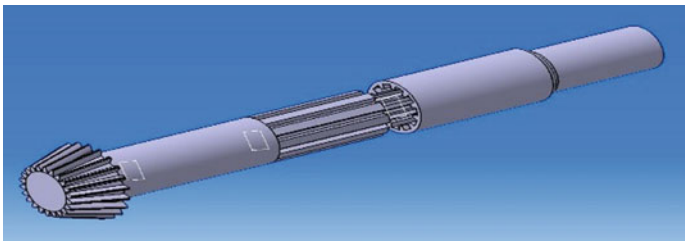

Fig. 5 Splined shaft (dissembled)

made which will adjust the position of gear by adjusting it using fasteners. Steering ratio is adjusted by changing one bevel gear in the system. Here, as the diameter of bevel gear changes, position of fixture is also changed. It is mandatory to change the position of fixture for changing bevel gear. Key slots are provided on shaft and bevel gear, for locking and assemble as well as dissemble the bevel and shaft. Bearings are press fitted in the fixture for rotational motion of shafts. The whole arrangement of system is shown in Fig. 6.

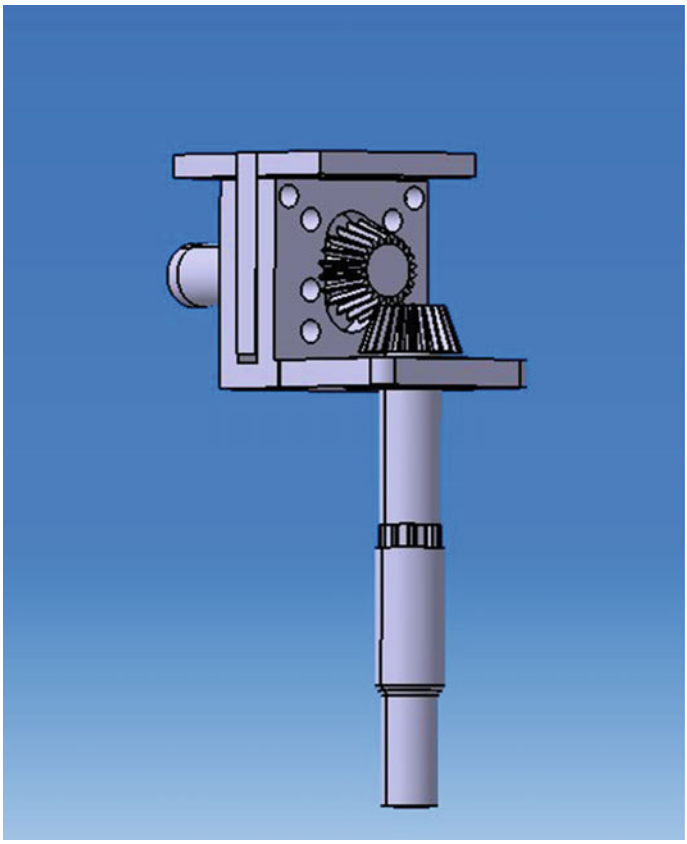

Fig. 6 Assembly of the proposed system

3 Conclusion

The study makes the system variable for making steering ratio adjustable, which in turn is reliable and comfortable for driver. In today's industrial field, gearing for power transmission with high efficiency is very important. This is the reason behind selecting bevel gears for system because of their better efficiency. Use of universal joints for steering system induces free play in arrangement. Use of this arrangement makes the steering system adjustable as well as efficient. One more advantage after using bevel arrangement is that there is no free play between steering wheel and steering column. Aggressive steering makes steering quickly.

References

1. Farrington JA (2010) Redesign of an FSAE race car's steering and suspension system. Int J Appl Eng 1(1):104–113. ISSN 0976-4259
2. Milliken WF, Milliken DF (1993) Race car vehicle dynamics, pp 709–723
3. FSAE rulebook 2017, pp 17, 21, 91, 106
4. Smith C (1978) Tune to win. Aero Publishers, pp 60–69. ISBN 0-87938-071-3
5. Bhishikar S (2014) Design and simulation of 4 wheel steering system. Int J Appl Eng Res 3(12):356. ISSN-0976-4259
6. Bhandari VB, Design of machine elements, 4th edn. Tata McGraw-Hill, New York, pp 711–723
7. www.matweb.com

Crack Propagation Behavior in Spur Gear by XFEM and Its Influence on Dynamic Characteristics

Jay Govind Verma, P. K. Kankar, and Sachin Kumar

Abstract This manuscript inspects the dynamic characteristics of a standard spur gear considering the effect of gear root crack and crack at pitch circle. Cracked gear pair is modeled through extended finite element method with the help of ANSYS software. This method enables the accurate approximation of solution for problems involving non-smooth features like crack within elements. Additionally, the effect of position and length of the crack on the gear structure is observed in terms of the dynamic characteristics, i.e., natural frequencies and vibration shapes. Due to the presence of crack, the natural frequency of the gear changes. These results create a worthy basis for the failure investigation and fault finding of gears.

Keywords Crack · Extended finite element method · Gear · Natural frequency · Vibration shape

1 Introduction

Gears are power transmission components, as the primary structure of mechanical transmission, used in several applications like windmills, aircraft engines, ships, vehicles, etc. Due to increasing applications and demand, the study of failure analysis and diagnosis in gear faults is very important. Gear tooth crack possibly occurs when a gear transmission train is working under excessive and/or long-term dynamic loads. The formation of cracks leads to the breakage of material's surface layer.

J. G. Verma (✉) · P. K. Kankar
PDPM Indian Institute of Information Technology, Design and Manufacturing, Jabalpur 482005, India
e-mail: royalgovindvrm@gmail.com

P. K. Kankar
e-mail: pkankar@iiti.ac.in

S. Kumar
Department of Mechanical Engineering, Indian Institute of Technology Ropar, Rupnagar 140001, India
e-mail: sachin@iitrpr.ac.in

V. K. Gupta et al. (eds.), *Reliability and Risk Assessment in Engineering*,
Lecture Notes in Mechanical Engineering,
https://doi.org/10.1007/978-981-15-3746-2_26

For gear crack detection and its behavior with gear's specifications, finite element method (FEM) has been frequently used [1, 2]. The FE model of gear pair requires a very fine mesh and detailed geometrical features, which makes it computationally expensive. An analytical model [3] is established to compute the mesh stiffness of gear pair by considering bending deflection, axial compression and Coulomb friction. In addition to that, shear energy terminology [4] is introduced to compute the mesh stiffness of spur gear. An analytical model [5] is developed to observe the effect of crack propagation and the rim thickness on the crack path. The decrease in mesh stiffness [6], due to the occurrence of crack, is determined by analytical method. They incorporated tooth foundation deformation suggested by Sainsot et al. [7]. The effect of gear crack propagation on the dynamic behavior [8] of a gear system with hole is inspected. They observed that the effect of vibration response of gear for the same length of crack is high for crack's trajectory along the rim than the crack trajectory along the tooth's root. Virtual crack extension method and the minimum strain density criteria were used to study crack propagation in two-dimensional contact surface [9]. A numerical study was carried out [10] to investigate the impact of different crack opening locations at the tooth's root and crack propagation due to different load positions. They validate the result with experiments and conclude that the concept of linear elastic fracture mechanics can be used for crack growth of gear. The enhancement of the fatigue life of gear [11] having a crack is studied by three-dimensional finite element analysis. They incorporated patches of boron/epoxy in layers for enhancement. Gear tooth crack propagation is analyzed using finite element method in most of the previous studies, which require fine mesh at the crack tip and re-meshing during the crack propagation. Also, the available literature on these studies does not consider about the flexibility dynamics' theoretical viewpoint, for flexibility dynamics model of cracked gears.

Therefore, in this paper, extended finite element method (XFEM) developed by Belytschko and Black [12] is employed to simulate the dynamic behavior of cracked gear. Cracks of different severity with different positions are considered for the simulation and compared. The dynamic characteristic of gear structure having crack is also inspected comprising natural frequency and vibration shapes.

2 Simulation of Cracked Gears

2.1 Modeling of Gear

The spur gear model for the crack opening discussed in this study is established on the continuum mechanics approach. For that, it is considered that material is isotropic and homogeneous. The standard spur gear with involute tooth profile is created in three-dimension as shown in Fig. 1a. The specifications for standard spur gear are listed in Table 1. Since the gear is immovable to the shaft in the real operational conditions, the internal circumference is established to restrict in all directions. A three-dimensional

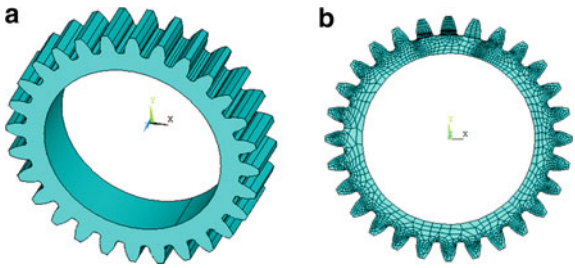

Fig. 1 Standard spur gear **a** three-dimension without mesh, **b** two-dimension with mesh

Table 1 Specifications of gear and pinion

Specification	Pinion	Gear
Number of teeth	28	25
Module (mm)	2	2
Face width (mm)	20	20
Contact ratio	1.63	1.63
Rotational speed (rpm)	2000	2400
Pressure angle (deg.)	20	20
Young's modulus (N/mm^2)	2×10^5	2×10^5
Poisson ratio	0.3	0.3

problem can be solved in two-dimensions if the boundary condition acts in the plane of the three-dimension with acceptable accuracy. In this study, the load is applied in the plane of the gear and evenly dispersed along the face width of the tooth. Moreover, there is no load concerned in the axial direction of spur gear. Thus, it is agreeable to create a two-dimensional model of the gear, to reduce computational cost as shown in Fig. 1b, Quad-4 elements are selected for the meshing. The defined thickness of the two-dimensional spur gear is equal to the tooth width, by choosing element behavior as plane stress with thickness. The length of cracks and its position in spur gear depend upon microstructure of the gear material and geometrical specification of structure and loading condition. The nucleation of cracks and crack propagation occurs due to local amassing of dislocations, high stresses/strain at local region, plastic deformation or other imperfections. During the periods of gear pair, a dissimilar combination of rolling and sliding contact takes place. According to the operating conditions, the crack was simulated at the root and nearby pitch circle of gear. The length of the crack is defined as crack depth, which is ratio of crack length to the tooth thickness as presented in Fig. 2. The values of crack depths are taken as 0.5 and 0.75 at the root and at the pitch circle crack, respectively. For longer crack, the value of stress concentration and fracture stress is lower.

Fracture comprises thorough interruption of continuity of a structure and begins with the opening of a crack. The opening of crack takes place if maximum stress at the crack tip is equal to the cohesive strength of structure. The stress can then

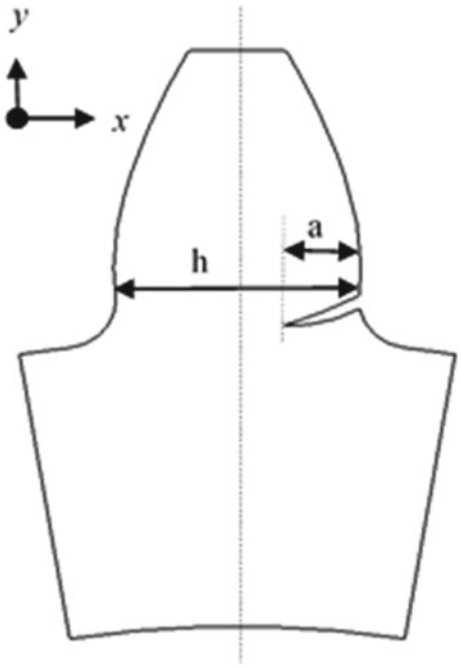

Fig. 2 Schematic illustration of crack in gear

be called fracture stress, which depends upon the kind of the crack and the loading characteristics.

This constant is known as fracture toughness of the structure of material which resists the fracture and is expressed by (K_{1C}). It is a material characteristic parameter. Thus, Eq. (1) can be modified in the form of Eq. (2). From Fig. 3, external stress is normal to the crack plane having crack length ($2a$). The stress distribution at the crack tip is determined using Eq. (3), where K_1 is the stress intensity factor for opening mode of fracture and θ is the crack propagation angle.

$$\sigma_c \sqrt{a\Pi} = \text{Constant} \tag{1}$$

$$\sigma_c \sqrt{a\Pi} = K_{1C} \tag{2}$$

$$\left.\begin{aligned} \sigma_x &= \tfrac{K_I}{\sqrt{2\Pi r}}\left\{\cos\tfrac{\theta}{2}\left(1-\sin\tfrac{\theta}{2}\sin\tfrac{3\theta}{2}\right)\right\} \\ \sigma_y &= \tfrac{K_I}{\sqrt{2\Pi r}}\left\{\cos\tfrac{\theta}{2}\left(1+\sin\tfrac{\theta}{2}\sin\tfrac{3\theta}{2}\right)\right\} \\ \tau_{xy} &= \tfrac{K_I}{\sqrt{2\Pi r}}\sin\tfrac{\theta}{2}\cos\tfrac{3\theta}{2} \end{aligned}\right] \tag{3}$$

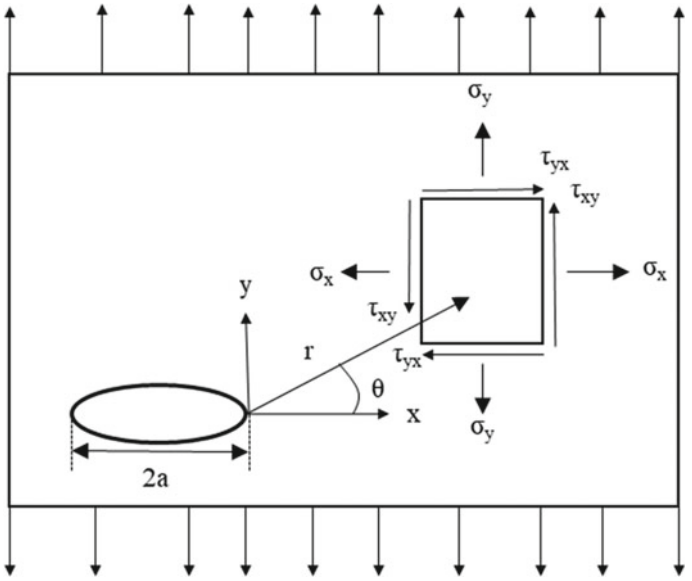

Fig. 3 Crack of mode-I

2.2 Creation of Cracked Model of Gear

XFEM is considered as an effective tool for the modeling of fracture problems. It supports the accurate estimate of solution that involves jumps, kinks, singularities and additional non-smooth characteristic in the elements. In XFEM, discontinuous enrichment functions like Heaviside functions, asymptotic functions, etc., are put together to the normal finite element estimation. Thus, XFEM extinguishes the need of re-meshing for discontinuous surface. It reduces the computational cost and the errors associated with finite element method. The displacement approximation for a cracked domain, at a particular node of interest in 2-D, can be written as [13].

$$u^h(x) = \sum_{i=1}^{n} N_i(X) \left[\overline{u_i} + \underbrace{\left\{ \begin{matrix} H(X) - \\ H(X_i) \end{matrix} \right\} a_i}_{i \in n_r} + \left\{ \underbrace{\sum_{\alpha=1}^{4} \left[\begin{matrix} \beta_\alpha(X) \\ -\beta_\alpha(X_i) \end{matrix} \right] d_i^\alpha}_{i \in n_A} \right\} R(X) \right] \quad (4)$$

where $N_i(X)$ and $\overline{u_i}$ are shape functions and nodal displacement vector at node i; n is the combination of all nodes in the mesh; n_r is the combination of nodes related with elements which are entirely cut by the crack. $H(X)$ is the Heaviside function, considered for those elements which are entirely cut by the crack, and whose value is $+1$ on one side of crack and -1 on the other side; a_i is the nodal enriched degree of freedom associated with $H(X)$. n_A is the combination of nodes connected with

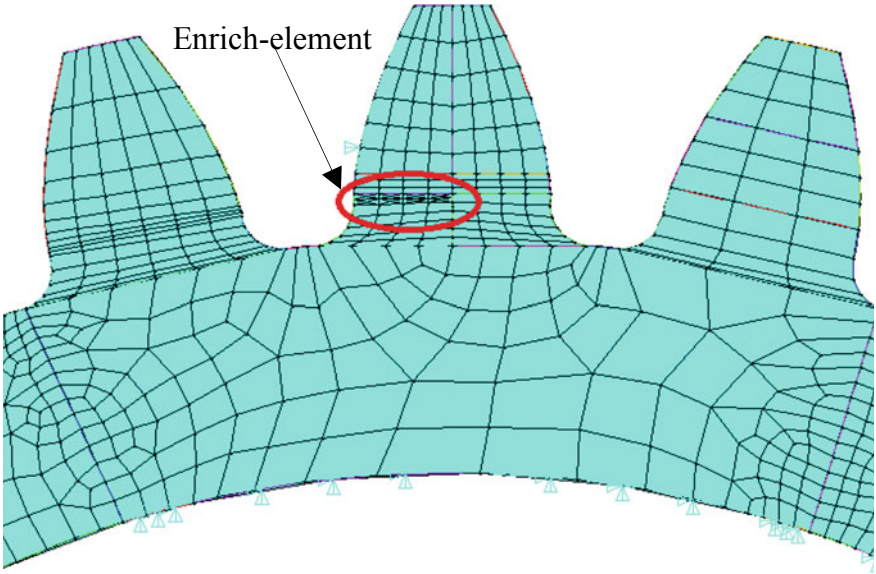

Fig. 4 Meshing of gear with enrichment

elements which are partially cut due to the crack; $R(X)$ is ramp function that is used for the blending elements [13]. d_i^{α} is the degrees of freedom for nodal enriched vector connected to enrichment function $\beta_{\alpha}(X)$ with crack tip. Taking into account a polar coordinate system with specification r and θ at the crack tip, enrichment functions for crack tip are asymptotic and can be written as [14],

$$\beta_{\alpha}(X) = \left[\sqrt{r}\sin\frac{\theta}{2}, \sqrt{r}\cos\frac{\theta}{2}, \sqrt{r}\sin\frac{\theta}{2}\cos\theta, \sqrt{r}\cos\frac{\theta}{2}\cos\theta\right] \tag{5}$$

XFEM-based computer program in ANSYS software is used to simulate the crack in gear body by Eq. (4). By incorporating the concept of XFEM, the gear mesh with enrichment element is shown in Fig. 4. The contact force in the meshed tooth with the crack is taken as 100 N. The displacement contour plot of a cracked tooth of a gear is shown in Fig. 5.

3 Discussion

The natural frequencies are distinct with the presence/absence of crack, as presented in Table 2. The deflection stiffness of gear is altered by crack position and crack length. Due to this, a small amount of decrement in natural frequency is observed

Fig. 5 Cracked tooth of gear

Table 2 Natural frequency of gear in Hz

Crack	Crack depth	First	Second	Third	Fourth	Fifth
Without crack	$\alpha = 0$	51.245	51.854	52.452	53.84	54.637
Root	$\alpha = 0.75$	51.085	51.85	51.908	53.835	54.058
	$\alpha = 0.5$	51.236	51.852	52.401	53.835	54.581
Pitch circle	$\alpha = 0.75$	51.24	51.852	52.424	53.84	54.606
	$\alpha = 0.5$	51.244	51.854	52.447	53.84	54.631

even for a small crack length. This decrement in natural frequency is more for a large crack length at the same position. Also, the value of natural frequency is noticeably higher if crack occurs near the pitch circle as compared to crack at tooth's root. This implies that the loss to the gear's stiffness is more for crack occurring at the tooth root as compared to crack found near the pitch circle of tooth. Figure 6 represents different vibration shape for different crack position and crack length.

4 Conclusions

The dynamic natural characteristics of structure of spur gear are affected due to the presence of crack and vary with length and position of cracks. When crack is at the tooth's root, the decrease in expected frequency is comparatively large than when it is near the pitch circle. Also, for large length of crack at the same position of the gear structure, corresponding decrement in natural frequency is high. The vibration shapes for corresponding natural frequencies of the gear with crack are very similar

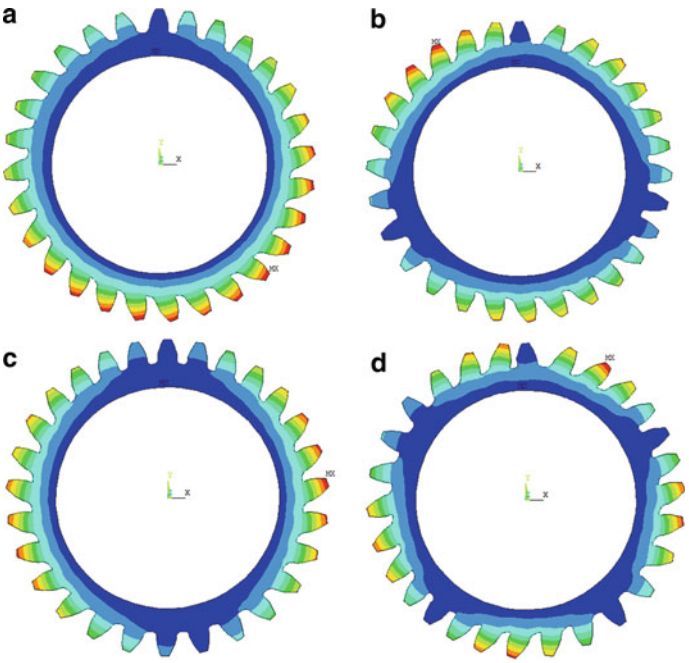

Fig. 6 Vibration shape of gear with crack **a** first order, $\alpha = 0.75$, root crack **b** third order, $\alpha = 0.75$, pitch circle crack **c** second order, $\alpha = 0.5$, root crack **d** fifth order, $\alpha = 0$, pitch circle crack

to the gear without crack. The findings obtained in the present study deliver a basic indication for detecting the cracks and diagnosing the damage.

References

1. Zouari S, Maatar M, Fakhfakh T, Haddar M (2007) Three-dimensional analyses by finite element method of a spur gear: effect of cracks in the teeth foot on the mesh stiffness. J Fail Anal Prev 7:475–481. https://doi.org/10.1007/s11668-007-9078-5
2. Wang J, Howard I (2005) Finite element analysis of high contact ratio spur gears in mesh. J Tribol 127:469. https://doi.org/10.1115/1.1843154
3. Yang DCH, Lin JY (1987) Hertzian damping, tooth friction and bending elasticity in gear impact dynamics. J Mech Transm Autom Des 109:189. https://doi.org/10.1115/1.3267437
4. Tian X (2004) Dynamic simulation for system response of gearbox including localized gear faults. MSc thesis, University of Alberta, Edmonton, Alberta, Canada
5. Pandya Y, Parey A (2013) Crack behavior in a high contact ratio spur gear tooth and its effect on mesh stiffness. Eng Fail Anal 34:69–78. https://doi.org/10.1016/j.engfailanal.2013.07.008
6. Chaari F, Fakhfakh T, Haddar M (2009) Analytical modelling of spur gear tooth crack and influence on gearmesh stiffness. Eur J Mech A/Solids 28:461–468. https://doi.org/10.1016/j.euromechsol.2008.07.007
7. Sainsot P, Velex P, Duverger O (2004) Contribution of gear body to tooth deflections—a new bidimensional analytical formula. J Mech Des 126:748. https://doi.org/10.1115/1.1758252

8. Ma H, Pang X, Zeng J, Wang Q, Wen B (2015) Effects of gear crack propagation paths on vibration responses of the perforated gear system. Mech Syst Signal Process 62:113–128. https://doi.org/10.1016/j.ymssp.2015.03.008
9. Fajdiga G, Ren Z, Kramar J (2007) Comparison of virtual crack extension and strain energy density methods applied to contact surface crack growth. Eng Fract Mech 74(17):2721–2734
10. Pehan S, Kramberger J, Flasker J, Zafosnik B (2008) Investigation of crack propagation scatter in a gear tooth's root. Eng Fract Mech 75(5):1266–1283
11. Ghaffari MA, Pahl E, Xiao S (2015) Three dimensional fatigue crack initiation and propagation analysis of a gear tooth under various load conditions and fatigue life extension with boron/epoxy patches. Eng Fract Mech 135:126–146
12. Belytschko T, Black T (1999) Elastic crack growth in finite elements with minimal remeshing. Int J Numer Methods Eng 45:601–620. https://doi.org/10.1002/(SICI)1097-0207(19990620)45:5%3c601:AID-NME598%3e3.0.CO;2-S
13. Singh IV, Mishra BK, Bhattacharya S, Patil RU (2012) The numerical simulation of fatigue crack growth using extended finite element method. Int J Fatigue 36:109–119. https://doi.org/10.1016/j.ijfatigue.2011.08.010
14. Kumar S, Singh IV, Mishra BK (2015) A homogenized XFEM approach to simulate fatigue crack growth problems. Comput Struct 150:1–22. https://doi.org/10.1016/j.compstruc.2014.12.008

Biomechanical Evaluation of Manual Material Handling Task in the Workplace: A Comprehensive Review

Anurag Vijaywargiya and Mahesh Bhiwapurkar

Abstract Human involvement, as a manual work, is still prevailing in modern manufacturing activities because of a limited workspace which does not allow the use of mechanical devices or robots. The manual materials handling (MMH) is an inefficient way of performing a task and is considered hazardous in addition to wastage of the great amount of human energy. Moreover, subsequent accidents and injuries can be physically and economically very disturbing and costly. Ergonomic evaluation of MMH has largely been based on task analysis approach, where the jobs are broken down into simpler tasks and studied. But there is the lack of clarity in the use of terms defining various MMH activities. Therefore, the need arises to minimize MMH tasks-related injury, using specific design approaches, so that its demand stays within the capacity of the worker. The aim of the present study is to demonstrate the applications of biomechanics and explain how the use of biomechanics can reduce the risk of an initial injury. The study also indicates the impact low back pain may have, on performing the task. To achieve this, a systematic review of specific design approaches (biomechanical, physiological, epidemiological, and psychophysical approaches) of various tasks in the workplace has been made to identify a situation that has a higher risk of workplace injury. This review of literature will be helpful to evaluate MMH task design or work practice so as to identify an effective and efficient solution, to ensure physical changes to the workplace. The study will also be helpful to provide a set of recommendations, to reduce or prevent the presence of musculoskeletal disorders and enhance production.

Keywords MMH · Biomechanics · Back pain · Musculoskeletal risks

A. Vijaywargiya (✉) · M. Bhiwapurkar
O.P. Jindal University, Raigarh, India
e-mail: anurag@opju.ac.in

V. K. Gupta et al. (eds.), *Reliability and Risk Assessment in Engineering*,
Lecture Notes in Mechanical Engineering,
https://doi.org/10.1007/978-981-15-3746-2_27

1 Introduction

From an ergonomics perspective, manual handling tasks are responsible for potential risks of workplace accidents and high-risk activities could lead to a spinal cord injury. The tasks for manual material handling incorporates varied activities with awkward motion and postures such as pushing, pulling, holding, carrying, lifting, lowering, and turning of weights. MMH is the most common cause of occupational fatigue, and major concern has been shown to low back injuries [1]. Depending on the nature of activity, MMH exposure results in physical stresses to the operator that may manifest individually or collectively as strains on the musculoskeletal, cardiovascular, and neurological system. If these strains exceed the capacity of the system, it leads to potential hazards such as discomfort, fatigue, or injury, which in turn may have detrimental effects on productivity.

The utilization of ergonomic principles in the workplace design and evaluation of human work can help to reduce physical stress on the body and preventing many potential workplace risks, disabling musculoskeletal disorders. A variety of ergonomics assessment methods are available for the evaluation of MMH tasks. To prevent the work-related musculoskeletal disorders (WMSDs) at a preliminary stage, the key step is the measurement and evaluation of physical loading of the musculoskeletal system, which helps to identify stressful job components, so that solutions can be developed and implemented. It also provides valuable information for the design of MH system, and decisions for redesigning are implemented.

The literature on the research issues of manual load lifting caused by frequent lifting and lowering tasks has grown rapidly in the past few decades. These researches implemented three approaches, namely physiological, psychophysical, and biomechanical. The present paper also discusses the epidemiological approach. A review of the literature has been carried out to synthesize and evaluate the limitations of and conflicts among these approaches so that areas which need further examination can be explored.

2 Material and Method

Based on the four main types of manual load lifting approaches, the review of literature was done. The various databases were used to find relevant literature and Internet sources include bibliographic database, Google Scholar, and several search engines. The literature was searched by using the keywords manual lifting, lower back pain, and musculoskeletal risk. The findings from the literature are presented in a well-organized manner. The capability/strengths and shortcomings/weaknesses of each approach are also presented.

2.1 MMH Task Design Approaches

Many efforts have been made by researchers to design the MMH tasks, using physiological, psychophysical, and biomechanical approaches. The assumptions that these approaches inherited (i) the inappropriate method that make manual handling of loads hazardous and increase the risk of musculoskeletal injury, particularly for low back pain, and (ii) lack of secured and accurate technique which was suitable for most of the population.

The vital examination of these approaches has been done in relation to worker characteristics (body weight, sex, age, and individual muscle strength); container/material characteristics (container size, weight of load, and coupling); task characteristics (comprised of distance of movement, duration/frequency, and dynamics of the activity); and the work practices involving working posture, position, lifting techniques, and safety functions.

The Biomechanical Approach The biomechanical approach refers to the study of mechanics, which investigates the effect of forces (internal and external) on human bodies in motion and at rest. The mechanical stresses are imposed on the musculoskeletal system (internal forces produce torques about joints, compressive and shear forces on the lower back) during a lifting action. These stresses serve as the criteria upon which capacity of the lift is based. The aim of any approach is to determine the maximal acceptable load so that the limit can be set on the acceptable physical stresses during lifting action. The most commonly used criteria considered in biomechanical approach are compression limits for the spinal L4/L5 or L5/S1 disk joints and/or maximum joint torques. The cadaver studies of spinal failures derived the compression limits for the L4/L5 or L5/S1 joints, while the result of empirical studies was used to derive maximum joint torques [2]. This approach is generally applicable for one-time loading situation or in worst-case scenario of a task. It can predict localized muscle fatigue only. This approach does not take into account the effect of duration and frequency of MMH task.

The Physiological or Cardiovascular Approach The physiological approach is concerned with the physiological response of the body to MMH tasks. It is based on work physiology principles. This approach selects physiological criteria such as energy expenditure and its upper limit. Based on that upper limit, lifting capacity data can be established. Typically, the physiological responses are closely linked with fatigue, related to a difficulty in performing voluntary tasks. This approach considers metabolic energy requirement of the MMH task. The aim is to keep metabolic rate less than 5 kcal/min for an eight hours' task. It takes into account rate and duration of MH and dynamic effect of body movement. However, injury may occur due to localized muscle or joint overload, which this method cannot isolate. Dempsey and Westfall [3] reported that the field measurement of oxygen consumption is not only expensive but also interferes with task performance. This criterion is better than the biomechanical criterion. This approach is well suited for repetitive tasks practice and less sensitive to infrequently performed tasks like holding loads, etc.

The Psychophysical Approach Psychophysics describes the relation between physical stimuli and its corresponding sensations. The subject adjusts the weight of the load of the object being lifted, until a maximum acceptable weight of lift (MAWL) is achieved. The maximum acceptable weight of lift is defined as the maximum weight an individual can lift according to his or her own perception of effort, repeatedly without undue stress or overtiring. As such, for the psychophysical approach, the criterion upon which capacity of the lift is based is the perceived stress by the subject. The psychophysical approach was chosen to determine lifting capacity. This approach assumes that the combined effects of biomechanical and physiological stresses are present in nearly all lifting tasks. Both these approaches are integrated or combined for the measurement of perception of stress. The main limitations of the psychophysical method are that it is a subjective measure and relies on assumption that selected workload by worker is below the threshold for injury, and it has not been validated. Furthermore, psychophysical approach provides limits that exceed the limits imposed by biomechanical and physiological assessment at low- and high-lifting frequencies [4].

Emanuel et al. [5] were allowed subjects to select loads that they felt could lift as a maximum. This work was expanded by Snook and Irvine [6–8] who demonstrated in determining the subject's preference of maximum acceptable weight of lift (MAWL) subjectively for lifting tasks based on assessing subjectively the feelings of exertion or fatigue of worker. Few years later, Switzer [9] collected data on one- and two-handed lifting capabilities of 75 subjects for three different vertical heights of lift, who pointed out they could lift standard containers with varying amounts of weight with 5, 10 or 20 lbs increments.

The Epidemiology Approach The epidemiological approach is used to identify and classify factors which influence injury. Epidemiological method has been designed to identify the cause and effect relationships, which were difficult to understand. Therefore, the epidemiological approach had paid insufficient attention as against other approaches, due to the difficulties in correlation between the work environment, workers, and accidents/injuries. Epidemiology is the study of disease occurrence in human population. The emphasis of this approach is on groups of people rather than the individual. In the context of MMH activities, the epidemiological approach investigates the circumstances and conditions that exist during an incident and attempts to develop a set of general conditions that may be associated with the hazards of MMH activities. Epidemiology attempts to answer questions such as 'why are there so many back injuries in the material handling occupations?', 'How can these injuries be prevented?', 'What are the common factors present in all, or most of these injuries?', etc. Several epidemiological studies have concluded that weight of the load and frequency of lifting it are among the most critical factors that determine the risk of injury [10]. Epidemiology is one of the most underestimated tools due to a lack of verification of MMH criteria. Therefore, further research is required toward area of MMH, primarily due to a lack of epidemiological verification and validity of the criteria based on different approaches [11].

2.2 Development of Job Severity Index

Two factors, the job demands and the operator capacity, determine whether a MMH job is injurious to the operator. Often, job demands describe each job in terms of actual weight of lift, frequency of lift, container size, and range of lift. The related capacity of the operator can be expressed by his or her lifting ability, as based on physiological, biomechanical or psychophysical criteria. The goal of ergonomics is to design the task, so that its demands stay within the capacities of the workers. Applying this to material handling, the goal is to design MMH tasks such that the weight of the lift required for a given frequency, range of lift, etc., does not exceed the operator's capacity of the lift. This notion was used in the lifting strength rating (LSR) which is the most stressful load lifted by a person on the job divided by the lifting strength of large strong man [10].

The concept was also used in the NIOSH lifting index (LI) [12] which is the ratio of actual load being lifted during a particular task, divided by recommended weight limit (RWL) [13, 14]. If the LI is less than unity, it indicates the safe lifting task. If LI is greater than 1, it poses an increased risk of lifting task. The job severity index (JSI) is conceptually similar to LSR and is a function of the ratio of job demands, to the lifting capacities of the person. A JSI as an engineering tool is used for the control of manual materials handling injury. During the development of the JSI, the capacity to lift was determined using psychophysical methods.

The NIOSH Equations In 1981, the National Institute for Occupational Safety and Health (NIOSH) established load limit recommendations designed to identify hazardous lifting jobs and provide recommendations to alleviate the hazardous elements associated with lifting jobs. Due to the limitation of 1981 equation to a limited number of lifting tasks, the equation was revised and expanded in 1991. Due to the inclusion of an asymmetry multiplier and coupling multiplier, the 1991 revised lifting equation covers a wider range of tasks and is more protective of workers compared with the 1981 equation. Though the equation was not fully validated, the RWL computed was generally lower than the MAWL as reported in literature [13].

The 1981 equation was limited to sagittal lifting task, whereas the revised lifting equation uses six variables which include horizontal location from the mid-point between the ankles, vertical location, vertical travel distance, asymmetric angle, lifting frequency, and coupling along with the load constant. The NIOSH lifting equation is an ergonomic intervention assessment tool, to assess the manual material handling risks associated with lifting without increasing the risk of musculoskeletal disorders (MSD) to the lower back. However, after cross-validation of the results for psychophysical, biomechanical, and physiological criteria used in establishing the NIOSH limits for manual lifting, Hidalgo et al. [15] reported that the biomechanical and physiological criteria were not in total agreement with the 1991 NIOSH model. Therefore, there is a need of further research to determine the association of estimate of risk for lifting with the lifting index [12].

2.3 Shortcomings and Conflict of Various Criterion

This section addresses the shortcoming of evaluating four approaches under study has been discussed. The conflicts that arise among these criteria have also been discussed, as these have some of the direction for future research efforts.

Biomechanical Concern A topic of biomechanical model whether it is static or dynamic is always debatable. Dynamic models are more representative of the lifting motions and, therefore, are preferred to static models. The static models ignore the forces due to inertia of the load and moments underestimated the internal loads in dynamic actions [16, 17]. The primary concern of dynamic model is the inability to predict the dynamic strength capability of a population, to judge the acceptability of a task [16]. Secondly, biomechanical model estimates compression force on the low back, while ignoring shear forces.

Epidemiological Concern While interpreting various epidemiological results that exist, it was found very difficult to derive valid criteria. It was observed from many studies that the combined effect of twisting and lifting task will amplify the risk of LBD, but found to be difficult quantitatively. The review results also implied that the inappropriate use of methods might result in uncertain exposure estimates of risk, which attributes to serious consequences for risk estimates arising from epidemiological studies.

While interpreting epidemiological results, it was observed that the investigation of several researchers was focused on a single variable and it was suggested that a number of factors such as characteristics of worker, material, task, and work practices should be considered in determining capacity data of MMH activities to investigate LBD, so as to predict effective and valid interventions model with potential interactions [3].

Physiological criteria Though the standard measure of aerobic capacity is directly related to the physical working capacity of an individual, the researchers were specified by setting energy expenditure limit as the maximum oxygen uptake (VO_2max). While specifying a physiological design criterion, the physiological demands should be related to an individual's maximum aerobic capacity, in order to determine what percent of that capacity a given lifting task requires [11].

Moreover, the lack of demonstrated association was observed between physiological load and injury rates. In MMH activities, work often involves many muscles in the neck, trunk, and abdomen, which may be necessary to keep balance of the body during work. While the oxygen uptake of the given task may be increased due to contraction of these accessory muscles, the maximum oxygen uptake may be lower during lifting due to compression of the abdomen and thorax. In the perspective of enhancing the performance of the MMH system, physiological criteria are necessary.

Psychophysical criteria The psychophysical approach is associated with the maximum work-related perceived exertion, to estimate his or her tolerance level, thereby

establishing the maximum acceptable lift of limit for different MMH activities. The psychophysical criterion provides limit by integrating both biomechanical and physiological sources of stresses imposed by the workload of lifting job [14]. It allows for realistic simulation of many types of material and can be used to study very intermittent manual handling tasks, generally found in the industry. Psychophysics uses a subjective method that relies upon perceived exertion by subject [18]. In psychophysical criteria, the limits established are higher for very high-frequency tasks than recommended metabolic criteria. The permissible loads for tasks requiring high effort should be related to metabolic criteria. The disadvantage of psychophysics is the lack of sensitivity to the bending and twisting motions occurring at the back. One potential limitation of psychophysics is that the subject adjusts the weight until it is acceptable for lifting over a specified time period, as required by the physiological burden of performing the task for an 8 h in a day [19, 20].

3 Conflict Between Criteria Based on the Various Approaches

The limits provided for MMH based on biomechanics, psychophysics, and physiology criteria are in considerable disagreement and in conflict. Unfortunately, these conflicts cause uncertainty for practitioners and troublesome for selecting a proper limit. The discrepancies among these criteria are shown in Fig. 1, which demonstrates the recommended loads with respect to frequency (lifts/min), lifting from floor to shoulder. The biomechanical fatigue criteria tend to minimize the load on the low back by selecting smaller weight and more frequent rate of lifts (to reduce stresses on the lower back). While metabolic fatigue criteria tend to choose larger load at

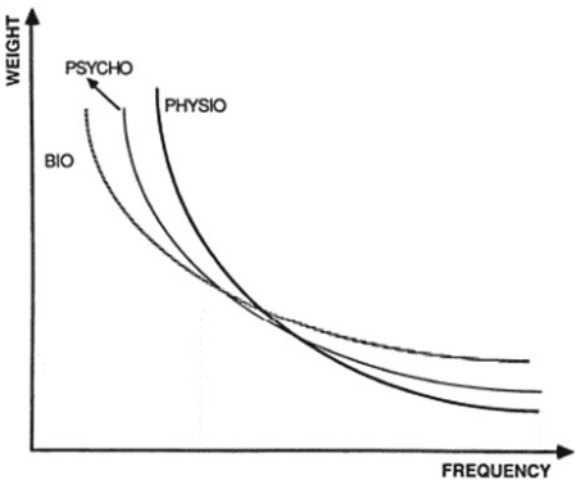

Fig. 1 Comparison of biomechanical, physiological, and psychophysical fatigue criteria [11]

less frequent rate of lift (to reduce metabolic energy expenditures), it is obvious that the recommendations based on the biomechanical approach are lower than those of the physiological approach at low frequencies ($\leq$3 lifts per minute) and higher at higher frequencies (>5 lifts per minute). Previous efforts to compare the psychophysical and physiological criteria for determining safe, acceptable weights have concluded that the weight recommendations based on the physiological approach are lower than psychophysical approach at high frequencies. The trend is reversed at low frequencies.

For the comparison purpose, Garg [16], Asfour, and Karwowski's models were used. Even though these three models work very well on real large data sets, most of the case, Garg's model overestimate the metabolic energy requirement and Asfour's model ignores the oxygen consumption rate for other's actual measurement of the metabolic energy. Karwowski's model gives quite accurate prediction of oxygen consumption. However, this model is restricted to the range from floor to knuckle heights of lifting activity. Developing a physiological model for metabolic energy expenditure for better estimation is necessary at this point.

4 Conclusions

This paper reviewed three criteria and provides the recommendation that has been useful to decrease the frequency and severity of MMH-related injuries. The application of different criteria has yielded different recommendations with regard to safe lifting capacity. Lifting is a task of an extremely complex nature, and because of this, it cannot be fully described or explained using only biomechanical or physiological criterion. Both physiological and biomechanical stresses, among others, are present in nearly every lifting task, and as such, the need exists for a means of determining lifting capacity that can accommodate all of these stresses. Technological advances and utilization of very sophisticated equipment are helping to progress our information of the anatomical responses of the body to work. At the present time, it is necessary to accept trade-offs, such as whether to minimize the spinal forces resulting from manual material handling or minimize the energy expenditure of a lift or be within the maximum permissible weight range. The combined effort of epidemiological studies with such technological advances explores the potential to improve and further widen criteria to prevent the related injuries of MMH.

References

1. National Institute of Occupational Safety and Health, USA (1997) Musculoskeletal disorders and workplace factors. DHHS (NIOSH) Publication No. 97–141
2. Dempsey PG (1998) A critical review of biomechanical, epidemiological, physiological criteria for designing manual materials handling tasks. Ergonomics 42(1):73–88

3. Dempsey PG, Westfall PHP (1997) Developing explicit risk models for predicting low back disability: a statistical perspective. Int J Ind Ergon 19(6):483–497
4. Dempsey PG, Ayoub MM (1999) The psychophysical approach to manual materials handling task design. Ergonomics 42(1):17–31
5. Emanuel I, Chaffee JW, Wing J (1956) A study of human weight lifting capabilities for loading ammunition into the F-86H aircraft. WADC Technical Report 56-367. Wright Air Force Base, OH
6. Snook SH (1978) The design of manual material handling tasks: ergonomics. Taylor and Francis, London
7. Snook SH, Irvine CHC (1967) Maximum acceptable weight of lift. Am Ind Hyg Assoc J 28(4):322–329
8. Snook SH, Ciriello VM (1991) The design of manual handling tasks: revised tables of maximum acceptable weights and forces. Ergonomics 34(9):1197–1213
9. Switzer SA (1962) Weight-lifting capabilities of a selected sample of human subjects. Technical Document Report No MRL-TDR-62-57, Aerospace Medical Research Laboratories, Wright-Patterson Air Force Base, OH
10. Chaffin DB, Park KS (1973) A longitudinal study of low back pain as associated with occupational weight lifting factors. Am Ind Hyg Assoc J 34(12):513–525
11. Ayoub MM, Dempsey PG, Karwowski W (1997) Manual materials handling. In: Handbook of human factors and ergonomics, 2nd edn. Wiley, New York
12. Waters TR, Putz-Anderson V, Garg A (1994) Applications manual for the revised NIOSH lifting equation. DHHS(NIOSH) Publication No. 94–110, NIOSH, Cincinnati
13. Ayoub MM, Selan BJL, Jiang C (1983) A mini-guide for lifting. Texas Tech University, Texas
14. Ayoub MM, Bethea N, Deivanayagam S, Asfour S, Bakken G, Liles D, Selan J, Sherif M (1978) Determination and modeling of lifting capacity. Final Report HEW (NIOSH) grant no 5R010H00545-02 NIOSH, Cincinati, OH
15. Hidalgo J, Genaidy A, Karwowski W, Christensen D, Huston R, Stambough J (1995) A cross-validation of the NIOSH limits for manual lifting. Ergonomics 38(12):2455–2464
16. Garg A, Chaffin DB, Freivalds A (1982) Biomechanical stresses from manual load lifting: a static vs. dynamic evaluation. IIE Trans 14(4):272–281
17. McGill SM, Norman RW (1985) Dynamically and statically determined low back moments during lifting. J Biomech 18(12):877–885
18. Mital A, Nicholson AS, Ayoub MM (1993) A guide to manual materials handling. Taylor & Francis, London
19. Fernandez JE, Ayoub MM, Smith JL (1991) Psychophysical lifting capacity over extended periods. Ergonomics 34(1):23–32
20. Mital A (1983) The psychophysical approach in manual lifting—a verification study. Hum Factors 25(5):485–491

Analysis of Causes of Rail Derailment in India and Corrective Measures

Prakash Kumar Sen, Mahesh Bhiwapurkar, and S. P. Harsha

Abstract Railways provide the cheapest and most convenient mode of passenger transport both for long distance and suburban traffic; also, it plays a significant role in the development and growth of industries. Even though there are several advantages and safety in railway transport, the frequency of train accidents is still increasing. A train derailment can result in severe injuries or even death to passengers, railroad employees and bystanders. In 2007, the Federal Railroad Administration (FRA) reported nearly 2000 derailments on tracks all over the country. Whereas approximately 373 train derailments were reported by Indian Railways from 2009 to 2015. In the same duration of 6 years, there were total 803 accidents in Indian Railways killing 620 people and injuring 1855 people. 47% of these accidents were due to derailment of trains. Therefore, the statistical analyses were conducted to examine the effects of accident causes in India for last ten years. The analysis showed that broken rails or welds were the leading cause of derailments. Because of the seriousness of railway accidents, the study also aims to suggest the possibilities of minimizing devastating consequences of vehicle derailments by appropriate measure.

Keywords Train derailment · Accident cause · Railroad · Collision

1 Introduction

The largest Railway network in Asia and second largest in the world, the Indian Railways transport more than 20 million passengers and over 7500 freight day in and day out. 11,000 trains race around the nation every day on a multi-gauge and a multi-suction system under one management. Spreading over the course of 65,500 km, the Indian Railways is branched into 16 zones consisting more than 7000 stations.

P. K. Sen (✉) · M. Bhiwapurkar
O.P. Jindal University, Raigarh, India
e-mail: prakashkumarsen@gmail.com

S. P. Harsha
Indian Institute of Technology Roorkee, Roorkee, India

V. K. Gupta et al. (eds.), *Reliability and Risk Assessment in Engineering*,
Lecture Notes in Mechanical Engineering,
https://doi.org/10.1007/978-981-15-3746-2_28

Railroad safety and risk analysis is an increasingly active research field which relies on accurate estimation of derailment rate. The derailment rate is a useful statistic to estimate the likelihood of a derailment and is defined as the number of derailments normalized by traffic exposure (train-miles, car-miles or gross ton-miles) [1–4]. This risk analysis is designed to help the industry to minimize the occurrence of accidents at railway turnouts. It is of keen interest to both the rail industry and the FRA to identify promising strategies for the prevention of train accidents.

The study conducted by Nayak et al. provides the comprehensive insight into the railroad accident rates in the USA [1]. The derailment rate per million train-miles in US railroad has declined from 8.98 derailments in 1980, to 1.63 in 2014, i.e., total 82% reduction [5]. Evans [6, 7] analyzed train collisions due to human error in Great Britain and the USA. Barkan et al. [8] found that the average number of cars derailed per train accident is associated with accident speed. The FRA identifies distinct accident causes organized into the categories of track defects, rolling stock failures, signaling failures, human errors, and other causes [9]. A higher speed may result in more cars derailed, given all other factors being equal. In addition to speed, Saccomanno and El-Hage [10] found that the point of derailment (the position of the first derailed car), train length, and accident cause also affect accident severity. Liu et al. [4] found that, on average, derailments caused by track failure typically resulted in more cars being derailed than in the case of mechanical failures. For example, broken rails resulted in an average of 13 cars derailed per freight train derailment, as compared to seven cars derailed from bearing failures [4].

Over the past few decades, the Indian Railways has been improving and introducing new schemes and facilities, but in recent times, accidents and derailments have seriously affected its credibility. A fatality from train derailments in 2016–2017 holds the highest death toll due to train derailments in a decade. 193 passengers died in these accidents despite the fewest train accidents over 10 years (104) ending March 2017; 78 of these accidents were derailments [11]. These incidents have brought the focus on Indian Railways grappling with safety issue.

Vast statistical data analyses about train derailment were found in literature, but to the author's knowledge, no published studies were explicitly found on Indian trains. Therefore, this paper aims to predict the number of trains' derailments in last ten years in India by railroad, and analyses the dominant causes of major derailment. The aim is also to suggest the possibilities of minimizing devastating consequences of train derailments by appropriate measures. Furthermore, literature-based recommendations are used to address the issues arising from risks. The research outcomes are expected to aid the rail industry in developing, evaluating, prioritizing, and gaining a different perspective of derailment to efficiently improve transportation safety. To understand better the work developed here, the authors obtained data from Ministry of Railways, India as data source, without comparing the results with another database. On the other hand, the database has been formed only of India-based reports.

2 Methods

The exposition of this paper is as follows. First, introduces the collection of accident data, traffic exposure data from Ministry of Railways, India. Second, this paper analyzes accident cause-specific train derailment rate by railroad in various zones on mainlines in India between 2003–2004 and 2015–2016. Third, this paper reviews the relevant literature on rail safety and risk analysis, to understand the state of the art in literature and to identify and fill knowledge gaps. Finally, this paper presents its major findings and suggests the possibilities of minimizing devastating consequences of train derailments by appropriate measure.

3 Results and Discussion

Number of train accidents and derailments during the period from 2003–2004 to 2015–2016 along with the casualties (killed/injured) are given in Fig. 1. Train accidents have occurred due to various factors, one of them is derailment. During 2003–2004, 202 accidents (84.51%) out of a total of 325 accidents occurred due to derailments. During the year, 2014–2015 out of total 135 train accidents, 63 (46.7%) were derailments. The trend was found similar during the previous years. In the year 2015–2016, out of total 107 train accidents, 65 (60.7%) train accidents were attributed to derailments. In the year starting from April 1, 2016 to February 28, 2017, out of total 99 train accidents over Indian Railways, 76 train accidents (76.7%) were attributed to derailments (not shown in the figure). During the last three years, i.e., 2013–2014, 2014–2015, 2015–2016 and the year up to February 28, 2017, altogether 459 train

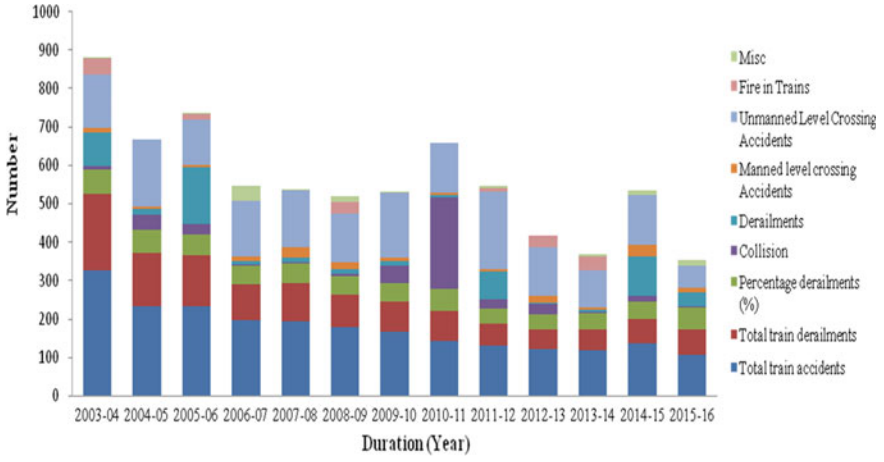

Fig. 1 Number of train accidents and derailments along with the casualties

accidents (including incidents at unmanned level crossings, mostly caused due to negligence of road vehicle users) occurred on Indian Railways.

During 2014–2015, out of 161 casualties, 103 (around 56%) were due to derailment. During 2015–2016, out of 64 casualties in various types of accidents, 36 (56%) were due to derailment.

The consequential train accidents, excluding unmanned level crossing incidents on Indian Railways, have declined substantially from 239 in 2003–2004 to 85 in 2014–2015. However, the trend is not positive in case of accidents at unmanned level crossings, where during 2003–2004, 86 accidents occurred while 50 such accidents occurred in 2014–2015. Further, during 2014–2015, out of 135 accidents, 50 accidents (around 37%) occurred at unmanned level crossings. It may simultaneously be observed from Fig. 1 that out of 291 casualties during 2014–2015, 130 (around 44%) and during 2015–2016, 58 casualties (48%) were at unmanned level crossing.

On November 20, 2016, 14 coaches of Indore–Patna Express derailed where 146 passengers lost their lives, while 58 passengers sustained grievous injuries and 122 passengers sustained simple injuries. During the course of evidence, the Chairman, Railway Board had stated that derailment may be on account of defect in the track or defect in the rolling stock.

The major causes of derailments might be due to rail fracture, weld failure, track defects, especially in curve/turnout areas, inappropriate worksite protection, defects arising in different types of rolling stock (wagon and coach defects), and overshoot the signal (Signal passing at danger) by loco pilots, etc.

The zone-wise and year-wise number of train accidents over Indian Railways during the last three years, i.e., 2014–2015, 2015–2016, 2016–2017 and the current year from April 1, 2017 to June 30, 2017 are shown in Fig. 2. The result clearly shows maximum train accidents in Northern zone, followed by East Central. The reason may be due to the maximum traffic flow in these zones.

A train accident is a type of disaster that often occurs as a result of miscommunication between the two trains moving on the same track; or an accident, when a train

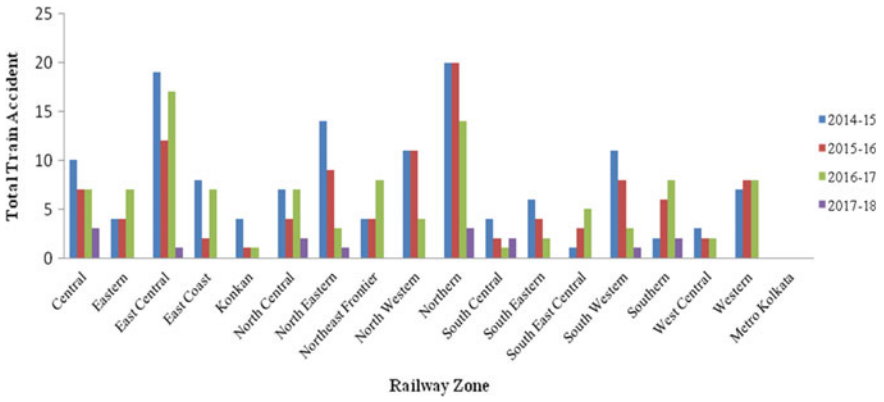

Fig. 2 Zone-wise and year-wise number of train accidents

wheel jumps off a track in a derailment. The train accidents occur due to a variety of causes such as collisions, derailments, fire in trains, and human error. The human error caused by driver distraction can have a terrifying impact on the victims of the accident. The overworked loco pilots easily doze off while working beyond their duty hours and this stressful work may lead to chronic fatigue and puts the life of thousands of commuters at risk, damage to railway property and affects the safety of train operations.

Indian Railways accord highest priority to safety in train operations. The number of train accidents increased from 117 during 2013–2014 to 135 during 2014–2015. However, accidents per million train kilometers are used as an important index reflecting the rate of accidents keeping the density of traffic on a particular railway in view. In respect of Indian Railways, the train accidents per million train kilometers have decreased from 0.28 in 2006–2007 to 0.10 in 2014–2015; despite quantum increase in the volume of traffic carried by Indian Railways over the years. Table 1 gives details of train accidents on Indian Railways since 2003. Data from the Railway Ministry [11] reveals that in the period of 4 years (2013–2017), more than 450 rail accidents have taken place killing over 800 people (Fig. 1). The majority of these accidents were due to train derailments followed by unmanned level crossings, excessive traffic, underinvestment, and shortcomings of the staff members.

Causes of train accidents from 2003–2004 to 2016–2017 are shown in Fig. 3. Of the 239 train accidents (except UMLCs), 161 accidents were caused due to failure of Railway Staff, 21 were due to failure on the part of other than Railway staff, 18 due to failure of equipment, 18 due to sabotage, 17 due to the incidental factors, 2 accidents occurred due to the combination of factors, and in 2 cases none has been held responsible. From the statement above, it is seen that during 2015–2016 out of 77 accidents, 55 accidents (about 70%) occurred due to failure on the part of railway staff. The figure for 2014–2015 shows a similar trend with failure of Railway Staff accounting for nearly 71% of the total consequential train accidents. The trend has been replicated throughout the years where failure of railway staff is the major cause of consequential railway accidents. Incidental causes act as natural calamities such as falling of boulders, sinking of track due to heavy rain, cattle run over, etc. [11].

4 Recommendation to Reduce Derailment of Vehicle

Improvement in safety and security is a continuous process. For improving safety, constant upgradation of technology is being incorporated in all spheres of railway operations and infrastructure to increase safety and prevent accidents. These include timely replacement of over-aged assets, adoption of appropriate technologies for upgradation and maintenance of track, elimination of unmanned level crossing, and the use of safety drives. The great emphasis should be given on training of officials and educate staff for observance of safe practices. The inspections should be done at regular intervals to monitor rolling stock, signaling, and interlocking systems.

Table 1 Train accidents on Indian railways since 2003–2016

Year	Collisions	Derailments	Manned level crossing	Unmanned level crossing	Fire in trains	Misc	Total	Movements of traffic, i.e., train km run (in Million)	Train accidents per million train km
2003–04	9	202	9	86	14	5	325	NA	NA
2004–05	13	138	5	65	10	3	234	NA	NA
2005–06	9	131	10	65	15	4	234	NA	NA
2006–07	8	96	7	72	4	8	195	825.4	0.28
2007–08	8	100	12	65	5	4	194	890.5	0.22
2008–09	13	85	7	62	3	7	177	905.2	0.2
2009–10	9	80	5	65	2	4	165	997.2	0.17
2010–11	5	80	5	48	2	1	141	1005.9	0.14
2011–12	9	55	7	54	4	2	131	1077	0.12
2012–13	6	49	5	53	9	0	122	1109.7	0.11
2013–14	4	53	4	47	7	3	118	1096	0.1
2014–15	5	63	6	50	6	5	135	1166.7	0.11
2015–16	3	65	6	29	0	4	107	NA	NA

NA not available

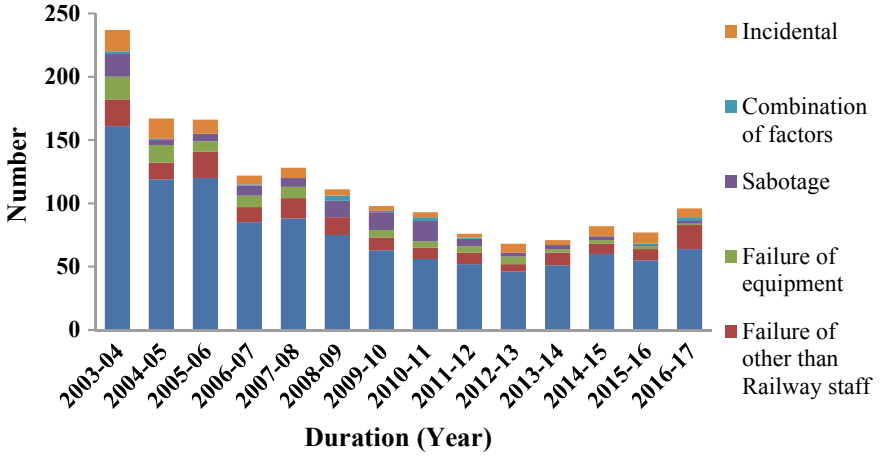

Fig. 3 Causes of consequential train accidents

It was observed that as most of the accidents at unmanned level crossings occur due to rash and careless driving of road users. It is, therefore, suggested that there should be a reduction in speed of road vehicles while crossing the unmanned level crossings. This can be accomplished by providing speed breakers to bring the speed substantially down, i.e., up to dead speed, so that the time for judgment will be sufficient for the driver of road vehicle to negotiate the level crossing safety. Moreover, there must be a provision of second whistle board (repeater) for level crossings for the loco drivers to whistle while approaching unmanned/manned level crossings to warn the road users. Overall it is also seen that deployment of Gate Mitras is helpful in reducing accident at unmanned level crossing by creating an additional layer of safety.

It was seen that nearly 71% of the total consequential train accidents occur due to railway staff. Therefore, it was suggested to adopt safety drive such as Block Proving by Axle Counters (BPAC), which is a solid-state system, used for controlling coordinated movements of train and eliminates manual co-operations. The provision of Auxiliary Warning System (AWS), alert the motorman via a display panel about some advance notification of upcoming signal aspects to avoid collisions between trains and reduce accident rates. Color light LED signals is a signal which displays lights of different colors, depending upon the aspect of the signal. The driver interprets the signal's indication and acts accordingly for the rail safety.

Similarly, Vigilance Control Device (VCD) is micro-controller-based equipment to enhance the safety of the locomotive operation by ensuring the alertness of the motorman. Besides the usage of 60 kg rails and pre-stressed concrete sleepers, long rail panels, better welding technology, progressive use of Linke Hofmann Busch (LHB) Coaches, Center Buffer Couplers with Integral Coach Factory (ICF) Coaches, etc., enhance the safety and prevents the accidents in the future.

The following corrective measures should also be considered to prevent derailment of trains:

- **Proliferation of Linke Hofmann Busch (LHB) coaches for improving safety**: LHB coaches are of a superior design that reduce the chances of derailment and mitigate the possibility of grievous injury or death in case of accidents. LHB coaches have superior body-bogie and wheel-bogie connections, anti-climbing features, tight lock coupling, provision of bump stop, superior braking, provision of yaw dampers to ensure better riding and comfort with lesser chances of dislocation of body from shell, destabilization and tilting of the coach, possibility of overriding of one coach over the other, uncoupling of coaches and consequent movement in an uncontrolled manner, etc., in case of accidents.
- **Progressive use of Air springs**: To maintain constant height at variable load, air spring should be used in secondary suspension of EMU/DMU coaches. These springs shall also be introduced in mainline and LHB coaches to enhance safety and reliability.
- **Center Buffer Coupler**: It is a mechanism for connecting rolling stock in a train to improve the safety of the railway coaches with a view to prevent the coaches from climbing over each other, in unfortunate event of an accident.
- **Track Renewal**: Track renewal process should be done stage by stage and stretches should be considered for renewal on age-cum-condition basis.
- **Modern track structure** consisting of pre-stressed concrete sleeper (PSC), 60 kg, 90 kg or higher, ultimate tensile strength (UTS) rails, fan-shaped layout turnout on PSC sleepers, steel channel sleepers on girder bridges should be used.
- **Long rail panels** of 260 M/130 M length should be manufactured at the steel plant or in flash butt welding plants to minimize the number of alumino-thermit (AT) joints in the track.
- **Ultrasonic Broken Rail Detection System (UBRDS)** used by South African Railway for detection of rail/weld fractures should be used in monitoring the tracks. This system works on the principle of guided ultrasonic waves and interrogates continuously welded rail in sections up to one kilometer long using ultrasound waves, and reports break at time intervals down to a few minutes.
- **Composite Sleepers, which are eco-friendly made from recycled plastic/PU**, having high resilience and requiring lesser maintenance input should be adopted for regular use.

Artificial intelligence system—a new approach: Indian Railways should undertake the remote condition monitoring of the system, to predict failures through the effective use of artificial intelligence. The system allows data to be transferred through a wireless medium and predict failures in the future through the use of artificial intelligence.

5 Conclusions

Over the past few decades, the Indian Railways has been improving and introducing new schemes and facilities, but in the recent times, accidents and derailments have seriously affected its credibility. These accidents, whether due to poor infrastructure,

human staff's shortcomings or other reasons, adversely impact people's safety, lead to loss of life, and ultimately shaking the common populace's faith on railways. The biggest reason behind most fatal train accidents recently is "failure of railway staff" accounting for nearly 71% of the total consequential train accidents, which might be due to careless working, poor maintenance cases, implementing short cuts, and disregard of the prescribed safety rules laid down.

Derailments are the consequences of track collapses, rail ruptures and other asset failures along with inappropriate management. There is a need for long welded rails, reducing the number of joints. Joint has one weak area where failure may cause accident. Therefore, it is suggested to adopt flash butt welds instead of thermit welds, which have proved to be better. To enhance safety and prevent derailment, regular inspection/maintenance of the tracks using large-scale mechanized ultrasonic testing of the rails and welds is the need of hour. There is also a need to address the backlog in rail/track renewals and the technology of rail welding. Advancement in technology would also reduce dependency on human resources.

References

1. Nayak PR, Rosenfield DB, Hagopian JH (1983) Event probabilities and impact zones for hazardous materials accidents on railroads, Report DOT/FRA/ORD-83/20. FRA, U.S. Department of Transportation
2. Treichel TT, Barkan CPL (1993) Working paper on mainline freight train accident rates. Research and test department, Association of American Railroads, Washington, DC
3. Anderson RT, Barkan CPL (2004) Railroad accident rates for use in transportation risk analysis. Transp Res Rec J Transp Res Board 1863:88–98. Transportation Research Board of the National Academies, Washington, DC
4. Liu X, Barkan C, Saat M (2011) Analysis of derailments by accident cause: evaluating railroad track upgrades to reduce transportation risk. Transp Res Rec J Transp Res Board 2261:178–185
5. Federal Railroad Administration (FRA) (2015) Office of safety analysis 3.01 accident trends–summary statistics. http://safetydata.fra.dot.gov/officeofsafety/publicsite/summary.aspx
6. Evans AW (2007) Rail safety and rail privatisation in Britain. Accid Anal Prev 39(3):510–523
7. Evans AW (2010) Rail safety and rail privatisation in Japan. Accid Anal Prev 42(4):1296–1301
8. Barkan C, Dick CT, Anderson R (2003) Railroad derailment factors affecting hazardous materials transportation risk. Transp Res Rec J Transp Res Board 1825:64–74. Transportation Research Board of the National Academies, Washington, DC
9. FRA Guide for Preparing Accident/Incident Reports (2011) U.S. Department of Transportation
10. Saccomanno FF, El-Hage S (1989) Minimizing derailments of railcars carrying dangerous commodities through effective marshaling strategies. Transp Res Rec 1245:34–51. TRB, National Research Council, Washington, DC
11. 12th Report: Safety and security in Railways, Standing Committee on Railways, 14 Dec 2016. http://164.100.47.193/lsscommittee/Railways/16_Railways_12.pdf

Artificial Neural Network (ANN)-Based Response Surface Approach for Passive System Reliability Assessment

R. B. Solanki, Harshwardhan Kulkarni, Suneet Singh, P. V. Varde, and A. K. Verma

Abstract Advanced designs of nuclear reactors deploy passive safety systems, in combination with active systems in order to enhance safety, to improve reliability, and to reduce human intervention. Substantive efforts are underway worldwide to estimate passive system reliability using different approaches, however, consensus of these approaches is not achieved so far. In most of the methods developed for passive system reliability assessment, the fundamental approach is to analyze thermal-hydraulic behavior of system for limited number of scenarios and develop mathematical relationship between set of input parameters and parameter of interest, normally known as 'Response Surface'. Multivariate linear/nonlinear regression is used for developing such relationships. This assumption may not be always true for complex systems, and hence, such assumptions for problem simplification could introduce uncertainty in reliability assessment. Furthermore, the input variables may be interrelated and that could introduce additional uncertainties. Artificial neural network (ANN) can eliminate need for such assumptions in predicting the relationship between the output and input parameters and thereby reducing the uncertainties in passive system reliability analysis. In this paper, the ANN approach is used for generating the response surface, which can then be used for estimating passive system reliability. A typical isolation condenser system, which operates in two-phase

R. B. Solanki (✉)
Atomic Energy Regulatory Board, Mumbai, India
e-mail: rajsolanki@aerb.gov.in

H. Kulkarni · S. Singh
Indian Institute of Technology, Mumbai, India
e-mail: harshkul@iitb.ac.in

S. Singh
e-mail: suneet@iitb.ac.in

P. V. Varde
Bhabha Atomic Research Center, Mumbai, India
e-mail: varde@barc.gov.in

A. K. Verma
Western Norway University of Aplied Sciences, Haugesund, Norway
e-mail: ajitkumar.verma@hvl.no

V. K. Gupta et al. (eds.), *Reliability and Risk Assessment in Engineering*,
Lecture Notes in Mechanical Engineering,
https://doi.org/10.1007/978-981-15-3746-2_29

natural circulation principle, is considered in this analysis. The system performance is analyzed for different combinations of input parameters. Latin hypercube method is used to select a random set of input parameters. For this set of input parameters, system performance is analysis using thermal-hydraulic code RELAP5/MOD3.2. Multivariate linear regression analysis is carried out for generating response surface. Similarly, response surface is generated using the ANN model developed on MATLAB tool. The comparison is made between two approaches and their effect on the response surface, which eventually have significant impact on the reliability estimates of passive system.

Keywords Artificial neural networks · Passive systems · Reliability analysis · REPAS · Response surface

1 Introduction

The passive systems are increasingly being deployed into advanced nuclear reactors designs in combination with active systems in order to enhance safety, to improve reliability, and to reduce human intervention. The operation of passive systems depends on the moderately weak driving forces such as natural circulation, gravity, and internal stored energy. Hence, phenomenon-logical failures become equally important as equipment mechanical failures in reliability assessment of passive systems. The worldwide research is underway on assessment of reliability for passive systems and their integration into PSA; however, consensus is not reached. Reliability Evaluation of Passive systems (REPAS) [1–3] and Assessment of Passive System Reliability (APSRA) methods [4, 5] are widely used methods for passive system reliability assessment.

The REPAS characterizes the performance of passive systems in an analytical way. Set of input parameters are identified, which governs the performance of the system. These parameters are expected to be within a definite range as fixed by designers. For the purpose of analysis, in absence of the adequate operational data, probability distribution functions are assigned for each of these parameters to represent the dynamic behavior of the passive system initial and boundary conditions, when the system is called upon during the accident conditions.

Thermal-hydraulic behavior of system is analyzed for limited number of cases to develop mathematical relationship between set of input parameters and parameter of interest. This mathematical function is normally known as ‘Response Surface’. Multivariate linear/nonlinear regression is used for developing such relationships. This assumption may not be always true for complex systems, and hence, such assumptions for problem simplification could introduce uncertainty in reliability assessment. Furthermore, the input variables may be interrelated and that could introduce additional uncertainties

Artificial neural network (ANN) can eliminate need for such assumptions in predicting the relationship between the output and input parameters and thereby reducing the uncertainties in passive system reliability analysis. In this paper, the ANN approach is used for generating the response surface, which can then be used for estimating passive system reliability. A typical isolation condenser system (ICS), which operate in two-phase natural circulation principle, is considered in this analysis. The system performance is analyzed for different combinations of input parameters. Latin hypercube method is used to select a random set of input parameters. For this set of input parameters, system performance is analyzed using thermal-hydraulic code RELAP5/MOD3.2 [6]. Multivariate linear regression analysis is carried out for generating response surface. On the same set of data, ANN model is developed in order to generate a mathematical relationship between input parameters and output parameters using the Neural Network Toolbox [7]. The comparison is made between two approaches and their effect on generation of response surface.

It is observed that ANN model fits the data much better than the linear regression method generally adopted in most of the methods being used for passive system reliability analysis. However, challenge is to derive this relationship into mathematical form, which can then be used as response surface to predict the system behavior for new sets of input parameters. This paper concludes that use of ANN model to generate response surface presents a promising approach, which would eliminate the need for using simplified assumptions, which may have significant impact on the overall estimate of passive system reliability.

2 Isolation Condenser System

Isolation condenser (IC) system currently being used in most of the innovative NPPs is considered for performance evaluation using APSRA and REPAS methods. The system is categorized as category D type as per IAEA classification scheme [8]. The safety function depends on the principle of natural circulation (passive means) except that internal 'intelligence' of actuation signal is not available in this system. At a pre-defined set point, valve opens automatically. The system is illustrated in Fig. 1. The system consists of steam drum (SD), heat exchanger, also known as isolation condenser (IC), a discharge valve in the return path of IC and associated piping. The IC is immersed in a large water pool, also known as Gravity Driven Water Pool (GDWP).

On opening of the valve, the system operates on two-phase natural circulation principle. The GDWP and IC are at higher elevation than the power source (i.e., SD). The objective of the system is to reject the core decay heat produced after reactor shutdown to the heat sink (GDWP) by condensing the primary fluid (steam) into the heat exchanger tube bundles (IC tubes).

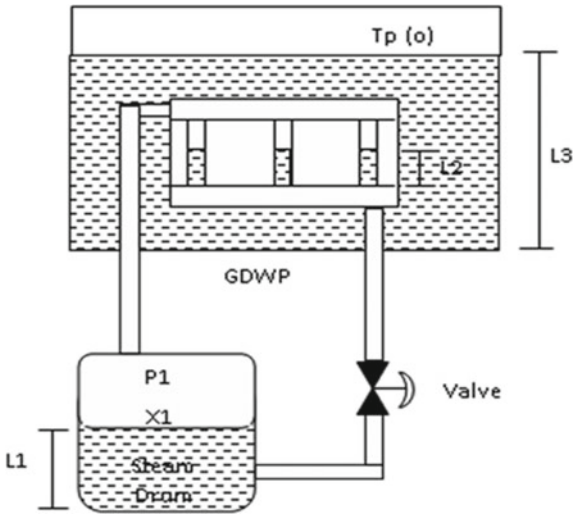

Fig. 1 Isolation condenser system [9]

3 REPAS Methodology—An Overview

The REPAS characterizes the performance of passive systems in an analytical way. Therefore, the methodology may provide numerical values that can be used in more complex safety assessment study and might be seen as the equivalent of the 'Fault-

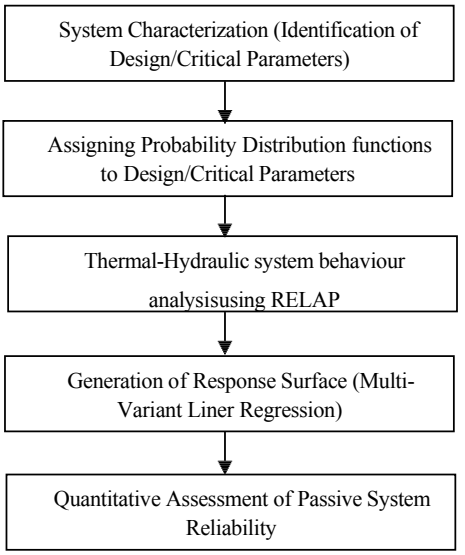

Fig. 2 REPAS methodology for passive system reliability assessment

Tree' analysis that is used as a support for a probabilistic safety assessment (PSA) study. Figure 2 provides major procedural steps involved in REPAS methodology for passive system reliability analysis.

The system is characterized using the design and critical parameters. The design parameters are the governing parameters. The critical parameters are those, which can affect the heat transfer capability and the natural circulation flow rates. The main design parameters identified are: steam drum pressure ($P1$), the liquid level in the steam drum ($L1$), the liquid level in GDWP ($L3$), and the GDWP temperature (Tp). The main critical parameters identified are: presences of non-condensable gases in steam drum ($X1$) and the liquid level in IC tubes ($L2$).

Once the design/critical parameters are identified, the probability distribution is assigned to these parameters for simulating different system configurations. For assigning the probability to the discrete initial parameter values, experts' judgment is used. All the input parameters should ideally acquire nominal values all the times. In other word the ideal value of pdf for each input parameter is unity and there is no uncertainty in value of any input parameter. However, there is a possibility that parameter values could be different from the nominal values when the system is actuated to operate on demand in response to accident sequence. In addition, the fluctuations in input parameters up to a certain extent arising during operation must be accounted.

The RELAP5 mode 3.2 computer code is used for assessing the thermal-hydraulic behavior of the ICS under different system configurations. The considerable computational time is required for detailed calculation. Hence, a limited but statistically meaningful number of system configurations are selected using Wilks' formula [10]. To assess the system performance, the success criteria need to be established first. In the present case study, the heat rejection capability of the isolation condenser system is considered as a parameter of interest during the reactor shutdown.

The ratio (integral power ratio) of cumulative heat rejected in a particular system configuration during the mission time and the same in a nominal configuration has been chosen as the failure criteria for the isolation condenser system performance evaluation.

$$\text{Integral Ratio} = \int_0^t W_2' \mathrm{d}t \Big/ \int_0^t W_{2\,\text{nominal}}' \mathrm{d}t$$

If the integral ratio falls below a fixed fraction of the 'nominal' configuration, it would be considered as system failure. From the input parameter values and integral ration estimates obtained from thermal-hydraulic analysis, an approximate mathematical model called 'Response Surface' is developed using multiple regression analysis. The system performance is simulated through this response surface, which is used to predict the integral ratio for new set of input parameters for large numbers of configurations. The probability of system failure is estimated from these configurations using an appropriate 'failure criteria' [11].

4 Artificial Neural Network

Linear relationship between input parameters and the output parameter assumed in REPAS methodology may not be always true for complex systems. Hence, such simplified assumptions could introduce uncertainty in reliability assessment. It is prudent to use an alternative approach such as artificial neural network (ANN), which can eliminate the need for assumption of the linear relationship between the output and input parameters.

Artificial neural network (ANN) is composed of many nonlinear computational elements operating in parallel and arranged in patterns similar to biological neural network. Massive parallelism is essential for high performance speech and image recognition. Each cell of ANN has multiple inputs and single output. ANN consists of large number of such cells arranged in multiple layers and interconnected with each other. It receives input from input devices or cells in previous layer. The input is them weighed, added, and the result is then transformed by a transfer function into output transfer functions [12].

Assessment of ANN performance depends on several considerations, such as design of network, adequacy of training data. Design considerations include the number of input and output nodes, number of hidden layers and number of nodes in each of these layers. Training considerations include determination of input and output parameters, selection of size of training data sets, initialization of network weights, selection of learning rate and stopping criteria for training. According to the nature of the problem, various working structures with or without feedback loops can be used. The most suitable structure for linear/nonlinear modeling is multi-layered perceptron structure.

The illustration of a typical ANN with multi-layered perceptron structure is shown in Fig. 3. It contains an input layer to accept the input, an output layer to calculate the final results, with several numbers of hidden/intermediate layers in between. In this

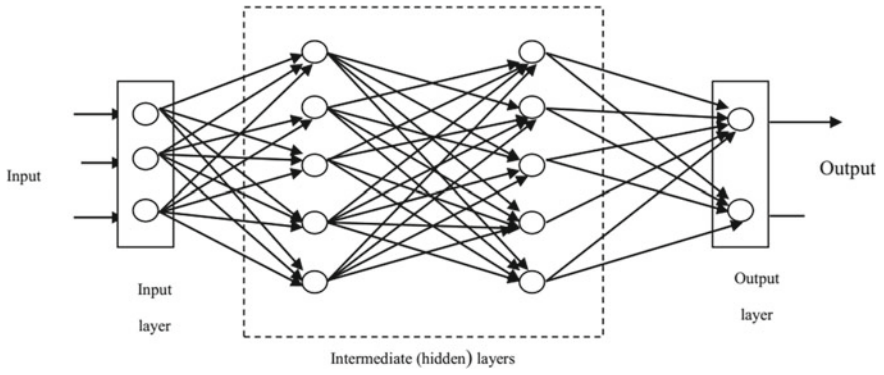

Fig. 3 A typical artificial neural network with multi-layered perceptron model

structure, each neuron output is connected to every other neuron in the subsequent layers connected in cascade with no connection between neurons in the same layer [13].

There are numerous applications of neural network approach in nuclear engineering. In the context of nuclear power plants and subsystems, neural networks are used in system diagnostics, transient identification, validation of sensors, plant-wide monitoring and to keep an eye on performance and efficiency. Virtually, it can be used for any application where large number of inputs is involved and near-instantaneous outputs are expected [14]. Bootstrapped ANN method is also suggested for uncertainty and sensitivity analysis of passive safety systems used in NPPs [15].

Other applications of ANN model include speed control of DC motors, diagnostics of faults in induction motor, sensor failure detection, operation of check valves in nuclear power plants, vibration monitoring in roller contact bearings, temperature control system, monitoring component's thermal performance in PWRs, and many more [16]. In a nuclear power plant, since every incident is an outcome of a pattern of preceding events, prediction of occurrence of an incident can be potentially considered as a pattern recognition problem [17].

5 ANN Approach for Response Surface Generation

The REPAS uses linear regression approach for generating mathematical relationship between input parameters and the output parameter. However, linear relationship between input parameters and output parameter may not be always true. The relationship could be nonlinear also. In such cases, more sophisticated machine learning tools are required. To make prediction about output parameter, there can be two approaches, namely (i) predict a complex nonlinear function and (ii) break the entire problem spectrum into multiple steps and solve for each step. The second approach leads to the use of artificial neural network (ANN).

Based on the Wilks' approach, sample size of 93 data set points was found to be adequate in order to affirm with 95% confidence coefficient that the output parameter would bind at least 95% of the population. The same data set is used both for REPAS method and ANN approach. Two-layer feedforward ANN network with 10 numbers of 'sigmoid hidden layer neurons' and 'linear output layer neurons' is developed in MATLAB. The 93 sets of input parameters were provided in ANN model as columns in a matrix. Ninety-three sets of output vectors (i.e., integral power ratios obtained from thermal-hydraulic analysis of ICS) were also provided in another matrix. The 'Levenberg–Marquardt' backpropagation algorithm is used as training function for the ANN model. Inside ANN model, the input vectors and target vector are randomly divided into three sets as follows:

- 70% (65 data) is used for training
- 20% (18 data) is used to validate ANN
- 10% (10 data) is used as a completely independent test of network generalization.

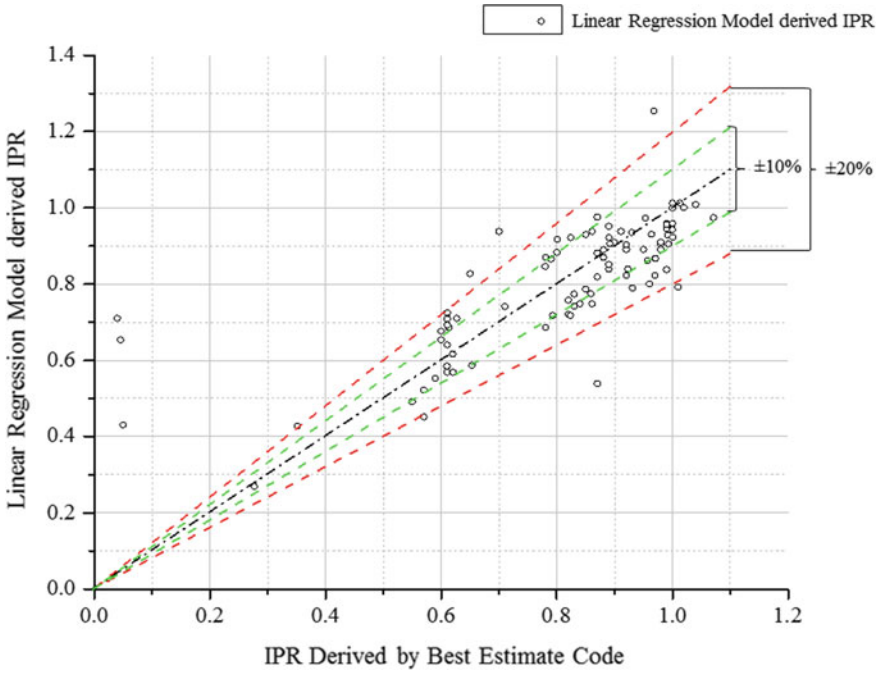

Fig. 4 Results of linear regression-based response surface approach

The threshold value of mean square error (MSE) was set at 0.001 as it is sufficient to demonstrate superiority of ANN method over linear regression.

Hence, iterations are run each time till MSE value reaches the threshold value. The results obtained through ANN model and REPAS generated response surface are compared and results are indicated asperity plots in Figs. 4, 5, 6, and 7.

Figure 4 indicates that

- Results remain within ±10% values obtained from best estimate codes for a limited stretch of success region of IPR, i.e., from 0.8 to 1.
- About 25% of points for which IPR is from region of 0.8 to 1.0 lie outside the high precision zone of ±10%.
- On either side of the threshold value of IPR (0.6), the accuracy of results is modest at ±20%.
- The model does not give satisfactory responses when IPR decreases below 0.3; however, data points with IPR values from 0 to 0.6 are too few to predict any correct results using a linear regression model.

Figure 5 indicates that

- Barring three outlying points, all results of ANN model remain within ±10% values obtained from best estimate codes.

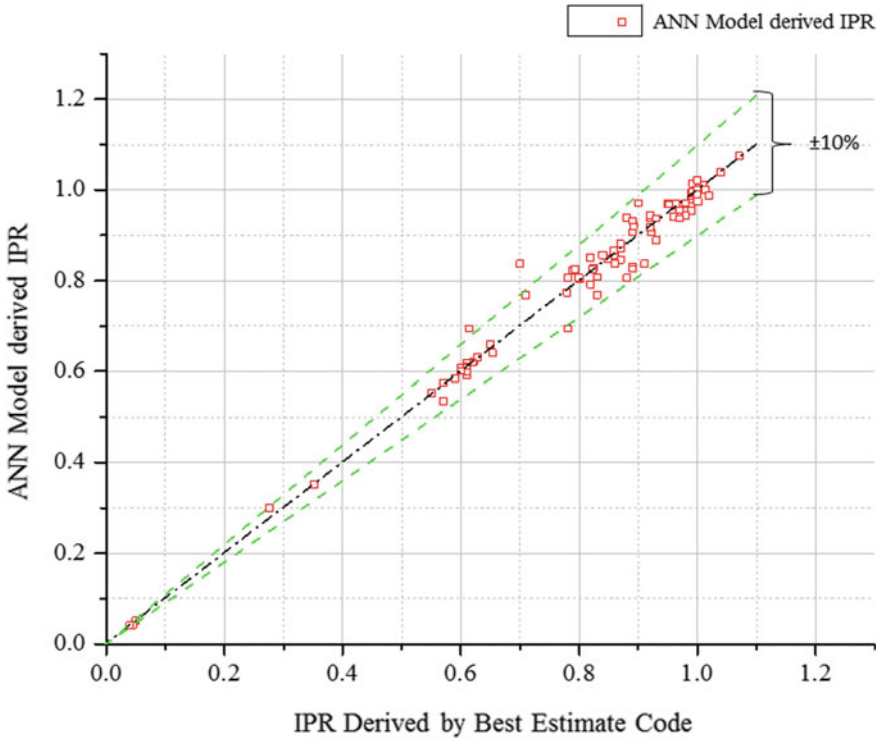

Fig. 5 Results of ANN-based response surface approach

- High precision zone spans over entire range of IPR unlike linear regression model which covers much smaller range.

ANN model predicts output fairly good despite 'inadequate' data points in failure region (IPR values from 0 to 0.6).

Figure 6 indicates that:

- For IPR values between 0.8 and 1, error is roughly equally divided into positive and negative halves. This indicates that error minimization in success region is possible with higher number of input points.
- For IPR values between 0.6 and 0.8, the linear regression model tends to overpredict the results.
- Accuracy of a linear regression model comes at the cost of increased initial computational effort, which is undesirable in any physical process or simulation.

Figure 7 indicates that error in both success and failure regions nearly hugs the 'zero error line' except a few errand points.

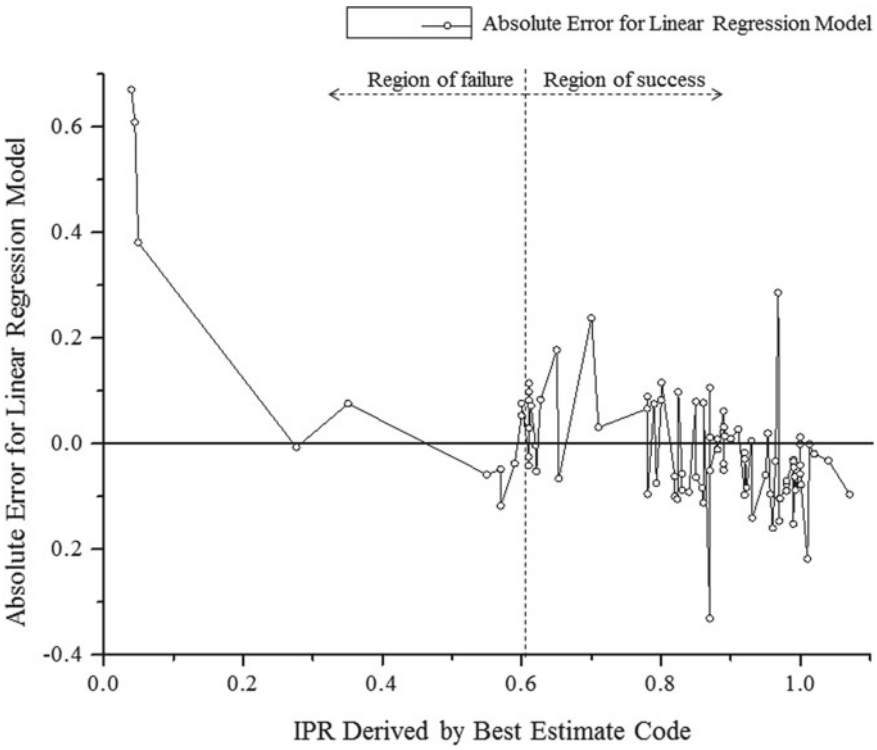

Fig. 6 Results of error analysis for linear regression-based response surface approach

6 Conclusions

The response surface provides the mathematical relationship between input parameters and output parameter, which serves as 'surrogate' prediction tool for the output parameter in order to reduce the calculation efforts that would have been required if the prediction is done with the help of deterministic analysis of the thermal-hydraulic behavior of the ICS using best estimate computer code (i.e., RELAP). The derivation of response surface is sensitive to the overall estimate of the reliability of the passive system. The linear regression-based approach is adopted in most of the prevailing methods is for simplifying the problem, which may not be necessarily providing the accurate prediction in all cases. The results of the case study indicate that the use of ANN approach for response surface generation provided improved results as compared to linear regression-based approach.

However, it is recognized that ANN approach is used in application of the safety case where the scoring population is significantly different as compared to training sample. It becomes important that data set used by ANN for 'training' and 'test' are related and that it covers the entire spectrum of input data set. There are still some open issues that need to be addressed in order to substantiate the claim that

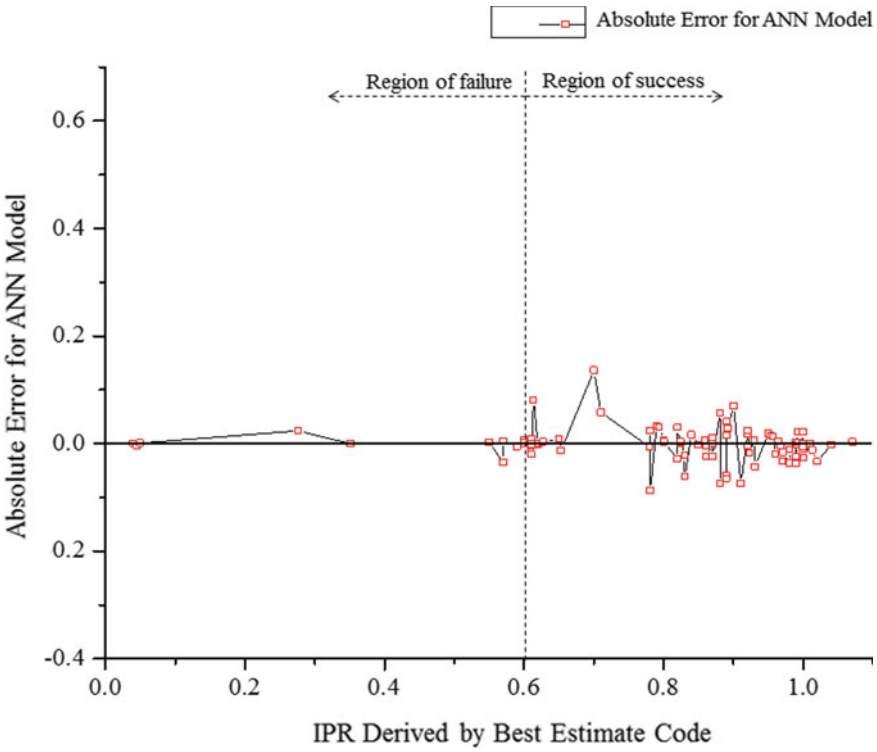

Fig. 7 Results of error analysis for ANN-based response surface approach

ANN approach provides the improved results, as compared to linear regression-based response surface approach for reliability assessment of passive systems.

References

1. Ricotti ME, D'Auria F, Caruso G (2002) The REPAS study: reliability evaluation of passive safety systems. In: International Conference on Nuclear Engineering, ICONE-10, Arlington
2. Jafari J, D'Auria F (2002) Passive system reliability analysis: a study of the isolation condenser. Nucl Technol 3–9
3. Burgaazi L (2011) Addressing the challenges posed by advanced reactor passive safety system performance assessment. Nucl Eng Des 1834–1841
4. Nayak AK, Gartia MR, Antony A, Vinod G, Sinha RK (2008) Passive system reliability analysis using APSRA methodology. Nucl Eng Des 1430–1440
5. Nayak AK, Jain V, Garita MR, Prasad H, Anthony A, Bhatia SK, Sinha RK (2009) Reliability assessment of passive isolation condenser system of AHWR using APSRA methodology. Reliab Eng Syst Saf 1064–1075
6. RELAP5/MOD3.2 Code manual (2001) Idaho National Laboratory, Idaho Falls, USA
7. Beale MH, Hagan MT, Demuth HB (2015) Neural network toolbox user's guide. The MathWorks, Inc., 3, Apple Hill Drive, Natick, MA, pp 01760–2098

8. International Atomic Energy Agency (1991) Safety related terms for advanced nuclear power plants. TECDOC-626
9. Solanki RB (2014) Inter-comparison of REPAS and APSRA methodologies for passive system reliability analysis. Life Cycle Reliab Saf Eng 3(3):25–32
10. Wilks SS (1941) Determination of sample sizes for setting tolerance limits. Ann Math Stat 12:91–96
11. Solanki RB, Pradhan SK, Kumar A, Gupta SK (2006) Reliability evaluation of thermal-hydraulic passive systems. In: 18th National and 7th ISHMT-ASME heat and mass transfer conference, Jan 4–6. IIT, Guwahati
12. Lippmann R (1987) An introduction to computing with neural nets. IEEE ASSP Mag 4–22
13. Meireles MRG, Almeida PEM, Simoes MG (2003) A comprehensive review for industrial applicability of artificial neural networks. IEEE Trans Ind Electron 50(3):585–601
14. Uhrig RE (1992) Analysis of complex systems using neural networks. In: Proceedings of the second international forum on expert systems and computer simulation in energy systems, 17–20 Mar. Erlangen, Germany
15. Zio E, Pedroni N (2011) How to effectively compute the reliability of a thermal-hydraulic nuclear passive system. Nucl Eng Des 241(1):310–327
16. Meireles MRG, Almeida PEM, Simoes MG (2003) A comprehensive review for industrial applicability of artificial neural networks. IEEE Trans Industr Electron 50(3):585–601
17. Guo Z, Uhrig RE (1992) Use of artificial neural networks to analyse nuclear power plant performance. Nucl Technol 99(1):36–42

Enhancement of Human Performance by Competency Development in High-Reliability Organizations (HROs)

K. S. Ramprasad and Prabhat Kumar

Abstract A high-reliability organization (HRO) is an organization that has succeeded in avoiding catastrophes in an environment where normal accidents can be expected due to risk factors and complexity of operations. The HROs are aviation and space organizations, nuclear power plants, oil and gas plants, chemicals processing plants, health care, construction industries, etc. The human performance and reliability plays a critical and vital role in the prevention of accidents in these industries. The study and review of past accidents few years back including Fukushima in HROs reveal that the human competence to handle the situations in all conditions (normal, emergency and accidental) needs to be upgraded to effectively prevent or mitigate or manage them. This necessitates the HROs to re-look and re-invent the gaps in human knowledge, skills and attitudes to enhance the standards of safety performance. A study analogous to prognostic and systematic approach to training (SAT) is envisaged/carried out to identify the gaps between the future demands and the present existing abilities in nuclear safety and regulatory functions of a service organization. The available documents of International Atomic Energy Agency (IAEA), International Organization for Standardization (ISO), etc., on the subject were studied and referred. The results of a pilot study with checklists conducted for about 187 personnel to assess the existing competencies in terms of knowledge, skills and attitudes (abilities) in the area of nuclear safety and regulations are presented. The gap analysis is based on the four-quadrant competence model to improve the human performance and reliability for the safe operation of HROs. A comprehensive training program is arranged to breach the gaps in a phased manner to develop human capabilities.

Keywords Checklists · High-reliability organization (HRO) · Human organizational and technical factors · Risk factors · Systematic approach to training (SAT)

K. S. Ramprasad (✉)
Sathyabama Institute of Science and Technology, Chennai 600119, India
e-mail: rprasad1905@gmail.com

P. Kumar
Bharatiya Nabhikiya Vidyut Nigam (BHAVINI), Kalpakkam, Tamilnadu, India
e-mail: prabhatbhavini@gmail.com

V. K. Gupta et al. (eds.), *Reliability and Risk Assessment in Engineering*,
Lecture Notes in Mechanical Engineering,
https://doi.org/10.1007/978-981-15-3746-2_30

1 Introduction

1.1 About High-Reliability Organizations (HROs)

A high-reliability organization (HRO) is an organization [1] that successfully prevents catastrophic/disastrous events in an environment where normal incidents are anticipated due to complexity and risks associated with the operations. In general, the HROs identified are aviation and space organizations, nuclear power plants, oil and gas plants, hazardous chemicals processing plants, health care, construction industries, etc. HROs by their nature are governed by statutory provisions and are required to comply with safety stipulations and specifications prescribed from time to time. The incidents in HROs arise due to 'systemic failures' resulting into personal injury and/or, damage to equipment and/or, environmental pollution, etc., which could have been prevented by robust design and technical controls.

The HRO under study is a nuclear service organization constituted by the executive order to carry out prescribed regulatory and safety functions under the statute. The authority and empowerment of the service organization are mainly derived from the rules, regulations, notifications, etc., promulgated under the relevant statutes. The organization works on the mission to ensure that the use of ionizing radiation and nuclear energy in India does not pose an undue risk to health and the environment.

The organization's typical functions can be listed as core and supporting. The core functions are consenting encompassing review and assessment including authorization; regulatory inspections and enforcement; development of safety regulations/documents. The supporting functions are safety research and development; emergency preparedness and response; international cooperation; communication with the public and other groups/interested parties; safety promotion; assets and resources management including knowledge management; administration and finance.

1.2 Genesis of HROs

The HROs have origin mainly in aviation and nuclear industry. In 1980s, the roots have widely spread into other hazardous industries. The research in these areas conducted by Weick [2] and Schulman [3] has given more stress and importance on HROs. The remarkable observation is that HROs may appear to be diverse and complex by nature but similarities are visible. Firstly, both operate in an unforgiving socio-political environment. Secondly, the technologies adopted are risky and have scope for systemic errors. Thirdly, the possible severe consequences that may arise from errors prohibit learning from experimentation. Finally, to prevent failures and enhance safety, HROs utilize complex processes and technologies. HROs possess many characteristics like highly skilled/trained manpower, continuous learning

through training, encouraging incentive system, frequent system audits, improvement on continuous basis, prevention of failures, diversity, redundancy, checks and balances against lapses, errors which are more prominent and common to high-performance-oriented organizations [4].

1.3 Features of HROs

The research study collates the empirical evidence about the unique features of HROs and also on the development of responsible care and concern for safety. The research studies suggest that the key parameters on HROs performance are complex technologies and risk management, environments, severe consequences of failures/errors, organizational commitment and responsibility for safety at all levels, prevalence of positive aspects of safety culture, improvement on continuous basis, promoting learning culture and motivating staff, highly skilled and trained personnel, innovative methods/ways to prevent errors, regular/periodic inspections and meetings, built in safety through redundancy, diversity, independence, error free, fault-tolerant processes, etc., and change management process. The safety of the HROs, especially nuclear power plants, is built and evolved around the above features.

1.4 Fundamentals of HROs

Weick and Sutcliffe [5] study enunciated that HROs are mindful in approach to safety which means that sensible in thinking, continuous evolving of thoughts of improvement and adaptive to change management. The five fundamentals for HROs in their aspiration to achieve high standards successfully in safety and risk management are as follows.

1. Recognition of potential failure—The HROs systems are complicated and can experience failures. The organization gives continuous and thorough attention to deviations/anomalies that could be the signs and symptoms of probable failures. The basic thought is that major failure does not take place instantly; they are preceded by minor deviations, problems or anomalies, or evidences which detected and given proper attention would prevent catastrophic failure.
2. Root cause analysis—In HROs, complex systems have many potential sources of failure and it is not viewed as general and isolated to address them. The attitude of management to consider a minor failure as trivial and a general cause as a solution is not encouraged in HRO. The occurrence of a failure is considered as an opportunity to delve deep into the details of the system involved to find the real cause.

3. Review of operations—HRO operates on a real-time basis; this includes both components and the system working together. The operations and their outcomes are observable. The HRO strives to continuously evaluate and reviews the operation outcomes to determine whether they accomplis the objectives of the organization. In true sense, they are treated as hands-on experiences from which lessons about the organization can be taken to further improve function in real time.
4. Resilience—The HROs are robustly designed with highly resilient/tolerant to faults/errors. Even the occurrence of an error/fault does not disable essential safety functions. HROs possess an adaptable and learning by experience culture. The HROs have the capability to continue to operate even under the degraded environmental conditions with a capacity to cope up/marshal resources to bring into the safe state of shutdown/operation. This condition demands the human and organizational resilience through the open-mindedness and willingness to react appropriately to conditions/observations arising under unexpected situations.
5. Resourcefulness—HRO has an imbibed principle of developing resourcefulness/expertise for assessment and response to high-risk circumstances/conditions arising during the operation. The involvement and participation are based on expertise in the area and not by hierarchy. The management should encourage persons possessing expertise to participate in the process improvement programs, rather than authority or position in the organization. The HRO culture should promote open-mindedness and justness.

All the above five principles are the basis for improvement of HRO's performance. In general nuclear, oil and gas processing, etc., organizations strive to improve their operational reliability by adapting the above. Over time, more and more organizations involved in health care, construction, etc., are also tending to follow these principles to improve their performance to join the band of HROs.

1.5 Human Competence

The term competence for the purpose of this study is the combination of **knowledge**, **skill** and **attitude** (KSAs) needed by a person to perform a particular job. All three are important and interrelated. **Knowledge** (**K**) is familiarity with a thing and can include facts, descriptions and information acquired through experience or education. It can refer to both the theoretical and the practical understanding of a subject. It can be gained explicitly or tacitly. **Skill** (**S**) is the learned capacity to perform a task to a specified standard. **Attitude** (**A**) is the feelings, opinions and ways of thinking, perceptions, values, behavior and interests of an individual which allow a job or task to be undertaken to the best ability of that individual. Attitudes cannot wholly be taught directly and are partly a consequence of the organizational culture [6]. The term competence development in the study broadly includes the development of

knowledge, skill and attitude (KSA) aspects. Competencies are the mental, physical and behavioral tools needed for performing an activity or a task.

1.6 Organizational Competence Development

The organization under our study is service-centered involved in nuclear safety and regulatory activities. The typical core and supporting functions are listed in the earlier paragraph. The management system [7] requirements are the determination of competences, training and awareness for personnel performing work affecting the organizational efficiency and quality. It also mentions about actions to acquire the necessary competence and evaluate the effectiveness of the actions taken.

The IAEA documents [8–12] also highlight about the practices/requirements of the service organizations/regulatory bodies to manage, develop and maintain the competence of its staff and a systematic analysis of the existing and expected competences of the regulatory body based on the functions and demands from time to time. The onus on management is to determine the competences and resources necessary to carry out the activities of the organization safely and shall also provide them.

2 Approach to Study

A pragmatic approach considering the lessons leant from the Fukushima Daiichi accident in 2011, the human and organizational factors responsible for the safe performance of the individual, group, leadership and the organization are considered. The qualitative assessment of competence needs by quantifying the measured level gaps. The systematic approach to training (SAT) which is globally accepted is used in the study to analyze the gaps and to develop competency by comprehensive training programs. The subject considered for this study is the enhancement of human reliability by development of personal competency to ensure safety of a nuclear or radiation facility at all stages, namely siting, construction, commissioning, de-commissioning and beyond by the competency gap analysis. The scheme is given in Fig. 1.

The seven-step approach in Fig. 1 is explained in brief below.

Step 1 (Regulatory Functions): The organization has the mandate to account of the present needs as well as the future aspirations arising from future demands, strategic view, etc., with corresponding functions. All anticipated needs are accounted for in the development of the training program, including the continuing development needs of personnel.

Step 2 (Specific Tasks): Once the main functions are identified, the next step is to describe the tasks that will be needed to perform the defined functions by each individual/group.

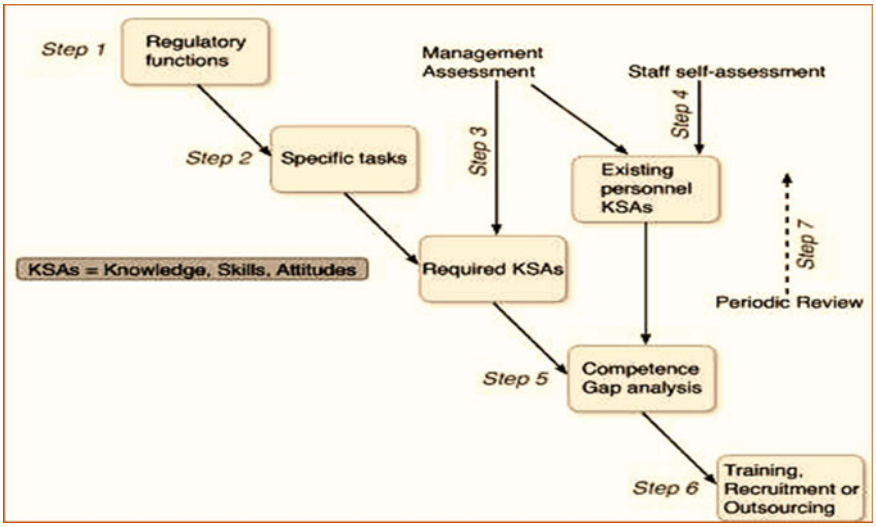

Fig. 1 Flow chart for competency gap analysis and assessment

Step 3 (Required KSAs): For every function, the responsible superior should specify for each position the level [basic competence (BC), applied competence (AC), & mentoring competence (MC)] of required KSAs. This is done at an individual level and at a superior level. The questionnaire format is used for determining the levels of KSAs needed to perform the core and supporting functions. The compilation of competences is carried out to assess the gap areas by superiors.

Step 4 (Existing KSAs): For each identified function, the KSA levels existing should be identified by the individual officer using definitions of the levels [basic competence (BC) & applied competence (AC), mentoring competence (MC)], with guidance but without knowing the required levels, to avoid bias. The applicable questionnaire format is used. At the end of this process, we have data on all the required KSAs and available KSAs, and we can proceed to assess the gaps. Table 1 represents the individual competence levels with attributes as well as theoretical and observed ranges.

Table 1 Individual competency levels

NC (No competence)	0	No expertise/experience
BC (basic competence)	1	Basic understanding
AC (applied competence)	2	Understanding and capability
MC (mentoring competence)	3	Expertise and capable to coach or mentor

Theoretical range $(R) = -3 \leq R \leq 3$
Observed range $(r) = -2 \leq r \leq 2$

Step 5 (Competence Gap Analysis): The senior officers analyze the gap (difference between the existing and the expecting level of competence) for each individual with respect to each function. The gap can be positive (+) or negative (−). The competency mapping exercise is carried for the whole organization.

Step 6 (Training, Recruiting or Outsourcing): The organization is in the process of prioritizing the gaps according to the importance to the functions and allocate resources to fill some of the gaps by recruitment, training and outsourcing, as shown in Fig. 1. In few cases of rare specialization and disciplines like human and organizational factors (HOFs), etc the gap is planned to be filled through consultancy/outsourcing; in such instances, at least one senior expert well-trained in the subject matter is available.

Step 7 (Periodic Review): Situations such as reorganization, assignment of new functions, recruitment of new staff may make it necessary to repeat the gap analysis process either for the whole organization or for affected parts. In addition, it is advisable to conduct a periodic assessment to check the effectiveness of the training program, design new training cycles and foster continuous improvement. The period for review planned is 3–5 years or earlier as required.

3 Methodology of Study

A pilot self-assessment competency mapping study to identify the gap areas and to enhance the levels of competency of personnel was conducted in 2014. The study was carried out only for the core functions as represented in the four-quadrant model (Fig. 2). A questionnaire format containing 139 customized questions covering all the four quadrants, namely legal and regulatory processes, technical disciplines, regulatory practices, personal and interpersonal effectiveness was administered to 187 (about 80%) personnel in the organization under study from entry level (0–2 years' experience) to a senior level (>15 years' experience) covering the core functions only. Based on the above competence model, the questionnaire formats for all the persons in technical divisions of the organization have been prepared. The competence data are collected from individual and the superior, compiled and analyzed. The outcome of the study is compiled in a format that the gap between the existing and the needed KSAs is worked out. The observations results of the study are presented in Table 2. The mode of filling the gap at individual/group level is planned (e.g., by induction of new staff or by re-training/upgrading existing staff/mentoring/coaching). The whole exercise stated above is carried out using an EXCEL format.

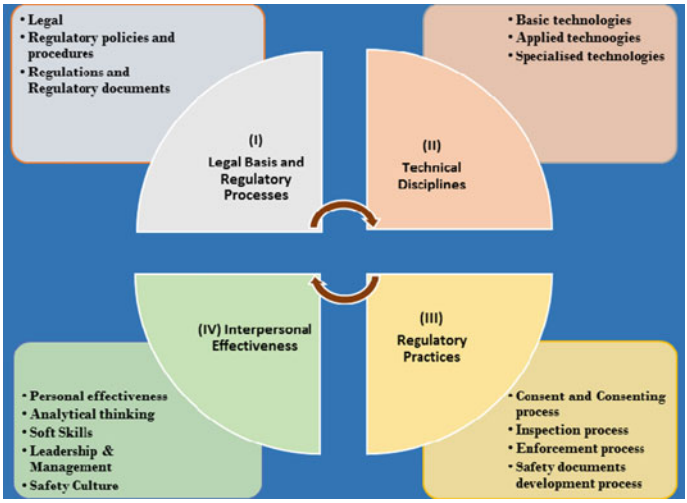

Fig. 2 Four-quadrant competency model

4 Results and Discussions

The total range (cumulative individual) of gaps found out in the study are presented in Table 2. In Quadrant 1 (legal basis) has a wide gap (deficit 21–55). The legal basis is not directly attributable to the functional competence except the consenting process. The in-house legal knowledge is enhanced by permitting six officers to pursue law course and training programs for the other personnel. The wide range gap (−54 to +11) is found in regulations and regulatory documents. The organization is involving the officers through in-house comprehensive review and understanding the regulations and regulatory documents. This process will improve the competence in assimilating the regulatory requirements in due course of time.

In Quadrant 2 (technical disciplines), the wide gap (−48 to +19) is visible in specialized technologies. The organization is exploring the possibility of deputing few officers for required/applicable identified specialized courses for acquiring competence. In Quadrant 3 (regulatory practices), the wide gaps are found in all the four areas. In-house training programs/mentoring/coaching are planned periodically to enhance the KSA and improve the competency. More emphasis is given in this aspect/areas by involving persons on the in-house review process.

In Quadrant 4 (personal and interpersonal effectiveness), the gap in personal effectiveness, analytical thinking and problem solving, soft skills and safety culture is narrow not significant), but the gap in strategic thinking, leadership and management is wide (−15 to +43). The management development programs (MDPs) have been organized in 2016 and 2017 to develop leadership and management. The senior officers were encouraged to mentor juniors in team building, group tasks, team commitment and involvement, etc.

Table 2 Competency gap analysis

Competency	Areas/number of questions	Total range		
		(−) gap	(+) surplus	(−) deficit
Quadrant 1 (Legal and regulatory processes)	Legal basis/6	44–72	16–30	21 to 55
	Regulatory policies and procedures/6	27–50	17–36	0 to 33
	Regulations and regulatory documents/5	26–78	21–41	54 to (+11)
Quadrant 2 (Technical disciplines)	Basic technologies/2	34–35	19–54	16 to (+20)
	Applied technologies/7	28–51	15–43	33 to (+15)
	Specialized technologies/16	15–61	15–61	48 to (+19)
Quadrant 3 (Regulatory practices)	Consent and consenting process/16	29–75	12–44	63 to (+11)
	Inspection process/17	32–70	15–52	53 to (+20)
	Enforcement process/15	26–66	18–43	48 to (+17)
	Safety documents development process/6	52–67	21–30	20 to 42
Quadrant 4 (Personal and interpersonal effectiveness)	Personal effectiveness/6	27–43	34–39	3 to (+9)
	Analytical thinking and problem solving/10	30–47	20–39	6 to 24
	Soft skills/6	36–52	25–33	5 to 27
	Strategic thinking, leadership and management/14	21–44	28–72	15 to (+43)
	Safety culture/7	25–42	35–51	7 to (+22)

Number of regulators analyzed (N) = 187
Total number of questions = 139

In the study, the working level (WL) and supervisory level (SL) are identified based on the nature of functions and seniority. The minimum expected level of competency in core and support functions for WL are in the range of (BC-AC) and for SL the range is (AC-MC) to perform functions and to discharge responsibilities. The SAT approach will be used to re-train and enhance competency in the gap areas required. This exercise is planned to be carried out once in 3–5 years after completing the initial gap-filling activity.

5 Conclusions

The organization under study as a HRO strives to have appropriately qualified and competent staff to handle core and supporting functions effectively and efficiently.

Human resources (HR) long-term plan is being developed with the best available methods, practices and techniques to ensure that an adequate number of officers with essential knowledge, skills and abilities (KSAs) are available to perform all the necessary regulatory functions from time to time. A process is being established by the organization to develop and maintain the necessary competence and skills of staff, as an element of knowledge management. The process includes the development of a specific training program on the basis of an analysis of the necessary gaps in competence levels periodically. The gaps are being planned to be filled by training or re-training program (which shall cover principles, concepts and technological aspects, as well as the procedures followed by the regulatory bodies for carrying out mandate/assignments) or mentoring or coaching or consultant engagement, recruiting, etc. for, assessing applications in authorization process, for inspecting facilities and activities and for enforcing regulatory requirements.

Acknowledgements The authors are grateful to the authorities and officers of the study organization who have supported and encouraged the study of competency mapping program for identifying the gap areas and developing training programs for enhancing the competency levels within the organization as well as for the publication of this paper.

References

1. https://en.wikipedia.org/wiki/High_reliability_organization
2. Weick KE, Roberts KH (1993) Collective mind in organizations: heedful interrelating on flight decks. Adm Sci Q 38:357–381
3. Schulman PR (1993) The negotiated order of organizational reliability. Adm Soc 25(3):353–372
4. Schulman PR (2004) General attributes of safe organizations. Qual Saf Health Care 13 (Supplement II):ii39-ii44
5. Weick K, Sutcliffe K (2015) Managing the unexpected: Sustained performance in a complex world, 3rd edn. Wiley, Hoboken, NJ, p 7–21
6. IAEA safety glossary: Terminology used in nuclear safety and radiation protection 2007 edition. International Atomic Energy Agency (IAEA), International Centre, Vienna, Austria (2007)
7. Indian standard (IS/ISO 9001: 2008/2015) quality management systems—Requirements. Bureau of Indian Standards (BIS), New Delhi
8. Training the staff of the regulatory body for nuclear facilities: A competency framework. International Atomic Energy Agency (IAEA), Technical Document (IAEA-TECDOC-1254), Vienna International Centre, Vienna, Austria (2001)
9. Systematic assessment of regulatory competence needs for regulatory bodies of nuclear facilities (SARCON) guidelines. International Atomic Energy Agency (IAEA), Vienna International Centre, Vienna, Austria (2011)
10. Governmental legal and regulatory framework for safety, Safety standards Series No. GSR Part 1 (Rev. 1), General safety requirements. International Atomic Energy Agency (IAEA), Vienna International Centre, Vienna, Austria (2016)
11. Leadership and management for safety, safety standards Series No. GSR Part 2, General safety requirements. International Atomic Energy Agency (IAEA), Vienna International Centre, Vienna, Austria, pp 12 (2016)
12. Managing regulatory body competence, Safety Reports Series No. 79. International Atomic Energy Agency (IAEA), Vienna International Centre, Vienna, Austria (2013)

Optimization and Machine Learning Techniques for Industrial Applications

Mechanical Fault Detection in Steel Plant with Infrared Thermography: Field Cases

Mahesh Bhiwapurkar

Abstract The intensity of the infrared radiation emitted by objects is mainly a function of their temperature. Infrared thermography stands as one of the most attractive and a successful non-destructive technique that has ability to detect the object's surface/subsurface defects remotely based on observing and measuring the surface's emitted infrared heat radiation by using an infrared camera. This work presents several case studies that illustrate the application of infrared thermography to detect mechanical faults during dynamic loading conditions of rotational machineries in plant equipments; all these cases are referred to steel and power plant unit and prove the potential of the technique to detect several types of mechanical failures (bearing faults, misalignments, belt transmission problems, etc.). The study proves that thermography is a viable technique to qualify and quantify the flaws where it is possible to indicate the faulty areas and their thermal variation characterized in thermal analysis.

Keywords Infrared thermography · Active thermography · Passive thermography · Temperature measurement · NDT

1 Introduction

Please note that the first paragraph the need for a decrease of major accidents, huge economic losses, maintenance costs, downtime and increase of reliability enforced the maintenance engineer to come up with better maintenance concepts. Several NDT techniques such as radiography, eddy current testing, ultrasonic testing, acoustic emission and vibration analysis are routinely used for condition monitoring. Each of these methods may be suitable for some applications but not for others. The choice of the method depends on the system to be monitored. Also, one of the important factors that differentiates these methods and affects the choice of the suitable method for each system is the detection horizon or the capability of early fault detection. Thus far,

M. Bhiwapurkar (✉)
O. P. Jindal University, Raigarh, India
e-mail: mahesh.bhiwapurkar@opju.ac.in

V. K. Gupta et al. (eds.), *Reliability and Risk Assessment in Engineering*,
Lecture Notes in Mechanical Engineering,
https://doi.org/10.1007/978-981-15-3746-2_31

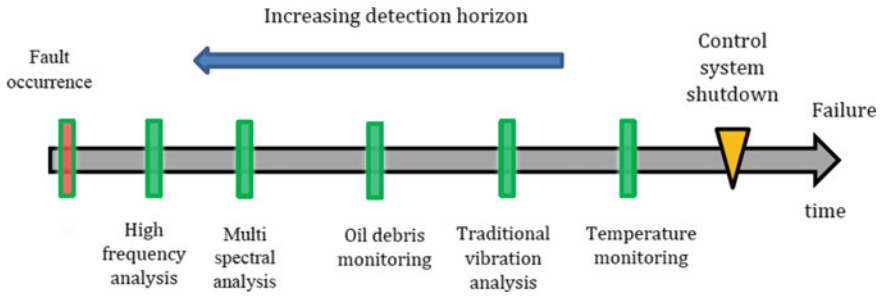

Fig. 1 Detection horizons of different condition monitoring methods [4]

it has been believed that temperature monitoring has the shortest detection horizon among all the existing condition monitoring methods [1–3].

Figure 1 shows the ranking of different condition monitoring methods in terms of the detection horizon length [4]. Heat emission is a phenomenon that accompanies almost every dynamic activity. However, using temperature monitoring for mechanical fault detection has been thought to be less effective than other methods, as discussed above. This is mainly because of the misperception that a temperature monitoring system has the shortest detection horizon among all the systems listed in Fig. 1.

Heat emission is a phenomenon that accompanies almost every dynamic activity. However, using temperature monitoring for mechanical fault detection has been thought to be less effective than other methods, as discussed above. This is mainly because of the misperception that a temperature monitoring system has the shortest detection horizon among all the systems listed in Fig. 1.

It is well known that temperature is one of the most useful parameter that indicates the structural health of an object [5]. Therefore, monitoring the temperature of machineries or a process is undoubtedly one of the best predictive maintenance methodologies. Infrared thermography is one of the more sophisticated NDT methods recently applied in detecting heat generating anomalies and has become a major player to achieve reliability and quality for both mechanical and electrical equipments.

Thermography offers non-contact, wide area detection of subsurface defects and can be used as an alternative or complement to conventional inspection technologies [6]. IRT has been successfully utilized for several condition monitoring applications such as civil structures [7, 8], inspection of electrical equipment [9], monitoring of plastic deformations [10], inspection of tensile deformation [11], evaluation of fatigue damages in materials [12], inspection of machineries [13–15], and weld inspection [16, 17]. Many references inferred that the change in temperature is not sensible until approaching the end of the monitored component life and even the whole system life [1, 2, 4]. Transient thermography, which employs pulse surface heating of an inspected component followed by acquisition of the thermal decay, was used for aircraft body inspection [18].

The rolling element bearings are widely used machine elements. Their failures are among the most frequently reported reasons for machine breakdowns. Recent studies on the application of thermography for bearing fault detection include those in [15–19]. Researchers also worked on the development of wireless sensors for direct measuring bearing cage temperature [20–22]. On the other hand, the most commonly used condition monitoring method, i.e., vibration analysis, is not free from pitfalls. Although vibration analysis has shown success in detecting some bearing faults, for other faults like lubrication problems and gradual wear it is much less effective. Also, it does not give a reliable indication of fault severity for many types of bearing faults.

The advancement of thermography as a temperature monitoring tool encourages the reconsideration of temperature monitoring for mechanical system fault detection. In addition to the improved accuracy and responsiveness, it has the advantage of non-contact monitoring which eliminates the need for complex sensor mounting and wiring especially for rotating components. Therefore, in current studies the thermography-based monitoring method is often used either as a distinct method or as a complementary tool to vibration analysis in an integrated condition monitoring system. In this article, the applications of IRT in the field of condition monitoring of mechanical equipment of steel plant with typical case studies are presented. It also describes the basics of IRT with theoretical background.

2 About Infrared Thermography

All objects emit infrared radiation as a function of their temperature. An infrared camera measures and images the infrared radiation emitted from an object. The fact that radiation is a function of object surface temperature makes it possible for the camera to calculate and display this temperature. However, the radiation measured by the camera does not only depend upon the temperature of the object, but is also a function of its emissivity. Radiation also originates from the surroundings and is reflected by the object. The radiation from the object and the reflected radiation will also be influenced by the absorption of the atmosphere. To measure temperature accurately, it is therefore necessary to compensate for the effects of a number of the different radiation sources. This is done online automatically by the camera. However, the following object parameters must be supplied for the camera: the emissivity of the object, the reflected temperature, the distance between the object and camera, and relative humidity.

Emissivity is a surface property that specifies the ability of that surface to emit energy; values of ε are between 0 (for a perfect reflector) to 1 (for a perfect emitter, called a "blackbody"). Emissivity has dependences with surface orientation, temperature, and wavelengths. A surface having a low emissivity acts as a mirror and makes measurements difficult since spurious radiations emitted by warm neighboring bodies perturb readings through reflections. Various techniques are deployed to solve

low or uneven emissivity problems. Among them, covering the inspected surface with a high emissivity flat paint ($\mathcal{E} \sim 0.9$) is the most common one for imaging applications [5].

Thermal energy is present with the operation of all machines. It can be in the form of friction or energy losses, as a property of the process media, produced by the actual process itself or any combination thereof. As a result, temperature can be a key parameter for monitoring the performance of machines, the condition of machines, and the diagnostics of machine problems. Infrared thermography is an ideal technology to do this temperature monitoring because it provides complete thermal images of a machine, or a machine component, with no physical attachments (non-intrusive), requires little setup, and provides the results in a very short period of time.

There are several recognized IR thermography techniques in use throughout industry. Comparative thermography (CT) is the most common technique, and it is normally used to provide the best available data in lieu of ideal, or absolute, thermal measurements. When encountering changing machinery operating conditions, the ability to perform rough emissivity estimates, and the ability to differentiate emissivity differences on machinery equipment, provides useful information for the condition monitoring and diagnostics of the machine under the less-than-ideal circumstances frequently encountered in the field. The confidence level of the information obtained depends on the thermography equipment used, the training and experience of the thermographer, and the detection method applied.

The comparative quantitative thermography method is an accepted and effective method for evaluating the condition of a machine or component by determining approximate temperatures. It is very difficult to determine precisely the actual temperatures of a component, using IRT in the field. This is due to a certain extent to the physics of IRT which must take into consideration the multiple parameters that enable a true absolute temperature measurement. These IRT considerations are: emissivity; reflectivity; and transmissivity. As a result, estimates of these IRT considerations can be readily made to obtain a component's approximate temperature, which in most cases is more than sufficient to determine the severity of an adverse condition.

2.1 Assessment Criteria

The infrared thermographer may use temperature difference criteria or classify the temperature severity of mechanical system anomalies. These criteria are usually reported as the temperature rise of the exception above the temperature of a defined reference.

2.2 Relative Temperature Criteria

An example of a set of severity criteria based on categories and temperature rises above established Ref. [6] is as follows:

Advisory: Up to a 10 °C rise above a reference or baseline
Intermediate: 10–20 °C rise above a reference or baseline
Serious: 20–40 °C rise above a reference or baseline
Critical: In excess of a 40 °C rise above a reference or baseline.

Reference temperatures should be based on temperatures specified by manufacturers of similar items or groups of equipment, or of components located on the same shaft. Baseline temperatures should be based on historical or statistically derived temperatures established from the specific item or machine groups when in the "ideal" condition.

3 Methods

All the main objective of the study is to identify the location of faults of various machineries by thermography method. The steel and power plant equipment's under study is bearing pedestal, ventilation blower of plate mill, motor bearing of fan and V-belt of a pulley. Infrared inspections were performed when environmental and physical conditions under which data acquired were consistent with normal conditions and favorable to gathering accurate data. The thermographer was ensure that all emissivity and reflected apparent temperature determinations are carried out. The infrared thermographer was use thermography equipment (Testo 885) with capabilities sufficient to meet the inspection requirements.

3.1 Image Interpretation

From a machinery viewpoint, thermal image interpretation essentially is a process of comparing absolute temperature and temperature profiles against design, manufacture, installation, operation and maintenance criteria. When using thermography for machinery condition monitoring purposes, the operating conditions at the time of each survey should be known in detail, as many changes in thermal profile are operating condition dependent. The design of a machine is essential to understanding component loading, which in turn is the primary contributor to thermal profile.

When using thermography to assess machine condition, it is important that the machine is viewed as a whole and that each image is analyzed as part of a series rather than as an individual representation of a localized condition.

4 Results and Discussion

Case 1: A problem was detected in the Bull Gear NDE (non-drive end) bearing pedestal. After inspecting the target point, the creepy sound was heard from the equipment. The infrared camera had detected a hot spot on the bearing block NDE side through thermal imaging (refer Fig. 2, real image, and thermal image). Hot spot meant some internal problem of the bearing block NDE side and that can be seen as friction that is produced in a mechanical system. In the case of mechanical drive systems, infrared camera can identify bearing problems quickly and easily as the bearings generate more heat as they become pitted, or when they are under-lubricated and sometimes over-lubricated. After taking corrective measures, the bearing blocks temperature found reduced from 47 to 39.7 °C.

Case 2: Drive end (DE) of the motor bearing of ventilation blower has been inspected. Thermal imaging of the DE motor showed that the temperature in the bearing portion of the motor has higher temperature than the adjacent parts. Lack of lubrication might have increased the temperature of the bearing case, as shown in Fig. 3.

Temperature monitoring can play a crucial role in such a system. To this end, the heat generation mechanism during the operations of the healthy bearings has to be well understood. The effect of bearing fault on heat generation should also

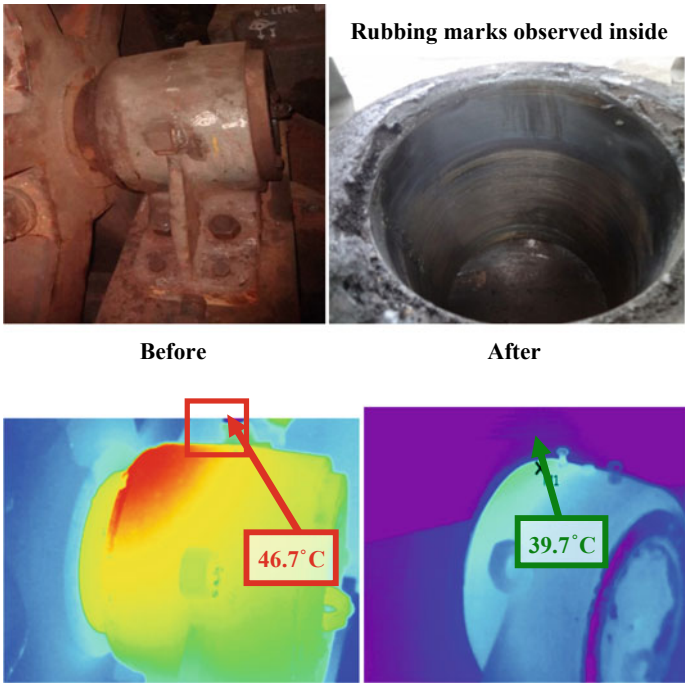

Fig. 2 Thermal imaging of the DE motor

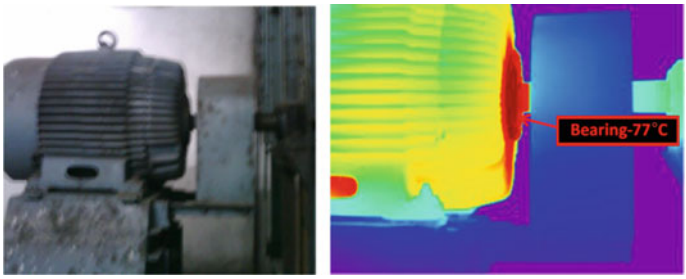

Fig. 3 Thermal imaging of the DE motor

be analyzed. The success also relies on accurate measurements and analyses of the temperature rise behavior for both healthy and faulty bearings using a high response temperature-sensing device, e.g., a thermal camera and infrared sensor.

Two important factors affecting energy losses in rolling element bearing are the properties of lubricant and its film thickness. It is thought that the energy losses during bearing operation are the result of the combined effect of friction forces, elastic deformation hysteresis losses, and drag force of lubricant film [23, 24].

Vibration-based condition monitoring systems have been used for bearing fault detection over several decades. However, they are effective mainly in the detection of physical bearing damages such as cracks and spalls and may not be easily used to detect several other undesirable conditions, in particular the lack of lubrication which eventually leads to physical damages of the bearing components. Even though the vibration-based methods are still the most popular approaches, temperature readings are used only for complementary purposes.

However, the potential of using temperature monitoring for the detection of both the physical bearing damages and lubrication problems has not yet been adequately addressed. The underlying cause that is hindering the use of thermal information for early fault detection for rotary machines in general and for bearings in particular is yet to be examined.

Case 3: The problem has been detected in the ventilation blower NDE bearing pedestal. After inspecting the target point, it recognizes creepy sound coming from the equipment. A hot spot was detected on the bearing block NDE side through thermal imaging by using its infrared thermal camera (refer to real image and thermal image of Fig. 4). Hot spot meant some internal problem of the bearing block NDE side.

The adaptor sleeve supports long shaft at more than two positions. The bearings are mounted on adapter sleeves, and a smooth shaft is probably the most popular arrangement especially for smaller bearings and provides an economic solution. The force to drive the bearing up on the sleeve is some 40% lower than for other types of sleeve mounting as friction only occurs between two mating surfaces.

Abnormal temperature rise at the bearing and shaft of the impeller end of the blower was observed, which may be attributed to excess heating due to defective gland packing due to over tightening. Thermal profile of Motor NDE bearing side body shows high-temperature distribution across the surface (max. 74.6 °C). The

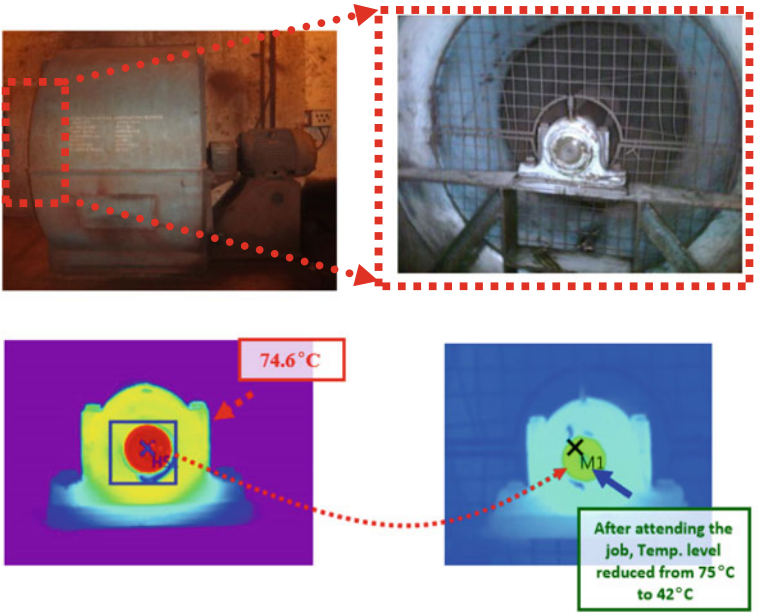

Fig. 4 Thermal imaging of the DE motor

hot spot is due to defective improper mounting of the bearing, and the abnormal temperature distribution bearing can be clearly seen from the respective thermal images. The corrective measures have been taken by tightening the adaptor sleeve; the temperature is reduced to 42 °C.

Case 4: The problem has been detected in the Fan DE bearing (motor side) of ER3 Thyristor room fan. After inspecting the target point, it recognized creepy sound coming from the equipment, and a hot spot has been detected on the Fan DE bearing (motor side) through thermal imaging (refer to real image and thermal image of Fig. 5). Hot spot meant some internal problem of the Fan DE bearing (Motor side).

Fan DE bearing (motor side) end indicates more temperature than Fan body side. There is difference of temperature more than 6–7 °C. Fan DE bearing is to be inspected for any kind of skewness inside the housing. The effect of skewness indicates that the load carrying capacity decreases as positive skewness increases, while negatively skewed roughness increases the load carrying capacity. The positive effect of the negatively skewed roughness is relatively more in the case of standard deviation, while there is a nominal adverse effect registered by standard deviation. From the previous research study [23], it was found that the maximum rise in temperature increased as the roughness and skewness increased.

Case 5: Thermal imaging of V-belts was done. The thermal profile of these V-belts indicated a unique feature in the sense that the outermost V-belt had the highest temperature (57 °C) while the innermost V-belt had the lowest temperature (45 °C). It was observed that the temperature profile of V-belts had a pattern showing decrease

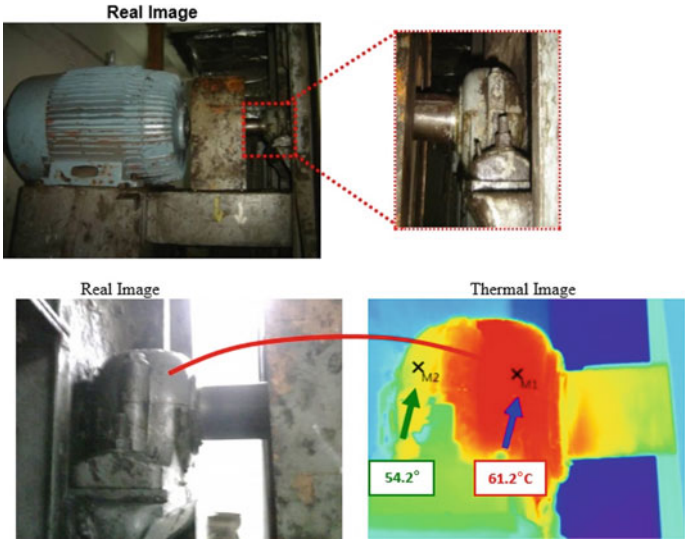

Fig. 5 Thermal imaging of the DE motor

in temperature from outside to inside of pulley, Fig. 6. This indicated that the V-belts were loose on the outer side and tight on the inner side. Thus, there is a probability of pulley misalignment. V-belt tension measurement was done, and it was observed that the outer three V-belts were loose as compared to the inner three V-belts. Pulley was realigned. Axial vibration level was checked using vibration meter and was found to reduce. Besides, V-belt abnormal sound found eliminated.

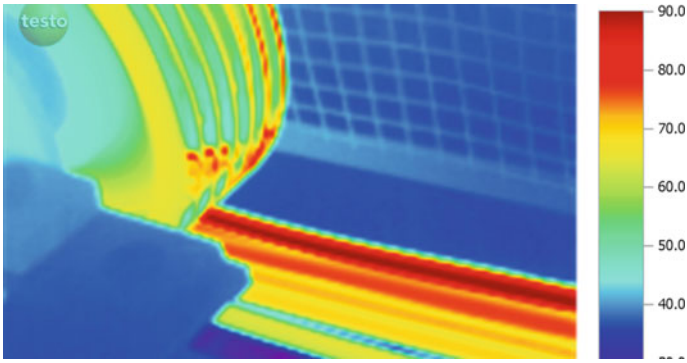

Fig. 6 V-belts temperature profile showing a pattern

5 Conclusion

In this article, the temperature profile of the equipments was analyzed through the contactless, non-destructive infrared thermography method. Based on the results, the real-time monitoring and abnormality diagnosis using the infrared thermography method were found to be applicable and useful for condition monitoring of rotating machine elements in the future. The above examples prove conclusively that IRT can produce important information where the possibilities of conventional diagnostic techniques have been exhausted. By monitoring the critical mechanical drives, problems can be identified at an early stage, and hence, reliability of a system can be improved.

References

1. Kurfess TR, Billington S, Liang SY (2006) Advanced diagnostic and prognostic techniques for rolling elements bearing. In: Wang L, Gao RX (eds) Condition monitoring and control for intelligent manufacturing. Springer, London, pp 153–181
2. Randall RB (2011) Vibration-based condition monitoring. Wiley, West Sussex, UK
3. Watson MJ, Byngton CS, Behbahani A (2007) Very high frequency monitoring system for engine gearbox and generator health management, SAE Paper No 2007-01-3878
4. Patrick R, Smith MJ, Zhang B, Byington CS, Vachtsevanos GJ, Rosario RD (2009) Diagnostic enhancements for air vehicle HUMS to increase prognostic system effectiveness. In: Vladimirova T (ed) Proceedings of the 14th IEEE aerospace conference, big sky, Montana, pp. 1–12
5. Epperly RA, Heberlein GE, Eads LG (1997) A tool for reliability and safety: predict and prevent equipment failures with thermography, In: IEEE petroleum and chemical industry conference, Banff, Alta, pp. 59–68
6. Maldague X (2001) Theory and practice of infrared technology for non destructive testing, laval. Wiley, Québec, QC
7. Meola C (2007) Infrared thermography for masonry structure. Infrared Phys Technol 49(3):228–233
8. Grinzato E, Bressan C, Marinetti S, Bison PG, Bonacina C (2012) Monitoring of the Scrovegni Chapel by IR thermography: Giotto at infrared. Infrared Phys Technol 43(3–5):165–169
9. Jadin MS, Taib S (2012) Recent progress in diagnosing the reliability of electrical equipment by using infrared thermography. Infrared Phys Technol 55(4):236–245
10. Badulescu C, Grediac M, Haddadi H, Mathias JD, Balandraud X, Tran HS (2011) Applying the grid method and infrared thermography to investigate plastic deformation in aluminium multicrystal. Mech Mater 43(1):36–53
11. Kumar J, Baby S, Kumar V (2008) Thermographic studies on IMI-834 titanium alloy during tensile loading. Mater Sci Eng 496(1):303–307
12. Pastor ML, Balandraud X, Grediac M, Robert JL (2008) Applying infrared thermography to study the heating of 2024-T3 aluminium specimens under fatigue loading. Infrared Phys Technol 51(6):505–515
13. Bagavathiappan S, Saravanan T, George NP, Philip J, Jayakumar T, Raj B (2008) Condition monitoring of exhaust system blowers using infrared thermography. Insight 50(9):512–515
14. Kim D, Yun H, Yang S, Kim W, Hong D (2010) Fault diagnosis of ball bearing within rotational machines using the infrared thermography method. J Korean Soc Nondestruct Test 30(6):570–575

15. Seo J, Yoon H, Ha H, Hong D, Kim W (2011) Infrared thermographic diagnosis mechanism for fault detection of ball bearing under dynamic loading conditions. Adv Mater Res 295–297:1544–1547
16. Meola C, Carlomagno GM, Squillace A, Giorleo G (2004) The use of infrared thermography for nondestructive evaluation of joints. Infrared Phys Technol 46(1–2):93–99
17. Kafieh R, Lotfi T, Amirfattahi R (2011) Automatic detection of defects on polyethylene pipe welding using thermal infrared imaging. Infrared Phys Technol 54(4):317–325
18. Plotinkov YA, Winfree WP (1999) Temporal treatment of a thermal response for defect depth estimation. In: Burgess CP, Myers RC (eds) proceedings of American institute of physics conference, vol 509. Montreal, Canada, pp 587–595
19. Kim W, Jinju S, Hong D (2012) Infrared thermographic inspection of ball bearing; condition monitoring. In: Diederichs R (ed) proceedings of the 18th world conference of non destructive testing, Durban, South Africa, pp 1–4
20. Marble S, Tow D (2006) Bearing health monitoring and life extension in satellite momentum/reaction wheels. In: Proceedings of the 11th IEEE aerospace conference, Big Sky, Montana, pp 1–7
21. Scott S, Kovacs A, Gupta L, Katz J, Sadeghi F, Peroulis D (2011) Wireless temperature microsensors integrated on bearings for health monitoring applications. In: Bohringer KF, Liwei L (eds) IEEE 24th international conference on micro electro mechanical systems (MEMS), Cancun, Mexico, pp 660–663
22. Henao-Sepulveda JA, Toledo-Quinones M, Jia Y (2005) Contactless monitoring of ball bearing temperature. In: Petriu EM (ed) Proceedings of the IEEE instrumentation and measurement technology conference Ottawa, Canada, pp 1571–1573
23. Palmgren A (1959) Ball and roller bearing engineering, 3rd edn. SKF Industries, Burbank, Philadelphia
24. Stolarski TA, Tobe S (2000) Rolling contacts. Professional Engineering, London

Feature Extraction and Classification from Texture Image of Machined Surfaces Using Multilevel Wavelet Decomposition and Logistic Regression

N. Dave, V. Vakharia, U. Kagathara, and M. B. Kiran

Abstract This manuscript aims to identify the texture images of the different machined operation, with the help of machine vision and artificial intelligence techniques. Texture of machined component, viz. electric discharge machining, milling, sand blasting and shaping is captured and segmented into sixteen equal, non-overlapping sub images and then discrete wavelet transform using Daubechies wavelet is applied on the sub images. Wavelet coefficients of sub images are decomposed up to fourth level, and five significant features are extracted from each level. Logistic regression, which is an artificial intelligent technique, is applied to get training and testing efficiency for identifying texture images. It is observed that the decomposition level 1 gives the 100% training identification as well as 92.3% testing identification. Results revealed that as level of decomposition is increased efficiency decreases and a number of incorrect classified instances rise drastically.

Keywords Daubechies · Discrete wavelet transform · Logistic regression · Texture

1 Introduction

In this competitive world, the quality of manufactured component is important in the field of manufacturing. To maintain the desirable quality of product, the trend toward automation is progressing. Improvement in quality and finishing of machined

N. Dave (✉) · V. Vakharia · U. Kagathara
Department of Mechanical Engineering, PDPU, Gandhinagar, India
e-mail: neildave999@gmail.com

V. Vakharia
e-mail: vinay.vakharia@sot.pdpu.ac.in

U. Kagathara
e-mail: udaykagathara@gmail.com

M. B. Kiran
Department of Industrial Engineering, PDPU, Gandhinagar, India
e-mail: MB.kiran@sot.pdpu.ac.in

V. K. Gupta et al. (eds.), *Reliability and Risk Assessment in Engineering*,
Lecture Notes in Mechanical Engineering,
https://doi.org/10.1007/978-981-15-3746-2_32

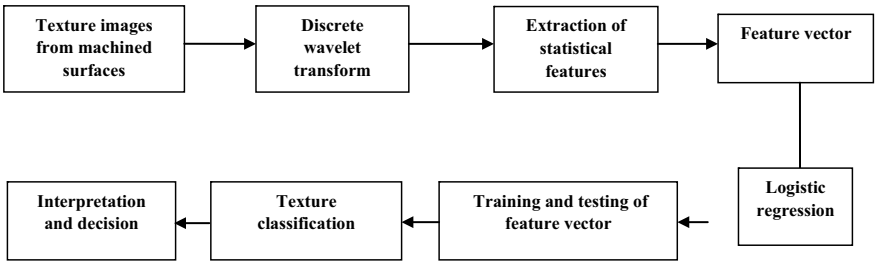

Fig. 1 Multilevel decomposition Daubechies wavelet-based texture recognize methodology

components can be achieved by the development of new tools and machining processes which must be economical. These improvements can be controlled and monitored with the help of tool condition monitoring (TCM). TCM emerges as a technique to identify the condition of tool, workpiece, etc., with reasonable accuracy. The aim of tool condition monitoring is to identify precisely the condition of tool with less human supervision [1]. An integrated monitoring system for classification consists of sensors, data acquisition system and signal conditioner. One-dimensional signal processing techniques were used with vibration-related investigations such as fault diagnosis and chatter detection, whereas 2D signal processing methods are known as image processing techniques. In machined components, the surface texture analysis is one of the significant areas of investigation [2]. Image processing technique is emerging as a promising technique for TCM, surface roughness prediction, etc., due to benefits like non-contact and non-destructive method. Machine vision is used to identify the different texture data by analyzing the images of the different machined surfaces. It was observed that different machining operations posses varied pattern of lines, roughness and elements. Authors [3, 4] have applied the application of image processing and artificial intelligence techniques to identify texture images. Discrete wavelet transform (DWT) is a widely used signal processing technique for the processing of various complex non-stationary signals [5]. Important feature of DWT is that it works on time and frequency domain simultaneously. DWT is used to calculate statistical features from the images which contain information about the machined operation. Feature vector is formed and is fed to classifier algorithms for the prediction of texture images. Artificial intelligence (AI) technique is one of the best techniques for classification, prediction, estimation with various applications like fault diagnosis [6, 7], EEG signals [8], current signature analysis, [9] etc. Various classifiers such as support vector machine, artificial neural network, Naive Bayes, random forest and logistic regression are widely used techniques for classification of data. An attempt has been made to predict the surface roughness values by varying feed, speed and depth of cut in end milling operation with back propagation neural network as a classifier [10].

In the present study, computer vision is used for identification of the surface texture images from machined surfaces, using electric discharge machining (EDM), shaping, milling and sand blasting with multiple levels of decomposition of wavelet

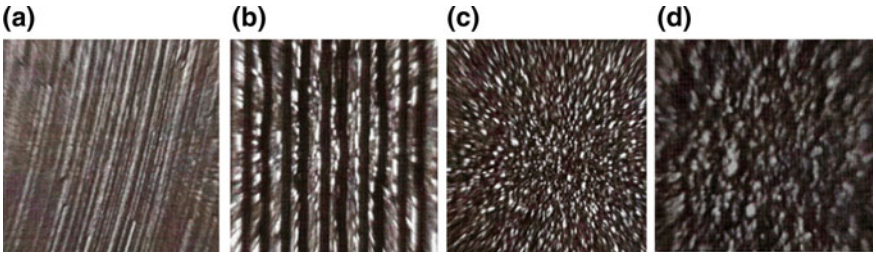

Fig. 2 Acquired images from machined surfaces. **a** Milling; **b** Shaping; **c** EDM; **d** Sand blasting

coefficients. Figure 1 shows the methodology of texture recognition, and Fig. 2 shows the acquired texture images from machined components.

2 Experimentation

For identification of texture images from machined surfaces, manufacturing operations like EDM, milling, shaping and sand blasting are performed. Images are acquired with charge-coupled device cameras (CCD) and image processor LC processing hardware with four frame buffers, Pulnix-TM6 and 1/30 s as a grabbing speed. Workpiece is illuminated by a white light source which is inclined at 45° with the respect to workpiece surface [11]. The captured images are magnified to 10× for proper texture analysis with image acquisition software. An industrial interface is used to convert the captured image into a digital image, and the processed image was displayed on the monitor. Figure 3 shows the schematic diagram of experimental setup used for conducting study.

3 Discrete Wavelet Transform and Feature Extraction

The wavelet transform is mainly used for the non-stationary signal from the different machined operation texture image, which involves varied time–frequency windows and can provide good localization in both the frequency as well as time domains at the same time. It has been widely used, as it is new mathematical approach that decomposes a time domain signal with a combination of different frequency groups. It offers a high reduction in computational time without losing useful information.

$$w(y) = (z * g)[y] = \sum_{k=-\infty}^{\infty} x(k)g[y-k] \tag{1}$$

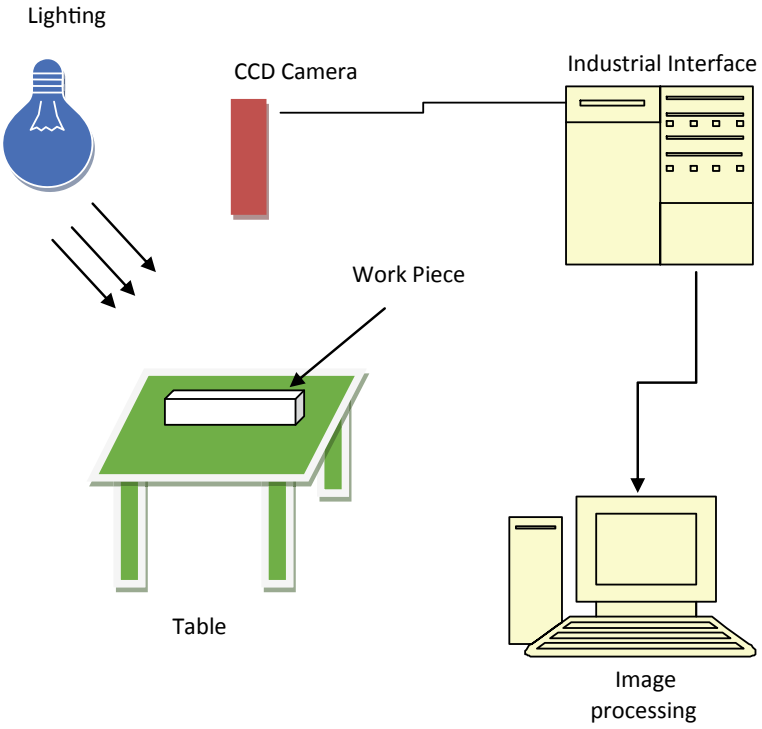

Fig. 3 Schematic diagram of the experimental setup

where $x(y)$ is the input signal, $w(y)$ is the output signal, which gives detail coefficients and approximation coefficients.

$$C_{nn}(y) = O\left(\sum_{y} x(y) l_n^*(y - 2^p q)\right) \tag{2}$$

$$C_n(y) = O\left(\sum_{y} x(y) h_n^*(y - 2^p q)\right) \tag{3}$$

Here C_n and C_{nn} are detailed coefficients and approximation coefficients, and n indicates the level of decomposition and scaling function. $l(y)$ and $h(y)$ indicate the low-pass and high-pass filter. O operator represents the down sampling of approximation coefficient which consists of the characteristic of low-frequency components of the texture image, while the detailed components consist of the characteristics of high-frequency components.

In discrete wavelet transform, several mother wavelets like Haar, Biorthogonal, Reverse Biorthogonal, Dmey, Symlet, Coiflets and Daubechies are present. In order to select mother wavelet function, Daubechies wavelet is considered as a mother

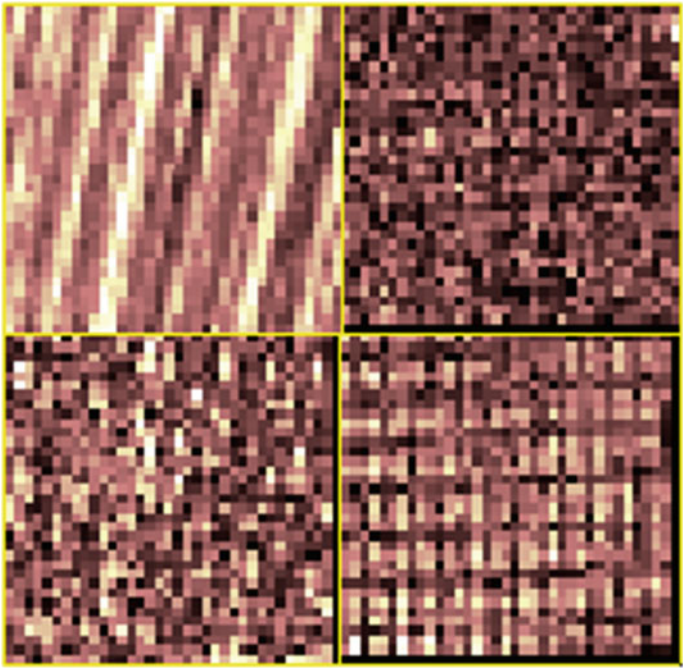

Fig. 4 Level 1 decomposition of texture image

wavelet. It belongs to an orthonormal wavelet family. However, this family is asymmetric about their midpoint. It has been decomposed to one, two, three and four levels of the wavelet, and signals are processed for feature extraction. The DWT coefficients are calculated at the first, second, third and fourth levels of decomposition. All the decomposition levels have been represented in Figs. 4, 5, 6 and 7.

The acquired machined images are pre-processed through discrete wavelet transform with different level. Statistical features are extracted from the wavelet coefficients obtained from various levels, which are explained below:

1. Mean: It is the ratio of the summation of the list of number to the length of list.
2. Maximum Energy: It represents the maximum available energy of the element.
3. Variance: Variances measure the distribution of data from the mean value of the element.
4. Shannon Entropy: The amount of information of each image forms an uncertainty whose expected value can be near to it.
5. Permutation Entropy: It is a measure based on the analysis of permutation patterns for arbitrary time series.

All different machined operation images are divided into 16 equal non-overlapping images, from original texture image, for detailed texture analysis. With

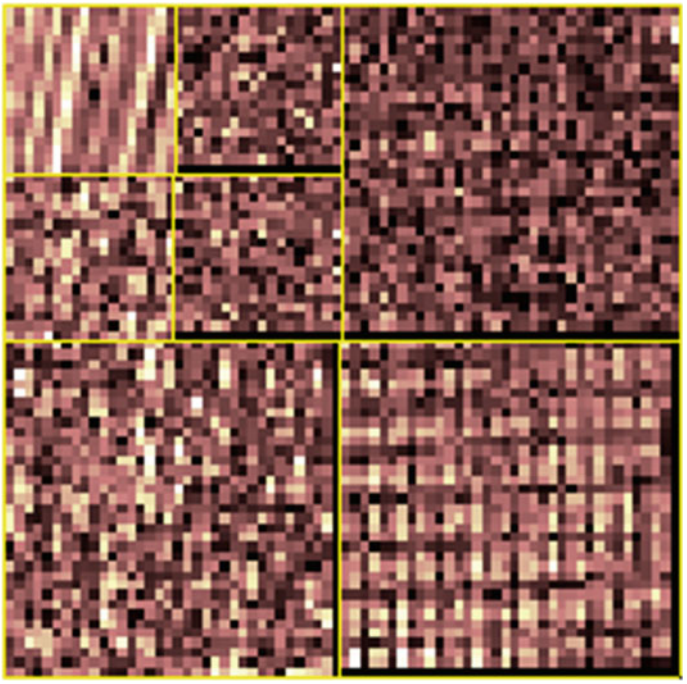

Fig. 5 Level 2 decomposition of texture image

this segmentation, in-depth characteristic details of texture surfaces will be known, which helps in the identification of texture images.

4 Logistic Regression

Logistic regression is used as a classifier and predictor for categorization of different textured images. It is a type of supervised model, for prediction of data as input by user, and applicable to data which is nonlinear in nature. In logistic regression, the variables may be binary or multinomial. Logistic curve is used for regression analysis to predict values. In the case of logistic regression, the odd ratio predicted from positive outcomes is expressed as sum of product, which is obtained after multiplying the values of coefficients and independent variables. The aim is to find out the relationship between outcome variable Y and set of input variables.

$$Y = (\beta_0 + \beta_1 \chi_1 + \beta_2 \chi_2 + \beta_3 \chi_3 + \cdots) \tag{4}$$

Here, χ_1, χ_2, χ_3 represent independent variables and β_0, β_1, β_2, β_3 represent the regression coefficients.

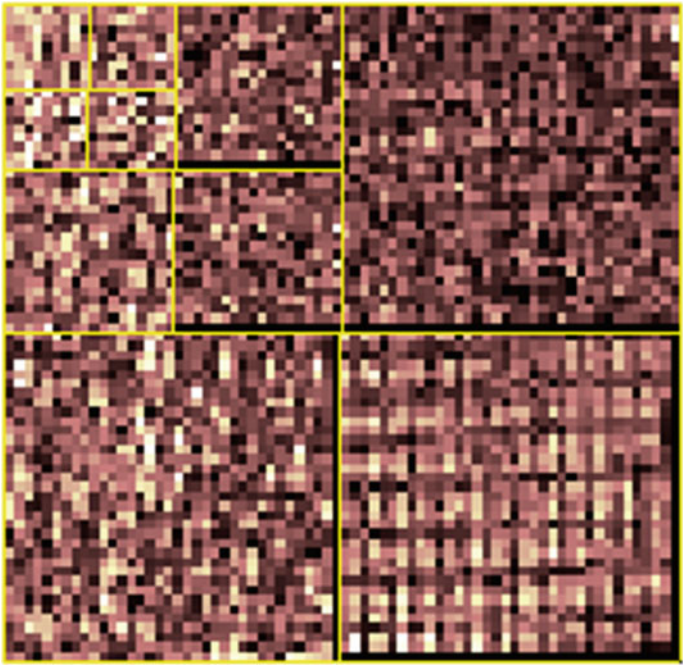

Fig. 6 Level 3 decomposition of texture image

The probability of occurrence is estimated by a function

$$p = e^Y / 1 + e^Y \tag{5}$$

5 Results and Discussion

In the present study, the texture image is identified from the multilevel decomposition of DWT with four different levels. Training and testing of the dataset have been carried out by the logistic regression classifier. Total 64 instances were considered with five significant features for the present study. From Fig. 8, it is observed that the features calculated from level 1 decomposition give high training accuracy of 100% in comparison with the other levels considered. The least training accuracy achieved was 79.68%. For the testing accuracy, one-fifth of the data has been taken from the input dataset. It has been observed that testing accuracy reduces as the level of decomposition is increased. Decomposition level 2 and 3 give the same accuracy. Level 4 gives least accuracy with testing (Fig. 9).

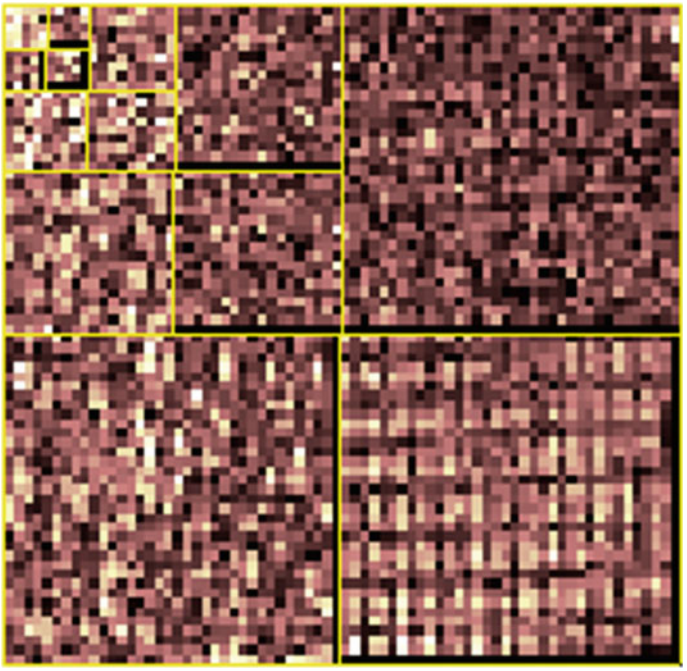

Fig. 7 Level 4 decomposition of texture image

Fig. 8 Training accuracy with logistic regression

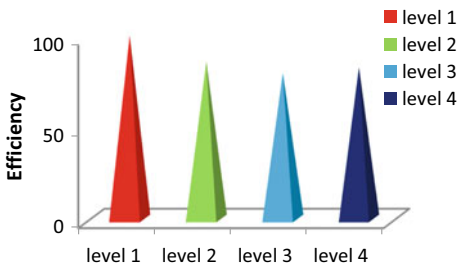

Fig. 9 Testing accuracy with logistic regression

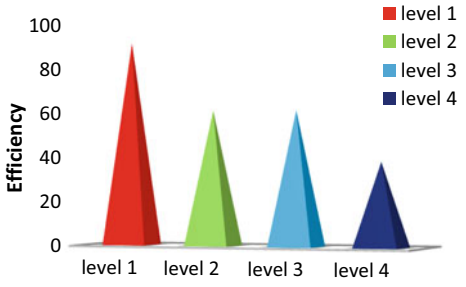

6 Conclusions

In this paper, identification of the different texture images obtained from machining operations is incorporated with the help of a discrete wavelet transform. Five features are calculated from five levels considering db1 as a base wavelet. After calculation of statistical features from machined texture images, the feature vector is formed. Training and testing accuracy of logistic regression classifiers are compared. It is observed that maximum training and testing accuracy of 100 and 93% were obtained with features calculated from level 1 decomposition. Experimental results show that level 1 is the best level for the calculation of statistical features. Methodology incorporated is useful for deciding optimal level for the calculation of statistical features from texture images.

Acknowledgements The authors would like to acknowledge the support of PDPU, Gandhinagar, for providing the infrastructure required for carrying out the experiments.

References

1. Dutta S, Datta A, Chakladar ND, Pal SK, Mukhopadhyay S, Sen R (2012) Detection of tool condition from the turned surface images using an accurate grey level co-occurrence technique. Precis Eng 36(3):458–466
2. Bhandari SH, Deshpande SM (2007) Feature extraction for surface classification—an approach with wavelets. Int J Comput Inf Eng 1(4):322–326
3. Venkat Ramana K, Ramamoorthy B (1996) Statistical methods to compare the texture features of machined surfaces. Pattern Recogn 29(9):1447–1459
4. Geetharamani R, Balasubramanian L (2016) Retinal blood vessel segmentation employing image processing and data mining techniques for computerized retinal image analysis. Biocybern Biomed Eng 36(1):102–118
5. Vakharia V, Gupta VK, Kankar PK (2017) Efficient fault diagnosis of ball bearing using Relief and Random Forest classifier. J Braz Soc Mech Sci Eng 39(8):2969–2982
6. Vakharia V, Gupta VK, Kankar PK (2015) Ball bearing fault diagnosis using supervised and unsupervised machine learning methods. Int J Acoust Vib 20:244–250
7. Vakharia V, Gupta VK, Kankar PK (2016) Bearing fault diagnosis using feature ranking methods and fault identification algorithms. Procedia Eng 144:343–350
8. Hassan AR, Bhuiyan MIH (2016) A decision support system for automatic sleep staging from EEG signals using tunable Q-factor wavelet transform and spectral features. J Neurosci Methods 271:107–118
9. Singh S, Kumar N (2014) Combined rotor fault diagnosis in rotating machinery using empirical mode decomposition. J Mech Sci Technol 28:4869–4876
10. Palani S, Natarajan U (2011) Prediction of surface roughness in CNC end milling by machine vision system using artificial neural network based on 2D fourier transform. Int J Adv Manuf Technol 54:1033–1042
11. Vakharia V, Kiran MB, Dave NJ, Kagathara U (2017) Feature extraction and classification of machined component texture images using wavelet and artificial intelligence techniques. In: Eighth international conference on mechanical and aerospace engineering (ICMAE), Prague, pp 140–144

Effect of Combining Teaching Learning-Based Optimization (TLBO) with Different Search Techniques

Jaydeep Patel, Vimal Savsani, and Vivek Patel

Abstract This paper investigates the effect to ensemble teaching learning-based optimization (TLBO) with other meta-heuristics methods like artificial bee colony (ABC), biogeography-based optimization (BBO), differential evolution (DE) and genetic algorithm (GA). Three different schemes to generate sub-population from the main population are proposed, and the effect of migration of solutions from one sub-population to the other is also explored. The experiments are performed on different unconstrained and constrained benchmark optimization problems. The results are investigated using the statistical test like Friedman rank test and Holm-Sidak post hoc test. The results reveal that the ensemble of different optimization methods is effective than the basic algorithms.

Keywords Artificial bee colony (ABC) · Biogeography-based optimization (BBO) · Differential evolution (DE) · Genetic algorithm (GA) · Sub-population · Ensemble of algorithms · Teaching learning-based optimization (TLBO)

1 Introduction

Sub-populations are based on the mechanics of natural flora and fauna. Nature is diversified with the existence of different species which compete to survive in the system. All the species follow different mechanism for the survival. Role of all the species is interconnected for preserving nature. A sub-population, also called niche, can be related as a subspace in the environment that can support different species. A species is defined as a group of individuals with similar genetic features. For each sub-population, the physical resources are finite and must be shared among the inhabitants of that sub-population only. In meta-heuristics, sub-population involves the formation of subgroups within a population where each subgroup updates the solutions with specific intension. Compared with the simple meta-heuristics, the

J. Patel · V. Savsani · V. Patel (✉)
Department of Mechanical Engineering, Pandit Deendayal Petroleum University, Gandhinagar, Gujarat 382007, India
e-mail: viveksaparia@gmail.com

V. K. Gupta et al. (eds.), *Reliability and Risk Assessment in Engineering*,
Lecture Notes in Mechanical Engineering,
https://doi.org/10.1007/978-981-15-3746-2_33

uniqueness of sub-population meta-heuristics lies in the fact that they preserve not only the highly fit individuals, but also weaker individuals so long as they belong to groups. If the main population is divided into sub-populations, they attempt to maintain a diverse population and are not as prone to converge prematurely.

Since the earliest sub-population approach, preselection was proposed in [4], and various other methods such as crowding [11, 14, 19, 21, 22], sharing [6–10, 20, 25, 33, 34] and clearing [17, 18, 26] have emerged. The main aim to produce niche by the above methods is to find different peaks of a multimodal function. So, the concentration was mainly focused to solve multimodal functions. However, to divide the main population into sub-population provides many advantages like parallel processing [1, 3], to combine different constraint handling techniques [23], to combine different search strategies of single algorithm [24], to solve multi-objective optimization [5], to find multiple optimum solutions and many more. This is also known as ensemble of different strategies [23]. Some optimization algorithms use sub-population approach as an integrated part of the algorithm [29]. Many works are reported for niche strategies and randomly selected sub-population from the main population, but the computationally effective procedures to create sub-population and its effects are still unexplored. So, very less work is reported to initialize sub-population in every generation. Moreover, no work is reported to apply different optimization search techniques for separate sub-population. However, so far, to solve a certain problem, only one meta-heuristic method is used at a time. It is often the case that we have to try out several methods and tune their parameters to find the best method and its best set of parameters to solve a given problem. Irrespective of the exhaustiveness of the parameter tuning, no one method can be the best for all problems as per no free lunch theorem (NFL).

To prevail over the above research gaps, this paper presents the investigation of ensemble of different meta-heuristics like teaching learning-based optimization (TLBO), artificial bee colony (ABC) optimization, biogeography-based optimization (BBO), differential evolution (DE) and genetic algorithm (GA). The purpose of selecting above methods is that all the algorithms are well established search techniques, and their effectiveness has been proved on a wide spectrum of engineering and science problems. Moreover, all the considered algorithms follow totally different search techniques, compared to each other. Three different schemes to obtain sub-population are also proposed and investigated on different unconstrained and constrained benchmark problems. The proposed schemes are also investigated with and without the migration of solutions from one sub-population to the other. In each generation, all sub-populations follow different search mechanisms of the considered algorithms, and the results thus obtained are combined at the end of each generation. The same procedure is repeated for the next generation.

2 Search Techniques for Different Algorithms

All the considered algorithms start the search process with a set of solutions known as population. The population is randomly created and is subjected to different search procedures which depend on the considered optimization techniques. All the techniques considered in this paper follow different natural phenomenon for its working. TLBO works on the basic philosophy of teaching and learning process, ABC mimics the natural food foraging behavior of a honey bee, BBO works on the natural behaviors of different species to immigrate and emigrate at different places, and GA is a well-known algorithm which works on the theory of evolution and survival of the fittest. DE is the special variant of GA and explores the search space by the vector difference theory. TLBO works in two phase, namely teaching and learning phase [27, 28]. New solutions are generated from the old solutions in the teaching phase by using the following equation:

$$X_{i,j}^{\text{new}} = X_{i,j}^{\text{old}} + r_i\left(X_{i,j}^{\text{best}} - T_F M_j\right) \tag{1}$$

where $X_{i,j}^{\text{best}}$ is the best solution present in the current solution, r_i is the random number between 0 and 1, T_F is the teaching factor, M_j is the mean of all design variables, $X_{i,j}^{\text{old}}$ is the current solution, and $X_{i,j}^{\text{new}}$ is the new solution generated. The new solution is accepted if it is better than the current solution. After evaluating all the solutions, it undergoes learner phase. In this phase, solution X_k is selected which is different than the current solution X_i. The solution is updated as follows:

$$\text{If } f(X_i) < f(X_k),\ X_{i,j}^{\text{new}} = X_{i,j}^{\text{old}} + r_i\left(X_{i,j} - X_{k,j}\right) \tag{2}$$

$$\text{Else, } X_{i,j}^{\text{new}} = X_{i,j}^{\text{old}} + r_i\left(X_{k,j} - X_{i,j}\right)$$

ABC starts its search by dividing the population into two parts, i.e., employed bees and onlooker bees [2, 15, 16]. So, the search of ABC follows two phases, i.e., employed bee phase and onlooker bee phase, but the search equation for both the phases is same. The solution is updated in the employed bee phase by the following equation.

$$X_{i,j}^{\text{new}} = X_{i,j}^{\text{old}} + R_i\left(X_{i,j} - X_{k,j}\right) \tag{3}$$

where R_i is a random number between -1 and 1. The solution is accepted if it is better than the previous solution. The updated solution thus produced is selected probabilistically depending on its fitness value for the onlooker bee phase. In the onlooker bee phase, the solution is updated using the same equation used in the employed bee phase. The solution is randomly changed if there is no improvement in the solution for specified number of count known as 'limit' in ABC. BBO updates the solution by exchanging different design variables among the population [31]. It uses the value of immigration rate and emigration rate to exchange the variables.

The procedure to exchange design variables can be found in [31]. DE modifies the solution using the following expressions [32]:

$$X_{t,j} = X_{3,j} + F(X_{1,j} - X_{2,j}) \tag{4}$$

where $X_{t,j}$ is the target solution generated from three randomly chosen solutions $X_{1,j}$, $X_{2,j}$ and $X_{3,j}$, and it replaces the current solution $X_{i,j}$ depending on the crossover probability CR. F is the constant factor. The target solution is compared with the randomly chosen solution, and the better solution replaces the current solution. GA is a very well-known technique, which selects the best solution probabilistically by using roulette wheel selection procedure [12]. The selected solution undergoes arithmetic crossover which is used in this work.

3 Different Schemes to Generate Sub-population

As mentioned above, many schemes to create niches are available in the literature, but all such schemes are computationally expensive and require extra computational efforts [30]. Other methods are also available such as to generate sub-population randomly and to generate by following some solutions with probability. However, the concept to initialize sub-population is poorly explored and requires more investigation, so as to have a method to generate sub-population with less computational efforts. Three different schemes are proposed in this paper known as biased sub-population, random sub-population and sequential sub-population. Migration is also an important term which is referred as the change of solutions among the sub-population. In this work, migration of the output of one sub-population to the other is also investigated. The understanding of all the methods is given as follows.

3.1 Biased Sub-population

In this method, all the sub-populations are created from the first best superior solutions, and thus, it provides the biasness to create sub-population. Pictorial representation of this method is shown in Fig. 1. As shown in Fig. 1, two sub-populations are required to be generated from one main population. Main population contains ten solutions arranged in ascending order from P1 to P10. In this method, both the sub-populations are assigned population from P1 to P5, i.e., the best five solutions. Solutions from P6 to P10 are removed without getting chance to move in the sub-population. That is why this method is called biased sub-population scheme. So, in this scheme all the sub-populations will have same solutions.

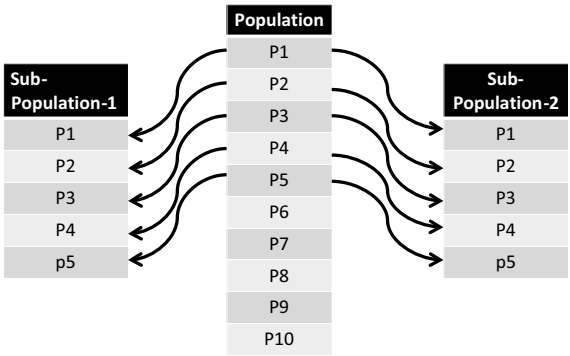

Fig. 1 Biased sub-population scheme

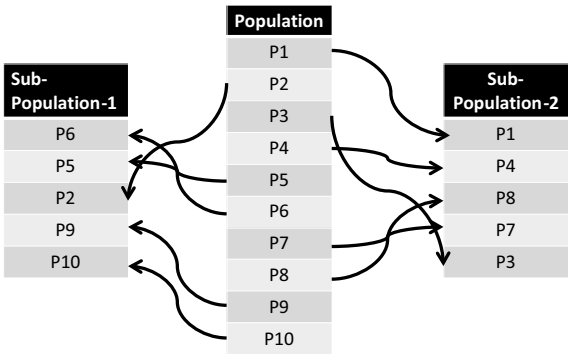

Fig. 2 Random sub-population scheme

3.2 Random Sub-population

In this method, the solutions are allotted randomly to all the sub-population from the main population. Pictorial representation of this method is shown in Fig. 2. It is observed from Fig. 2 that no particular methodology is followed to assign solution to the sub-population. Here, sub-population-1 is assigned P1, P4, P8, P7 and P3 and rest are assigned to sub-population-2. Care should be taken to avoid the repetition of solutions in the sub-population to maintain diversity. So, in this method all the sub-populations will have different solutions.

3.3 Sequential Sub-population

In this method, sub-population is created by allotting one by one solution to each sub-population from the ascending ordered main population. Pictorial representation of this method is shown in Fig. 3. It is observed form Fig. 3 that P1, P3, P5, P7 and P9 are assigned to sub-population-1 and P2, P4, P6, P8 and P10 are assigned to

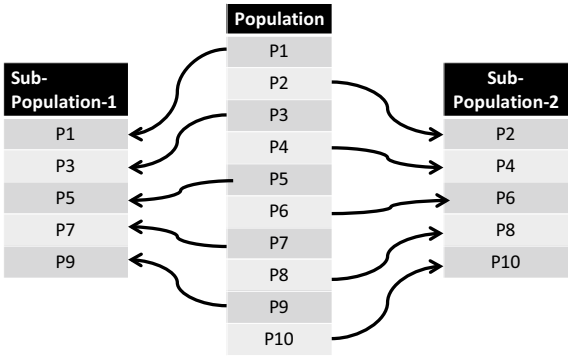

Fig. 3 Sequential sub-population scheme

sub-population-2. So, this is a structured method to form a sub-population and here also all the sub-populations will be different.

In this work, the ensemble is done by considering the combinations of two, three, four and five algorithms independently, by keeping TLBO as a common algorithm. Thus, there are 15 different possibilities to ensemble considered meta-heuristics with TLBO. These possibilities are listed as follows: ensemble of two algorithms [TLBO-ABC (T-A), TLBO-DE (T-D), TLBO-BBO (T-B), TLBO-GA (T-G)], ensemble of three algorithms [TLBO-ABC-DE (T-A-D), TLBO-ABC-BBO (T-A-B), TLBO-ABC-GA (T-A-G), TLBO-DE-BBO (T-D-B), TLBO-DE-GA (T-D-G), TLBO-BBO-GA (T-B-G)], ensemble of four algorithms [TLBO-ABC-DE-BBO (T-A-D-B), TLBO-ABC-DE-GA (T-A-D-G), TLBO-ABC-BBO-GA (T-A-B-G), TLBO-DE-BBO-GA (T-D-B-G)] and ensemble of five algorithms [TLBO-ABC-DE-BBO-GA (ALL)]. It is observed from the list above that first four possibilities will have two sub-populations, next six will have three sub-populations, next four will have four sub-populations, and last will have five sub-populations. As mentioned, this work is concentrated to investigate the effect of sub-dividing the population into small groups and to explore these sub-populations by different search mechanisms. Moreover, it is possible to investigate the effect of considering more than one algorithm for the evaluations of different sub-populations.

The effect of passing the solution from one sub-population to the other is also investigated in this study. To pass the solution from one sub-population to the other, initially only the first sub-population is generated where it follows the search mechanism of that sub-population, and the obtained output is passed to the next sub-population where it follows the search mechanism of other algorithm. For example in TLBO-ABC, initially the sub-population of TLBO is generated, and the solutions are updated with the search mechanism of TLBO. The output of this sub-population is given to the sub-population of ABC where the solution is updated by the search mechanism of ABC. So, this leads to five different schemes for the sub-population, biased scheme (B), biased scheme with passing (BS), random scheme (R), random scheme with passing (RS) and sequential scheme (S).

4 Performance of Proposed Methods

For the comparison of proposed ensemble-TLBO, following performance criteria evaluations are considered for the benchmark problems: population size = 60, function evaluations = 30,000, number of runs = 25; for BBO: immigration rate = emigration rate = 1, mutation factor = 0.01; for ABC: number of employed bees = number of onlooker bees, limit = number of generations; for DE: $F = 0.5$, CR= 0.5; for GA: crossover = arithmetic crossover, selection = roulette wheel selection, crossover probability = 0.8, mutation probability = 0.005.

Experimentation is done on 13 unconstrained and 24 constrained benchmark problems. All the considered benchmark problems are of different characteristics. To check the effectiveness of any proposed optimization algorithms, it is a good practice to test the algorithm on such benchmark problems. Results are obtained for all benchmark problems by using all 15 algorithms, considering all three different schemes with and without passing, for 25 independent runs. The results are obtained in the form of an 'error' calculated as $|f(X_{\text{opt}}) - f(X)|$, where $f(X_{\text{opt}})$ is the known optimum value for the particular benchmark problem and $f(X)$ is the objective function value obtained by the optimization algorithm. The results are compared for the 'best error value' and the 'mean error value' obtained in 25 runs. Thus, the result for the unconstrained benchmark problems contains 13×15 data points for different sub-population schemes, like random sub-population scheme with (RP) and without passing (R), best sub-population scheme with (BP) and without passing (B) and sequential sub-population scheme (S). Hence, total result data consists of $5(13 \times 15)$ points for unconstrained problems and $5(24 \times 15)$ for constrained benchmark problems. As the obtained result consists of large data, it is very difficult to quantify the performance of the algorithms without the use of statistical tests. Thus, to identify the best performing algorithm, Friedman rank test is implemented on the results. Firstly, the performance of each proposed algorithm is checked to identify which method of sub-population is well suited on the benchmark problems. The results of the Friedman rank test [13], based on best error values and mean error values, for unconstrained benchmark problems, obtained by using each proposed sub-population method, are illustrated in Table 1.

It is observed from the results that out of all the five proposed sub-population methods, sequential sub-population is more effective for unconstrained problems as it has shown better performance on ten algorithms for best solutions and on nine algorithms for obtaining mean solutions. Friedman rank test is also performed in the similar way for constrained benchmark problems, and results are illustrated in Table 2. It is observed from the results that, for constrained benchmark functions, sequential sub-population is effective for all the 15 proposed algorithms. Thus, it can be said that out of all the proposed schemes for the sub-population, sequential sub-population is the best-suited method for the unconstrained and constrained benchmark problems.

Now, it is required to find the best algorithm from the sequential sub-population scheme. The best algorithm is obtained by performing Friedman rank test on the

Table 1 Friedman rank test for individual ensemble algorithm considering all the sub-population

UC	Best					Mean				
	B	BP	R	RP	S	B	BP	R	RP	S
T-A	26.5	36.5	51.5	63	**17.5**	27.5	37.5	47.5	64	**18.5**
T-B	43.5	39	50	39.5	**23**	44	41	48	40	**22**
T-D	27.5	42.5	46.5	63	**15.5**	27	42.5	45.5	65	**15**
T-G	31.5	**30.5**	56	31	46	32.5	**27.5**	55	31	49
T-A-B	31.5	38	44	61	**20.5**	29	38.5	44.5	63	**20**
T-A-D	27.5	38	47.5	65	**17**	26.5	39.5	48.5	65	**15.5**
T-A-G	**25.5**	27	56	52.5	34	**22.5**	34.5	50	56	32
T-D-B	33	39.5	44.5	61	**17**	34	43	37	62	**19**
T-D-G	**28**	29	56.5	51	30.5	**27**	31	52.5	55.5	29
T-B-G	38.5	**30.5**	58	32.5	35.5	41.5	30.5	60	**27.5**	35.5
T-A-D-B	33	33	48.5	63	**17.5**	30.5	40.5	42.5	64	**17.5**
T-A-D-G	**25**	33	51	61	**25**	28	34	51	59	**23**
T-A-B-G	45	**28.5**	53	37	31.5	44.5	**28**	58	34.5	30
T-D-B-G	44.5	32.5	54	**32**	**32**	51.5	29	55.5	**28.5**	30.5
ALL	43.5	44.5	51	32	**24**	42.5	44.5	53	30	**25**

The bold letters indicates the best scheme

Table 2 Friedman rank test for individual ensemble algorithm considering all the sub-population methods (constrained problems)

C	Best					Mean				
	B	BP	R	RP	S	B	BP	R	RP	S
T-A	63	61.5	93	101	**41.5**	68	68	85	96	**43**
T-B	77.5	55.5	87	93	**47**	70.5	69	78.5	85	**57**
T-D	70	60	88.5	102	**39.5**	72	62.5	88.5	96	**41**
T-G	78.5	70	97	73	**56.5**	75	88	87.5	59.5	**50**
T-A-B	65	79	81.5	89.5	**45**	78	87	73.5	82.5	**39**
T-A-D	67.5	73	88.5	96.5	**34.5**	71.5	77.5	76.5	95	**39.5**
T-A-G	66	70	86	90	**48**	76	83.5	76	83	**41.5**
T-D-B	72	65.5	87.5	98.5	**36.5**	88.5	80	71	84	**36.5**
T-D-G	68	83	83	76.5	**49.5**	80	90	76.5	69	**44.5**
T-B-G	68	74.5	85	83	**49.5**	85.5	80.5	72	70.5	**51.5**
T-A-D-B	75	85.5	76	82.5	**41**	83	92	70	79.5	**35.5**
T-A-D-G	82.5	81	83	82	**31.5**	95.5	86.5	68.5	72	**37.5**
T-A-B-G	67	76.5	113	67	**36.5**	86.5	85.5	68.5	72.5	**47**
T-D-B-G	77.5	91	66.5	82	**43**	89.5	91	71	64.5	**44**
ALL	87	87.5	68.5	78	**39**	88.5	97.5	60	72.5	**41.5**

The bold letters indicates the best scheme

Table 3 Friedman rank test for sub-population method considering all the ensemble algorithms (unconstrained problems)

	Unconstrained		Constrained	
	Best	Mean	Best	Mean
T-A	1.66	1.38	**1.18**	**1.33**
T-B	1.56	1.31	1.44	1.83
T-D	**1.09**	**1.00**	**1.00**	**1.00**
T-G	3.52	3.15	1.77	2.13
T-A-B	1.20	**1.03**	1.49	1.78
T-A-D	1.41	1.08	**1.01**	**1.26**
T-A-G	3.47	2.96	1.84	1.62
T-D-B	**1.16**	1.23	1.38	1.58
T-D-G	3.11	2.70	1.75	1.78
T-B-G	2.61	2.18	1.78	2.36
T-A-D-B	**1.00**	**1.02**	1.55	1.52
T-A-D-G	3.09	2.55	1.38	1.57
T-A-B-G	2.32	1.92	1.57	1.92
T-D-B-G	2.03	1.61	1.71	2.00
ALL	1.66	1.34	1.75	2.03

The bold letters indicates the best scheme

results of unconstrained and constrained benchmark problems of sequential sub-population scheme, and the results are given in Table 3. The algorithm is judged on its ability to perform consistently in every runs. The consistent performance is measured by the mean value of the best solution obtained in all the runs. So, it is observed from Friedman rank value of Table 3 that T-D is the best performing algorithm for the unconstrained and constrained benchmark problems. For unconstrained problems, T-D is followed by T-A-D-B, T-A-B and T-A-D, while for the constrained problems T-D is followed by T-A-D, T-A and T-A-D-B. It is also noted that the presence of GA in the ensemble algorithm deteriorates the performance of the algorithm compared to other algorithms in the same category, e.g., T-A, T-B and T-D are more effective than T-G. Similarly, T-A-B, T-D-B and T-A-D have produced better results than T-A-G, T-D-G and T-B-G. It can also be observed from the results that the performance of the algorithm ensemble by two algorithms is better than the algorithm ensemble by three algorithms, i.e., T-D is better than T-A-D, while T-A-D is better than T-A-D-B.

5 Conclusions

The effect to ensemble different meta-heuristics algorithms like ABC, DE, BBO and GA with TLBO is investigated in this paper. Different schemes to generate

sub-population like biased, random and sequential are proposed and investigated on different unconstrained and constrained benchmark problems. It is observed from the results that the sequential sub-population scheme is more effective than biased and random scheme. Also, migration of solutions from one sub-population to the other is not effective compared to the method without migration. Combination of TLBO and DE is more effective than other combinations. Most of the ensemble algorithms with the sequential scheme are better than the parent algorithms. Effectiveness of basic TLBO increases if it is combined with the search technique of DE.

References

1. Alba E, Troya JM (1999) A survey of parallel distributed genetic algorithms. Complexity 4(4):31–52
2. Basturk B, Karaboga D (2006) An artificial bee colony (ABC) algorithm for numeric function optimization. In: IEEE Swarm Intelligence Symposium, Indianapolis, Indiana, USA, 12–14 May
3. Cantú-Paz E (1998) A survey of parallel genetic algorithms. Calc Paralleles Reseauxet Syst Repartis 10(2):141–171
4. Cavicchio DJ (1970) Adaptive search using simulated evolution. Doctoral Dissertation, University of Michigan, Ann Arbor
5. Deb K, Pratap A, Agarwal S, Meyarivan TAMT (2002) A fast and elitist multiobjective genetic algorithm: NSGA-II. IEEE Trans Evol Comput 6(2):182–197
6. Dilettoso E, Salerno N (2006) A self-adaptive niching genetic algorithm for multimodal optimization of electromagnetic devices. IEEE Trans Magn 42:1203–1206
7. Gan J, Warwick K (1999) A genetic algorithm with dynamic niche clustering for multimodal function optimization. In: Proceedings of the 4th international conference on artificial neural nets and genetic algorithms, pp 248–255
8. Goldberg DE, Richardson JJ (1987) Genetic algorithms with sharing for multimodal function optimization, Genetic algorithms and their application. In: Proceedings of the 2nd international conference on genetic algorithms, pp 41–49
9. Goldbergand DE, Wang L (1997) Adaptive niching via coevolutionary sharing. Genet Algorithms Evol Strat Eng Comput Sci 21–38
10. Dunwei G, Fengping P, Shifan X (2002) Adaptive niche hierarchy genetic algorithm. In: TENCON '02. proceedings of IEEE region 10 conference on computers, communications, control and power engineering, pp 39–42
11. Harik G (1994) Finding multiple solutions in problems of bounded difficulty. IIIiGAL Report No. 94002, University of Illinois at Urbana-Champaign
12. Holland J (1975) Adaptation in natural and artificial systems. University of Michigan Press, Ann Arbor
13. Joaquín D, Salvador G, Daniel M, Francisco H (2011) A practical tutorial on the use of nonparametric statistical tests as a methodology for comparing evolutionary and swarm intelligence algorithms. Swarm Evol Comput 1(1):3–18
14. Jong KA (1975) An analysis of the behavior of a class of genetic adaptive systems. Doctoral Dissertation, University of Michigan
15. Karaboga D (2005) An idea based on honey bee swarm for numerical optimization. Technical Report-TR06, Erciyes University, Engineering Faculty, Computer Engineering Department
16. Karabogaand D, Akay B (2009) Artificial bee colony (ABC), harmony search and bees algorithms on numerical optimization. In: IPROMS-2009, Innovative Production machines and systems virtual conference, Cardiff, UK

17. Kim JK, Cho DH, Jungand HK, Lee CG (2002) Niching genetic algorithm adopting restricted competition selection combined with pattern search method. IEEE Trans Magn 38(2):1001–1004
18. Lee C, Choand D-H, Jung H-K (1999) Niching genetic algorithm with restricted competition selection for multimodal function optimization. IEEE Trans Magn 35(3):1722–1725
19. Li M, Wang Z (2009) A hybrid coevolutionary algorithm for designing fuzzy classifiers. Inf Sci 179(12):1970–1983
20. Lin C-Y, Wu W-H (2002) Niche identification techniques in multimodal genetic search with sharing scheme. Adv Eng Softw 33(11–12):779–791
21. Mahfoud SW (1992) Crowding and preselection revisited. Parallel Probl Solving Nat 2:27–37
22. Mahfoud SW (1995) Niching methods for genetic algorithms. Ph.D. thesis, IlliGAL Report No. 95001, University of Illinois at Urbana-Champaign
23. Mallipeddi R, Suganthan PN (2010) Ensemble of constraint handling techniques. IEEE Trans Evol Comput 14(4):561–579
24. Mallipeddi R, Suganthan PN, Pan QK, Tasgetiren MF (2011) Differential evolution algorithm with ensemble of parameters and mutation strategies. Appl Soft Comput 11(2):1679–1696
25. Miller BL, Shaw MJ (1996) Genetic algorithms with dynamic niche sharing for multimodal function optimization. In: Proceedings of IEEE international conference on evolutionary computation, New York, USA, pp 786–791
26. Pétrowski A (1996) A clearing procedure as a niching method for genetic algorithms. In: Proceedings of the IEEE international conference on evolutionary computation, New York, USA, pp 798–803
27. Rao RV, Savsani VJ, Vakharia DP (2011) Teaching-learning-based optimization: a novel method for constrained mechanical design optimization problems. Comput Aided Des 43(3):303–315
28. Rao RV, Savsani VJ, Vakharia DP (2012) Teaching-learning-based optimization: an optimization method for continuous non-linear large scale problems. Inf Sci 183:1–15
29. Ray T, Liew KM (2003) Society and civilization: an optimization algorithm based on the simulation of social behaviour. IEEE Trans Evol Comput 7:386–396
30. Sareni B, Krahenbuhl L (1998) Fitness sharing and niching methods revisited. IEEE Trans Evol Comput 2(3):97–106
31. Simon D (2008) Biogeography-based optimization. IEEE Trans Evol Comput 12:702–713
32. Stornand R, Price K (1997) Differential evolution—a simple and efficient heuristic for global optimization over continuous spaces. J Glob Optim 11:341–359
33. Talatahari S, Azar BF, Sheikholeslami R, Gandomi AH (2012) Imperialist competitive algorithm combined with chaos for global optimization. Commun Nonlinear Sci Numer Simul 17(3):1312–1319
34. Yin X, Germay N (1993) A fast genetic algorithm with sharing scheme using cluster analysis methods in multi-modal function optimization. In: Proceedings of the international conference on artificial neural nets and genetic algorithms, pp 450–457

Fault Diagnosis of Ball Bearing Using Walsh–Hadamard Transform and Random Tree Classifier

Vipul Dave and V. Vakharia

Abstract Bearing failure may result in the breakdown of machinery or possibly damage the human being operating the machinery. It is therefore necessary to diagnose bearing faults at an early stage. This paper presents the application of Walsh–Hadamard transform and tree-based classifier for detecting bearing faults. An experimental was conducted from the Case Western Reserve University bearing data center. At the initial stage, coefficients from inner race fault, outer race fault, ball fault, and healthy bearing were calculated from the measured signal. Twenty-five statistical features are calculated from the acquire signals with different speeds and fault sizes. Feature vector form is used for classification purpose using various classifiers, i.e., random tree and logistic model tree. Training and testing of classifier are done, and the result revealed that 100% fault identification accuracy is obtained with random tree for both training and testing. Similarly, 98.43% training and 100% fault identification accuracy are obtained with logistic model tree. The result shows that the methodology adopted is effective to diagnose various bearing faults.

Keywords Logistic model tree · Random tree · Walsh–Hadamard transform

1 Introduction

The rolling element bearings are extensively used rotating component in industrial and domestic applications. The utility of rolling element bearings in rotating machinery is to support load and minimize friction [1]. The dent caused by the rotating elements generates cracks in the components of bearing. Misalignment, insufficient lubrication, friction, corrosion, etc., are some of the sources through which faults are developed in bearing [2]. During maintenance activity, it is observed that the fault in rotating components needs to be identified at the initial stage

V. Dave (✉) · V. Vakharia (✉)
Pandit Deendayal Petroleum University, Gandhinagar 320007, India
e-mail: vipul.dphd16@sot.pdpu.ac.in

V. Vakharia
e-mail: vinay.vakharia@sot.pdpu.ac.in

V. K. Gupta et al. (eds.), *Reliability and Risk Assessment in Engineering*,
Lecture Notes in Mechanical Engineering,
https://doi.org/10.1007/978-981-15-3746-2_34

to avoid the probability of critical failure of machinery [3]. Various methods are used to distinguish fault associated with bearings like infrared thermograph, acoustic emission, wear, vibration, etc. Vibration-based signal processing method for diagnosis of bearing fault is reported by various authors [4, 5]. Various signal processing methods such as time domain, frequency domain (FFT), time–frequency (wavelet) domain are used to detect faults. It is observed that the features extracted from time domain signals are unable to give sufficient information, since these features contain noise. Fourier transform is good for a spectral analysis to determine which frequency components occurred in signal, but at the same time, it will not give information about which time or location a failure occurs. It is difficult to diagnose faults from traditional methods. Wavelet transform and discrete wavelet transform are advance signal processing methods used by many researchers for fault diagnosis of ball bearings [5]. The Hadamard transform, also known as Walsh–Hadamard transform (WHT), is an example of generalized class of Fourier transform. It performs an orthogonal symmetric, involute, linear operation on 2 m real numbers. WHT decomposes a signal into a set of orthogonal, rectangular waves from Walsh function. The Hadamard transform is used by many authors working in data encryption, signal processing and data compression algorithms, etc. The advantage of WHT is fast computation of Walsh–Hadamard coefficients, requires less storage space, and fast signal construction [6]. To identify the type of fault or classification, different pattern recognition methods are applied by various authors [4, 5]. Pattern recognition or artificial intelligence techniques are broadly classified as supervised method and unsupervised method. Support vector machine, artificial neural network, naïve Bayes, and random forest are some of the common methods for fault pattern identification.

In the present paper, Walsh–Hadamard transform (WHT) is used as a signal processing technique for feature extraction from various fault cases of ball bearings. In computational mathematics, fast Walsh–Hadamard transform (FWHTh) is an efficient algorithm to calculate the Walsh–Hadamard transform coefficients. The proposed technique is applied to the Case Western Reserve University (CWRU) bearing data center [7], and faults are identified with the help of random tree classifier.

2 Experimental Procedures and Feature Extraction

The experimental data from the Case Western Reserve University for diagnosis of bearing faults are used to investigate the utility of Walsh–Hadamard transform and random forest. Vibration signals are captured from 6205 ball bearings from drive end of bearing. Schematic diagram shown in Fig. 1 consists of 2HP three-phase induction motor, coupling attached with dynamometer, and torque transducer with accelerometer to measure vibration signals [8]. Faults are seeded into various bearing components utilizing electric discharge machining with variation in fault diameters as 0.1778, 0.3556, 0.5334, and 0.7112 mm, respectively. Fault conditions of bearings considered are healthy bearing (HB), inner race fault (IRF), outer race fault (ORF),

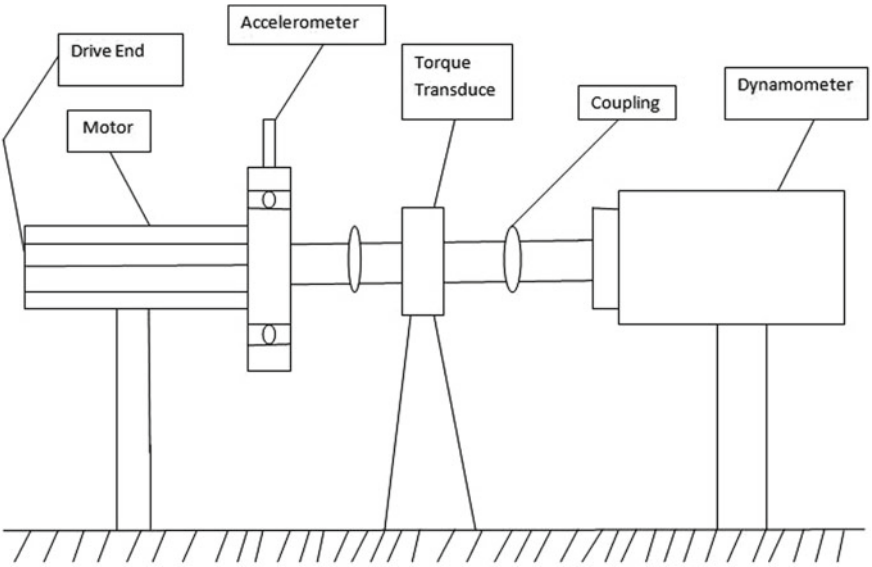

Fig. 1 Schematic diagram of experimental setup

and ball fault (BF). The rotational speed of shaft varied as 1730, 1750, 1772, and 1797 rpm, and the sampling frequency was set to 12 kHz [8] (Fig. 2).

Nonlinearity exists in the vibration signals collected from faulty as well as healthy components of bearings. Possible reasons are frequency modulation due to the existence of shaft, motor, couplings, etc. To detect nonlinearity, some parameters like permutation entropy with wavelet transform were used for detection of faults [1]. Kurtosis, skewness, root mean square, mean value, and Shannon entropy are frequently used features which are calculated from vibration signals [8]. The difficulty that arose from the features extracted from time domain method is that it is unfit to detect faults at an initial stage. Therefore, in the present study, a wide

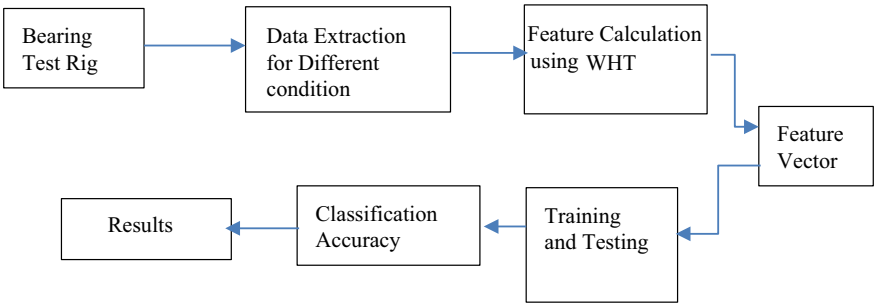

Fig. 2 Ball bearing fault diagnosis methodology

range of statistical features are calculated from the coefficients of Walsh–Hadamard transform. Some features are explained below:

1. Average: It represents the general significance of a set of unequal values.
2. Average deviation: It generally represents dispersion, which is calculated by arithmetic mean of the absolute values of the deviation of the function values from central values.
3. Minimum value: Represent lowest value in signal.
4. Maximum value: Represent highest value in signal.
5. Variance: It is the expectation of the squared deviation of a random variable from its mean.
6. Kurtosis: It is a measure of whether the data are peaked or flat relative to normal distribution.
7. Skewness: It is a measure of the asymmetry of the probability distribution of a real-valued random variable about its mean.

$$\text{Skewness} = \frac{\sum_{i=1}^{n}\left(X_i - \overline{X}\right)^3}{(n-1)s^3} \tag{1}$$

8. Geometric mean: It is defined as the central number in a geometric progression.
9. RMS value: It is the square root of the arithmetic mean of the squares of the original values.
10. Peak value: It is the maximum value of the signal which reaches above a reference value.
11. Crest factor: It is a value obtained after dividing peak value of signal to its RMS value.
12. Form factor: It is a value obtained after dividing RMS value to average value of signal.
13. RSSQ: The root-sum-of-square (RSS) level of a signal X_i is

$$\text{RSSQ} = \sqrt{\sum_{i=1}^{n} |X_i|^2} \tag{2}$$

3 Fault Classification Techniques

3.1 Random Tree

Random tree is a type of supervised learning technique to recognize the condition of machinery component. A random set of data is constructed after employing bagging which is considered as an ensemble of learning algorithm. In random tree, each node

is divided using the best among the subset of predicators, randomly chosen at that node [9]. It can be used for classification and regression. In case of classification, the feature vector is fed as an input to the classifier, classifies it with each potential tree in a set of forest, and generates output in terms of class labels which receives majority of votes.

3.2 Logistic Model Tree

It is a type of supervised learning algorithm that uses the combination of logistic prediction and decision tree with logistic regression functions at the leaves. The goal of supervised algorithm is to optimally determine the subdivision of subspace into the regions labeled with the target class. In principle, logistic model tree (LMT) predicts a numeric value which is defined over a fixed set of attributes. A piecewise linear approximation function is constructed using model trees, and prediction, for instance, is obtained after sorting down to a leaf with numerous iterations until the final decision is obtained.

4 Results and Discussion

In the present paper, random tree and logistic model were used by authors to detect the presence of various bearing faults. Four fault cases are considered, i.e., ORD, IRD, BALL, and HB, respectively. In total, 64 instances and 25 features are considered. Rotor speed varied from 1730 to 1797 rpm. Feature set from extracted statistical features is formed and fed into the tree-based algorithm, for identification of bearing faults. To get an insight about classwise fault identification accuracy, confusion matrix is used. Tables 1, 2, 3 and 4 show the confusion matrix for training and testing using random tree and logistic model tree. Confusion matrix is used to predict individually various bearing faults with the help of random tree and logistic model tree. From Tables 1 and 2, it is evident that since 100% accuracy is achieved, so classwise prediction rate is also 100% with random tree classifier. When logistic model tree is used for training, then it is observed that 100% fault identification is achieved for ORD, BF and HB whereas 94% fault identification is achieved for IRD

Table 1 Confusion matrix with random tree for training

S. No.	ORD	IRD	BF	HB	Identification result
1	28	0	0	0	ORD
2	0	16	0	0	IRD
3	0	0	16	0	BF
4	0	0	0	4	HB

Table 2 Confusion matrix with random tree for testing

S. No.	ORD	IRD	BF	HB	Identification result
1	1	0	0	0	ORD
2	0	2	0	0	IRD
3	0	0	2	0	BF
4	0	0	0	1	HB

Table 3 Confusion matrix with logistic model tree for training

S. No.	ORD	IRD	BF	HB	Identification result
1	28	0	0	0	ORD
2	1	15	0	0	IRD
3	0	0	16	0	BF
4	0	0	0	4	HB

Table 4 Confusion matrix with logistic model tree for testing

S. No.	ORD	IRD	BF	HB	Identification result
1	1	0	0	0	ORD
2	0	2	0	0	IRD
3	0	0	2	0	BF
4	0	0	0	1	HB

as observed from Table 3. Table 4 shows confusion matrix obtained, when LMT is used for testing, and 100% classwise prediction is obtained when 10% features are used for testing purpose. Training and testing results for both classifiers are shown in Fig. 3.

5 Conclusion

This paper proposes methodology to identify bearing faults using WHT fault identification algorithm. Twenty-five statistical features were calculated from Walsh–Hadamard transform coefficients from various bearing fault cases. Training and testing of feature vector were done using classifiers. Results were compared using logistic model tree and random tree classifiers. It was observed from experimental study that 100% percentage split validation accuracy is obtained by using random tree classifier. The methodology proposed is useful for development of online fault diagnosis system.

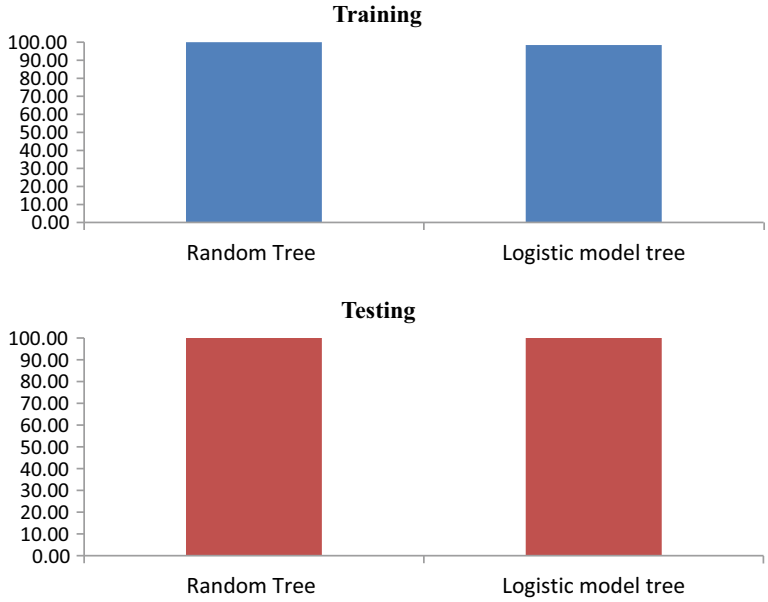

Fig. 3 Training and testing efficiency

Acknowledgements The authors would like to thank the Case Western Reserve University and Professor K. A. Loparo for providing bearing vibration data sets which is used in the present study to detect bearing faults. The authors would like to acknowledge the support of PDPU, Gandhinagar, for providing the infrastructure required for carrying out the study.

References

1. Vakharia V, Gupta VK, Kankar PK (2016) Bearing fault diagnosis using feature ranking methods and fault identification algorithms. Procedia Eng 144:343–350
2. Shah DS, Patel VN (2014) A review of dynamic modeling and fault identifications methods of rolling element bearing. Procedia Technol 14:447–456
3. Azizi R, Attaran B, Hajnayeb A, Ghanbarzadeh A, Changizian M (2017) Improving accuracy of cavitation severity detection in centrifugal pumps using a hybrid feature selection technique. Measurement 108:9–17
4. Kavathekar S, Upadhyaya N, Kankar PK (2016) Fault classification of ball bearing by rotation forest technique. Procedia Technol 23:187–192
5. Vakharia V, Gupta VK, Kankar PK (2015) Ball bearing fault diagnosis using supervised and unsupervised machine learning methods. Int J Acoust Vib 20:244–250
6. Banerjee A, Dutta A (2013) Performance comparison of cosine, haar, walsh hadamard, fourier and wavelet transform for shape based image retrieval using fuzzy similarity measure. Procedia Technol 10:623–627
7. Loparo KA (2017) Bearing vibration data set. Case Western Reserve University, Available at: www.eecs.cwru.edu/laboratory/bearing. Accessed Aug 2017

8. Vakharia V, Gupta VK, Kankar PK (2017) Efficient fault diagnosis of ball bearing using Relief and Random Forest classifier. J Braz Soc Mech Sci Eng 39(8):2969–2982
9. Yıldırım P (2016) Pattern classification with imbalanced and multiclass data for the prediction of albendazole adverse event out-comes. Procedia Comput Sci 83:1013–1018

Air Engine Efficiency Improvement Using Control System

N. J. Chotai, Vimal Savsani, and Vivek Patel

Abstract Current research of compressed air-powered engine is mainly focused on air engine system, its simulation and mathematical model of power calculations. However, concentration on efficiency improvement is narrow which restricts the use of renewable powered air engine in the automobile industry. Compressed air-powered air engine is modified from the conventional four-stroke engine. Fast switching valve takes the position of cam mechanism and works to source and exhaust compressed air. Expansion of compressed air makes possible to get output torque by pushing the piston in the cylinder. In this paper, a new approach is pointed to overall efficiency improvement of air engine using control systems. Control system predicts exhaust pressure at every degree rotation of crank and consequently gives feedback to intake port to close supply of compressed air which restricts the flow of uncompressed air at exhaust port which argues in efficiency improvement.

Keywords Air engine · Air engine efficiency · Air engine flow chart · Controller of air engine · Predicted exhaust pressure

1 Introduction

Use of compressed air is not limited to transportation even great future in the field of temporal energy stored system without toxic wastage. Compressed air energy storage (CAES) is used as a secondary source of the backup power system, and

N. J. Chotai
Department of Mechanical Engineering, Marwadi Education Foundation Group of Institutions, Rajkot, India
e-mail: nikhil.chotai@gmail.com

V. Savsani · V. Patel (✉)
Department of Mechanical Engineering, Pandit Deendayal Petroleum University, Raysan, Gandhinagar, Gujarat, India
e-mail: viveksaparia@gmail.com

V. Savsani
e-mail: vimal.savsani@gmail.com

V. K. Gupta et al. (eds.), *Reliability and Risk Assessment in Engineering*,
Lecture Notes in Mechanical Engineering,
https://doi.org/10.1007/978-981-15-3746-2_35

storing compressed air at 30 MPa and at a power rating of 2 kw gives less maintenance system for 30 years [1]. Air engine will become the heart of future local transportation owed for low emission, zero pollution and answer of fossil fuel crisis at stipulation of efficiency improvement of compressed air engine. A convention four-stroke petrol engine converted into a two-stroke engine, changing camshaft gear system and having an equal rotation of crankshaft and camshaft. Fast switching valve reduces the power loss in friction leads to higher efficiency. In this camless compressed air engine, 15% of power reduction is achieved [2].

Pulse width modulation (PWM) technique-based valve switching time is about 4.5 ms at 460 l/min flow rate as a replacement for same for high switching time of 3.5 ms at a flow rate of 400 l/min with the integrated electronic circuit in valve is utilized to meet high rotation of camshaft [3]. Presented designed circuit with 3/2 direction control valve enables to control engine inlet and outlet port at high frequency and to operate engine at high speed.

2 Working System of Air Engine Section

Controlled air engine system is shown in Fig. 1. Working model of air engine rotary encoder is used to measure crank angle rotation, later used to measure real-time cylinder instantons volume. High-frequency pressure sensor to measure min pressure

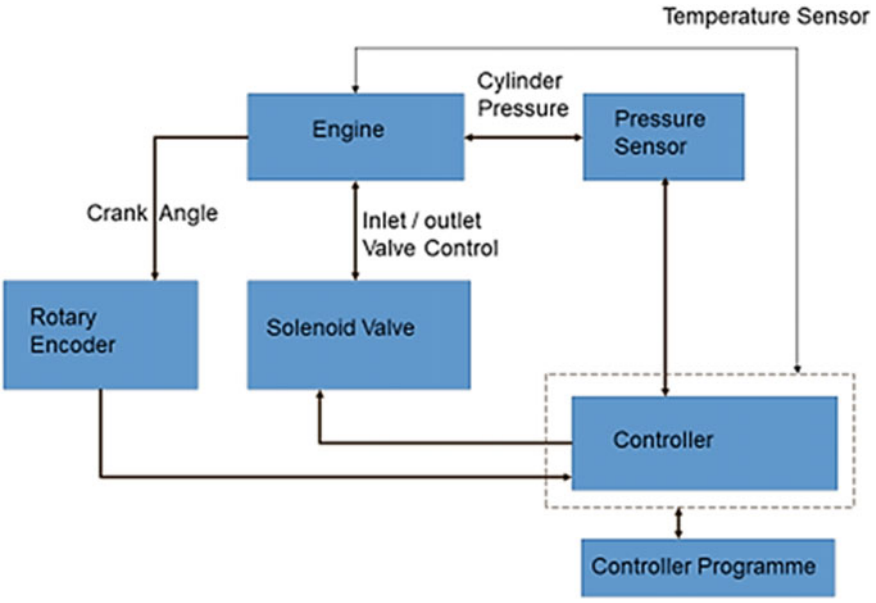

Fig. 1 Controlled air engine system

in the cylinder and temperature sensor are used at compressed air inlet port and at exhaust port to catch real-time polytropic index of the process.

Controller with high frequency is realistic to control the switching of the solenoid valve. In a conventional camless engine, power is supplied to solenoid to open it between 0° to 180° of crank angle. Same time exhaust port will have no active condition. Just after crank of 180°, exhaust port will open up to 360°. This may leads to loss of air power in terms of higher exhaust pressure. To overcome these losses, controller with exhaust pressure prediction system came in the picture (Fig. 2).

Prediction of exhaust air pressure is governed by laws of thermodynamics and the structural equation of piston, connecting rod and crankshaft. In compressible flow, exact relation between pressure and specific volume is required. Here, exhaust air flow process is considered polytropic and obeys relations as below:

$$PV^n = \text{Constant} \tag{1}$$

Compressed air expands in cylinder and exhausts from the outlet port, and considering this process as polytropic process and using geometrical parameters of engine, instantaneous volume is calculated, and finally, exhaust air predicted pressure is predicted at every moment using following equation [4]:

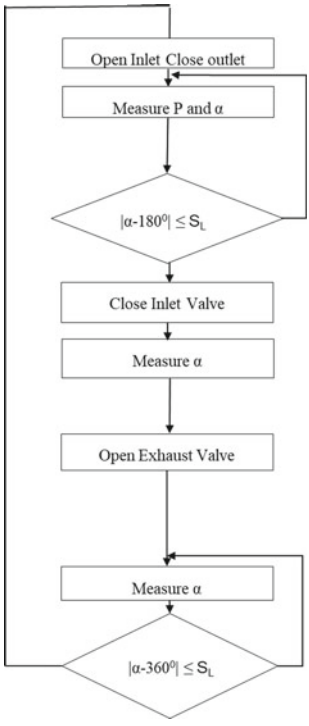

Fig. 2 Flow chart of the ideal air engine

$$P_{2e} = P_1\left[\frac{r}{S_{\text{Length}}}\left\{1 - \cos\phi + \frac{1}{\lambda}\left(1 - \sqrt{1 - \lambda^2 \sin^2\phi}\right)\right\}\right]^n \tag{2}$$

where r is the crank radius, S_{Length} is the stroke length and L is the length of connecting rod, and these all are the geometric parameters of the engine. The geometrical relationship of the piston, connecting rod and crank angle is shown in Fig. 3.

The controller working is described using flow chart in Fig. 4. At an initial condition, inlet valve and outlet valve are in closed conditions. Once the power supply is on, controller gets instantaneous feedback of pressure (P_1) and crank angle (α) and controls the solenoid valve. At 0° of crankshaft, inlet valve switches the position of port and allows the compressed air to enter into the cylinder from a supply tank. Threshold limit (T_{RL}), which is decided considering the delay of sensors and atmospheric pressure, predicted exhaust pressure (P_{2e}) is calculated at every degree rotation of the shaft. Once predicted pressure exceeds the limit, the controller passes the signals and cut off the power supply of inlet solenoid valve and inlet valve closes. Further on crankshaft rotation angle feedback outlet valve be active and switching of port allowed to exhaust air to the atmosphere after 180° of the crankshaft. Thus, the loss of energy in terms of higher exhaust pressure is restricted. Sensor limit (S_L) is the range helps to give sufficient time to control and operate solenoid valve.

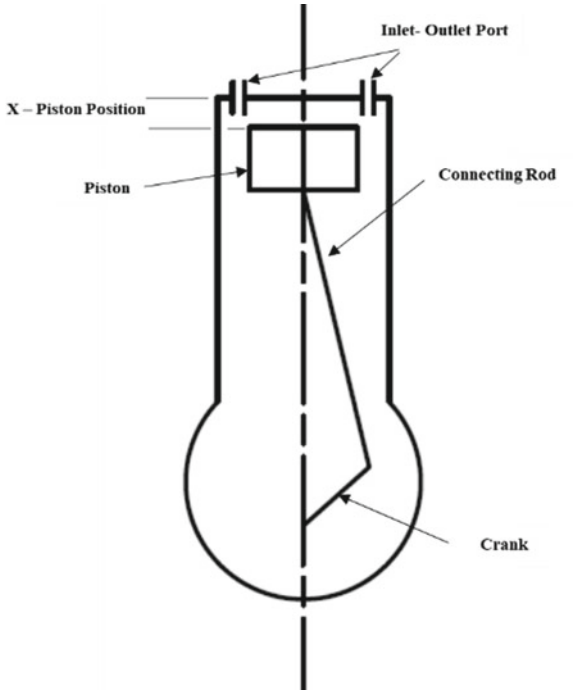

Fig. 3 Geometric relationship of piston displacement and crank angle

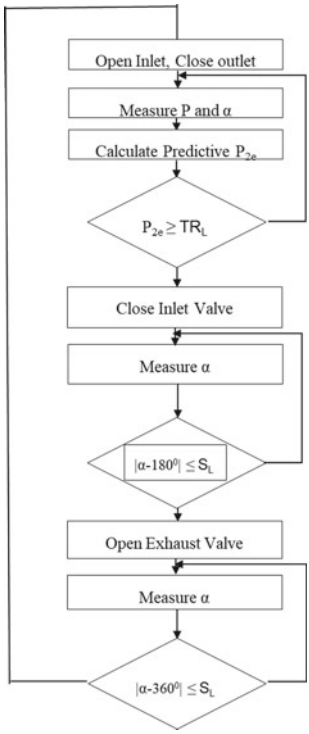

Fig. 4 Flow chart of predicted pressure controlled air engine

3 Mathematical Model

A mathematical model is based on the mass flow of compressed air enters into the engine and expands into the cylinder and gives force to head of piston to move them downwards which rotates the crank, and due to inertia force, piston moves back upward and air flow outs from exhaust point.

To simplify the research, there are some assumptions are made as follows:

1. Ideal gas laws are applied to working air.
2. Assumed that there is no heat transfer through cylinder wall and there is no leakage.
3. The flow of air into the cylinder, and outflow is one dimensional.
4. There is no friction between the piston, piston ring and cylinder.

3.1 Input Power

Supplied compressed air power is a function of flow rate and pressure difference at supply point and cylinder mean pressure as follows.

$$\text{Power}_{in} = Q * \Delta P \tag{3}$$

where

$$\Delta P = P_{in} - P_c \tag{4}$$

where Q is flow rate measure using air flow sensor and P_{in} is the compressed air supply pressure and P_c is the cylinder instantaneous pressure.

3.2 Output Power

Mechanical output power can be derived from output torque and rotational speed as well can be derived from PV diagram of actual cycle also.

3.3 Efficiency of Air Engine

Engine efficiency is the ratio of output shaft power to input power in terms of compressed air flow and pressure difference (ΔP) [5].

$$n = \frac{T * w}{Q * \Delta P} \tag{5}$$

4 Solenoid Valve Diagram to Meet High-Frequency Operation

Here, in pneumatic circuit, 3/3 solenoid valve is required, and its availability with high frequency is rare. 3/3 solenoid valve requirement is solved by using two 2/2 high-frequency valve as shown in Fig. 5. Pneumatic diagram of 3/2 solenoid valve using two DCV valve is shown in Fig. 5.

5 Result

Predicted pressure controller flow chart presented in Fig. 4 describes the mechanism of control system to control compressed air flow through inlet valve according to

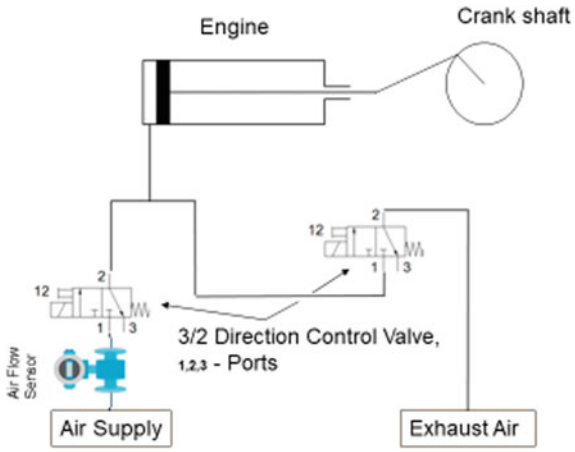

Fig. 5 Pneumatic diagram of 3/2 solenoid valve using two DCV valve

predicted exhaust pressure losses calculated from the feedback of piston position and mean pressure. Pneumatic circuit diagram labelled in Fig. 5 describes methodology achieves high operational speed of engine.

6 Discussion

Controller flow charts support to design controller and experimental setup and to examine the engine output parameters. Optimization of system and parameters are important to increase effectiveness, but efficient fundamental design improves overall efficiency of systems. Though this design requires high-frequency sensors and feedback system with a controller, it helps to increase the practicality of air engine.

7 Conclusions

Based on mathematical model of air engine efficiency and working principle, core controlling parameters are identified, and controller system is designed to reduce exhaust compressed air energy loss. This research report has introduced an approach of the efficient environmental-friendly engine system.

Acknowledgements This research was supported by Marwadi Education Foundation Group of Institutions and Pandit Deendayal Petroleum University. We thank our colleagues from MEFGI who provided insight and expertize that greatly assisted the research.

References

1. Zhang X, Xu Y, Xu J, Xue H, Chen H (2016) Study of a single-valve reciprocating expander. J Energy Inst 89(3):400–413
2. Wong VW, Tung SC (2016) Overview of automotive engine friction and reduction trends–Effects of surface, material, and lubricant-additive technologies. Friction 4(1):1–28
3. Topçu EE, Yüksel I, Kamiş Z (2006) Development of electro-pneumatic fast switching valve and investigation of its characteristics. Mechatronics 16(6):365–378
4. Song R, Fu X, Cai M (2013) Non-dimensional modeling and simulation analysis of air powered engine. 280:307–314
5. Yu Q, Cai M, Shi Y, Yuan C (2015) Dimensionless study on efficiency and speed characteristics of a compressed air engine. J Energy Resour Technol 137:(4)

Parametric Analysis of Genetic Algorithm Toolbox for Truss Problem Optimization

Akash Vasani, Rhythm Patel, Vimal Savsani, and Poonam Savsani

Abstract Genetic algorithms (GA) are powerful and efficient methods of evolutionary optimization algorithms which conduct search and optimization based on the Darwinian principles of natural genetics and natural selection. They have been extensively used in the recent past for optimization problems of the truss structures. However, for obtaining the best and robust solutions, it is necessary to choose proper GA operators depending upon the type and complexity of the problem. In this research study, genetic algorithm toolbox of MATLAB is used for the optimizing truss structures. The stress and deflections in various members of the truss are obtained using commercially available FEA software ANSYS. An interface has been established between MATLAB and ANSYS for parametric modelling of the problem. The GA operators tested are selection functions, crossover functions and mutation functions. We made use of five selections functions, six crossover functions and three mutation functions to find best set of combination which can be used further for optimization of truss structure.

Keywords ANSYS · Genetic algorithm · MATLAB · Optimization · Truss

1 Introduction

Truss optimization has become a prominent field in the structural optimization due its exhaustive use in the engineering applications. It can be broadly classified into size, shape and topology optimization. Size optimization aims to find out the optimum cross-sectional areas of the truss structure [1], whereas shape optimization works on changing the nodal position of the truss structure, to find the best possible solution [2]. In topology optimization, the nodes and the elements get added or removed to find out the best possible topology of the structure [3, 4]. In the last three decades, there has been great contribution by various researchers around the globe towards

A. Vasani (✉) · R. Patel · V. Savsani · P. Savsani
Department of Mechanical Engineering, Pandit Deendayal Petroleum University, Gandhinagar, Gujarat 382007, India
e-mail: vasani.akash5@gmail.com

V. K. Gupta et al. (eds.), *Reliability and Risk Assessment in Engineering*,
Lecture Notes in Mechanical Engineering,
https://doi.org/10.1007/978-981-15-3746-2_36

the development of an efficient optimization method for size, shape and topology optimization.

Tanskanen [5, 6] has proposed a two-stage optimization process. In the first stage, optimization of truss structures is carried out for optimum topology. In the second stage, optimized topology obtained in the previous stage is further optimized for size problem. But Zhou et al. [7] said the results obtained are of questionable nature, as the topology obtained in the first stage may not be favourable after size optimization process. Hence, the best solution can be obtained by combining the two stages into a single stage and performing simultaneous optimization of topology and size.

Topping proposed the ground structure method for the topology optimization [8]. Ground structure is a structure with all the nodes and possible members connected between any two nodes. Topology optimization problem is generally a combinatorial problem with 0–1 variables for the presence of different members. The members with vanishing cross-sectional area correspond to 0, which essentially means the member is absent in the resulting structure. Variable value of 1 indicates the presence of the member. Hence, the optimal structure is found for continuous area variables and members with cross-sectional areas less than the specified critical area ε are removed in the resulting topology. Shrestha and Ghaboussi [9] proposed physical design space methodology which is free from ground structure; however, this method requires huge computational work.

In this research study, parametric analysis for the various GA operators is carried out for the topology optimization of the benchmark 6 node, 11 bar truss problem. Ground structure method has been used for the topology optimization. The FEA analysis of each newly generated truss structure by the GA is done on the ANSYS module. In a truss structure, some nodes are necessary and must exist in the design of truss structures. These nodes are known as basic nodes and are usually supplied by the designer as an input during initial phase. Hence, the optimization process is used to find which members of the truss should be present and its cross-sectional areas to minimize the weight of the overall structure under the various constraints (usually maximum stress and maximum displacement constraints).

2 Problem Formulation

With the above-mentioned procedure, the formulation of optimization problem is as given below:

$$\text{minimize } f(A) = \sum_{j=1}^{m} \rho_j A_j l_j \tag{1}$$

Subject to

G1 Truss is acceptable and does not violate any basic node violation
G2 Truss is not a mechanism

G3 Truss is kinematically stable
G4 $S_j - \sigma_j(A) \geq 0, \ \ j = 1, 2, 3, \ldots, m$
G5 $\delta_j^{\max} - \delta_j(A) \geq 0, \ \ j = 1, 2, 3, \ldots, m.$

where,

ρ Density of the material,
A Area of the member,
l Length of the member,
S_j Allowable strength in jth member,
$\delta_j^{\max}$ Allowable deflection in jth member.

The weight of the overall structure is taken as the objective function in this work. The constraints are explained in detail as below:

Constraint G1. In this constraint, the truss is checked for the absence of the basic nodes specified by the user. If any of the basic nodes are absent, then a large penalty is assigned to the solution and no further calculation of objective function and constraints is done.
Constraint G2. In this constraint, the truss is checked if it is a mechanism or not according to the Grubler's criterion: [10]

$$\text{Degree-of-freedom} = 2n - m - nl \tag{2}$$

If the corresponding DOF is non-positive, the corresponding truss is not a mechanism. If the truss is a mechanism, then a large penalty is assigned with no further calculation of objective function and constraints.
Constraint G3. In this constraint, the truss is checked for kinematic stability by checking for the positive definiteness of the stiffness matrix. If the matrix is not positive definite, then a large penalty is assigned to the solution with no further calculation of objective function and constraints.
Constraint G4. In this constraint, the truss is checked for any maximum stress violation in any member. A maximum allowable strength is predefined and the maximum stress value generated in any member should be within the permissible limit.
Constraint G5. In this constraint, the truss is checked for any maximum displacement violation in any member. A maximum allowable displacement is predefined and the maximum displacement value generated in any member should be within the permissible limit.

Hence, the objective function in our problem becomes:

$$f(A) = \sum_{j=1}^{m} \rho_j A_j l_j + \text{penalty}, \tag{3}$$

where,

$$\text{penalty} = \begin{cases} 10^9, & \text{if G1 is violated} \\ 10^8, & \text{if G2 is violated} \\ 10^7, & \text{if G3 is violated} \\ 10^6, & \text{if G4 or G5 is violated} \\ 0, & \text{otherwise} \end{cases}$$

2.1 Optimization Method

The above-mentioned problem formulation has been used to develop the following algorithm as shown in Fig. 1.

2.1.1 6 Node, 11 Bar Benchmark Truss Problem

The 6 node, 11 bar truss of Fig. 1 is a commonly used benchmark. The truss is composed of aluminium, with a Young's modulus of 68.9 GPa (104 ksi). Density is taken to be 2700 kg/m^3 (0.1 lb/in^3). The static loads P1 and P2 have a nominal value of 444.8 kN (100 kip). The design variables, represented by genes, are the areas of each member. The problem is to minimize the total weight of the truss without violating any constraint. Constraints are imposed on member stresses that may not exceed 172.4 MPa (25 ksi). The allowable limits for stresses are set for both tension and compression. The allowable maximum deflection in both horizontal and vertical directions is 0.0508 m (2 in). The search range for the design variables is limited to between -0.0225806 m^2 (-35 in^2) and 0.0225806 m^2 (35 in^2) (Fig. 2).

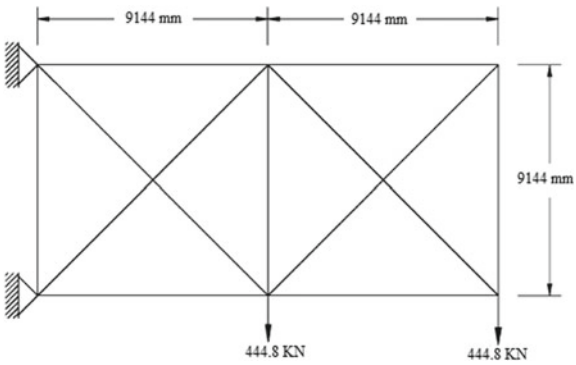

Fig. 1 6 node, 11 bar truss problem

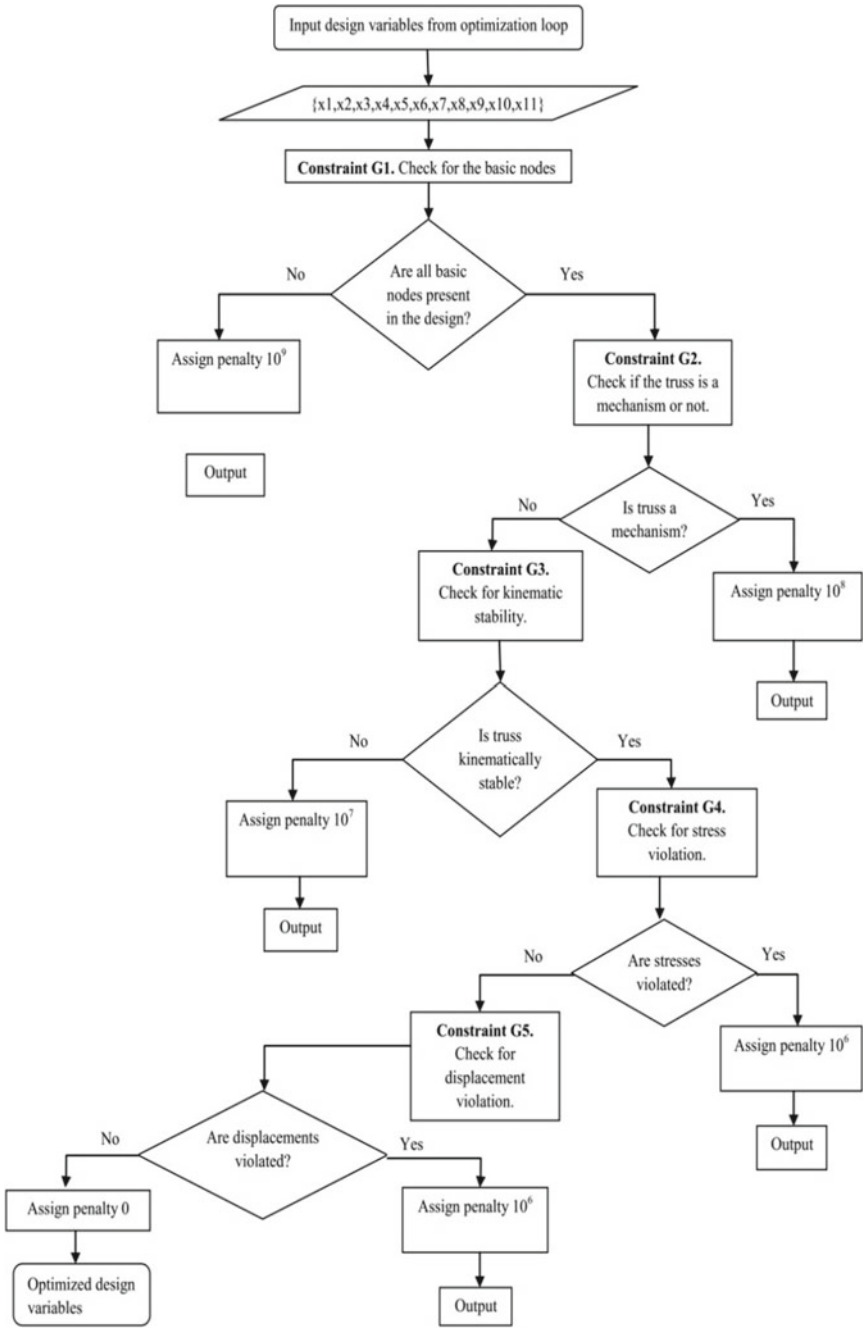

Fig. 2 Flowchart of the problem design

3 Results and Discussion

3.1 Parametric Analysis of GA Toolbox of MATLAB

A parametric analysis was done for the 6 node, 11 bar truss problem. As the result of a genetic algorithm largely depends upon the genetic parameters, the solution process was explored using various parameters of GA toolbox of MATLAB as stated below:

- Selection functions: Remainder, Roulette, Stochastic Uniform, Tournament, Uniform
- Crossover functions: Arithmetic, Heuristic, Intermediate, Scattered, Single point, Two point
- Mutation function: Adaptive, Feasible, Gaussian, Uniform.

The population size was defined to be 200 and maximum generations were limited to 200. So $5 \times 6 \times 3 = 90$ different sets of genetic operators were explored. For each set of genetic parameter, a total of 30 independent solutions were obtained. So, in total of $5 \times 6 \times 3 \times 30 = 2700$ independent computational experiments were executed in total. The results are as shown in Table 1 and the optimal topology obtained is as shown in Fig. 3.

The fifth column of the above table comprises the mean of all the best values obtained from 30 independent solutions for each set of genetic operators. From the above table and graph, the following points could be concluded:

1. The best optimal result is 2169.152347 kg and was obtained for index number 13.

   Mutation Function: Adaptive Feasible
   Selection Function: Stochastic Uniform
   Crossover Function: Intermediate

2. The worst result is 235129.5965 kg and was obtained for index number 83.

   Mutation Function: Uniform
   Selection Function: Stochastic uniform
   Crossover Function: Singlepoint

3. The highly abnormal values were obtained for the combinations corresponding to the index number 25, 81, 83, 84 and 85.
4. The result obtained with default function parameters of MATLAB's GA toolbox is 2182.492441 kg. This is 0.6% greater than the best value obtained.

Table 1 Result of parametric analysis

Index No.	Mutation	Crossover	Selection	Mean of best values (kg)
1	Aptfeasible	Arithmetic	Remainder	2335.977393
2	Aptfeasible	Arithmetic	Roulette	2375.773176
3	Aptfeasible	Arithmetic	Stochunif	2361.212611
4	Aptfeasible	Arithmetic	Tournament	2359.145486
5	Aptfeasible	Arithmetic	Uniform	3060.098838
6	Aptfeasible	Heuristic	Remainder	2241.984033
7	Aptfeasible	Heuristic	Roulette	2170.674065
8	Aptfeasible	Heuristic	Stochunif	2241.984033
9	Aptfeasible	Heuristic	Tournament	2170.674065
10	Aptfeasible	Heuristic	Uniform	2217.688998
11	Aptfeasible	Intermediate	Remainder	2170.332789
12	Aptfeasible	Intermediate	Roulette	2527.539719
13	Aptfeasible	Intermediate	Stochunif	2169.152347
14	Aptfeasible	Intermediate	Tournament	2241.984033
15	Aptfeasible	Intermediate	Uniform	3197.406243
16	Aptfeasible	Scattered	Remainder	2212.090382
17	Aptfeasible	Scattered	Roulette	2173.9935
18	Aptfeasible	Scattered	Stochunif	2182.492441
19	Aptfeasible	Scattered	Tournament	2185.879516
20	Aptfeasible	Scattered	Uniform	2300.721589
21	Aptfeasible	Singlepoint	Remainder	2207.557924
22	Aptfeasible	Singlepoint	Roulette	2187.091508
23	Aptfeasible	Singlepoint	Stochunif	2197.403123
24	Aptfeasible	Singlepoint	Tournament	2337.321335
25	Aptfeasible	Singlepoint	Uniform	102135.1424
26	Aptfeasible	Twopoint	Remainder	2202.232115
27	Aptfeasible	Twopoint	Roulette	2206.431925
28	Aptfeasible	Twopoint	Stochunif	2188.258825
29	Aptfeasible	Twopoint	Tournament	2279.891651
30	Aptfeasible	Twopoint	Uniform	2294.258332
31	Gaussian	Arithmetic	Remainder	2256.267465
32	Gaussian	Arithmetic	Roulette	2248.904153
33	Gaussian	Arithmetic	Stochunif	2188.593799
34	Gaussian	Arithmetic	Tournament	2370.45642
35	Gaussian	Arithmetic	Uniform	2277.789763
36	Gaussian	Heuristic	Remainder	2253.703868

(continued)

Table 1 (continued)

Index No.	Mutation	Crossover	Selection	Mean of best values (kg)
37	Gaussian	Heuristic	Roulette	2277.441962
38	Gaussian	Heuristic	Stochunif	2284.411564
39	Gaussian	Heuristic	Tournament	2180.454458
40	Gaussian	Heuristic	Uniform	2201.335285
41	Gaussian	Intermediate	Remainder	2253.163686
42	Gaussian	Intermediate	Roulette	2229.125188
43	Gaussian	Intermediate	Stochunif	2192.022899
44	Gaussian	Intermediate	Tournament	2194.069054
45	Gaussian	Intermediate	Uniform	2219.942303
46	Gaussian	Scattered	Remainder	2173.201619
47	Gaussian	Scattered	Roulette	2171.028885
48	Gaussian	Scattered	Stochunif	2184.692812
49	Gaussian	Scattered	Tournament	2176.96753
50	Gaussian	Scattered	Uniform	2279.169122
51	Gaussian	Singlepoint	Remainder	2238.093666
52	Gaussian	Singlepoint	Roulette	2208.260453
53	Gaussian	Singlepoint	Stochunif	2214.742561
54	Gaussian	Singlepoint	Tournament	2206.155043
55	Gaussian	Singlepoint	Uniform	2248.181175
56	Gaussian	Twopoint	Remainder	2233.360569
57	Gaussian	Twopoint	Roulette	2176.761126
58	Gaussian	Twopoint	Stochunif	2217.749378
59	Gaussian	Twopoint	Tournament	2176.658823
60	Gaussian	Twopoint	Uniform	2235.263076
61	Uniform	Arithmetic	Remainder	2207.124526
62	Uniform	Arithmetic	Roulette	2613.109208
63	Uniform	Arithmetic	Stochunif	2301.945792
64	Uniform	Arithmetic	Tournament	2257.470938
65	Uniform	Arithmetic	Uniform	2677.763911
66	Uniform	Heuristic	Remainder	2617.396577
67	Uniform	Heuristic	Roulette	2218.677152
68	Uniform	Heuristic	Stochunif	2302.96692
69	Uniform	Heuristic	Tournament	2229.188136
70	Uniform	Heuristic	Uniform	2212.906478
71	Uniform	Intermediate	Remainder	2251.2366
72	Uniform	Intermediate	Roulette	2224.274069

(continued)

Table 1 (continued)

Index No.	Mutation	Crossover	Selection	Mean of best values (kg)
73	Uniform	Intermediate	Stochunif	2242.932177
74	Uniform	Intermediate	Tournament	2227.142132
75	Uniform	Intermediate	Uniform	2349.502868
76	Uniform	Scattered	Remainder	2211.485658
77	Uniform	Scattered	Roulette	2230.442502
78	Uniform	Scattered	Stochunif	2230.601051
79	Uniform	Scattered	Tournament	2270.948136
80	Uniform	Scattered	Uniform	2206.090807
81	Uniform	Singlepoint	Remainder	68875.24851
82	Uniform	Singlepoint	Roulette	2361.459114
83	Uniform	Singlepoint	Stochunif	235129.5965
84	Uniform	Singlepoint	Tournament	35580.23513
85	Uniform	Singlepoint	Uniform	35636.00405
86	Uniform	Twopoint	Remainder	2266.182203
87	Uniform	Twopoint	Roulette	2289.12485
88	Uniform	Twopoint	Stochunif	2289.365256
89	Uniform	Twopoint	Tournament	2242.932177
90	Uniform	Twopoint	Uniform	2381.053098

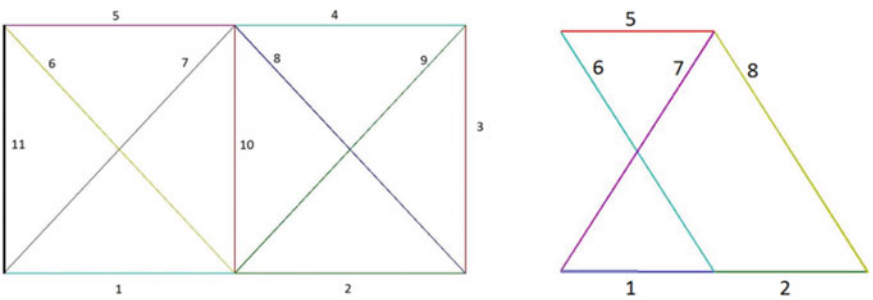

Fig. 3 Optimal topology obtained

4 Conclusion

During this study, we identified a research gap in Truss Topology Optimization problem using genetic algorithm. No previous work on parametric analysis of built in functions of MATLAB's GA Toolbox has been reported. In this study, we have carried out a detailed analysis of the same and following conclusions were drawn out from the study.

- The best result was obtained for Adaptive Feasible, Stochastic Uniform and intermediate of Mutation, Selection and Crossover function, respectively.
- The worst solution was obtained for Uniform, Single point and Stochastic Uniform of Mutation, Selection and Crossover function, respectively.
- The default values of Mutation, Selection and Crossover function in MATLAB's GA toolbox gives fairly satisfactory results when compared to the best combination.

References

1. Goldberg DE, Samtani MP (1986) Engineering optimization via genetic algorithms. In: Proceedings of the ninth conference on electronic computations, ASCE, Birmingham, Alabama, pp 471–482
2. Imai K, Schmith LA (1981) Configuration optimization of trusses. J Struct Div ASCE 107:745–756
3. Krish U (1989) Optimal topologies of truss structures. Comput Methods Appl Mech Eng 72:15–28
4. Ringertz UT (1985) On topology optimization of trusses. Eng Optim 9:209–218
5. Tanskanen P (2006) A multiobjective and fixed elements based modification of the evolutionary structural optimization method. Comput Methods Appl Mech Eng 196(1–3):76–90
6. Tanskanen P (2002) The evolutionary structural optimization method: theoretical aspects. Comput Methods Appl Mech Eng 191(47–48):5485–5498
7. Zhou M, Pagaldipti N, Thomas HL, Shyy YK (2004) An integrated approach to topology, sizing and shape optimization. Struct Multidiscip Optim 26(5):308–317
8. Topping BHV (1992) In shape and layout optimization of structural systems and optimality criteria methods. Math Program Tech Shape Optim Skelet Struct, 349–375
9. Shrestha SM, Ghaboussi J (1998) Evolution of optimum structural shapes using genetic algorithm. J Struct Eng ASCE 124(11):1331–1338
10. Ghosh A, Mallik AK (1988) Theory of mechanisms and machines. Affiliated East-West Press, New Delhi

An Industrial Heat Exchanger Optimization from Economic View Point

B. D. Raja, Jaydeep Patel, and Vivek Patel

Abstract This study explores the application of heat transfer search (HTS) algorithm, a recently developed advanced optimization technique, for design optimization of an industrial shell and tube heat exchangers from economic viewpoint. Minimization of total annual cost is considered as an objective function, and eleven design variables are considered for optimization. Pressure drop, tube-side flow velocity and length of the heat exchanger to shell diameter ratio constraints are included in the procedure. Reliability and maintenance due to fouling are also taken into account. A case study is also presented to demonstrate the effectiveness and accuracy of the proposed algorithm. The results of optimization obtained using HTS algorithm is compared with those obtained by using other optimization algorithms.

Keywords Genetic algorithm · Heat transfer search algorithm · Optimization · Particle swarm optimization · Shell and tube heat exchanger

1 Introduction

Heat exchangers are used in industrial process to recover heat between two process fluids. Shell and tube heat exchanger (STHE) is the most widely used heat exchangers in refineries, petrochemical industries, power generation, refrigeration, HVAC and medical applications because of their adaptability to different operating conditions [1–3]. Design optimization of STHE requires an integrated understanding of thermodynamics, fluid dynamics and cost estimation [4, 5]. Generally, objectives involved in the design optimization of STHE are focused on economic aspects (i.e., minimum cost, minimum pressure drop, minimum weight, maximum heat transfer rate). The industrial design of STHE includes the knowledge of thermodynamics, fluid dynamics, cost estimation and optimization [6]. The conventional design

B. D. Raja
INDUS University, Ahmedabad, Gujarat, India

J. Patel · V. Patel (✉)
Pandit Deendayal Petroleum University, Gandhinagar, Gujarat, India
e-mail: viveksaparia@gmail.com

V. K. Gupta et al. (eds.), *Reliability and Risk Assessment in Engineering*,
Lecture Notes in Mechanical Engineering,
https://doi.org/10.1007/978-981-15-3746-2_37

approach for STHE is time-consuming and does not guarantee an optimal solution. Hence, the application of evolutionary and swarm intelligence-based algorithms has gained much attention in the design optimization of STHE.

Previously, several investigators had used different optimization techniques with different methodologies and objective functions to optimize STHE. Mohanty [7] applied gravitational search algorithm for economic optimization of STHE. The author focuses on optimization of the total annual cost of STHE. Wong et al. [8] carried out the optimization of capital cost and operating cost of STHE by adapting NSGA-II. Amin and Bazargan [9] optimized eleven design variables of STHE for maximum heat transfer rate and minimum total cost of the heat exchanger by using genetic algorithm. Hadidi and Nazari [10] solved three case studies of STHE for cost minimization of heat exchanger. The authors employed biogeography-based optimization (BBO) in their optimization investigation. Rao and Patel [11] applied modified teaching learning-based optimization algorithm for the optimization of heat transfer rate and total cost of the STHE. Wen et al. [12] optimized the heat transfer rate and total cost of the helical baffle STHE. The authors also demonstrated the comparison between optimized and conventional STHE design. Hajabdollahi et al. [13] employed genetic algorithm for economic optimization of STHE. The authors considered nine design variables of STHE in their optimization investigation. Khosravi et al. [14] investigatesd the performance of three different evolutionary algorithms for economic optimization of STHE. Selbas et al. [4] used genetic algorithm for minimization of the total cost of STHE with pressure drop constraint. Ozcelik [15] proposed mixed-integer nonlinear programming problem of STHE and applied genetic algorithm for minimization of capital cost and exergetic cost of STHE. Wildi-Tremblay and Gosselin [16] optimized total cost of heat exchanger with maintenance consideration by adapting genetic algorithm. Rao and Patel [17] used particle swarm optimization and civilized swarm optimization for the economic optimization of shell and tube heat exchanges. Caputo et al. [18] carried out heat exchanger design, based on economic optimization using genetic algorithm. Caputo et al. [19] carried out comparison between actual installed heat exchangers, designed resorting to a leading commercial software tool and the corresponding equipment configurations obtained by a genetic algorithm-based software tool, developed for optimal heat exchangers design. Several other investigators [17, 20, 21] used different strategies for various objectives to optimize shell and tube heat exchanger design.

The main objectives of this study are to optimize the influential parameter of STHE from economic point of view using recently developed heat transfer search (HTS) algorithm. The ability of the considered algorithm is demonstrated using a case study. The results obtained using the HTS are compared with those obtained by using genetic algorithm (GA), particle swarm optimization (PSO) and civilized swarm optimization (CSO) for the same case study.

2 Mathematical Modeling of Shell and Tube Heat Exchanger

Evolution of heat exchanger performance in the present work is based on Bell-Delaware method. Moreover, the attention is also given to classical straight tubes with fixed tube sheet heat exchanger (TEMA E).

2.1 Tube-Side Heat Transfer and Pressure Drop

The tube-side heat transfer coefficient (h_t) is computed from following correlation,

$$h_t = 0.024 \frac{k_t}{d_i} \mathrm{Re}_t^{0.8} \mathrm{Pr}_t^{0.4} \left(\frac{\mu_t}{\mu_w} \right)^{0.14} \quad \text{For } 2500 \leq \mathrm{Re}_t \leq 1.24 \times 10^5 \tag{1}$$

Tube-side pressure drop includes distributed pressure drop along the tube length and concentrated pressure losses in elbows and in the inlet and outlet nozzle [1].

$$\Delta P_t = \frac{\rho_t v_t^2}{2} \left(\frac{L}{d_i} f_t + p \right) N_p \tag{2}$$

Constant p is given different values by different authors. Kern [1] suggested $p = 4$, and the same value is utilized in the present work.

2.2 Shell-Side Heat Transfer and Pressure Drop

The present work relies on Bell-Delaware method for the calculation of the shell-side heat transfer coefficient h_s. In this method, an ideal heat transfer coefficient h_i is determined and corrected by correction factors to take into consideration the shell geometry and various leakage and bypass streams [3].

$$h_s = h_i J_c J_l J_b J_s J_r \tag{3}$$

$$h_i = j C_{ps} \mathrm{Pr}_s^{-2/3} A_{o,cr}^{-1} \tag{4}$$

where j is the Colburn factor and $A_{o,cr}$ is the flow area at or near the shell centerline for one cross-flow section. A curve-fit correlation is available to compute the values of j.

As per Bell-Delaware method, shell-side pressure drop is given by [3],

$$\Delta P_s = \left[(N_b - 1)\Delta P_b \gamma_b + N_b \Delta P_w\right]\gamma_0 + 2\Delta P_b \left(1 + \frac{N_{r,cw}}{N_{r,cc}}\right)\gamma_b \gamma_s \tag{5}$$

where $N_{r,cw}$ is the number of effective tube rows in cross-flow in the window section. $N_{r,cc}$ is the effective number of tube rows crossed. ΔP_b is the ideal pressure drop in the central section. ΔP_w is the pressure drop associated with an ideal one window section.

2.3 Cost Estimation

Total cost C_{tot} of a heat exchanger can be seen as the combination of two major costs: the initial cost C_{ic} and the operating cost C_{oc}. The initial cost of a heat exchanger is estimated from the following correlation

$$C_{ic} = \delta_M \delta_P \delta_T PC \tag{6}$$

where PC is the purchase cost of the equipment in \$ and δ_M, δ_P and δ_T are the correction factor for the material of construction, operating pressure and temperature. All the correction factors are obtained from Ref. [16]. The operating cost depends on the pumping power required for driving the hot and cold fluids through the exchanger. The operating cost can be determined from,

$$C_{oc} = \frac{(E_s + E_t) \times op \times ec}{1000} \tag{7}$$

where E_s and E_t are the required pumping powers in watt for the shell and the tube sides, respectively. Finally, the total cost of the heat exchanger is expressed as [16],

$$C_{tot} = C_{ic} \frac{i(1+i)^{ny}}{(1+i)^{ny} - 1} + C_{oc} \tag{8}$$

where i is the fractional interest rate per year and ny is the expected lifetime of the heat exchanger.

2.4 Objective Function

Minimization of total cost C_{tot} is taken as the objective function, but the geometry which results in minimum total cost also satisfies the pressure drop, minimum flow velocity and heat exchanger length to shell diameter ratio constraint [16]. So, considering all the constraints, objective function is formulated as below

$$\mathrm{OF} = C_{\mathrm{tot}} + \gamma_1[\Delta P_{\mathrm{s}} - \Delta P_{\mathrm{cs}}] + \gamma_2[\Delta P_{\mathrm{t}} - \Delta P_{\mathrm{ct}}] + \gamma_3 v_{\mathrm{t}} + \gamma_4\left[\frac{L}{D_{\mathrm{s}}}\right] \tag{9}$$

where γ_1, γ_2, γ_3 and γ_4 are penalty factors used to penalize the objective function when the pressure drop, flow velocity or ratio of tube length to shell diameter exceed the allowable limit.

3 Heat Transfer Search Algorithm (HTS)

Heat transfer search (HTS) [22] is a recently developed optimization algorithm inspired from the law of thermodynamics and heat transfer. The fundamental law of thermodynamics states that any system always tries to achieve thermal equilibrium with its surroundings. In order to achieve this, a system transfers heat to surroundings as well as to different parts of the system through conduction, convection and radiation. Therefore, the HTS algorithm composes with the 'conduction phase,' 'convection phase' and 'radiation phase' to reach an optimum solution. In HTS, a population is akin to molecules of the system, temperature levels of the molecules represent the value of design variables, and energy level of the system represents the fitness value of the objective function. The best solution is treated as the surrounding, and rest of the solutions are part of the system. Each phase of the HTS algorithm executes with equal probability during the course of optimization. Equal probability is controlled by a parameter '*R*' in each generation, which is a uniformly distributed random number, and varies between 0 and 1. Working of each phase of HTS algorithm is explained below for minimization problem. Here, size of the population, number of design variables and generation number are denoted by '*n*,' '*m*' and '*g*' respectively.

3.1 Conduction Phase

This phase simulated the conduction heat transfer between molecules of the substance. In conduction heat transfer, higher energy-level molecules transmit heat to adjacent lower energy-level molecules. In the course of optimization with HTS algorithm, higher and lower energy-level molecule analogues to a population having higher and lesser objective function value. During conduction phase, solutions are updated according to the following equation [22].

$$\begin{cases} X_{j,i}^{\mathrm{new}} = X_{k,i}^{\mathrm{old}} - R^2 X_{k,i}^{\mathrm{old}} & \text{If } f\left(X_j\right) > f(X_k) \\ X_{k,i}^{\mathrm{new}} = X_{j,i}^{\mathrm{old}} - R^2 X_{j,i}^{\mathrm{old}} & \text{If } f(X_k) > f\left(X_j\right) \end{cases}; \quad g \le g_{\max}/\mathrm{CDF}$$
$$\begin{cases} X_{j,i}^{\mathrm{new}} = X_{k,i}^{\mathrm{old}} - r_i X_{k,i}^{\mathrm{old}} & \text{If } f\left(X_j\right) > f(X_k) \\ X_{k,i}^{\mathrm{new}} = X_{j,i}^{\mathrm{old}} - r_i X_{j,i}^{\mathrm{old}} & \text{If } f(X_k) > f\left(X_j\right) \end{cases}; \quad g \le g_{\max}/\mathrm{CDF} \tag{10}$$

where $j = 1, 2, \ldots, n, j \neq k, k \in (1, 2, \ldots, n)$ and $i \in (1, 2, \ldots, m)$. Further, k and i are randomly selected solution and design variables. $R \in [0, 0.3333]$ is the probability for selection of conduction phase; $r_i \in [0, 1]$ is a uniformly distributed random number and CDF is the conduction factor.

3.2 Convection Phase

This phase simulates convection heat transfer between system and surroundings. In convective heat transfer, surrounding temperature interacts with mean temperature of the system. In the course of optimization with HTS algorithm, the best solution is assumed as a surrounding, while rest of the solutions compose the system. So, the design variable of the best solution interacts with the corresponding mean design variable of the population. In this phase, solutions are updated based on the following equation [22].

$$X_{j,i}^{\text{new}} = X_{j,i}^{\text{old}} + R * (X_{\text{s}} - X_{\text{ms}} * \text{TCF})$$
$$\begin{cases} \text{TCF} = \text{abs}(R - r_i) & g \leq g_{\max}/\text{COF} \\ \text{TCF} = \text{round}(1 + r_i) & \text{If } g > g_{\max}/\text{COF} \end{cases} \tag{11}$$

where $j = 1, 2, \ldots, n$, $i = 1, 2, \ldots, m$, X_{s} is the temperature of surrounding and X_{ms} is mean temperature of the system. $R \in [0.3333, 0.6666]$ is the probability for selection of convection phase; $r_i \in [0, 1]$ is a uniformly distributed random number; and COF is the convection factor.

3.3 Radiation Phase

This phase simulates the radiation heat transfer within the system as well as between system and surrounding. Radiation heat transfer takes place between the system and surrounding as well as within the different part of the system also. In the course of optimization with HTS algorithm, this situation represents the update of any solution with the help of best solution or any other randomly selected solution. In this phase, the solutions are updated as given below [22].

$$\begin{cases} X_{j,i}^{\text{new}} = X_{j,i}^{\text{old}} + R * \left(X_{k,i}^{\text{old}} - X_{j,i}^{\text{old}}\right) & \text{If } f\left(X_j\right) > f(X_k) \\ X_{j,i}^{\text{new}} = X_{j,i}^{\text{old}} + R * \left(X_{j,i}^{\text{old}} - X_{k,i}^{\text{old}}\right) & \text{If } f(X_k) > f\left(X_j\right) \end{cases}; \quad \text{If } g \leq g_{\max}/\text{RDF} \tag{12}$$

$$\begin{cases} X_{j,i}^{\text{new}} = X_{j,i}^{\text{old}} + r_i * \left(X_{k,i}^{\text{old}} - X_{j,i}^{\text{old}}\right) & \text{If } f\left(X_j\right) > f(X_k) \\ X_{j,i}^{\text{new}} = X_{j,i}^{\text{old}} + r_i * \left(X_{j,i}^{\text{old}} - X_{k,i}^{\text{old}}\right) & \text{If } f(X_k) > f\left(X_j\right) \end{cases}; \quad \text{If } g \le g_{\max}/\text{RDF} \tag{13}$$

where $j = 1, 2, \ldots, n$, $j \neq k$, $k \in (1, 2, \ldots, n)$ and $i \in (1, 2, \ldots, m)$. Further, k is a randomly selected solution. $R \in [0.6666, 1]$ is the probability for selection of radiation phase; $r_i \in [0, 1]$ is a uniformly distributed random number; and RDF is the radiation factor.

4 Case Study, Results and Discussion

The effectiveness of the present approach using HTS is assessed by analyzing 5 MW duty, heavy gas oil–crude oil exchanger which were earlier analyzed using GA, PSO and CSO. Hot heavy gas oil at a temperature of 319 °C enters into the heat exchanger and needs to cool down to 269 °C by crude oil which enters into the heat exchanger at 209 °C. The flow rate of gas oil and crude oil are 29.36 kg/s and 102.12 kg/s, respectively. Heat load of the heat exchanger between two fluids is 5 MW which means that the leaving temperature of crude oil is 226 °C.

Fluid inlet and outlet temperatures, flow rates, number of pass divider lane, number of seal strip pairs and width of the pass divider lane are considered as design specifications. Tube outer diameter (d_o), shell diameter (D_s), shell-to-baffle diametrical clearance (δ_{sb}), tube-to-baffle diametrical clearance (δ_{tb}), tube bundle outer diameter (D_{otl}), baffle spacing at center (L_{bc}), baffle spacing at inlet and outlet (L_{bi} and L_{bo}), baffle cut (B_c), tube pitch (P_T) and number of tube passes (N_P) are considered as design variables which need to optimize for minimum total cost of the heat exchanger. The lower bound and upper bound of the design variables are listed in Table 1, while Fig. 1 indicates the heat exchanger geometry along with all the design variables.

Table 1 Search ranges of design variables

Design variables	Lower bound	Upper bound
Shell diameter (D_s) (mm)	300	1000
Tube outer diameter (d_o) (mm)	15.87	63.5
Tube pitch (P_T)	1.25 d_o	1.5 d_o
Tube layout pattern	30°	90°
Number of tube passes (N_P)	1	4
Baffle spacing at center (L_{bc})	0.2 D_s	0.55 D_s
Inlet and outlet baffle spacing (L_{bi}, L_{bo})	L_{bc}	1.6 L_{bc}
Baffle cut (B_c)	25%	45%
Shell-to-baffle diametrical clearance (δ_{sb})	0.01 D_s	0.1 D_s
Tube-to-baffle diametrical clearance (δ_{tb})	0.01 d_o	0.1 d_o

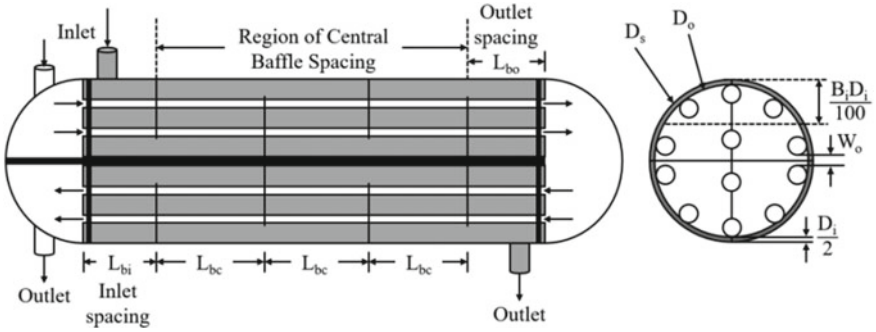

Fig. 1 Geometry of shell and tube heat exchanger

Table 2 Process input

Process input	Tube side	Shell side
Fluid	Heavy gas oil	Crude oil
Flow rate (kg/s)	29.36	102.12
Operating pressure (Pa)	1×10^6	3×10^6
Allowable pressure drop (Pa)	1×10^4	1×10^4

The design specifications, shown in Table 2, are supplied as an input to the heat exchanger case study. Further, the following values are considered to compute the operating cost of heat exchanger: lifetime of the heat exchanger (ny) = 20 year; annual interest rate (i) = 5%; energy cost (ec) = 0.1 \$/kWh; annual operating period (op) = 5000 h/year; and pumping efficiency (η) = 0.85. The correction factor for the operating temperature, pressure and material is taken as 1.6, 1.2 and 1, respectively.

Table 3 shows the optimized parameters of the case study obtained using HTS algorithm and its comparison with the earlier approaches. It is observed from the results that HTS approach results in minimum heat exchanger area as compared to other approaches. Because of the reduction in heat exchanger area, the capital investment is also decreased in the present approach as compared to previous approaches. However, higher tube-side and shell-side pressure drop in the present approaches increases the annual pumping cost. Overall, the reduction in the total cost of about 4.33% (compared to GA), 0.82% (compared to PSO), 0.32% (compared to CSO) is observed using the proposed algorithm. Figure 2 shows the convergence of the objective function using all the approaches.

One of the most encountered problems in STHE is the inside and outside fouling of tubes. Fouling increases the thermal resistance, diminishing the overall heat transfer coefficient and augmenting the pressure drop. Wildi-Tremblay and Gosselin [16] suggested that system should be somewhat over design for minimizing the number of maintenance cleanings. Oversurface design is presented by surface coefficient I_s as

Table 3 Comparison of heat exchanger design

Output parameters	GA [9]	PSO [9]	CSO [9]	HTS
Shell diameter	900	752.7	741.2	739.25
Tube diameter	15.9	15.87	15.87	15.87
Number of tubes	1010	600	607	603
Tube layout	90	45	45	45
Center baffle spacing	495	414	407.7	406.6
Inlet/outlet baffle spacing	792	414	547.9	406.6
Baffle cut	25	25	25	25.65
Shell-side pressure drop	8490	8670	9980	9990
Tube-side pressure drop	8760	9610	9180	9270
Operating cost	928.7	965.9	1064.8	1066.84
Initial cost	9660.4	9247.9	9098.3	9063.6
Total cost	10,589.1	10,213.8	10,163.1	10,130.44

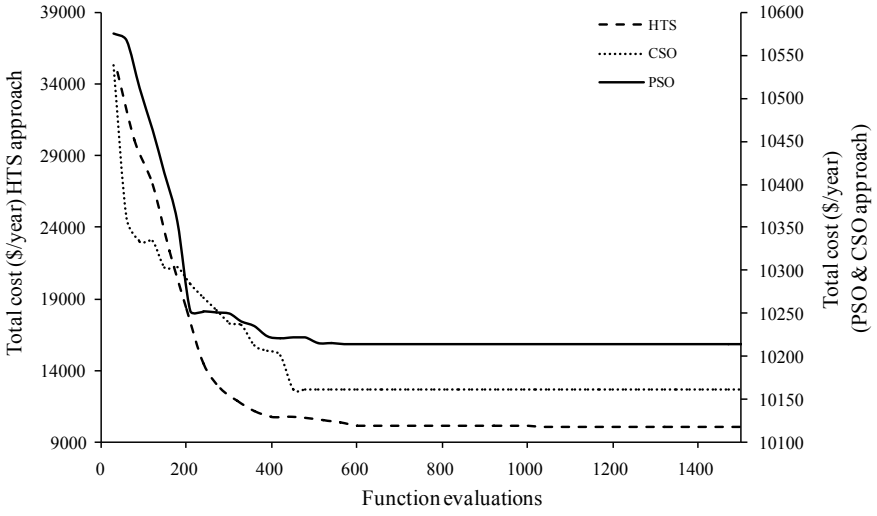

Fig. 2 Convergence of comparative algorithms

$$I_s = \left(\frac{A - A_c}{A_c} \right) \tag{14}$$

where A is the total surface area that was calculated previously, and A_c is the total surface area when fouling resistance is zero. High value of I_s indicates more maintenance cleanings, while small value of I_s results in an excessively expensive heat exchange [16].

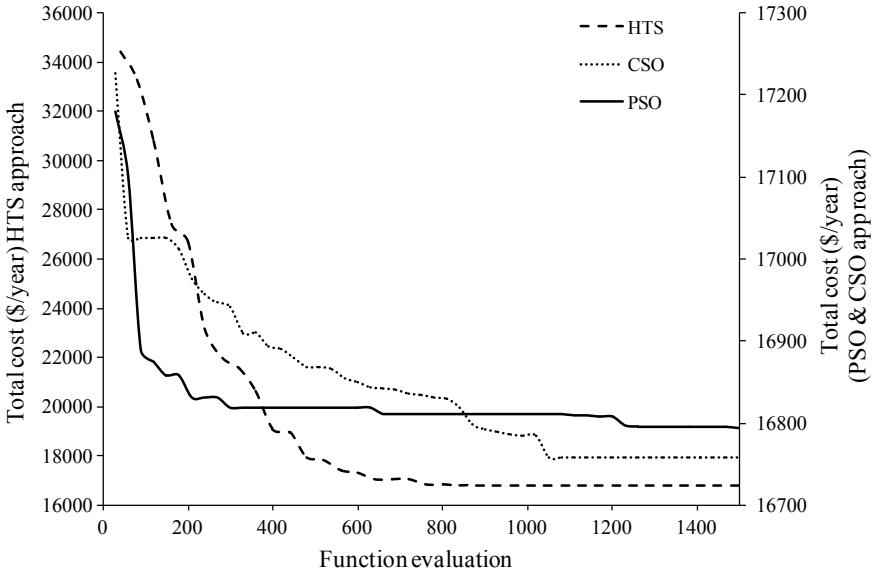

Fig. 3 Convergence of HTS, PSO and CSO algorithms

Table 4 shows the new geometry of the 5 MW duty heavy gas oil–crude oil exchanger with maintenance consideration along with results obtained by previous researchers. Result shows that a reduction of the total cost of about 0.92% (compared to GA), 0.56% (compared to PSO) and 0.35% (compared to CSO) is observed using

Table 4 Comparison of heat exchanger design with maintenance consideration

Output parameters	GA [9]	PSO [9]	CSO [9]	HTS
Shell diameter	1000	1000	1000	1000
Tube diameter	50.8	25.87	21.87	16.15
Tube layout	90	90	90	90
Number of tube passes	2	4	4	4
Center baffle spacing	550	308	299.4	403
Inlet/outlet baffle spacing	880	492	479	645
Baffle cut	30	25	25	25
Shell-side pressure drop	3970	5300	4940	2420
Tube-side pressure drop	678.49	3300	3200	4740
Operating cost	347.43	527.2	492.1	452.32
Initial cost	16,505	16,266	16,266	16,245.19
Total cost	16,852.43	16,793.2	16,758.1	16,697.51
I_s factor (%)	25	25	25	25

the proposed algorithm. Figure 3 shows the convergence of the objective function using all the approaches.

5 Conclusions

This study demonstrates the successful application of heat transfer search algorithm for the optimal design of TEMA-E STHE from economic viewpoint. In the present work, eleven design variables were optimized in order to identify the cheapest possible solution which had to consider a pressure drop constraint on both shell and tube side. The algorithm's ability was demonstrated using a case study, and the performance is compared with GA, PSO and CSO approaches. Referring to results, saving in total cost be observed using HTS as compared to GA, PSO and CSO approaches. Furthermore, for minimizing the number of maintenance cleanings on heat exchanger and provide a more robust and reliable design, maintenance of heat exchanger was also considered. This can be taken into account by I_s factor. Here, again HTS algorithm gives better results compared to other approaches.

References

1. Kern DQ (1950) Process heat transfer. McGraw-Hill, New York
2. Hewitt GF (1998) Heat exchanger design handbook. Begell House, New York
3. Shah RK, Sekulic DP (2003) Fundamentals of heat exchanger design. Wiley, New York
4. Selbas R, Kizilkan O, Reppich M (2006) A new design approach for shell- and-tube heat exchanger using genetic algorithm from economic point of view. Chem Eng Process 45:268–275
5. Fesanghary M, Damangir E, Soleimani I (2009) Design optimization of shell and tube heat exchangers using global sensitivity analysis and harmony search algorithm. Appl Therm Eng 29:1026–1031
6. Serna M, Jimenez A (2004) An efficient method for the design of shell and tube heat exchangers. Heat Transfer Eng 25:5–16
7. Mohanty DK (2016) Gravitational search algorithm for economic optimization design of a shell and tube heat exchanger. Appl Therm Eng 107:184–193
8. Wong JYQ, Sharma S, Rangaiah GP (2016) Design of shell-and-tube heat exchangers for multiple objectives using elitist non-dominated sorting genetic algorithm with termination criteria. Appl Therm Eng 93:888–899
9. Amini M, Bazargan M (2014) Two objective optimization in shell-and-tube heat exchangers using genetic algorithm. Appl Therm Eng 69:278–285
10. Hadidi A, Nazari A (2013) Design and economic optimization of shell-and-tube heat exchangers using biogeography-based (BBO) algorithm. Appl Therm Eng 51:1263–1272
11. Rao RV, Patel VK (2013) Multi-objective optimization of heat exchangers using a modified teaching-learning-based optimization algorithm. Appl Math Model 37:1147–1162
12. Wen J, Yang H, Jian G, Tong X, Li K, Wang S (2016) Energy and cost optimization of shell and tube heat exchanger with helical baffles using Kriging meta-model based on MOGA. Int J Heat Mass Tran 98:29–39
13. Hajabdollahi H, Naderi M, Adimi S (2016) A comparative study on the shell and tube and gasket-plate heat exchangers: the economic viewpoint. Appl Therm Eng 92:271–282

14. Khosravi R, Khosravi A, Nahavandi S, Hajabdollahi H (2015) Effectiveness of evolutionary algorithms for optimization of heat exchangers. Energy Convers Manage 89:281–288
15. Ozcelik Y (2007) Exergetic optimization of shell and tube heat exchanger using a genetic based algorithm. Appl Therm Eng 27:1849–1856
16. Wildi-Tremblay P, Gosselin L (2007) Minimizing shell and tube heat exchanger cost with genetic algorithms and considering maintenance. Int J Energy Res 31:867–885
17. Rao RV, Patel VK (2011) Design optimization of shell and tube heat exchangers using swarm optimization algorithms. Proc Inst Mech Eng Part A: J Power 225:619–634
18. Caputo AC, Pelagagge PM, Salini P (2009) Heat exchanger design based on economic optimization. Appl Therm Eng 28:1151–1159
19. Caputo AC, Pelagagge PM, Salin P (2015) Heat exchanger optimized design compared with installed industrial solutions. Appl Therm Eng 87:371–380
20. Patel VK, Rao RV (2010) Design optimization of shell-and-tube heat exchanger using particle swarm optimization technique. Appl Therm Eng 30:1417–1425
21. Hajabdollahi H, Hajabdollahi Z (2016) Assessment of nanoparticles in thermo-economic improvement of shell and tube heat exchanger. Appl Therm Eng 106:827–837
22. Patel VK, Savsani VJ (2015) Heat transfer search (HTS): a novel optimization algorithm. Inform Sci 324:217–246

Exploring the Effect of Passing Vehicle Search (PVS) for the Wind Farm Layout Optimization Problem

Jaydeep Patel, Vimal Savsani, Vivek Patel, and Rajesh Patel

Abstract The wind farm layout optimization (WFLO) is a challenge that helps to alter the position of wind turbines and arrange in such a way that the assembly of the turbines has reduced wake effect, which improves the power output and overall efficiency of a wind farm. In the present study, a novel optimization tool, a passing vehicle search (PVS) technique has been used for optimizing the positioning of turbines to maximize the power yield and improved overall efficiency of a wind farm for a given set of turbines. The PVS algorithm is applied to square wind farm considering the multi-directional unvarying wind velocity and variable wind velocity. The numerical results indicate that PVS is leading to maximum power extraction from a wind farm, even on using the same number of turbines, despite of the substantial variations in wind speed and direction.

Keywords Metaheuristic · Passing vehicle search (PVS) · Wind energy · Wind farm layout optimization

1 Introduction

The wind energy is converted into electric energy using wind turbines. A cluster of turbines is setup at the wind farm site to generate energy and also to reduce O&M cost [1]. When the wind passes the turbine, it creates the rotational motion of the turbine and produces the wake region behind the wind turbines [2]. When the turbines are placed in this wake region, the performance of that affected turbine is reduced and produces less energy than predicted because of the wake effect caused by the upstream turbine. The wake effect on performance of downstream turbine can be reduced by placing the turbine in such a way that the swept area of turbine rotor and wake radius produced by the upstream turbine does not overlap. Hence, effective

J. Patel (✉) · V. Savsani · V. Patel · R. Patel
Department of Mechanical Engineering, Pandit Deendayal Petroleum University, Gandhinagar 382007, India
e-mail: Jaydeeppatel028@gmail.com

V. K. Gupta et al. (eds.), *Reliability and Risk Assessment in Engineering*,
Lecture Notes in Mechanical Engineering,
https://doi.org/10.1007/978-981-15-3746-2_38

positioning of turbines, that lessen the wake effect and maximizes the energy yield of a wind farm, is imperative.

The phenomenon of placement of wind turbines in a wind farm can be converted in the form of an optimization problem, to find the optimal placement of wind turbines to achieve the required objectives. The objective of the problem is to maximize the power generation and minimize the cost of energy produced by the wind farm. Such type of wind turbine placement problem is classified as a 'wind farm layout optimization (WFLO)' problem. The WFLO approach was first addressed by Mosetti et al. [3]. They used Jensen's wake decay model [4] for the development of a wake behind the rotor. The genetic algorithm was applied to 10 × 10 grid space and employed to find the optimal placement of turbines. In addition to this, the genetic algorithm for layout optimization with the same objective was also used with 1 m × 1 m discrete grid space for turbine placement [5]. In addition to this, advanced genetic algorithm approaches, i.e., a hybrid GA [6], a distributed genetic algorithm (DGA) [7], and hybrid DGA [8] had been used to solve the discrete wind farm layout optimization problems. Apart from genetic algorithm, many other stochastic meta-heuristic methods such as mixed integer nonlinear discrete combinatorial optimization algorithm [9], ant colony optimization algorithm (ACO) [10], particle swarm optimization [11], greedy randomized adaptive search procedure (GRASP) [12], simulated annealing (SA) [13], teaching–learning-based optimization [14], quadratic optimization (QO), and mixed integer linear (MIL) method [2] had also been tested to solve the wind farm layout optimization problems.

The goal of the present study is to maximize the energy yield produced by the wind farm. Present study uses an effective optimization method, passing vehicle search (PVS), for WFLO problem. The results of PVS are compared with the results available in literature for grid-based placement of turbines.

2 Problem Formulation

The kinematic wake model developed by the Jensen [4] is one of the oldest and most widely used wake models. It assumes a linearly expanding wake with a velocity deficit that is only dependent on the distance behind the turbine. This wake decay model uses the law of conservation of mass to calculate the consequence of wake of the upstream turbine on the downstream turbine. This wake effect leads to lower the velocity of the downstream turbine and can be estimated by a linearly increasing wake decay model as visualized in Fig. 1.

The goal of the WFLO is to reduce the cost of energy yield per unit produced. This can be achieved when the energy extracted by the wind farm is maximum.

Hence, the WFLO problem is described as:

$$\text{Minimize} \frac{\text{Cost}}{P_{\text{wf}}} = \frac{N_{\text{T}}\left(\frac{2}{3} + \frac{1}{3}\text{e}^{-0.00174N_{\text{T}}^2}\right)}{\sum_{i=1}^{N_{\text{T}}} 0.3v_i^3} \tag{1}$$

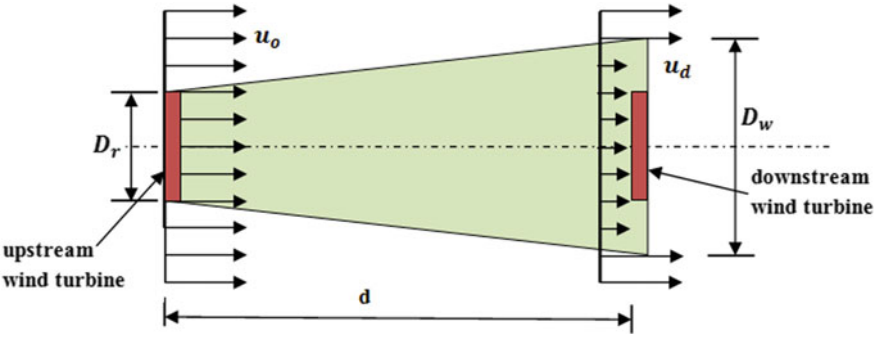

Fig. 1 Representation of the Jenson wake decay model

where, $v_i = v_0$, (when turbine is under no wake)

$$v_i = v_o\left[1 - \left[\frac{1 - \sqrt{1 - \mathrm{CT}}}{\left(1 + \frac{d}{\ln(h/h_0)D_\mathrm{r}}\right)^2}\right]\right], \text{(when turbine is under single wake)}$$

$$v_i = v_o\left[1 - \sqrt{\sum_{n=1}^{N_w}\left(1 - \left(\frac{v_n}{v_0}\right)\right)^2}\right], \text{(when turbine is under many wake)}$$

N_T is number of turbines, P_wf is the net power produced by the wind farm, v_i is velocity at turbine i, C_T is thrust coefficient of turbines, d is the distance between two turbines, h is the hub height of turbines, h_o is the surface roughness of a site, and D_r is the diameter of a rotor.

3 Application of Passing Vehicle Search (PVS) Algorithm

The passing vehicle search (PVS) algorithm is a population-based stochastic global search metaheuristic algorithm developed by Savsani and Savsani [15] from the inspiration of an idea of the vehicle passing mechanism on a two-lane highway. The safe overtaking of the vehicle is the most vital consideration on a two-lane highway. This depends on many independent and inter-related complex parameters such as speed and acceleration of individual vehicles, driver's skill, the characteristics of the traffic, availability of gaps in the opposing traffic flow, type of journey, road geometry, and weather conditions. The PVS algorithm considers the three vehicles (i.e., oncoming vehicle (OV), back vehicle (BV), and front vehicle (FV)) that are involved in the vehicle passing mechanism on a two-lane highway. The back vehicle wants to pass the front vehicle, which is only possible if the front vehicle is slower than the back vehicle. If the speed of FV is more than BV, then no passing is possible.

Moreover, passing depends on the distance between BV, FV, and OV, the position and speed of OV, and their velocities. The PVS algorithm is free from the algorithm parameters.

In PVS algorithm, population reassembles different vehicles on two-lane highways, whereas design variable indicates the position of the vehicle on a highway. The objective function value is analogous to vehicles velocity, i.e., solution with better fitness value is considered as a vehicle with high velocity. So, PVS algorithm starts with a set of solutions called the population of vehicles, out of which three vehicles (solutions) are selected at random. Among these three selected vehicles, the current solution is correlated as BV and other two can be OV and FV randomly. The basic steps of PVS algorithm are summarized in Fig. 2.

4 Results and Discussion

Experimental investigations were carried out to show the strength and effectiveness of the proposed algorithms. The algorithms were coded using MATLAB. The wind turbine positioning has been obtained with two different wind scenarios. The first scenario (case (a)) was assumed to have multi-directional unvarying wind velocity and the second scenario (case (b)) was considered with multi-directional variable wind velocities. The size of wind farm is 2000 m $\times$ 2000 m which is further divided into the 10 $\times$ 10 grid. The characteristic of turbine used in present study is given in Table 1. The results were obtained for ten different runs with a population size of 50 and the function evaluations of 50,000. The best values obtained out of ten runs have been presented as the optimum solutions for the WFLO problem.

4.1 Results for Multi-directional Unvarying Wind Velocity [Case (a)]

This case considers the unvarying wind velocity of 12 m/s. The wind is flowing across the 36 rotational directions with equal probability of occurring in each direction. The result obtained for each direction are equally weighted and combined. The number of turbines to be placed in the wind farm area is considered as 39. The optimization process was carried out for 39 turbines, and results in the form of power output and efficiency were obtained and compared with the results reported in Refs. [2, 16]. The illustration of the location of turbines in a wind farm is visualized in Fig. 3. The comparative results are summarized in Table 2, where the results are presented in the form of objective function value, total power, and efficiency of a wind farm. It is observed from Table 2 that total power output obtained by the PVS algorithm is higher, compared to the layout suggested in Refs. [2, 16]. The efficiency of wind farm obtained by the PVS algorithm is 90.85% and power output is 18,368 kW. Grady

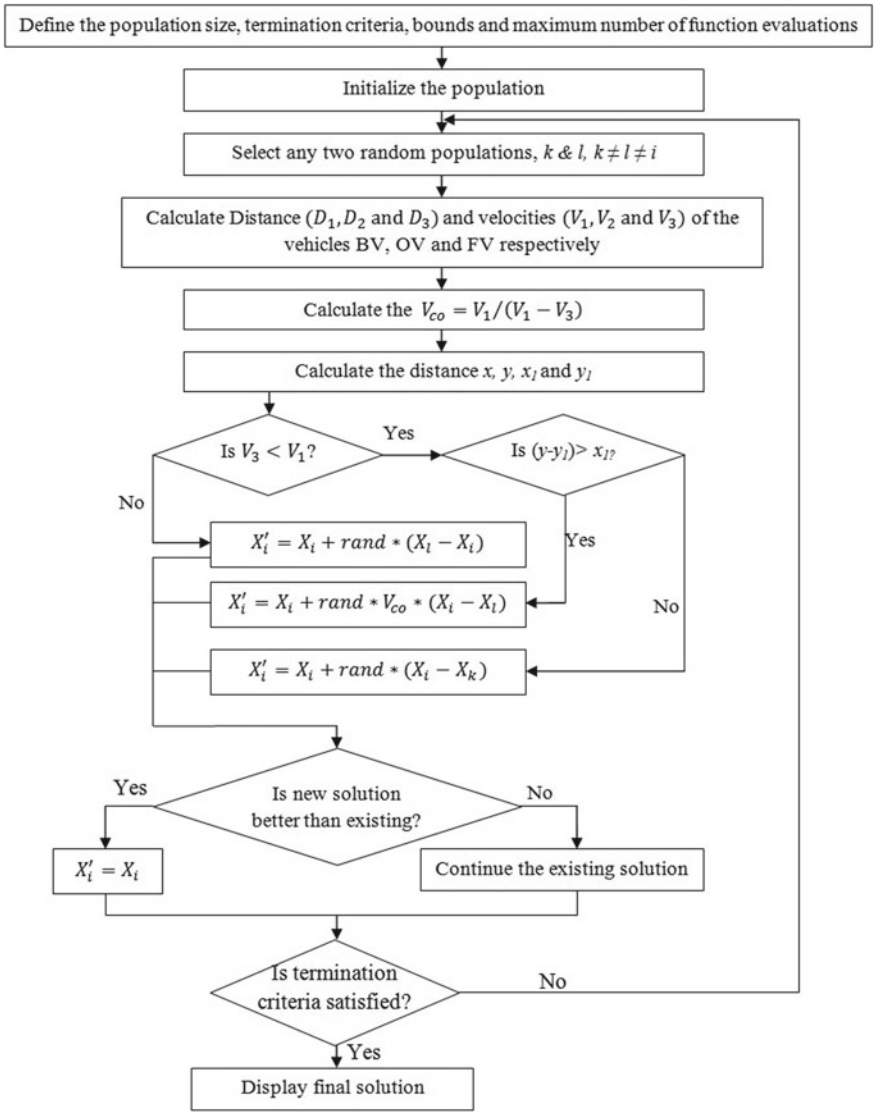

Fig. 2 Flowchart of PVS algorithm

Table 1 Wind turbine characteristics

Hub height of turbine (h)	60 m
Rotor diameter of turbine (D_r)	40 m
Turbine thrust coefficient (C_T)	0.88
Ground surface roughness (h_o)	0.3

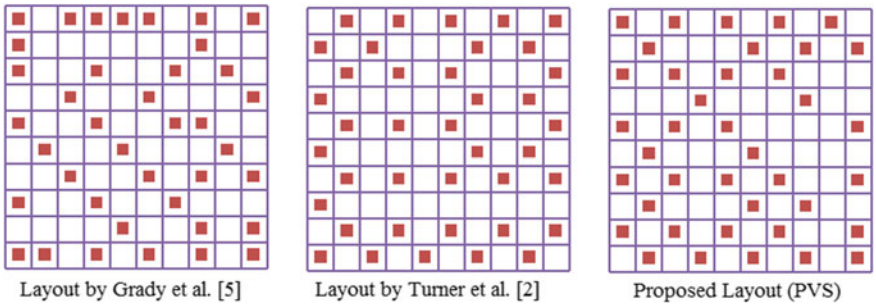

Fig. 3 Wind farm layout configuration for case (a)-39 wind turbine

Table 2 Performance comparison for case (a): (i) Turner et al. (ii) Grady et al. (iii) Present study (PVS)

	(i)	(ii)	(iii)
Objective function value	0.00147	0.001567	0.001447
Number of turbines (N_T)	39	39	39
Efficiency (%)	90.7	85.17	90.85
Power output (P_{wf})	18,336	17,220	18,368

et al. [16] and Turner et al. [2] had reported the efficiency of 85.17% and 90.7% and power output 17,220 kW and 18,336 kW, respectively.

4.2 Results for Multi-directional Unvarying Wind Velocity [Case (a)]

This case is a more realistic approach of wind environment where the multi-directional variable velocities of 8, 12, and 17 m/s were considered. The wind is flowing from 36 rotational directions with an unequal probability of occurrence, at each wind velocity, in each direction, as shown in Fig. 4. The results obtained for each direction are weighted as per likelihood of occurrence at each wind velocity

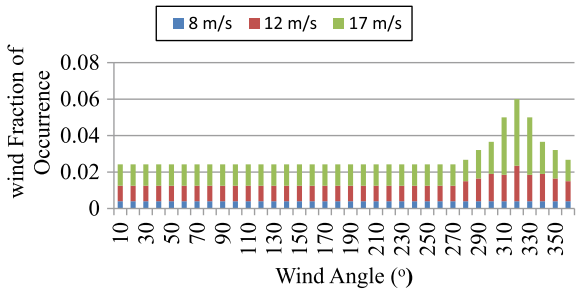

Fig. 4 Bar graph of multi-directional variable wind velocity

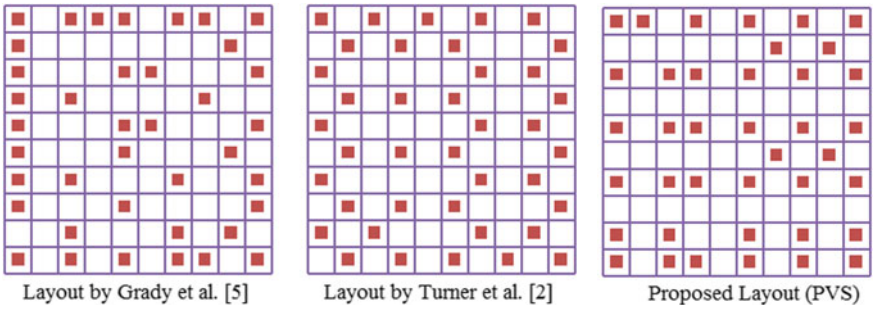

Fig. 5 Wind farm layout configuration for case (b)-39 wind turbine

Table 3 Performance comparison for case (b): (i) Turner et al. (ii) Grady et al. (iii) Present study (PVS)

	(i)	(ii)	(iii)
Objective function value	0.00082	0.00083	0.000798
Number of turbines (N_T)	39	39	39
Efficiency (%)	87.73	86.74	91.22
Power output (P_{wf})	32,453	32,086	33,741

and combined. The optimization process was carried out for 39 turbines, and results in the form of power output and efficiency were obtained and compared with the results reported in Refs. [2, 16].

The illustration of the position of wind turbines in a wind farm is visualized in Fig. 5. The comparative performances of the results are summarized in Table 3, where the results are presented in the form of objective function value, total power, and efficiency of a wind farm. It is observed from Table 3 that total power output obtained by the PVS algorithm is higher compared to the layout suggested in Refs. [2, 16] for the multi-directional variable wind speed. The efficiency of wind farm obtained by the PVS algorithm is 91.22% and power output is 33,741 kW. The power obtained by the PVS algorithm is higher by 3.97% and 5.16% compared to Turner et al. [2] and Grady et al. [16], respectively. The distribution given by Grady et al. [16] produces a total power of 32,086 kW with an efficiency of 86.74%, while the distribution provided by Turner et al. [2] produces a total power of 32,453 kW with an efficiency of 87.73%.

5 Conclusions

Present study explores the passing vehicle search (PVS) optimization algorithm for solving the WFLO problem. Based on the results, it can be summarized that PVS algorithm had outperformed or it is at par with other algorithms. It is concluded that the PVS algorithm can get better placement of wind turbines in wind farm

than previous studies with minimum energy losses without being trapped in local optimum. Moreover, PVS requires less computational efforts than other algorithm for WFLO problem. So, it can be outlined that PVS algorithm is indeed effective and can produce better results on challenging problems. However, the proposed method needs to be investigated for other challenging problems.

References

1. Pookpunt S, Ongsakul W (2013) Optimal placement of wind turbines within wind farm using binary particle swarm optimization with time-varying acceleration coefficients. Renew Energy 55:266–276
2. Turner SDO, Romeo D, Zhang PY, Amon CH, Chan TCY (2014) A new mathematical programming approach to optimize wind farm layouts. Renew Energy 63:674–680
3. Mosetti G, Poloni C, Diviacco B (1994) Optimization of wind turbine positioning in large wind farms by means of a genetic algorithm. J Wind Eng Ind Aerodyn 51(1):105–116
4. Jensen NO (1983) A note on wind generator interaction
5. Mittal A (2010) Optimization of the layout of large wind farms using a genetic algorithm. Dissertation, Case Western Reserve University
6. Rahbari O, Vafaeipour M, Fazelpour F, Feidt M, Rosen MA (2014) Towards realistic designs of wind farm layouts: application of a novel placement selector approach. Energy Convers Manag 81:242–254
7. Huang HS (2007) Distributed genetic algorithm for optimization of wind farm annual profits. In: Proceedings of intelligent systems applications to power systems. IEEE
8. Huang HS (2009) Efficient hybrid distributed genetic algorithms for wind turbine positioning in large wind farms. In: IEEE international symposium on industrial electronics. IEEE
9. Ozturk UA, Norman BA (2003) Heuristic methods for wind energy conversion system positioning. Electr Power Syst Res 70(3):179–185
10. Eroğlu Y, Seçkiner SU (2012) Design of wind farm layout using ant colony algorithm. Renew Energy 44:53–62
11. Chowdhury S, Zhang J, Messac A, Castillo L (2012) Unrestricted wind farm layout optimization (UWFLO): investigating key factors influencing the maximum power generation. Renew Energy 38(1):16–30
12. Yin PY, Wang T-Y (2012) A GRASP-VNS algorithm for optimal wind-turbine placement in wind farms. Renew Energy 48:489–498
13. Bilbao M, Alba E (2009) Simulated annealing for optimization of wind farm annual profit. In: Proceedings of international symposium on logistics and industrial informatics, IEEE
14. Patel J, Savsani V, Patel V, Patel R (2017) Layout optimization of a wind farm to maximize the power output using enhanced teaching learning based optimization technique. J Clean Prod 158:81–94
15. Savsani P, Savsani V (2016) Passing vehicle search (PVS): a novel metaheuristic algorithm. Appl Math Model 40(5):3951–3978
16. Grady SA, Hussaini MY, Abdullah MM (2005) Placement of wind turbines using genetic algorithms. Renew Energy 30(2):259–270

Process Parameters Optimization for Inconel-825 in WEDM Using TLBO Algorithm

D. Saikiran, Arun Kumar Rouniyar, and Pragya Shandilya

Abstract To achieve best manufacturing conditions, we have to manufacture quality products at minimum cost and minimum manufacturing lead time, and this can be done with optimization. The effective optimization of machining process parameters dramatically affects the cost and production time of machined components as well as the quality of the final products. Wire electrical discharge machining (WEDM) is a specialized thermal machining process capable of accurately machining parts of hard materials with complex shapes. Owing to its complex process, selection of optimal parameter values enhances the performance of the WEDM. The present work deals with single optimization in minimizing the surface roughness of Inconel-825 alloy, in WEDM process using teaching–learning-based optimization (TLBO) algorithm. Three input process parameters of Wire EDM (i.e. pulse on time, pulse off time and peak current) are used to study their effects on the surface roughness. The optimal solution of process parameters is obtained by using TLBO approach.

Keywords Inconel · Process parameters · Surface roughness · Teaching–learning-based optimization · WEDM

1 Introduction

Inconel-825 is a nickel–iron–chromium super alloy which is used in various industrial-related applications such as marine, aerospace, automobile and medical industries due to their high temperature mechanical strength and high corrosion resistance properties [1]. Inconel-825 when heated forms a thick yet stable oxide layer that protects its outer surface from further attack. This makes it the ideal choice for extreme temperature and pressure applications, where steel and aluminium would

D. Saikiran (✉) · A. K. Rouniyar · P. Shandilya
Department of Mechanical Engineering, Motilal Nehru National Institute of Technology, Allahabad, Allahabad Uttar Pradesh, 211004, India
e-mail: rme1602@mnnit.ac.in

P. Shandilya
e-mail: pragya20@mnnit.ac.in

V. K. Gupta et al. (eds.), *Reliability and Risk Assessment in Engineering*,
Lecture Notes in Mechanical Engineering,
https://doi.org/10.1007/978-981-15-3746-2_39

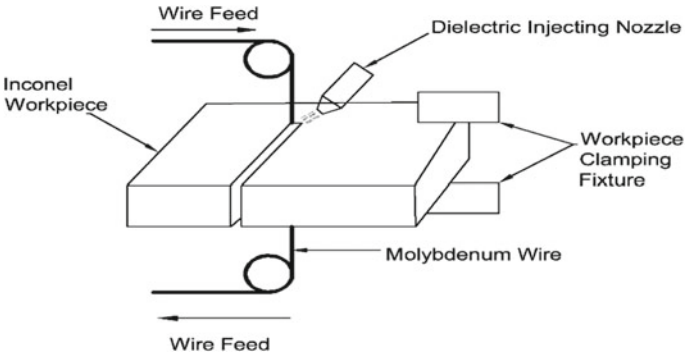

Fig. 1 Schematic diagram of WEDM

succumb to thermal creep [2]. However, machining of Inconel-825 by traditional process possess various difficulties such as poor thermal diffusivity generates high temperature at the tool tip affecting the tool life adversely. Owing to all these difficulties, non-traditional machining of Inconel-825 is preferred and among them, wire EDM gives better surface finish and burr-free surfaces [3].

Wire electrical discharge machining is a non-traditional machining process which uses a thin, electrically charged moving brass or copper wire electrodes to cut any conductive material, which are difficult to cut as well as for intricate profiles [4]. WEDM processes are broadly used in various industrial applications such as in aerospace, medical and automotive industries for cutting due to better dimensional accuracy and surface finish, burr-free surfaces, as well as no post-finishing operation required [5]. Removal of material occurs as a result of spark erosion when the wire electrode is fed, from a fresh wire spool, through the workpiece separated by a thin film of dielectric medium as depicted in schematic diagram of Fig. 1.

2 Literature Review

Some researchers have carried out cutting of difficult to cut conductive material by WEDM process to investigate the influence of process parameters on cutting performance measures such as material removal rate, surface roughness, overcut and white layer. For example, Sarkar et al. [6] developed a feed-forward backpropagation neural network to determine the optimal combination of control parameters on cutting the γ-titanium aluminide alloy by wire electrical discharge machining. Ramakrishnan and Karunamoorthy [7] performed multi-objective optimization of the WEDM process for the machining of heat-treated tool steel on response material removal rate, wire wear ratio and surface roughness using multi-response S/N ratios. Sarkar et al. [8] developed an analytical model during cutting cylindrical job to understand the mechanism of the wire-lag phenomenon. It was observed that the inaccuracy

level due to wire lag was higher for job with smaller radius. Rajyalakshmi and Ramaiah [1] used Taguchi along with grey relational analysis to determine the optimal cutting parameters on machining the Inconel-825 on spark gap, surface roughness and material removal rate. Li et al. [9] focused on the effect of discharge energy on surface integrity on main cut and trim cuts of Inconel-718. At high discharge energy, thick white layer observed was nonuniform and discontinuous. Chen et al. [10] analysed and reduced the geometrical inaccuracy of rough corner cutting, observed reduction in corner wear by more than 50% and an elliptic fitting method was proposed to be the best in describing the wire electrode centre trajectory. Zhang et al. [11] performed optimization by integrated RSM and non-dominated sorting genetic algorithm-II (NSGAII) to determine the optimal set of process parameters on cutting SKD-11 steel on the response surface quality and material removal rate. Kumar et al. [12] varied different WEDM process parameters to study the influence on material removal rate and overcut on cutting the pure titanium by using brass wire electrode. Model to predict the response was developed using response surface methodology. Chalisgaonkar and Kumar [13] performed optimization using traditional utility method in combination with the weight assignment concept in trim cutting the pure titanium by wire electrical discharge machining. Shandilya et al. [14] machined the SiCp/6061 Al metal matrix composite using wire EDM and performed modelling using ANN and RSM to predict the response MRR and kerf width in terms of process parameters and observed better results with ANN.

Worldwide researchers have investigated WEDM of difficult to cut conductive materials such as Inconel-718, pure titanium and SKD-11 steel. Researchers have focused on the influence of cutting parameters such as pulse off time, pulse on time, gap voltage and peak current on material removal rate, wire wear ratio, surface roughness, white layer thickness, etc. Very less work has been reported on WEDM of Inconel-825. In the present study, single-objective optimization is performed to determine the optimum set of process parameters, namely angle of cutting, pulse on time, pulse off time and peak current to minimize the surface roughness in WEDM of Inconel-825. Regression model is developed to predict the surface roughness.

3 Experimental Setup and Methods

3.1 Experimental Material

Inconel-825 of dimension 160 mm × 160 mm × 10 mm is selected as workpiece material, molybdenum wire as electrode of diameter 180 μm and de-ionized water as dielectric fluid was used for performing experiments. In all the experiments, triangular profile cutting was performed of side 10 mm. The chemical composition and mechanical properties of Inconel-825 are shown in Tables 1 and 2.

Table 1 Chemical composition of Inconel-825

Element	Ni	Cr	Fe	Ti	Cu
% weight	39.72	20.08	24.09	0.88	0.18

Table 2 Mechanical properties of Inconel-825

Properties	Density	Thermal conductivity	Modulus of elasticity	Ultimate tensile strength
Units	Kg/m^3	W/m K	GPa	MPa
Values	8140	11.1	193	95

Fig. 2 Experimental setup of wire EDM

3.2 Experimental Equipment

The experiments were performed on Wire Electric Discharge Machine model—"EX7732" present in workshop in Mechanical Engineering Department of MNNIT, Allahabad. Figure 2 depicts the experimental setup of WEDM.

3.3 Design of Experiments

Three levels and four process parameters are selected for this present experimental work. Range and levels of process parameters are selected on the basis of machine specification range, preliminary experiments conducted considering one factor at a

Table 3 Range of the process parameters used and their levels

Process parameters	Units	Levels		
		1	2	3
Pulse on time (T_{on})	μs	30	35	40
Pulse off time (T_{off})	μs	7	12	17
Peak current (IP)	A	1	2	3
Angle (AN)	Degree	30	45	60

time and literature review of various researchers as depicted in Table 3. For this present experiment, Box–Behnken Design (BBD) is considered as experimental design.

3.4 Performance Characteristics

Surface roughness is considered as performance characteristics for this experimental analysis and single-objective optimization is performed using TLBO approach. Surface roughness is measured at three different locations using Mitutoyo SJ-410 surface roughness tester and average of them is taken for analysis purpose. A cone-shaped diamond stylus with tip angle of 90° and diameter of 5 μm was used. Total sampling length of 4 mm, cut off length as 0.8 mm and traverse speed of 0.5 mm/s were kept constant throughout the measurement.

TLBO is an optimization technique to obtain global solutions for continuous as well as discrete problems involving single-objective or multi-objectives introduced by R. V. Rao for high consistency with less computational effort, as it does not require any algorithm-specific parameters. The algorithm work defines the relationship between teachers and learners where the teachers influence the quality of results of learners. The following steps are carried out according to TLBO approach to obtain the optimal solutions [15, 16, 17].

TLBO Steps:

Step 1: Define the population size, design variables, range, objective function and number of iterations.
Step 2: Prepare a table with the values of design variables, objective functions of given population size and find the mean of all design variables.
Step 3: Find the teacher values based on the objective function values.
Step 4: Update other variable values based on the teacher values.
Step 5: Compare the new and corresponding old objective function values and update the table.
Step 6: Select and compare random learners to improve their value.

Step 7: Compare the new and corresponding previous objective function values and update the table.
Step 8: Do the iteration upto termination criteria.

4 Results and Discussion

The measured data obtained from the experiments was used to develop the response surface regression model using design expert software V9.0.1 calculating the regression coefficients. Single-objective optimization was performed to determine the optimal set of solutions for process parameters for response surface roughness. Using MATLAB R2013a, computer code was developed for the parametric optimization in WEDM process considering the population size of 29 and numbers of generations 20.

Response surface regression model depicted in Eq. (1) developed is used for calculating the optimized values of surface roughness in teacher and learner phase:

$$\begin{aligned}\text{Surface Roughness (SR)} &= 0.82 - 0.0543 \times \text{AN} + 1.800 \times \text{IP} \\ &+ 0.0734 \times T_{\text{on}} - 0.2737 \times T_{\text{off}} + 0.000595 \times \text{AN} \times \text{AN} \\ &- 0.1023 \times \text{IP} \times \text{IP} + 0.00036 \times T_{\text{on}} \times T_{\text{on}} + 0.00953 \times T_{\text{off}} \times T_{\text{off}} \\ &- 0.00033 \times \text{AN} \times \text{IP} + 0.000057 \times \text{AN} \times T_{\text{on}} - 0.000027 \times \text{AN} \times T_{\text{off}} \\ &- 0.02710 \times \text{IP} \times T_{\text{on}} + 0.00155 \times \text{IP} \times T_{\text{off}} + 0.00057 \times T_{\text{on}} \times T_{\text{off}} \end{aligned} \quad (1)$$

The RSM-based Eq. (1) contains independent, quadratic and interactive terms which shows the effect of the terms on the considered responses. Coefficients of these equations show the comparative importance of different terms testing process.

From the graph as shown in Fig. 3, it was observed that the curve is always a decreasing curve that is surface roughness value is decreasing from iteration to its successive iteration. More the number of iterations more close to the optimized value. Optimized values for surface roughness are obtained in fourteenth iteration. The optimized set of process parameters for the minimum surface roughness was obtained as shown in Table 4.

5 Conclusions

This experimental study aims at single-objective optimization investigation to determine the optimal set of solution for minimum surface roughness on cutting the Inconel-825 by wire EDM process. Box–Behnken design of experiments was used along with teaching–learning-based optimization algorithm as optimizing technique

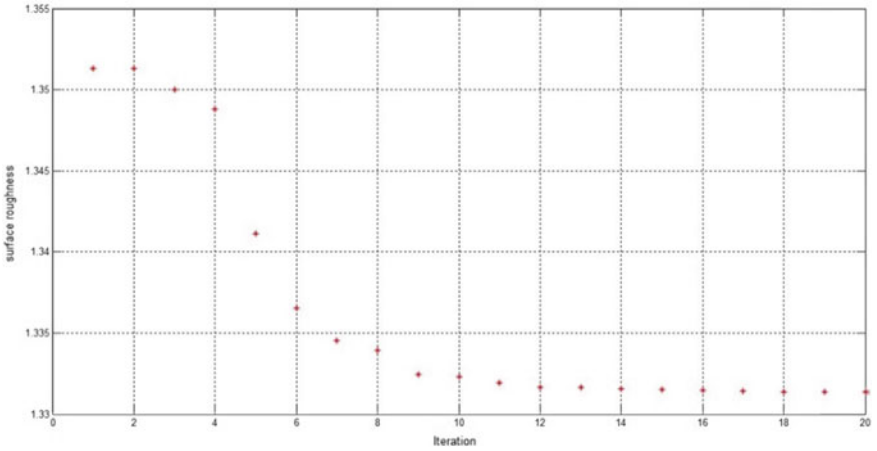

Fig. 3 Effect on surface roughness with number of iterations

Table 4 Optimized value of process parameters using TLBO algorithm

Iteration	Peak current (A)	Pulse on time (μs)	Pulse off time (μs)	Angle (°)	Surface roughness (μm)
14	1	30	13.39245	44.656060	1.331415

for cutting the Inconel-825. Following conclusions have been drawn from the present study:

1. Response surface model was developed to predict the surface roughness.
2. The optimal set of process parameters was obtained at fourteenth iteration for peak current of 1 A, pulse on time of 30 μs, pulse off time of 13.39245 μs and angle of 44.656060° for minimum surface roughness using the TLBO algorithm.

Acknowledgements First author (D. Saikiran) would like to acknowledge Motilal Nehru National Institute of Technology, Allahabad, for providing financial support towards carrying out this research work.

References

1. Rajyalakshmi G, Ramaiah PV (2016) Multiple process parameter optimization of wire electrical discharge machining on Inconel-825 using Taguchi grey relational analysis. Int J Adv Manuf Technol 69(5–8):1249–1262
2. Guo Q, Li Y, Qian J, Yu H, Chen C (2017) Study of the pitting corrosion at welding joints of Inconel-625 alloy under high temperature and high H_2S/CO_2 partial pressure. Int J Electrochem Sci 8929–8943

3. Munde V, Pansare V (2017) Flank wear measurement of Inconel-825. Int Res J Eng Technol 4(8):1343–1351
4. Nair SS, Joshi N (2014) Trends in wire electrical discharge machining (WEDM): a review. Int J Eng Res Appl 4(12):71–76
5. Lin CT, Chung IF, Huang SY (2001) Improvement of machining accuracy by fuzzy logic at corner parts for wire-EDM. Fuzzy Sets Syst 122(3):499–511
6. Sarkar S, Mitra S, Bhattacharyya B (2006) Parametric optimization of wire electrical discharge machining of γ titanium aluminide alloy through an artificial neural network model. Int J Adv Manuf Technol 27:501–508
7. Ramakrishnan R, Karunamoorthy L (2006) Multi response optimization of wire EDM operations using robust design of experiments. Int J Adv Manuf Technol 29:105–112
8. Sarkar S, Sekh M, Mitra S, Bhattacharyya B (2011) A novel method of determination of wire lag for enhanced profile accuracy in WEDM. Precis Eng 35(2):339–347
9. Li L, Guo YB, Wei XT, Li W (2013) Surface integrity characteristics in wire-EDM of Inconel-718 at different discharge energy. Proc CIRP 6:220–225
10. Chen Z, Huang Y, Zhang Z, Li H, Ming W, Zhang G (2014) Ananalysis and optimization of the geometrical inaccuracy in WEDM rough corner cutting. Int J Adv Manuf Technol 74:917–929
11. Zhang G, Zhang Z, Ming W, Guo J, Huang Y, Shao X (2014) The multi objective optimization of medium-speed WEDM process parameters for machining SKD-11 steel by the hybrid method of RSM and NSGA-II. Int J Adv Manuf Technol 70:2097–2109
12. Kumar A, Kumar V, Kumar J (2015) Semi-empirical model on MRR and overcut in WEDM process of pure titanium using multi-objective desirability approach. J Braz Soc Mech Sci 37:689–721
13. Chalisgaonkar R, Kumar J (2015) Multi-response optimization and modeling of trim cut WEDM operation of commercially pure titanium considering multiple user's preferences. Eng Sci Technol Int J 18:125–134
14. Shandilya P, Jain PK, Jain NK (2016) Modelling and process optimisation for wire electric discharge machining of metal matrix composites. Int J Mach Machin Mater 18(4):377–391
15. Rao RV (2015) Teaching learning based optimization algorithm and its engineering applications. Springer, Berlin
16. Tiwari A, Pradhan MK (2017) Applications of TLBO algorithm on various manufacturing processes: a review. Mater Today Proc 4:1644–1652
17. Rao RV (2016) Review of applications of TLBO algorithm and a tutorial for beginners to solve the unconstrained and constrained optimization problems. Dec Sci Let 5:1–30

Internet of Things: A Review on Major Challenges and Applications

Chintan Patel and Nishant Doshi

Abstract Internet of Things has created high opportunities for industries to enhance their manufacturing, servicing and supplying capabilities. Industrial Internet of Things (IIoT) will add innovation and smartness in industrial capabilities. Internet of Things helps the industry to generate the critical and decidedly big data. Generated big data will be analyzed by various data mining algorithms and will generate knowledge out of data. Generated knowledge will create smooth decision making for smart machines by machine learning. Radio frequency identification (RFID) and a quick response code (QR code)-based object tagging has created an easy identification environment for various things in the industry. Most security algorithms are implemented in the Industrial Internet of Things for the purpose of authentication and access control mechanism. IoT has created revolution in the healthcare industry, in terms of data availability and analytics. Similarly, many IoT devices and IoT-based services are implemented in various industries for their day-to-day tasks. In this paper, we have studied various recent applications of IoT in industry in terms of machine learning, security, and services and challenges faced by industries in the deployment of IoT-based services. Mainly, this paper will summarize the current state of an Industrial Internet of Things in a systematic manner and rate of data stream by sliding window and tumbling window, respectively.

Keywords Data analytics · Machine learning · Security · Radio frequency identification (RFID) · Quick response code (QR code) · Wireless communication protocols · Near-field communication · Zigbee

C. Patel (✉) · N. Doshi
Pandit Deendayal Petroleum University, Gandhinagar, Gujarat 382007, India
e-mail: chintan.p592@gmail.com

V. K. Gupta et al. (eds.), *Reliability and Risk Assessment in Engineering*,
Lecture Notes in Mechanical Engineering,
https://doi.org/10.1007/978-981-15-3746-2_40

1 Introduction

As shown in Fig. 1, the revolution of industry commenced in the eighteenth century utilizing mechanization, dihydrogen monoxide power, and steam power was considered as industry 1.0, and in industry 2.0, electricity and its power has engendered high impact. Industry 3.0 was injected with computer and automation. Computerization of manufacturing and automation of data generation is the rudimentary motive of the German regime for industry 4.0. Industry 4.0 is a coalescence of five enabling technologies. This includes Internet of Things, cyber-physical system, M2M communication, cognitive computing, and sizable voluminous data [1]. Most of the entrepreneurs from ecumenical companies are aiming toward the re-establishment of their businesses utilizing perspicacious technologies.

Power of 1% preserving by utilizing Internet of Things is flattering famous in the world. 1% preserving of fuel in the aviation industry leads toward preserving of $ 30 billion. In industry 4.0, the impact of implementation is soothsaying afore the implementation, so it can avail sundry industries and academics to focus toward felicitous designing. For the implementation of industry 4.0, many industries need to regenerate their business model and SWOT analysis. Integration of factory with Internet of Things will lead toward keenly intellectual factory [2]. Internet-enabled radio frequency identification tag (RFID) is leading technology to make industry 4.0 as a true game changer. RFID tag can work as a unique identity for the sundry objects of astute factories. There are so many researchers who are working in the cyber world of things and its impact on society. In [3], the author has discussed the generic structure of IoT and key challenges that Internet of Things will face during implementations. In [4], the author has discussed key enabling technologies. They have additionally discussed IoT three-layer architecture, IoT elements, IoT standards, and communication protocols like MQTT and 6LoWPAN. In [5], researchers have fixated on IoT vision, accommodation-oriented architecture, various application domains for IoT, and sundry open issues including security and privacy.

Industry 4.0 needs to fixate on Amalgamated Nations 17 sustainable development goals. In these goals, UN has fixated to build resilient infrastructure, promote sustainable industrialization, and foster innovation in ninth goal. In that, it targets on promoting inclusive and sustainable industrialization and, by 2030, significantly raises industry's quota of employment and gross domestic product, in line with national circumstances, and double its share in the least developed countries. It believes

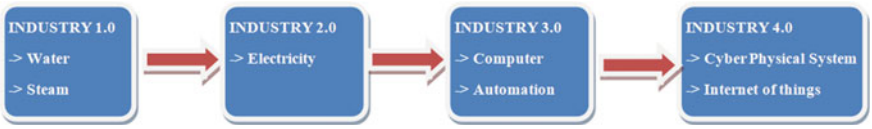

Fig. 1 Industrial revolutions

that Internet of Things and the cyber-physical system will surely play a paramount role in this goal.

This paper is organized as follows. In Sect. 2, we have discussed background of Internet of Things and the current research on Industrial IoT. In these sections, we have discussed numerous IoT research projects carried out by several countries and companies. In Sect. 3, we have discussed IoT architectures. In Sect. 4, applications of IoT on critical industries are discussed. In Sect. 5, we have discussed research challenges and opportunities in IIoT. Section 6 is conclusions followed by references.

2 Internet of Things and Current Research on IIoT

Morgan Stanly refers an "Industrial Internet of Things as robots and machinery connected with Internet, sensors, and software". In Industrial Internet of Things, astute machines or manufacturing contrivances will transmit authentic-time data to the engineers and scientists to work on that. A survey by Morgan Stanly brought to notice that amending operational efficiency is one of the most critical tasks for manufacturers adopting IIoT. According to Stanly's survey, more than 46% of the industry feels that cyber security is another most immensely colossal threat to their business.

In Fig. 2, identity-enabled machines can be any objects inside the industry. All the machines will be equipped with particular identity and utilizing that identity they will communicate among themselves as well as other contrivances. Identity for the contrivances can be achieved utilizing radio frequency identification or near-field communication. RFID provides the capability of communication without physical interconnect. So, with the avail of RFID, it becomes facile to group the product, to identify and track the product, as well as to map the product. Near-field NFC with NFC tag provides capabilities to store identification data. Sharing, pairing, and transaction are a consequential area in which NFC can be utilized. NFC requires

Fig. 2 IIoT basic architecture [6]

less amount of computation compared to other technologies. One session–one key mechanism makes NFC more congruous option for payment technologies [7].

IoT will engender wireless mesh network at the above layer, communicating with possibly a wired or wireless bus or ring network at ground level. A fog computing [8, 9] provides the capability to gateway contrivances for processing data and engendering capabilities to convert it into information. In [9], fog computing is defined as a "Model to complement the cloud for decentralizing the concentration of computing resources like servers and accommodations in data center toward users for ameliorating the quality of accommodations and their experiments."

Overall fog computing will amend the quality in terms of efficiency and performance of computing. Zigbee (IEEE 802.15.4) is radio frequency communication [10]. Rudimentally, two types of Zigbee contrivances are utilized 1. RFD and 2. FFD. Reduced function contrivances (RFD) of Zigbee is capable enough to connect meters, actuators, and sensors, but reduced function contrivances cannot do the communication among themselves. Full function contrivances (FFD) of Zigbee are capable enough to do intercommunication as well as communication with meters, actuators, and sensors [10]. Another protocol that can be utilized by superseding Zigbee predicated on applications domains is 6LoWPaN (IPv6 predicated low-power personal area network) that utilizes the wide identity allocation capability from IPv6.6LoWPaN, RFC 4919 [11] fortifies minute packet size, 16-bit and 64-bit media access control database, Low bandwidth, topology like start and mesh, low puissance, low cost, the astronomically immense number of contrivances deployment. IEEE 802.15.1, Bluetooth, is additionally utilized for minuscule range contrivances communications. M2M (machine-to-machine communication) includes factory machines, enabling actuators or sensors to transfer recorded data to software application that can utilize it for mining the data and engender the erudition for decision making.

XMPP, REST, COAP, and MQTT are protocols utilized at IoT application layer. XMPP, RFC 3920 [12] is extensible messaging and passing protocol. XMPP uses extensible markup language to communicate between Web objects. XMPP follows client-server architecture for communication. Constrained application protocol (COAP) [13] is the Web-predicated protocol that fortifies resource unearthing predicated on representation state protocol (REST).

Lack of unique standardization is one of the most immensely colossal challenges that industries are facing in adopting Internet of Things. Currently, for the development of IoT-predicated business solutions, developer needs to identify felicitous hardware and predicate on hardware felicitous protocols, the desideratum to develop the software. IoT will need mainly three types of standards, software standardization which includes protocols for communication (wireless as well as wired), security, data maintenance, data mining and application development; hardware standardization which includes motherboard designing, sensor manufacturing, gateway development, and cables manufacturing; licitness standardization which includes policies matter for confidentiality, access control, authentication, and privacy preserving. Open connectivity foundations (OCF) is working toward providing open-source designations, code, and certification program. OCF provides accommodations to mainly

three entities, manufacturers, developers, and users. It provides frameworks for secure interoperability for multiple operating systems, communication protocols, platforms, and use cases.

OneM2M is ecumenical industry which fixates on development of architecture, security solutions, and interoperability solutions for machine-to-machine and Internet of Things developments. It is working toward providing accommodations to sundry industries like healthcare, automation, and astute home. There are other organizations working for the standardization of sundry entities in IoT establishment like International Engineering Task Force, IEEE, International Telecommunication Unit, China Electronics and Standardization Institute, and National Institute for standardization for technology [14, 15].

3 IoT Architecture and Industrial Applications

In Fig. 3, we have discussed basic four-layer IoT sensor and service (S&S)-based architecture. In 2010, [16], Wu et al. have proposed three-layer architecture for the Internet of Things. Later on in [3], Khan et al. have discussed five-layer architecture for the Internet of Things. Recently, in 2016, IEEE has launched new project, IEEE P2413 Project, for the development of architecture and standards for Internet of Things, which aims to provide an architecture outline which seizures the unities across diverse fields and provides a foundation for instantiation of existing IoT architectures. Authors in [17] and [18] had also discussed industrial IoT based architectures and applications.

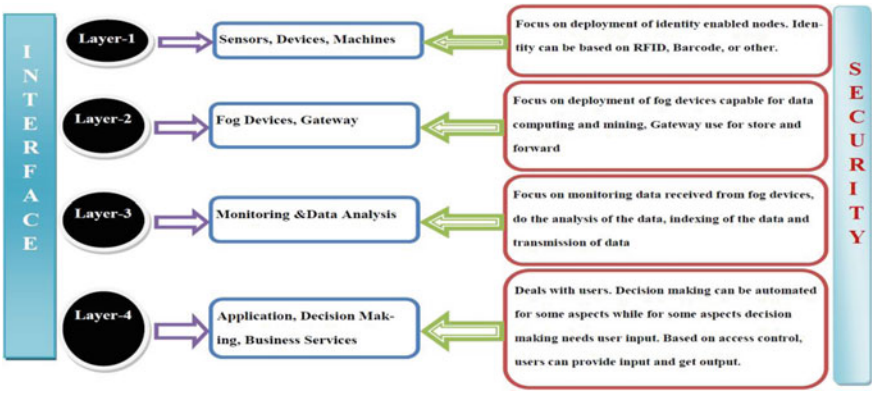

Fig. 3 IoT sensors and service (S&S)-based architecture [6]

3.1 Sensors, Devices and Machine

Layer 1 is the base layer of the IoT architecture. This layer is additionally considered as information accumulating layer. This layer will fixate on standardization and accommodations for physical aspects of sundry "THINGS" involved in the Industrial Internet of Things. For the manufacturing phase, sundry machines are involved starting from input of raw material, followed by processing of raw material, and packaging of the product. These machines are identity-enabled and equipped with sundry sensors and actuators. Actuators are contrivances capable to perform predication on the input of sensors. Perspicacious grid architecture [19] deploys sensor at transmission station, distribution station, load accommodating station, energy storage, and so on.

3.2 Fog Devices and Gate Way

Layer 2 is the "store," "filter," and "forward" layer of the IoT Architecture, sundry fog contrivances "which are considered as perspicacious routers" capable of data processing and accumulating the data from sundry sensors. Fog computing is a component of distributed computing. Distributed computing aims to reduce overhead of cloud server for data processing. Feasibility of fog computing is discussed in [9], and fog computing leads toward amelioration in the quality of accommodations. According to [9], data transmission between layer 1 contrivances and cloud server is reduced by 90% due to fog computing, and response time is incremented by 20%. So, this layer is very much consequential in terms of "qualitative" distribution of accommodations.

3.3 Monitoring and Analysis

Layer 3 is the "cloud and information mining" layer of the IoT architecture. This layer will process the information and will convert this information into "knowledge." Knowledge is also considered as indexed data or decisions. This device will communicate with applications as well as fog devices. Various entities like Google and Amazon provide cloud services to various business entities. Amazon provides virtual server services via Amazon EC2, Amazon S3 provides a facility for scalable storage, Amazon RDS provides relational database services, and Amazon API Gateway provides a facility for building, deploying, and managing application program interfaces. This layer will be capable of implanting recommender system which will be the outcome of data processing. Amazon Greengrass performs local computer messaging and sync for devices.

3.4 Application, Decision Making, and Business Services

Layer 4 is the interconnecting layer between utilizer and business. Development of the technology-vigilant business model will be required for the better servicing to the customers. Mobile API will work as a key interface for the business. Prosperous deployment of the technology-cognizant business model will lead toward better profit model. This layer will work as a consummate business management layer for the promoters while it will work as accommodation achieving for the customers. This layer will avail in analyzing and decision taking for the ordinate dictation-supply ratio of the enterprise. Concurrently, it will avail the customer to fine-tune deals and negotiations for the sundry enterprise accommodations. Enhanced mobile applications development will be the key capability requisite for the qualitative implementation of this layer.

4 Key Industrial IoT Application

Smaller finite sets from unbounded data stream procreate window, which become significant by applying operations such as aggregation and joins. Among them, aggregation is a common important feature in streaming applications. Such applications often need an aggregated summary of the most recent data in a stream, which is deemed the most relevant. A poorly chosen algorithm can cause high latencies and high memory consumption, leading to losses, missed opportunities, and quality-of-service violations. Aggregation operation depends on its window, which aims the most efficient algorithm. The most commonly used aggregation algorithms are discussed in the following sections.

4.1 Healthcare Industry

The medical industry had most magnetized and adopted IoT technology compared to any other industry. One of the mundane goals that we keep in mind during the development of applications is "more automation." A survey by Islam et al. [20] discusses security, wearable contrivances, sizable voluminous data, e-Health policies, and their economic impact. Increasing death ratio by sudden heart attacks, road accidents, and diabetic diseases has led toward the necessity of technological amelioration in the medical industry. Internet of Things (IOT)-predicated applications in the healthcare will reduce the accommodation time to the patient, will reduce the cost, and ameliorate the quality of life. TechNet topology discussed in [20] shows the rudimentary structure of connectivity between sundry components involved in IoT healthcare. The health-care based IoT discussed in [21] shows iMedBox as an open platform-predicated astute medicine box and iMedpack as a perspicacious

pharmaceutical packaging and wearable bio-medical sensor contrivances. In e-Health, human equipped with wearable contrivances or/and bio-chip will perpetually send the data to the remote server via the base station.

4.2 Smart City

Urbanization in the world engendered the most immensely colossal challenge for the sundry countries. The major challenge includes engendering a sustainable and pollution-free environment, open and safe conveying system, renewable and low-cost energy solutions, innovative inculcation system, innovative solutions for supply chain management including dihydrogen monoxide supply, oil and gas supply, and so on. To provide the better solution and facile life, astute city initiatives are taken by both public and private sector and commenced to contribute to that. Kaa is a open source and flexible IoT platform for the development of end to culminate solutions. It provides perspicacious meter network, perspicacious city lighting, perspicacious grid automation, ecology monitoring solutions, ad-sultry traffic balancing, and perspicacious public safety engenderment. Libelium reported about sundry perspicacious cities in their white paper [21]. "Sensing the city" project aims to monitor authentic-time air quality parameter in Glasgow city. Carbon track and trace project aims at reducing carbon dioxide emissions in Nordic countries. Vicrea with Libelium technology launched a project to manage canal traffic in the Netherlands city.

4.3 Production, Mining, and Manufacturing

Cumbersomely hefty equipment utilized in mining, manufacturing, agriculture, construction, and logging is becoming more keenly intellective day-by-day. In the above verbally expressed operation, safety and autonomy is the major parameter. Manual mining of coal, gold, or ceramic is one of the perilous tasks in the engendered world. Safety can be achieved by preparing human-less devices. Rio Tinto's automated truck is utilized in autonomous haulage system as well as autonomous drill systems. The general motor commenced manufacturing of driverless cars with cruise automation system. Rolls Royce aerospace is celling engine power by "power by the hour" model, and they utilize sensors built into jet plants to identify users. Various challenges in the adoption of keenly intellective manufacturing include interoperability, safety, cost and profit, regulation, security, the colossal data, and usability [22]. IBM Watson, a cloud platform of IBM, provides industrial data analytics and support system for decision making. A Sandvik Coromant, a tooling giant, has engendered scalable accommodation model with Microsoft IoT Suit and Azure to provide standard quality of accommodation to its customers.

4.4 Research Challenges in Industrial Internet of Things

Industrial IoT research challenges can be divided into two components. 1. Researchers will fixate on research challenges associated with obligatory ideological aspects like standardization, adaptability, modularity, and secure business model. 2. Researcher will fixate on technological aspects and its developments. An IoT also has many security challenges which are surveyed by Patel et al. in [23].

4.5 Adaptability

Manufacturing of sundry sensors engendered sundry options for the utilizer to develop astute objects. Sundry industry bellwethers are converging for the engenderment of prevalent standards, prevalent architecture, and mundane platforms. Better adaptability will engender better interoperability. Better interoperability will open the door for more expeditious deployment of the cyber world of things. Efficient interoperability will provide innovation and cost reduction in deployment [22]. Modular adaptability will lead toward the development of each different module and will not engender conflict. Modules can be additionally considered as a four-layer architecture discussed above. Industrial IoT will be the relatively closed environment and will communicate within a company. According to the survey, more than 85% of data communication will transpire within company contrivances. So, interoperability of data formats is withal a paramount aspect and its needs standardization for data representations. Hardware-level adaptability additionally needs to take care.

4.6 Data Transmission Latency

Latency is considered as a delay in transmission of data signal and control signals. Development of low weight communication model inside the large industry for the faster operations is also an important need of industry. A message received few seconds late may become useless sometimes in the IoT architecture where devices are miles apart. So, it becomes necessary to secure company operations from creating unnecessary collision inside the network. Congestion control mechanism can help in this.

4.7 Security Challenges

In most of the currently available IoT security systems, the authentication between devices occurs through device-to-device (D2D). The D2D authentication takes more

time and computation, so we find that there is a strong need to find a solution like level-dependent authentication through which we can authenticate and secure multiple IoT devices at a time.

5 Conclusions

In this paper, we have reviewed the current status of industry 4.0 and its function. We also proposed IoT's general architecture as well as sensor and service (S&S)-based IoT layered architecture. We have also discussed various application domains closely related to the Industrial Internet of Things. Industrial IoT was the focus of this paper. We have discussed research challenges associated with IIoT. So, overall, this paper presents precise survey about the industrial Internet of Technology.

References

1. Hermann M, Pentek T, Otto B (2016) Design principles for industrie 4.0 scenarios
2. Kagermann H, Wahlster W, Helbig J (2013) Recommendations for implementing the strategic initiative industrie 4.0
3. Khan R (2012) Applications and key challenges future internet: the internet of things architecture, possible applications and key challenges. In: Proceedings of international conference on frontiers of information technology, pp 257–260
4. Al-fuqaha A, Guizani M, Mohammadi M, Aldheri M, Ayyash M (2015) Internet of Things: a survey on enabling technologies, protocols, and applications. IEEE Commun Surv Tutor 17(4):2347–2376
5. Atzori L, Iera A, Morabito G (2010) The Internet of Things: survey. Comput Netw 54(15):2787–2805
6. Patel C, Doshi N (2018) Internet of things security: challenges, advances, and analytics. Auerbach Publications, New York, NY
7. Husni E, Kuspriyanto, Basjaruddin N, Purboyo T, Purwantoro S, Ubaya H (2011) Efficient tag-to-tag near field communication (NFC) protocol for secure mobile payment. In: Proceedings of international conference on instrumentation, communications, information technology, and biomedical engineering, pp 97–101
8. Dastjerdi AV, Buyya R (2016) Fog computing: helping the Internet of Things realize its potential
9. Varghese B, Wang N, Nikolopoulos DS, Buyya R (2017) Feasibility of fog computing
10. Gill K, Yang SH, Yao F, Lu X (2009) A ZigBee-based home automation system. IEEE Trans Consum Electron 55(2):422–430
11. 6lowpan RFC, pp 1–12 (2007)
12. Andre PS (2004) XMPP RFC 3920, pp 1–77
13. Hornsby A, Belimpasakis P, Defee I (2009) XMPP-based wireless sensor network and its integration into the extended home environment. In: IEEE international symposium on consumer electronics, pp 794–797
14. Singh S, Singh N (2016) Blockchain: future of financial and cyber security. In: Proceedings of 2nd international conference on contemporary computing and informatics, pp 463–467
15. Atzori L, Iera A, Morabito G (2010) The Internet of Things: a survey. Comput Netw 54(15):2787–2805

16. Wu M, Lu TJ, Ling FY, Sun J, Du HY (2010) Research on the architecture of internet of things. In: Proceedings of the 3rd international conference on advanced computer theory and engineering, vol 5, pp 484–487
17. Wan J, Humar I, Ferrari D (2016) Industrial IoT technologies and applications
18. Xu LD, He W, Li S (2014) Internet of Things in industries: a survey. IEEE Trans Ind Inform 10(4):2233–2243
19. Albrecht K, Michael K (2013) Connected: to everyone and everything. IEEE Technol Soc Mag 32:31–34
20. Islam SMR, Kwak D, Kabir MH, Hossain M, Kwak KS (2015) The Internet of Things for health care: a comprehensive survey. IEEE Access 3:678–708
21. Yang G et al (2014) A health-IoT platform based on the integration of intelligent packaging, unobtrusive bio-sensor, and intelligent medicine box. IEEE Trans Ind Inform 10(4):2180–2191
22. Bloede K, Mischou G, Senan A, Tilow A (2017) The industrial Internet of Things making factories 'smart' for the next industrial revolution, p 124
23. Patel C, Doshi N (2019) Security challenges in IoT cyber world. Security in smart cities: models, applications, and challenges. Springer, Cham, pp 171–191

Development of Computational Decision Making Tool for Predicting the Growth and Development of Rice Crop Using Location Specific Diurnal Air Temperature Data

A. Alagesan, P. Vaishnavi, and R. Karthikeyan

Abstract Temperature plays an active role in growth and development of any plant. From sowing till maturity, the plant has to undergo different phenological phases called crop growth stages/plant growth stages. Measuring growing degree days (GDD) is employed to assess the growth and development of any plants provided all other factors required for the growth of the plants are conducive. The plant growth may cease if the plant experiences a certain low temperature specific to each plant species called base temperature. Keeping in view that each plant species and crop varieties has its own requirement of growing degree days from sowing to till harvest, a study was undertaken to assess the GDD requirement for rice crop varieties ADT 38 and CR 1009 during kharif and rabi, respectively, in South India The objective of this study is to (1) calculate GDD on daily basis (2) develop a mathematical model to forecast crop growth stage and maturity date based on AGDD (3) verify the model using field data and (4) provide farmers with a forecast tool to estimate crop growth and crop maturity date well in advance. The results revealed that the two cultivars attained physiological maturity at 134 and 154 days after sowing, respectively. Variation in the growing degree days was observed between cultivars. The growing degree days (GDD) of both the varieties of rice indicated that the variety CR 1009 availed more GDD (2481.3) as compared to variety ADT 38 (2207.9) due to longer duration of the variety.

Keywords Crop growth · Growing degree days · Prediction tool · GDD · AGDD

A. Alagesan (✉)
A. D. Agricultural College & Research Institute, Tamil Nadu Agricultural University, Tiruchirappalli, India
e-mail: alagesan2000@gmail.com

P. Vaishnavi (✉) · R. Karthikeyan
Anna University Chennai—BIT Campus, Tiruchirappalli, India
e-mail: vaishmk@gmail.com

R. Karthikeyan
e-mail: karthee.r@gmail.com

V. K. Gupta et al. (eds.), *Reliability and Risk Assessment in Engineering*,
Lecture Notes in Mechanical Engineering,
https://doi.org/10.1007/978-981-15-3746-2_41

1 Introduction

Measuring growing degree days (GDD) is employed to assess the growth and development of any plants provided all other factors required for the growth of the plants are conducive. The plant growth may cease if the plant experiences a certain low temperature specific to each plant species called base temperature [1]. The concept of GDD is being used by many researchers to study the different growth phases of plants during different growing seasons [2]. The agriculture field and applications of GDD find its role (1) to depict the changes in air temperature on plant growth and development [3]; (2) to take planting decisions [4, 5]; (3) as a measure to assess the role of plating date on crop performance [6]; (4) to make agronomic management decisions based on improved crop growth [7]; (5) to predict the decomposition of crop residue and to study the nutrient release pattern [8] and (6) to study the seasonal variation of climatic factors and crop growth and yield [9]. Dynamics of GDD during the growth period of plants may act as an important tool to assess the impact of climate change on crop plants. Keeping in view that each plant species and crop varieties has its own requirement of growing degree days from sowing to till harvest, a study was undertaken to assess the GDD requirement for rice crop varieties ADT 38 and CR 1009 during kharif and rabi, respectively, in South India The objective of this study is to (1) calculate GDD on daily basis (2) develop a mathematical model to forecast crop growth stage and maturity date based on AGDD (3) verify the model using field data (4) and provide farmers with a forecast tool to estimate crop growth and crop maturity date well in advance.

2 The Concept of Growing Degree Days

Temperature plays an active role in growth and development of any plant. From sowing till maturity, plant has to undergo different phenological phases called crop growth stages/plant growth stages. The plant requires/consumes heat for its growth and development. For successfully completing each plant growth stage, the plant requires heat energy. The required heat energy for plant is called as growing degree days (GDD); GDD is also called as thermal time, degree days and growth unit by some researchers. The GDD is calculated using daily diurnal air temperature data using different methods, viz. (i) averaging method (ii) Baskerville-Emin (BE) method—mathematical curve fitting method using calculus and (iii) electronic real-time air temperature data collection.

The calculation for GDD is provided as $\text{GDD} = (T_{\max} + T_{\min})/2 - T_{\text{b}}$, where $T_{\max}$ and $T_{\min}$ are daily maximum and minimum air temperature in degrees centigrade

and T_{base} is the base threshold temperature in degrees below which the process of growth does not progress. The formula of the GDD is a summation formula for each day of the growing season.

Temperature affects plant root growth, nutrient uptake and water uptake photosynthesis, respiration and photosynthates. Temperature also affects plants morphology, growth pattern, maturity and also the time required to reach various plant growth stages. On the method of determining the most suitable sowing date, the method involves computing GDD for each day of the year, then to compare it to the acceptable range of GDD values, there are many concepts and methods have been used to predict various growth stages of crop plant; however, growing GDD concept is found superior for adoption under different agroclimatic condition. For seasonal accumulation, the daily GDD values were summed as AGDD throughout the season. T_{base} varies among species and possibly cultivars and likely varies with the growth stage under consideration.

3 Data Acquisition and Analysis

Data sources and datasets description: The voluminous quality controlled historic daily weather data, viz. daily maximum and minimum temperature for each location from India Meteorological Department forms the integral part of the base data. The data will be updated on daily time step from local weather station. The data from the computational global circulation model form the part of future climate change scenarios. The crop-specific thermal data on base temperature and crop phenology data from published research form the base of crop data. The computational model computes the GDD for each selected crop sowing date and calculates AGDD to a particular crop and particular location to reach different growth stages. This can also be used to predict the performance of different crops under future climate change scenarios.

The system shall be programmed to provide the output of the daily GDD in the form of graph on daily basis and also the AGDD on the growth stage basis. The research based on each crop specific required AGDD at which maturity will be reached has to be incorporated into the programming so as to forecast the crop plan's maturity date for each crop. On the method of determining the most suitable sowing date, the method involves computing GDD for each day of the year, then to compare it to the acceptable range of GDD values, and hence, specifying the suitable sowing dates. This requires 365 evaluations of GDD equation that requires long calculation times, in addition to the need of accessing the climate database to find T_{max} and T_{min} of each day of the year and storing a massive amount of data in the computer's memory. The predicted maturity date depends on actual AGDD up to the date the model is queried and the predicted AGDD for the remainder of the season using the long-term average GDD values (Fig. 1).

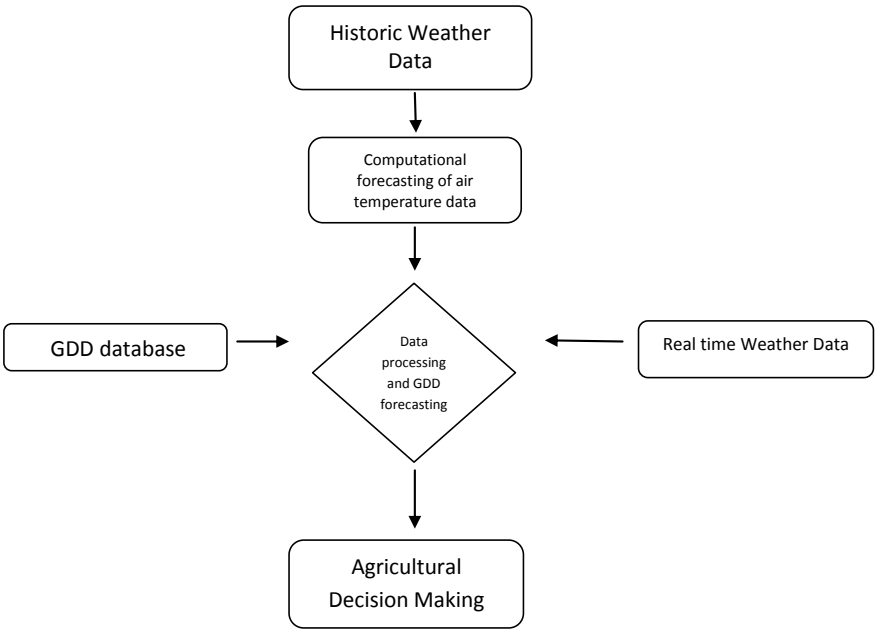

Fig. 1 Schematics of GDD-based decision making

4 Results

The GDD requirement for selected rice variety ADT 38 and CR 1009 for rabi season in Tamil Nadu was calculated. This is an arithmetic accumulation of daily mean temperature above the threshold temperature where the degree days are equal to [maximum temperature + minimum temperature/2] base temperature. The warmth of 12 °C was considered as a base temperature for rice for calculating the degree days. The growing degree (heat units) required to attain different phonological stage was computed and presented in Table 1.

Table 1 Growing degree days to attain different phonological stages

No.	Phenological stages	ADT 38	CR 1009
1.	Sowing—transplanting	500.05	628.75
2.	Transplanting—panicle initiation	636.90	739.25
3.	Panicle initiation—heading	466.70	488.10
4.	Heading—50% flowering	109.15	116.95
5.	50% flowering—maturity	428.10	418.05
6.	Maturity—harvest	67.05	90.25
Total		2207.95	2481.35

The two cultivars attained physiological maturity at 134 and 154 days after sowing, respectively. Variation in the growing degree days was observed between cultivars. The growing degree days (GDD) of both the varieties of rice indicated that the variety CR 1009 availed more GDD (2481.3) as compared to variety ADT 38 (2207.9) due to longer duration of the variety.

5 Conclusion

Each plant species is having its own distinct physiological crop stages. With respect to agricultural crops, crop management practices were done based on the crop growth stage attained by the specific crops. The crop plant attains its different growth stages after experiencing/receiving a specified quantum of heat units in the form of the accumulated thermal unit/growing degree days. For a better crop management and attaining maximum crop yield, it is wise to predict the date of succeeding crop growth stage, thereby suitable crop management practices can be programmed to satisfy the crop input need for achieving higher yield. The crop growth stages can be predicted using computational prediction technique using historic air temperature data in combination with computational model prediction. Once the future air temperature data is predicted, using the crop-specific GDD one can make informed decision for managing the agricultural crops for achieving higher yield. In this study, the GDD requirement for selected rice variety ADT 38 and CR 1009 for rabi season in Tamil Nadu was calculated. The growing degree days (GDD) of both the varieties of rice indicated that the variety CR 1009 availed more GDD (2481.3) as compared to variety ADT 38 (2207.9) due to longer duration of the variety.

References

1. Cleland EE, Chuine I, Menzel A, Mooney HA, Schwartz MD (2007) Shifting plant phenology in response to global change. Trends Ecol Evol 22(7):357–365
2. Bollero GA, Bullock DG, Hollinger SE (1996) Soil temperature and planting date effects on corn yield, leaf area, and plant development. Agron J 88(3):385–390
3. Kadioğlu M, Şaylan L (2001) Trends of growing degree-days in Turkey. Water Air Soil Pollut 126(1–2):83–96
4. Griffin TS, Honeycutt CW (2000) Using growing degree days to predict nitrogen availability from livestock manures. Soil Sci Soc Am J 64(5):1876–1882
5. Lu H-Y, Lu C-T, Chan L-F, Wei M-L (2001) Seasonal variation in linear increase of taro harvest index explained by growing degree days. Agron J 93(5):1136–1141
6. Esparza A, Gowda P, Baumhardt R, Marek T, Howell T (2007) Heat unit avail-ability for cotton production in the Ogallala Aquifer region of the United States. J Cotton Sci 11:110–117
7. Thomison P, Nielson R (2002) Impact of delayed planting on heat unit requirements for seed maturation in maize. Pontificia Universidad Católica de Chile. Departamento de Ciencias Vegetales. Seminario Internacional Semillas: comercialización producción y tecnología, Santiago, vol 15, pp 140–164

8. Nielsen RL, Thomison PR, Brown GA, Halter AL et al (2002) Delayed planting effects on flowering and grain maturation of dent corn. Agron J 94(3):549
9. Hassan QK, Bourque CP, Meng F-R, Richards W (2007) Spatial mapping of growing degree days: an application of MODIS-based surface temperatures and enhanced vegetation index. J Appl Remote Sens 1(1):013511–013512

Comparative Analysis of Multi-objective Algorithms for Machining Parameters of Optimization of EDM Process

Vimal Savsani, T. Ramprabhu, Mohak Sheth, N. Radadia, S. Parsana, N. Sheth, and R. K. Mishra

Abstract Recently, several evolutionary algorithms have been formulated with multi objective optimization capabilities. Evolutionary algorithms (EAs) are gaining popularity with the increasing computational resources. Moreover, in the field of non-conventional manufacturing processes, evolutionary algorithms are emerging as a powerful tools for their highly efficient population based optimal searches. However, in most cases selection of algorithms is based on empirical understanding and no standard resources exist for comparing the performance of such algorithms relevant to the manufacturing domain. This paper compares results of five advanced evolutionary algorithms- Non-dominated Sorting Genetic Algorithm-III (NSGA-III), Strength Pareto Evolutionary Algorithm-II (SPEA-II), Multi-objective Evolutionary Algorithm Based on Decomposition (MOEA/D), Pareto Envelope-based Selection Algorithm-II (PESA-II), and Passing Vehicle Search (PVS) algorithm. The performance of EAs are compared using three cases of EDM process. In each case, solution sets for all five optimization methods are recorded. These solution sets are used to

V. Savsani · N. Radadia · S. Parsana · N. Sheth
Pandit Deendayal Petroleum University, Gandhinagar, Gujarat, India
e-mail: vimal.savsani@gmail.com

N. Radadia
e-mail: nradadia96@gmail.com

S. Parsana
e-mail: sparsana2@gmail.com

N. Sheth
e-mail: 107nps@gmail.com

T. Ramprabhu
Materials and Manufacturing Processes, Panchami Punchapadam, Palakkad, Kerala 678633, India
e-mail: ramprabhu.t@gmail.com

R. K. Mishra
CEMILAC, Defence R&D Organization, Bangalore, India
e-mail: rkmishra.drdo@gmail.com

M. Sheth (✉)
Canadore college, North Bay, Canada
e-mail: vimal.savsani@canadorecollege.ca

V. K. Gupta et al. (eds.), *Reliability and Risk Assessment in Engineering*,
Lecture Notes in Mechanical Engineering,
https://doi.org/10.1007/978-981-15-3746-2_42

plot Pareto optimal plots for visual comparison of performances. To quantitatively ascertain the performance of an algorithm based on the generated solution sets, seven performance metrics are considered—Generational Distance, Inverted Generational Distance, Spacing, Spreading, Hypervolume, and Pure Diversity which are coded using MATLAB. The combination of these performance metrics determines the cardinality, accuracy and diversity of solution sets in each case. Preliminary studies have shown that NSGA-III has better performances measure in overall terms among the five algorithms. Thus, the results of this study will help researchers in selecting appropriate optimization technique based on the established performance measures of that algorithm.

Keywords Evolutionary algorithms · Optimization · Pareto fronts · Passing-vehicle search · Performance metrics

1 Introduction

Surface finish and dimensional accuracy are related to high precision manufacturing processes for the automotive and aerospace industry. Electrical Discharge Machining (EDM) is an advanced non-conventional machining method widely utilized in the fabrication of precision components from extremely hard materials [1]. Machining parameter optimization for different class of materials is practiced to achieve high quality output at a minimal cost. It is even more critical for processes like EDM where the relationship of control variables (like pulse duration, peak current, etc.) is stochastic in nature and no analytical relationship could be established. Statistical models are widely developed for EDM process responses (Material removal rate (MRR), surface roughness, etc.) individually for different workpiece materials. Optimization schemes used so far mostly consider single objectives at a time and there is a lack of multi-objective approaches for response models in EDM. Evolutionary algorithms have been hugely successful in solving applied multi-objective problems, especially in engineering [2]. Several algorithms have been developed in this regard.

Non-dominated Sorting Genetic Algorithm-III (NSGA III) demonstrates satisfactory results for many objective constraint optimization problems (2–15 objectives) using well spread reference points. Difficulty in handling many objective problems using other Evolutionary multi-objective algorithms such as non-dominance of large fraction of population, computationally expensive evaluation of diversity and inefficiency of recombination operator can be solved using NSGA III [3]. Strength Pareto Evolutionary Algorithm-II (SPEA-II) contemplates convergence and diversity which outperforms the weakness of other evolutionary algorithms. It incorporates improvement in fitness assignment scheme, density estimation technique for the precise search process and a new archive truncation method to perpetuate boundary solutions [4]. Pareto Envelope-based Selection Algorithm-II (PESA-II) proposed the region based selection, rather than individual based selection to ensure a good spread of

development along the pareto frontier. The unit of selection is a hyper box in the objective space and the resulting selected individual is randomly chosen from this hyper box [5]. In Multi-objective Evolutionary Algorithm based on Decomposition (MOEA/D), the optimization problem is decomposed into a number of scalar optimization sub-problems and optimizes them simultaneously. It surmounts other evolutionary algorithms in terms of lower computational complexity and incorporation of the normalization techniques for disparately scaled objectives [6]. PVS developed [7] is primarily a single objective optimization algorithm. The authors have modified the PVS algorithm to allow multi-objective optimization using priori articulation of preferences and normalization of different output function technique. The weighted sum method was implemented on objective functions thereby transforming them into a single function. Functions can be permuted by dividing that response with the modulus of function maxima, thus forming a non-dimensional objective function [8]. However, there is a research gap in determining the suitability of multi-objective approaches based on the nature of problem. Although many quantitative measurement assessments have been proposed, they have not been used for describing the performance characteristics of manufacturing problems.

The results of multi-objective optimization are obtained in the form of Pareto fronts. These frontiers may be concave, convex, linear and discontinuous depending on the type of objective function and optimal solution space. Simple visual inspection may not yield sufficient information about the quality of solution sets. Quantitative measurement tools must be used for the comprehensive evaluation of Pareto solution sets. Okabe et al. [9] concluded that single indicators should not be relied upon to compare different algorithms. The algorithm is considered better if it (i) predicts solutions as close to the best optimal (or true) Pareto frontier, and/or (ii) find solutions with high cardinality and diversity in the non-dominated space. However, the comparisons are made on common algorithmic parameters for uniformity. The authors have employed the following performance metrics for comparing the results obtained:

- Generational Distance (GD): It was proposed by [10]. It evaluates the average distance between solutions of given Pareto frontier (Q) with respect to true Pareto (P*) frontier.
- Inverted Generational Distance (IGD): It is similar to GD but it is not Pareto compliant, so its conclusions may vary depending on the size of the reference front. However, it is computationally better than GD.
- Spacing: Spacing was proposed by J. Scott [11]. It computes the relative distances between the consecutive solutions in the non-dominated solution set. A lower value of spacing is desired for solutions to be uniformly spaced in the solution space.
- Spreading: This metric was suggested by Deb et al. [12] to measure the spread of solution over the solution space. It describes the extent of spread achieved among the obtained solutions.
- Hypervolume: Hypervolume indicator computes the union of the hypercubes of the domination regions described by the elements of Pareto solution sets [10]. It

provides information about convergence, as well as the diversity of solutions in Pareto front. It is only known estimator that combines pareto dominance by using the proximity test and distribution test of Pareto solutions. The authors use the formulation of Cheng et al. [13] which has simplicity and robustness. Large values of hypervolume values suggest better converged results for least scaled objectives.

- Pure Diversity (PD): It is the sum of the dissimilarity in solutions to the remaining population in a greedy order, with solutions having maximal dissimilarity being the highest priority to account for its dissimilarity [14]. PD is used to study the diversity maintenance performance of algorithms through their solution sets. A higher value of PD is useful in achieving a more random distribution of solutions in objective space.

In this paper, the authors have developed a multi-objective capable-Passing Vehicle Search (PVS) Algorithm and used six different performance assessment tools for four other popular multi-objective algorithms. Empirical results fully demonstrate the superiority of our proposed method.

2 Methodology

2.1 Case Studies

Table 1 shows the summary of all case studies which are analyzed for comparing Pareto fronts. Also, the algorithm parameters are fixed for uniformity in comparison and are shown in Table 2. Eiben et al. [15] described a framework to tune such parameters for evolutionary algorithms. To find an appropriate combination of parameters, this methodology alongside trial and error is adopted to save time.

Table 1 Summary of case studies [16–18]

Parameters	Case 1	Case 2	Case 3
Material	Standard high speed steel	SiC/Al composites	AISI 5160
Machining parameters	Current, pulse on time, pulse-off time	Peak current, pulse-on time, pulse-off time, servo voltage	Pulse on time, pulse-off time, peak current, flushing mode
Response variables	MRR, surface roughness	MRR, surface roughness	MRR, surface roughness
Statistical modeling	Support vector machine	Multivariable regression model	Central composite design
Lower limit	[6, 50, 50]	[1, 3, 2, 65]	[100, 30, 1, 1]
Upper limit	[15, 200, 200]	[6, 7, 7, 75]	[500, 390, 12, 5]

Table 2 Algorithm parameters valid for all the optimization techniques

Algorithm parameters	Value
Population size	200
Maximum number of iteration	50
Crossover percentage	0.995
Mutation percentage	0.005
Mutation rate	0.02

Henceforth, authors used mathematical models for three cases (multi-objective optimization) to evaluate the performance of evolutionary algorithms mentioned below vis-à-vis each case:

Case 1 Objective Functions [16] is given in Eqs. (1) and (2):

$$\text{Material Removal Rate} = e^{-0.9421} * \text{Current}^{1.5264} * T_{on}^{0.4418} * T_{off}^{-0.5176} \quad (1)$$

$$\text{Average Surface Roughness} = e^{-0.1080} * \text{Current}^{0.5484} * T_{on}^{0.1203} * T_{off}^{0.0238} \quad (2)$$

Case 2 Objective Functions [17] is given in Eqs. (3) and (4):

$$\begin{aligned}\text{Material Removal Rate} = {} & -4.76 + 0.2201 * \text{Current} + 0.620 * T_{on} + 0.352 * T_{off} \\ & + 0.0720 * \text{Servo voltage} + 0.01976 * \text{Current}^2 \\ & - 0.012401 * \text{Current} * T_{off} + 0.0182 * T_{on} * T_{off} \\ & - 0.00976 * T_{on} * \text{Servo voltage} \\ & - 0.00586 * T_{off} * \text{Servo voltage} \end{aligned} \quad (3)$$

$$\begin{aligned}\text{Surface Roughness} = {} & -59.4 + 3.001 * \text{Current} - 0.1053 * T_{on} - 1.441 * T_{off} \\ & + 1.73 * \text{Servo voltage} + 0.1026 * T_{off}^2 \\ & - 0.01145 * \text{Servo voltage}^2 + 0.10321 * \text{Current} * T_{off} \\ & - 0.03961 * \text{Current} * \text{Servo voltage} \end{aligned} \quad (4)$$

Case 3 Objective Functions [18] is given in Eqs. (5) and (6):

$$\begin{aligned}\text{Material Remova Rate} = {} & 0.76 + 0.21 * T_{on} - 0.20 * T_{off} - 0.13 * \text{Current} \\ & + 0.078 * \text{FM} - 0.053 * T_{on} * T_{off}\end{aligned}$$

$$+ 0.15 * T_{on} * \text{FM} - 0.048 * T_{off} * \text{FM} + 0.021 * T_{on}^2 - 0.074 * T_{off}^2 - 0.049 * \text{Current}^2 \quad (5)$$

$$\text{Surface Roughness} = +4.56 + 0.74 * T_{on} - 0.70 * T_{off} - 0.57 * \text{current} + 0.34 * \text{FM} + 0.63 * T_{on} * \text{FM} \quad (6)$$

where T_{on} is Pulse On time, T_{off} is Pulse off time, FM is flushing method taken into consideration for all cases.

3 Results and Discussion

The Pareto fronts obtained from algorithms are combined in Fig. 1 to commence the comparative analysis to determine the true Pareto front. By fixating some particular values of the output parameter, the values of other parameters predicted by all Pareto fronts can be evaluated and based on the design requirement, the best Pareto (or most dominant) front can be selected. This process is iteratively performed and the most suitable graph of all five algorithms may be accorded the true Pareto front. This approximation is well suited for graphs where a clear distinction between the design points are visible, as more overlapping of graphs would make it difficult to assert a clear true Pareto front. This is used for calculations involving GD and IGD.

Figure 1 represents the Pareto frontier of MRR (mm^3/min) with Surface roughness (microns) as predicted by all algorithms without any refinements for Case 1. Table 3 shows the performance metrics values for all algorithms which depicts that NSGA-III dominates (at same surface roughness, higher MRR) all other algorithms through

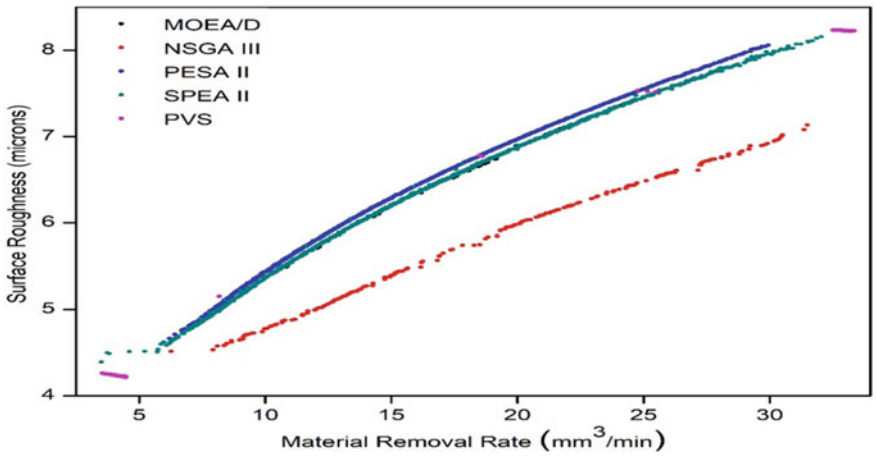

Fig. 1 Pareto fronts for surface roughness versus MRR for Case 1

Table 3 Performance metrics for surface roughness versus MRR for Case 1

P. Metrics	Algorithms				
	MOEA/D	NSGA-III	SPEA-II	PESA-II	PVS
IGD	1.713	0	0.815	0.916	2.417
Spacing	0.005	0.129	0.035	0.018	0.148
Spreading	1.017	0.710	0.760	0.723	1.420
GD	0.030	0	0.023	0.030	0.064
Hypervolume	110.5	94.540	113.2	90.510	112.926
Pure diversity	9.55E+03	1.40E+04	1.79E+04	1.76E+04	1.23E+04

MRR range of 10–30 (mm^3/min) and hence, NSGA-III is assumed as true Pareto frontier. So, the value of GD and IGD for NSGA-III is zero. Further, it can be seen from low values of GD that algorithms do converge to portions predicted by NSGA-III at lower values of both axes. In terms of diversity of solutions, the performance of SPEA-II is incomparable (as can be seen from hypervolume and PD) and it has clearly predicted the highest cardinality of solutions. Thus, it can be concluded that designers could prefer NSGA-III for the most accurate solutions with less diversity. SPEA-II has the highest pure diversity in solution space. PVS has poor spread of solutions but the solutions dominate a higher volume of space than NSGA-III as seen from hypervolume values.

Figure 2 represents the Pareto frontier of all algorithms for Case 2. The PVS Pareto is better than other graphs at the extremities. All algorithms predict more close and uniform solutions for MRR: 0.6–1.8(mm^3/min) after which spacing is not uniform. NSGA-III again dominates most of the region in 2-D space and hence considered as true Pareto front. Table 4 shows the performance metrics values in case 2. However,

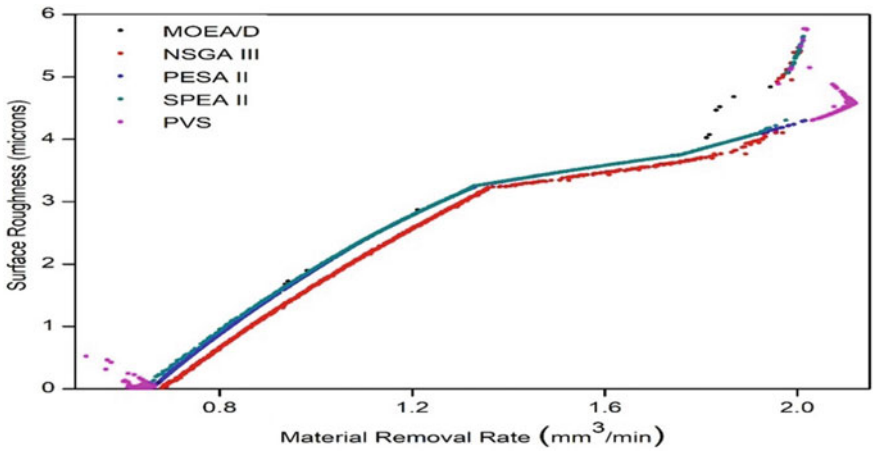

Fig. 2 Pareto fronts for surface roughness versus MRR for Case 2

Table 4 Performance metrics for surface roughness versus MRR for Case 2

P. Metrics	Algorithms				
	MOEA/D	NSGA-III	SPEA-II	PESA- II	PVS
IGD	0.073	0	0.053	0.063	1.027
Spacing	0.002	0.005	0.005	0.003	0.008
Spreading	1.011	0.602	0.717	0.857	1.224
GD	0.002	0	0.000	0.002	0.006
Hypervolume	9.538	9.160	9.508	9.431	10.089
Pure diversity	4.21E+03	4.18E+03	4.14E+03	5.37E+03	3.78E+03

other algorithms also predict solutions very close to NSGA-III indicated by very low values of GD and IGD. Again, the spread of solutions are best in NSGA-III. PESA-II has the most diverse sets of solutions so it can be considered in case when decision making is more relaxed. The performance of PVS is good in terms of hypervolume but suffers from the poor spreading of solutions. Overall, all algorithms fare better with spacing and pure diversity in solution sets.

Figure 3 represents the Pareto front and Table 5 shows performance metrics values for all algorithms in Case 3. As in the above cases, PVS solutions are better converged at the extremities of Pareto fronts than other algorithms. The frontiers are uniform mostly throughout and follow an almost linear pattern. NSGA-III is again assumed to be the true Pareto front although the frontiers are very close to each other as shown by low GD values. The metrics values are best for NSGA-III amongst all algorithms. It has predicted rich diverse solutions with better convergence in most regions of Pareto frontier. PVS, on the other hand, performs better in terms of hypervolume and diversity while yielding poor performance measures against the rest of the indices.

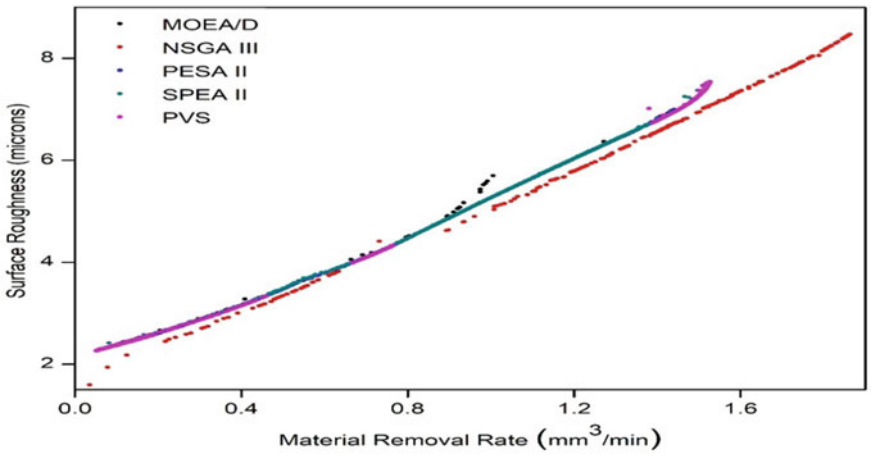

Fig. 3 Pareto fronts for MRR versus surface roughness for Case 3

Table 5 Performance metrics for MRR versus surface roughness for Case 3

P. Metrics	Algorithms				
	MOEA/D	NSGA-III	SPEA-II	PESA-II	PVS
IGD	0.607	0	0.173	0.312	0.402
Spacing	0.030	0.048	0.006	0.004	0.005
Spreading	1.206	0.802	0.829	0.824	1.117
GD	0.004	0	0.002	0.003	0.004
Hypervolume	13.805	15.566	14.112	13.464	14.111
Pure diversity	2.63E+03	5.85E+03	5.23E+03	4.08E+03	4.02E+03

SPEA-II followed by PESA-II can be considered predicting the next best algorithm with good performance in terms of all indices.

Finally, it can be seen that NSGA-III could be suited for designers focusing on maximum solution sets to responses of MRR and surface roughness. However, it also depends on problem formulations which are mostly polynomial approximation for statistical models. PVS should be used when designers are more inclined towards getting solutions from the extremities. SPEA-II and PESA-II may be useful in cases where diversity of solutions are imperative and the designers intend to focus on any particular range of solution set. MOEA/D is not found particularly useful for such applied statistical models, although no evolutionary multi-objective algorithm is completely better or completely worse than another, for all problems [19].

4 Conclusion

Authors have developed a multi objective optimization algorithm—PVS to compare with the other four popular algorithms. Performance evaluation for all algorithms are presented in quantitative terms through six metrics. It is observed that NSGA-III performs better on overall terms, while SPEA-II and PESA-II generate more diverse regions in solution space. PVS predicts better results when one of the objectives is considered much more important than another. MOEA/D algorithm has shown poor performance than the rest of the algorithms on case problems chosen by authors. However, it is not advisable to generalize the results for all cases, since the performance of evolutionary algorithms is case sensitive. For future research, a substantial amount of test problems may be used with more than two objectives to determine the performance measures.

References

1. Abbas NM, Solomon DG, Bahari F (2007) A review on current research trends in electrical discharge machining 47:1214–1228
2. Coello CAC, Lamont GB, Van Veldhuizen DA (2007) Evolutionary algorithms for solving multi-objective problems, 2nd edn.
3. Jain KDH (2014) An evolutionary many-objective optimization algorithm using reference-point based nondominated sorting approach, Part II: handling constraints and extending to an adaptive approach. IEEE Trans Evol Comput 18(4):602–622
4. Zitzler E, Laumanns M, Thiele L (2001) SPEA2: Improving the strength pareto evolutionary algorithm. In: Evolutionary methods for design, optimization and control with applications to industrial problems, pp 95–100 (2001)
5. Corne D, Jerram N, Knowles JD, Oates M, Martin J (2001) PESA-II: region-based selection in evolutionary multi-objective optimization. In: Proceedings of the genetic and evolutionary computation conference, pp 283–290
6. Zhang HLQ (2007) MOEA/D: a multiobjective evolutionary algorithm based on decomposition. Evol Comput IEEE Trans 11(6):712–731
7. Savsani P, Savsani V (2015) Passing vehicle search (PVS): a novel metaheuristic algorithm. Appl Math Model 1–28
8. Prabhu TR, Savsani V, Parsana S, Radadia N, Sheth M, Sheth N (2018) Multi-objective optimization of EDM Process parameters by using passing vehicle search (PVS) algorithm. In: Defect and diffusion forum, vol 382, pp 138–146
9. Okabe T, Jin Y, Sendhoff B (2003) A critical survey of performance indices for multi-objective optimisation. In: Proceedings of 2003 congress on evolutionary computation, vol 2, pp 878–885
10. Zitzler E, Thiele L, Laumanns M, Fonseca CM, da Fonseca VG (2003) Performance assessment of multi-objective optimizers: an analysis and review. Evol Comput 7(2):117–132
11. Schott J (1995) Fault tolerant design using single and multicriteria genetic algorithm optimization. Massachusetts Institute of Technology, Cambridge, Massachusetts
12. Srinivas N, Deb K (1995) Muiltiobjective optimization using nondominated sorting in genetic algorithms. Evol Comput 2(3):221–248
13. Cheng R, Li M, Tian Y, Zhang X, Yang S, Jin Y, Yao X (2017) Benchmark functions for CEC'2017 competition on evolutionary many-objective optimization, pp 1–20
14. Ulrich T, Bader J, Thiele L (2010) Defining and optimizing indicator-based diversity measures in multi-objective search. In: Parallel problem solving from nature, PPSN XI. Springer, Berlin, pp 707–717
15. Eiben AE, Smit SK (2011) Parameter tuning for configuring and analyzing evolutionary algorithms. Swarm Evol Comput 1(1):19–31
16. Aich U, Banerjee S (2016) Application of teaching learning based optimization procedure for the development of SVM learned EDM process and its pseudo Pareto optimization. Appl Soft Comput J 39:64–83
17. Ming W, Ma J, Zhang Z, Huang H, Shen D, Zhang G, Huang Y (2016) Soft computing models and intelligent optimization system in electro-discharge machining of SiC/Al composites. Int J Adv Manuf Technol 1–17
18. Kanagarajan D, Karthikeyan R, Palanikumar K, Davim JP (2008) Optimization of electrical discharge machining characteristics of WC/Co composites using non-dominated sorting genetic algorithm (NSGA-II). Int J Adv Manuf Technol 36(11–12):1124–1132
19. Zitzler E, Deb K, Thiele L (2013) Comparison of multi-objective evolutionary algorithms: empirical results. Evol Comput 8(2):173–195

Performance/Failure Analysis of Materials in Service

Deformation-Induced Surface Roughness and Global Spring Back Resulted with Different Plastic Strain Levels in Incremental Forming of Original and Preheated Sheet Samples

Parnika Shrivastava and Puneet Tandon

Abstract Single point incremental forming (SPIF) process has gained considerable popularity in the field of manufacturing when it comes to the fabrication of complex and customized products. Flexibility of the process, due to the elimination of die, makes the process viable for rapid prototyping applications. The dieless and localized nature of the process, however, induces the limitations in formed parts in the form of surface irregularities and geometrical inaccuracies. These surface and geometrical limitations question the reliability of the process and still hinder the process to become industrially worthwhile. The manuscript targets and unfolds the complex deformation-induced outer surface roughness and spring back behavior after unloading and unclamping of the SPIF parts. The investigation utilizes original and preheated sheet samples with an aim to analyze the surface roughness on the outer free surface and global spring back in the SPIF parts formed with different levels of strain. It was analyzed that increase in strain level and preheating resulted in lower depth recovery phenomena and thus, reduced spring back in the parts. However, deformation-induced surface roughness increases with the preheating of the sheet. The present investigation provides an insight into the overall quality of the parts obtained by SPIF, so that the process can be further reliably implemented for industrial applications.

Keywords Single point incremental forming · Deformation-induced surface roughness · Spring back · Preheating

P. Shrivastava
Mechanical Engineering Department, National Institute of Technology Hamirpur, Hamirpur, India

P. Tandon (✉)
Mechanical Engineering Department, PDPM Indian Institute of Information Technology, Design and Manufacturing, Jabalpur, India
e-mail: ptandon@iiitdmj.ac.in

V. K. Gupta et al. (eds.), *Reliability and Risk Assessment in Engineering*,
Lecture Notes in Mechanical Engineering,
https://doi.org/10.1007/978-981-15-3746-2_43

1 Introduction

The recent trend in the sheet metal industry is to fabricate unique, complex and customized products. Conventional forming techniques, which are more suitable for mass production, are unable to satisfy the current industrial needs. The proved solution to the abovementioned issue is single point incremental forming (SPIF) process. The process facilitates the forming of highly complex and unique three-dimensional products. The process is beneficial as it eliminates the usage of die and thus upsurges the flexibility and cost-effectiveness. Another benefit of the process is the enhanced formability which is due to the highly localized nature of the deformation in comparison with conventional forming techniques. The process strategically imparts local plastic deformation with the help of a simple hemispherical tool, which moves in predefined tool path trajectory, generated as per the desired shape of computer-aided design (CAD) model [1]. Studies have been done in order to make the process viable as per the rapid prototyping and small series production demands of automobile, aerospace and medical industries. Enhanced formability (more than 300% in comparison with traditional techniques) offered by the process also brings out of the limitation of the process in terms of plastic deformation-induced surface roughening of the parts' surface.

The present-day need of vehicle and aerospace industries is to form high strength/low weight alloys. In such applications, reliably predicting the evolved surface heterogeneities is of the utmost importance. In SPIF, various studies have been done in order to analyze the surface topography defect due to the variations in various process parameters like, tool dimensions/design, incremental step depth, lubrication, sheet material, sheet thickness and tool revolution speed and feed [2]. Hagan and Jeswiet [3] have also designed tool path to improve the internal surface finish. Most of the past studies are based on the analysis of internal surface roughness resulted due to the effect of process parameters and minimal attention is given to the surface topography evolved due to plastic straining of the free external surface.

In SPIF, efforts have been made to form the product geometrically as accurate as ideal CAD model. Discrepancies in the geometric deviations occur may be due to predominant bending, pillow effect and spring back phenomenon etc. Spring back is due to the elastic recovery of the material once the unloading has been done [4]. This effect can be attributed to the 'Bauschinger effect' which explains the tendency of the material to follow dissimilar paths during loading and unloading cycles [5]. This tendency induces the residual stress in the formed material as a result material after unloading tends to return to its original shape. Thus, investigation of spring back effect in SPIF is essential so that process improvements can be done in order to compensate the dimensional errors. Geometric deviation analysis is also essential when the materials to be formed are having higher ratios of yield strength to elastic modulus as these materials suffer from dominant spring back [6].

Previously, researches have been carried out to minimize geometrical errors by adopting strategies like optimization of tool path trajectory, use of flexible backing, use of counter pressure, back drawing and multiple point incremental forming [7]. In

SPIF, various feature-based tool paths are developed to predict and later modified to compensate the pillow effect and errors caused due to spring back. Further, techniques have also been developed by coupling artificial neural network (ANN) and finite element method for simulation and prediction of spring back in response to changes in the processing parameters [8, 9]. Both, surface inhomogeneity and residual stresses (which causes spring back) in SPIF, are the major causes of crack initiation and ultimate failure of the formed part. The strength of the material ultimately suffers due to the trapped stresses and surface heterogeneity.

The manuscript targets and unfolds the complex outer surface roughness and spring back behavior generated with respect to the different levels of plastic straining in SPIF. The formed parts were investigated after unloading and unclamping from the setup. The original and preheated sheet samples were incrementally formed with different levels of strain to investigate the effect on surface roughness on the outer free surface and global spring back in the SPIF parts. Roughness and depth recovery parameters were calculated resulted due to the different amount of imposed strain and preheating. One of the major necessities of the process is to form components with desired geometrical accuracy and surface finish without the failure of the component. Therefore, the present work attempts to unfold the relationship between formability (imposed strain), surface morphology and geometrical accuracy in SPIF. The present investigation provides an insight into the overall quality of the parts obtained by SPIF, so that the process can be further reliably implemented for industrial applications

2 Materials and Methods

2.1 Material

The material used in the work is aluminum alloy sheet (AA1050A H14). The chemical composition and physical properties of the sheet material are presented in Tables 1 and 2.

Table 1 Chemical composition of aluminum alloy sheet (AA1050A H14)

Element	wt%
Manganese (Mn)	0.0–0.05
Iron (Fe)	0.0–0.40
Copper (Cu)	0.0–0.05
Magnesium (Mg)	0.0–0.05
Silicon (Si)	0.0–0.25
Zinc (Zn)	0.0–0.07
Titanium (Ti)	0.0–0.05
Aluminum (Al)	Balance

Table 2 Physical properties of AA1050A H14

Property	Value
Density	2.71 kg/m^3
Melting point	660 °C
Thermal expansion	24 × 10^{-6}/K
Modulus of elasticity	71 GPa
Thermal conductivity	222 W/m K

Preheating of the sheets at 150, 300 and 450 °C was performed for the time duration of one hour to reform the mechanical properties of cold-rolled and work-hardened sheets. Further, the samples were furnace cooled and brought back to room temperature before forming.

2.2 Single Point Incremental Forming

The SPIF experimentation was performed by utilizing three-axis CNC milling machine. The setup is shown in Fig. 1. The values of referred ISF parameters are given in Table 3. In order to track the evolution of deformation-induced surface roughness and spring back in SPIF part, instead of forming the single component in phases

Fig. 1 SPIF setup

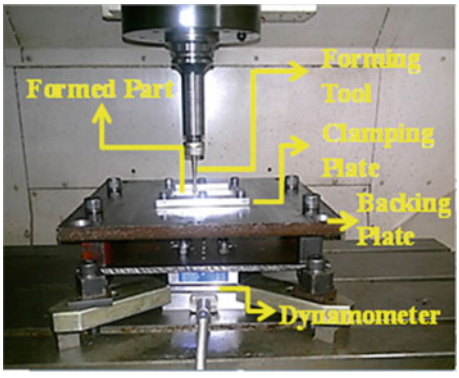

Table 3 Incremental sheet forming parameters

Tool diameter (mm)	Vertical step size (mm)	Rotational speed (RPM)	Tool feed rate (mm^{-1})	Lubricating oil	Tool path	Sheet thickness (mm)
8	0.2	200	1000	Hydraulic oil (grade-68)	Spiral	0.91

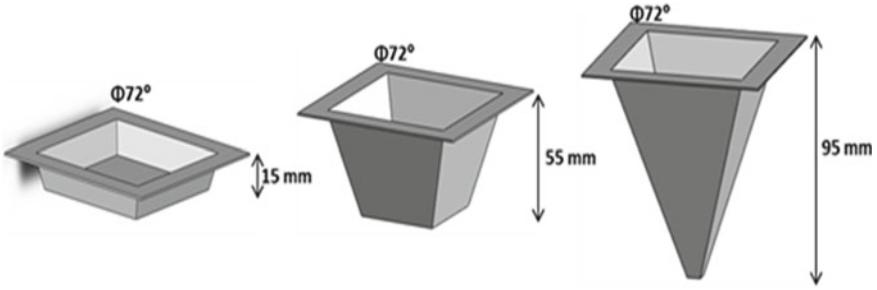

Fig. 2 CAD part showing different SPIF stages

and analyzing, three different components with different extent of deformation were formed and analyzed separately. Intermediate analysis of the single component when it attains different stages of deformation requires clamping and unclamping of the sheet and thus causes distortion in the component. Therefore, different strategy is adapted where forming of three different components with different deformation stages is done to investigate the effect of incremental deformation on roughness and spring back in SPIF. This was done because clamping of the sheet and unclamping of the component and again clamping causes distortion in the component.

The first test specimen geometry considered here was a truncated pyramid component, with major square base of 70 * 70 mm, wall inclination angle of 72°, formed by clamping a square metal blank of 90 * 90 mm. Three different components were formed with forming depth of 15 mm (minimum deformation level), 55 mm (medium deformation level) and 95 mm (maximum deformation level). The computer-aided design (CAD) of the parts is shown in Fig. 2.

2.3 Evaluation of Spring Back and Deformation-Induced Outer Surface Roughness

To measure spring back in the formed geometry, digitization of the component was carried out. In order to acquire point cloud data of the formed geometry and to compare with 3D CAD parts, highly sophisticated ATOS Compact Scan blue light scanner and ATOS Professional—3D Scanning and Inspection Software were utilized, respectively. The global spring back value was calculated as the differences in the depth of ideal CAD profile (desired component depth) and extracted depth of the formed products, which is as given in Eq. (1).

$$\text{Spring back} = D_0 - D_i \tag{1}$$

For respective deformation stages, D_0 represents desired depth of the formed component, as obtained from the CAD model, while D_i represents the actual depth

of formed component. The formed components were compared with the respective CAD geometries having same level of deformation.

Rugosurf 10G v.2.96 profilometer was used to measure the average surface roughness of the outer formed surface in the direction perpendicular to the tool advancing direction. For each stage of deformation, three measurements were taken and average value was considered.

3 Results and Discussion

3.1 Evolution of Spring Back in SPIF

Three-dimensional deviation analyses from respective CAD parts reveal that global spring back in SPIF increases with increase in deformation. The preheating of the sheets resulted in lower spring back and the results are given in Table 4.

The geometric deviation analysis is done between the respective CAD and formed part which is shown in Fig. 3. Figure 4 shows the deviation analysis result for the different stages of deformation in SPIF.

It can be analyzed that formed part suffers major deviation in the two different zones of the parts. One of the major regions of the deviation is near the major base of the component which is due to bending and other at the top surface of the component which is due to global spring back or depth recovery phenomena. The enhanced capability of the SPIF process is to impart higher amount of strain in comparison to conventional forming operation. However, with increase in imposed strain and depth of formation, there is an increment in global spring back or depth recovery index. Figure 5 depicts the variation in depth recovery index with preheating for different stages of deformation in SPIF. The increase in plastic strain also increases the tendency of the elastic recovery of the material and this may be the reason for the increased amount of the spring back in the components [10]. Further, preheating of the sheets causes the reduction in the yield strength of the material and this results in reduced spring back in SPIF parts [11].

Table 4 Geometric deviation in SPIF parts in comparison with ideal CAD part

Deformation level	Imposed strain	Depth of formation (mm)	Unloading depth of formation (mm)	Spring back (mm)	Spring back after preheating		
					150 °C	300 °C	450 °C
Low	1.1	15	14.912	0.088	0.087	0.085	0.083
Medium	2.6	55	54.840	0.160	0.150	0.146	0.139
High	3.8	95	94.711	0.289	0.280	0.272	0.195

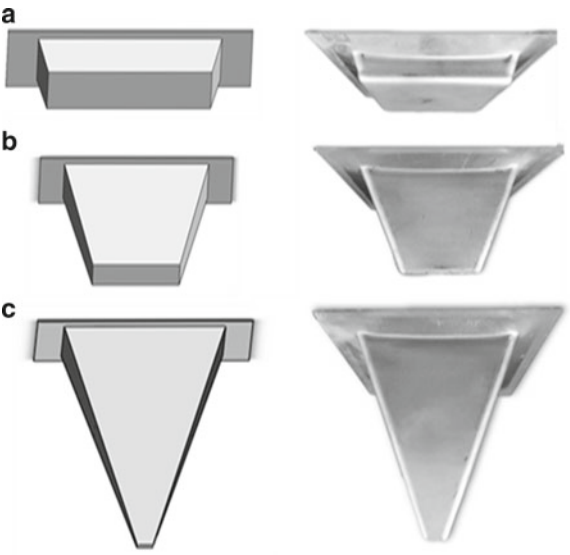

Fig. 3 CAD and respective formed parts subjected to different levels of deformation in SPIF **a** low, **b** medium and **c** high

3.2 Evolution of Outer Surface Roughness with Deformation in SPIF

For the different strain values in SPIF, the deformation induced roughness of the outer formed surface was measured. The obtained results are provided in Fig. 6. The result reports the increase in roughness values with the increment in strain-level in SPIF.

4 Conclusion

The present manuscript reports the evolution of geometrical accuracy and outer surface roughness induced in single point incremental forming (SPIF) process. For the purpose, three different SPIF components were formed with different levels of imposed strain or depth of formation as low, medium and high.

SPIF parts suffer from geometric deviation from the ideal CAD part especially due to depth recovery phenomena. Elastic recovery tendency of the material leads to spring back in SPIF parts. SPIF components show higher spring back or depth recovery tendency when formed up to higher strain levels. Preheating of sheets reduces the elastic recovery tendency of the formed parts, and thus, lower spring back is reported irrespective of imposed strain.

Deformation-induced roughness which increased with the increase in level of deformation further increased with preheating. Preheating leads to grain reformation, and as a result, grain size increases which in turn increases the surface roughness due to orange peel on the outer surface.

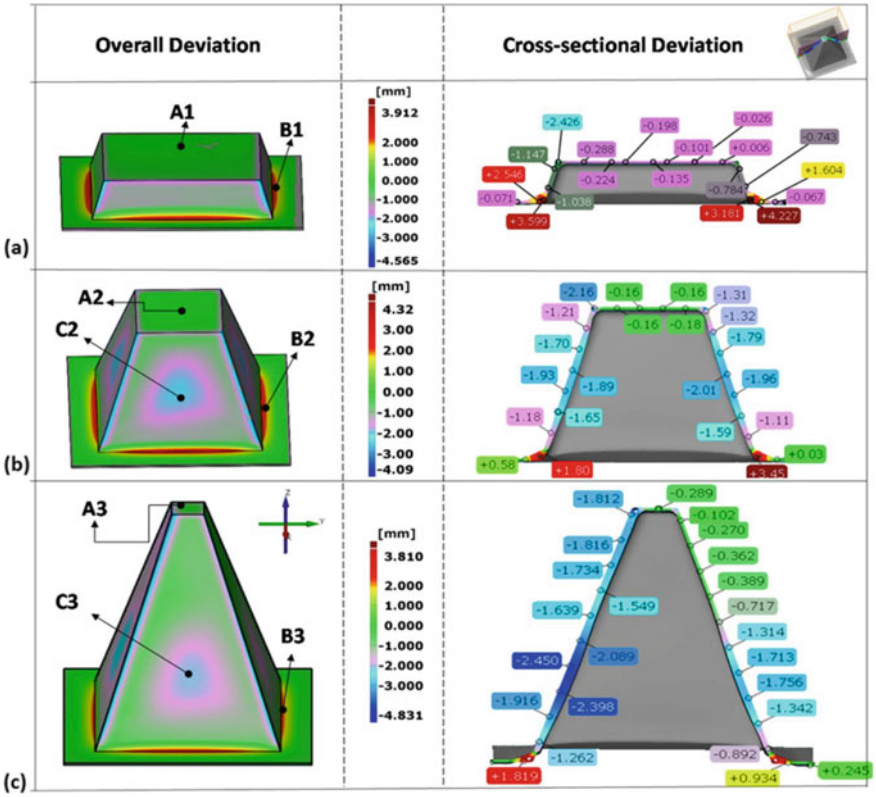

Fig. 4 Three-dimensional deviation evolve with different levels of deformation in SPIF **a** low, **b** medium and **c** high

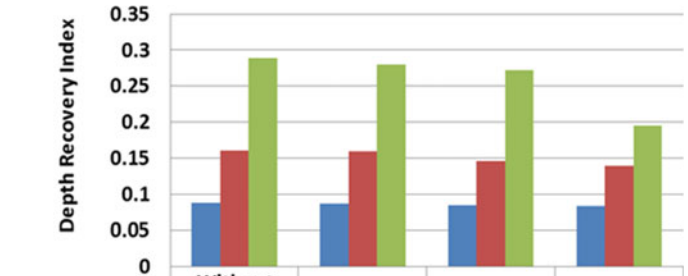

	Without preheat	150°C	300°C	450°C
Low Strain	0.088	0.087	0.085	0.0832
Medium Strain	0.16	0.159	0.146	0.139
High Strain	0.289	0.28	0.272	0.195

Fig. 5 Depth recovery index resulted after preheating and different levels of deformation in SPIF

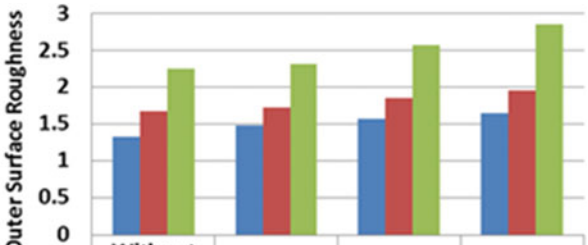

	Without preheat	150°C	300°C	450°C
Low Strain	1.324	1.485	1.564	1.642
Medium Strain	1.67	1.724	1.854	1.954
High Strain	2.248	2.314	2.57	2.85

Fig. 6 Deformation-induced surface roughness resulted with different strain levels and preheating in SPIF

Although SPIF process facilitates the forming of components at much higher strain in comparison with conventional forming, it leads to geometrical inaccuracy and deformation-induced roughness in the parts. Preheating can be one solution to reduce the elastic tendency of the formed parts. The present investigation provides an insight into the overall quality of the parts obtained by SPIF, so that the process can be further reliably implemented for industrial applications.

References

1. Echrif SBM, Hrairi M (2011) Research and progress in incremental sheet forming processes. Mater Manuf Processes 26:1404–1414
2. Echrif SB, Hrairi M (2014) Significant parameters for the surface roughness in incremental forming process. Mater Manuf Processes 29:697–703
3. Jeswiet J, Micari F, Hirt G, Bramley A, Duflou J, Allwood J (2005) Asymmetric single point incremental forming of sheet metal. CIRP Ann Manuf Technol 54:88–114
4. Hussain G, Gao L, Hayat N (2011) Forming parameters and forming defects in incremental forming of an aluminum sheet: correlation, empirical modeling, and optimization: part A. Mater Manuf Processes 26:1546–1553
5. Chung K, Lee MG, Kim D, Kim C, Wenner ML, Barlat F (2005) Spring-back evaluation of automotive sheets based on isotropic-kinematic hardening laws and non-quadratic anisotropic yield functions: Part I: theory and formulation. Int J Plast 21:861–882
6. Jiang CP (2014) Initial grain size effect on mechanical properties and spring back behavior of thin metal sheets with varying rolling reduction ratios. Int J Precis Eng Manuf 15:291–297
7. Micari FA, Ambrogio G, Filice L (2017) Shape and dimensional accuracy in single point incremental forming: state of the art and future trends. J Mater Process Technol 191:390–395
8. Fu Z, Mo J, Han F, Gong P (2013) Tool path correction algorithm for single-point incremental forming of sheet metal. Int J Adv Manuf Technol 64:1239–1248

9. Lu B, Chen J, Ou H, Cao J (2013) Feature-based tool path generation approach for incremental sheet forming process. J Mater Process Technol 213:1221–1233
10. All FF (2001) Finite element and experimental studies of spring back in sheet metal forming. National Library of Canada, Canada
11. Hatch JE (1984) Aluminum: properties and physical metallurgy. ASM International, USA

Safety Assessment of Femur

Shivdayal Patel, Mradul Awasthi, and Suhail Ahmad

Abstract Femur is the longest and strongest bone in the human body. It is subjected to various loads created during different physiological activities. Stresses developed in the femur depend upon the material property, which depends upon the density of the femur and the load (body weight) acting on it. The femur density and body weight varies from person to person. Stochastic finite element analysis of the femur has taken care of all the uncertainties present in the material properties and forces acting on the femur head. Prediction of the stability of the femur depends upon the choice of the failure criteria, material properties, and loading condition. Thus, the focus of the present study is on three basic aspects. Firstly, the finite element model, determination of critical load on the femur as per the gait cycle, modeling of the load application, and boundary conditions. Secondly, stochastic finite element analysis of the femur as per the limit state derived from the maximum strain failure criteria, in which probabilistic material properties are employed. Third part deals with the computational efficiencies of the various methods employed to obtain the probabilities of failure and corresponding safety assessment of the femur for normal and osteoporotic patients. Further, the scope of the study covers the effect of a range of scatters (in terms of standard deviation) of random variables on probabilities of various cases.

Keywords Stress analysis · Reliability · Safety · Stochastic finite element method · Computed tomography · Biomechanics

S. Patel (✉)
Indian Institute of Information Technology Design and Manufacturing, Jabalpur 482005, India
e-mail: shivdayal@iiitdmj.ac.in

M. Awasthi · S. Ahmad
Indian Institute of Technology Delhi, New Delhi 110016, India

V. K. Gupta et al. (eds.), *Reliability and Risk Assessment in Engineering*,
Lecture Notes in Mechanical Engineering,
https://doi.org/10.1007/978-981-15-3746-2_44

1 Introduction

Femur is a natural composite material. It is a mixture of collagen fibers in hydroxyl apatite matrix. Femur tissues are generally classified as cortical and trabecular. The main difference in the two portions is due to the porosity of the femur. Cortical femur is the outer portion of the femur, which is much denser and less porous than the inner one called trabecular. The femur is also called as the thigh femur that joins the hip to the knee. It is the strongest and the longest bone in the skeletal system. The material properties of the femur depend upon the porosity of the femur, which differs within the femur and with respect to the age of the individual. The properties of the femur can be obtained from the computed tomography (CT) images. The average Hounsfield unit (HU) number is calculated from CT images which in turn can be used to calculate density and Young's modulus using the empirical relationships. Yang et al. [1] performed a 3D FE model of the femur and the material properties of the femur were determined from the computed tomography (CT) scanning of femur. The average HU number of the CT images was obtained to calculate the density and elastic Young's modulus of femur. A total of 165 material property cards were defined and each element of the meshed model of the femur was assigned with a material card. Due to the presence of these uncertainties in material properties and loading criteria, reliability analysis is needed to calculate the actual performance of femur. Taddei et al. [2] and Viswanath et al. [3] presented a sensitivity analysis of a human femur. FE model is derived by computed tomography (CT) data to determine the stochastic response for the femur. Laz et al. [4] and New et al. [5] performed a probabilistic analysis on a femur using strain-based criteria and taking random variables as femur stiffness, implant stiffness, load angle, and load. The load angle and implant stiffness do not seem to affect the results significantly. The study suggested that the number of simulations, the proper selection of random variables, and geometry are very important for the reliability of both the probability values and the sensitivity analyses. Yoshibash et al. [6] investigated the yield prediction capabilities of different femur models using different yield criteria and the spread in the predicted load between the isotropic and orthotropic material models. Subject-specific finite element models of two human femurs were developed from CT scan data with orthotropic or isotropic material properties and loaded with a simple compression force at the head. Maximum principal strain criteria in combination with the orthotropic model best predicted both the yield force and fracture location as compared with other criteria.

Francis and Kumar [7], Singh and Ahmed [8], and Baca et al. [9] developed a 3D finite element model for three different patients of different ages from CT images using commercial MIMICS software. A finite element analysis of the femur was carried out for different body weights and for different inclination angles of the load acting at the hip-joint. The study determined that the total deformation and Von-stress were found to be increasing with an increase in inclination angle. The quantitative assessment of stress under combined bending and compression loads has been carried out by Zhao et al. [10]. The study was carried out for static loading at the hip-joint of

the femur, where four different points at the femoral head were considered to include the variation in bending moment. It was concluded that neck portion and the upper end of the femur shaft are the weakest parts due to higher stress concentration and the femur stress increases significantly with bending moment.

Accurate prediction of long-term behavior of hip-implant system is very important not only for patient comfort but also for elimination of any revision surgery due to the failure of implant. Failure of implant means loosening of stem which allows relative motion of the implant stem and femur, causing pain and mechanical instability of total hip Arthroplasty. Both loosening and fracture of stem are related to mechanical stresses created in the joint, bone–implant interface. These mechanical stresses are the result of uncertainties present in properties of bone and implant and loading conditions. The response of hip-implant under different physical activities and the variation of material properties raise a need to generate a realistic computer model used for stress analysis as well as deterministic and probabilistic analyses of the femur with and without implant. Femoral neck is the most critical fracture site, especially for old age people suffering from osteoporosis disease. It is essential to examine its failure behavior under static load situation and the fracture risk involved in it for a complete range of motion. The uncertainties involved in the geometric and material properties play a very dominant role in the finite element (FE) analysis of the femur. The response of femur under critical physical activities and the variation of material properties motivated to carry out finite element analysis and probabilistic analysis of the human femur. Probability of failure depends upon the failure criteria, material properties used, and the loading conditions.

Recently, FE modeling has been combined with probabilistic design methods to allow randomness and variability in the system parameters to be taken into account [11]. The probabilistic finite element analysis is carried out considering the scatters of material properties (elastic modulus) and loading conditions. Discretization of material properties of random nature is modeled using Karhunen–Loeve (KL) expansion series method. First-order reliability method (FORM) is used to calculate the Pf for femur neck region. Comparison of Pf is also carried out for FORM, advanced mean value method (AMV), and MCS methods. The maximum principle strain failure criterion for femur neck is adopted to establish the limit state function in a more realistic fashion.

2 Probabilistic Analysis

Reliability analysis is strongly recommended by various international codes especially to achieve challenging design targets for satisfactory service and survival. It is because, the factor of safety approach does not account for the natural scatter in the input data. The probabilistic approach explicitly quantifies the extent of safety or probability of failure. Many a time design standards recommend a threshold of target reliability for satisfactory design. Probabilistic approach is, all the more, significant to assess the safety of femur. The material properties of femur inherently

exhibit a scatter or uncertainty due to their inhomogeneity, anisotropic characteristics, and manufacturing defects. In the conventional approach, deterministic input data is assumed to participate and associated uncertainties are accounted for by using the deterministic factor of safety. This factor of safety is too uncertain up to a greater extent. Hence, there is a persistent need to quantify its performance in a realistic fashion by taking into account the actual mean and statistics data.

2.1 Random Input Parameters

In deterministic analysis, the inputs defined in a problem are single valued, while in probabilistic analysis, there is a range of input parameters which follow a particular type of distribution. These random parameters must be defined in terms of their mean value, standard deviation, and distribution types. The values of elastic modulus of cortical and trabecular femur and the joint contact loads in terms of their mean value, standard deviation, and distribution type are defined to perform the probabilistic study of femur. Discretization of material properties of random nature is modelled using Karhunen–Loeve (KL) decomposition technique as suggested by Patel et al. [11]. Detailed information of the KL expansion method for generating the random fields for the composite materials is explained by Patel et al. [12–15]. The current results include the randomness of material properties: EC, EPY, ET, JCF1, JCF2, and JCF3.

2.2 Stochastic Stiffness Matrix

The global stiffness matrix **C** is determined after assembling the element stiffness matrices.

$$\mathbf{C} = \int_{\mathbf{V}} \mathbf{B}^{\mathbf{T}} \cdot \mathbf{C}(\mathbf{x}, \theta) \cdot \mathbf{B} \mathbf{dV} \tag{1}$$

Here, **B** is the strain–displacement matrix, $\mathbf{C}(\mathbf{x}, \theta)$ is the approximated elasticity matrix, and **V** represents the volume of the element. Suppose the material properties are represented by Gaussian fields, the elasticity matrix at point x can be given as:

$$\mathbf{C}(\mathbf{x}, \theta) = \mathbf{C_0}(\mathbf{1} + \mathbf{w}(\mathbf{x}, \theta)) \tag{2}$$

C_0 represents a random field of materials constant over the domain and $w(x, \theta)$ represents the approximate random field, modelled as per KL technique.

Strength properties such as S_{22}, S_{13}, $S_{12,}$ and S_{23}, etc. represented in a probabilistic fashion given

$$\mathbf{R}(\mathbf{x}, \theta) = \mathbf{R_0}\mathbf{w}(\mathbf{x}, \theta) \tag{3}$$

Here, R_0 is the mean value of the random parameters such as (S_{22}, S_{13}, S_{12}, and S_{23}).

2.3 Limit State Function

Limit state function defines the failure and safe zones. Essentially, the failure criterion is same as limit state functions. The limit state function is used in the evaluation of joint probability function, to find out the failure probability, and cumulative probability distribution. The selection of the output or failure criterion plays an important role in the results. The maximum strain-based failure criteria are considered for the limit state function in the present study.

The maximum principle strain failure criterion for femur neck is adopted to establish the limit state function in a more realistic fashion.

3 Numerical Modeling

3.1 Geometry of Femur

The finite element model of a human femur is obtained from a public database of VAKHUM project. The use of the data is free for academic purpose. The model is in a PATRAN neutral file format which is converted into an ABAQUS compatible file and is truncated to analyze only the proximal part. The geometry of the femur is then imported in ABAQUS 6.13. The 3D model of the femur consists of 3466 elements of type C3D8I (eight-noded incompatible brick element) and 9806 nodes (Fig. 1).

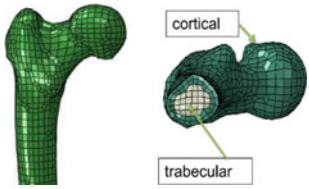

Fig. 1 Femur geometry

3.2 *Loading and Boundary Conditions*

The femur, in physiological conditions, is subjected to a spontaneous loading pattern that can be quite complex due to the involvement of many muscle forces which are created due to the body movement of the person. The magnitude and direction of these loads may change considerably with time and the type of movement being performed. The force acting due to hip-joint on the femoral head acts on 70% of area of the head [10] and the reaction force provided by the muscles acts on the greater trochanter region. To model these forces, two sets of nodes are created on the femoral head and greater trochanter as shown in Fig. 2. The respective forces are applied to each node set and a fixed boundary condition is applied at the distal portion of the femur. To perform the static analysis of the femur, the peak static loads are considered which occur during the gait cycle [16] of brisk walking and normal walking. During the gait cycle of brisk walking and normal walking, the load variation for a 75 kg person with time at the hip-joint is shown in Fig. 3. The load, when the heel is grounded, increases and then decreases when the foot is taken off the ground till the next step. This load is completely dependent upon the body weight.

The abductor muscle force, which acts on the greater trochanter part, is 0.62 times of the force acting on the head. Other muscle forces are negligible as compared to the abductor muscle force. The magnitude of all the forces is given in Table 1.

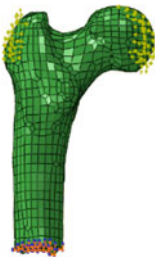

Fig. 2 Loading and boundary conditions

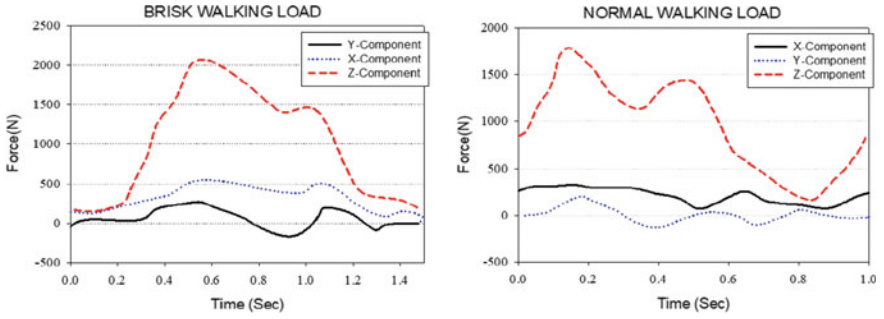

Fig. 3 Load variation during gait cycle of brisk walking and normal walking

Table 1 Magnitude of hip-joint and muscle force

Force component	Brisk walking	Normal walking
F_x	489° N	341.18° N
F_y	372° N	268.64° N
F_z	2135° N	1837.7° N

In order to apply the body forces on the femur head and trochanter region, two different node sets are created. Node sets have 60 and 42 nodes, respectively, to simulate the loading on the femur head and the trochanter region.

3.3 Material Properties

Isotropic properties (Table 2) are considered for an osteoporotic patient. Static analysis is performed for the peak load, which occurs in the gait cycle (Fig. 3) of brisk walking activity of the subject. The load is applied to the hip-joint and greater trochanter region with the help of appropriate modeling of load distribution and node selection. Due to existing uncertainties and variability in geometric and material properties in femur, it is important to perform probabilistic analysis of this system to find out the probability of failure with maximum strain failure criteria. Sensitivity analysis of probability of failure with respect to random variables is also important for characterizing their influence on the safe behavior of femur.

4 Discussions of Results

The deterministic FE analysis considers the mean values of all the random variables involved in the limit state function, as given in Table 2. It is essential to carry out a general finite element analysis to obtain the state and magnitude of stress and strain at the critical locations of the femur. The respective results help in relating the study of the relative behavior of femur in the probabilistic analysis. The influence of joint probability assessment of failure in comparison to the deterministic response is studied. As the material properties play an important role in the analysis, the actual spatially varying properties are employed for the analysis. A finite element analysis has been performed to get the critical location around neck for probabilistic analysis.

Table 2 Distribution of material properties

Material properties	Cortical	Trabecular	COV
Young's modulus	12,600 MPa	880 MPa	9%
Yield strain	0.73%	0.73%	
Yield strength	134 MPa	110 MPa	

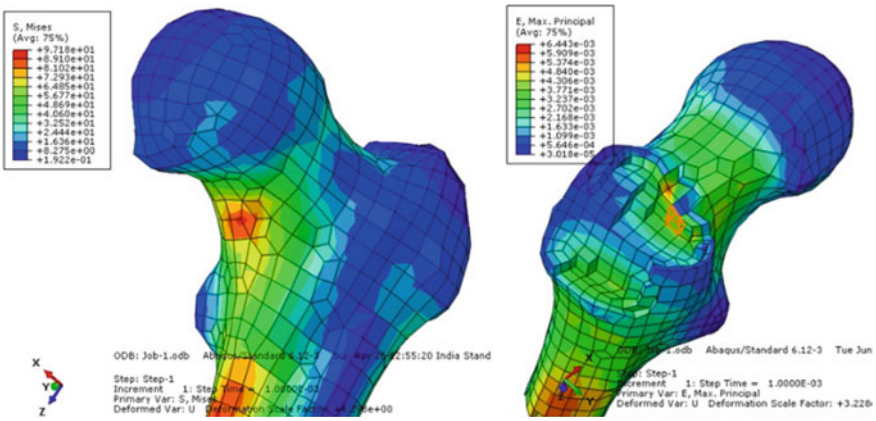

Fig. 4 Location of critical point

For that purpose, a static analysis is performed using isotropic properties for the osteoporotic patient as shown in Table 2 for osteoporotic femur using the peak load occurs in the gait cycle of brisk walking activity given in Table 2. The location of maximum stress and maximum principal strain around the femur is shown in Fig. 4.

4.1 Maximum Principal Strain Criteria

The probabilistic analysis is carried out by using maximum principal strain criteria. From the deterministic finite element analysis (Fig. 4), it is clearly mentioned that the probability of failure of the upper portion of neck in tension is higher than the probability of failure of compressive failure in bottom neck portion.

4.2 Cumulative Distributive Function (CDF)

From the deterministic finite element analysis, it is clearly mentioned that maximum tensile strain occurs in the upper portion of the neck and compressive strain occurs in the lower portion of the neck. However, the failure first occurs in a tension zone of the femur, as the permissible strain is lesser in that area. Analyses were performed using the Monte Carlo and advanced mean value (AMV) methods within reliability code. Briefly, the efficient AMV method combines optimization and reliability techniques to determine the most probable point (MPP), which represents the combination of parameter values that predict performance at a specific probability level. Monte Carlo simulation is also performed for different number of cycles to get convergence. At 6000 cycles, the result obtained by Monte Carlo simulation technique matches the

Table 3 Probability of failure and computation time of various methods

Method	Brisk walking	Normal walking	Computation time (h)
FORM	0.0493	0.0081	5
AMV	0.0486	0.0068	4
MONTE CARLO	0.0474	0.0073	38

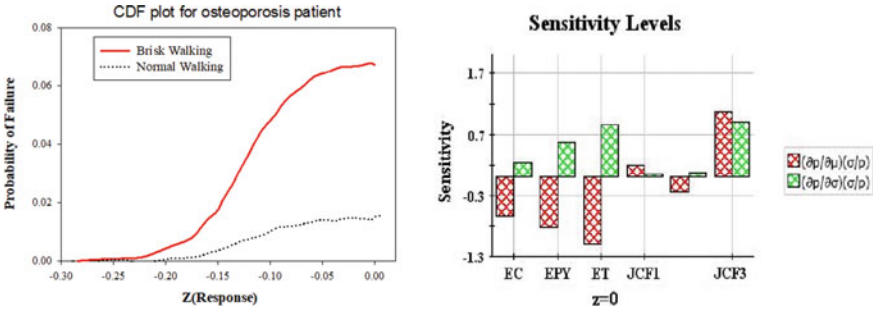

Fig. 5 CDF and sensitivity analysis for osteoporotic patient using maximum principal strain criteria

results obtained by AMV and FORM methods. The values of the probability of failure at $\mathbf{z} = 0$ or at a strain value of 0.73% obtained from all the three methods are given in Table 3.

Figure 5 shows the probability of failure (Pf) at different values of z or different values of strain. For example, for strain value of 0.59%, 0.64%, and 0.68%, the probability of failure are 1%, 4%, and 6.2%, respectively.

4.3 Sensitivity Analysis

The sensitivity plot at z (input parameters) $= 0$ is shown in Fig. 5, which shows the critical parameter which affects the Pf. The femur maximum strain was most sensitive to hip-joint force in z-direction, followed by the stiffness of trabecular femur and cortical stiffness and other force components. It is very similar to sensitivity plot obtained for normal femur using the same failure criteria. The difference is only in the levels of the bars presenting the sensitivity of Pf with respect to random variables.

Influence of Young's Modulus: The derivatives of the Pf with respect to the mean value of Young's modulus of cortical and trabecular femur are showing the negative sensitivity, which is same as sensitivity plot obtained by Viswanath et al. [3]. This pattern occurs because the femur strain is inversely proportional to the young's modulus of femur and increase in the value of the Young's modulus will result in a decrease in the probability of failure.

It can also be seen from Fig. 5 that the partial derivatives of Pf with respect to standard deviations of EC and ET are showing the positive value of sensitivity bar. It is because, as scatter increases, the area under the curve also increases which results in an increase of the failure region, leading to an increase of probability of failure. Thus, if the scatter in the distribution of Young's modulus increases, it will enhance the probability of failure.

Influence of Hip-Joint Force: The derivative of the probability of failure (Pf) with respect to the mean value of hip-joint force in Z (JCF3)-direction is showing the positive value of sensitivity, which implies that by increasing the mean value of this parameter, will enhance the probability of failure. JCF3 tends to bend the neck of the femur due to which the bending stresses in the femur is developed. The bending stresses in the neck increases subsequently by an increase in the mean value of JCF3, which may enhance the chances of fracture.

The sensitivity of the other two components is very small as compared to sensitivity of JCF3 because the magnitude of JCF1 and JCF2 are very small as compared to JCF3. The effects of scatter of all the components are same as the scatter effect of Young's modulus, for the given combination of random variable, in the limit state function.

5 Conclusions

The stochastic analysis is performed from the femur neck to determine the actual failure behavior for the femur. The study concluded with the following important orthopedic findings, which may provide vital safety information to the clinics of orthopedic treatment. The advanced mean value method provides good results in agreement with the Monte Carlo simulation technique that taken significantly reduced computation time. The influence of mean values and standard deviation of femur random properties on its probability of failure mainly depend on the limit state function that provides the joint probability distribution. The optimal values of random variables control or govern the safety criteria. From the sensitivity analysis, it is found that the joint contact force in normal direction due to the body weight and the elastic modulus of femur are the most sensitive parameters that influence the probability of failure. Young's modulus of cortical femur shows the positive influence in case of stress failure, while it shows the negative influence in the case of strain failure criteria for the given properties. As the Young's modulus of femur increases, its stiffness increases, which will result in a decrease in strain and an increase in the stress, due to the probability of failure of the femur is more in stress than in strain. It is mainly due to the limit state function. The methodology presented may be effectively used for the design optimization of hip-implant and material selection for the same.

References

1. Yang HS, Guo TT, Wu JH, Ma X (2009) Inhomogeneous material property assignment and orientation definition of transverse isotropy of femur. J Biomed Sci Eng 2(6):419–424
2. Taddei F, Martelli S, Reggiani B (2006) Finite-element modeling of femurs from ct data: sensitivity to geometry and material uncertainties. IEEE Trans Biomed Eng 53(11):2194–2200
3. Viswanath Y, Ahmad S, Pankaj P, Mahajan P (2014) Static analysis and strength reliability of human femur. In: Proceedings of the 12th biennial conference on engineering systems design and analysis, vol 1. Copenhagen, Denmark
4. Laz PJ, Easley SK, Tomaszewski PR, Petrella AJ, Rullkoetterand PJ, Pal S (2007) Finite element-based probabilistic analysis tool for orthopaedic applications. Comput Methods Programs Biomed 85(1):32–40
5. New AM, Dopico-González C, Browne M (2009) Probabilistic analysis of an uncemented total hip replacement. Med Eng Phys 31(4):470–476
6. Yosibash Z, Tal D, Trabesial N (2010) Predicting the yield of the proximal femur using high-order finite-element analysis with inhomogeneous orthotropic material properties. Philos Trans Royal Soc A Math, Phys Eng Sci 368:2707–2723
7. Francis A, Kumar V (2012) Computational modeling of human femur using CT data for finite element analysis. Int J Eng Res Technol 1(6):1133–1156
8. Singh V, Ahmed S (2014) Probabilistic analysis of human femur under dynamic loading. In: Proceeding of the national workshop on structure-property relations: from 3D imaging to computation modelling RDC-SASE. Chandigarh
9. Baca V, Horak Z, Mikulenka P, Dzupa V (2007) Comparison of an inhomogeneous orthotropic and isotropic material models used for FE analyses. Med Eng Phys 85(1):924–930
10. Zhao J, Ma S, Wei X (2009) Finite element analysis of femur stress under bending moment and compression load. In: 2nd international conference on biomedical engineering and informatics. Tianjin, China, pp 1–4
11. Patel S, Ahmad V, Mahajan P (2014) Reliability analysis of a composite plate under low velocity impact using the Gaussian response surface method. Int J Comput Methods Eng Sci Mech 15(3):218–226
12. Patel S, Soares C (2017) Guedes, System probability of failure and sensitivity analyses of composite plates under low velocity impact. Compos Struct 180:1022–1031
13. Patel S, Ahmad S (2017) Probabilistic failure of graphite epoxy composite plates due to low velocity Impact. ASME J Mech Des 139(4):044501–044504
14. Patel S, Soares C (2018) Guedes, Reliability assessment of glass epoxy composite plates due to low velocity impact. Compos Struct 200:659–668
15. Patel S, Ahmad S, Mahajan P (2016) Probabilistic finite element analysis of S2–glass epoxy composite beams for damage initiation due to high velocity impact. ASME J Risk Uncertainty Part B: Mechanical Engineering 2(4): 044504–044504-3
16. Heller M, Bergamnn G (2001) Hip contact forces and gait patterns from routine activities. J Biomech 34(7):859–871

Finite Element Analysis and Failure Mechanisms of Porous Biomaterial Architecture for Prosthetic Device

Prashant Athanker and Amit Singh

Abstract Many researchers have studied that porous unit cell-based architecture design and fabrication by additive manufacturing technique is proven to achieve similar mechanical characterization of trabecular bone. In this article, the micro-stress-strain distribution and failure mechanisms of bio-metal at four different types of porous architecture, chosen as X, Star, Cross and Octet lattice structures, with defined pore size, are studied. The unit cell-based structures have been modeled using INTRALATTICE CAD software, with specific pore size, strut aspect ratio (radius/length) and unit cell size. INTRALATTICE is capable of an efficient unit cell shape modeling and part design. For linear and nonlinear finite element (FE) analysis of above porous architectures, commercial CAE ANSYS and HyperMesh software have been used. 1D Beam and 3D tetra elements have been used to model the structure under compressive loads. The finite element (FE) results of all the unit cell-based architectures have been compared and identify which architecture has less stiffness response during the compressive loads. Subsequently, the micro-stress-strain distribution behaviors of all four porous structures have been illustrated through Johnson-Cook (nonlinear) FE model. This methodology has been used for estimating the structural response and failure mechanisms of unit cell geometry. Consequently, the unit cell type and size were modified to encountered desired Young's modulus and yield stress under compressive loading condition. At last of this investigation, to check the CAE software reliability, for which validation part has been done with previously reported literature, that was performed both experimental and FE study.

Keywords Unit cell-based architecture · Finite element · Micro-stress-strain

P. Athanker (✉) · A. Singh
Department of Mechanical Engineering, MNIT, Jaipur, Rajasthan 302017, India
e-mail: pathanker71@gmail.com

A. Singh
e-mail: asingh.mech@mnit.ac.in

V. K. Gupta et al. (eds.), *Reliability and Risk Assessment in Engineering*,
Lecture Notes in Mechanical Engineering,
https://doi.org/10.1007/978-981-15-3746-2_45

1 Introduction

The design and development of cellular (unit cell-based architecture) porous biomaterial with defined porosity and pore sizes are used for patient-specific implants. The metallic porous biomaterials like foam and unit cell-based architecture are of biomimetic and technological interest because it can make bounding relationship with a bone-implant interface. For the growth of bone, tissue, organs and for the replacement of injured or diseased bone, porous biomaterial structure has been introduced with desired porosity, and which has same mechanical characterization as the host bone [1]. In particular, the biomimetic material design and the selection of fabrication process which fabricates fully reliable, cellular, porous, engineered materials for orthopedic implants, is the main area of interest [2]. Today, there is a need for achieving high strength porous biomaterials, therefore, unit cell-based architecture bio-metal is commonly used for implants fabrication [3]. However, dense bio-metals implants pose the problem of stress shielding, due to their high modulus compared to bones. The pores of unit cell-based bio-metal structures have design parameters, such as pore size, strut aspect ratio, interconnectivity arrangement of the unit cell, unit cell size and porosity. Thus, porous bio-metal implant structures can behave as host bone [4]. The human bone cross-section architecture has non-uniform structure, classified into two categories (i) cancellous or trabecular bone and (ii) cortical bone [5]. Bones are porosity graded architecture materials; spongy in the middle having high porosity (cancellous) and dense on the outer (cortical bone) [6, 7]. To match the microstructures of bones in non-uniform porosity, with the porous biomaterial implants mechanical properties, is a challenging task nowadays. Therefore, the new series of porous bio-metals have been developed and are used in orthopedic surgery, including stainless steel, cobalt–chromium alloys, titanium, titanium–nickel and tantalum. The above bio-metals review discusses the biomaterial properties of traditional and highly micro-level porous metals used in orthopedics application [8, 9].

Over the mechanical properties comparison of ceramic and polymer porous biomaterials, bio-metal have enhanced the load-bearing property for orthopedic applications. However, complex metallic micro-lattice (unit cell-based) architectures are being fabricated by additive manufacturing (AM) techniques, such as selective laser melting (SLM) and electron beam melting (EBM) [10]. To contrast traditional manufacturing technique, AM can fabricate bio-metal microporous structures that mimic the same mechanical properties as of natural bone. Micro-lattice-based structures provide inherent advantages over foams, due to their lightweight and strong material [11].

This paper approaches to design microporous structures, which have been considered along with the four different unit cell topologies. The main objective of this work is to estimate mechanical responses of four different unit cell-based architectures under compression loads using finite element analysis. A methodology framework is developed to comprehend the deformation (linear and nonlinear analysis) response and failure mechanisms (buckling analysis) of microporous (unit cell-based) structures under compressive loads. The mechanical responses of the above-considered

porous bio-metal were studied using finite element (FE) models. For FE analysis, Ti6Al4V material physical properties were used as an input parameter. ANSYS and HyperMesh commercial CAE software's were used for FE simulation. Both 1D beam and 3D tetra elements were designed FE model for estimating the above-mentioned mechanical response. Consequently, this methodology has been used to demonstrate the response and failure mechanisms of micro-unit cell-based architecture and estimating structural properties of unit cell topology, i.e., Young's modulus, plateau stress and strain. At last, the result of methodology was compared with the results of experimental works in reported literature for the confirmation and validation.

2 Modeling Methodology

This section describes the modeling method to create the 3D-CAD model (both wireframe and solid). Initially, four different unit cell (X, Star, Cross and Octet) porous cellular structures were selected with same design variables (i.e., pore size, strut radius). Figure 1 demonstrates the four different types of unit cell spatial configuration. It has a certain number of strut or line arrangement, i.e., X, Star, Cross and Octet unit cells (lattice) are 8, 20, 24 and 36, respectively. For modeling, INTRALATTICE software was used, developed by McGill's Additive Design & Manufacturing Laboratory (ADML, 2016) [12] and is based on Grasshopper—a graphics algorithm editor for Rhino CAD software (Rhino 5, 2016) [13, 14]. In preliminary, the common geometric variables are selected for all four unit cells models, such as strut length (2 mm), pore size (1.5 mm) and strut diameter (0.3 mm). The unit cell of X, Star, Cross and Octet shape are patterned in the all three directions of design space ($5 \times 5 \times 5$) (Fig. 2). The geometrical properties are summarized in Table 1.

INRALATTIC is a plugin which is based on Grasshopper. Grasshopper is a visual programming tool which provides an ideal interface for systematic design. In this visual interface, parameters and function components are combined sequentially to

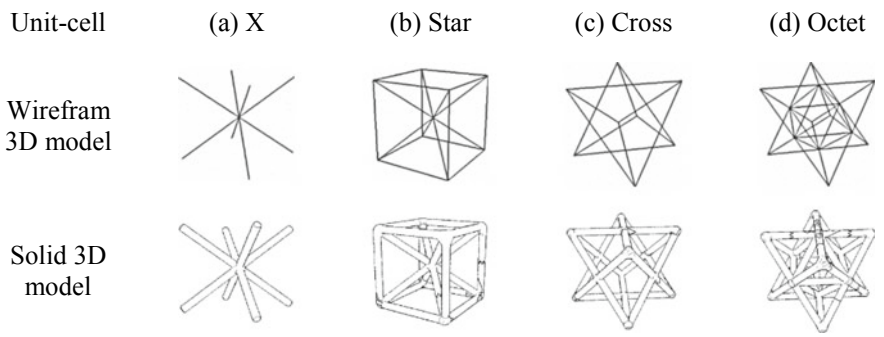

Fig. 1 Unit cell spatial configuration in 3D wireframe and 3D solid model **a** X; **b** Star; **c** Cross; **d** Octet

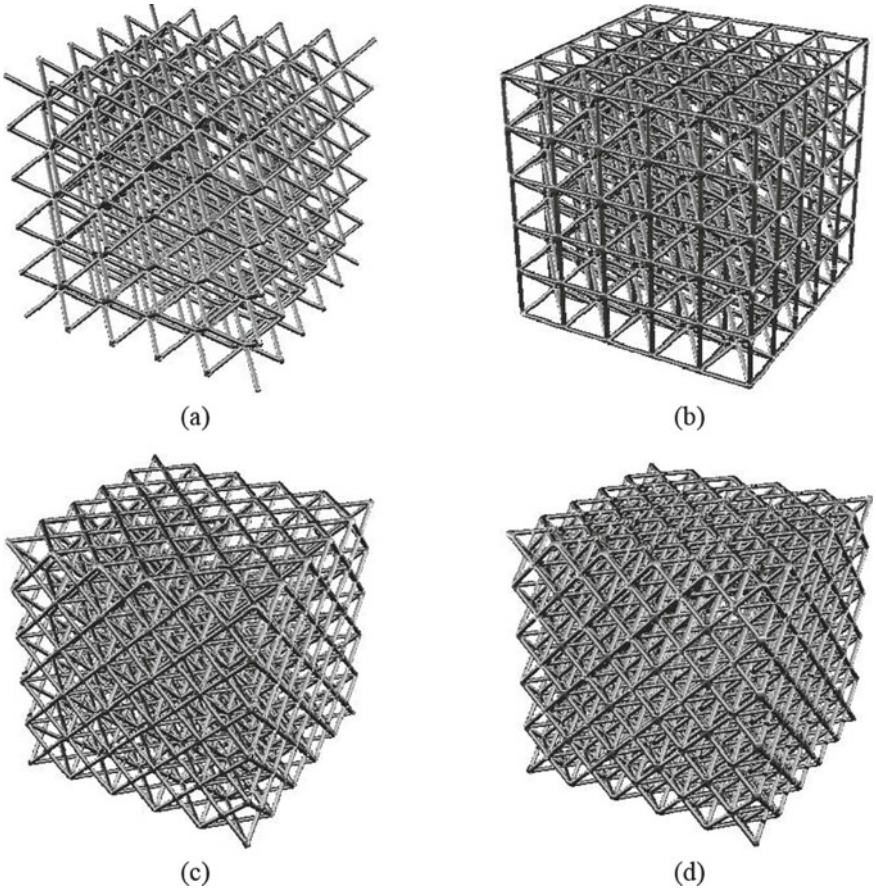

Fig. 2 A 5 × 5 × 5 unit cell 3D array arrangement **a** X; **b** Star; **c** Cross; **d** Octet

carry out the design of 3D CAD models generating into Rhinoceros 5. The geometric details of unit cell spatial configuration are representing in the graphics panel including such as vertices, face counting and mesh report (zero naked edges, proper manifold and solid (Fig. 3).

2.1 Finite Element Modeling

The numerical investigations of all micro-unit cell-based architectures were carried out by the CAE software package (HyperMesh) [15]. The numerical techniques are good for estimating the structural response under boundary constraints and loading condition. In this section, two FE model methods are presented. The first method used 3D beam elements (2 nodes) to demonstrate the unit cell strut arrangement.

Table 1 Geometric properties of X, Star, Cross and Octet unit cell-based architectures

S. No.	Unit cell topology	Strut length (SL)	Strut diameter (SD)	Pore size (PS)	Number of unit cell pattern in X, Y and Z direction			Total lattice block dimensions approx.		
					X_n	Y_n	Z_n	Length	Width	Height
		(All dimension in mm)						(All dimension in mm)		
1	X	2	0.3	1.7	5	5	5	10.03	10.03	10.03
2	Star									
3	Cross									
4	Octet									

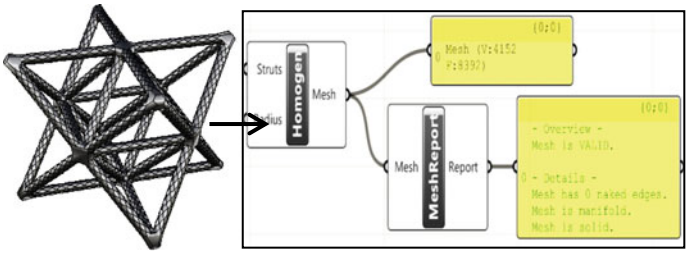

Fig. 3 Details of unit cell spatial configuration

Computationally this method has less information concerning the stress-strain distribution in the unit cell-based architecture [16]. The second method is 3D tetra elements (4 nodes) to demonstrate both unit cell geometry and stress-strain distribution information.

Beam element model

Initially, 2-node (IJ) beam elements were used to simplify the unit cell-based architecture with an arbitrary cross-section, but it deforms only in directions perpendicular to its axis (Fig. 4). Each strut in the unit cell-based structure is meshed using BEAM188 element which behaves as a Timoshenko beam. Timoshenko beam elements defined with quadratic interpolation functions are used for bending and transverse shear deformations. The 1D beam elements were used for investigated mechanical responses using commercial CAE software (ANSYS).

3D Tetra Element Model

The solid unit cell-based CAD model is meshed using 3D tetra elements, where four nodes surround each element. While meshing using HyperMesh software, the solid model is used for finite element numerical study. The element type chosen is tetrahedral, because for cylindrical shape strut region should properly fill the gaps between meshes in neighboring regions [17]. To ensure that the 3D elements quality is good for the particular type of FE analysis, (i.e., no free edges were found, selected elements should be enclosed the part volume).

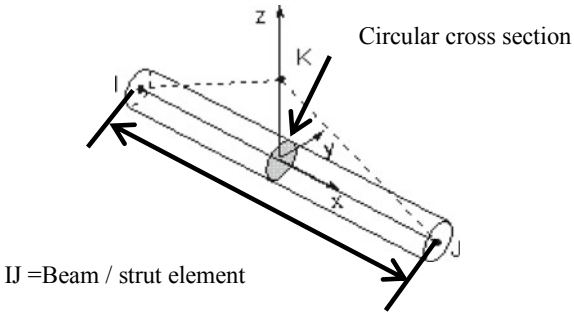

Fig. 4 Schematic beam element with the circular cross-section

Table 2 Ti6Al4V material composition and mechanical properties [18]

Metal	Main alloying composition	Mechanical properties					
		YS	UTS	YM	PR	TM	Max. elongation
Ti6Al4V (F136) (ASTM, 2008)	Ti; (5.5–6.75), Al; (3.5–4) V; (0.08), C; (0.2O) (wt%)	795 MPa	860 MPa	116 GPa	0.34	1000 MPa	10%

Table 3 Number of node and element of two FE models (Octet unit cell)

Model type	Number of strut for octet unit cell	Number of elements	Number of nodes
1D beam element	36	252	230
2D trias element (facet)	36	12,832	6372
3D tetra element	36	32,364	8994

2.2 Material Model

For FE modeling of unit cell-based architecture behavior, under different uniaxial loading and boundary condition, static linear, implicit geometric nonlinear and failure mechanisms analysis was implemented. A Ti6Al4V elastic-plastic material model property was used for modeling the mechanical behavior of the metal (Table 2). In this section, the material behavior is supposed to be bilinear. The density of 4320 kg/m^3 was used for the analysis.

2.3 Structure Model

Table 3 represents the key properties of three FE models of octet unit cell, where strut diameter and strut length are 0.3 mm and 2 mm, respectively. For 1D mesh of each strut of single unit cell are minimum ten beam elements, which gave better structure results under different loading condition.

3 Validation

Strength value obtained in this section demonstrates a validation of FEA, Merkt, S., et al. (2015) investigated the influence of strain rate in quasi-static compression test and to find the mechanical response of TiAl4V lattice structure. The f2cc-z structure was fabricated using selective laser melting (SLM) technique [19]. The f2cc-z lattice

Table 4 Geometric properties of all unit cell-based architectures

S. No.	Unit cell type	Number of unit cell in array arrangement	SL	SR	SD	PS	Volume of porous part	Bounding box volume of porous part	Apparent porosity	Compressive yield stress	Young's modulus
		$n \times n \times n$	mm	mm	mm	mm	mm^3	mm^3	%	MPa	GPa
1	X	$5 \times 5 \times 5$	2	0.15	0.3	1.7	96.97	1121.62	91	68	5.12
2	Star		2	0.15	0.3	1.7	154.07	1102.30	86	84	3.56
3	Cross		2	0.15	0.3	1.7	139.01	1108.71	87	87	3.23
4	Octet		2	0.15	0.3	1.7	241.22	1108.71	78	92	2.56

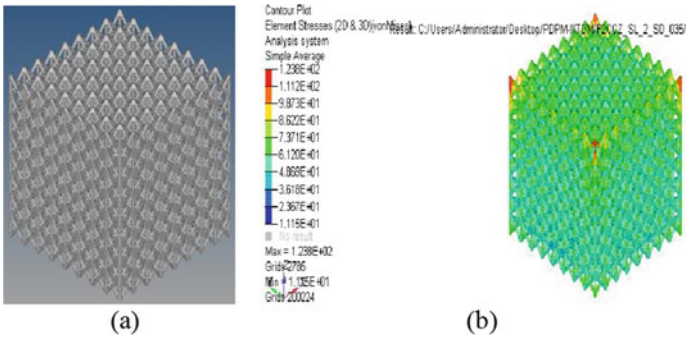

Fig. 5 **a** 8 × 8 × 8 of f2cc-z unit cell 3D CAD model; **b** von Mises stresses

comprised of an 8 × 8 × 8 array, with a strut diameter of 0.35 mm and a cell width (strut length) of 2 mm. Experimentally, Merkt reported that the Young's Modulus and compressive yield stress are 1.5 GPa and 47 MPa, respectively. In this study, same validation model has been created using INTRALATTICE software and performed nonlinear FE analysis. Although, FE simulation study was done using OptiStruct Solver (HyperMesh), and the Young's Modulus and compressive yield is 2.51 GPa and 55 MPa, respectively. Figure 5 represents the 3D CAD model of f2cc-z unit cell-based structure and FE analysis result

4 Results and Discussion

The static linear, nonlinear and buckling failure FE results of Ti6Al4V micro-unit cell-based structures, octet were selected as the best among the four-unit cell-based structure. The mechanical properties are affected due to the change in the design variables of micro-lattice structures. For the generation of human bone tissues, pore size and porosity of micro-cellular porous biomaterial structures play an important role. For achieving the desired mechanical properties of all porous cellular structure in the biomedical application, the pore size and porosity should be appropriate. Using FE analysis was done to estimate the mechanical response in both static and dynamic condition. It was found that the high porosity of micro-lattice structure has high Young's Modulus and low yield stress value. To reduce the stress-shielding effect, the micro-cellular porous bio-metallic structure has low Young's Modulus which is same as human bone. The results are interpreted in terms of the elasto-plastic (nonlinear) behavior of all mentioned structures. The apparent porosity percentage was measured using CAD software, compressive yield stress, and Young's Modulus was FE analysis results. It is demonstrated in Table 4.

5 Conclusion

As results of the FE analysis, it has been found that 'octet' has high yield strength and low Young's modulus as compared to X, Star, and Cross unit cell-based structures. For static linear analysis, high stiff unit cell-based architecture (octet) was identified. Similarly, through implicit geometric nonlinear (elasto-plastic) FE analysis using Johnson-Cook material model, the micro-stress-strain distribution curve of all above-mentioned architecture is described with initial yield stress and ultimate stress due to uniaxial compressive load. At last, failure mechanisms (critical buckling load) were calculated.

Based on FE simulation results, it was found that the porosity intensely affected the mechanical response of micro-unit cell-based architectures. The proposed work illustrates that all four micro-cellular porous structures exhibited Young's Modulus value between 2.56 and 5.12 GPa, which is same as in the range of human trabecular bone. The results suggest that with changing design variables the desired mechanical properties have potential for cellular-based metallic porous implant design.

References

1. Nouri A, Hodgson PD, Wen C (2010) Biomimetic porous titanium scaffolds for orthopedic and dental applications. In: Biomimetics, learning from nature, pp 415–450
2. Torres-Sánchez C (2010) Definition of a periodically distributed porosity gradient in functionally graded materials to be used as bone scaffolds. In: Proceedings of UK MMSG Strathclyde, pp 1–23
3. Arabnejad S, Johnston RB, Pura JA, Singh B, Tanzer M, Pasini D (2016) High-strength porous biomaterials for bone replacement: a strategy to assess the interplay between cell morphology, mechanical properties, bone ingrowth and manufacturing constraints. Acta Biomaterialia 30:345–356
4. Miao X, Sun D (2010) Graded/gradient porous biomaterials. Materials 3(1):26–47
5. Marin E, Fedrizzi L, Zagra L (2010) Porous metallic structures for orthopaedic applications: a short review of materials and technologies. Eur Orthop Traumatol 1(3–4):103–109
6. Wieding J, Jonitz A, Bader R (2012) The effect of structural design on mechanical properties and cellular response of additive manufactured titanium scaffolds. Materials 5(8):1336–1347
7. Heinl P, Müller L, Körner C, Singer RF, Müller FA (2008) Cellular Ti-6Al-4V structures with interconnected macro porosity for bone implants fabricated by selective electron beam melting. Acta Biomater 4(5):1536–1544
8. Levine B (2008) A new era in porous metals: applications in orthopaedics. Adv Eng Mater 10(9):788–792
9. Davis ME (2002) Ordered porous materials for emerging applications. Nature 417(6891):813–821
10. Yan C, Hao L, Hussein A, Raymont D (2012) Evaluations of cellular lattice structures manufactured using selective laser melting. Int J Mach Tools Manuf 62:32–38
11. Ashby MF, Evans AG, Fleck NA, Gibson LJ, Hutchinson JW, Wadley HNG (2000) Metal Foams : a design guide. Butterworth-Heinemann Publication
12. Intralattice (2016) http://adml.lab.mcgill.ca.html, Last accessed 2016
13. http://www.grasshopper3d.com.html
14. https://www.rhino3d.com.html

15. HyperMesh. http://www.altairhyperworks.com, HyperMesh.aspx, AltairHyperWorks
16. Smith M, Guan Z, Cantwell WJ (2013) Finite element modelling of the compressive response of lattice structures manufactured using the selective laser melting technique. Int J Mech Sci 67:28–41
17. Nguyen J, Park S, Rosen DW, Folgar L, Williams J (2012) Conformal lattice structure design and fabrication. In: Proceedings of 23rd annual international solid freeform fabrication symposium—an additive manufacturing conference, SFF, pp 138–161
18. Hermawan H, Ramdan D, Djuansjah JRP (2011) Metals for biomedical applications. In: Biomedical engineering—from theory to applications, pp 411–430
19. Merkt S, Hinke C, Bültmann J, Brandt M, Xie YM (2015) Mechanical response of TiAl6V4 lattice structures manufactured by selective laser melting in quasistatic and dynamic compression tests. J Laser Appl 27(S1):S17006

Investigation of Human Errors Using Fuzzy-Bayesian Belief Networks

M. Karthick, C. Senthil Kumar, and T. Paul Robert

Abstract It is an on-going process for the nuclear industry to implement newer safety measures based on lessons learnt from operating experience in both engineering and operation (such as establishing new regulations and providing additional measures for backup safety actions during external hazards). Even minor safety incidents in NPP are viewed critically and appropriate safety measures are undertaken to prevent such occurrences. Nevertheless, human errors are found to be one of the key contributors to accidents in NPPs. This is due to various reasons such as complex interfaces, workloads, and dynamic situations. Moreover, human error data is hard to be collected and classified; the factors which influence human behaviour are difficult to be identified. When attempting to reduce human error in such complex systems, cognitive dimensions (attention, memory, etc.), behavioural variables, environmental factors, organizational and technical factors associated with incidents/accidents must be clearly addressed. Though a number of methods are available to analyse and investigate the causes of human error, it seems that most of the existing methods are insufficient for comprehensive analysis of human activity-related contextual aspects of accidents. For this reason, the present study proposes a proactive modelling approach that combines fuzzy analytical hierarchy process (FAHP) and Bayesian belief networks (BBNs) with human factors analysis and classification system (HFACS), in order to identify the role of human errors. HFACS is a validated method to classify errors from current investigative records and to document the full range of potential human factor data in complex industries, such as avionics, rail and chemicals. FAHP implementation strengthens the HFACS system by offering an empirical context to ensure the quantitative evaluation of nuclear accidents. The proposed model is comprised of three stages. The first step is the empirical study of accident-related human factors, which utilizes HFACS to distinguish active or latent failures. In the next stage, which is a statistical analysis using BBN, the hierarchy of human factors defined in the first phase offers

M. Karthick (✉) · C. Senthil Kumar
AERB-Safety Research Institute, Kalpakkam, India
e-mail: msv.karthiktce@gmail.com

M. Karthick · T. Paul Robert
College of Engineering, Anna University, Chennai, India

V. K. Gupta et al. (eds.), *Reliability and Risk Assessment in Engineering*,
Lecture Notes in Mechanical Engineering,
https://doi.org/10.1007/978-981-15-3746-2_46

input for analysis. BBN strengthens HFACS capability by assessing the degree of human factors relationships. The fuzzy analytical hierarchy process methodology is introduced in the final phase to compute the conditional probabilities. BBN enhances the ability of HFACS by measuring the degree of relationships among the human factors. The application of fuzzy networks adopted in this study is to effectively model (1) uncertainty in human error (2) variations attributed to assessment by experts, (3) performance influencing variables and (4) cognitive human behaviour. A case study illustrates the model and indicates that the proposed model is capable of looking for critical contextual factors related to human activity that is not easily obtainable by using existing methods. Some of the advantages of implementing these accident analysis approaches are discussed. Finally, some considerations, including further work, associated with the FAHP-HFACS-BBN are discussed and concluded in this paper. The study of human reliability in the nuclear field focuses on understanding the causes and propagation mechanisms of operator errors and its implications for effective modelling in risk assessment studies.

Keywords Human error probability · Fuzzy Bayesian belief networks · Nuclear power plant · Human factor analysis and classification system · Human reliability analysis

1 Introduction

Several nuclear human factor safety regulations have been developed after the occurrence of serious nuclear accidents of Three Mile Island in 1979 and Chernobyl in 1986. Such incidents were primarily caused by human error. The International Atomic Energy Agency (IAEA), nuclear regulatory agency, has started looking into human factors from a different perspective after these events. Modern and emerging innovations are often implemented in nuclear industry based on lessons learned from the operational past. New and advanced technologies are introduced periodically in nuclear industry based on the lessons learned from the operating experience. Nevertheless, in the past decade, several accidents and incidents are reported which are mainly due to human and organizational factors from Alvarenga et al. [1]. Several researchers have insisted that the study of the human factor and its contribution to accidents are essential in the complex industries especially in nuclear industries, as human error is contributed to 50–70% of the nuclear accidents from Griffith and Mahadevan [2]. The operator errors, viz. slips due to perception, lapses due to memory, mistakes due to attention, exceptional and routine violations in a nuclear power plant, are often cited as reasons for reactor trip, plant shutdown, loss of coolant accident, heat removal system failure and various incidents [3]. Moreover, human errors due to organization also need to be considered. For example, in a typical control room environment, during an abnormal situation three important cognitive tasks to be performed by an operator, viz. identify the abnormal event, diagnose the causes

of event and execute steps for bringing the plant to a safe state from Hilliard and Jamieson [4]. During an abnormal event, the operator's attention is directed towards mitigation of the event by appropriate actions. Failure/inappropriate action during these situations will lead to system failure, so plant safety may get affected. So, a systematic human factor study is required to minimize the human error in nuclear power plants (NPP) to improve the plant's safety.

Human reliability analysis (HRA) is accounted for the human factor study in NPPs. To quantify the human error probability, there have been several methods available in HRA, viz. Technique for Human Error Rate Prediction (THERP) [5], Cognitive Reliability and Error Analysis Method (CREAM) [6] and A Technique for Human Error ANAlysis (ATHEANA) [7] in general. In addition to that, there are a number of Human Error Identification (HEI) tools available to systematically identify and classify the human error in human reliability analysis, viz. Systematic Human Error Reduction and Prediction Approach (SHERPA) [8], Korean-version HPES (K-HPES) [9], The Technique for the Retrospective and Predictive Analysis of Cognitive Errors (TRACEr) [10], Systems Theoretic Accident Modelling and Processes (STAMP) and and Human Factors Analysis and Classification System (HFACS) [11]. These tools specify a prescriptive process for collecting, analysing and integrating data related to human-related accidents. Among them, HFACS is adopted for two reasons: (1) analysis of the human errors with four levels of causal factors, viz. unsafe acts, preconditions of unsafe acts, unsafe supervision and organizational influences, and (2) predetermined set of causal factors.

Prioritization of human factor is a Multi-Criteria Decision Making (MCDM) problem. A multi-criteria decision problem can help us find the critical factors affecting the performance of the several factors (main criteria) and factors affecting the main criteria (sub-criteria). Some common methods to solve multi-criteria problems are analytic hierarchy process (AHP), analytic network process (ANP) and technical order preference by similarity to ideal solution (TOPSIS). These are well-structured methods and used to compare and evaluate the alternatives on the objectives systematically. Due to interaction effects and dependencies of elements at various levels, ANP and TOPSIS cannot be used in most of the practical decision-making problems [12–15]. This situation necessitated a holistic approach. A holistic approach like AHP overcomes the limitations of ANP and TOPSIS and accepts attributes and alternatives networked in a system. There are two types of AHP available: conventional and fuzzy type [14, 15]. A 9-point Saaty's scale is used in the conventional AHP and pairwise comparisons at each level with respect to the objective used for factor identification selection. The conventional AHP has some limitations, viz. crisp decision-making, unbalanced judgement scale and imprecise and subjective judgement. Due to the vagueness and uncertain decision-making with conventional AHP, the concept of fuzzy AHP is found to be advantageous. Fuzzy AHP replaces the hierarchies into a networked structure, in which all elements are interlinked. For this reason, fuzzy AHP is adopted in this study. Because these are qualitative analysis only, quantification analysis cannot be done using fuzzy AHP and HFACS [16, 14].

Quantitative research, compared to qualitative research, not only helps in making decisions about the progress of human factors, but also reinforces the investigative process of quantitative research incidents and provides judgements [17]. For example, HFACS model can be combined with BBN, which can provide statistical interrelationships and quantify numerical values of the likelihood of occurrence [18]. A Bayesian belief network (BBN) is an ideal method of quantitative risk analysis as this model can do both predictive and diagnostic analyses. The BBN consists of two parts: qualitative and quantitative parts. The qualitative component is a directed acyclic graph in which the process variables are represented by nodes and the arcs are the association of causes and effects of the variables [19]. In BBN, the conditional probability table (CPT) is generated for each node using opinions from experts in the reference domain and these values generally vary from expert to expert. Incorporating fuzzy sets and BBNs can help to reduce the uncertainty of observed evidence associated with the defined variable and differences related to expert evidence in CPT construction [20]. Nonetheless, it may be difficult for experts to determine precise probability values for the association of nodes [21].

In this study, the HFACS taxonomy integrated with fuzzy AHP is used to analyse the human and organizational factor in the recent nuclear disaster of Fukushima-Daiichi accident. The objective is to identify the human factors contributed/involved in the Fukushima accident in terms of unsafe acts, preconditions of acts, unsafe supervision and organizational errors and also to prioritize the human factors based on their level of contribution. Moreover, the prioritization of human errors is done using fuzzy AHP. Subsequently, human error is quantified by BBN. This would help regulators to make necessary step to minimize the human error in nuclear plants and particularly useful to develop an advanced risk model for accident scenarios.

2 Literature Review

The literature review is carried out by referring to various journals in three different domains: (1) applications of HFACS, (2) applications of fuzzy AHP and (3) applications of Bayesian belief networks, which are briefly described in Tables 1, 2 and 3, respectively.

2.1 Research Gap and Problem Domain

The common approach adopted in human reliability analysis is to identify the critical factors affecting human performance. Various techniques are proposed in the literature for identifying these factors. Among them, HFACS adopts factors at different level and one of the factors analysed is organizational factor. In general, human factors-related research is complicated due to vagueness and ambiguity in nature, so researchers go for expert's opinion. In such cases, BBN can be used as the

Table 1 Literature survey on applications of HFACS

Research articles	Sector	Contributions
Li et al. (2008) [22]	Aviation	Reason's organizational model-based analytical HFACS was designed to examine the role of human error in aviation accidents. Analysis of 41 civil aviation accidents indicates the most contributing factors are unsafe supervision and organizational influences
Patterson and Shappell (2010) [23]	Mining	A revised HFACS model is used to evaluate incident and accident reports from across Queensland state to identify human factor patterns and system vulnerabilities within mining
Chen et al. (2013) [24]	Maritime application	'*Why-because*' graph-based human factors analysis and classification system for maritime accidents (HFACS-MA) is proposed for maritime accidents. Results show that pre-condition of unsafe act was the most susceptible part of the system
Diller et al. (2013) [25]	Healthcare applications	Reason's theory-based modified version of human factors analysis classification system is proposed for identification of the causes of error in healthcare application. Investigation of 105 serious events shows that cognitive errors such as attention and memory are the root causes of errors
Madigan et al. (2016) [26]	Rail industry	To investigate the active and latent failures in rail industry accidents, a conventional HFACS is applied for 74 incidents. The results indicate that the active failures such as errors and violations are found higher in work-related distraction and environmental factors

best alternative tool due to the nature of minimizing the subjectivity. Since the basic nature of critical factor identification is an MCDM problem, techniques like fuzzy AHP are found to be suitable.

3 Research Methodology

The methodology followed in this study is shown in Fig. 1. The study begins with the literature review on human error identification models, MCDM and applications of BBN. A conceptual model for human factor prioritization has been designed. After developing the conceptual model, a suitable nuclear accident for the case study

Table 2 Literature survey on applications of fuzzy AHP

Research articles	Sector	Contributions
Lee et al. (2008) [27]	IT department performance evaluation	An integration model of FAHP and balanced scorecard (BSC) is proposed for performance evaluation of IT industries in Taiwan. The results of the proposed model are analysed with four different perspectives of financial, customer, internal business process and learning and growth shows that customer and internal business process are the most important factors to be focused
Choudhary and Shankar (2012) [28]	Thermal power plant location selection	A new framework of STEEP-fuzzy AHP-TOPSIS is proposed for evaluation and selection of optimal locations for thermal power plants. Parameters for location selection considered in this study were ranked by the proposed model and the appropriate location was identified
Naghadehi et al. (2009) [16]	Mining industry	FAHP approach based on a new model is proposed to select the optimum mining method. The weights of the criteria assigned by decision-makers to select the mining method are ranked by the proposed model and the suitable model was selected.
Taylan et al. (2014) [29]	Construction	A hybrid approach of fuzzy AHP and fuzzy TOPSIS is proposed to prioritize the project risks in the construction industry. FAHP is used to create favourable weights for the fuzzy linguistic variable of construction projects' overall risk
Dagdeviren and Yuksel (2008) [30]	Manufacturing organization	To determine the level of faulty behaviour risk in work system, FAHP-based approach is proposed

has been selected, and necessary data is collected. Then, HFACS and fuzzy AHP are used for human factor identification and for prioritization based on the human factors weighted index (HFWI). Subsequently, BBN is adopted for quantification of human errors. The human factors weighted index (HFWI) generated by the fuzzy AHP is prioritized. The results are validated to demonstrate its feasibility for applying in a real-world scenario.

Table 3 Literature survey on applications of Bayesian belief networks

Research articles	Sector	Contributions
Li et al. (2012) [31]	Nuclear power plants	A conceptual framework model of BN approach is developed for the quantification of organizational errors in HRA frameworks. The most likely root causes are identified and reliability of human operator is measured by the proposed model
Wang et al. (2011) [32]	Cargo	A hybrid and convergence model of HFACS and BBNs is proposed to define the HOF failure in vapour incidents. Findings suggest that the model is capable of looking for important human and organizational errors and conducting statistical accident analysis
Francis et al. (2014) [33]	Pipe industry	BBN-based knowledge model is constructed for drinking water distribution to find the pipe breaks in a water zone to prevent water loss and water quality deterioration
Martins and Maturana (2013) [34]	Oil industry	To study the internal factors (IFs), skills, and management and organizational factors (MOFs) in the operation of an oil tanker, on the risk of collision accidents, BBN-based methodology is proposed
Trucco et al. (2008) [35]	Maritime industry	A Bayesian belief network (BBN) is integrated with fault tree analysis (FTA) to model the maritime transport system (MTS) on a collision in open sea hazard of technical elements to model the influences of organizational functions and regulations

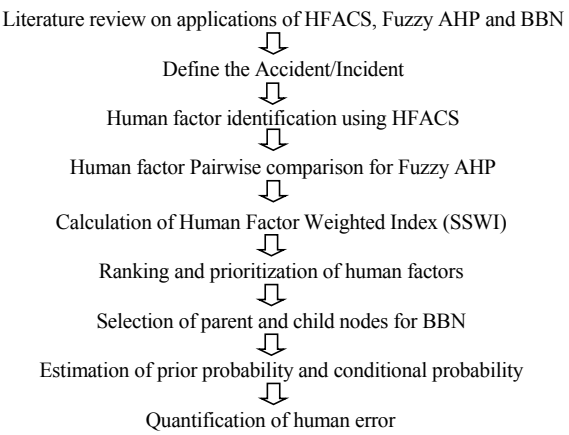

Fig. 1 Research methodology

3.1 Literature Review on Applications of HFACS, Fuzzy AHP and BBN

Research papers in the applications of fuzzy AHP, HFACS and BBN in different safety should be thoroughly studied.

3.2 Define the Accident/Incident

The accident to be investigated is clearly described in this step.

3.3 Human Factor Identification Using HFACS

Through implementing HFACS, operators and organization errors recognize active or latent errors. This research adopts Shappell and Wiegmann [11]. HFACS typically has four-level hierarchical structure: unsafe acts, preconditions of unsafe acts, unsafe supervision and organizational influences. These are briefly explained in following sections. For better understanding, readers can see HFACS framework in Shappell and Wiegmann [11].

3.3.1 Level 1: Unsafe Acts

This is the lowest and first level of the HOF system. This level includes operator's errors and violations. These are considered intentional accidents, leading directly to an incident, rendering them the most noticeable to investigators. In the error category, decision error (DE), skill-based error (SBE) and perceptual error (PE) are listed. Routine violation (RV) and exceptional violations (EV) are classified as violations.

3.3.2 Level 2: Preconditions of Unsafe Act

The second level of HFACS outlines the preconditions for unsafe acts. This level has three sub-categories: the condition of the operator (CO), personnel factors (PF) and environmental factors (EF). The condition of the operator category comprises three causal classes identifying conditions where the operator is overwhelmed or unable to perform the required task. The operator may suffer from an adverse mental state (AMS) due to excessive tiredness and stress. An adverse physiological state (APS) arises if the worker is acutely ill, wounded or otherwise temporarily unable to perform the vital tasks of the job healthy. The operator may have long-term or lifelong physical or mental limitations (PML). An example is bad vision.

Experts can proceed to investigate the "preconditions for unsafe acts" errors with the "unsafe acts" errors listed in level, which influences the human and organizational factors (HOFs) of level 1. The second subtype is personal factors comprising two explanatory groups and operator actions that lead to the adverse event. The most prevalent causal classification is crew resource management (CRM) which results in specific miscommunication between operators or in the absence, incompleteness or inaccessibility of data. Personal readiness (PR) allows for those times where operators do not sleep sufficiently, report to work while ill and auto-medicate for appropriate medications, which contribute to reduced operational capacities that can lead to errors. Such forms of complications can also be defined as an adverse physiological state. Finally, environmental factors explain the environmental impact of human error and may contribute to adverse events. There are two casual types, including the physical environment (PE) (e.g., lighting, sound, room layout) and the technical environment (TE) that affect device and control design, screen or software features, checklist design and automation.

3.3.3 Level 3: Unsafe Supervision

The third level of HFACS addresses supervision's role in adverse events. Those at the front lines of the nuclear control room are responsible for their actions; furthermore, they are beneficiaries of a number of implicit deficiencies due to their supervisors in some instances. This level includes four subtypes: inadequate supervision (IS), planned inappropriate actions (PIA), operational planning, failure to correct known problem (FCP) and supervisory violations (SV).

3.3.4 Level 4: Organizational Influences

The fourth and final phase of HFACS involves organizational impacts, where poor management decisions have a direct impact on supervisors and the operators they oversee. However, traditional RCAs often ignore these organizational forces. HFACS identifies three organizational failures: resource management (RM), organizational climate (OC) and organizational process (OP).

3.4 Human Factor Pairwise Comparison for Fuzzy AHP

Structure the AHP template hierarchically centred on the variables defined at Step 3.3. Fuzzy pairwise comparison matrix of correlations between different factors found in different levels is established. Eigenvector should be computed for the formed matrix.

3.5 Calculation of Human Factor Weighted Index (HFWI)

Determine local and global weights for key factors and auxiliary factors with comparative metrics on a pairwise basis. The fuzzy scale for relative weight measurement should be properly configured. This scale is to be converted into an appropriate fuzzy triangular number (TFN) based on appropriate α-cut value.

The operations in fuzzy AHP of given any two numbers are given below.

$T_1 = (l_1, m_1, u_1)$ and $T_2 = (l_2, m_2, u_2)$, and a positive real number r, some useful operations on triangular fuzzy numbers.

T_1 and T_2 can be expressed as follows:

$$T_1 \oplus T_2 = (l_1 + l_2, m_1 + m_2, u_1 + u_2)$$
$$T_1' \otimes T_2' = (l_1 \times l_2, m_1 \times m_2, u_1 \times u_2)$$
$$(T_1)^{-1} = \left(\frac{1}{u_1}, \frac{1}{m_1}, \frac{1}{l_1}\right)$$

3.6 Ranking and Prioritization of Human Factors

Based on the human factor weighted index, the global fuzzy number for each factor should be calculated. The global fuzzy number is then converted to crisp weight value using the Buckley's method [36] as follows.

The fuzzy weight matrix is calculated by,

$$\text{Geometric mean } r_i = (C_{i1} \otimes C_{i2} \otimes \cdots \otimes C_{ij})^{1/n} \tag{1}$$

$$\text{Weighted fuzzy Matrix } W_i = r_i \otimes (r_1 \oplus r_2 \oplus r_3 \oplus \cdots \oplus r_n)^{-1} \tag{2}$$

$$\text{De-fuzzification } W_i' = \frac{W_l + W_m + W_u}{3} \tag{3}$$

Importance of effects of individual factors

$$W_x = \frac{W_i'}{\sum_{i=1}^{n} W_i'} \tag{4}$$

whereas

C_{ij} = cost vector in the initial pairwise matrix
n = number of respondents.

3.7 Selection of Parent and Child Nodes

The appropriate parent and child nodes are selected based on the ranking factors from FAHP. The parent nodes are root nodes having prior probabilities and child nodes are leaf nodes which are having conditional probabilities based on the results of FAHP.

3.8 Estimation of Prior Probability and Conditional Probability

Estimate prior and conditional probability values by using the fuzzy membership to characterize expert probabilities. An example is the possibility to assign a probability value with the fuzzy membership function (1/2, 1/4, 1/5). In this case, a triangular fuzzy number (l, m, u) is used to represent the probabilities where l, m and u represent the highest, most likely and lowest.

BBN follows the Bayes' theorem as given below,

$$\text{Posterior probability } P(A \mid B) = L(B \mid A) * P(A) \tag{5}$$

whereas

$P(A)$, $P(B)$ = prior probabilities
$L(B \mid A)$ = Likelihood estimator.

3.9 Quantification of Human Error Using BBN

Finally, human error can be quantified after all the CPTs are elicited. The Bayesian inference depends on the specific goals of each accident analysis.

4 Case Study

In this section, a case study of Fukushima-Daiichi [37] is presented to demonstrate the application of the proposed model. The analysis of critical HOFs in the case study is presented in Sect. 4.1.

4.1 Large Radioactivity Release at Fukushima-Daiichi

Fukushima has six units, located in Japan, the oldest type of BWR (boiling water furnace) and BWR3/4 reactor. The main components of a pressure vessel (PV), a container (CV), a furnace building (RP) and a spent fuel tank (SFP) are located on the ground floor of the reactor building. Three units 1–3 were in operation during the earthquake, while the remaining 3 units of 4–6 were shut down for regular maintenance. Unit 4 has just been stopped and fuel has been passed to SFP. Units 1–3 are stopped automatically by the sensor of emergency diesel generators (EDGs) and the idle cooling system is initiated. Nevertheless, an earthquake disrupted the internal AC transmission line to the NPPs, leading to a tsunami that arrived some 50 min later and overwhelmed the EDGs and the sea pumps. The tsunami was triggered by destruction of the external AC system. High levels of radioactivity were released into the environment at that time, and it was estimated to be 1.6 × 1017 by the Nuclear Industry Safety Agency (NISA) [38, 39]. Several studies were carried out to determine the cause of the Fukushima nuclear accident. Including mechanical defects, the findings have considered human and organizational factors also to be a cause [40]. For example, failure to provide training can be defined as organizational errors; insufficient knowledge is described as the human-level errors. Such considerations are inherently linked to the performance of the operator and should be addressed when designing and implementing safety management practices in NPPs.

4.2 Applying the Proposed Model

4.2.1 Literature Review on Applications of HFACS, Fuzzy AHP and BBN

Research papers in the applications of fuzzy AHP, HFACS and BBN in different applications were thoroughly studied and well explained in Sect. 2.

4.2.2 Define the Accident/Incident

After reviewing the accident report from various research publications and Nuclear Regulatory Guidelines (NUREG), the accident is defined as “Human and Organizational errors at Fukushima”.

4.2.3 Human Factor Identification Using HFACS

Depending on the category, the classification system can be a two- or three-step process when using HFACS as a classification tool. The four tiers of HFACS are unsafe actions (Tier 1), preconditions for unsafe acts (Tier 2), unsafe supervision

Table 4 Fuzzy number to fuzzy scale conversion

Numeric scale	Conceptual scale	Triangular fuzzy number (TFN)	Reciprocal TFN
1	Equal	(1, 1, 1)	(1, 1, 1)
3	Moderate	(2, 3, 4)	(1/2, 1/3, 1/4)
5	Strong	(4, 5, 6)	(1/4, 1/5, 1/6)
7	Very strong	(6, 7, 8)	(1/6, 1/7, 1/8)
9	Absolute	(8, 9, 10)	(1/8, 1/9, 1/10)

(Tier 3) and organizational process (Tier 4). The causes of the accident can all be easily identified by the classification given in the HFACS system. For example, if an operator does not wear the recommended shoes and clothing during his operational work, he may run the risk of being exposed to radiation. As a result, this finding was labelled as unsafe acts and evaluated using the HFACS framework.

4.2.4 Human Factor Pairwise Comparison for Fuzzy AHP

A questionnaire is developed based on the HFACS for human factors pairwise comparison. A nine-point scale has been used for performing pairwise comparisons and shown in Table 4. Three experts (probabilistic safety assessment (PSA) expert, human reliability analysis researcher and PSA analyst) have been asked to respond to a sequence of pairwise comparisons by employing triangular fuzzy numbers. Triangular fuzzy numbers (1, 3, 5, 7, and 9) have been used to indicate the relative importance of each pair of entities at the same level. Eigenvector matrix for fuzzy pairwise comparison is shown in Tables 5, 6, 7 and 8.

α-Cut for the TFN is as follows,

Table 5 Fuzzy comparison matrix for dependencies in "unsafe acts" criteria

Factors	SB	DE	PE
SB	1	4	5
DE	1/4	1	5
PE	1/5	1/5	1

Factors	RV	EV
RV	1	4
EV	1/4	1

Table 6 Fuzzy comparison matrix for dependencies in "preconditions of unsafe acts" criteria

Factors	AMS	APS	PML
AMS	1	6	5
APS	1/6	1	5
PML	1/5	1/5	1
Factors	PE	TE	
PE	1	5	
TE	1/5	1	
Factors	CRM	PR	
CRM	1	7	
PR	1/7	1	

Table 7 Fuzzy comparison matrix for dependencies in "unsafe supervision" criteria

Factors	IS	PIA	FCP	SV
IS	1	5	5	5
PIA	1/5	1	7	7
FCP	1/5	1/7	1	1/7
SV	1/5	1/7	7	1

Table 8 Fuzzy comparison matrix for dependencies in "organizational influences" criteria

Factors	RM	OC	OP
RM	1	6	6
OC	1/6	1	4
OP	1/6	1/4	1

$$
\begin{aligned}
1\alpha &= [1, 3 - 2\alpha] \\
3\alpha &= [1 + 2\alpha, 5 - 2\alpha] \\
5\alpha &= [3 + 2\alpha, 7 - 2\alpha] \\
7\alpha &= [5 + 2\alpha, 7 - 2\alpha] \\
9\alpha &= [7 + 2\alpha, 11 - 2\alpha] \\
3\alpha^{-1} &= [1 + 2\alpha, 5 - 2\alpha] \\
5\alpha^{-1} &= [3 + 2\alpha, 7 - 2\alpha] \\
7\alpha^{-1} &= [5 + 2\alpha, 9 - 2\alpha] \\
9\alpha^{-1} &= [7 + 2\alpha, 11 - 2\alpha]
\end{aligned}
$$

where α is confidence level, whose value is substituted as $\alpha = 0.5$.

The fuzzy scale regarding relative importance to measure the relative weights is given in Table 4. This scale is proposed by Saaty [41] used for solving fuzzy decision-making problems.

4.3 Calculation of Human Factor Weighted Index (HFWI)

The human factor weighted index has been calculated for all pairwise comparisons in HFACS. The calculation of geometric mean and HFWI for "unsafe acts" is shown in Tables 9, 10, 11 and 12. Similarly, the geometric mean and HFWI are computed for all factors in all levels in HFACS and shown in Table 13.

4.4 Selection of Parent and Child Nodes

The parent and child nodes are selected from the ranking factors from fuzzy HFACS. Knowledge-based errors, cognitive factors, fail to correct known problems and organizational process are selected as parent nodes, and the child node is considered as the human error. The marginal distribution for the parent node is obtained from fuzzy AHP results.

4.5 Estimation of Prior Probability and Conditional Probability

The values of prior and conditional probabilities are given by using the fuzzy membership to describe the probabilities given by experts. The marginal destruction probability value and conditional probability table are obtained from the fuzzy membership function (l, m, u) from Tables 8, 9 and 10.

4.6 Quantification of Human Error Using BBN

Finally, the quantification of human error is done for using BBN. From the fuzzy AHP results, the prior and conditional probability values are elucidated and results are obtained.

The quantification of human error for the Fukushima with prior probability is shown in Fig. 2. The prior probabilities are calculated from the expert's opinion. This figure shows the results of prior probability values.

Table 9 Geometric mean for comparison matrix of the sub-criteria under criteria "errors"

Factors	SB			DE			PE		
	l	*m*	*u*	*l*	*m*	*u*	*l*	*m*	*u*
SB	1	1	1	0.368	0.437	0.550	0.144	0.168	0.203
DE	1.817	2.289	2.714	1	1	1	0.131	0.150	0.177
PE	4.932	5.944	6.952	5.646	6.649	7.652	1	1	1

Table 10 Geometric mean for comparison matrix of the sub-criteria under criteria "violations"

Factors	RV			EV		
	l	*m*	*u*	*l*	*m*	*u*
RV	1	1	1	0.909	1.197	1.494
EV	0.669	0.836	1.101	1	1	1

Table 11 Eigenvector for comparison matrix of the sub-criteria under criteria "unsafe acts"

Factors	*l*	*m*	*u*
SB	1.512	1.605	1.753
DE	2.961	3.458	3.917
PE	10.865	12.89	14.90
RV	1.909	2.197	2.494
EV	1.6694	1.836	2.101
Total	18.916	21.98	25.17
Inverse	0.053	0.045	0.040
Ascending order	0.040	0.045	0.053

Table 12 Final eigenvector for HFWI of the sub-criteria under criteria "unsafe acts"

Factors	*l*	*m*	*u*	Average	Normalized
SB	0.060	0.073	0.093	0.075	0.090
DE	0.118	0.157	0.207	0.161	0.192
PE	0.432	0.586	0.788	0.602	0.718
RV	0.076	0.100	0.132	0.103	0.122
EV	0.066	0.083	0.111	0.087	0.104

The posterior probability of each parameter also estimated for the Fukushima accident is also done by setting evidence of accident probability as 100%, and the posterior estimation is shown in Fig. 3.

5 Results and Discussions

A qualitative and quantitative analysis of the proposed model of FAHP-HFACS-BBN is carried out using a case study of Fukushima accident. The analysis of the case study indicates that knowledge-based errors (priority weight 0.708) are the primary cause at the first level of the HFACS framework. Lack of training and inadvertent errors are the common errors identified in the knowledge-based errors. Routine violation is the next highest contributor (priority weight 0.122) in the level one category of unsafe acts. This indicates that knowledge-based operators sometimes violate the

Table 13 Final weights for contributing human factor in Fukushima-Daiichi accident

Level	Category	Sub-category	HFWI
Unsafe acts	Errors	SB	0.090
		RB	0.192
		KB	0.718
	Violations	RV	0.122
		EV	0.104
Preconditions of unsafe acts	Conditions of operators	AMS	0.388
		APS	0.112
		PML	0.049
	Environment factors	PE	0.203
		TE	0.036
	Personal factors	CRM	0.176
		PR	0.037
Unsafe supervision		IS	0.094
		PIA	0.198
		FCP	0.367
		SV	0.341
Organizational influences		RM	0.199
		OC	0.188
		OP	0.613

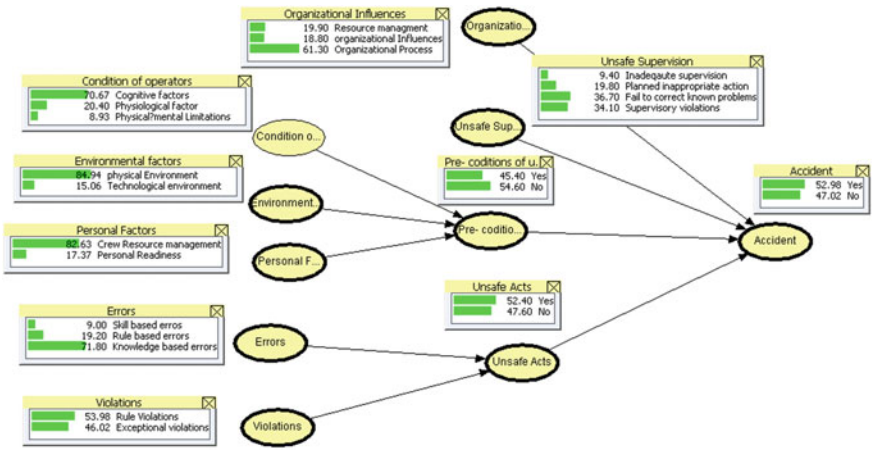

Fig. 2 Graphical representation based on prior probability for "Fukushima accident"

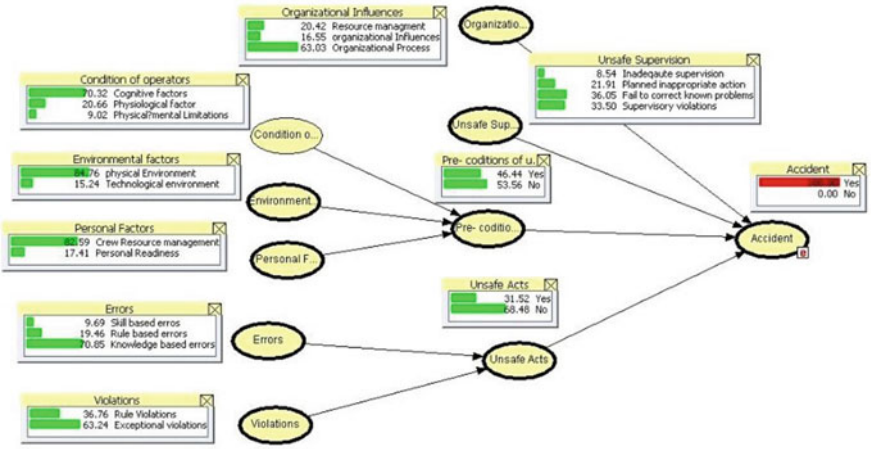

Fig. 3 Posterior probability estimation for "Fukushima accident"

rules and do not follow the manuals. In the second level of preconditions of unsafe acts, cognitive factors, physical environment and crew resource management are the most predominant errors for the accident. Among them, cognition-based errors are the highest contribution (priority weight 0.388) in the analysis. This indicates that cognitive factors such as attention, perception and memory influence more on the operators during abnormal condition. Physical environment has a priority weight of 0.203 followed by crew resource management which is 0.176. The above results indicate that a system should be designed with appropriate physical conditions such as visual display, lighting and alarms with reliable communication for operators. Failure to use available resources is the factor identified as crew resource management category. In the third level of HFACS, failure to correct problems (priority weight 0.31) has more weight. The fourth-level analysis shows that the root causes of this nuclear accident appear to be significant shortfalls in the execution of organizational processes (priority weight 0.613) such as time pressure, schedules and deficient planning, especially in an emergency situation and resource management (priority weight 0.199) including proper training of operator. Bayesian belief network is employed here to quantify the human factors identified by fuzzy AHP-HFACS. The prior probabilities of each factor are taken from the fuzzy AHP results. By using these values, the probability of human error is estimated as 52.99% for the accident. The posterior probability of each factor is estimated by setting evidence of 100% probability of accident. For example, the posterior probability of preconditions of unsafe acts is increased to 46.44 from 45.30 which means if preconditions of unsafe acts contribute 46.44%, the probability of accident is 100%.

6 Conclusions

A systematic model to identify and analyse human factors contributing to the human reliability analysis is proposed. From the results, it can be concluded that the model is useful in investigating HOFs in nuclear safety installations. The application of HFACS enables a comprehensive way of identifying active and latent human actions which are likely to lead to unsafe situations. The BBN model used in this study allows to make quantitative assessment of the human error. Fuzzy AHP minimizes the uncertainties while making judgements made by experts. The integration of BBN with HFACS allows the investigators or experts to quantify the degree of relationships among the human factors. In the results, the highly contributing factors at each level are derived based on weights. These highest weighting factors are considered as the critical and predominant factors contributing to the accident. By this analysis, weak links in the human performance in critical operations can be identified which is expected to aid designers for making suitable remedial measures to minimize the probability of accidents.

As future work, the study can be extended to analyse more number of accidents for decisions on significant human errors. Commercial software available for fuzzy AHP appears to be less, and future work may include development of specific software which facilitates the application of fuzzy AHP.

Acknowledgements This work was supported and funded by Safety Research Institute, Atomic Energy Regulatory Board, India. The authors would like to express sincere thanks to Director, NSARG, SRI-AERB, for his continuous support to do this research.

Compliance with Ethical Standards

Conflict of interest: The authors declare that they have no conflict of interest.

Ethical approval: Data collection for the study involving human participants was in accordance with the institutional ethical standards. This article does not contain any studies with animals performed by any of the authors.

Informed consent: Informed consent was obtained from all the experts included in the study.

References

1. Alvarenga MAB, Frutuoso e Melo PF, Fonseca RA (2014) A critical review of methods and models for evaluating organizational factors in human reliability analysis. Prog Nucl Energy 75:25–41
2. Griffith CD, Mahadevan S (2011) Inclusion of fatigue effects in human reliability analysis. Reliab Eng Syst Saf 96:1437–1447
3. Senthil Kumar C, John Arul A, Singh OP, Rao KS (2005) Reliability analysis of shutdown system. Ann Nucl Energy 32(1):63–87
4. Hilliard A, Jamieson GA (2015) Representing energy efficiency diagnosis strategies in cognitive work analysis. Appl Ergon 59:602–611
5. Swain AD, Guttmann HE (1983) Handbook of human reliability analysis with emphasis on nuclear power plant applications (NUREG/CR-1278). U.S. Nuclear Regulatory Commission

6. Hollnagel E (1998) Chapter 6—CREAM—a second generation HRA method. In: Cognitive reliability and error analysis method (CREAM)
7. Forester J, Kolaczkowski A, Cooper S, Bley D, Lois E (2007) ATHEANA user's guide final report (NUREG-1880). U.S. Nuclear Regulatory Commission Office of Nuclear Regulatory Research, Washington, DC
8. Pasquale VD, Miranda S, Iannone R, Riemma S (2015) A Simulator for Human Error Probability Analysis (SHERPA). Reliab Eng Syst Saf 139:17–32
9. Kim JN (1997) The development of K-HPES: a Korean-version human performance enhancement system. In: Human factors and power plants, pp 16–20
10. Shorrock ST, Kirwan B (2002) Development and application of a human error identification tool for air traffic control. Appl Ergon 33(4):319–336
11. Shappell S, Wiegmann DA (2000) The Human Factors Analysis and Classification System—HFACS. U.S. Department of Transportation Federal Aviation Administration
12. Dağdeviren M, Yüksel I, Kurt M (2008) A fuzzy analytic network process (ANP) model to identify faulty behavior risk (FBR) in work system. Saf Sci 46(5):771–783
13. Kubler S, Robert J, Derigent W, Voisin A, Traon YL (2016) A state-of-the-art survey & testbed of fuzzy AHP (FAHP) applications. Expert Syst Appl 65:398–422
14. Vinodh S, Anesh Ramiya R, Gautham SG (2011) Application of fuzzy analytic network process for supplier selection in a manufacturing organisation. Expert Syst Appl 38(1):272–280
15. Karthick M, Senthil Kumar C, Paul Robert T (2017) BAYES-HEP: Bayesian belief networks for estimation of human error probability. Life Cycle Reliab Saf Eng 6(3):187–197
16. Naghadehi MZ, Mikaeil Reza, Ataei Mohammad (2009) The application of fuzzy analytic hierarchy process (FAHP) approach to selection of optimum underground mining method for Jajarm Bauxite Mine, Iran. Expert Syst Appl 36(4):8212–8226
17. Karthick M, Senthil Kumar C, Paul Robert T (2020) Investigation of human factors using HFACS framework—a case study for unintended reactor trip events in NPP. In: Varde P, Prakash R, Vinod G (eds) Reliability, safety and hazard assessment for risk-based technologies. Lecture notes in mechanical engineering. Springer, Singapore
18. Chen ST, Chou YH (2012) Examining human factors for marine casualties using HFACS—Maritime Accidents (HFACS-MA). In: 12th international conference on ITS telecommunications, ITST, pp 391–396
19. Soner Omer, Asan Umut, Celik Metin (2015) Use of HFACS-FCM in fire prevention modelling on board ships. Saf Sci 77:25–41
20. Celik M, Cebi S (2009) Analytical HFACS for investigating human errors in shipping accidents. Accid Anal Prev 41(1):66–75
21. Nikki O, Williamson A (2017) Application of classification principles to improve the reliability of incident classification systems: a test case using HFACS-ADF. Appl Ergon 63:31–40
22. Li WC, Harris D, Yu CS (2008) Routes to failure: analysis of 41 civil aviation accidents from the Republic of China using the Human Factors Analysis and Classification System. Accid Anal Prev 40(2):426–434
23. Patterson JM, Shappell SA (2010) Operator error and system deficiencies: analysis of 508 mining incidents and accidents from Queensland, Australia using HFACS. Accid Anal Prev 42(4):1379–1385
24. Chen ST, Wall A, Davies P, Yang Z, Wang J, Chou YH (2013) A human and organisational factors (HOFs) analysis method for marine casualties using HFACS-Maritime Accidents (HFACS-MA). Saf Sci 60:105–114
25. Diller T, Helmrich G, Dunning S, Cox S, Buchanan A, Shappell S (2013) The human factors analysis classification system (HFACS) applied to health care. Am J Med Qual 29(3):181–190
26. Madigan R, Golightly D, Madders R (2016) Application of Human Factors Analysis and Classification System (HFACS) to UK rail safety of the line incidents. Accid Anal Prev 97:122–131
27. Lee AHI, Chen WC, Chang CJ (2008) A fuzzy AHP and BSC approach for evaluating performance of IT department in the manufacturing industry in Taiwan. Expert Syst Appl 34(1):96–107

28. Choudhary D, Shankar R (2012) An STEEP-fuzzy AHP-TOPSIS framework for evaluation and selection of thermal power plant location: a case study from India. Energy 42(1):510–521
29. Taylan O, Bafail AO, Abdulaal RMS, Kabli MR (2014) Construction projects selection and risk assessment by fuzzy AHP and fuzzy TOPSIS methodologies. Appl Soft Comput J 17:105–116
30. Dagdeviren M, Yuksel I (2008) Developing a fuzzy analytic hierarchy process (AHP) model for behavior-based safety management. Inf Sci 178(6):1717–1733
31. Li P, Chen GH, Dai LC, Zhang L (2012) A fuzzy-Bayesian network approach to improve the quantification of organizational influences in HRA frameworks. Saf Sci 50(7):1569–1583
32. Wang YF, Roohi SF, Hu XM, Xie M (2011) Investigations of human and organizational factors in hazardous vapor accidents. J Hazard Mater 191:1–3
33. Francis RA, Guikema SD, Henneman L (2014) Bayesian belief networks for predicting drinking water distribution system pipe breaks. Reliab Eng Syst Saf 130:1–11
34. Martins MR, Maturana MC (2013) Application of Bayesian belief networks to the human reliability analysis of an oil tanker operation focusing on collision accidents. Reliab Eng Syst Saf 110:89–109
35. Trucco P, Cagno E, Ruggeri F, Grande O (2008) A Bayesian belief network modelling of organisational factors in risk analysis: a case study in maritime transportation. Reliab Eng Syst Saf 93(6):823–834
36. Buckley JJ (1985) Fuzzy hierarchical analysis. Fuzzy Sets Syst 17(3):233–247
37. Kim MC (2014) Insights on accident information and system operations during Fukushima events. Sci Technol Nucl Install 2014
38. Baba M (2013) Fukushima accident: what happened? Radiat Meas 55:17–21
39. Steinhauser G, Brandl A, Johnson TE (2014) Comparison of the Chernobyl and Fukushima nuclear accidents: a review of the environmental impacts. Sci Total Environ 470:800–817
40. Saghafi M, Ghofrani MB (2016) Accident management support tools in nuclear power plants: a post-Fukushima review. Prog Nucl Energy 92:1–14
41. Saaty TL (1990) How to make a decision: the analytic hierarchy process. Eur J Oper Res 48(1):9–26

Reliability Issues in Electrical Distribution Systems

Distinctive Architecture Against Conspiring Attacks on Network Layer Over MANET Smart Grid Management

P. Vaishnavi, G. Vidhyalakshmi, and S. Vaishnavi

Abstract In the Recent decades, there is a vast requirements to lead the expanded network connectivity interms of connection, coordination and contribution. MANET serves as a mean to provide connectivity in such geographical locations, where connectivity through conventional mobile nodes is challenging. MANET is excellent communication systems in disaster-hit areas, as well as location of critical mission applications like military conflicts. Due to high dynamism and mobility, mobile networks are vulnerable to unauthorized access and malicious attacks. The strong challenge for MANET is to exhibit robust security solution even in the presence of malicious nodes. In this paper we propose distinctive architecture for MANET smart grid management along with consequence of conspiring attacks (Blackhole, Greyhole, Wormhole).

Keywords Blackhole attack · Greyhole attack · Wormhole attack · Mobile ad hoc network (MANET)

1 Introduction

A mobile ad hoc network (MANET) is moderately new communication model. MANET is considered as the most prominent technique. In initial stage research, wireless network was considered more comfortable to environment. The major issue in wireless channel is accessing and multi-hop routing. Although mobile ad hoc networks have several merits over wired networks, it has challenges to the security design than wired networks.

P. Vaishnavi (✉) · G. Vidhyalakshmi · S. Vaishnavi
Department of Computer Applications, Anna University, Chennai—BIT Campus, Tiruchirappalli, India
e-mail: vaishmk@gmail.com

G. Vidhyalakshmi
e-mail: ugvidhyalakshmicse@gmail.com

S. Vaishnavi
e-mail: vishruthsv@gmail.com

V. K. Gupta et al. (eds.), *Reliability and Risk Assessment in Engineering*,
Lecture Notes in Mechanical Engineering,
https://doi.org/10.1007/978-981-15-3746-2_47

MANET has no infrastructure network; all nodes of it are free to move. It has an ability to configure and maintain itself without assisting the centralized node. During the natural calamities, the nodes in MANET will frequently form a routing pattern to communicate the messages for disaster mitigation. The basic security issues in MANET at the primary stage are bits of data transfer, from one node to another. The nodes are connected virtually during communication. Each and every node transmission creates virtual connections. Routing protocol leads a way. Nodes act like router in ad hoc network. The advanced technique in wireless channels paved a way to both user and attackers. It shows that single solution never removes the boundaries. The existing proposals are vulnerable, so they try to detect the security threat and also improvise the proposal to overcome the threat. The present communication is an attempt to configure strong security management MANET against Blackhole, Greyhole and wormhole over MANET.

2 Related Works

Generally, attacks are not induced to follow the path of the node. It will decrease the performance of the network, and hence, to secure the network, watchdog mechanism has been used [1]. The Routing protocol AODV is prominent protocol used in MANET to detect the malicious attacks. The NS2 simulation software endorses the performance of the network with or without attacks. The wormhole attacks are reduced based on RTT and PFT tests [2]. The simulation results obtained in the proposed model are compared between DSR and AODV algorithms [2]. In order to defend the wormhole attack, a trust-based approach is also reported [3]. Finally, the proposed technique is integrated with IIRD which helps to identify and prevent the hole attacks in MANET. To prevent the hole attack, a signature technique has also been developed [4]. This verification and validation technique is used and relies on encryption types to ensure authentication. In order to strengthen the security of MANET preventing from blackhole and wormhole attack, an algorithm was developed based on ANT colony optimization framework [5]. The packet leash mechanism is used to detect and defend wormhole attacks. Hybrid cryptography, which gives a bit higher security for the networks, has also been proposed [6]. The digital signature algorithm-based RSA and DES are used in the proposed approach to overcome the problems in the existing system. Hybrid cryptography demonstrates higher detection rates and increases the network performance [7]; the proposed approach holds a technique to detect blackhole methodology included in AODV protocol so that when malicious node is detected then alarm is triggered. A MANET architectural model [8] describes the MANET's specific issues.

3 Proposed System Architecture

In MANET, routing the data packets to the destination node is the serious operation of the network because quite often the network breaks the links due to which it encounters change in transmission characteristics of intermediate nodes, from symmetrical links to asymmetrical links. The weakness of MANET, during routing are the unwrapped medium, un-trusted, cooperative environment leads to severe conspiring attacks in the network layer. The proposed system leads to design the Distinctive Architecture against the conspiring attacks on network layer over MANET smart grid management as an automated control for distribution and repairs.

In Blackhole attack the node act as malicious and it responds to request from the source node to broadcast the packets also it pretends as if it is the shortest path to destination. The greyhole attack similar to blackhole and difference is it drops the packets selectively. The performance of network layer are highly affected by this attack [8]. During the data packet transmission, some types of malicious nodes create a tunnel between the source and destination and either misguide or change the data packet, which is known as wormhole attack.

The proposed system architecture has been designed to detect and prevent the conspiring attacks of blackhole, greyhole and wormhole. New intention technique with AODV protocol is described in two stages: one is route discovery and another is route monitoring. The QoS parameters like throughput, end-to-end delay and packet delivery ratio have been calculated. The throughput has been determined by the total number of packets passed over the total simulation time. The end-to-end delay is calculated by the time taken for delivering the data packet across a network from source to destination. The packet delivery ratio is determined by calculating the no. of data packets received within the period of time by the destination node.

Algorithm for route discovery to identify the path and malicious node

Step 1: The source node delivers the broadcast test packet (source and destination fake address, i.e., not present in the network).
Step 2: If malicious node is present in the network, it receives test packet, does not check its route table and delivers reply with highest sequence number to the source node, then
Check 1: The source receives the reply from some nodes and identifies whether it is a malicious node using the details of highest sequence number.
Check 2: The source adds this particular malicious node to the block list table.
Step 3: Else, the source node will broadcast the request packet to the destination node through intermediate nodes.
Step 4: The destination node delivers the reply with acknowledged data packet to the source node.
Step 5: The source node receives the replied packet and establishes a path between source and destination with optimal path (Fig. 1).

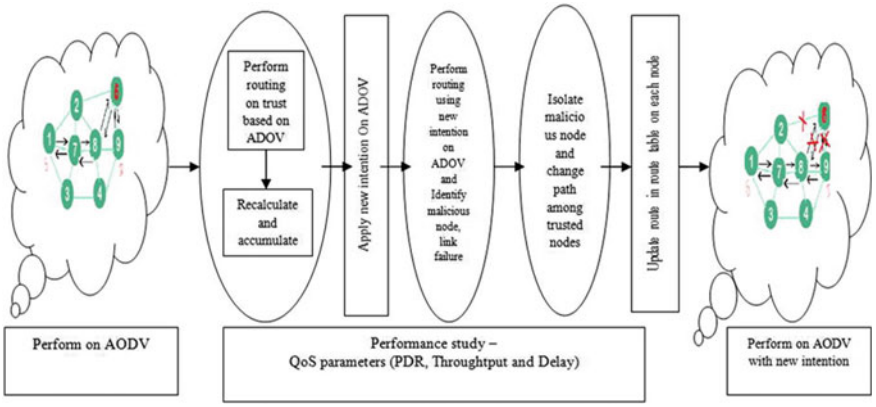

Fig. 1 Proposed system architecture

Algorithm for route monitoring to isolate the malicious node

Step 1: The source node delivers data packet to the destination node.
Step 2: The destination node receives the data packet in normal and sends acknowledgment (ack) to the source node.
Step 3: The source node receiveds the acknowledgment from the destination node.
Step 4: During data transmission on path, every node monitors its neighboring node.
If there is increase in ratio of drop data packets than the threshold value and also there no ack received by the source node then,

(i) node will send alert message, i.e., error message to the source node
(ii) Isolate the malicious node
(iii) Add to block list table
Go to route discovery
Else if path link failure due to dynamic topology
Then, send error messages and go to route discovery.

4 Conclusions

In this paper, a strong plan for MANET network layer security is proposed to protect the routing and packet forwarding techniques. The overall idea of the plan is to detect and prevent the attacks, which disrupt the communication network during critical operations. The developed system presents a distinctive architecture against the attacks of the blackhole, greyhole and wormhole over MANET smart grid management, which can be implemented and tested in the future for more number of

attacks, by increasing the nodes in the network. The main priority of the algorithm is to send the data through reliable route. Our distinctive architecture is suitable for any application such as emergency situation, rescue process, military battlefield. The quality of service parameters have been calculated between AODV and our new technique was working with AODV. For future enhancement, it is needed to be improved and updated more techniques for cost management and increased performance of MANET.

References

1. Vidhyapathi CM, Sundar S, Pal H, Punia K (2013) Securing MANETs from black hole and worm hole attacks. Int J Eng Technol (IJET) 5(3)
2. Behzad S, Fotohi R, Dadgar F (2015) Defense against the attacks of the black hole and worm hole in MANETs based on RTT and PFT. Int J Comput Sci Netw Solut 3
3. Grewal AK, Singh G (2017) Detection and prevention of grayhole, blackhole and wormhole attacks in MANET using IIRD. Int J Innov Res Comput Commun Eng 5(9)
4. Monika S, Gupta S (2015) Detection and prevention of black hole & gray hole attack in MANET using digital signature techniques. Int J Eng Comput Sci 4:13268–13272
5. Radhika A, Haritha D (2016) Detection and prevention of blackhole attack, wormhole attack in MANET using ACO. Int Natl J Eng Appl Sci (IJEAS) 3
6. Kulkarni P (2016) Novel hybrid techniques in EAACK for prevention of attacks in MANETS. Int Res J Eng Technol (IRJET) 03
7. Sharma N, Bisen AS (2016) Detection as well as removal of black hole and gray hole attack in MANET. In: International conference on electrical, electronics, and optimization techniques (ICEEOT)
8. A MANET architectural model (research report) (2007). HAL Id: inria-00136862. https://hal.inria.fr/inria-00136862v1. Submitted 15 Mar 2007 (v1), last revised 10 Jan 2007 (v3)

Steady-State Analysis of Self-excited Induction Generator to Enhance Reliability in Isolated Mode

Ashish Gupta and Arvind Kumar Jain

Abstract Nowadays, global warming is the main issue throughout the world because the temperature is surging due to increase in consumption of fossil fuels like coal and petroleum products. Therefore, renewable energy sources are getting attention among researchers to supply electric power for the modern world. Due to reduced cost, less maintenance, rugged and without brush construction, the self-excited induction generator (SEIG) is recommended for distributed generation. One of the most promising renewable energy sources is wind energy which is used as prime mover to self-excited induction generator (SEIG) located in remote areas in isolated mode. This paper presents steady-state reliability analysis of three-phase SEIG considering constant-frequency, constant-speed and variable-speed frequency-generating schemes. Simulation result reveals that SEIG-based electric system yields higher output for low and high wind speeds, it is free from synchronization problem, and frequency is constant for load variation at a particular rotational speed. Therefore, SEIG is useful for residential and commercial load, mini and micro hydro power plant and resistance heating load.

Keywords Self-excited induction generator · Generating schemes · Isolated system · Distributed generation

1 Introduction

An externally driven induction machine with a reasonable value of capacitor bank can be used as a generator [1]. This system is called self-excited induction generator (SEIG). Self-excited induction generators (SEIGs) have been found to be suitable for energy conversion for remote locations. Such generators can usually be used in remote rural areas where it is not possible to pull from transmission lines. These

A. Gupta (✉) · A. K. Jain
Discipline of Electrical Engineering, NIT Agartala, Barjala, Jirania, Agartala, Tripura, India
e-mail: ashishgupta97@gmail.com

A. K. Jain
e-mail: arvindj@nita.ac.in

V. K. Gupta et al. (eds.), *Reliability and Risk Assessment in Engineering*,
Lecture Notes in Mechanical Engineering,
https://doi.org/10.1007/978-981-15-3746-2_48

machines can be used to meet the local demand of remote areas in the absence of grid [2, 3]. SEIG has several advantages over synchronous generators: brushless (squirrel-cage rotor), reduced size, rugged and low cost. But the induction generator provides poor voltage regulation, and its value depends on the prime mover speed, capacitor bank and load [4]. The use of an induction machine as a generator is becoming more and more popular for renewable sources [5]. In the paper [6], the susceptibility theory-based sliding mode control (STSMC) algorithm has been proposed to increase the power quality to a single-phase micro grid. The proposed algorithm consists of a self-excited induction generator (SEIG), PV array and a battery system. STSMC was explained in real time using DSP controller. The proposed system significantly improves the reliability of micro grid. Paper [7] has proposed analytical and iterative methods to determine the critical excitation capacitor value to self-excite an induction generator to analyze steady-state performance. The paper [8] represents a steady-state analysis of a three-phase self-excited induction generator (SEIG) with shunt compensation. The forward conductance of the excitation potential of SEIG is determined in both the load and unload states.

2 System Configuration

SEIG is operated by prime mover. The generator supplies an isolated three-phase four-wire load. When an induction machine moves at a speed greater than synchronous speed (negative slip) through an external prime mover, the direction of the induced torque reverses and theoretically starts to operate as an induction generator. From the circle diagram of the induction machine in the negative slip region [9], it is seen that the machine draws current, which is lags by a voltage greater than 90°. This means that the actual power excites the machine, but the machine requires reactive power. In order to produce a voltage across the generator terminals, excitation must be provided in some ways. Therefore, the induction generator can operate in two modes. In the case of grid-connected modes, the induction generator can draw reactive power from the grid by connecting a capacitor bank to the generator terminals [10, 11]. For a discrete mode, an appropriate capacitor bank must be connected to the generator terminals. This phenomenon is known as capacitor self-excitation, and the induction generator is called “SEIG” [12]. Figure 1 shows a schematic arrangement of self-excited induction generator as a separate system.

3 Steady-State Modeling

The steady-state analyses of SEIG are of interest from both design and operational points of view. In isolated power systems, both the terminal voltage and frequency are unknown and have to be calculated for a given speed, capacitance and load impedance. In the present paper, the standard steady-state equivalent circuit of SEIG

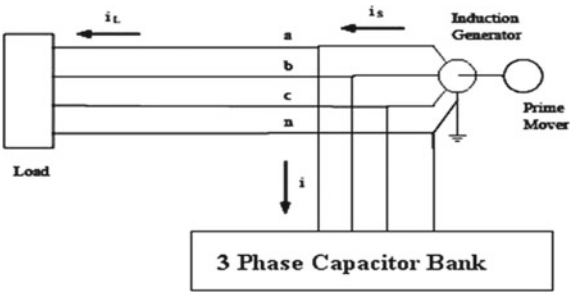

Fig. 1 Self-exited induction generator system

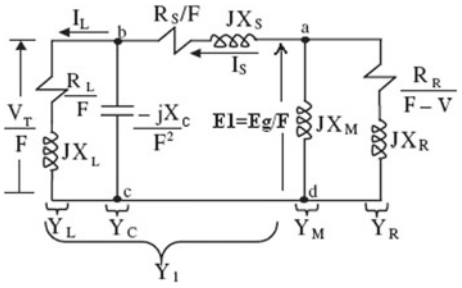

Fig. 2 Per-phase equivalent circuit of a SEIG

with the general assumptions, considering the variance of magnetizing reactance with saturation as the basis for calculation. The circuit is normalized to equal the base frequency by dividing all the parameters by the PU. The frequency is shown in Fig. 2.

The total current at node "a" in the above figure can be written as

$$E_1(Y_1 + Y_M + Y_R) = 0 \tag{1}$$

Therefore, under steady-state self-excitation, the total admittance must be zero,

$$(Y_1 + Y_M + Y_R) = 0 \tag{2}$$

where

$$Y_1 = \frac{(Y_C + Y_L)(Y_S)}{Y_C + Y_L + Y_S}, \quad Y_C = \frac{1}{-(jX_C/F^2)}, \quad Y_L = \frac{1}{(R_L/F)},$$
$$Y_S = \frac{1}{(R_S/F) + jX_S}, \quad Y_M = \frac{1}{jX_M}, \quad Y_R = \frac{1}{\frac{R_R}{F-V} + jX_R}$$

By separating the real and imaginary components of Eq. (2) and putting separately equal to zero, two equations are obtained in terms of machine parameters' shaft speed and generated frequency.

$$G_0(F) = A_5F^5 + A_4F^4 + A_3F^3 + A_2F^2 + A_1F + A_0 = 0 \tag{3}$$

$$H_0(V) = B_2V^2 + B_1V + B_0 = 0 \tag{4}$$

The coefficients (A_0–A_5) and (B_0–B_2) of two characteristics equation are obtained by solving the above two equations mathematically and given in Appendix 2, and X_M can be obtained from imaginary parts of Eq. (2) as

$$X_M = -1/\left\{\frac{X_R}{[R_R/(F-V)]^2 + X_R^2} + \frac{X_{ac}}{R_{ac}^2 + X_{ac}^2}\right\} \tag{5}$$

where

$$X_{ac} = X_s - X_{bc}, \quad R_{ac} = \frac{R_s}{F} + R_{bc},$$

$$X_{bc} = R_L^2X_C/(F^2R_L^2 + X_C^2), \quad R_{bc} = R_LX_C^2/[F(F^2R_L^2 + X_C^2)]$$

Now, by solving the equivalent circuit of SEIG, the analysis of machine is simple and straight. Branch currents, terminal voltage input power and output power are computed as under:

$$P_{\text{in}} = \frac{-3R_RF|I_R|^2}{F-V} \tag{6}$$

$$P_{\text{out}} = 3|I_L|^2R_L \tag{7}$$

where

$$I_S = \frac{E_g/F}{\frac{R_S}{F} + jX_S - \frac{jX_CR_L}{F^2R_L - FX_C}}, I_R = \frac{-E_g/F}{\frac{R_R}{F-V} + X_R}, \quad I_L = \frac{-jX_CI_S}{R_LF - jX_C}.$$

4 Simulation Results

Depending upon the prime movers used (constant speed or variable speed) and their locations (near to the power network or at isolated places), generating schemes can be broadly classified as under:

- Constant-frequency schemes
- Constant-speed schemes
- Variable-speed variable-frequency schemes.

4.1 Constant-Frequency Schemes

The variable-speed operation of the wind power system achieves high output for both low and high wind speeds. This results in higher annual energy yields per installed capacity. Both horizontal and vertical axis wind turbines exhibit this advantage under variable-speed operation. For constant frequency, shaft speed and magnetization response will vary with load and be taken as variable and calculated using Eqs. 8 and 9.

$$H_0(V) = B_2V^2 + B_1V + B_0 = 0 \tag{8}$$

$$X_M = -1/\left\{\frac{X_R}{[R_R/(F-V)]^2 + X_R^2} + \frac{X_{ac}}{R_{ac}^2 + X_{ac}^2}\right\} \tag{9}$$

The rating and datasheet of the induction generator considered in the present work are given in Appendix 1. The coefficients B_0–B_2 for this generator are obtained and discussed in Appendix 2. Using Eqs. 8 and 9, the load range and speed regulation for constant frequency of 60 Hz are computed and are summarized in Table 1.

The variation between rotational speed and load is shown in Fig. 3. The figure indicates that speed decreases with increment in load. The variation in magnetizing reactance with respect to load is also studied and is shown in Fig. 4. It can be clearly observed from Fig. 4 that magnetizing reactance changes for light load

Table 1 Load impedance and shaft speed of SEIG with constant output frequency

S. No.	Load impedance at unity power factor (in Ω)	Shaft speed (pu)	Output frequency (pu)
1	1.80	1.0379	0.9
2	5.40	1.0105	0.9
3	10.20	1.0037	0.9
4	13.80	1.0016	0.9
5	21.00	0.9996	0.9
6	24.60	0.9991	0.9
7	29.40	0.9985	0.9
8	33.00	0.9982	0.9
9	37.20	0.9979	0.9
10	39.60	0.9978	0.9
11	43.80	0.9976	0.9
12	52.80	0.9973	0.9
13	56.40	0.9972	0.9
14	61.20	0.9971	0.9

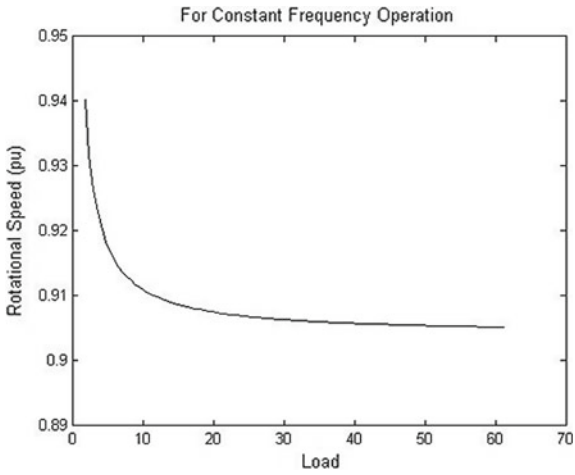

Fig. 3 Variation of rotational speed and load

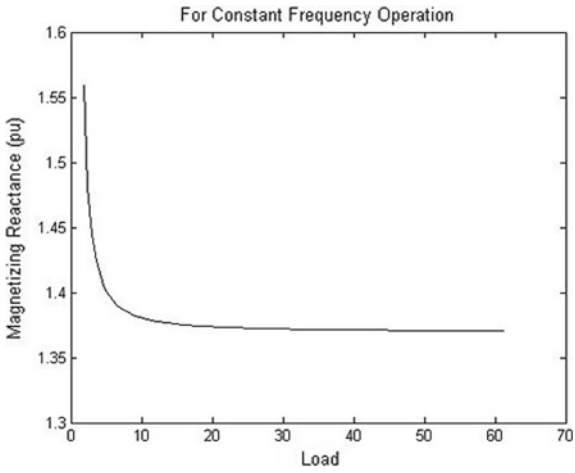

Fig. 4 Variation of magnetizing speed with load reactance and load

but remains almost constant for medium and large load. Therefore, the constant-frequency scheme is used in wind park for supplying both the residential and commercial loads.

The variation between rotational speed and load is shown in Fig. 3. The figure indicates that speed decreases with increment in load. The variation in magnetizing reactance with respect to load studied and is shown in Fig. 4. It can be clearly observed that magnetizing reactance changes for light load but remains almost constant for medium and large load. Therefore, constant-frequency scheme is used in wind park for supplying both the residential and commercial loads.

4.2 Constant-Speed Schemes

To achieve constant-speed operation, the generator must be powered by a fixed shaft speed turbine. In this scheme, the prime mover speed is kept constant by continuously adjusting the pitch and/or generator characteristics of the blade. For constant shaft motion, the generated frequency and magnetization response will vary with load and be taken as a variable and calculated using Eqs. 10 and 11.

$$G_0(F) = A_5F^5 + A_4F^4 + A_3F^3 + A_2F^2 + A_1F + A_0 = 0 \tag{10}$$

$$X_M = -1/\left\{\frac{X_R}{[R_R/(F-V)]^2 + X_R^2} + \frac{X_{ac}}{R_{ac}^2 + X_{ac}^2}\right\} \tag{11}$$

The coefficients (A_0–A_5) are given in Appendix 2. The load range and frequency regulation for constant speed are summarized in Table 2. The variation between generated frequency and load is shown in Fig. 5. Similarly, the variation between magnetizing reactance and load is obtained and is shown in Fig. 6.

An induction generator can operate on an infinite bus strip 1–5% above synchronous speed. Induction generators are simpler than synchronous generators. They are easy to operate, control and maintain, have no synchronization issues and are economical. Therefore, the scheme is used in mini and micro hydro power plants.

Table 2 Load impedance and output frequency of SEIG with constant shaft speed

S. No.	Load impedance at unity power factor (in Ω)	Output frequency (pu)	Shaft speed (pu)
1	1.80	0.7632	0.95
2	5.40	0.7699	0.95
3	10.20	0.7715	0.95
4	13.80	0.7720	0.95
5	21.00	0.7725	0.95
6	24.60	0.7726	0.95
7	29.40	0.7727	0.95
8	33.00	0.7728	0.95
9	37.20	0.7728	0.95
10	43.80	0.7729	0.95
11	52.80	0.7730	0.95
12	56.40	0.7730	0.95
13	61.20	0.7730	0.95

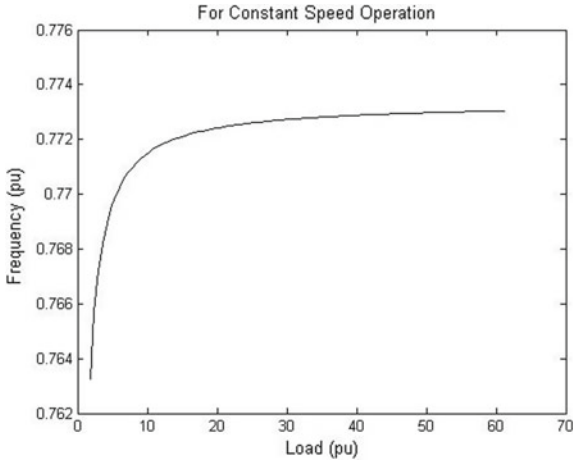

Fig. 5 Variations of generated frequency with load for constant speed operation

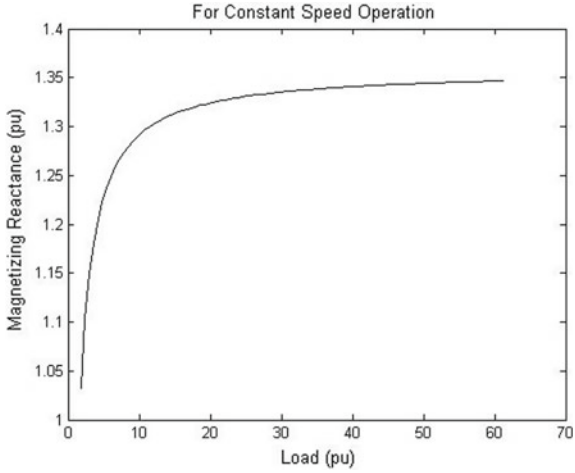

Fig. 6 Variation of magnetizing reactance with load for constant speed operation

4.3 Variable-Speed Variable-Frequency Schemes

For variable speeds corresponding to varying derivative speeds, SEIG can easily be used for resistive heat loads, which are essentially frequency insensitive. The scheme is gaining importance for stand-alone wind energy applications. In this, both the operation-generated frequency and the magnetizing reaction load and shaft speed will be taken as variables and calculated using Eqs. 12–14.

$$G_0(F) = A_5F^5 + A_4F^4 + A_3F^3 + A_2F^2 + A_1F + A_0 = 0 \tag{12}$$

$$H_0(V) = B_2V^2 + B_1V + B_0 = 0 \tag{13}$$

$$X_M = -1/\left\{\frac{X_R}{[R_R/(F-V)]^2 + X_R^2} + \frac{X_{ac}}{R_{ac}^2 + X_{ac}^2}\right\} \tag{14}$$

The coefficients (A_0–A_5) and (B_0–B_2) are given in Appendix 2. The variation between generated frequency and load at different speed is shown in Fig. 7. Similarly, the variation between magnetizing reactance and load is shown in Fig. 8. Figure 9 shows the variation between generated frequency and rotational speed.

It can be clearly observed that magnetizing reactance increases with load up to saturation, whereas the frequency is constant for the load variation from very small to large at a particular rotational speed. Therefore, this scheme is used in resistance heating.

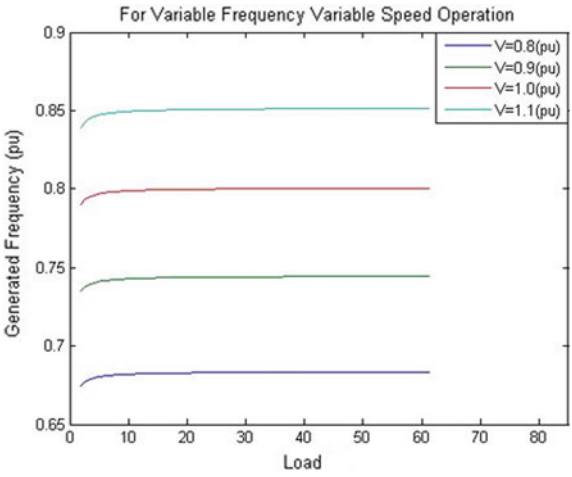

Fig. 7 Variations of generated frequency with load variable-speed variable-frequency operation

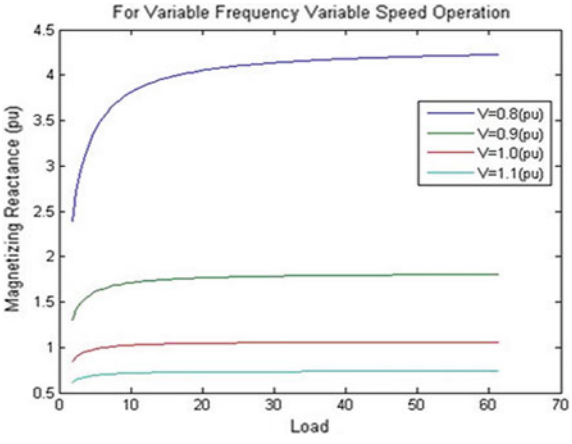

Fig. 8 Variation of magnetizing reactance with load variable-speed variable-frequency operation

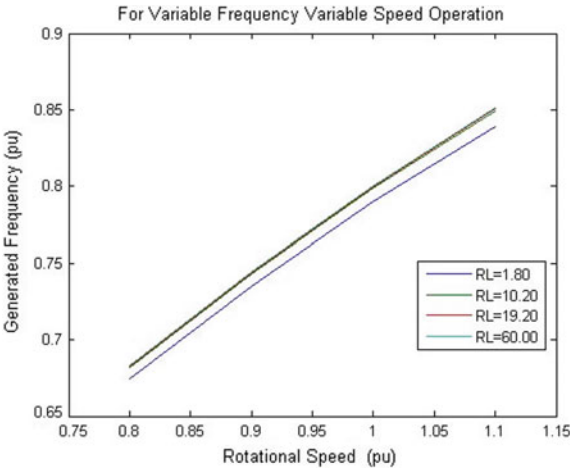

Fig. 9 Variations of generated frequency with rotational speed

5 Conclusions

Induction generators are simpler than synchronous generators. They are easy to operate and control, economical and do not have any synchronization problems. Therefore, several operating schemes of SEIG are discussed in this work, which are useful for setting SEIG on a different mode. From the results, it has been observed that self-excited induction generator is a perfect choice for remotely ventilated locations for power supply in a reliable manner. In addition, the proposed analysis can be helpful for researchers to think on the implementation of such generators successfully in remote locations of air and in various mini and micro hydro plants.

Appendix 1

The details of induction machine are:

- Specifications: three-phase, four-pole, 60 Hz, star-connected, squirrel-cage induction machine, 1 kW, 380 V, 2.27 A.
- Parameters: The equivalent circuit parameters for the machine are $R_S = 0.1$, $X_S = 0.2$, $R_R = 0.06$, $X_R = 0.2$;
  Base voltage = 219.3 V; base current = 2.27 A;
  Base impedance = 96.6 Ω; base frequency = 60 Hz;
  Base speed = 1800 rpm.

  The magnetization curve is represented mathematically as

$$\frac{E_g}{F} = 1.12 + 0.078X_M - 0.146X_M; \quad 0 < X_M < 3$$

Appendix 2

Coefficients (A_0–A_5) of equation $\boldsymbol{G}_0(\boldsymbol{F})$

$$A_0 = -VR_R\left(\frac{R_3}{R_L}\right)^2, \quad A_1 = R_R\left(\frac{R_3}{R_L}\right)^2 + R_3\left(\frac{R_R}{R_L}\right)^2 + V^2R_3\left(\frac{X_R}{R_L}\right)^2$$

$$A_2 = -2VR_3\left(\frac{X_R}{R_L}\right)^2 - VR_R\left\{\left(\frac{R_S}{X_C}\right)^2 + \left(\frac{X_S}{R_L}\right)^2 - 2\left(\frac{X_S}{X_C}\right)\right\}$$

$$A_3 = R_R\left[\left(\frac{X_S}{R_L}\right)^2 + \left(\frac{R_S}{X_C}\right)^2 - 2\left(\frac{X_S}{X_C}\right)\right] + R_3\left(\frac{X_R}{R_L}\right)^2 + R_S\left(\frac{R_R}{X_C}\right)^2 + V^2R_S\left(\frac{X_R}{X_C}\right)^2$$

$$A_4 = -V\left[R_R\left(\frac{X_S}{X_C}\right)^2 + 2R_S\left(\frac{X_R}{X_C}\right)^2\right], \quad A_5 = R_R\left(\frac{X_S}{X_C}\right)^2 + R_S\left(\frac{X_R}{X_C}\right)^2,$$

where $R_3 = R_S + R_L$.

Coefficients (B_0–B_2) of equation $\boldsymbol{H}_0(\boldsymbol{V})$

$$B_0 = R_RF(R_{ac}^2 + X_{ac}^2) + R_{ac}(R_R^2 + F^2X_R^2), \quad B_1 = -[R_R(R_{ac}^2 + X_{ac}^2) + 2FR_{ac}X_R^2],$$

$$B_2 = R_{ac}X_R^2.$$

References

1. Bassett ED, Potter FM (1935) Capacitive excitation for induction generators. AIEE Trans Electr Eng 54:540–545
2. Joshi D, Sandhu KS, Soni MK (2009) Voltage control of self-excited induction generator using genetic algorithm. Turk J Electr Eng Comput Sci 17(1). https://doi.org/10.3906/elk-0610-1
3. Joshi D, Sandhu KS (2009) Excitation control of self excited induction generator using genetic algorithm and artificial neural network. Int J Math Models Methods Appl Sci 3(1)
4. José AB, Griñó R (2006) Analysis of voltage control for a self-excited induction generator using a three-phase four-wire electronic converter. Departamento de Ingeniería Eléctrica, Electrónica y Automática ETSE, Universitat Rovira i Virgili Avinguda Països Catalans, 26, 43007 Tarragona (España)
5. Bansal RC, Bhatti TS, Kothari DP (2003) A bibliographical survey on induction generators for application of nonconventional energy systems. IEEE Trans Energy Convers 18(3):433–439
6. Kalla UK, Singh B, Murthy SS (2017) Slide mode control of microgrid using small hydro driven single-phase SEIG integrated with solar PV array. IET Renew Power Gener 11(11):1464–1472
7. Chermiti D, Khedher A (2017) Two reliable approaches to determine the critical excitation capacitor value for a SEIG operating in stand-alone. In: 2017 international conference on green energy conversion systems (GECS)

8. Bouchiba N, Sallem S, Kammoun MBA (2015) Three-phase self-excited induction generator analysis in stand-alone mode. In: 2015, 6th international renewable energy congress (IREC)
9. Nagrath IJ, Kothari DP (1997) Electrical machines, 2nd edn. Tata McGraw-Hill, New York
10. Bansal RC (2005) Three phase self excited induction generator: an overview. IEEE Trans Energy Convers 20(2)
11. Bansal RC, Kothari DP, Bhatti TS (2000) Some aspects of grid connected wind electric energy conversion systems. In: Proceedings of 24th national renewable energy conversion, Bombay, India, Nov 30–Dec 2
12. Jayadev TS (1976) Windmills stage a comeback. IEEE Spectr 13(11):45–49

Ashish Gupta received his B.Tech. and M.Tech. in Electrical Engineering from Madhav Institute of Technology and Science, Gwalior (MP), India. Presently, he is an Assistant Professor at RustamJi Institute of Technology (RJIT), BSF, Tekanpur, Gwalior (MP), India. His research interest includes distributed generation, optimal placement of FACTs devices and power electronics applications to power system.

Arvind Kumar Jain received his M.Tech. and Ph.D. in Electrical Engineering from Indian Institute of Technology Kanpur, Kanpur (UP), India. Presently, he is an Associate Professor at National Institute of Technology (NIT) Agartala (Tripura), India. His research interest includes demand response, power system economics and optimization, distributed generation, reactive power management and power system restructuring.